Science

8 March 2013 | $10

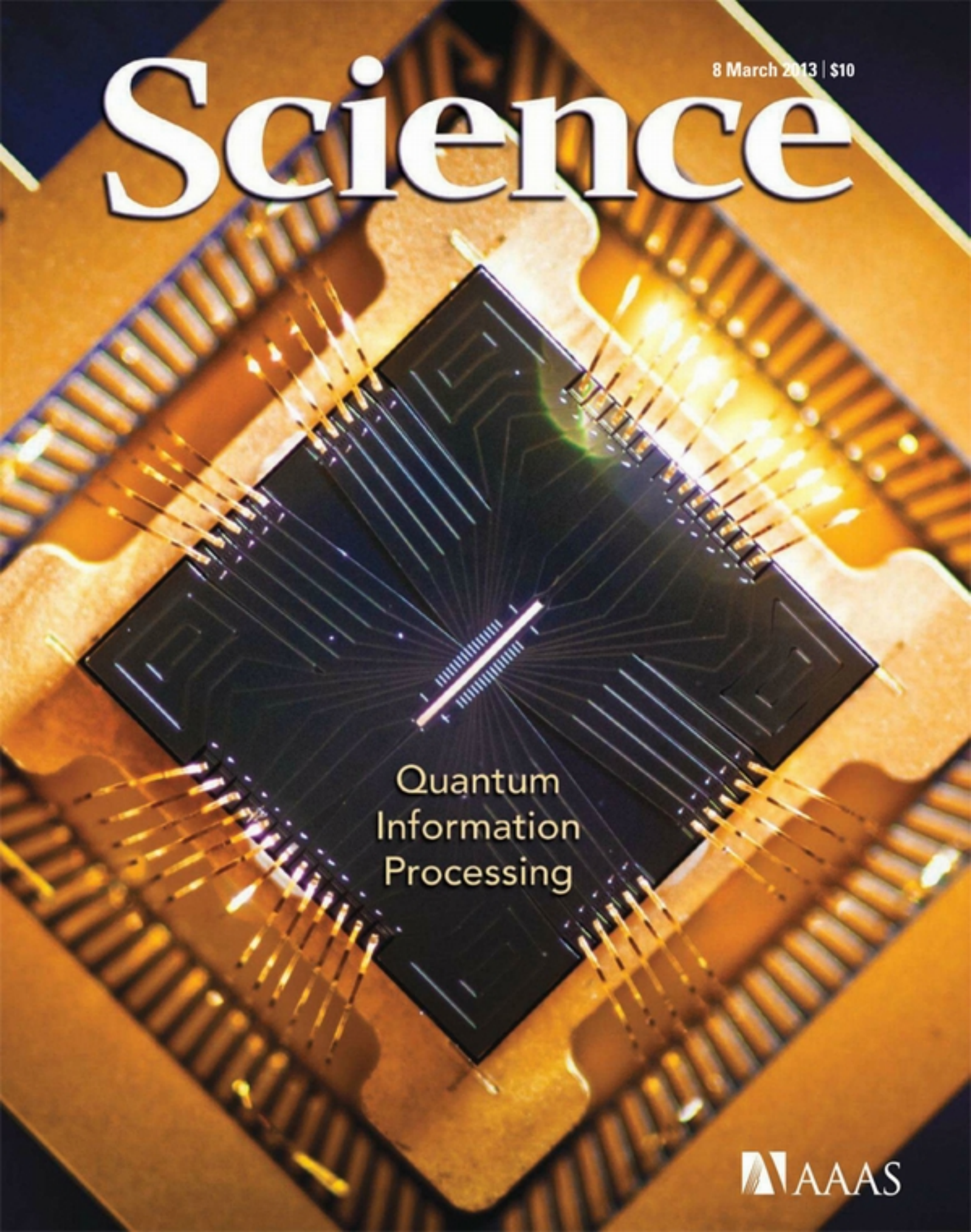

Quantum Information Processing

AAAS

Volume 339 Issue 6124

SPECIAL SECTION

Quantum Information Processing

INTRODUCTION

1163 The Future of Quantum Information Processing

REVIEWS

1164 Scaling the Ion Trap Quantum Processor
C. Monroe and J. Kim

1169 Superconducting Circuits for Quantum Information: An Outlook
M. H. Devoret and R. J. Schoelkopf

1174 Quantum Spintronics: Engineering and Manipulating Atom-Like Spins in Semiconductors
D. D. Awschalom et al.
>> Science *Podcast*

1179 Topological Quantum Computation—From Basic Concepts to First Experiments
A. Stern and N. H. Lindner

page 1138

EDITORIAL

1123 Denial of Catastrophic Risks
Martin Rees
>> Science *Podcast*

NEWS OF THE WEEK

1130 A roundup of the week's top stories

NEWS & ANALYSIS

1134 Early Treatment May Have Cured Infant of HIV Infection

1135 Siberian Meteor Spurs Dash for Data, Calls for Safeguards

1136 At Home on the Range: Prairie Rodents Yield Their Secrets to a Dogged Observer
>> *Report p. 1205*

NEWS FOCUS

1138 A Sea Change for U.S. Oceanography
The New Generation of Sea Scientist
Ahoy, Telepresence
>> Science *Podcast*

1144 Europe's Science Superwoman Struggles to Get Off the Ground

LETTERS

1148 The Other Revolution in the Life Sciences
C. De Duve

Museums' Role: Increasing Knowledge
G. C. Mayer et al.

Museums' Role: Pollen and Forensic Science
S. Warny

1149 CORRECTIONS AND CLARIFICATIONS

BOOKS *ET AL.*

1150 The Emergence of Organizations and Markets
J. F. Padgett and W. W. Powell, Eds., reviewed by M. Macy

1151 2052
J. Randers, reviewed by R. E. Horn

POLICY FORUM

1152 Behavioral Economics and the Retirement Savings Crisis
S. Benartzi and R. H. Thaler
>> Science *Podcast*

PERSPECTIVES

1154 With a Little Help from Prokaryotes
E. P. C. Rocha
>> *Report p. 1207*

1155 (De)Personalized Medicine
R. I. Horwitz et al.

1156 Red Wine, Toast of the Town (Again)
H. Yuan and R. Marmorstein
>> *Report p. 1216*

1157 Caffeine Boosts Bees' Memories
L. Chittka and F. Peng
>> *Report p. 1202*

1159 Getting the Jump on Explosive Percolation
R. M. Ziff
>> *Report p. 1185*

1160 Guilty by Association
N. S. Joshi and T. Jacks
>> *Report p. 1219*

1161 Exceptional Properties by Design
M. Zhou
>> *Report p. 1191*

CONTENTS continued >>

Explore our rich online offerings, including multimedia, news, *Science* Careers, and our two research journals—*Science Signaling* and *Science Translational Medicine*—at www.sciencemag.org

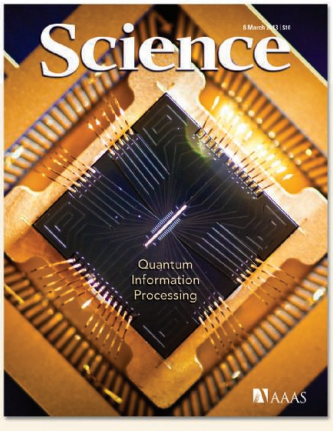

COVER

Photograph of a silicon chip (area of entire chip: 33 mm^2) that levitates individual atoms. Static and radio frequency voltages are applied to the array of electrodes at the center, creating an electric confinement for individual atomic ions, which hover ~0.1 mm above the chip. Such trapped ion systems are a leading physical implementation for quantum information processing. See the special section beginning on page 1163.

Photo: Curt Suplee and Emily Edwards, Joint Quantum Institute and University of Maryland; Chip fabrication: Sandia National Laboratories with support from the Intelligence Advanced Research Projects Activity

DEPARTMENTS

1121 This Week in *Science*
1125 Editors' Choice
1128 *Science* Staff
1225 New Products
1226 *Science* Careers

Published by AAAS

REPORTS

1185 Avoiding a Spanning Cluster in Percolation Models
Y. S. Cho et al.
In a percolation model that avoided bridge bonds, the continuity of transitions depends on lattice dimensionality.
>> Perspective p. 1159

1187 Emergence of a Measurement Basis in Atom-Photon Scattering
Y. Glickman et al.
The scattering of single photons from a trapped ion may shed light on the process of decoherence and quantum measurement.

1191 A Transforming Metal Nanocomposite with Large Elastic Strain, Low Modulus, and High Strength
S. Hao et al.
The use of a shape-memory metal alloy as a matrix better exploits the inherent elastic properties of niobium nanowires.
>> Perspective p. 1161

1194 Terrestrial Accretion Under Oxidizing Conditions
J. Siebert et al.
Earth's core formed under conditions similar to those that formed the most common meteorites.

1198 A Reconstruction of Regional and Global Temperature for the Past 11,300 Years
S. A. Marcott et al.
Current global average surface air temperature is warmer than that for all but a small fraction of the past 11,300 years.

1202 Caffeine in Floral Nectar Enhances a Pollinator's Memory of Reward
G. A. Wright et al.
Caffeine at concentrations found in flowers helps individual honeybees remember where to find associated nectar.
>> Perspective p. 1157

1205 Prairie Dogs Disperse When All Close Kin Have Disappeared
J. L. Hoogland
Long-term observation reveals that the presence of family members keeps a new generation of prairie dogs close to home.
>> News story p. 1136

1207 Gene Transfer from Bacteria and Archaea Facilitated Evolution of an Extremophilic Eukaryote
G. Schönknecht et al.
A mosaic of genes acquired from various phyla enable a red alga to grow abundantly in hot, acidic, and toxic niches.
>> Perspective p. 1154

1210 Cell Death from Antibiotics Without the Involvement of Reactive Oxygen Species
Y. Liu and J. A. Imlay

1213 Killing by Bactericidal Antibiotics Does Not Depend on Reactive Oxygen Species
I. Keren et al.
Tests of the oxidative damage mechanism for antibiotic killing do not support the generality of the hypothesis.

1216 Evidence for a Common Mechanism of SIRT1 Regulation by Allosteric Activators
B. P. Hubbard et al.
An interaction of the deacetylase SIRT1 with its substrate offers a possible explanation for some effects on aging.
>> Perspective p. 1156

1219 Aire-Dependent Thymic Development of Tumor-Associated Regulatory T Cells
S. Malchow et al.
Prostate tumors in mice recruit thymus-derived regulatory T cells that are specific for tissue autoantigens.
>> Perspective p. 1160

page 1150

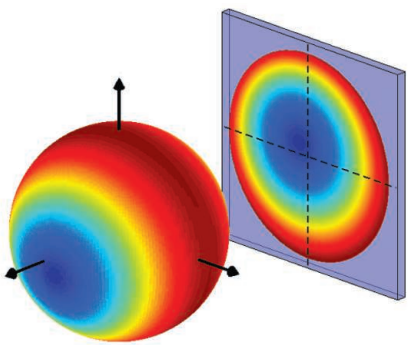

page 1187

pages 1157 & 1202

CREDIT: (BOTTOM) GERALDINE A. WRIGHT

SCIENCE (ISSN 0036-8075) is published weekly on Friday, except the last week in December, by the American Association for the Advancement of Science, 1200 New York Avenue, NW, Washington, DC 20005. Periodicals Mail postage (publication No. 484460) paid at Washington, DC, and additional mailing offices. Copyright © 2013 by the American Association for the Advancement of Science. The title SCIENCE is a registered trademark of the AAAS. Domestic individual membership and subscription (51 issues): $149 ($74 allocated to subscription). Domestic institutional subscription (51 issues): $990; Foreign postage extra: Mexico, Caribbean (surface mail) $55; other countries (air assist delivery) $85. First class, airmail, student, and emeritus rates on request. Canadian rates with GST available upon request, GST #1254 88122. Publications Mail Agreement Number 1069624. **Printed in the U.S.A.**

Change of address: Allow 4 weeks, giving old and new addresses and 8-digit account number. **Postmaster:** Send change of address to AAAS, P.O. Box 96178, Washington, DC 20090–6178. **Single-copy sales:** $10.00 current issue, $15.00 back issue prepaid includes surface postage; bulk rates on request. **Authorization to photocopy** material for internal or personal use under circumstances not falling within the fair use provisions of the Copyright Act is granted by AAAS to libraries and other users registered with the Copyright Clearance Center (CCC) Transactional Reporting Service, provided that $30.00 per article is paid directly to CCC, 222 Rosewood Drive, Danvers, MA 01923. The identification code for *Science* is 0036-8075. *Science* is indexed in the *Reader's Guide to Periodical Literature* and in several specialized indexes.

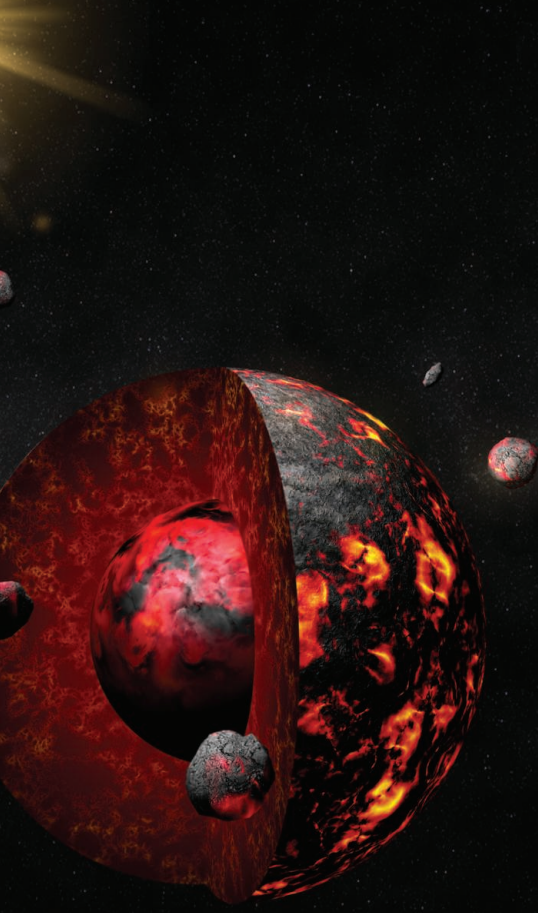

Earth's Ingredients

What was the composition of the earliest terrestrial starting blocks? The answer lies in understanding how Earth's interior separated into mantle and core components. **Siebert *et al.*** (p. 1194, published online 10 January) performed a series of high pressure and temperature experiments to track how chromium and vanadium, which have a slight affinity for iron, partition into metal and silicate fractions. Combined with accretionary models, the data suggest that Earth accreted under the same relatively oxidizing conditions under which the most common types of meteorites formed. Transferring oxygen in the form of FeO from the mantle to the core could have gradually reduced the mantle to its present-day oxidation state.

CREDITS (TOP TO BOTTOM): ANTOINE PITROU/INSTITUT DE PHYSIQUE DU GLOBE DE PARIS; SCHÖNKNECT *ET AL.*

Characterizing Quantum Measurement

In the classical world, the result of measurement is often viewed as independent of the experimental apparatus. In the quantum world, however, the act of measurement has an effect through processes such as back-action, entanglement, and decoherence. Looking at the scattering of single electrons from a single ion and the evolution of the spin state of that ion, **Glickman *et al.*** (p. 1187) probed how these processes are intertwined and characterize how the result of quantum measurement emerges from the system's interaction with its environment.

S-T-R-E-T-C-H Me

Most metals show elastic strain limits well below 1%, beyond which permanent plastic deformation occurs. Metal nanowires can be elastically stretched to much higher strains, on the order of 4 to 7%. However, when placed inside a metal matrix to form a composite, these nanowires can no longer be stretched to the same extent, even when the nanowires are well distributed and show good bonding with the matrix. **Hao *et al.*** (p. 1191; see the Perspective by **Zhou**) used a shape memory alloy as the matrix material to produce a much better (more elastic) composite.

Exceptional Now

The climate has been warming since the industrial revolution, but how warm is climate now compared with the rest of the Holocene? **Marcott *et al.*** (p. 1198) constructed a record of global mean surface temperature for more than the last 11,000 years, using a variety of land- and marine-based proxy data from all around the world. The pattern of temperatures shows a rise as the world emerged from the last deglaciation, warm conditions until the middle of the Holocene, and a cooling trend over the next 5000 years that culminated around 200 years ago in the Little Ice Age. Temperatures have risen steadily since then, leaving us now with a global temperature higher than those during 90% of the entire Holocene.

Bees Get That Caffeine "Buzz"

Caffeine improves memory in humans, millions of whom find that their daily dose enhances clarity, focus, and alertness. The human relationship with caffeine is relatively recent, however, and thus its impact on our brains is likely a by-product of its true ecological role. Caffeine occurs naturally in the floral nectar of *Coffea* and *Citrus* plants. **Wright *et al.*** (p. 1202; see the Perspective by **Chittka and Peng**) found that caffeine presented at naturalistic levels significantly improved the ability of bees to remember and locate a learned floral scent and potentiated the responses of neurons involved in olfactory learning and memory.

Hot, Toxic Eukaryote

Unusually, the single-celled eukaryote red alga, *Galdieria sulphuraria*, can thrive in hot, acidic springs. This organism is endowed with extraordinary metabolic talents and can consume a variety of strange carbohydrates, as well as turn on photosynthesis when the food runs out. **Schönknecht *et al.*** (p. 1207; see the Perspective by **Rocha**) discerned from phylogenetic analysis of its genome that during its evolution, *G. sulphuraria* appears to have commandeered at least 75 bacterial and archaeal genes by horizontal gene transfer and then applied gene expansion to boost its metabolic repertoire.

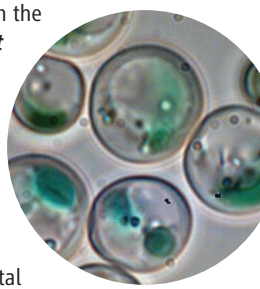

It's a SIRT

Intense attention has focused on the SIRT1 deacetylase as a possible target for anti-aging drugs. But unexpected complications in assays of SIRT1 activity have made it unclear whether compounds thought to be sirtuin-activating compounds (STACs) are really direct regulators of the enzyme. Further exploration of these effects by **Hubbard *et al.*** (p. 1216; see the Perspective by **Yuan and Marmorstein**) revealed that interaction of SIRT1 with certain substrates allows activation of SIRT1 by STACs and identified critical amino acids in SIRT1 required for these effects. Mouse myoblasts reconstituted with SIRT1 mutated at this amino acid lost their responsiveness to STACs.

On the Origin of Tumor T_{regs}

The tumor microenvironment is often seeded with regulatory T cells (T_{regs}), which inhibit antitumor immunity. Using mice with genetically driven prostate cancer, **Malchow *et al.*** (p. 1219; see the Perspective by **Joshi and Jacks**) found a population of T_{regs} that were enriched in the prostate of tumor-bearing mice. Surprisingly, these cells were also present in female mice and were found to be specific, not for a tumor-specific antigen, but rather for an antigen normally expressed in the prostate. Prostate antigen–specific T_{regs} arose in the thymus and their selection was dependent on Aire, a protein that drives the expression of tissue-specific antigens in the thymus. Thus, T_{regs} that seed tumors likely arise in the thymus, are not necessarily tumor-specific, and are recruited and/or expand in an organ when a tumor arises.

Additional summaries

Still Living in Their Mother's House

Dispersal, movement away from an organism's natal site, is a critical stage in the development of a juvenile into an adult and several drivers of this process have been proposed. A classic hypothesis put forward by Hamilton and May argues that individuals disperse away from kin in order to avoid competing with similar phenotypes. Many species have been shown to follow this pattern, and it is generally accepted that most organisms disperse well away from the sites where they were born. However, not all species follow this pattern and some display a distinct tendency to remain within their mother's home range. **Hoogland** (p. 1205) studied populations of three species of prairie dogs over more than three decades and found that the presence of close kin in these highly social rodents actually led young animals to remain on their natal site, whereas dispersal away from it occurred almost exclusively when close female kin were absent. This suggests that sociality may in fact result in individuals remaining with their close kin in order to benefit from cooperation and that longer-distance dispersal may instead occur when the opportunity for cooperation does not exist.

CREDIT: ELAINE MILLER BOND

Limits in Percolation Models

Slight changes in the number of connections within a network that form at random (for example, connections in social networks) can lead to a huge increase in connectivity, a phenomenon termed "explosive percolation." These percolation transitions are often studied with Erdös and Rényi models, in which edges connecting pairs of vertices in a network are added randomly or according to a rule. Whether these transitions are continuous in nature has been the subject of several recent studies. **Cho *et al.*** (p. 1185; see the Perspective by **Ziff**) examined the effect of avoiding bridge bonds that create a spanning cluster (one that completes the percolation path) on the continuity of transitions for a d-dimensional lattice (up to six dimensions). Analytical arguments and numerical studies reveal a critical value for the number of bonds m below which the percolation transition is continuous and above which it is discontinuous. The critical value depends on d and on the fractal dimension of the bridge bonds of the clusters.

Antibiotic Mechanisms Revisited

Several recent studies have suggested that bactericidal antibiotics kill cells by a common mechanism involving reactive oxygen species (ROS). Two groups tested this hypothesis using diverse experiments, with both finding that quinolone, lactam, and aminoglycoside antibiotics had similar efficacy for killing in the presence or absence of oxygen (or nitrate). **Liu *et al.*** (p. 1210) saw no increase in hydrogen peroxide production in antibiotic-exposed cells and found no association between antibiotic exposure and the expected symptoms of oxidative damage, such as the breakdown of iron-sulfur clusters in enzymes or of hydroxyl radical injuries to DNA. Similarly, **Keren *et al.*** (p. 1213) found no correlation between the production of ROS, inferred from hydroxyphenyl fluorescein dye measurements, and bacterial survival, nor was there any significant protective effect engendered by thiourea. The results do not support a common mode of action for bactericidal antibiotics mediated by ROS.

Published by AAAS

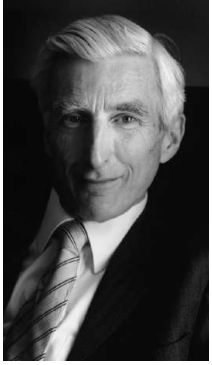

Martin Rees is a member of the United Kingdom's House of Lords and Astronomer Royal. He is cofounder, with Huw Price and Partha Dasgupta, of a prospective research program at Cambridge University, UK, on "existential risks." E-mail: mjr@ast.cam.ac.uk.

Denial of Catastrophic Risks

IN A MEDIA LANDSCAPE SATURATED WITH SENSATIONAL SCIENCE STORIES AND "END OF THE WORLD" Hollywood productions, it may be hard to persuade the wide public that real catastrophes could arise as unexpectedly as the 2008 financial crisis, and have a far greater impact. Society could be dealt shattering blows by the misapplication of technologies that exist already or could emerge within the coming decades. Some of the scenarios that have been envisaged may indeed be science fiction, but others may be disquietingly real. I believe these "existential risks" deserve more serious study. Those fortunate enough to live in the developed world fret too much about minor hazards of everyday life: improbable air crashes, possible carcinogens in food, low radiation doses, and so forth. But we should be more concerned about events that have not yet happened but which, if they occurred even once, could cause worldwide devastation.

The main threats to sustained human existence now come from people, not from nature. Ecological shocks that irreversibly degrade the biosphere could be triggered by the unsustainable demands of a growing world population. Fast-spreading pandemics would cause havoc in the megacities of the developing world. And political tensions will probably stem from scarcity of resources, aggravated by climate change. Equally worrying are the imponderable downsides of powerful new cyber-, bio-, and nanotechnologies. Indeed, we're entering an era when a few individuals could, via error or terror, trigger societal breakdown.

Some threats are well known. In the 20th century, the downsides of nuclear science loomed large. At any time in the Cold War era, the superpowers could have stumbled toward Armageddon through muddle and miscalculation. The threat of global annihilation involving tens of thousands of hydrogen bombs is thankfully in abeyance, but now there is a growing concern that smaller nuclear arsenals might be used in a regional context, or even by terrorists. We can't rule out a geopolitical realignment that creates a standoff between new superpowers. So a new generation may face its own "Cuba," and one that could be handled less well or less luckily than was the 1962 crisis.

What are some new concerns stemming from fast-developing 21st-century technologies? Our interconnected world depends on elaborate networks: electric power grids, air traffic control, international finance, just-in-time delivery, and so forth. Unless these are highly resilient, their manifest benefits could be outweighed by catastrophic (albeit rare) breakdowns cascading through the system. Social media could spread psychic contagion from a localized crisis, literally at the speed of light. Concern about cyberattack, by criminals or hostile nations, is rising sharply. Synthetic biology likewise offers huge potential for medicine and agriculture, but in the sci-fi scenario where new organisms can be routinely created, the ecology (and even our species) might not long survive unscathed. And should we worry about another sci-fi scenario, in which a network of computers could develop a mind of its own and threaten us all?

Online
sciencemag.org
Podcast interview with author Martin Rees (http://scim.ag/ed_6124).

Some would dismiss such concerns as an exaggerated jeremiad: After all, societies have survived for millennia, despite storms, earthquakes, and pestilence. But these human-induced threats are different—they are newly emergent, so we have a limited time base for exposure to them and can't be so sanguine that we would survive them for long, or that governments could cope if disaster strikes. That is why a group of natural and social scientists in Cambridge, UK, plans to inaugurate a research program to identify the most genuine of these emergent risks and assess how to enhance resilience against them. True, it is hard to quantify the potential "existential" threats from (for instance) bio- or cybertechnology, from artificial intelligence, or from runaway climatic catastrophes. But we should at least start figuring out what can be left in the sci-fi bin (for now) and what has moved beyond the imaginary.

– Martin Rees

10.1126/science.1236756

CREDITS: (TOP) LUCINDA DOUGLAS-MENZIES; (RIGHT) ISTOCKPHOTO/FEDOR KONOPLIN

Downloaded from www.sciencemag.org on March 8, 2013

Published by AAAS

CHEMISTRY

Plasmonic Water Splitting

One issue in harvesting the energy in sunlight to split water for hydrogen generation is utilizing the lower-energy visible-light component. Mubeen *et al.* report on an integrated platform in which plasmons excited in gold nanorods (~50 nm in diameter) create electron-hole pairs for driving the reaction. The nanorods are capped with a thin layer of titanium dioxide decorated with platinum nanoparticles, which act as the hydrogen generation catalysts. The sides of the nanorods are decorated with an inorganic cobalt-based oxygen evolution catalyst, so the nanorod also acts as the wire that completes the circuit. The plasmonic nature of the excitation generation was verified by showing that when operated as a photocathode (no cobalt catalyst but with a counterelectrode), the current generated tracked the changes in visible light intensity with wavelength. Indeed, the device operates less efficiently when illuminated only in the ultraviolet. Although the photon-to-hydrogen conversion efficiency is still low (~0.1%), improvements such as increasing the surface area devoted to the platinum catalyst could be made. The device could also be used in tandem with devices that are more efficient in the ultraviolet than in the visible range. — PDS

Nat. Nanotechnol. 10.1038/nnano.2013.18 (2013).

ATMOSPHERIC SCIENCE

Not Our Fault

The stratosphere contains a large inventory of aerosol particles. These aerosols are composed largely of sulfuric acid droplets, the precursors of which originate in the troposphere. Thus, the question has been asked whether anthropogenic emissions of sulfur-containing compounds such as sulfur dioxide have contributed substantially to the aerosol content of the stratosphere. Neely *et al.* report that changes in the concentration of stratospheric aerosols during the period from 2000 to 2010 were caused mostly by moderate volcanic eruptions and that the large increase in SO_2 emissions from China and India had no significant impact on it. They also conclude that the middle and upper stratosphere (which contains the bulk of the ozone layer) was not measurably affected by increased anthropogenic emissions of SO_2 from Asia during that interval. — HJS

Geophys. Res. Lett. 10.1002/grl.50263 (2013).

ECOLOGY

A Good Hiding Place

Dormancy in seeds is a common feature of plants, allowing seeds to be dispersed and to survive through unfavorable seasons before germinating. Dormancy can be physiological, terminated by some environmental cue; or it can be physical, whereby germination is prevented by the presence of a hard outer seed coat and is only achieved when the coat is ruptured. Paulsen *et al.* proposed an additional or alternative explanation for the function of hard seed coats, whereby escape from seed predators (rather than facilitation of dormancy) has been the selective force behind their evolution. An experimental system was used to compare the success of hamsters in detecting buried hard and soft dimorphic seeds of legume species. Soft seeds were located more easily owing to their production of a cocktail of volatile compounds that give their presence away. The authors suggest that hard seeds, even if detected, may be able to survive a second dispersal event when re-cached or pilfered by hoarding rodents, whereas soft seeds constitute a "payment" for dispersal services. The fact that hard/soft seed dimorphism has evolved at least six times provides further support for this interpretation. — AMS

New Phytol. 10.1111/nph.12191 (2013).

CREDITS (TOP TO BOTTOM): GETTY IMAGES/HEMERA; TORBJØRN R. PAULSEN

PHYSICS

Correcting for Quantum Collapse

The predicament faced by Schrödinger's cat is, perhaps, a broadly known if not wholly understood example of quantum mechanics that illustrates well the weirdness of the quantum world and the kinds of barriers faced by those now trying to control and manipulate it. The rules of quantum mechanics dictate that the mere measurement of a quantum system, describable mathematically in terms of a wavefunction, results in the irreversible collapse of that wavefunction and forces a definitive answer—the cat being either dead or alive. In quantum computing, wavefunction collapse presents a real issue because errors induced by unavoidable interactions with its environment look very much like measurements and can lead to a breakdown of the very quantum state you are trying to do a computation with. Methods have been introduced to correct those errors, which are then fed back into the system to keep the quantum state functional. Schindler *et al.* show that such error correction strategies can be used to undo a quantum measurement. Using a system of cold atoms and a series of laser

Continued on page 1127

Downloaded from www.sciencemag.org on March 8, 2013

Continued from page 1125

pulses, they distributed some of the knowledge they had of the quantum state of the atom of interest across the whole system. In doing so, they have shown that the state of a particular atom can be measured, but that it can be returned to the same superposition state (being both alive and dead) that it was in before the measurement. Such manipulations should lead to Schrödinger's cats with more than nine lives and, perhaps, simpler architectures for quantum processors. — ISO

Phys. Rev. Lett. **110**, 070403 (2013).

MICROBIOLOGY

AMPs In Action

Antimicrobial peptides (AMPs) provide an important first-line defense against bacteria and fungi in multicellular organisms. They do so by targeting the microbial cell membrane, but their precise mechanisms of action are not well understood. Song *et al.* used a combination of x-ray crystallography, electrophysiology, and molecular dynamics simulations to better understand the mechanism of one such AMP: dermcidin (DCD). DCD is secreted into human sweat and found on the skin. It is active against a range of bacteria, including methicillin-resistant *Staphylococcus aureus* and *Mycobacterium tuberculosis*. The authors' analysis revealed that DCD forms a hexameric barrel-like channel of elongated α helices in bacterial membranes. Stabilization of the channel required the presence of zinc. The channel formed was highly permeable to water and ions and so was a major membrane disruptor. This ability to disrupt the transmembrane potential of bacterial cell membranes can lead to rapid cell death and thus provide protective antimicrobial activity to the host. — KLM

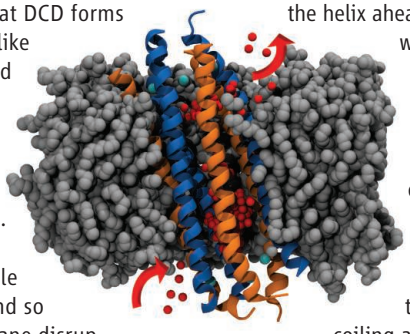

Proc. Natl. Acad. Sci. U.S.A. **110**, 10.1073/pnas.1214739110 (2013).

EDUCATION

Owning Up

One argument in favor of inquiry-based instruction is that it provides students with a sense of ownership over their learning. How do we characterize student ownership? Hanauer *et al.* examined the idea of project ownership among undergraduates involved in different types of laboratory experiences. A quantitative method for assessing project ownership was developed using both content and computational linguistic analysis of transcribed student interviews. A set of 14 elements, both positive and negative, that influenced the degree of project ownership experienced by a student was constructed. Five elements were found to foster student project ownership: facilitating personal agency, personal significance of the research project, scientific value of the scientific inquiry, social interaction and mentorship, and research that demands problem solving. Because the interviews for this study were conducted in 2008, the degree of student ownership could be correlated with the persistence of a scientific career. Students that expressed a higher level of project ownership also persisted further in science. — MM

CBE—Life Sci. Educ. **11**, 378 (2012).

MOLECULAR BIOLOGY

Mapping Supercoils

During transcription, the two strands of double-helical DNA must be locally separated, so that the RNA polymerase can transcribe the DNA, and then the helix must be resealed again. Opening the two strands and then moving this opening along the DNA as the template DNA strand is fed through the polymerase causes the helix ahead of the opening to be over-wound (positively supercoiled) and the helix behind the opening to be under-wound (negatively supercoiled). Either state has the potential to generate a topological impediment to transcription.

Kouzine *et al.* developed a method using the DNA cross-linking agent psoralen to map transcription-dependent supercoiling across the genome of human tissue culture cells. They find that, on average, negative supercoiling is prominent up to 1.5 kb upstream of the transcription start sites (TSSs) of moderately or strongly activated genes. Dynamic supercoiling was not associated with enhancers, regardless of the distance from their associated promoters. Topoisomerase I and II, enzymes that can dissipate supercoils, were found to act redundantly at moderately active genes, whereas topoisomerase II acted preferentially at the TSS of highly active genes. The results suggest that dynamic supercoiling is caused by frictional restriction of DNA twist diffusion and that it does not seem to be confined by fixed boundaries in chromatin. — GR

Nat. Struct. Mol. Biol. **20**, 10.1038/nsmb.2517 (2013).

CREDIT: CHEN SONG

Published by AAAS

Downloaded from www.sciencemag.org on March 8, 2013

www.sciencemag.org

Science

1200 New York Avenue, NW
Washington, DC 20005
Editorial: 202-326-6550, FAX 202-289-7562
News: 202-326-6591, FAX 202-371-9227
Bateman House, 82-88 Hills Road
Cambridge, UK CB2 1LQ
+44 (0) 1223 326500, FAX +44 (0) 1223 326501

Subscription Services For change of address, missing issues, new orders and renewals, and payment questions: 866-434-AAAS (2227) or 202-326-6417, FAX 202-842-1065. Mailing addresses: AAAS, P.O. Box 96178, Washington, DC 20090-6178 or AAAS Member Services, 1200 New York Avenue, NW, Washington, DC 20005

Institutional Site Licenses please call 202-326-6755 for any questions or information

Reprints: Author Inquiries 800-635-7181
Commercial Inquiries 803-359-4578

Permissions 202-326-7074, FAX 202-682-0816

Member Benefits AAAS Travels: Betchart Expeditions 800-252-4910; Apple Store www.store.apple.com/us/go/eppstore/aaas; NASA Federal, 1-888-NASA-FCU (1-888-627-2328) or www.nasafcu.com; Cold Spring Harbor Laboratory Press Publications www.cshlpress.com/affiliates/aaas.htm; GEICO Auto Insurance www.geico.com/landingpage/go51.htm?logo=17624; Hertz 800-654-2200 CDP#343457; Office Depot https://bsd.officedepot.com/portalLogin.do; Seabury & Smith Life Insurance 800-424-9883; Subaru VIP Program 202-326-6417; VIP Moving Services www.vipmayflower.com/domestic/index.html; Other Benefits: AAAS Member Services 202-326-6417 or www.aaasmember.org.

science_editors@aaas.org (for general editorial queries)
science_letters@aaas.org (for queries about letters)
science_reviews@aaas.org (for returning manuscript reviews)
science_bookrevs@aaas.org (for book review queries)

Published by the American Association for the Advancement of Science (AAAS), *Science* serves its readers as a forum for the presentation and discussion of important issues related to the advancement of science, including the presentation of minority or conflicting points of view, rather than by publishing only material on which a consensus has been reached. Accordingly, all articles published in *Science*—including editorials, news and comment, and book reviews—are signed and reflect the individual views of the authors and not official points of view adopted by AAAS or the institutions with which the authors are affiliated.

AAAS was founded in 1848 and incorporated in 1874. Its mission is to advance science, engineering, and innovation throughout the world for the benefit of all people. The goals of the association are to: enhance communication among scientists, engineers, and the public; promote and defend the integrity of science and its use; strengthen support for the science and technology enterprise; provide a voice for science on societal issues; promote the responsible use of science in public policy; strengthen and diversify the science and technology workforce; foster education in science and technology for everyone; increase public engagement with science and technology; and advance international cooperation in science.

Information for Authors
See pages 716 and 717 of the 8 February 2013 issue or access www.sciencemag.org/about/authors

EDITOR-IN-CHIEF **Bruce Alberts**
EXECUTIVE EDITOR **Monica M. Bradford**
NEWS EDITOR **Colin Norman**
MANAGING EDITOR, RESEARCH JOURNALS **Katrina L. Kelner**
DEPUTY EDITORS **Barbara R. Jasny, Andrew M. Sugden, Valda J. Vinson**

Editorial senior editors/commentary Lisa D. Chong, Brad Wible; **senior editors** Gilbert J. Chin, Pamela J. Hines, Paula A. Kiberstis (Boston), Marc S. Lavine (Toronto), Beverly A. Purnell, L. Bryan Ray, Guy Riddihough, H. Jesse Smith, Phillip D. Szuromi (Tennessee), Jake S. Yeston, Laura M. Zahn (San Diego); **associate editors** Melissa R. McCartney (Education Projects), Kristen L. Mueller, Jelena Stajic, Sacha Vignieri (Oregon), Nicholas S. Wigginton (Michigan); **book review editor** Sherman J. Suter; **associate letters editor** Jennifer Sills; **editorial manager** Cara Tate; **senior copy editors** Jeffrey E. Cook, Cynthia Howe, Harry Jach, Lauren Kmec, Barbara P. Ordway, Trista Wagoner; **copy editor** Chris Filiatreau; **senior editorial coordinators** Carolyn Kyle, Beverly Shields; **editorial coordinators** Joi S. Granger, Anita Wynn; **publications assistants** Ramatoulaye Diop, Aneera Dobbins, Jeffrey Hearn, Lisa Johnson, Dona Mathieu, Le-Toya Mayne Flood, Shannon McMahon, Scott Miller, Jerry Richardson, Teresa R. Sakon, Brian White; **editorial assistant** Patricia M. Moore; **executive editorial assistant** Yolanda O'Bannon (San Francisco); **executive assistant** Alison Crawford; **administrative support** Maryrose Madrid

Editorial director, web and new media Stewart Wills; **senior web editor** Sarah Crespi; **web editor** Kerry Klein; **web development manager** Martyn Green; **web developer** Corinna Cohn

News deputy news editors Robert Coontz, Elizabeth Culotta, David Grimm (Online), Eliot Marshall, Jeffrey Mervis, Leslie Roberts, Richard Stone, John Travis; **contributing editor** Polly Shulman; **news writers** Yudhijit Bhattacharjee, Adrian Cho, Jennifer Couzin-Frankel, Carolyn Gramling, Jocelyn Kaiser, Richard A. Kerr, David Malakoff, Elizabeth Pennisi, Robert F. Service (Pacific NW), Erik Stokstad, Emily Underwood; **web developer** Daniel Berger; **social media strategist** Meghna Sachdev; **intern** Lizzie Wade; **contributing correspondents** John Bohannon, Jon Cohen (San Diego, CA), Ann Gibbons, Sam Kean, Eli Kintisch, Andrew Lawler, Mitch Leslie, Charles C. Mann, Virginia Morell, Gary Taubes; **copy editors** Melissa Raimondi, Kara Estelle; **administrative support** Scherraine Mack; **bureaus** San Diego, CA: 760-942-3252, FAX 760-942-4979; Pacific Northwest: 503-963-1940

Production director Wendy K. Shank; **assistant manager** Rebecca Doshi; **senior specialists** Steve Forrester, Christopher Redwood, Anthony Rosen; **Preflight director** David M. Tompkins; **manager** Marcus Spiegler; **specialists** Jason Hillman, Tara Kelly

Art director Yael Fitzpatrick; **associate art director** Laura Creveling; **senior illustrators** Chris Bickel, Katharine Sutliff; **illustrator** Yana Hammond; **senior art associates** Holly Bishop, Preston Huey; **art associates** Kay Engman, Garvin Grullón, Chrystal Smith; **photo editor** Leslie Blizard

***Science* International**

Europe (science@science-int.co.uk) **editorial: international managing editor** Andrew M. Sugden; **senior editor/commentary** Julia Fahrenkamp-Uppenbrink; **senior editors** Caroline Ash, Stella M. Hurtley, Ian S. Osborne, Peter Stern; **associate editor** Maria Cruz; **contributing editor** Helen Pickersgill; **editorial support** Rachel Roberts, Alice Whaley; **administrative support** Janet Clements, Michelle Pegrume, John Wood; **news: deputy news editor, u.k.** Daniel Clery; **contributing editor, europe** Martin Enserink; **contributing correspondents** Michael Balter (Paris), Kai Kupferschmidt (Berlin), Gretchen Vogel (Berlin)

Asia Japan Office: Asca Corporation, Tomoko Furusawa, Rustic Bldg. 7F, 77 Tenjin-cho, Shinjuku-ku, Tokyo 162-0808, Japan; +81 3 6802 4616, FAX +81 3 6802 4615, inquiry@sciencemag.jp; **contributing editor, asia** Mara Hvistendahl [China: mhvisten@aaas.org]; **contributing correspondents** Dennis Normile [Japan: +81 (0) 3 33910630, FAX +81 (0) 3 5936 3531; dnormile@gol.com]; Hao Xin [China: cindyhao@gmail.com]; Pallava Bagla [South Asia: +91 (0) 11 2271 2896; pbagla@vsnl.com]

EXECUTIVE PUBLISHER **Alan I. Leshner**
PUBLISHER **Beth Rosner**

Fulfillment Systems and Operations (membership@aaas.org); **customer service supervisor** Pat Butler; **specialists** LaToya Casteel, Michelle Ofordire, April Marshall; **manager, data entry** Mickie Napoleoni; **data entry specialists** JJ Regan, Jaimee Wise, Fiona Giblin

Business Operations and Administration director Deborah Rivera-Wienhold; **business systems and financial analysis director** Randy Yi; **systems analyst** Nicole Mehmedovich; **manager, business analysis** Eric Knott; **manager, business operations** Jessica Tierney; **business analysts** Cory Lipman, Celeste Troxler; **financial analyst** Jeremy Clay; **rights and permissions: administrator** Emilie David; **associate** Elizabeth Sandler; **marketing director** Ian King; **marketing managers** Alison Chandler, Julianne Wielga, Justin Sawyers; **marketing associates** Mary Ellen Crowley, Elizabeth Sattler, Rebecca Riffkin; **senior marketing executive** Jennifer Reeves; **director, site licensing** Tom Ryan; **director, corporate relations** Eileen Bernadette Moran; **senior publisher relations specialist** Kiki Forsythe; **publisher relations manager** Catherine Holland; **publisher relations, eastern region** Keith Layson; **publisher relations, western region** Ryan Rexroth; **customer relations manager** Iquo Edim; **customer relations analysts** Simon Chong, Lana Guz; **marketing manager** Christina Schlecht; **marketing associates** Paulina Curto, Mitchell Edmund; **electronic media: director** Lizabeth Harman; **assistant manager** Lisa Stanford; **production specialists** Antoinette Hodal, Nichele Johnston, Lori Murphy, Kimberly Oster; **web and new media: senior project manager** Trista Smith, **project leader** Luke Johnson **computer specialists** Walter Jones, Kai Zhang, **web developer** Chris Coleman; **program director, AAAS member central** Peggy Mihelich

director, global collaboration, custom publications, advertising Bill Moran
editor, custom publishing Sean Sanders: 202-326-6430
assistant editor, custom publishing Tianna Hicklin 202-326-6463
associate director, collaboration, custom publications/china/taiwan/korea/singapore Ruolei Wu +86-1367-101-5294

Product (science_advertising@aaas.org); **midwest** Rick Bongiovanni: 330-405-7080, FAX 330-405-7081; **east coast/e. canada** Laurie Faraday: 508-747-9395, FAX 617-507-8189; **west coast/w. canada** Lynne Stickrod: 415-931-9782, FAX 415-520-6940; **uk europe/asia** Roger Goncalves: TEL/FAX +41 43 243 1358; **japan**, Makiko Hara: +81 (0) 3 6802 4616, FAX +81 (0) 3 6802 4615; ads@sciencemag.jp; **china/taiwan** Ruolei Wu: +86 1367 1015 294 rwu@aaas.org

worldwide associate director of *Science* Careers Tracy Holmes: +44 (0) 1223 326525, FAX +44 (0) 1223 326532

Classified (advertise@sciencecareers.org); **u.s./canada/south america** Tina Burks: 202-326-6577; **sales administrator** Marci Gallun; **europe/row sales** Lucy Nelson; **sales assistant** Kelly Grace; **japan** Yuri Kobayashi +81 (0)90-9110-1719; careerads@sciencemag.jp; **china/taiwan** Ruolei Wu: +86 1367 1015 294 rwu@aaas.org; **advertising support manager** Karen Foote: 202-326-6740; **advertising production operations manager** Deborah Tompkins; **senior production specialist/graphic designer** Amy Hardcastle; **production specialist** Yuse Lajiminmuhip; **senior traffic associate** Christine Hall; **sales coordinator** Shirley Young; **marketing manager** Allison Pritchard; **marketing associate** Aimee Aponte

AAAS Board of Directors retiring president, chair William H. Press; **president** Phillip A. Sharp; **president-elect** Gerald R. Fink; **treasurer** David Evans Shaw; **chief executive officer** Alan I. Leshner; **board** Bonnie L. Bassler, May R. Berenbaum, Claire M. Fraser, Elizabeth Loftus, Stephen L. Mayo, Raymond Orbach, Sue V. Rosser, Inder M. Verma

AAAS
ADVANCING SCIENCE, SERVING SOCIETY

SENIOR EDITORIAL BOARD

A. Paul Alivisatos, *Lawrence Berkeley Nat'l. Laboratory*
Cori Bargmann, *The Rockefeller Univ.*
Ernst Fehr, *Univ. of Zurich*
Erin O'Shea, *Harvard Univ.*
Michael S. Turner, *University of Chicago*

BOARD OF REVIEWING EDITORS

Adriano Aguzzi, *Univ. Hospital Zürich*
Takuzo Aida, *Univ. of Tokyo*
Leslie Aiello, *Wenner-Gren Foundation*
Sonia Altizer, *Univ. of Georgia*
Sebastian Amigorena, *Institut Curie*
Angelika Amon, *MIT*
Kathryn Anderson, *Memorial Sloan-Kettering Cancer Center*
Siv G. E. Andersson, *Uppsala Univ.*
Peter Andolfatto, *Princeton Univ.*
Meinrat O. Andreae, *Max Planck Inst., Mainz*
Paola Arlotta, *Harvard Univ.*
Johan Auwerx, *EPFL*
David Awschalom, *Univ. of California Santa Barbara*
Ben Barres, *Stanford Medical School*
Jordi Bascompte, *Estación Biológica de Doñana, CSIC*
Facundo Batista, *London Research Inst.*
Ray H. Baughman, *Univ. of Texas, Dallas*
David Baum, *Univ. of Wisconsin*
Mark Bear, *Massachusetts Inst. of Technology*
Yasmine Belkaid, *NIAID, NIH*
Philip Benfey, *Duke Univ.*
Stephen J. Benkovic, *Penn State Univ.*
Christophe Bernard, *Aix-Marseille Univ.*
Gregory C. Beroza, *Stanford Univ.*
Gabriele Bergers, *Univ. of California, San Francisco*
Peer Bork, *EMBL*
Bernard Bourdon, *Ecole Normale Superieure de Lyon*
Chris Bowler, *Ecole Normale Supérieure*
Ian Boyd, *Univ. of St. Andrews*
Christian Büchel, *Universitätsklinikum Hamburg-Eppendorf*
Joseph A. Burns, *Cornell Univ.*
William P. Butz, *Population Reference Bureau*
Gyorgy Buzsaki, *New York Univ., School of Medicine*
Mats Carlsson, *Univ. of Oslo*
Mildred Cho, *Stanford Univ.*
David Clapham, *Children's Hospital, Boston*
David Clary, *Univ. of Oxford*
Jonathan D. Cohen, *Princeton Univ.*
Robert Cook-Deegan, *Duke Univ.*
James Collins, *Boston Univ.*
Alan Cowman, *Walter & Eliza Hall Inst.*
Robert H. Crabtree, *Yale Univ.*
Wolfgang Cramer, *Mediterranean Inst. of Biodiversity and Ecology*
Jeff L. Dangl, *Univ. of North Carolina*
Tom Daniel, *Univ. of Washington*
Frans de Waal, *Emory Univ.*
Stanislas Dehaene, *Collège de France*
Robert Desimone, *MIT*
Claude Desplan, *New York Univ.*
Ap Dijksterhuis, *Radboud Univ. of Nijmegen*
Dennis Discher, *Univ. of Pennsylvania*
Gerald W. Dorn II, *Washington Univ. School of Medicine*
Jennifer A. Doudna, *Univ. of California, Berkeley*
Julian Downward, *Cancer Research UK*
Bruce Dunn, *Univ. of California, Los Angeles*
Christopher Dye, *WHO*
David Ehrhardt, *Carnegie Inst. of Washington*
Tim Elston, *Univ. of North Carolina at Chapel Hill*
Gerhard Ertl, *Fritz-Haber-Institut, Berlin*
Barry Everitt, *Univ. of Cambridge*
Paul G. Falkowski, *Rutgers Univ.*
Ernst Fehr, *Univ. of Zurich*
Tom Fenchel, *Univ. of Copenhagen*
Michael Feuer, *The George Washington Univ.*
Alain Fischer, *INSERM*
Susan Fiske, *Princeton Univ.*
Anne C. Ferguson-Smith, *Univ. of Cambridge*
Peter Fratzl, *Max Planck Inst.*
Elaine Fuchs, *Rockefeller Univ.*
Wulfram Gerstner, *EPFL Lausanne*
Andrew Gewirth, *Univ. of Illinois*
Karl-Heinz Glassmeier, *TU Braunschweig*
Elizabeth Grove, *Univ. of Chicago*
Kip Guy, *St. Jude's Children's Research Hospital*
Taekjip Ha, *Univ. of Illinois at Urbana-Champaign*
Christian Haass, *Ludwig Maximilians Univ.*
Steven Hahn, *Fred Hutchinson Cancer Research Center*
Gregory J. Hannon, *Cold Spring Harbor Lab.*
Martin Heimann, *Max Planck Inst., Jena*
Yka Helariutta, *Univ. of Finland*
Isaac Held, *NOAA*
James A. Hendler, *Rensselaer Polytechnic Inst.*
Janet G. Hering, *Swiss Fed. Inst. of Aquatic Science & Technology*
Ray Hilborn, *Univ. of Washington*
Michael E. Himmel, *National Renewable Energy Lab.*
Kai-Uwe Hinrichs, *Univ. of Bremen*
Kei Hirose, *Tokyo Inst. of Technology*
David Hodell, *Univ. of Cambridge*
David Holden, *Imperial College*
Lora Hooper, *UT Southwestern Medical Ctr at Dallas*
Jeffrey A. Hubbell, *EPFL Lausanne*
Thomas Hudson, *Ontario Inst. for Cancer Research*
Ray Huey, *Univ. of Washington*
Steven Jacobsen, *Univ. of California, Los Angeles*
Kai Johnsson, *EPFL Lausanne*
Peter Jonas, *Universität Freiburg*
Matt Kaeberlein, *Univ. of Washington*
William Kaelin Jr., *Dana-Farber Cancer Inst.*
Daniel Kahne, *Harvard Univ.*
Daniel Kammen, *Univ. of California, Berkeley*
Joel Kingsolver, *Univ. of North Carolina at Chapel Hill*
Robert Kingston, *Harvard Medical School*
Roberto Kolter, *Harvard Medical School*
Alberto R. Kornblihtt, *Univ. of Buenos Aires*
Leonid Kruglyak, *Princeton Univ.*
Thomas Langer, *Univ. of Cologne*
Mitchell A. Lazar, *Univ. of Pennsylvania*
David Lazer, *Harvard Univ.*
Virginia Lee, *Univ. of Pennsylvania*
Ottoline Leyser, *Cambridge Univ.*
Marcia C. Linn, *Univ. of California, Berkeley*
Jianguo Liu, *Michigan State Univ.*
Luis Liz-Marzan, *CIC biomaGUNE*
Jonathan Losos, *Harvard Univ.*
Ke Lu, *Chinese Acad. of Sciences*
Christian Lüscher, *Univ. of Geneva*
Laura Machesky, *CRUK Beatson Inst. for Cancer Research*
Anne Magurran, *Univ. of St Andrews*
Oscar Marin, *CSIC & Univ. Miguel Hernández*
Charles Marshall, *Univ. of California, Berkeley*
Chris Marshall, *Inst. of Cancer Research*
Martin M. Matzuk, *Baylor College of Medicine*
C. Robertson McClung, *Dartmouth College*
Graham Medley, *Univ. of Warwick*
Yasushi Miyashita, *Univ. of Tokyo*
Richard Morris, *Univ. of Edinburgh*
Edvard Moser, *Norwegian Univ. of Science and Technology*
Sean Munro, *MRC Lab. of Molecular Biology*
Thomas Murray, *The Hastings Center*
Naoto Nagaosa, *Univ. of Tokyo*
James Nelson, *Stanford Univ. School of Med.*
Daniel Neumark, *Univ. of California, Berkeley*
Stuart Newman, *New York Medical College*
Timothy W. Nilsen, *Case Western Reserve Univ.*
Pär Nordlund, *Karolinska Inst.*
Helga Nowotny, *European Research Advisory Board*
Luke O'Neill, *Trinity College, Dublin*
Stuart Newman, *New York Medical College*
N. Phuan Ong, *Princeton Univ.*
Joe Orenstein, *Univ. of California, Berkeley & Lawrence Berkeley National Lab*
Harry Orr, *Univ. of Minnesota*
Andrew Oswald, *Univ. of Warwick*
Steve Palumbi, *Stanford Univ.*
Jane Parker, *Max-Planck Inst. of Plant Breeding Research*
Donald R. Paul, *Univ. of Texas at Austin*
P. David Pearson, *Univ. of California, Berkeley*
John H. J. Petrini, *Memorial Sloan-Kettering Cancer Center*
Simon Phillpot, *Univ. of Florida*
Joshua Plotkin, *Univ. of Pennsylvania*
Philippe Poulin, *CNRS*
Colin Renfrew, *Univ. of Cambridge*
Trevor Robbins, *Univ. of Cambridge*
Jim Roberts, *Fred Hutchinson Cancer Research Ctr.*
Barbara A. Romanowicz, *Univ. of California, Berkeley*
Jens Rostrup-Nielsen, *Haldor Topsoe*
Mike Ryan, *Univ. of Texas, Austin*
Shimon Sakaguchi, *Kyoto Univ.*
Miquel Salmeron, *Lawrence Berkeley National Lab*
Jürgen Sandkühler, *Medical Univ. of Vienna*
Alexander Schier, *Harvard Univ.*
Randy Seeley, *Univ. of Cincinnati*
Vladimir Shalaev, *Purdue Univ.*
Joseph Silk, *Institut d'Astrophysique de Paris*
Denis Simon, *Arizona State Univ.*
Alison Smith, *John Innes Centre*
Davor Solter, *Inst. of Medical Biology, Singapore*
Peter Sorger, *Harvard Medical School*
John Speakman, *Univ. of Aberdeen*
Allan C. Spradling, *Carnegie Institution of Washington*
Jonathan Sprent, *Garvan Inst. of Medical Research*
Paula Stephan, *Georgia State Univ. and National Bureau of Economic Research*
Elsbeth Stern, *ETH Zürich*
V. S. Subrahmanian, *Univ. of Maryland*
Ira Tabas, *Columbia Univ.*
Yoshiko Takahashi, *Kyoto University*
Sarah Teichmann, *Cambridge Univ.*
John Thomas, *Duke Univ.*
Herbert Virgin, *Washington Univ.*
Bert Vogelstein, *Johns Hopkins Univ.*
Cynthia Volkert, *Univ. of Göttingen*
Bruce D. Walker, *Harvard Medical School*
Douglas Wallace, *Dalhousie Univ.*
Ian Walmsley, *Univ. of Oxford*
David A. Wardle, *Swedish Univ. of Agric Sciences*
David Waxman, *Fudan Univ.*
Jonathan Weissman, *Univ. of California, San Francisco*
Kathy Willis, *Oxford Univ.*
Ian A. Wilson, *The Scripps Res. Inst.*
Timothy D. Wilson, *Univ. of Virginia*
Rosemary Wyse, *Johns Hopkins Univ.*
Jan Zaanen, *Leiden Univ.*
Kenneth Zaret, *Univ. of Penn. School of Medicine*
Jonathan Zehr, *Univ. of California, Santa Cruz*
Maria Zuber, *MIT*

BOOK REVIEW BOARD

John Aldrich, *Duke Univ.*
David Bloom, *Harvard Univ.*
Angela Creager, *Princeton Univ.*
Richard Shweder, *Univ. of Chicago*
Ed Wasserman, *DuPont*
Lewis Wolpert, *Univ. College London*

AROUND THE WORLD

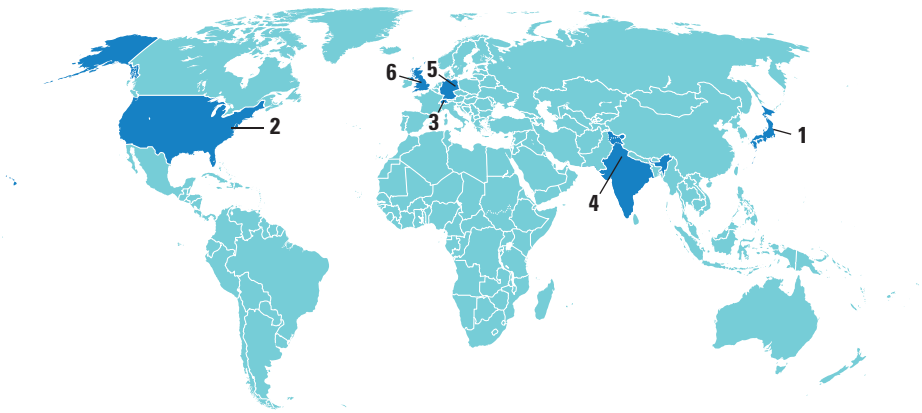

Okuma, Japan **1**

WHO: Fukushima Caused Minimal Cancer Risk

The World Health Organization (WHO) on 28 February released a report saying that the Fukushima nuclear disaster will cause no observable increases in cancer rates among residents of other countries and a very minimal increased risk of cancer among residents in the vicinity of the power plant. Workers who battled problems at the plant do face higher risks for some cancers. The WHO team estimated the increased lifetime risk of leukemia, thyroid cancer, and female breast cancer based on earlier estimates of radiation exposure in different locations around the power plant, which experienced multiple meltdowns and explosions in the aftermath of the 11 March 2011 earthquake and tsunami.

Inspectors at a Fukushima reactor building in May 2012.

Greenpeace condemned the report, stating that it "shamelessly downplays the impact of early radioactive releases from the Fukushima disaster on people inside the 20 km evacuation zone who were not able to leave the area quickly." But Kazuo Sakai, a radiation biologist at Japan's National Institute of Radiological Sciences, believes that the risks are overestimated, noting that the dose estimates used were based on preliminary data; actual measurements have shown the dose levels to be lower. **http://scim.ag/WHOcan**

Washington, D.C. **2**

A Budget Race Without A Finish Line

The sequester has begun. But when and where will it end?

U.S. government agencies are still trying to figure out how to apply the $85 billion in mandatory budget cuts that went into effect on 1 March. And Congress could soften the blow later this month when it takes up emergency legislation to extend a temporary spending measure for the remaining 7 months of the current fiscal year.

The sequester, part of a 10-year, $1.2 trillion deficit reduction package agreed to in August 2011, wasn't supposed to happen because its across-the-board mechanism was thought to be too onerous. But now that never is here, domestic science agencies are calculating how to save 5% through some combination of reducing the number of new grants, shrinking existing grants, lowering administrative costs, and downsizing ongoing programs. See some scientists' reactions to the "sciquester" on page 1133, and stay tuned.

Zurich, Switzerland **3**

Secure Test Site for GM Crops

The Swiss government will create a permanently protected area on federal land for experiments with genetically modified (GM) crops, which is intended to reduce the risk of vandalized fields as well as security costs. In a paper published on 28 February in *Trends in Biotechnology*, scientists from the Agroscope Reckenholz-Tänikon research station and the University of Zurich detailed the plan, which was approved by the Swiss Parliament and officially announced on 7 February. The Swiss Federal Council approved spending €600,000 annually from 2014 to 2017 to create a protected field site of approximately 3 hectares at the Reckenholz research station, 10 kilometers north of Zurich. Researchers will initially use it to test GM wheat with resistance to powdery mildew, a fungal disease.

In 2008, masked activists threatened researchers at another experimental site near Reckenholz and destroyed about one-third of the plants there. In 2009, researchers used grant funds to install surveillance cameras, build a double fence with barbed wire and motion sensors, and hire security guards. The study estimates that Swiss researchers running recent GM trials spent 78% of their research funds on security. **http://scim.ag/SwissGM**

New Delhi **4**

A Flat Science Budget for 2013

Indian scientists face belt-tightening: On 28 February, the government sent to Parliament for approval a $12 billion budget for science and technology in 2013, ending several years of substantial increases for S&T. The flat budget, which reflects the government's desire to reduce an almost $85 billion deficit, will equate to spending reductions with inflation running at about 5%.

Among the few highlights in the budget proposal is a new, $50 million fund for projects aiming to lift people out of poverty. The National Innovation Council will manage the new fund; the kinds of projects it will sup-

Science LIVE

Join us on Thursday, 14 March, at 3 p.m. EDT for a live chat with experts on **how arts education affects the brain**. **http://scim.ag/science-live**

CREDITS (TOP TO BOTTOM): ROLAND FISCHER/WIKIMEDIA COMMONS; *THE YOMIURI SHIMBUN* VIA AP IMAGES

Downloaded from www.sciencemag.org on March 8, 2013

Published by AAAS

port have not been revealed. But the fund's size will surely limit its impact, says physicist and Indian National Science Academy President Krishan Lal. "While the intent is correct, for a country of 1.2 billion people, this is only a drop in the ocean."

Meanwhile, major planned initiatives will go ahead, including India's maiden mission to Mars and the launch of the country's first military satellite. Grants to individual researchers are likely to bear the brunt of cuts necessary to offset big science spending. Parliament must pass the budget before the start of the next fiscal year on 1 April.
http://scim.ag/Indbud

Lower Saxony, Germany **5**

Genetic Engineering School Project Cut Off

One of the largest states in Germany is closing school laboratories as part of a strategy to "keep Lower Saxony free of genetic engineering." The new regional government of Social Democrats and Greens announced that it would end support of the HannoverGEN initiative, a project that installed and equipped four school laboratories in the state, allowing pupils to perform experiments in genetic engineering such as isolating DNA from tomatoes. The project, which started in 2008, was seen as a success by the previous government, which planned to expand it to 100 schools.

However, Greenpeace and other NGOs claimed that the learning materials gave a biased view of the debate about genetic engineering. The new government adopted that view and resolved in its coalition agreement to end the project. Hans-Jörg Jacobsen, a plant geneticist at the University of Hannover and one of the initiators of the project, said that termination was a mistake because the project "allowed pupils to make up their own minds based on knowledge." Students in the program have also protested the decision, and the project's coordinators and the schools' principals have started an online petition requesting that the state's prime minister visit a lab before deciding its future.

United Kingdom **6**

Ranking Countries' Health

The United Kingdom hasn't kept up with its European neighbors in health over the past 2 decades. In a paper published online by *The Lancet* on 4 March, Christopher Murray of the Institute for Health Metrics and Evaluation (IHME) at the University of Washington, Seattle, and more than a dozen U.K. public health experts report that although life expectancy increased by 4.2 years between 1990 and 2010, disability due to being overweight or obese has increased dramatically.

The overall health numbers place the United Kingdom below average when compared with the original 15 members of the European Union, Australia, Canada, Norway, and the United States. *The Lancet* paper comes at the same time that IHME published online analyses for 187 countries of its vast collection of data on disease burden and mortality due to 291 diseases (*Science*, 14 December 2012, p. 1414). Public health experts—and the general public—can sift through the findings at www.healthmetricsandevaluation.org.

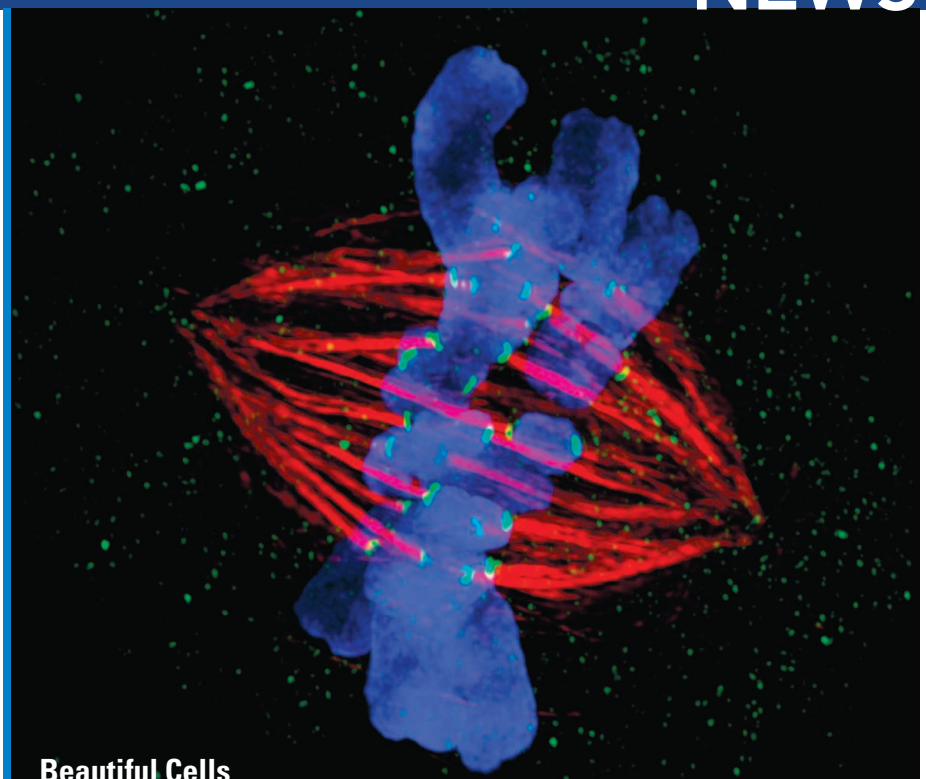

Beautiful Cells

The winners are in—and they're colorful. On 27 February, GE Healthcare Life Sciences announced the winners of its 2012 Cell Imaging Competition, chosen by public vote with more than 15,000 votes cast. Cell biologist and cancer researcher Jane Stout of Indiana University (IU), Bloomington, took the award in the High- and Super-Resolution Microscopy category for this image of metaphase epithelial cells (microtubules are in red, kinetochores in green, and DNA in blue). Research scientist Anushree Balachandran of Genea Limited, based in Sydney, Australia, won the High-Content Analysis category, while cell biologist Markus Posch of the University of Dundee in the United Kingdom was the regional winner in Microscopy.

Stout's image was taken with the university's DeltaVision OMX imaging system—nicknamed the "OMG" microscope by IU researchers. The image will also light up New York City's Times Square this April when it appears on the famed electronic billboard known as the big screen.

NEWSMAKERS

Moniz Tapped for DOE, McCarthy for EPA

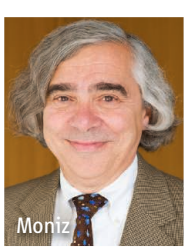

This week President Barack Obama tapped an academic scientist with a long Washington resume to lead the Department of Energy (DOE) and a data-hungry policy wonk who's already in town to run the Environmental Protection Agency (EPA).

Physicist **Ernest Moniz**, head of a high-profile energy think tank at the Massachusetts Institute of Technology, served as DOE's undersecretary and a senior White House science aide under President >>

CREDITS (TOP TO BOTTOM): COURTESY OF INDIANA UNIVERSITY; MASSACHUSETTS INSTITUTE OF TECHNOLOGY

Downloaded from www.sciencemag.org on March 8, 2013

Published by AAAS

>>NEWSMAKERS

Bill Clinton in the 1990s, and is a member of Obama's science advisory council. His wild, wavy locks prompted *The Washington Post*'s gossip column to suggest he'd have "the most iconoclastic hair in Cabinet history." He would replace Steven Chu at DOE if confirmed by the U.S. Senate.

McCarthy

Gina McCarthy, an air pollution specialist who is already a senior EPA official, worked for Mitt Romney, Obama's Republican opponent in the 2012 election, when he was governor of Massachusetts. She is known for a tough approach to crafting data-driven regulations—and for quips delivered in a thick New England accent. She would replace Lisa Jackson if confirmed.

Heart Researcher Wins Developmental Bio Prize

Olson

Insights into the mysteries of the heart have earned **Eric Olson** the 2013 March of Dimes Prize in Developmental Biology. He will receive the $250,000 prize in Washington, D.C., in May.

Olson studies the genetic signals that control heart development at the University of Texas Southwestern Medical Center in Dallas. He and his colleagues have shown that newborn mouse hearts can regenerate to a surprising degree in the first week after birth (*Science*, 25 February 2011, p. 1078). They have also found a suite of proteins and microRNAs that promote regeneration in older mouse hearts.

Outside the lab, Olson plays guitar and harmonica in a rock band called the Transactivators. One of their songs, "Mamas, Don't Let Your Stem Cells Grow Up to Be Cowboys," was inspired by a supporter of his work: Olson holds the Annie and Willie Nelson Professorship in Stem Cell Research.

Evolving Landscapes Through Artists' Eyes

Bright orange flames burn through the spruce trees, leaving behind a forest of curling gray smoke and blackened trunks. These are artist Ree Nancarrow's impressions of Alaska's Denali National Park, stitched into a quilt as part of an unusual collaboration between creative artists and scientists.

Denali Park is home to the Bonanza Creek Long-Term Ecological Research (LTER) site, one of 26 National Science Foundation (NSF) study areas chronicling change in the flora, fauna, and environment over decades. Bonanza Creek is also one of 11 LTERs that has invited artists to reflect on these changing landscapes in oils, watercolors, fiber art, photographs, essays, poems, and other media.

"We are, in a way, collecting humanities data," says Fred Swanson, a retired U.S. Forest Service scientist who worked at an Oregon LTER, HJ Andrews Experimental Forest, and now coordinates its Long-Term Ecological Reflections program.

Some of the works are on display at NSF's headquarters in Arlington, Virginia. Photographs from Baltimore chronicle plants that thrive in the city; paintings from Konza Prairie in Kansas capture the heat and drama of wildfires; a poem describes a stare-down with a spotted owl. In one installation, rows of plastic cups each cradle a live mangrove sprout that will eventually be used to restore mangrove forests in Florida.

The exhibit is not open to the public, but Swanson hopes one day to display the works of the 39 artists where anyone can enjoy them. Meanwhile, you can see some of them online at ecologicalreflections.com.

FINDINGS

Dietary Salt Linked to Autoimmune Diseases

Salt in food may increase the risk of autoimmune diseases, according to provocative results reported this week in *Nature*. Immunobiologist David Hafler of the Yale School of Medicine and colleagues determined that a pinch of salt triggered cultures of unspecialized T cells to produce large numbers of destructive T_H17 cells, which have been implicated in diseases such as psoriasis, rheumatoid arthritis, and multiple sclerosis. They also showed that a salt-rich diet makes mice more susceptible to experimental autoimmune encephalomyelitis (EAE), a rodent illness similar to multiple sclerosis.

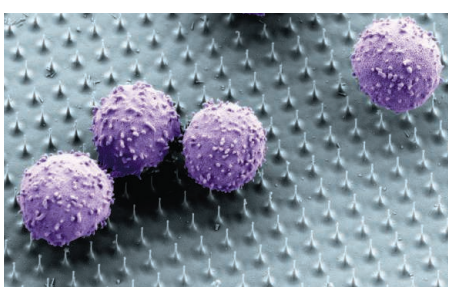

A salt connection also crystallized when computational biologist Aviv Regev of the Broad Institute in Cambridge, immunologist Vijay Kuchroo of Harvard Medical School in Boston, and colleagues pieced together the molecular circuit that controls specialization of T_H17 cells. An influential gene was *SGK1*, which helps cells manage sodium levels. And mice on high-salt rations developed a milder form of EAE if they lacked *SGK1*. The work doesn't establish that salt drives human autoimmune diseases, but "the stage is set to do precise experiments to test the hypothesis," Kuchroo says.
http://scim.ag/saltimm

Tweet, Shriek: On the Origin Of Language

The complex amalgam that is human language had humble beginnings: An analysis of bird songs and monkey calls suggests

CREDITS (TOP TO BOTTOM): BRIAN COATS/UT SOUTHWESTERN; EPA; N. YOSEF *ET AL.*, *NATURE* **495** (6 MARCH) © 2013 NATURE PUBLISHING GROUP; REE NANCARROW, DENALI PARK, AK; (PHOTO) ERIC NANCARROW

Downloaded from www.sciencemag.org on March 8, 2013

Published by AAAS

Random Sample

Doc Comic

Niche markets abound in the world of comic books: Whether you're interested in golden-age superheroes, 20th century history, or zombies, there's a comic for you. Now, there's "Missed It"—a new comic created by a clinician for clinicians.

There's a cultural hunger for medical storytelling, as the success of TV shows like *House* and *Grey's Anatomy* can attest, says bioethicist and professor of medicine Michael J. Green at the Pennsylvania State College of Medicine in Hershey. But "Missed It" goes a step further, depicting real-life tales from the emergency room, as written by Green and illustrated by artist Ray Rieck.

The first installment of the comic, which appears in the 5 March issue of *Annals of Internal Medicine*, follows a young doctor as he works his way through a medical puzzle. (How often the comic strip will run is still to be decided.) Green says he based the story on a personal experience with a seemingly routine case of chronic obstructive pulmonary disease—a lung disease that inhibits breathing—which he encountered during his medical residency in the 1990s.

"I have long felt that comics are an ideal way to tell stories that have an emotional impact," Green says. "Doctors are accustomed to telling and listening to stories, and I thought the time was ripe to try new ways to tell these stories."

that it may have evolved from a combination of simpler systems.

Our language has two layers: the words we use (the lexical structure) and how we organize those words (the expression structure). We're the only animal to combine the two, but some animals do use one or the other. Vervet monkeys use different alarm calls for different predators—a lexical structure with no grammar. And although nightingales can sing up to 200 different melodies, the individual notes have no meaning—an expression structure with no words.

Similar preexisting systems could have combined to form human language, researchers posited online last month in *Frontiers in Psychology*. "Evolution can work in different ways, and one way would be that existing mechanisms are combined into something new," says Johan Bolhuis, a biologist at Utrecht University in the Netherlands who was not involved with the study.

Still, he cautions, "we simply don't know enough about the evolution of all these systems to know if that is really the case."
http://scim.ag/langevol

Shared Genetics Could Drive Psychiatric Disorders

Finding genes behind psychiatric disorders has been a struggle, but a massive new study of about 60,000 cases and controls offers additional clues. The study took an unusual tack, lumping together five conditions generally considered to be distinct. Lo and behold, it found a handful of gene variants shared by all of the disorders. Reporting last week in *The Lancet*, the researchers, part of a collaboration called the Psychiatric Genomics Consortium, describe three variants that correlate with autism spectrum disorder, attention deficit-hyperactivity disorder, bipolar disorder, major depressive disorder, and schizophrenia. A fourth gene variant surfaced more often in people with either bipolar disorder or schizophrenia than in controls. Two variants are linked to calcium channels, which help cells communicate.

The Lancet report is the largest yet to dig for genes underlying these conditions. As is common in so-called genome-wide association studies, the variants raise risk only slightly, by about 10%. But some researchers say that identifying them adds to growing evidence that psychiatric conditions, even those that present very differently in patients, might share common molecular causes that could help better define and treat them.

THEY SAID IT

*Science*NOW asked readers to share how the U.S. sequester might affect their research and careers. For more comments, visit http://scim.ag/sciquester—and keep us posted with #sciquester.

I'm a young scientist who applied for 2 post-doctoral fellowships...with new grants being cut, my future is compromised #sciquester
—@Frank_Leibfarth

#sciquester is a science career killer at a time when the government is calling for more scientists
—@sciencegeist

Biology research dont take well to "stops and starts", cell cultures and longitudinal studies need continuous care & assessment. #sciquester
—@mksin149

CREDITS: (TOP) FROM "MISSED IT," WRITTEN BY MICHAEL J. GREEN, AND ILLUSTRATED BY RAY RIECK, PUBLISHED IN *ANN INTERN MED* 2013; **158**(5):357-361 (WWW.ANNALS.ORG). REPRODUCED WITH PERMISSION BY THE AMERICAN COLLEGE OF PHYSICIANS © 2013. ALL RIGHTS RESERVED.; (BOTTOM) CHRISTINE DANILOFF/MIT

Downloaded from www.sciencemag.org on March 8, 2013

Published by AAAS

>>NEWSMAKERS

Bill Clinton in the 1990s, and is a member of Obama's science advisory council. His wild, wavy locks prompted *The Washington Post*'s gossip column to suggest he'd have "the most iconoclastic hair in Cabinet history." He would replace Steven Chu at DOE if confirmed by the U.S. Senate.

McCarthy

Gina McCarthy, an air pollution specialist who is already a senior EPA official, worked for Mitt Romney, Obama's Republican opponent in the 2012 election, when he was governor of Massachusetts. She is known for a tough approach to crafting data-driven regulations—and for quips delivered in a thick New England accent. She would replace Lisa Jackson if confirmed.

Heart Researcher Wins Developmental Bio Prize

Olson

Insights into the mysteries of the heart have earned **Eric Olson** the 2013 March of Dimes Prize in Developmental Biology. He will receive the $250,000 prize in Washington, D.C., in May.

Olson studies the genetic signals that control heart development at the University of Texas Southwestern Medical Center in Dallas. He and his colleagues have shown that newborn mouse hearts can regenerate to a surprising degree in the first week after birth (*Science*, 25 February 2011, p. 1078). They have also found a suite of proteins and microRNAs that promote regeneration in older mouse hearts.

Outside the lab, Olson plays guitar and harmonica in a rock band called the Transactivators. One of their songs, "Mamas, Don't Let Your Stem Cells Grow Up to Be Cowboys," was inspired by a supporter of his work: Olson holds the Annie and Willie Nelson Professorship in Stem Cell Research.

Evolving Landscapes Through Artists' Eyes

Bright orange flames burn through the spruce trees, leaving behind a forest of curling gray smoke and blackened trunks. These are artist Ree Nancarrow's impressions of Alaska's Denali National Park, stitched into a quilt as part of an unusual collaboration between creative artists and scientists.

Denali Park is home to the Bonanza Creek Long-Term Ecological Research (LTER) site, one of 26 National Science Foundation (NSF) study areas chronicling change in the flora, fauna, and environment over decades. Bonanza Creek is also one of 11 LTERs that has invited artists to reflect on these changing landscapes in oils, watercolors, fiber art, photographs, essays, poems, and other media.

"We are, in a way, collecting humanities data," says Fred Swanson, a retired U.S. Forest Service scientist who worked at an Oregon LTER, HJ Andrews Experimental Forest, and now coordinates its Long-Term Ecological Reflections program.

Some of the works are on display at NSF's headquarters in Arlington, Virginia. Photographs from Baltimore chronicle plants that thrive in the city; paintings from Konza Prairie in Kansas capture the heat and drama of wildfires; a poem describes a stare-down with a spotted owl. In one installation, rows of plastic cups each cradle a live mangrove sprout that will eventually be used to restore mangrove forests in Florida.

The exhibit is not open to the public, but Swanson hopes one day to display the works of the 39 artists where anyone can enjoy them. Meanwhile, you can see some of them online at ecologicalreflections.com.

FINDINGS

Dietary Salt Linked to Autoimmune Diseases

Salt in food may increase the risk of autoimmune diseases, according to provocative results reported this week in *Nature*. Immunobiologist David Hafler of the Yale School of Medicine and colleagues determined that a pinch of salt triggered cultures of unspecialized T cells to produce large numbers of destructive T_H17 cells, which have been implicated in diseases such as psoriasis, rheumatoid arthritis, and multiple sclerosis. They also showed that a salt-rich diet makes mice more susceptible to experimental autoimmune encephalomyelitis (EAE), a rodent illness similar to multiple sclerosis.

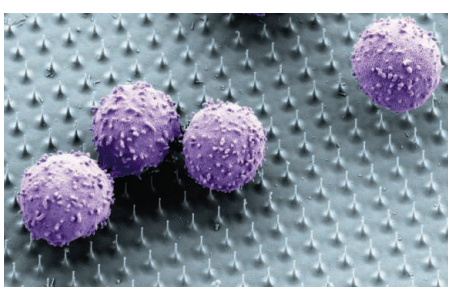

A salt connection also crystallized when computational biologist Aviv Regev of the Broad Institute in Cambridge, immunologist Vijay Kuchroo of Harvard Medical School in Boston, and colleagues pieced together the molecular circuit that controls specialization of T_H17 cells. An influential gene was *SGK1*, which helps cells manage sodium levels. And mice on high-salt rations developed a milder form of EAE if they lacked *SGK1*. The work doesn't establish that salt drives human autoimmune diseases, but "the stage is set to do precise experiments to test the hypothesis," Kuchroo says.
http://scim.ag/saltimm

Tweet, Shriek: On the Origin Of Language

The complex amalgam that is human language had humble beginnings: An analysis of bird songs and monkey calls suggests

CREDITS (TOP TO BOTTOM): BRIAN COATS/UT SOUTHWESTERN; EPA; N. YOSEF *ET AL.*, *NATURE* **495** (6 MARCH) © 2013 NATURE PUBLISHING GROUP; REE NANCARROW, DENALI PARK, AK; (PHOTO) ERIC NANCARROW

Downloaded from www.sciencemag.org on March 8, 2013

Published by AAAS

Random Sample

Doc Comic

Niche markets abound in the world of comic books: Whether you're interested in golden-age superheroes, 20th century history, or zombies, there's a comic for you. Now, there's "Missed It"—a new comic created by a clinician for clinicians.

There's a cultural hunger for medical storytelling, as the success of TV shows like *House* and *Grey's Anatomy* can attest, says bioethicist and professor of medicine Michael J. Green at the Pennsylvania State College of Medicine in Hershey. But "Missed It" goes a step further, depicting real-life tales from the emergency room, as written by Green and illustrated by artist Ray Rieck.

The first installment of the comic, which appears in the 5 March issue of *Annals of Internal Medicine*, follows a young doctor as he works his way through a medical puzzle. (How often the comic strip will run is still to be decided.) Green says he based the story on a personal experience with a seemingly routine case of chronic obstructive pulmonary disease—a lung disease that inhibits breathing—which he encountered during his medical residency in the 1990s.

"I have long felt that comics are an ideal way to tell stories that have an emotional impact," Green says. "Doctors are accustomed to telling and listening to stories, and I thought the time was ripe to try new ways to tell these stories."

that it may have evolved from a combination of simpler systems.

Our language has two layers: the words we use (the lexical structure) and how we organize those words (the expression structure). We're the only animal to combine the two, but some animals do use one or the other. Vervet monkeys use different alarm calls for different predators—a lexical structure with no grammar. And although nightingales can sing up to 200 different melodies, the individual notes have no meaning—an expression structure with no words.

Similar preexisting systems could have combined to form human language, researchers posited online last month in *Frontiers in Psychology*. "Evolution can work in different ways, and one way would be that existing mechanisms are combined into something new," says Johan Bolhuis, a biologist at Utrecht University in the Netherlands who was not involved with the study.

Still, he cautions, "we simply don't know enough about the evolution of all these systems to know if that is really the case."
http://scim.ag/langevol

Shared Genetics Could Drive Psychiatric Disorders

Finding genes behind psychiatric disorders has been a struggle, but a massive new study of about 60,000 cases and controls offers additional clues. The study took an unusual tack, lumping together five conditions generally considered to be distinct. Lo and behold, it found a handful of gene variants shared by all of the disorders. Reporting last week in *The Lancet*, the researchers, part of a collaboration called the Psychiatric Genomics Consortium, describe three variants that correlate with autism spectrum disorder, attention deficit-hyperactivity disorder, bipolar disorder, major depressive disorder, and schizophrenia. A fourth gene variant surfaced more often in people with either bipolar disorder or schizophrenia than in controls. Two variants are linked to calcium channels, which help cells communicate.

The Lancet report is the largest yet to dig for genes underlying these conditions. As is common in so-called genome-wide association studies, the variants raise risk only slightly, by about 10%. But some researchers say that identifying them adds to growing evidence that psychiatric conditions, even those that present very differently in patients, might share common molecular causes that could help better define and treat them.

THEY SAID IT

*Science*NOW asked readers to share how the U.S. sequester might affect their research and careers. For more comments, visit http://scim.ag/sciquester—and keep us posted with #sciquester.

I'm a young scientist who applied for 2 post-doctoral fellowships...with new grants being cut, my future is compromised #sciquester
—@Frank_Leibfarth

#sciquester is a science career killer at a time when the government is calling for more scientists
—@sciencegeist

Biology research dont take well to "stops and starts", cell cultures and longitudinal studies need continuous care & assessment. #sciquester
—@mksin149

CREDITS: (TOP) FROM "MISSED IT," WRITTEN BY MICHAEL J. GREEN, AND ILLUSTRATED BY RAY RIECK, PUBLISHED IN *ANN INTERN MED* 2013; **158**(5):357-361 (WWW.ANNALS.ORG). REPRODUCED WITH PERMISSION BY THE AMERICAN COLLEGE OF PHYSICIANS © 2013. ALL RIGHTS RESERVED.; (BOTTOM) CHRISTINE DANILOFF/MIT

Downloaded from www.sciencemag.org on March 8, 2013

Published by AAAS

Surprising success. Deborah Persaud found only traces of apparently defective HIV in a toddler infected at birth.

HIV/AIDS

Early Treatment May Have Cured Infant of HIV Infection

ATLANTA—A baby in rural Mississippi appears to have been cured of an HIV infection, likely because doctors started treatment 30 hours after birth. This is "the first well-documented case" of its kind, said pediatrician Deborah Persaud at the 20th Conference on Retroviruses and Opportunistic Infections here this week. Persaud, who works at the Johns Hopkins Children's Center in Baltimore, Maryland, did not treat the child herself but did extensive analyses of blood samples. She and her colleagues concluded that unusually early administration of anti-HIV drugs may have enabled the now 2-and-a-half-year-old to clear an established infection.

As Persaud explained, the child was born in July 2010 after 35 weeks of gestation. Doctors did not learn about the mother's HIV infection until she was in labor, and she did not receive antiretroviral drugs. (The baby's gender and caretakers aren't being identified for privacy reasons.) Because of the premature birth, doctors decided to move the baby to the University of Mississippi Medical Center (UMMC) in Jackson, which performed two separate blood tests on the 2-day-old infant and found HIV RNA and DNA. UMMC pediatrician Hannah Gay decided to begin a cocktail of AZT and two other anti-HIV drugs 31 hours after birth. Typically, Persaud noted, up to 6 weeks can pass before tests confirm an HIV infection in newborns.

Laboratory tests at 6, 12, and 20 days repeatedly found HIV in the baby. But by 29 days, the virus was undetectable on standard tests. For unknown reasons, the baby's caretakers decided to stop treatment at 18 months. In the fall of 2012, when the 21-month-old came in for a checkup, Gay couldn't find HIV antibodies or the virus. "It was quite unbelievable," Persaud said. Gay then contacted immunologist Katherine Luzuriaga at the University of Massachusetts Medical School in Worcester for help, who in turn asked Persaud's group at Hopkins to scour the blood samples for evidence of HIV persistence.

Persaud's team, which has ongoing studies of babies who start treatment early, uses an array of ultrasensitive screens for HIV. The researchers first tested the toddler's blood 24 months after birth and found only a single copy of HIV RNA in the plasma. To assess whether the child still harbored intact virus, or whether the RNA represented defective versions of the virus that can't copy themselves, they mixed the child's blood with uninfected CD4 cells—HIV's main target—to see if the cells produced new virus. They did not. Further tests at 26 months again found tiny genetic traces of the virus, but it did not appear to have integrated into cells, which it must do to copy itself. "We're very excited and planning new studies to assess this," says Lynne Mofenson, who heads the maternal and pediatric infectious disease branch of the U.S. National Institute of Child Health and Human Development in Bethesda, Maryland, and was not involved in this analysis.

Persaud suspects that the early treatment prevented the establishment of a reservoir of long-lived CD4 cells that harbor latent HIV infections; these infected cells avoid immune detection and are impervious to antiretroviral drugs. Such reservoirs are a central reason why the virus persists even after decades of antiretroviral treatment.

In the history of the AIDS epidemic, researchers have convincingly shown that only one HIV-infected person, Timothy Brown (*Science*, 13 May 2011, p. 784), has been cured. Brown had leukemia and received bone marrow transplants from a donor whose CD4 cells had a mutation that made them resistant to HIV infection. "We believe this is our Timothy Brown case to spur research interest and get us on the road toward a cure for HIV-infected children," Persaud said.

Persaud acknowledges that, like Brown, this is a single case, and the child may still harbor an undetected infection. Even so, "this has very important implications for pediatric HIV infection and the ability to achieve cure."

Effective antiretroviral treatment of pregnant women has made transmission of HIV to infants rare everywhere it's used. But Mofenson, who gave a presentation here on mother-to-child transmission, noted that some 330,000 new pediatric infections occurred worldwide in 2011. Even in the United States, where fewer than 200 HIV-infected babies are born each year, mother-to-child transmission occurs when treatment guidelines aren't followed, as happened in this case.

Mofenson cautions that it will be far easier to promptly diagnose HIV infection and treat babies early in wealthy places like the United States. "It will be very difficult to actually implement it in developing countries," she says. "The key to elimination of pediatric HIV is to prevent infection in the first place."

–JON COHEN

CREDIT: J. COHEN/*SCIENCE*

Published by AAAS

METEORITICS

Siberian Meteor Spurs Dash for Data, Calls for Safeguards

When a meteor shot through the dawn sky over Chelyabinsk, Russia, on 15 February, people rushed to windows and watched the contrail gradually dissipate. "They didn't know what was about to hit them," says Michael Hedlin, a geophysicist at University of California (UC), San Diego. About 2 minutes after the bolide streaked past at 18 kilometers a second—Mach 50—its shock waves reached Chelyabinsk, shattering windows and blowing down walls. About 1500 people were injured, mostly by flying glass.

Could the injuries have been prevented?

In the aftermath of the Chelyabinsk bolide, scientists are crafting proposals for an air-burst warning system. By stepping up surveillance for impactors small enough to elude surveys of dangerous near-Earth objects (NEOs) but big enough to penetrate deep into the stratosphere before shattering or exploding, researchers hope to spot threats hours before they reach Earth and forecast their paths in time for authorities to issue warnings.

The Chelyabinsk meteor is thought to have been the biggest rock to strike Earth since a cosmic object exploded over the Tunguska region of Siberia in 1908, leveling and scorching 2000 square kilometers of taiga forest. This time, scientists were treated to an unprecedented show. The Chelyabinsk meteor's death throes emitted the most powerful infrasound waves ever recorded. "We're doing seismology in the atmosphere," says David Simpson, president of Incorporated Research Institutions for Seismology, a consortium in Washington, D.C. Shock waves from the air burst set off magnitude-2.7 tremors in the ground below. "The event was just astounding," Simpson says.

Hedlin and his wife, geophysicist Catherine de Groot-Hedlin of the Scripps Institution of Oceanography, are analyzing the recordings to vet models of how the speed of sound varies with temperature, wind speed, and other factors. Hedlin says that they're also "working feverishly" to use infrasound data to refine estimates of the blast's yield, pegged at about 440 kilotons of TNT. (Tunguska was about 10 times as big: hydrogen-bomb scale.) "This is a once-in-a-lifetime opportunity," Hedlin says.

Meanwhile, on the ground, meteorite recovery and analysis teams are focusing on frozen Lake Chebarkul, 70 kilometers southwest of Chelyabinsk, where locals found a hole in the ice and putative meteorites. Gunther Kletetschka, an astrobiologist at Charles University in Prague, rushed to the site last week, aiming to lay hands on meteorites big enough to contain organic compounds. He hopes to test the panspermia hypothesis: that life on Earth arose after the oceans were seeded with organic chemicals from space. Larger meteorites at the bottom of Chebarkul "may be the most pristine," Kletetschka says, because the clayey sediments would cocoon them from contamination by lake water.

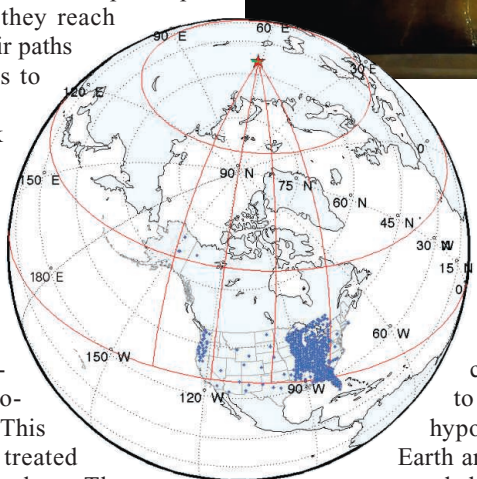

Silent scream. USArray infrasound stations picked up the inaudible octaves of the Chelyabinsk meteor as it broke apart.

NEO specialists estimate that a rock the size of the Chelyabinsk meteor—17 to 20 meters across—hits Earth roughly once a century, while Tunguska was once-a-millennium. Experts like Mark Boslough, a computational physicist at Sandia National Laboratories in Albuquerque, New Mexico, see last month's near-calamity as a shot across the bow. None of the nearly 1000 known "civilization killers"—asteroids 1 kilometer across or wider—in their present orbits will collide with Earth, but surveys are generally blind to the thousands of asteroids that are less than 100 meters across.

An early warning system is feasible. Boslough points to 2008 TC3, a 4-meter-wide asteroid that the Catalina Sky Survey spied 20 hours before its arrival—the first time an object on a collision course with our planet had been spotted in space. Astronomers trained their scopes on 2008 TC3, enabling NASA and others to predict that the small meteor would explode high in the stratosphere, safely above the Nubian Desert in Sudan. 2008 TC3, however, approached in the night sky; dayside objects obscured by the sun's glare would have to be spotted farther out with more powerful telescopes.

Once an incoming cosmic object is in the crosshairs, gauging the hazard will be tough. Its size and composition and, therefore, its mass will be highly uncertain, making it hard to predict the magnitude of the air burst, Boslough says. Also complicating the picture are unknown rates of ablation and fragmentation as friction eats away at the bolide. Still, Boslough says, scientists will be able to calculate an incoming object's orbital dynamics and issue a National Hurricane Center–style forecast, allowing authorities to advise people in the predicted impact zone to take shelter or evacuate.

An early warning system "wouldn't be that difficult to implement" and could be run out of NASA's NEO office, says Boslough, who was in Chelyabinsk last week performing stellar calibrations to narrow the location of the terminal air burst. A global array of inexpensive telescopes, he says, could be set up to detect smaller impactors. The size of objects spotted, how much forewarning can be provided, and how precisely the orbital dynamics are worked out, says Raymond Jeanloz, a geophysicist at UC Berkeley, "will depend on how much money is spent on hardware, analysis, and length of time doing the observing."

Boslough will pitch such a system at next month's Planetary Defense Conference in Flagstaff, Arizona. "I see a huge opportunity here for the private sector," he says. "How much would someone pay for a seat on a charter flight to witness such an event from a safe distance? I would love to see private investors funding survey telescopes with such a plan in mind."

–RICHARD STONE

CREDITS (TOP TO BOTTOM): AP; COURTESY OF CATHERINE DEGROOT-HEDLIN/UNIVERSITY OF CALIFORNIA, SAN DIEGO

Downloaded from www.sciencemag.org on March 8, 2013

Published by AAAS

Prairie dog passion. John Hoogland has intensively studied these colonial rodents for 40 years.

BEHAVIORAL ECOLOGY

At Home on the Range: Prairie Rodents Yield Their Secrets to a Dogged Observer

To say that John Hoogland is passionate about prairie dogs is an understatement. Fanatic is more like it. A behavioral ecologist, he has studied these North American colonial rodents for 40 years, spending months at a time sitting in a blind from dawn to dusk recording the activities of each individual in a colony. "Catch 'em. Mark 'em. Watch 'em," is his motto; he rarely does experiments with the animals. "His style is a throwback to the old days of living with your organism and getting to know them really well, and in the process you get insights that are simply not possible otherwise," says Tim Clutton-Brock, a behavioral ecologist at the University of Cambridge in the United Kingdom. "That approach is increasingly rare."

On page 1205, Hoogland, 64, who works at the Appalachian Laboratory of the University of Maryland Center for Environmental Science in Frostburg, describes his latest insight: that young female prairie dogs move out of their territories when their close kin go missing. He finds this tendency in three species, even though long-accepted wisdom holds that relatives tend to disperse to avoid competing with each other. "John has sort of turned this old idea on its ear," says Charles Brown, a behavioral ecologist at the University of Tulsa in Oklahoma. The result helps illuminate how competition and cooperation both play out in the life of a prairie dog and "flies in the face of a lot of mathematical modeling," adds F. Stephen Dobson, a behavioral ecologist at Auburn University in Alabama.

Other researchers have studied mammals for decades, but few have done so with Hoogland's unflagging fervor. Early each spring, he heads to a remote study site, usually in the U.S. Southwest, to catch the animals as they emerge from hibernation. Prairie dogs live in colonies of a dozen to thousands of individuals, sharing burrows with their close relatives. Hoogland stays at the sites for 4 months, until the last pups have started to spend their days above ground and are weaned. To survive sitting still all day in frigid towers at 2600 meters elevation at his current site in New Mexico, he wears 11 layers on his torso, eight pairs of pants, snowmobile boots, and two wool hats. "I usually don't even notice the cold, there's so much going on," he says. But Hoogland repeatedly warns his three or four seasonal undergraduate assistants that in the field, they will be the coldest they have ever been.

The researchers catch pups as they emerge from underground nests, then place permanent tags on their ears and dye a number or unique marking on their flanks to easily identify them from afar. Twice a year, Hoogland sets out 500 live traps for several weeks to recapture and remark the adults.

Hoogland started out in Wyoming in 1974 with black-tailed and white-tailed prairie dogs, two of the five species in North America, trying to assess the costs and benefits of colonial life by looking at differences between small and large colonies. He then spent 15 years observing a 200-member black-tailed prairie dog colony at Wind Cave National Park in South Dakota, 7 years watching Gunnison's prairie dogs in Petrified Forest National Park in Arizona, 7 years studying white-tailed prairie dogs in Arapaho National Wildlife Refuge in Colorado, and 11 years with Utah prairie dogs in Bryce Canyon National Park in Utah. Now, he's back with Gunnison's prairie dogs, this time at Valles Caldera National Preserve in New Mexico.

Starting in 1978, Hoogland and his undergraduates discovered that in each prairie dog species studied, a female is receptive to breeding just 1 day a year for about 6 hours. During that time most females try to mate with multiple males. Hoogland's long-term data on reproductive success indicate that polyandrous females are more likely to get pregnant and wean larger litters with offspring that are more likely to live at least a year. But these advantages come at a cost, as the females themselves are less likely to survive to the next mating season, he will report later this year in the *Journal of Mammalogy*.

Spying on prairie dog romances "is better than watching *Grey's Anatomy*," the TV show, he says. Males compete intensely with each other, biting and chasing off rivals. Successful suitors go to great lengths to try to keep females from mating a second time. Tracking this prairie dog soap opera, Hoogland has racked up more than 60 papers, several in influential journals, and written two books. "I just wish every biologist in the world could spend 1 day watching prairie dogs during the mating season," Hoogland says. "It would blow them away."

These front row seats to prairie dog biol-

CREDIT: ELAINE MILLER BOND/WWW.ELAINEMILLERBOND.COM

Downloaded from www.sciencemag.org on March 8, 2013

Published by AAAS

ogy demanded sacrifices both personal and professional, however. After a postdoc at the University of Minnesota, Hoogland spent 6 years as an assistant professor at Princeton University but failed to get tenure. "They really wanted me to be on campus for more of each year, but my research was going so well that I wouldn't give up on the prairie dogs," he says.

He quickly landed at the University of Maryland satellite lab in Frostburg, where he can spend 5 months away at his field sites. But the center is hundreds of kilometers away from the main campus, and Hoogland has only one Ph.D. student, from the Princeton days, in his pedigree.

To keep his family together, Hoogland's wife, Judy, homeschooled their four children. The kids grew up watching prairie dogs with their dad and with open spaces as their playground. "We were like gypsies, leaving [home] each spring," Hoogland says.

His 1985 finding that closely related lactating females will kill their relative's newborn pups, presumably to eliminate competition, drives home the value of such dedication. This was "a gargantuan surprise," Hoogland recalls, as most of the time, related prairie dog females seem to help each other out. The team witnessed infanticide only once every 300 hours of observation. But Hoogland has many thousands of such hours under his belt and spent a season with a backhoe to dig out burrows to find dead pups. He was able to document that more than one-third of litters have some or all of its members killed by other prairie dogs. The finding demonstrates that fierce competition lurks beneath the prairie dogs' communal life (*Science*, 29 November 1985, p. 1037).

Hoogland's world. By marking prairie dogs on their flanks (*top*) and watching them in all sorts of weather from towers (*middle*), Hoogland has gleaned insights into these animals' family dynamics (*bottom*).

CREDITS: ELAINE MILLER BOND/WWW.ELAINEMILLERBOND.COM (3)

Hoogland can thank his wife for his latest surprise. Among prairie dogs, young males often leave their birthing ground while females stay put, forming a family unit called a clan with the mother, her daughters, sisters, and sometimes cousins. But a few exceptional females left their territories, and these sparked Judy's curiosity. "I said it's so rare, it's not worth looking at," Hoogland recalls. But she wore him down.

When Hoogland did the analysis in black-tailed prairie dogs, he found that females with no mother, sisters, or brothers nearby were 12.5 times more likely to move away than females with a close relative around. In Gunnison's prairie dogs, such dispersal was 5.5 times more likely, and in Utah prairie dogs, 2.5 times, he reports.

The results are very convincing because Hoogland has such a large sample size—the data were drawn from recorded movements of 744 males and 907 females from 1093 litters—says Dirk Van Vuren, a behavioral ecologist at the University of California, Davis. And the findings were unexpected. "This [result] is contrary to the predictions made by two of behavioral ecology's superstars," Hoogland says.

In 1977, William Donald Hamilton and Robert May argued that close kin disperse to avoid competing with one another. They used mathematical models to evaluate the effect of relatedness on animal behavior and predicted that if two sisters stayed in the same place, for example, competition for resources would lower the fitness of both. In theory, one sister should leave. Research in scores of species, including mice, wasps, and lizards, has supported this idea.

Instead, Hoogland finds that "cooperation with other kin can counterbalance the amount of competition that close relatives have," Dobson comments. That counterbalance may help explain family groups in other animals, such as wolves, dolphins, and primates. Prairie dogs are indeed cooperative: They sound off to warn each other of approaching predators, and once the young emerge from nests, females nurse them irrespective of parentage. When the services provided by their close kin disappear, young females may leave to seek out territories with more food where cooperation is not as crucial to their survival or reproductive success, Hoogland suggests. Alternatively, the absence of kin may simply signal that the area is no longer a good place to live.

Prairie dog researcher Con Slobodchikoff, a behavioral ecologist who is now officially retired from Northern Arizona University in Flagstaff, is hesitant about these results, however. He suggests that genetic data would help guarantee that individuals sharing a territory really are closely related. But Hoogland thinks that his observations are enough to establish kinship.

Clutton-Brock is satisfied with Hoogland's observational approach. "There's a big push throughout science to focus on experimental results," he explains. Hoogland's work "shows how top level science can be done without experimenting."

Analyzing the effects of competition and cooperation in prairie dogs may help explain the behavior of other species, too, adds Ana Davidson, a conservation ecologist at Stony Brook University in New York. "Uncovering all these exciting insights into the world of the prairie dog is teaching us a lot about social behavior of animals in general."

–ELIZABETH PENNISI

Downloaded from www.sciencemag.org on March 8, 2013

Published by AAAS

A Sea Change for U.S. Oceanography

Marine scientists are confronting declining budgets and a shrinking research fleet as torrents of data from new technologies remake their field

SINCE 1996, OCEANOGRAPHER KIPP Shearman has relied on a duo known around the lab as Bob and Jane to measure chlorophyll and other environmental parameters in the ocean off the Oregon coast. Roaming the sea for 3 to 5 weeks at a time, the pair never complains and comes up for air just every 6 hours. They're 2-meter-long automated submersibles called gliders, and the reams of data they've collected have allowed Shearman's team at Oregon State University, Corvallis, to make novel insights into changing marine ecosystems.

The gliders are cheaper than sending scientists out in ships to make measurements, Shearman says, and they can remain at sea nearly indefinitely. He named the machines after some senior colleagues, and, "We kid them that we're replacing them with robots."

There's a glimmer of truth to that notion. Two cultural shifts are simultaneously shaking the foundations of oceanography in the United States—and fueling a debate about the future direction of a fast-changing field. Fewer scientists are going to sea as a result of a shrinking science fleet, flat budgets, and skyrocketing costs. At the same time, oceanographers are using a growing array of high-tech devices—such as satellites, gliders, and vast networks of sensors tethered to the sea floor—to remotely collect more data than ever before without getting wet.

The trends are helping to transform oceanography "from small science to big science," says technologist James Bellingham of Monterey Bay Aquarium Research Institute (MBARI) in Moss Landing, California. That shift, in turn, is affecting how researchers study an increasingly urgent set of problems, including overfishing, ocean warming, and acidifying seas. It is also altering the culture of oceanography, including how scientists share data and how young oceanographers are trained.

Online
sciencemag.org
Podcast interview with author Eli Kintisch (http://scim.ag/pod_6124).

The churning is prompting contradictory emotions, however. The decline of the U.S. science fleet is "a catastrophe that's happening in slow motion," warns Bruce Appelgate, who heads ship and marine operations at the Scripps Institution of Oceanography in San Diego, California. But "we've entered a new era in oceanography, and it's for the best," declares oceanographer Sydney Levitus of the U.S. National Oceanic and Atmospheric Administration (NOAA) in Silver Spring, Maryland.

A waning fleet

A symbol of the changes remaking marine science floats alongside the dock at the Woods Hole Oceanographic Institution (WHOI) in Massachusetts. In its glory days, the research vessel *Atlantis* boasted adventures that kept it at sea for 10 months a year. Last year, it was out of port for only 8 months. Idle, the 84-meter-long vessel has the vacant feel of an abandoned steel office building, albeit a floating one. Labs and workshops sit empty; just a few crew members and students were busy during a recent visit. "We've had our thumb out looking for work," says Captain A. D. Colburn. He was "grateful" that Canadian scientists hired the ship for a monthlong mapping mission this past summer. But fewer U.S. researchers are using *Atlantis* as a result of funding issues and because its equipment is undergoing recertification tests to deploy its celebrated partner craft, the piloted submersible *Alvin*. So Colburn is confronting "a lot of face time with my computer," he says glumly, echoing a common refrain these days among oceanographers.

The dormancy is a product of decades-long policy shifts. During the Cold War, the U.S. Navy was the main benefactor of the nation's marine scientists, whose studies on ocean mixing and sound scattering served

CREDIT: TRISTAN PEERY, OREGON STATE UNIVERSITY

Downloaded from www.sciencemag.org on March 8, 2013

Published by AAAS

Robot overboard. Gliders offer scientists like Kipp Shearman a nearly permanent presence at sea.

military needs such as for undersea warfare. As the Navy has steadily reduced its support for academic oceanography, researchers have pieced together support from up to nine federal agencies; NOAA, the National Science Foundation (NSF), and the Navy are now the main funders. The fraction of federal research funding devoted to ocean sciences plummeted as the Cold War wound down, from roughly 7% in the 1970s to 3.5% in the 2000s, analysts estimate.

While budgets have stagnated, the U.S. science fleet has shrunk and the price tag for expeditions has skyrocketed. Academic oceanographers rely largely on government-built vessels operated by the University-National Oceanographic Laboratory System (UNOLS), a consortium of 62 universities and government laboratories. In 2001, UNOLs boasted 28 ships; now there are 19, and fleet officials project that there will be 13 in 2025, barring new federal commitments. Meanwhile, operating costs for the five largest UNOLS ships, which can support dozens of scientists for months at a time, have doubled in the last decade to roughly $36,000 per day. Daily costs for smaller ships have increased by 50%, to about $8000 per day. Such increases—along with hefty investments in new technologies—are reshuffling marine science budgets: This year, for the first time, NSF's Division of Ocean Sciences, a major UNOLS funder, expects to spend more of its $352 million budget on ships and infrastructure than on support for research grants.

One result is that, in a bid to pinch pennies, funding agencies have been urging scientists to use smaller, less expensive ships for their work when possible. That can create problems, researchers say. As part of a 2005 geological study of Hawaiian volcanoes, for instance, geologists deployed 35 seafloor seismometers using one of the larger UNOLS vessels, the 85-meter-long *Melville* operated by Scripps. When they returned the following year to retrieve them, NSF stipulated that the researchers use the smaller and less-costly *Ka'imikai-o-Kanaloa*, operated by the University of Hawaii, which lacks the *Melville*'s heft and ability to maneuver laterally. The downsizing contributed to two mishaps in rough seas, says Scripps geophysicist Gabi Laske, the cruise leader. In one, a 200-kg seismometer smashed against the side of the vessel as the crew tried to haul it on deck, causing minor damage to a sensor. "It's extremely unlikely this would have happened with a larger ship," Laske says. "It's these little things that make science in the ocean more dangerous and more difficult."

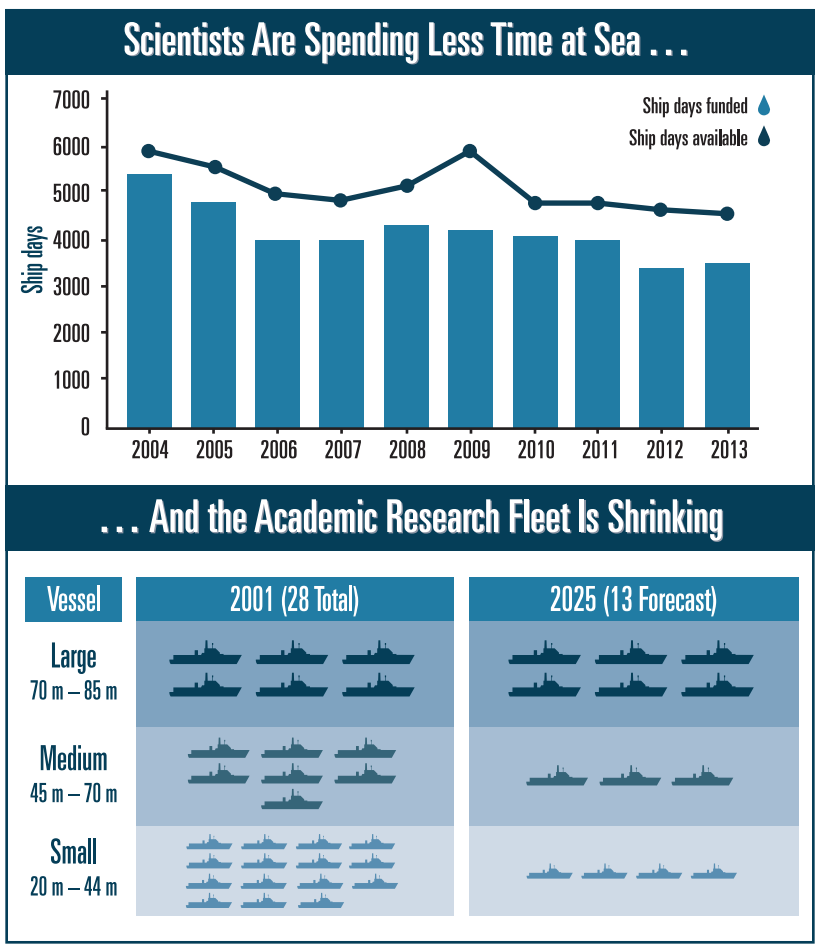

Landlocked? Fewer ships and less money mean getting to sea is increasingly challenging for university researchers.

The combination of fewer ships, increasing costs, and stagnating budgets is also creating a worrying feedback loop. Researchers interested in going to sea say they are having a harder time getting their proposals funded—and NSF has in the past suggested that requests that don't include costly ship time might have a better chance of winning approval. Discouraged, some researchers have simply stopped trying to do science aboard ships. "The last thing we want to do is spend a lot of time working on a proposal that is not going to be successful," says biological oceanographer Dennis McGillicuddy of WHOI.

In 2011, a UNOLS survey of 355 oceanographers found that 62% had at some point been "reluctant" to ask for at-sea funding, citing a "perception of low award rate for proposals with ship time." Ironically, that reluctance could further hasten the decline of the fleet, because it reduces demand and funding for the vessels. Indeed, officials say the demand for ship time is declining.

Many UNOLS vessels, some of which are 40 years old, are also showing their age or suffering from underfunded maintenance programs. Last year, three of the fleet's four large vessels operating from Pacific ports had serious technical problems. The 84-meter-long *Thomas G. Thompson*, for instance, was sidelined for half a year with a busted main thruster, a calamity that was "very disruptive" for several major cruises, says official Douglas Russell of the University of Washington (UW), Seattle, which manages the ship. (Some blame availability of parts, not the maintenance schedule, for the problem.) And in early 2012, the U.S. Coast Guard had to rescue the *Kilo Moana*, a 57-meter-long vessel operated by the University of Hawaii, after corrosion punched a 6-centimeter hole in its hull. "Not only are we losing ships, but the condition of the ships is such that they're breaking down," says Peter Wiebe, an oceanographer at WHOI and former UNOLS chair.

The prospects for major improvements are relatively bleak. A 2001 UNOLS plan called for building 10 new ships by 2020 for a fleet size of 16. The proposed additions included seven large ones, to "maintain fleet capacity" (*Science*, 21 January 2005, p. 338). So far, however, replacements have come more slowly than envisioned and just three new

CREDITS: UNOLS

Downloaded from www.sciencemag.org on March 8, 2013

Published by AAAS

ones have appeared, including two large ships with less range than the vessels they replaced. Three are getting tested or are under construction, and three others are on the drawing board but unfunded. If those three fail to materialize, vessel retirements would shrink the fleet to 13 vessels in 2025. A smaller fleet will be "increasingly unable to meet science user demands," concluded a 2009 UNOLS report. "[M]ulti-ship operations" would be more difficult to schedule, it warns, as would "expeditions in remote areas."

Even stabilizing the fleet at 13 vessels could become a stretch given current U.S. budget problems. This past June, NSF and Navy officials recommended that UNOLS retire some smaller ships sooner than planned in order to create savings that "would be used to bolster the schedules of the remaining vessels." That framework troubles researchers who primarily work in coastal and nearshore waters, where the smaller ships are an advantage. The plan will create "a big gap" in the fleet, McGillicuddy says.

The downsizing doesn't necessarily mean disaster, says Rodey Batiza, an official with NSF's ocean research branch. Modern ships feature more capable laboratory spaces than their predecessors and can deploy robotic payloads that can roam widely, enabling vessels to collect "1000 times more data in a day than they did a decade ago," Batiza says. But many oceanographers are not persuaded. "The ocean is undersampled now, and it was undersampled when we had 28 ships," McGillicuddy says. "The new tools don't obviate the need for research vessels."

The bottom line, believes former UNOLS Chair Bruce Corliss, dean of the Graduate School of Oceanography at the University of Rhode Island (URI), Narragansett Bay, is that "we have a significant crisis for the UNOLS fleet."

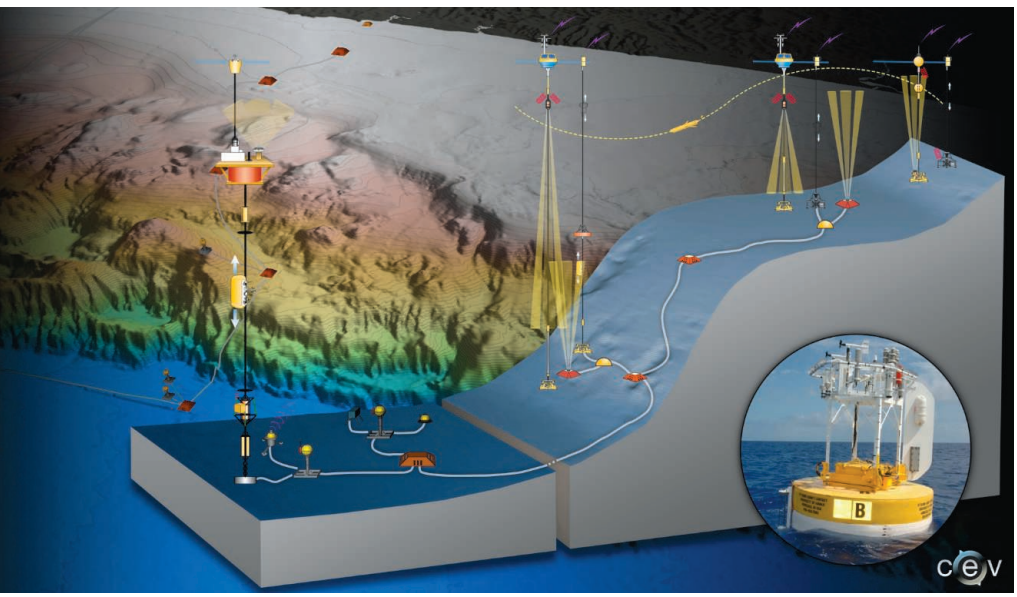

Wired sea floor. A panoply of sensors and robots will provide fully powered, real-time data through the Ocean Observatories Initiative.

CREDIT: OOI REGIONAL SCALE NODES PROGRAM AND THE CENTER FOR ENVIRONMENTAL VISUALIZATION, UNIVERSITY OF WASHINGTON

The marine tech revolution

The fleet's woes are all the more striking in contrast to the dazzling new data-gathering tools that oceanographers now deploy. Walk the deck of a research vessel built in the 1970s, and you'll find shiny new submersibles, buoys, and other devices sporting the latest in batteries, communications, and cameras, often built by graduate students half as old as the ships. These are the tools of a technological revolution in oceanography that began some 3 decades ago, with the 1978 launch of SEASAT, the first civilian oceanographic satellite. During just 3 months in orbit, NASA estimates SEASAT collected as much data—including sea surface temperatures, wind speeds, and ice conditions—as had been acquired by all ships during the previous century.

Now, automated devices are gathering even more data from more places, including far below the top centimeter of seawater that satellites can probe. Since 2004, for example, the global Argo program, comprised of 3500 drifting devices packed with electronics, has extensively profiled the oceans to a depth of 2000 meters (*Science*, 27 April 2012, p. 405). Costing roughly $10,000 each, the floats measure temperature, pressure, and salinity as they rise and sink over a 10-day cycle, reporting data continually by satellite. The floats collect some 120,000 profiles each year, dwarfing the 15,000 or so that ships collected just a few decades ago. Researchers slicing and dicing Argo data have already produced more than 1100 scientific publications, including papers with new insights into the ocean's heat content and major currents.

Physical and chemical oceanographers have benefited most, but biologists are eager to catch up. "We have physics envy," says biological oceanographer David Karl of the University of Hawaii, Manoa. He is just one researcher hoping to benefit from the next generation of Argo floats, which will include sensors able to monitor biological activity, such as the rate of marine photosynthesis.

Other cutting-edge automated instruments are essentially floating laboratories. The Lexus of these devices is called the Environmental Sample Processor (ESP), developed by MBARI. About the size of a large trash can, the ESP usually hangs roughly 20 meters below the ocean surface off a moored buoy. Inside, a robot draws in water samples, extracts RNA from them, and uses a microarray to detect certain microorganisms' genes. MBARI recently commercialized the machine and researchers hope to use it to monitor fisheries, sewage pollution, and harmful algal blooms. The ESP is "really the only show in town" when it comes to high-tech remote biological oceanography, Karl says.

The ESP costs roughly $175,000, but its more affordable robotic brethren "democratize" the ability to do studies once within the reach of only larger laboratories, says MBARI's Bellingham. For example, submersible gliders like Oregon State's Bob and Jane can cost $125,000 to $150,000 each, making them "something that under a normal research grant you can buy," he says.

Falling technology prices are also spurring innovation. One barrier to developing new marine science gear has been the cost of the cruises needed to test it at sea. But many gliders, robotic submersibles, and floats now can be tested off small vessels near shore. At URI, marine engineer Chris Roman and colleagues are using that approach to develop a new device on a relatively small budget of $1 million. The tubular float snaps one high-resolution photo of the ocean floor every second as it drifts in shallow waters, where floats like Argo can't operate. "We approached it as: 'What could we do with a very simple instrument?'" Roman says. If it works, the floating photographer could make the weekly chore of catching and counting fish in nearby Narragansett Bay far less arduous for graduate students.

The marine technology renaissance isn't just about tinkerers building single instru-

Downloaded from www.sciencemag.org on March 8, 2013

Published by AAAS

ments; it is also enabling researchers to envision and install vast instrument networks that are linked to land by kilometers of fiber optic cable. The wired ocean includes a new Japanese 20-site seismology network, a 12-site network that will ultimately dot European seas, and a U.S. network that connects several coastal sensor arrays. The most ambitious project is the Ocean Observatories Initiative (OOI), an international, Internet-connected network featuring 804 physical, chemical, and biological sensors in six separate arrays from Greenland to southern Chile (*Science*, 16 November 2007, p. 1056). Whereas battery-powered seafloor sensors can conk out, sensors on the OOI network, now under construction, will get a steady supply of power from land. With an estimated cost of $770 million, scientists predict that OOI, which is scheduled to go live in the deep ocean next year, will give them immediate access to data, a rare treat. In the process they'll get a front-row seat to ephemeral or fast-moving seafloor phenomena, such as undersea methane burps, that can be hard to capture during relatively brief research cruises.

These new systems will produce unprecedented torrents of data. And like space and genome scientists before them, oceanographers now face the challenge of efficiently storing, using, and sharing their largess. One difficult task will be learning how best to combine and properly label incompatible data sets, says URI oceanographer Peter Cornillon. Another will be making sure all the data get used; it's becoming increasingly common that some data go unanalyzed after a cruise or project—a notion that would have been unthinkable just a few years ago.

New day. Three-thousand-five-hundred Argo floats provide unprecedented daily ocean data.

The arrival of big oceanography is engendering a new commitment to sharing data. Traditionally, scientists jealously guarded their data for 2 years after collection, giving them time to publish, says John Gould of the National Oceanography Centre in Southampton, U.K. Some geochemical data collected on cruises during the 1990s "didn't see the light of day for 10 years," he notes. Now, raw satellite, Argo, and glider data are available nearly instantly online, and sharing is becoming the norm.

A new process

Such changes are helping reshape and enhance a variety of oceanographic projects, which generally fall into two broad categories. One is "process" studies, which examine specific phenomena through experiments that can last days, weeks, or perhaps a month. The other includes monitoring or survey efforts that gather data over a long period in different places, or annually at the same spot, in order to track changing conditions.

Process experiments highlight the growing capabilities of modern ships, which can host big, multidisciplinary teams working in clean, roomy labs equipped with devices, such as DNA sequencers or mass spectrometers, that were previously available only on land.

The New Generation of Sea Scientist

Veteran oceanographer Margaret Leinen fondly remembers the regular stream of lengthy ocean cruises that she and her fellow students enjoyed during their training in the 1970s—and the outsized demand for their labor. Senior scientists asked: "How many times can we get students to go to sea before they rebel?" recalls Leinen, director of Harbor Branch Oceanographic Institute in Fort Pierce, Florida.

Now, however, "seafaring adventures are a much smaller part of the way we perceive our careers than those who are 15 or 20 years older," says Rebecca Walsh Dell, who recently received a doctorate from the Woods Hole Oceanographic Institution (WHOI) in Massachusetts. Of the five students who joined her Ph.D. program the same year, only one, who focuses on biology, has relied on data collected on ocean cruises for their graduate research, she says. The others have used remote sensing data, modeling studies, or data from the Argo network. "The traditional model—design an experiment, deploy equipment, collect the data, spend 2 years writing the paper—none of us did that." The students eventually made it on a cruise, she says, "but only to see how the sausage gets made."

Core curriculum. Time at sea is no longer a mandatory part of oceanographic education.

That doesn't mean young scientists don't still dream of exploring the high seas. A summer fellowship that trains graduate students to lead research cruises has "more students signing up than we can accommodate," says Bruce Appelgate, who runs the program at the Scripps Institution of Oceanography in San Diego, California. "We've got a tremendous interest among students in getting out to sea."

Overall, about 45% of the approximately 2500 graduate students in U.S. oceanography programs saw time at sea the year before, according to a 2011 survey conducted by the University-National Oceanographic Laboratory System. It also found that 75% of U.S. ocean scientists within 4 years of completing their postgraduate training planned to request future ship time. Still, that is less than the 85% of scientists with more than 20 years of experience who said the same. And WHOI oceanographer Peter Wiebe is dismayed that the institute's graduate students routinely turn down invitations to take a berth on an upcoming cruise. "We end up bringing European or Asian students," he says.

That's a danger sign for some oceanographers. Kipp Shearman of Oregon State University, Corvallis, says that the master's degree students he supervises "get real skilled real fast" at programming gliders and interpreting the data they provide. But that can't replace "the experience of doing ship-based research." John Gould of the National Oceanography Centre in Southampton, U.K., worries that data are being "handed on a plate to young scientists on the Web sites, and there might be this tendency [not to question] the numbers." But "turn the clock back 20 years," he says, and "you went out and collected your own data, you applied your own expertise to it, and you had to question whether things [were] what they seemed."

–E. K.

CREDITS (TOP TO BOTTOM): ADAM Ü/PICASA/NOAA; 2012 SCRIPPS INSTITUTION OF OCEANOGRAPHY/UNIVERSITY OF CALIFORNIA, SAN DIEGO

Downloaded from www.sciencemag.org on March 8, 2013

Published by AAAS

They also emphasize the evolving role of the research vessel as a mother ship for an array of mobile technologies. In 2011, for example, a 50-scientist team used a pair of big ships to help launch a study called LatMix that used a phalanx of tools to study surface stirring—a fundamental ocean process poorly described by computer models. Working in the Gulf Stream off the coast of Cape Hatteras, North Carolina, the researchers released tracking dyes, robotic submersibles, and floats, and even called in an airplane to help keep a close eye on moving water masses. The "impressive" project set a recent scientific meeting abuzz, says Rebecca Walsh Dell, a postdoctoral researcher at Scripps.

Similarly, MBARI researchers have deployed ships, robot submersibles, and ESP, their floating gene analyzer, in multifaceted efforts to study California's Monterey Bay. In one 2009 campaign, the scientists used real-time data from an ESP to guide the submersibles to interesting sampling locations. Combining the data revealed in new and startling spatial detail how zooplankton flock to otherwise invisible boundaries between warm and cold water masses.

Autonomous or remotely controlled assets are also allowing researchers to collect data in rough seas or remote areas that can be too dangerous for ships. When Superstorm Sandy hit the New Jersey coast last year, for example, Rutgers University researchers were able to deploy a glider that offered a unique look at how the storm scrambled near-shore sediments and water layers (*Science*, 9 November 2012, p. 728).

Biological oceanographers are also hoping to chart new territory, for example by building devices that can track individual organisms. Measuring biological activity has often meant sampling creatures as they waft by one particular spot in the ocean. Advanced sensors and software, however, could enable a submersible to follow visual, chemical, or biological cues. "Smarts on board—that's the nirvana we'd like to move towards," says Oregon State's Mark Abbott.

The closest thing so far is a torpedo-shaped robot called *Tethys* which combines aspects of a propeller-driven submersible and a buoyancy-driven glider. It can wait for weeks in areas of interest before racing to a specific site—and it travels four times faster than previous gliders. One of its designers, MBARI's Bellingham, hopes that similar tools will one day travel alone to an algae bloom during its initial stages of development and then monitor its growth and decline, which generally takes a month.

A watchful eye

The growing mix of technologies is also reenergizing the once relatively obscure world of long-term monitoring studies, enabling what Hawaii's Karl calls a shift from the "snapshot view of the ocean to the full-length movie perspective."

As recently as the 1990s, "environmental monitoring" was seen as anathema to funders interested in big experiments focused on specific questions, Karl says, and "something you would never put in a proposal, especially to NSF." But now, analyzing how ocean ecosystems influence and react to climate change, pollution, and overfishing have become important to researchers and policymakers alike. And that means developing baseline information on the ocean's "normal" conditions—such as water chemistry and seasonal fluxes in plankton—and then keeping an eye on how things change.

Human-crewed ships will continue to be essential for some survey projects, such as a global effort to understand climate variability called CLIVAR, because only they can perform complex measurements at sea, such as genetic and chemical isotope analyses. But automated devices, such as the Argo float network, are also demonstrating the value of monitoring for monitoring's sake. In part, that's because the floats go places that ships often don't, with the network covering every ice-free region of the open ocean. "The Southern Hemisphere has been so poorly observed almost anything we find will be new," says NOAA oceanographer Levitus, a member of the Argo science team.

And Argo is extending into new frontiers,

Ahoy, Telepresence

One way oceanographers are coping with dwindling ship time is by using "telepresence" video technology to connect landlocked scientists with colleagues at sea. Last summer, one such virtual cruise marked the first time the technique was used to help direct an autonomous submersible mission.

The 3-week expedition explored seafloor seeps near the Blake Ridge, roughly 500 km off the South Carolina shore. The research team was split between a small group of scientists and engineers aboard the National Oceanic and Atmospheric Administration vessel *Okeanos Explorer*, which features a suite of cutting-edge video and data communication tools, and about a dozen scientists and students on shore at the University of Rhode Island, Narragansett Bay. To find seeps, the shipboard team deployed an autonomous robotic submersible called *Sentry* each evening and retrieved it the following morning.

Screen time. Scientists on shore wave to colleagues at sea during a telepresence cruise.

Sentry's sonar, image, and sensor data were sent daily via satellite to the scientists in Rhode Island for analysis. The shipboard team, meanwhile, analyzed ship sonar data for clues to possible seep areas. Together, the two groups used the information to identify promising areas for *Sentry*'s daily dive and plan the spacing of its zigzag search pattern. Scientists call the virtual cruise a modest scientific success, noting that it discovered five new seeps in an area previously known to contain only one.

Equally important, perhaps, was that the effort demonstrated how virtual cruises can enhance training for students, even undergraduates. It's tough for a college student to get a spot on a research cruise, notes one of the students on the shore team, junior Meghan Rose Jones of the University of Miami in Florida. So it "was an opportunity which would have not been otherwise possible," she says. Even if she had gotten a berth, Jones thinks she might have spent many more hours standing watch than analyzing data. Instead, she learned to use two mapping software programs and participate in research decision-making.

By the end of the cruise, Jones and several graduate students "were the ones discovering what the seafloor was like" and making dive plan suggestions, says lead scientist Cindy Van Dover, director of the Duke University Marine Laboratory in Beaufort, North Carolina. The team expects to get even more out of a 5-day return expedition next year to Blake Ridge. It will feature the *Jason* tethered submersible, which can collect samples of water, rocks, and sea life. **–E. K.**

CREDIT: ALEX DECICCIO/INNER SPACE CENTER, URI

Downloaded from www.sciencemag.org on March 8, 2013

Published by AAAS

as polar scientists begin to deploy new rugged floats below sea ice. Argo is also helping eliminate a seasonal bias in oceanographic data, created by the tendency of researchers to avoid cold weather cruises. "A main finding has been that the ocean is more variable than we thought," Levitus says. Charting those changes and fluctuations is helping researchers do weather, climate, and fisheries "forecasting much better than we have ever done in the past," he adds.

Evolving technology is underscoring the power of sustained monitoring in other ways. In the late 1980s, researchers established sites near Bermuda and Hawaii, dubbed BATS and HOT, where ships and moored instruments take monthly readings. The sites have played a key role in helping scientists determine the fluctuating physical, chemical, and biological patterns that make up the ocean's baseline. But even monthly readings may not be enough to detect certain phenomena, researchers say. In 2011, for example, UW's Matthew Alford published new findings that suggest the breaking of seafloor waves happen more rarely than expected. Key to that finding were readings from a moored profiler he deployed on a cable at the HOT site that sampled the whole water column each hour for more than 2 years. "Most of the time, monthly readings taken from ships will completely miss the phenomenon" he says. Other researchers say the success of BATS and HOT suggest that it would be worth setting up new monitoring sites in areas important to global climate, such as the Arctic or northern mid-Atlantic.

Seafloor scientists are hoping to literally see fireworks with some of their new monitoring tools. Researchers have never witnessed an undersea volcanic eruption from beginning to end, notes oceanographer John Delaney of UW Seattle, one of OOI's leaders. But the payoff could be so great that researchers have built one section of the groundbreaking sensor network on the Axial Seamount, an active underwater volcano about 500 kilometers west of the Washington state coast that erupts every 10 to 15 years. "Next time it erupts we can be there," Delaney says. He's got his fingers crossed that the sensor array, which includes video, chemical, and seismic equipment, can survive the harsh environment.

Biologists are also eager to examine the exotic bacteria that the volcano spews with an underwater mass spectrometer and DNA sequencer. "By the time we [usually] get there, they've diluted or wafted away," Delaney says. Now, researchers can relax on shore in comfort, knowing OOI is always watching.

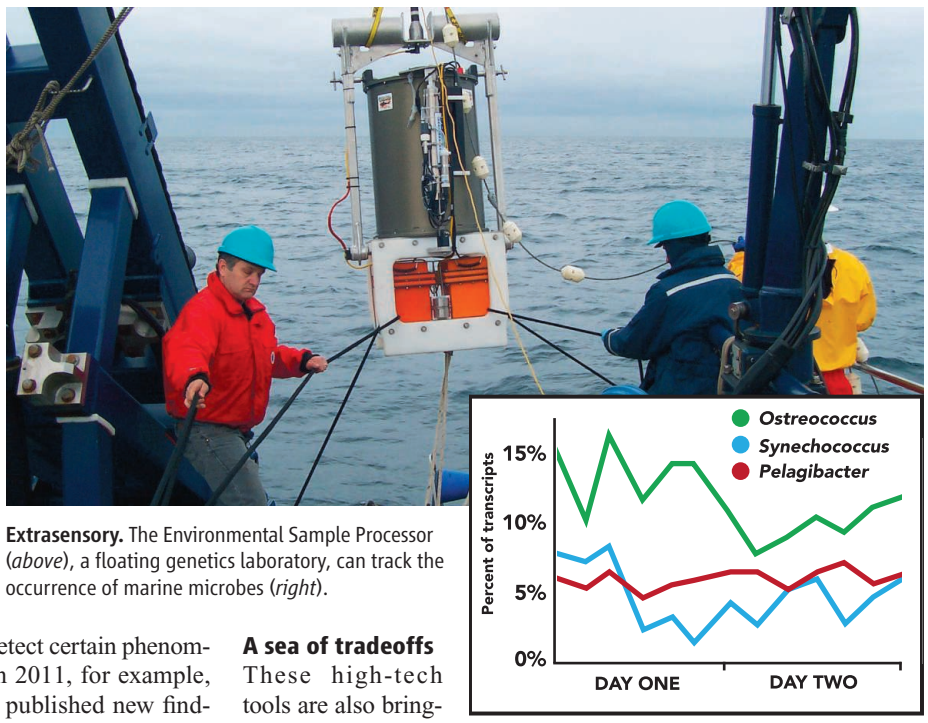

Extrasensory. The Environmental Sample Processor (*above*), a floating genetics laboratory, can track the occurrence of marine microbes (*right*).

CREDITS: MBARI; (INSET) ADAPTED FROM OTTESEN *ET AL.*, *PNAS* 110 (5 FEBRUARY)

A sea of tradeoffs

These high-tech tools are also bringing some contentious issues to the surface: The relatively high cost of systems like OOI is forcing U.S. oceanographers to confront difficult choices over how to spend limited funds. The unfolding debate sometimes pits building bigger ships against smaller ones, or ships against unmanned robotic craft—or mobile robots against static sensor networks. Deciding which tradeoffs to make will be "very, very important," UW's Delaney says. Researchers might "go to sea less," for instance, "but the data flow from these new systems is around the clock, 365 24/7, for decades."

Others are challenging the ship-centric mindset that dominates planning in marine science. At URI, for instance, Cornillon has weighed in on a campus debate about what sort of vehicle should eventually replace the university's 38-year-old research ship, *Endeavor*, which it operates for NSF. He's not against obtaining a new vessel, but says his colleagues should focus on "very quickly" evolving oceanography technologies. "The development of these will be as or more important to an institution such as URI than having its own ship," Cornillon says. He and his colleagues have envisioned a scenario for 2030 in which phalanxes of airborne drones and submersibles conduct a tightly choreographed analysis of sea-air interactions, with a ship's role undefined. Colleagues applaud such creativity, but questioning the need for a big vessel has made Cornillon "not terribly popular with many," he admits.

There's also disagreement about the value of large seafloor observatories like OOI. Floats, gliders, and robotic submersibles are well-suited for tough economic times, advocates say, because of their relatively low prices and flexibility. In contrast, OOI will require expensive ship time for maintaining the network, which could command as much as 16% of the NSF Division of Ocean Science's budget beginning in 2015. The project "really is a huge tax on everything," Alford says. "Are there other places that we haven't seen that we could be studying instead?" asks WHOI engineer Dana Yoerger. "There's a whole world to explore."

To help set priorities, the U.S. government's main ocean research advisory panel is working on a report, due next year, that will review fleet needs. At NSF, ocean science chief David Conover wants scientists to go even further. He'd like the field's diverse constituencies to write a consensus "decadal survey" with numbered priorities for projects, as scientists in astronomy and other facilities-intensive fields have done. "It's not just about how you slice the pie, it's about making the case to grow the pie," he says.

That's certainly a case researchers feel has been poorly made in Washington. "Studying the oceans should be funded comparable to research in outer space," says UW's Delaney. But with a depressing budget outlook and the oceanographic community at odds over its future path, that's "a dialogue nobody has the guts to be having."

–ELI KINTISCH

Downloaded from www.sciencemag.org on March 8, 2013

Published by AAAS

ments; it is also enabling researchers to envision and install vast instrument networks that are linked to land by kilometers of fiber optic cable. The wired ocean includes a new Japanese 20-site seismology network, a 12-site network that will ultimately dot European seas, and a U.S. network that connects several coastal sensor arrays. The most ambitious project is the Ocean Observatories Initiative (OOI), an international, Internet-connected network featuring 804 physical, chemical, and biological sensors in six separate arrays from Greenland to southern Chile (*Science*, 16 November 2007, p. 1056). Whereas battery-powered seafloor sensors can conk out, sensors on the OOI network, now under construction, will get a steady supply of power from land. With an estimated cost of $770 million, scientists predict that OOI, which is scheduled to go live in the deep ocean next year, will give them immediate access to data, a rare treat. In the process they'll get a front-row seat to ephemeral or fast-moving seafloor phenomena, such as undersea methane burps, that can be hard to capture during relatively brief research cruises.

These new systems will produce unprecedented torrents of data. And like space and genome scientists before them, oceanographers now face the challenge of efficiently storing, using, and sharing their largess. One difficult task will be learning how best to combine and properly label incompatible data sets, says URI oceanographer Peter Cornillon. Another will be making sure all the data get used; it's becoming increasingly common that some data go unanalyzed after a cruise or project—a notion that would have been unthinkable just a few years ago.

New day. Three-thousand-five-hundred Argo floats provide unprecedented daily ocean data.

The arrival of big oceanography is engendering a new commitment to sharing data. Traditionally, scientists jealously guarded their data for 2 years after collection, giving them time to publish, says John Gould of the National Oceanography Centre in Southampton, U.K. Some geochemical data collected on cruises during the 1990s "didn't see the light of day for 10 years," he notes. Now, raw satellite, Argo, and glider data are available nearly instantly online, and sharing is becoming the norm.

A new process

Such changes are helping reshape and enhance a variety of oceanographic projects, which generally fall into two broad categories. One is "process" studies, which examine specific phenomena through experiments that can last days, weeks, or perhaps a month. The other includes monitoring or survey efforts that gather data over a long period in different places, or annually at the same spot, in order to track changing conditions.

Process experiments highlight the growing capabilities of modern ships, which can host big, multidisciplinary teams working in clean, roomy labs equipped with devices, such as DNA sequencers or mass spectrometers, that were previously available only on land.

The New Generation of Sea Scientist

Veteran oceanographer Margaret Leinen fondly remembers the regular stream of lengthy ocean cruises that she and her fellow students enjoyed during their training in the 1970s—and the outsized demand for their labor. Senior scientists asked: "How many times can we get students to go to sea before they rebel?" recalls Leinen, director of Harbor Branch Oceanographic Institute in Fort Pierce, Florida.

Now, however, "seafaring adventures are a much smaller part of the way we perceive our careers than those who are 15 or 20 years older," says Rebecca Walsh Dell, who recently received a doctorate from the Woods Hole Oceanographic Institution (WHOI) in Massachusetts. Of the five students who joined her Ph.D. program the same year, only one, who focuses on biology, has relied on data collected on ocean cruises for their graduate research, she says. The others have used remote sensing data, modeling studies, or data from the Argo network. "The traditional model—design an experiment, deploy equipment, collect the data, spend 2 years writing the paper—none of us did that." The students eventually made it on a cruise, she says, "but only to see how the sausage gets made."

Core curriculum. Time at sea is no longer a mandatory part of oceanographic education.

That doesn't mean young scientists don't still dream of exploring the high seas. A summer fellowship that trains graduate students to lead research cruises has "more students signing up than we can accommodate," says Bruce Appelgate, who runs the program at the Scripps Institution of Oceanography in San Diego, California. "We've got a tremendous interest among students in getting out to sea."

Overall, about 45% of the approximately 2500 graduate students in U.S. oceanography programs saw time at sea the year before, according to a 2011 survey conducted by the University-National Oceanographic Laboratory System. It also found that 75% of U.S. ocean scientists within 4 years of completing their postgraduate training planned to request future ship time. Still, that is less than the 85% of scientists with more than 20 years of experience who said the same. And WHOI oceanographer Peter Wiebe is dismayed that the institute's graduate students routinely turn down invitations to take a berth on an upcoming cruise. "We end up bringing European or Asian students," he says.

That's a danger sign for some oceanographers. Kipp Shearman of Oregon State University, Corvallis, says that the master's degree students he supervises "get real skilled real fast" at programming gliders and interpreting the data they provide. But that can't replace "the experience of doing ship-based research." John Gould of the National Oceanography Centre in Southampton, U.K., worries that data are being "handed on a plate to young scientists on the Web sites, and there might be this tendency [not to question] the numbers." But "turn the clock back 20 years," he says, and "you went out and collected your own data, you applied your own expertise to it, and you had to question whether things [were] what they seemed."

–E. K.

CREDITS (TOP TO BOTTOM): ADAM Ü/PICASA/NOAA; 2012 SCRIPPS INSTITUTION OF OCEANOGRAPHY/UNIVERSITY OF CALIFORNIA, SAN DIEGO

Downloaded from www.sciencemag.org on March 8, 2013

Published by AAAS

They also emphasize the evolving role of the research vessel as a mother ship for an array of mobile technologies. In 2011, for example, a 50-scientist team used a pair of big ships to help launch a study called LatMix that used a phalanx of tools to study surface stirring—a fundamental ocean process poorly described by computer models. Working in the Gulf Stream off the coast of Cape Hatteras, North Carolina, the researchers released tracking dyes, robotic submersibles, and floats, and even called in an airplane to help keep a close eye on moving water masses. The "impressive" project set a recent scientific meeting abuzz, says Rebecca Walsh Dell, a postdoctoral researcher at Scripps.

Similarly, MBARI researchers have deployed ships, robot submersibles, and ESP, their floating gene analyzer, in multifaceted efforts to study California's Monterey Bay. In one 2009 campaign, the scientists used real-time data from an ESP to guide the submersibles to interesting sampling locations. Combining the data revealed in new and startling spatial detail how zooplankton flock to otherwise invisible boundaries between warm and cold water masses.

Autonomous or remotely controlled assets are also allowing researchers to collect data in rough seas or remote areas that can be too dangerous for ships. When Superstorm Sandy hit the New Jersey coast last year, for example, Rutgers University researchers were able to deploy a glider that offered a unique look at how the storm scrambled near-shore sediments and water layers (*Science*, 9 November 2012, p. 728).

Biological oceanographers are also hoping to chart new territory, for example by building devices that can track individual organisms. Measuring biological activity has often meant sampling creatures as they waft by one particular spot in the ocean. Advanced sensors and software, however, could enable a submersible to follow visual, chemical, or biological cues. "Smarts on board—that's the nirvana we'd like to move towards," says Oregon State's Mark Abbott.

The closest thing so far is a torpedo-shaped robot called *Tethys* which combines aspects of a propeller-driven submersible and a buoyancy-driven glider. It can wait for weeks in areas of interest before racing to a specific site—and it travels four times faster than previous gliders. One of its designers, MBARI's Bellingham, hopes that similar tools will one day travel alone to an algae bloom during its initial stages of development and then monitor its growth and decline, which generally takes a month.

A watchful eye

The growing mix of technologies is also reenergizing the once relatively obscure world of long-term monitoring studies, enabling what Hawaii's Karl calls a shift from the "snapshot view of the ocean to the full-length movie perspective."

As recently as the 1990s, "environmental monitoring" was seen as anathema to funders interested in big experiments focused on specific questions, Karl says, and "something you would never put in a proposal, especially to NSF." But now, analyzing how ocean ecosystems influence and react to climate change, pollution, and overfishing have become important to researchers and policymakers alike. And that means developing baseline information on the ocean's "normal" conditions—such as water chemistry and seasonal fluxes in plankton—and then keeping an eye on how things change.

Human-crewed ships will continue to be essential for some survey projects, such as a global effort to understand climate variability called CLIVAR, because only they can perform complex measurements at sea, such as genetic and chemical isotope analyses. But automated devices, such as the Argo float network, are also demonstrating the value of monitoring for monitoring's sake. In part, that's because the floats go places that ships often don't, with the network covering every ice-free region of the open ocean. "The Southern Hemisphere has been so poorly observed almost anything we find will be new," says NOAA oceanographer Levitus, a member of the Argo science team.

And Argo is extending into new frontiers,

Ahoy, Telepresence

One way oceanographers are coping with dwindling ship time is by using "telepresence" video technology to connect landlocked scientists with colleagues at sea. Last summer, one such virtual cruise marked the first time the technique was used to help direct an autonomous submersible mission.

The 3-week expedition explored seafloor seeps near the Blake Ridge, roughly 500 km off the South Carolina shore. The research team was split between a small group of scientists and engineers aboard the National Oceanic and Atmospheric Administration vessel *Okeanos Explorer*, which features a suite of cutting-edge video and data communication tools, and about a dozen scientists and students on shore at the University of Rhode Island, Narragansett Bay. To find seeps, the shipboard team deployed an autonomous robotic submersible called *Sentry* each evening and retrieved it the following morning.

Screen time. Scientists on shore wave to colleagues at sea during a telepresence cruise.

Sentry's sonar, image, and sensor data were sent daily via satellite to the scientists in Rhode Island for analysis. The shipboard team, meanwhile, analyzed ship sonar data for clues to possible seep areas. Together, the two groups used the information to identify promising areas for *Sentry*'s daily dive and plan the spacing of its zigzag search pattern. Scientists call the virtual cruise a modest scientific success, noting that it discovered five new seeps in an area previously known to contain only one.

Equally important, perhaps, was that the effort demonstrated how virtual cruises can enhance training for students, even undergraduates. It's tough for a college student to get a spot on a research cruise, notes one of the students on the shore team, junior Meghan Rose Jones of the University of Miami in Florida. So it "was an opportunity which would have not been otherwise possible," she says. Even if she had gotten a berth, Jones thinks she might have spent many more hours standing watch than analyzing data. Instead, she learned to use two mapping software programs and participate in research decision-making.

By the end of the cruise, Jones and several graduate students "were the ones discovering what the seafloor was like" and making dive plan suggestions, says lead scientist Cindy Van Dover, director of the Duke University Marine Laboratory in Beaufort, North Carolina. The team expects to get even more out of a 5-day return expedition next year to Blake Ridge. It will feature the *Jason* tethered submersible, which can collect samples of water, rocks, and sea life. **–E. K.**

CREDIT: ALEX DECICCIO/INNER SPACE CENTER, URI

Downloaded from www.sciencemag.org on March 8, 2013

Published by AAAS

PROFILE: ANNE GLOVER

Europe's Science Superwoman Struggles to Get Off the Ground

The first chief science adviser for the European Commission's president speaks her mind and some call her "inspiring," but can she influence policy?

BRUSSELS—On her first day as Scotland's chief science adviser, Anne Glover almost lost her life. It was summer 2006 and on the way to catch an early morning train, the biologist lost control of her car in a bend, spun off the street, and crashed into a stone wall. The front and back of the small car were destroyed, she says. Somehow she emerged with hardly a scratch. Most people would have called it a day. Not Glover. "I arrived late" to work, she says. "But I did show up."

Now, Glover is the European Union's first chief scientific adviser and her resilience is being tested in other ways. Instead of 5 million Scots, her constituency is 500 million Europeans who are deeply divided on modern technologies and increasingly distrustful of scientists. A 2010 poll found that nearly 60% of Europeans felt scientists could no longer be trusted on controversial issues. And although her E.U. job did not start with a car accident, it has been challenged by the financial crash blighting Europe and by the complexities of her position.

Glover took office on 1 January 2012 and her duties only start with providing the European Commission's president with expert advice "on any aspect of science, technology and innovation." Her official tasks also include analyzing major policy proposals, liaising with institutions such as the European Union's food safety authority, helping with emergency planning, and giving early warning "on issues that might arise when scientific progress entails either opportunity or threat for the EU." Speaking recently in Sussex, U.K., Glover said that her brief evoked superwoman "flying through the treetops of Brussels."

European Commission President José Manuel Barroso, the driving force behind the creation of her position, hasn't bestowed superpowers on Glover, however. On the contrary, after years of discussions in Brussels, the science adviser's office became a "casualty" of austerity measures, Glover says. She has no budget of her own and just five staff members—one-half of the size of her team in Scotland.

Some European science policy analysts wonder if, under those constraints, Glover can wield any influence here in Brussels. "Unless you really anchor the position somehow," says Helga Nowotny, president of the European Research Council, Europe's science adviser "will not become a powerful position comparable to the U.S." And Peter Tindemans, secretary general of the researchers' organization Euroscience, says that although he is happy the job was created, giving it so little support was a mistake.

Indeed, Glover's influence is hard to discern so far. She has deliberately steered clear of the debate over the size of Horizon 2020; the European Union's primary science program for the next 7 years is slated to receive far less money than many scientists had hoped (*Science*, 15 February, p. 745). Glover defines her role as one of injecting science into policymaking rather than shaping policy for science. Still, some are waiting for those injections. "She hasn't yet singled out a small number of key issues on which she would like to make a difference," Tindemans says.

She *is* fighting for something. With less than 2 years left until Barroso's term expires, Glover is pressing hard to raise the profile of science and evidence in European politics. Among other initiatives, she's pushing for all E.U. members to have their own chief science advisers, and she has convened what she hopes will be a permanent advisory council on science and technology

CREDIT: COURTESY OF THE EUROPEAN UNION

Downloaded from www.sciencemag.org on March 8, 2013

Published by AAAS

for the commission. She is right to devote much time to this, Tindemans says. "How much power she can effectively wield also depends very much on her establishing solid ties with scientific advisers or persons or bodies with a similar role in member states."

Glover has already convinced some that a science adviser is important to Europe's future. Robert Madelin, the European Union's director-general for communications networks, content and technology, says that he "cannot imagine a future for Europe where the president of the commission would not want a high-level scientific adviser."

Rise of the science advisers

Born in Arbroath, Scotland, Glover, 56, trained as a microbiologist in Edinburgh and Cambridge, U.K., before joining the University of Aberdeen in 1983, where she ultimately became a professor in 2001. Her interest in politics started the same year, after she was appointed as a member of the Natural Environment Research Council, a U.K. body that funds research and training. "I found it really satisfying because you saw you made a difference," Glover says. In 2006, she became the Scottish chief science adviser. A friend had flagged the opening, suggesting it was the "perfect job" for Glover. "I wasn't sure what the job was," she says, "But then I don't think the Scottish government knew what the job was either."

No one foresaw how much work it would be. The part-time job ate away at the hours she could spend in her Aberdeen lab. But she persisted with her research, which is on stress responses in the worm *Caenorhabditis elegans*. She has continued that tradition in Brussels, running her lab mostly via Skype. Although it is hard to be productive this way, it's important, she says, to "have credibility as a working scientist."

On a recent morning here in the Berlaymont building, the European Commission's massive headquarters, Glover, reddish hair piled into a flaming sculpture, glasses perched on top, bubbled with enthusiasm as she talked about astronomy, physics, nanotechnology, and microbiology. She also loves *Star Trek* (though unlike her assistant Jan Marco Müller, she has no Starfleet uniform at home) and enjoys spotting the International Space Station as a hobby. "There is an app for that. Isn't that amazing?" she says.

About once a month, Glover takes the elevator up, from her 8th floor office to the 13th floor, to the true nerve center of the European Commission. There, she briefs Barroso on a variety of topics, including supercomputers, space weather, and dengue fever. The minutes that Glover spends on that floor are the currency in which her political power can be measured, and it is hardly enough to choreograph big changes in Brussel's legendary bureaucracy. She attributes her lack of clout to the newness of the position. "You cannot just arrive and expect everyone to be constantly knocking on your door," she says.

Contrast Glover's access with that of John Holdren, the latest in a long list of éminence grises tapped to advise U.S. presidents. At the annual meeting of AAAS (*Science*'s publisher) in Boston last month, Glover says that Holdren told her that he was in and out of Barack Obama's office up to four times a day in the run-up to important decisions.

Glover's position within the European Union is also unusual in that she reports directly to the president. The commission is a very hierarchical structure, says Müller, who is a veteran of European science politics. "In some ways, Anne is outside of that. She is a freelance artist." That allows her the freedom to operate a bit differently or to say things that other people are afraid to say. "Coming from outside the hierarchy can be an advantage if the holder of the position knows how to use it well. And Anne knows how to use it well," Nowotny says.

A case in point, in a magazine interview in July, Glover argued that eating genetically modified food was no riskier than eating conventionally farmed food—a stance at odds with the beliefs of many Europeans. She says she wanted to give evidence a voice. "By all means, people can say, for ethical reasons, for philosophical reasons, for economical reasons, for political reasons, I am not keen on that," she says. "But you cannot say it is dangerous, when it isn't."

The interview sparked a debate in the European Parliament and an official request by one of its members asking whether the commission agreed with Glover's stance. The reply was telling. The chief science adviser, the commission wrote in its answer, "has a purely advisory function and no role in defining Commission policies. Therefore, her views do not necessarily represent the views of the Commission." The tempest over her remarks and the commission's pallid response hasn't cowed Glover.

GM debate. Science adviser Anne Glover advocates research into genetically modified crops, despite protests such as ones staged by Greenpeace outside the European Commission's headquarters (*below*) and by members of the European Parliament.

"The way I interpret it, is that I have independence within the commission, which is a rare advantage."

Science advisers have always sat uneasily at the intersection of politics and science. Those in government "have overriding political considerations and sometimes the science is in the way," says Neal Lane, a public policy expert at Rice University in Houston, Texas, who served as Bill Clinton's science adviser.

Still, Glover's appointment is a sign of a shift. For decades, only the United States and United Kingdom found a use for science advisers. Surprised by the Soviet launch of Sputnik, U.S. President Dwight Eisenhower created the position in 1957. The United Kingdom followed suit in 1964. But in recent years, the concept has gained ground. New Zealand appointed its

CREDITS (TOP TO BOTTOM): VINCENT KESSLER/REUTERS/LANDOV; EPA/LANDOV

Downloaded from www.sciencemag.org on March 8, 2013

Published by AAAS

first chief science adviser in 2009, and the United Nations and Japan are planning similar posts. "Among the reasons for the trend are the number of policy issues that have a technical or scientific aspect to them and the assertion of authority by scientists themselves," says Roger Pielke Jr. of the Center for Science and Technology Policy Research at the University of Colorado, Boulder, who has studied the history of science advisers.

In Glover's office, a picture of the flame nebula, a colorful swirl of gas, dust, and stars in the constellation Orion, evokes how she has been lobbying to strengthen that trend. "This is a very interesting part of the sky, because this is a star nursery," she says, pointing to a few bright dots in the top half. Just like a core of gas and dust attracts more and more matter to form a star, Glover hopes her position will spawn similar jobs in every E.U. member state, beyond the three that currently employ a chief science adviser: the United Kingdom, Ireland, and the Czech Republic.

Glover's discussions with E.U. members appear to have paid off: A network of science advisers could be in place by the end of the year, she says. Having comrades in arms, she acknowledges, would help her and her successors exert greater influence. Last week, the commission announced another step in that direction: the creation of a president's science and technology advisory council. Glover will chair the 15-member group, which includes climate change expert Hans-Joachim Schellnhuber from Germany and Nobel Prize winner Ada Yonath from Israel. It will meet with the E.U. president three to four times a year to offer ideas on how to stimulate societal debates about science.

Atmospheric control. Glover has visited countless labs in Europe, such as this Italian one focused on air pollution monitoring, to establish ties with scientists.

CREDIT: COURTESY OF THE EUROPEAN UNION

Persuading the public

In a private dining room at an elegant Brussels restaurant, Glover takes on another key duty of her position. "There is a risk in eating food," she says as waiters place a salad in front of each of the 30-odd people in the room, members of an industry lobby group called the European Risk Forum. Some people have food allergies, some plants contain toxins, and sometimes food is ill-prepared, she notes. "But there is a bigger risk in not eating: certain death." Her point is that risk is everywhere, but we manage it through rational decisions. Europeans are too risk-averse, she contends—and it is holding the continent back. "Ask Europeans for their association to the word 'risk' and most would answer 'danger,' " Glover says. "I would say 'reward.' "

Glover speaks from experience. At the end of the '90s, she co-founded a company called Remedios that used biosensors to identify contaminated land and suggest clean-up technologies. In Europe, the response was measured, she says, as regulators hesitated to embrace something completely new. In the United States, on the other hand, the response was enthusiastic, she says. "In North America there is this race to be first and in Europe we are racing to be second all the time," Glover laments.

She has pounded that message over and over since becoming science adviser. She says that calling out Europe on its tepid support for innovation is fundamental to her mandate "to enhance public confidence in science and technology." It is a part of her job that she clearly enjoys and is very good at.

It's vital that science advisers are visible, says Miles Parker, former deputy chief science adviser to the U.K. Department for Environment, Food and Rural Affairs. Glover's hard work at creating a public persona seems to have succeeded. *Nature* named her a person to watch in 2013, and a panel of journalists and politicians convened by a BBC radio station recently voted her among the 20 most powerful women in the United Kingdom.

Despite rising to become the face of science in Europe, Glover says that she has encountered subtle sexism throughout her academic career. That's why she wants to use her newfound prominence to shine a light on women in science. Some E.U. members have a reputation for being better than the United States at letting female scientists juggle family and careers, but Glover believes Europe overall must do more. She argues, for example, that stronger maternal care provisions are needed for E.U. researchers. (Glover herself has no kids.) "Europe is in real danger of falling behind by being utterly careless in retaining their best assets of highly qualified and able women," she says.

Glover's profile will get another boost later this year, when Europe's Emergency Response Centre opens. Glover will be the center's science spokesperson. The next time European air traffic is disrupted by a volcano, for instance, or a disease emerges on the continent, expect Glover to be in front of the press explaining the science and Europe's response to the crisis.

Such an on-camera role would be part of Glover's ongoing audition for more time as Europe's top scientist. When Barroso steps down at the end of next year, her future will also be decided. "If we do our job well, the next president will want a chief scientific adviser as well, maybe even the same one," Müller says.

At the lunch meeting with the risk forum, a young business woman, a little flustered, thanks Glover after her speech. "The way you talk and the energy you have is so … ," she pauses, searching for a word, "inspiring." It is an unlikely word to describe a Brussels bureaucrat, but it is one often heard when people describe Glover. She may not have superpowers, but her charisma may be enough to endow the science adviser position with staying power.

–KAI KUPFERSCHMIDT

Downloaded from www.sciencemag.org on March 8, 2013

Published by AAAS

How relations make actors 1150

Adaptation with a difference 1154

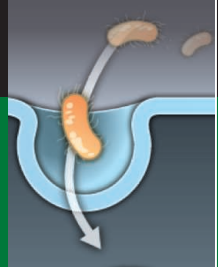

LETTERS | BOOKS | POLICY FORUM | EDUCATION FORUM | PERSPECTIVES

LETTERS

edited by Jennifer Sills

The Other Revolution in the Life Sciences

IN HIS PERSPECTIVE "THE REVOLUTION IN THE LIFE SCIENCES" (14 DECEMBER 2012, P. 1427), S. Brenner refers to the celebrated book *What Is Life?*, published in 1944 by the Austrian physicist Erwin Schrödinger, best known for the development of wave mechanics (*1*). Brenner focuses on only one of the two properties of life considered by Schrödinger in his definition, namely its ability to store, replicate, transfer, and express genetic information. Schrödinger, unaware of the as-yet-undiscovered DNA double helix with its base-pairing, attributed this mysterious property to an "aperiodic crystal." That Schrödinger's insight highlighted a fundamental property of life is undeniable. I can still vividly remember my immediate sense of being witness to a key event in the history of science when I read Watson and Crick's brief note titled "A structure for deoxyribonucleic acid" in a 1953 issue of *Nature* (*2*). Although that publication had been preceded 9 years earlier by the identification of the pneumococcal "transforming factor" as DNA by Avery *et al*. (*3*), the earlier landmark paper had had relatively little impact because of a prevailing bias that favored proteins as the information carrier in chromosomes. By identifying DNA base pairing as the universal mechanism of biological information transfer, the historic Watson and Crick publication indeed added a new paradigm in the Kühnian sense, as Brenner points out.

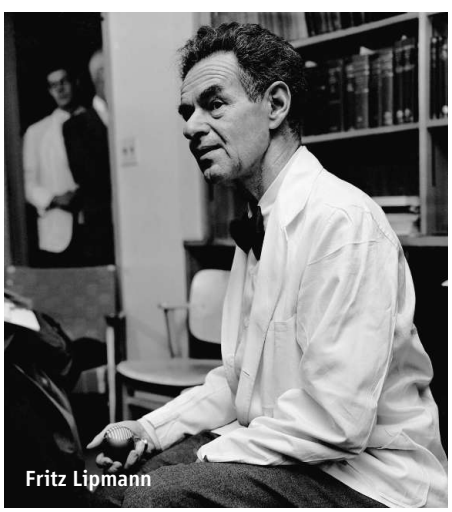

Fritz Lipmann

I have been witness to another revolution in the life sciences that Brenner did not mention. I experienced an earlier comparable feeling of excited illumination when I first read the paper by Fritz Lipmann titled "Metabolic generation and utilization of phosphate bond energy" (*4*). This historic paper introduced the notion of the "high-energy phosphate bond," symbolized by Lipmann's famous "squiggle," together with the accompanying key concepts of group potential and group transfer. This paper, even though published 3 years before Schrödinger's celebrated book, was most probably unknown to him. It clarified for the first time the second property singled out by Schrödinger in his definition of life: its ability to extract "negative entropy," better known to chemists as "free energy," from the environment and convert it into chemical and other forms of work.

This second paradigmatic element of Schrödinger's definition of life is arguably as fundamental as the first one and, in fact, preconditions it. Without group transfer and the support of high-energy phosphate bonds—to which must be added Mitchell's "chemiosmotic" mechanism (*5*), another conceptual jump that took everyone by surprise—living organisms would be unable to carry out any of the instructions conveyed by way of base pairing. They would be unable to replicate DNA and to express the information it carries into RNA and proteins and, through these, all of the other components of life.

It is even possible, probable in my opinion, that bioenergy preceded information in the origin of life. Before Gilbert's widely publicized "RNA world" (*6*), there may have been Baltcheffsky's "pyrophosphate world" (*7*), Wächtershäuser's "iron-sulfur world" (*8*), or my "thioester world" (*9*). In one or more of these worlds, ATP and the related GTP, CTP, and UTP may well have arisen as conveyers of energy before they became precursors of information-bearing RNA (*10*).

CHRISTIAN DE DUVE

Emeritus professor at the Catholic University of Louvain, Belgium, and at the Rockefeller University, New York. Present address: de Duve Institute, B-1200 Brussels, Belgium. E-mail: deduve_private@icp.ucl.ac.be

References

1. E. Schrödinger, *What Is Life?* (Cambridge Univ. Press, Cambridge, 1944).
2. J. D. Watson, F. C. Crick, *Nature* **171**, 737 (1953).
3. O. T. Avery, C. M. MacLeod, M. McCarty, *J. Exp. Med.* **79**, 137 (1944).
4. F. Lipmann, *Adv. Enzymol.* **1**, 99 (1941).
5. P. Mitchell, *Biol. Rev. Camb. Phil. Soc.* **41**, 445 (1966).
6. W. Gilbert, *Nature* **319**, 618 (1986).
7. H. Baltcheffsky, M. Lundin, C. Luxemburg, P. Nyren, M. Baltcheffsky, *Chem. Scr.* **26B**, 259 (1986).
8. G. Wächtershäuser, *System. Appl. Microbiol.* **10**, 207 (1988).
9. C. de Duve, *Blueprint for a Cell* (Neil Patterson Publishers, Burlington, NC, 1991).
10. C. de Duve, *Singularities* (Cambridge Univ. Press, Cambridge, 2005).

Museums' Role: Increasing Knowledge

GREAT NATURAL HISTORY MUSEUMS ARE among the world's premier institutions of scientific research, training, and education. The research produced by these museums, based on their collections of biological, geological, and anthropological specimens, has been of incalculable importance in formulating and testing the most fundamental theories and principles of these and related disciplines. In the biological sciences, for instance, contributions from past curators of these collections form the pillars of modern evolutionary biology [e.g., (*1*–*3*)].

We therefore read with deep concern of plans to drastically reduce the role of scientific research at one of the world's greatest museums of natural history, Chicago's Field Museum ("Budget crunch to shrink science

CREDIT: AP PHOTO

Downloaded from www.sciencemag.org on March 8, 2013

Published by AAAS

Practicing personalized medicine 1155

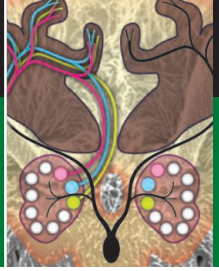

Caffeine for the bees 1157

programs at Chicago's Field Museum," V. Morell, News & Analysis, 4 January, p. 19). The collections of the Field Museum are an irreplaceable scientific resource, and the scientists who care for, augment, and make them available for study by others are also renowned contributors to science in their own right. Their loss would be a blow not just to the Museum, but to the scientific enterprise as a whole.

In making the bequest that endowed the Smithsonian, James Smithson epitomized what has become the mission of modern natural history museums: They are institutions for "the increase and diffusion of knowledge" (*4*). Many science museums can mount exhibits for the diffusion of knowledge, but only museums such as the Field, with its collections and scientists, can contribute so much to its increase. For the Field Museum to abandon this duty would be unconscionable. We urge the Museum's authorities and supporters to find a way to prevent such a calamity.

GREGORY C. MAYER,[1]* JERRY A. COYNE,[2] JONATHAN B. LOSOS,[3] JOHANNES FOUFOPOULOS,[4] NEIL SHUBIN,[5] DOUGLAS J. FUTUYMA,[6] BENJAMIN C. CAMPBELL,[7] SCOTT V. EDWARDS[3]

[1]Department of Biological Sciences, University of Wisconsin–Parkside, Kenosha, WI 53141, USA. [2]Department of Ecology and Evolution, University of Chicago, Chicago, IL 60637, USA. [3]Museum of Comparative Zoology, Harvard University, Cambridge, MA 02138, USA. [4]School of Natural Resources and Environment, University of Michigan, Ann Arbor, MI 48109, USA. [5]Department of Organismal Biology and Anatomy, University of Chicago, Chicago, IL 60637, USA. [6]Department of Ecology and Evolution, Stony Brook University, Stony Brook, NY 11794, USA. [7]Department of Anthropology, University of Wisconsin–Milwaukee, Milwaukee, WI 53201, USA.

*To whom correspondence should be addressed. E-mail: mayerg@uwp.edu

Letters to the Editor

Letters (~300 words) discuss material published in *Science* in the past 3 months or matters of general interest. Letters are not acknowledged upon receipt. Whether published in full or in part, Letters are subject to editing for clarity and space. Letters submitted, published, or posted elsewhere, in print or online, will be disqualified. To submit a Letter, go to www.submit2science.org.

References

1. E. Mayr, *Systematics and the Origin of Species* (Columbia Univ. Press, New York, 1942).
2. G. G. Simpson, *Tempo and Mode in Evolution* (Columbia Univ. Press, New York, 1944).
3. B. Rensch, *Neuere Probleme der Abstammungslehre* (Enke, Stuttgart, 1947).
4. J. Smithson, "James Smithson makes his will" (1826); http://siarchives.si.edu/collections/siris_sic_638.

Museums' Role: Pollen and Forensic Science

IN HER NEWS & ANALYSIS STORY, "BUDGET crunch to shrink science programs at Chicago's Field Museum" (4 January, p. 19), V. Morell reports that Chicago's Field Museum's science program will be slashed by $3 million. Now more than ever, it is essential to convey the importance of natural history research collections to forensic science. For example, museum collections are crucial to the application of pollen evidence in criminology.

Because each region on Earth has a specific plant population, and each plant produces a specific pollen or spore that is morphologically unique to the parent plant, pollen can be used as a geolocation tool (*1*). The association (diversity and relative abundance) of pollen and spore types found at a specific location, called the pollen print, links trace pollen evidence to its source location (*2*). Pollen can thus help track the provenance of illegally imported art, drugs, medicine, or food, as well as items obtained from crime scenes or terrorism investigations, including bodies, clothes, and weapons. Pollen can also provide clues to the timing of events, because pollination occurs at specific times each year.

Tying pollen prints from trace evidence to a location of origin depends on both highly trained palynologists and comprehensive collections and samples for reference. For instance, the geographic source of items such as illegal drugs brought into the United States can be identified if pollen grains from the geographic regions of interest are available for comparison. The Louisiana State University Museum of Natural Science has 4598 samples collected from 564 unique localities spread across all 31 Mexican states and its Federal District (*3*). This collection represents more than 100 years of fieldwork by several generations of curators and graduate students. The specimens not under moratorium are available upon request; scientists or community members can come to the Museum or borrow samples for research. Government agencies such as the National Oceanic and Atmospheric Administration (*4*) or the NSF-funded GeoMapApp at Columbia University (*5*) host pollen data, but for the most part do not curate the samples.

Although using pollen as a forensic tool (forensic palynology) is common in Europe and Australia, the United States lags far behind (*6*). This does not need be to be the case, because U.S. palynological collections are among the world's best. Yet, these collections can be lost in an instant with one major budget cut.

SOPHIE WARNY

Louisiana State University, Baton Rouge, LA 70803, USA. E-mail: swarny@lsu.edu

References

1. G. D. Jones, *Grana* **51**, 206 (2012).
2. V. M. Bryant, G. Jones, D. C. Mildenhall, *Palynology* **14**, 193 (1990).
3. S. Warny, *AASP–The Palynological Society Newsletter* **46**, 22 (2013).
4. National Climatic Data Center, Global Pollen Database (www.ncdc.noaa.gov/paleo/gpd.html).
5. Marine Geoscience Data System, GeoMapApp (www.geomapapp.org).
6. D. Mildenhall, P. Wiltshire, V. M. Bryant, *Forensic Sci. Int.* **163**, 161 (2006).

CORRECTIONS AND CLARIFICATIONS

New Focus: "Reversal of misfortunes" by J. Cohen (22 February, p. 898). The article mistakenly reversed the first and last name of Martin Tshipuk. The HTML and PDF versions online have been corrected.

Letters: "Give shark sanctuaries a chance" by D. D. Chapman *et al.* (15 February, p. 757). The second author is Michael G. Frisk, not Michael J. Frisk. The HTML and PDF versions online have been corrected.

Editors' Choice: "Bombs below" by N. S. Wigginton (18 January, p. 253). The last sentence of the story didn't accurately describe the conclusions of the paper. The corrected sentence should read "Based on their simulations, the Xe signal from the 26 March 1992 test would have met previous criteria for a nuclear weapon only if the test had taken place at certain locations within the Nevada Test Site." The HTML and PDF versions online have been corrected.

Editors' Choice: "A washable MOF" by M. S. Lavine (4 January, p. 12). The reaction between the potassium salt of PTC and the specific metal acetate could readily be done on multigram scales, not milligram scales as stated in the summary. The HTML and PDF versions online have been corrected.

News Focus: "The year in news" (21 December 2012, p. 1534). The first June item incorrectly stated that Lonesome George was the last Galapagos giant tortoise. George was the last of the subspecies *Chelonoidis nigra ssp. abingdoni*, but other subspecies persist on the islands. The HTML version online has been corrected.

Downloaded from www.sciencemag.org on March 8, 2013

Published by AAAS

SOCIAL SCIENCES

The Chemistry of Social Life

Michael Macy

How did life emerge from lifeless chemicals? A possible answer is a chemical reaction that catalyzes its own reproduction (*1*). In their edited volume, *The Emergence of Organizations and Markets*, John Padgett and Walter Powell explore the possibility that autocatalysis may also explain the genesis of social life and the emergence of novel forms of social organization. "Chemistry, especially regarding the origins of life, does not provide all of the answers, but it at least asks the right questions—for social science as well as for biology."

The Emergence of Organizations and Markets
John F. Padgett and Walter W. Powell, Eds.
Princeton University Press, Princeton, NJ, 2012. 607 pp. $120. ISBN 9780691148670. Paper, $45. ISBN 9780691148878.

The book's relational paradigm will feel familiar to readers of Harrison White [e.g., (*2*)], to whom Padgett and Powell dedicated this edited collection of theoretically integrated historical case studies. The book carries White's imprint analytically, methodologically, and stylistically, but the method the editors employ, derived from models of autocatalytic chemical reactions, is not your father's social network analysis. The book's intellectual genesis is traceable to the interdisciplinary ferment at the Sante Fe Institute, with which both editors are affiliated.

Following the editors' introductory overview, three chapters explain biochemical autocatalysis in language intended to engage social scientists. Chemical reactions can be thought of as interactions embedded in networks, with paths not only between reactants but also between reactants and the paths between reactants—an arrow that targets an arrow. A special case is an arrow from a chemical that targets another arrow that targets the chemical—an interaction that catalyzes its own reproduction. Things get even more complicated when the catalytic agent is not a single node in a single network but an autocatalytic set that overlaps multiple networks, in which no single element of the set is sufficient to catalyze itself but the sum total of the interactions becomes self-sustaining.

The remainder of the book comprises a series of detailed historical case studies (the majority authored or coauthored by one of the editors) in network autocatalysis. Although the book's analytical framework is inspired by biopoietic models of prebiotic chemical autocatalysis, the historical applications more closely resemble speciation rather than abiogenesis. The universality of DNA suggests that biotic life may have evolved from a single common ancestor, with subsequent evolutionary branching. The book's historical cases involve the emergence of new organizational forms from Renaissance Florence to the present, a process that has more in common with the subsequent branching of cellular life rather than its Eoarchean genesis. Perhaps a closer life-science parallel is not the emergence of a nucleotide chain out of prebiotic chemistry, but repeated episodes of massive evolutionary jumps in response to global environmental changes, such as the oxygen content of the atmosphere.

Early evidence of organization. Stromatolites formed by cyanobacteria biofilms.

The editors use the case studies to illustrate "network-folding mechanisms of organizational genesis," in which parts of multiple social networks (e.g., economic, political, and kinship) are folded together in novel ways, analogous to Mendel's mechanisms that govern genetic recombination. In a quartet of chapters, Padgett considers "early capitalism and state formation." The second of these, "Transposition and refunctionality," traces the diffusion of the master-apprentice relationship from local guilds to merchant finance in Renaissance Florence, leading to a new organizational form, the business partnership. Another depicts "migration and homology" in Spanish Netherlands, where the joint-stock company can be traced to the massive influx of Protestant merchants and artisans from Antwerp. In the fourth, Jonathan Obert and Padgett explore the organizational genesis of 19th-century Germany as geographically disparate principalities under a novel constitutional troika that welded together democratic and autocratic political currents.

The next section examines "processes of organizational innovation and invention in the communist bloc through the end of the 1990s." Its opening chapter, comparing economic reform in the Soviet Union and China, discusses "robust action," which refers to efforts to keep strategic options open in the face of constraints imposed by political and organizational adversaries. Padgett shows how Deng Xiaoping initiated economic development (including market expansion and liberalization) in response to initiatives by his political opponents, through strategic applications of political patronage that encouraged entrepreneurship at the local administrative level. The chapter also describes "purge and mass mobilization," in which organizational elites are displaced by a rising core of younger officials, as in Stalin's Great Terror and Mao's Cultural Revolution.

The last and longest section takes up the development of today's science- and technology-based sectors. In "Chance, nécessité, et naïveté," Walter Powell and Kurt Sandholtz document the transposition of the life-sciences lab from the university to the business world, leading to the creation of the biotechnology firm. Turning to information technology, Lee Fleming, Lyra Colfer, Alexandra Marin, and Jonathan McPhie consider the roles of social

The reviewer is at the Social Dynamics Laboratory, 372 Uris Hall, Cornell University, Ithaca, NY 14853–7601, USA. E-mail: m.macy@cornell.edu

CREDIT: MICHAEL C. RYGEL/WIKIMEDIA COMMONS

Downloaded from www.sciencemag.org on March 8, 2013

Published by AAAS

networks and "regional agglomeration" in the emergence of industrial districts in Silicon Valley and Boston.

In their concluding chapter, Padgett and Powell acknowledge the absence of attention to perturbation as a source of novelty, which is an essential but empirically challenging piece of their theoretical framework. They see the "percolation of perturbations" through complex networks as the next research frontier in the program of study that they propose, and they hope their initial forays in *The Emergence of Organizations and Markets* will inspire readers across the sciences to pick up the torch. If that happens, this theoretically innovative contribution to social science will have catalyzed the regeneration of historical applications of complexity science.

References

1. S. Kauffman, *The Origins of Order: Self-Organization and Selection in Evolution* (Oxford Univ. Press, Oxford, 1993).
2. H. C. White, *Identity and Control: A Structural Theory of Social Action* (Princeton Univ. Press, Princeton, NJ, 1992).

10.1126/science.1232679

SOCIAL SCIENCES

Business as Usual —or Not?

Robert E. Horn

Four decades ago, the furiously debated *The Limits to Growth* presented a set of computer model–based visions of the future (*1*). Its authors' views were widely dismissed until recently, when the accuracy of a great many of the findings of their standard reference scenario was recognized (*2*). The authors were also extensively but incorrectly criticized for forecasting a single future. Now one of them, Jorgen Randers, does just that in *2052: A Global Forecast for the Next Forty Years.*

To prevent being blindsided, businesses and governments ordinarily desire a group of scenarios that covers a diverse range of plausible futures. Nonetheless, the single, highly detailed depiction of our future Randers provides this time is welcome and helpful in the midst of the proliferation of climate, energy, and sustainability models, the totality of which often feels more like noise than signal. Anyone interested in the profound social, economic, political, and climate challenges confronting us will want to consider his predictions—either to agree with him or to show convincingly how their future world will differ from the one he presents.

2052
A Global Forecast for the Next Forty Years
by Jorgen Randers
Chelsea Green, White River Junction, VT, 2012.
414 pp. $34.95.
ISBN 9781603584678.
Paper, $24.95.
ISBN 9781603584210.

Randers (BI Norwegian Business School) argues strongly for the impact of business as usual on our future. He believes our course over the next 40 years will be strongly shaped by five big issues: capitalism (surviving but modified); economic growth (continuing but affected by decreasing resources); democracy (holding on but with changes, some toward authoritarianism, forced by ecosystem decline); intergenerational harmony (ending as the young seek to change their lot); and climate stability (ending, but mostly after 2052).

Helpfully, Randers documents and extensively discusses the assumptions that underlie his forecast, which allows other scenario-makers to check their assumptions against his. He is extremely gifted at explicating the consequences of his assumptions, models, educated guesses, and results. And while he relies on a "backbone" of a couple of systems dynamics models (*3*), as did *Limits*, Randers uses his experience and judgment to carefully qualify and sometimes amend outcomes of the quantitative results. In this way, he allows his personality and vast experience with quantitative models to come through.

Some of Randers's predictions differ from those of most standard or reference models of the future. He expects lower per capita consumption in rich countries. For 2052, he foresees 8 billion people (a billion below the United Nations Population Bureau's median estimate). His forecast has no apocalyptic overshoot and collapse due to climate change before 2052 but posits a rapid downturn beginning very soon afterward.

In keeping with the business-as-usual perspective, we find no major discontinuities or wild cards. Rather, Randers depicts the huge momentum of industrial society and the inertia of modern thought (growth, progress, democracy, capitalism, free trade, etc.); modern life (keeping on doing what we have been doing because it is very difficult to change our personal ways); and structural aspects of society and, especially, governance. Randers's picture includes technological improvement and innovation at about the same rate as for the past 40 years. Thus, forecasters favoring more breakthrough technology and exponential growth scenarios face considerable challenges in the book's rigorous assumptions and theories of change.

After reflecting on his global forecast, Randers offers a closer view of the futures of five "regions": the United States; the remaining Organization for Economic Cooperation and Development countries; China; Brazil, Russia, India, South Africa, and 10 big emerging economies; and the rest of the world. He then compares his predictions with results from simulations using two earlier dynamic world models. His closing chapter ("What should you do?") offers 20 "pieces of personal advice" for individuals (e.g., know the problems your location is going to face), in business (e.g., distinguish between growth in volume and in profits), and in politics (e.g., seek benefits that can be gained in the short term).

One successful ingredient in the book is the inclusion of two- to four-page "Glimpses" of trends and consequences, written by 34 invited experts from around the world (e.g., Chandran Nair, Mathis Wackernagel, Herman Daly, and Catherine Cameron). Randers agrees with many of the points they raise and uses some for qualified distinction, amplification, and disagreement. This rhetorical move works well, and rather than making the book choppy, it adds liveliness and specificity.

I was surprised that Randers omitted mention of his "one degree war plan"—an investigation that described the emergency changes needed to keep civilization on a sustainable path of no more than 1ºC increase in average global temperature over preindustrial levels (*4*).

In the final chapter of *2052*, Randers advises us to "Learn to live with impending disaster without losing hope." He reminds readers, "Anyone who is the least interested knows well what must be done.… Global society needs to (a) increase energy efficiency; (b) shift to renewable energy; (c) stop destroying the forests; and (d) build carbon capture and storage." And he points out that "[a]ll of these actions are technically feasible and not particularly expensive." But in his forecast, the inertia and momentum of business as usual rule.

References

1. D. H. Meadows *et al.*, *The Limits to Growth: A Report for the Club of Rome's Project on the Predicament of Mankind* (Universe, New York, 1972).
2. G. M. Turner, *Glob. Environ. Change* **18**, 397 (2008).
3. The models and data are available at www.2052.info.
4. J. Randers, P. Gilding, *J. Global Responsibility* **1**, 170 (2010).

10.1126/science.1235035

The reviewer is at the Human Sciences and Technology Advanced Research Institute, Stanford University, Stanford, CA 94305, USA. E-mail: hornbob@earthlink.net

Downloaded from www.sciencemag.org on March 8, 2013

Published by AAAS

ECONOMICS

Behavioral Economics and the Retirement Savings Crisis

Behavioral economics can be scaled up to have a major, positive impact on certain behaviors, such as retirement savings.

Shlomo Benartzi[1,2]* and Richard H. Thaler[3]

Many countries are facing a retirement savings crisis. In the United States, for example, the fraction of workers at risk of having inadequate funds to maintain their lifestyle through retirement is estimated to have increased from 31% to 53% from 1983 to 2010 (*1*). Roughly half of U.S. employees (78 million) have no access to retirement plans at their workplace (*2*). Fortunately, there are solutions to these problems. We simply have to change the choice architecture of retirement plans by utilizing the findings of behavioral economics research (*3*) and make such plans available to all workers. We describe a large-scale field demonstration of the potential impact of such research-based changes in how we save.

One reason for the savings crisis is the ongoing shift in the private sector from defined benefit pension plans (DB, where retirement benefits are formulaic and known in advance) to defined contribution plans (DC, where benefits depend on investment outcomes). This trend is spreading to the public sector as well and is likely to quicken given the dire underfunding of many state and local pension plans (*4*). The United States is not alone in facing these problems. The UK is launching the National Employment Savings Trust, a national payroll savings plan similar to the New Zealand KiwiSaver program.

Making a payroll-based savings plan available to everyone is essential because it is the most effective way for the middle class to save. But having a plan offered at the workplace is not sufficient. Even for those with access to an employer-sponsored plan, almost a quarter fail to join, and among those who do join, many save too little (*5*).

There are four essential ingredients to any comprehensive plan to facilitate adequate saving for retirement: availability, automatic enrollment, automatic investment, and automatic escalation.

Availability. Every U.S. worker should have easy access to a payroll deduction–based DC plan. The Obama Administration has proposed a universal program called the auto-IRA (Individual Retirement Account), which will require employers who do not offer a retirement plan to auto-enroll their employees in an IRA account. Of course, workers can opt out. The state of California has passed a similar plan called the California Secure Choice Retirement Savings Trust.

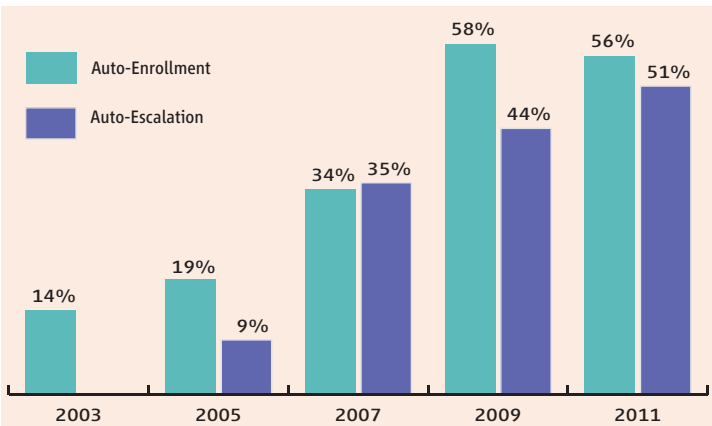

The percentage of U.S. employers who offer 401(k) plans that automatically enroll employees and escalate savings rates. Automatic saving escalation programs are also shown. See (*10*).

Automatic enrollment. In traditional DC plans, participants must make an active decision to enroll, including picking a savings rate and an investment portfolio. Many employees intend to join but never get around to it. There is now conclusive evidence that automatic enrollment, where employees are automatically signed up unless they opt out, is extremely successful in overcoming the procrastination that can impede signing up. Opt out rates average about 10% (*5*, *6*).

Automatic investment. If employees are automatically enrolled, there has to be a default investment option. Fortunately, since the Department of Labor established the criteria for qualified default investment vehicles, both employers and asset managers have worked to create a variety of investment vehicles that provide employees with sensible diversification and an asset allocation mix that is automatically rebalanced when stock prices change (thus, buying stocks in 2009 when the market bottomed), as well as adjusting the portfolio as the employee ages.

Automatic escalation. About three-quarters of automatic enrollment plans use an initial saving rate of just 3% of income (*7*). Research shows that when offered the default rate many passively accept it but had they been forced to make a choice on their own, some would have selected a higher rate (*6*). Automatic enrollment does a good job of getting people started, but employees can be stuck for years saving at an insufficient rate.

We argue that the solution to the problem of saving too little is automatic escalation, a generic term for a plan we devised called Save More Tomorrow (SMT), based on behavioral economics research (*8*). The original SMT program has three components. First, employees are invited to commit now to increase their saving rate later, perhaps next January or a few months in the future. Self-control is easier to accept if delayed rather than immediate. Second, planned increases in the saving rate are linked to pay raises. This is meant to diminish the effect of loss aversion—the tendency to weigh losses larger than gains (*9*). Because the increase in the savings rate is just a portion of the pay raise, employees do not see their pay fall. Third, once employees sign up for the plan they remain in it until they reach a preset limit or choose to opt out. This uses inertia to keep people in the system.

At the first company that implemented SMT, employees who elected to join (and 78% of those offered the plan did) ended up almost quadrupling their saving rate from 3.5% to 13.6% in slightly less than 4 years (*8*). This evidence of success stimulated employers and administrators to adopt the Save More

[1]Professor and Cochair of the Behavioral Decision-Making Group, Anderson School of Management, University of California, Los Angeles, CA 90095, USA. [2]Chief Behavioral Economist, the Allianz Global Investors Center for Behavioral Finance, New York, NY 10019, USA. [3]Ralph and Dorothy Keller Distinguished Service Professor of Behavioral Science and Economics, University of Chicago Booth School of Business, Chicago, IL 60637, USA.

*Author for correspondence. E-mail: benartzi@savemoretomorrow. org

Downloaded from www.sciencemag.org on March 8, 2013

Published by AAAS

Tomorrow plan (or the generic version, automatic escalation, which does not link savings increases to pay increases). Take-up then increased considerably, helped by the passage of the Pension Protection Act of 2006, which encouraged firms to adopt a combination of automatic enrollment and automatic escalation. How automatic enrollment and automatic escalation have spread among U.S. employers is shown in the chart. By 2011, 56% of employers who offer 401(k) plans automatically enrolled employees, and 51% offered automatic escalation (*10*).

The ideas are spreading, but has retirement saving actually increased? To address this question, we estimated the effect of automatic escalation, because automatic enrollment can have an ambiguous effect on the average saving rate. We contacted the largest 25 companies that administer retirement plans, which service roughly 90% of participants in DC plans according to the 2012 Pensions and Investments directory of retirement plan providers (*11*, *12*) [supplementary materials (SM)]. We asked each plan provider for the following data as of the end of year 2011: the number of plan participants they serve who are currently making contributions to their plan (N); the number of plan participants who are enrolled in a SMT or other automatic escalation program (S).

We received data from 13 of the 25 plan providers, covering 55% of plan participants according to the Pensions and Investment directory (*13*) (SM). Of the 20,628,702 contributing participants in our data, 2,268,726 are enrolled in an automatic escalation program, yielding a utilization rate (S/N) of 11%. If this utilization rate is applied to the entire universe of participants, we estimate that there are already about 4.1 million participants who are having their savings rates automatically increased.

We calculated the effect of automatic escalation on retirement plan saving rates, based on the conservative assumption that salary deferral rates are increased automatically by just 1 percentage point per year for only 3 years. These are the minimum requirements set by the Pension Protection Act of 2006. Some plans go beyond this minimum, either in the rate at which deferrals are increased or in the number of years such increases are continued, so our estimate of the increase in savings is biased downward. Our estimate is also biased downward because we do not include the effect of additional matching contributions by employers, typically 50% up to some cap. At the current utilization level of automatic escalation, 11% of participants boost their salary deferral rates by 3% over 3 years, which results in an average increase of 0.33% for the universe of plan participants (11% penetration times 3% increase in deferral rate). To put this 0.33% effect in perspective, the average deferral rate is 6.2%, as reporfted by the Plan Sponsor Council of America (*14*). We interpret this as showing that the intervention is having a noticeable effect, even at the currently low take-up rate by employees. We estimate that automatic escalation boosted annual savings by $7.4 billion, if we assume an average annual compensation of $60,000 and a 3% increase in deferral rates (*15*).

The next step is to increase program utilization. There are three simple ways to achieve this goal. First, it should be easier for workers to join the plan. Of the employees offered the original version of SMT, 78% signed up, in part due to the ease of doing so (employees met with a financial adviser who took all necessary steps to join). Take-up rates in most plans are much lower, in part because employees do not know the option exists or find the sign-up procedure cumbersome. Making the option more salient and making it easier to enroll will likely pay dividends. Alternatively, automatic escalation can be made the default, both for new and existing employees who are stuck at a low savings rate. Of course, in this case, opting out must be easy.

Second, this feature can be included in existing DC plans offered to government workers. For example, the Save More Tomorrow Act of 2012 proposes to offer this feature to federal government workers in their existing Thrift Savings Plan.

Third, automatic escalation should be included in the new plans targeting employees without a savings plan at work such as the auto-IRA and the California Secure Choice Retirement Savings program. Automatically enrolling employees at a low initial savings rate without incorporating automatic escalation is simply bad policy.

One question about these efforts has until recently been impossible to answer. Does inducing larger contributions to retirement saving actually increase total saving, or does it simply shift saving from one place (say, a bank account) into another? However, new work using Danish data that include measures of household wealth suggests that when employees are automatically enrolled into a retirement savings plan, 85% of that savings is new, rather than shifted (*16*).

Lessons from this savings example can be applied in other domains. For example, much of the rise in health care spending in the United States is not just a problem with the health care–delivery system but also inadequacies in the ways by which we encourage people to be healthy. Dealing with obesity and its health consequences, is first and foremost a behavior problem (*17*). If we can nudge people toward a healthier diet and more exercise, we will end up spending less delivering treatments. Similarly, in stressing incentives to encourage patients to economize, we can miss more important determinants of health outcomes. For some patients, the most important way to improve health outcomes is to make sure patients take their prescribed medicines, but many do not (*18*). Charging high copays in such situations is counterproductive. Choice architecture can have profound impacts on behavior, more powerful than might be achieved merely with financial incentives.

References and Notes

1. A. H. Munnell, A. Webb, F. N. Golub-Sass, The national retirement risk index: An update (Center for Retirement Research at Boston College, Chestnut Hill, MA, 2012).
2. A. H. Munnell, R. C. Fraenkel, J. Hurwitz, The pension coverage problem in the private sector: An update (Center for Retirement Research at Boston College, Chestnut Hill, MA, 2012).
3. R. H. Thaler, C. R. Sunstein, *Nudge: Improving Decisions About Health, Wealth, and Happiness* (Yale Univ. Press, New Haven, CT, 2008).
4. R. Novy-Marx, J. Rauh, *J. Finance* **66**, 1211 (2011).
5. S. Benartzi, R. Lewin, *Save More Tomorrow: Practical Behavioral Finance Solutions to Improve 401(k) Plans* (Penguin, New York, 2012).
6. B. C. Madrian, D. F. Shea, *Q. J. Econ.* **116**, 1149 (2001).
7. Vanguard Group, *How America Saves* (Vanguard, Valley Forge, PA, 2012).
8. R. H. Thaler, S. Benartzi, *J. Polit. Econ.* **112**, (suppl. 1), S164 (2004).
9. D. Kahneman, A. Tversky, *Econometrica* **47**, 263 (1979).
10. Data provided by Aon Hewitt, which tends to focus on larger plans that are generally more innovative, so the numbers could be biased upward. By comparison, the Plan Sponsor Council of America reports in their 54th Annual Survey (*19*) that 46% of plans had automatic enrollment in 2011. Owing to confidentiality concerns, Aon Hewitt analyzed data on authors' behalf and only provided summary statistics displayed in the chart.
11. Pensions and Investments (2012); www.pionline.com/specialreports/dc-record-keepers/20120402.
12. According to 2010 Department of Labor data (*20*), the pensions and investments universe of plan providers covers more than 90% of all plan participants in the United States.
13. Firms shared data on condition of anonymity, so data are stripped of identifying information.
14. Plan Sponsor Council of America, 55th Annual Survey, 2012; www.psca.org/55th_survey.
15. At the authors' request, a large-plan administrator calculated a median income of $62K and average income of $93K for 1.8 million contributing participants in its plans, which suggests that our calculation may be conservative.
16. R. Chetty *et al.*, Active vs. passive decisions and crowd-out in retirement savings accounts: Evidence from Denmark (NBER Working Paper No. 18565, National Bureau of Economic Research, Cambridge, MA, 2012).
17. K. G. Volpp *et al.*, *JAMA* **300**, 2631 (2008).
18. K. G. Volpp *et al.*, *Health Serv. Res.* **8**, 272 (2008).
19. Plan Sponsor Council of America, 54th Annual Survey, 2011; www.psca.org/54th-annual-survey.
20. U.S. Department of Labor, www.dol.gov/ebsa/PDF/2010pensionplanbulletin.PDF.

Supplementary Materials
www.sciencemag.org/cgi/content/full/339/6124/1152/DC1

10.1126/science.1231320

Downloaded from www.sciencemag.org on March 8, 2013

Published by AAAS

EVOLUTION

With a Little Help from Prokaryotes

Red algae can adapt to extreme conditions through horizontal gene transfer from free-living prokaryotic extremophiles.

Eduardo P. C. Rocha[1,2]

Organisms need to innovate to tackle new challenges. This can be achieved by tinkering with their genetic repertoires. Gene or genome duplications followed by evolution into new functions have thus shaped eukaryotic genomes (*1*). Alternatively, organisms may acquire other organisms' innovations by horizontal gene transfer. Bacteria and Archaea (Prokaryotes) adapt predominantly by transfer (*2*), and closely related strains of the same species can differ by a large fraction of their genes repertoires (*3*). On page 1207 of this issue, Schönknecht *et al.* (*4*) present evidence of massive gene transfers from Prokaryotes to a eukaryote, the unicellular red alga *Galdieria sulphuraria*.

Horizontal transfers were long thought to be specific to Prokaryotes, with the exception of the spread of transposable elements among closely related species and of intracellular transfer from mitochondria and plastids to the nuclear genome (*5*, *6*). Recent studies report an increasing number of transfers into eukaryotic genomes from other, less ancient organelles (*7*), endosymbionts (*8*), and free-living organisms (*9*), showing that genetic diversification by horizontal transfer propels eukaryotic evolution (see the figure). For example, more than 5% of the gene repertoire of the diatom *Phaeodactylum tricornutum* probably originated from bacteria, and half of these genes were incorporated in the last 90 million years (*8*). However, few clear-cut cases of niche adaptation by horizontal gene transfer in eukaryotes have been found.

The massive gene transfers from prokaryotes and possibly fungi to *G. sulphuraria* enabled its adaptation to niches that are hot, acidic, and toxic to most eukaryotes. Such environments are colonized almost exclusively by prokaryotes called extremophiles. From their genomes, *G. sulphuraria* acquired a wide range of enzymes and transporters, providing the capacity to tackle arsenic and high salinity, reduce mercury, and tolerate high temperatures. The large number of transfers and the diversity of bacterial or archaeal origins strongly suggest that transfer occurred from free-living bacteria and not from endosymbionts.

Evolutionary innovation is ongoing in parallel in all species. Innovations by gene duplication and horizontal gene transfer differ in that the latter profits from the massively parallel adaptation processes occurring on the planet. Furthermore, gene duplication depends solely on information encoded in the genome, whereas horizontal transfer depends on ecological opportunities (*10*). Gene duplication gives rise to new functions at a slow pace, whereas horizontal gene transfer can produce rapid and dramatic phenotypic shifts. Thus, duplication and horizontal transfer offer very different evolutionary mechanisms of adaptation.

These differences can have profound effects on the evolution of biological systems, because recently duplicated genes share the same biological networks, contrary to homologs arising from recent horizontal transfer (*3*). The differences between the two mechanisms of genetic innovation might lead them to play distinct roles in evolution. But the two mechanisms can also work together. For example, the red coloration of pea aphids is caused by enzymes for carotenoid biosynthesis that were transferred from fungi and then duplicated (*11*). Horizontal transfer from bacteria followed by extensive duplication shaped the repertoire of degrading enzymes of nematodes (*12*). The *G. sulphuraria* genome encodes a vast repertoire of membrane transport proteins, providing exceptional metabolic versatility (*9*). A number of these transporters arose by horizontal transfer and were then subject to duplication. Duplication after transfer allows both functional diversification and rapid adaptation of the genes to the new host genome (*13*).

Organisms that experience horizontal transfer encode genes with very different evolutionary histories. This has fueled controversy on the relevance of tree-like representations of life diversity and on the possibility of reconstructing a tree of life. Paradoxically, recent data suggest that transfers may facilitate the tracking of important adaptive events and may help to calibrate evolutionary trees (*14*).

A number of outstanding questions regarding horizontal transfer in Eukaryotes provide fertile ground for research. For example, the frequency of transfer and the variables that influence its rate remain unknown. Analysis of larger genome data sets to detect horizontal gene transfer could reveal more cases of prokaryotic contributions to eukaryotic evolution. Questions also remain regarding the mechanisms of transfer. Endosymbiosis and phagocytosis might facilitate transfer (*15*), but cases such as those of *G. sulphuraria* or *P. tricornutum* suggest that transfer also occurs between free-living cells. Many models in evolutionary systems biology assume duplication as the key process of genetic and biochemical innovation. But innovation by gene transfer takes different paths, and these should be incorporated in the models. The adaptation of genes to the cell machineries of the new host also deserves further study. Genes of bacterial origin in *G. sulphuraria* have fewer introns and atypical sequence compositions, suggesting ongoing adaptation to the host genome. The dynamics of this process are as yet unexplored.

Genes involved in ecological interactions

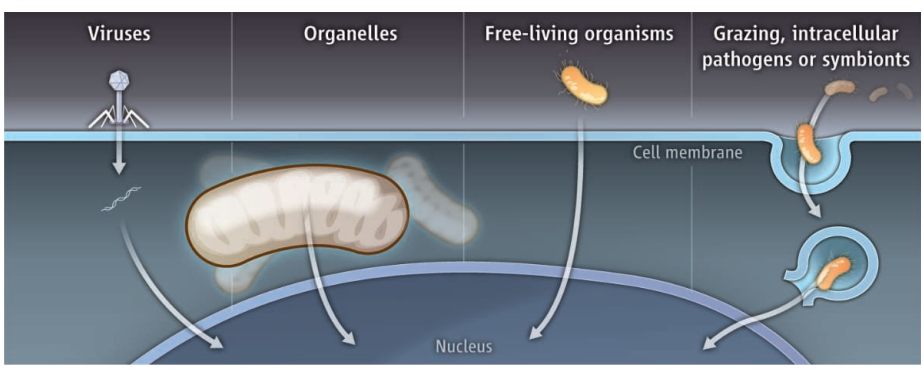

Pathways of genetic transfer. Eukaryotic genomes can incorporate DNA from different origins. Contrary to most previous analyses, Schönknecht *et al.* show massive gene transfer from free-living prokaryotes, suggesting a pathway of direct transfer between these very distant clades.

[1]Institut Pasteur, Microbial Evolutionary Genomics, Département Génomes et Génétique, F-75015 Paris, France. [2]CNRS, UMR3525, F-75015 Paris, France. E-mail: erocha@pasteur.fr

CREDIT: C. BICKEL/SCIENCE

Downloaded from www.sciencemag.org on March 8, 2013

Published by AAAS

and niche shifts in Prokaryotes, such as those encoding virulence factors, antibiotic resistance, and adaptation to high temperature, are frequently transferred. Schönknecht *et al*.'s study of *G. sulphuraria* shows that gene acquisition from Prokaryotes allowed this alga to invade a niche typically nonpermissible to Eukaryotes. Hence, horizontal gene transfer also drives rapid and radical adaptation of eukaryotic genomes.

References

1. J. S. Taylor, J. Raes, *Annu. Rev. Genet.* **38**, 615 (2004).
2. H. Ochman, E. Lerat, V. Daubin, *Proc. Natl. Acad. Sci. U.S.A.* **102** (suppl. 1), 6595 (2005).
3. T. J. Treangen, E. P. Rocha, *PLoS Genet.* **7**, e1001284 (2011).
4. G. Schönknecht *et al*., *Science* **339**, 1207 (2013).
5. A. Sánchez-Gracia, X. Maside, B. Charlesworth, *Trends Genet.* **21**, 200 (2005).
6. P. M. Shih *et al*., *Proc. Natl. Acad. Sci. U.S.A.* **110**, 1053 (2013).
7. E. C. Nowack, A. R. Grossman, *Proc. Natl. Acad. Sci. U.S.A.* **109**, 5340 (2012).
8. J. C. Dunning Hotopp *et al*., *Science* **317**, 1753 (2007).
9. C. Bowler *et al*., *Nature* **456**, 239 (2008).
10. C. S. Smillie *et al*., *Nature* **480**, 241 (2011).
11. N. A. Moran, T. Jarvik, *Science* **328**, 624 (2010).
12. E. G. Danchin *et al*., *Proc. Natl. Acad. Sci. U.S.A.* **107**, 17651 (2010).
13. P. A. Lind, C. Tobin, O. G. Berg, C. G. Kurland, D. I. Andersson, *Mol. Microbiol.* **75**, 1078 (2010).
14. G. J. Szöllosi, B. Boussau, S. S. Abby, E. Tannier, V. Daubin, *Proc. Natl. Acad. Sci. U.S.A.* **109**, 17513 (2012).
15. W. F. Doolittle, *Trends Genet.* **14**, 307 (1998).

10.1126/science.1234938

MEDICINE

(De)Personalized Medicine

Ralph I. Horwitz,[1] Mark R. Cullen,[2] Jill Abell,[3] Jennifer B. Christian[4]

Integration of clinical, social, and environmental data with genomic and molecular information is needed to develop a personalized approach to medicine.

Personalized medicine is often described as genomics-based knowledge that "promises the ability to approach each patient as the biological individual he or she is" (*1*). This is an appealing description, yet unless clinical, social, and environmental features that affect the outcomes of disease are also incorporated, the current approach may be carving a path to "depersonalized" medicine, both in its science and its relevance to medical practice.

One of the earliest demonstrations of personalized medicine concluded that the outcomes of diffuse large B cell lymphoma (DLBCL) were a function of both the tumor's gene expression and clinical features of the affected patients (*2*). Shortly afterwards, the compound imatinib achieved high rates of clinical remission by acting on a biological pathway that was "causally" related to chronic myeloid leukemia (CML) (*3*). The distinct frameworks of these examples—probabilistic (DLBCL and gene expression profiles) and deterministic (CML and imatinib)—contain the seed of the current concept of personalized medicine. The former, which estimates average effects in groups of patients, has proven successful in separating useful from useless therapies. However, there are differences in scientific inference embedded in these frameworks, as illustrated by data from the Beta-Blocker Heart Attack Trial (BHAT) (*4*).

In the BHAT, patients with myocardial infarction who received the drug propranolol had a mortality rate of 7.2% compared to 9.8% for those who received a placebo; the relative risk and relative risk reduction were 0.74 and 26%, respectively. Although these kinds of statistics are typically used to describe the results of therapeutic trials, the findings can also be described differently. In the case of the BHAT, the results could also be reported as the absolute difference in mortality between the experimental and control groups (2.6%) and the number of patients needed to treat to prevent one heart attack (38, calculated as the inverse of the risk difference times 100). These two ways of expressing the same data lead to profoundly different interpretations. Under the deterministic model, only one of 38 patients would benefit from the treatment; but because there is incomplete knowledge, the single patient cannot be identified. Under the probabilistic model, all who took propranolol have a 26% reduction in the risk of dying after a heart attack; however, it is unclear who benefits—and there is a degree of belief about an outcome that is stochastically, not biologically, determined (*5*).

Neither the probabilistic nor deterministic framework is independent of the other. For example, although 53 of the initial 54 patients with CML who were treated with imatinib showed a hematologic response (*3*), subsequent clinical trials reported lower cytogenetic response rates for the drug. So, even though the molecular mechanism is known and a targeted treatment applied, we cannot "determine" the desired outcome for every patient nor know whether treatment failures are due to stochastic processes or incomplete biologic understanding. This example reflects the need to measure a greater range of features to determine the risk for disease and the response to treatment. Indeed, at the core of clinical medicine lies substantial variation in clinical response linked to the extraordinary heterogeneity of individual experience. This consideration of clinical heterogeneity in treatment response is critical for the integration of features of individual experience for personalized medicine.

When treatments have large effects, variations in outcome—whether due to clinical, environmental, or genetic factors, or to chance—are usually within the overall range of predicted benefit (quantitative interaction). As effect size becomes smaller, differences that are opposite to the overall beneficial effect may also occur (qualitative interaction). The latter are considered uncommon, and when observed, may be viewed as "random" deviations from the average benefit. Yet, one argument underlying personalized medicine is that a deeper understanding of mechanisms can identify subgroups in which risk for disease and response to treatment are different from the overall average results not because of the play of chance, but because of the impact of human biology. In fact, a shortcoming of the genomic or molecular approach to personalized medicine is the failure to incorporate the full range of a patient's clinical, social, and environmental features—diet, behaviors, stress, and socioeconomic factors, as examples—that determines an individual's risk for disease and response to treatment.

Just as statistics can sometimes force a focus on groups and ignore individuals, so too

[1]Clinical Evaluation Sciences, GlaxoSmithKline King of Prussia, PA 19406, USA. [2]Division of General Medical Disciplines, Stanford University School of Medicine, Stanford, CA 94305, USA. [3]Clinical Effectiveness and Safety, GlaxoSmithKline, King of Prussia, PA 19406, USA. [4]Clinical Effectiveness and Safety, GlaxoSmithKline, Research Triangle Park, NC 27709, USA. E-mail: mrcullen@stanford.edu

CREDIT: J. SWANEPOEL/ISTOCKPHOTO

Downloaded from www.sciencemag.org on March 8, 2013

Published by AAAS

can a singular focus on genetic and molecular mechanisms fail to account for meaningful differences in patients' risk of disease. Consider the genetically homogeneous Berbers of Morocco as an example of the intersection of human physiology, culture, and environment. When gene expression in peripheral white blood cells was examined among nomadic, mountain agrarian, and coastal urban persons, up to one-third of the "transcriptome" was associated with different environments (*6*).

In many instances, environmental features dominate genetic ones. For example, in cardiovascular disease, traditional risk factors (such as blood pressure and serum cholesterol concentration) are more influential than genetic factors (alterations in genes associated with the condition) for predicting disease susceptibility (*7*). Yet even traditional risk factors are insufficient to capture the complexity of human experience. A patient that experiences acute stress provokes certain homeostatic adjustments that affect that person's risk for disease; likewise, someone suffering from chronic stress could experience an array of certain allostatic adjustments in his or her physiology that could have deleterious health effects. Even though there are genetic and molecular markers for conditions such as cardiovascular disease—markers that are the current backbone of personalized medicine—they do not reflect the array of personal features that make up the richness of clinical variation in patients and affect the risk for disease and response to treatment.

Consider the implications of a genomics-based approach to "personalized" treatment of diabetic risk in a native American Pima Indian with known high genetic susceptibility (that is, they have a genetic profile that predisposes them to diabetes). Treatment in an era when most Pima Indians ate native diets (and the rate of diabetes was low) would have resulted in exaggerated risk assessment and overtreatment. This strategy would be equally inappropriate for the patient if used in the era of epidemic diabetes when most Pima Indians are on Western diets that promote diabetes. Although this is a classic example of gene-environment interaction, it is evident that the best approach to "personalized" treatment is to consider other features, not just genetic factors.

Several factors are threatening to create a path to "depersonalized" medicine despite advances both in fundamental science and clinical therapeutics. The tendency to focus on statistics for the group rather than the individual clinical features of patients is one factor. Another is the neglect of social and behavioral features that have been long disparaged as "soft" in measurement (because they often rely on subjective reports and physician assessment). The failure to give suitable weight to clinical variation is not the fault of the statistical paradigm any more than it is the fault of the molecular orientation of contemporary medicine. The problem lies with the atrophy of clinical science. Physician investigators whose clinical knowledge equips them to create the needed clinical taxonomies have been distracted by quantitative models or reductionist science. What is needed to complement the power of genomics is an emphasis on personal attributes of patients and their environments, and to incorporate these features into an enriched approach to personalized medicine.

References

1. A. E. Guttmacher, M. E. Porteous, J. D. McInerney, *Nat. Rev. Genet.* **8**, 151 (2007).
2. A. A. Alizadeh *et al.*, *Nature* **403**, 503 (2000).
3. B. J. Druker *et al.*, *N. Engl. J. Med.* **344**, 1031 (2001).
4. *JAMA* **247**, 1707 (1982).
5. S. N. Goodman, *Ann. Intern. Med.* **130**, 604 (1999).
6. Y. Idaghdour *et al.*, *Nat. Genet.* **42**, 62 (2010).
7. W. Burke, B. M. Psaty, *JAMA* **298**, 1682 (2007).

10.1126/science.1234106

BIOCHEMISTRY

Red Wine, Toast of the Town (Again)

Hua Yuan and Ronen Marmorstein

The debate may be over on whether resveratrol and other small molecules directly activate an enzyme implicated in longevity.

Sirtuin proteins were once only of interest to yeast geneticists studying transcriptional regulation. That changed when their conserved effects on extending life span in yeast, worms, and flies were reported (*1–3*). Attention widened even more at the possibility of small-molecule activators of sirtuins increasing human health span and perhaps also life span (see the figure). Then came resveratrol, a natural compound found in red wine that could reportedly activate SIRT1, a human member of the sirtuin family. But just as quickly as red wine became the toast of the town, the biochemical assays used to identify resveratrol and other sirtuin-activating compounds (STACs) were called into question. Speculation that the cellular effects of STACs are achieved not through direct SIRT1 binding, but instead through other proteins, gave pause to wine enthusiasts, among others. Glasses may be lifted once again, however. On page 1216 of this issue, Hubbard *et al.* (*4*) demonstrate that SIRT1 can indeed be activated by resveratrol and other STACs in vitro, but only under certain conditions.

Sirtuins are nicotinamide adenine dinucleotide (NAD^+)–dependent protein deacetylases, although some members carry out other related enzymatic reactions (*5*). Humans have seven sirtuins, with SIRT1 the most similar to yeast Sir2, the first sirtuin shown to increase life span. SIRT1 targets a wide range of protein substrates and has been shown to play a role in many age-related diseases including cancer, Alzheimer's disease, and type 2 diabetes. In 2003, resveratrol and other STACs were identified as sirtuin activators through a biochemical assay that used recombinant SIRT1 and a fluorophore-tagged p53 substrate (*6*). Subsequent studies using a related fluorophore identified an unrelated family of synthetic STACs that were more potent than resveratrol (*7*). However, several groups reported that resveratrol and the other STACs failed to activate SIRT1 in vitro when non–fluorophore-tagged substrates were used (*8–11*). Despite these contradictory in vitro results on the ability of STACs to directly activate SIRT1, other studies demonstrated that in cells, STACs caused pharmacological changes consistent with SIRT1 activation (*6*, *7*, *12*, *13*). The question was raised of whether STACs work indirectly to activate SIRT1 by binding to other proteins.

Hubbard *et al.* demonstrate that SIRT1 can be activated by STACs in vitro on substrates without a fluorophore tag, but only on certain natural peptide substrates. The authors hypothesized that the fluorophore tag attached to the substrates employed for the original SIRT1 activation screen might mimic hydrophobic amino acids of natural substrates at the same position as the fluorophore (+1 relative to the acetylated lysine). Hubbard *et al.* thus found that natural SIRT1 substrates with a large hydrophobic residue (Trp, Tyr, or Phe) at positions +1 and +6 [such as the substrate peroxisome proliferator-activated receptor γ coactivator 1α, acetylated on lysine at position 778 (PGC-1α-K778)] or +1 [such as the substrate forkhead box protein O3a acety-

Wistar Institute, Philadelphia, PA 19104, USA. E-mail: marmor@wistar.org

Published by AAAS

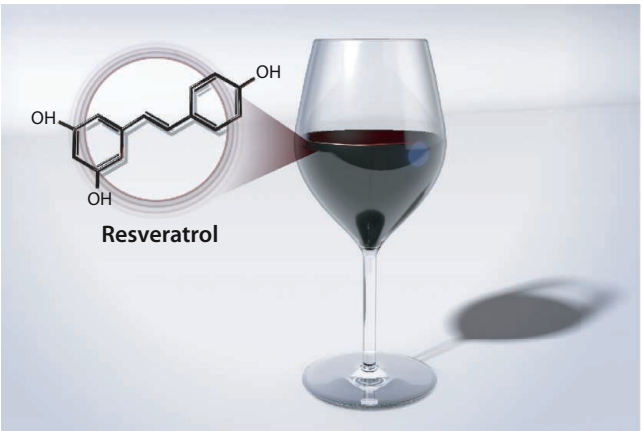

Cheers. Resveratrol, the natural compound in red wine, and other small molecules are allosteric activators of SIRT1, an enzyme with roles in many biological processes (including DNA repair, metabolism, programmed cell death, and inflammation) that affect human life span.

lated on lysine at position 290 (FOXO3a-K290)], as well as other peptides that conformed to this substrate signature, were selectively activated by several STACs. Kinetic analysis of SIRT1 activation by STACs in the presence of these peptide substrates revealed that rate enhancement was mediated primarily through an improvement in peptide binding (lowering of peptide K_M), consistent with an allosteric mechanism of activation. When Hubbard *et al*. screened for SIRT1 mutants resistant to activation by STACs, they identified a single-residue mutation ($Glu^{230} \rightarrow$ Lys; E230K) just to the amino-terminal side of the conserved sirtuin catalytic core. Biophysical studies indicated that in addition to the conserved catalytic core domain and a carboxyl-terminal segment, a small amino-terminal region encompassing Glu^{230} also played a structural role for SIRT1 function. This is consistent with previous studies demonstrating a role for this region in catalysis by SIRT1 (*14*). Moreover, cultured cells lacking endogenous SIRT1 but expressing the mutant enzyme (mouse SIRT1-E222K, the murine equivalent of human SIRT1-E230K) did not respond to several STACs, in contrast to cells expressing wild-type SIRT1. Together, the findings of Hubbard *et al*. demonstrate that STACs can increase the catalytic activity of SIRT1 toward certain substrates through an allosteric mechanism involving an amino-terminal region near the catalytic core, and through direct binding to SIRT1 or a SIRT1-protein complex both in vitro and in cells.

The finding of Hubbard *et al*. has important implications for the further development of SIRT1 modulators. Allosteric activation of SIRT1 through a nonconserved amino-terminal region suggests that SIRT1-selective activators can be developed. Although the current STACs only work against a subset of SIRT1 substrates that contain hydrophobic amino acids at position +1 to the acetylated lysine, this is likely due to the bias of the initial screen that contained a hydrophobic residue mimic (the fluorophore tag) at this position in the substrate peptide. Another screen that is not biased in this way may identify STACs for SIRT1 substrates that contain other sequence signatures. Moreover, if allosteric activators can be developed, then appropriate modifications of these molecules could lead to the development of allosteric SIRT1 inhibitors with comparable protein selectivity. Structural details of the SIRT1 catalytic domain and amino-terminal segment bound to these STACs would facilitate a rational approach to the development of such molecules. That some STACs, like resveratrol, modulate the activity of other molecules (*9*, *15*) is further argument for such structural insights.

There are also implications for understanding some of the seemingly contradictory findings on SIRT1 biology. For example, SIRT1 has been reported to have dual roles—in cell survival with properties of an oncoprotein, and in cell death with properties of a tumor suppressor (*16*). It may be that particular cellular effectors modulate SIRT1 to deacetylate certain protein targets, just as STACs can increase the ability of SIRT1 to deacetylate proteins that contain hydrophobic residues at certain amino acid positions. One could imagine that other stimuli might promote SIRT1 deacetylation of other substrates. Indeed, the amino-terminal segment of SIRT1—the region critical to activation by STACs—might be an important regulatory switch for SIRT1 function, consistent with the ability of the amino-terminal segment of SIRT1 to potentiate the enzyme's deacetylase activity (*14*). Along the same lines, a carboxyl-terminal segment of SIRT1 has also been shown to be important for optimal SIRT1 activity and may have an important regulatory function (*14*, *17*). One thing is now clear—SIRT1 activation by STACs has made a comeback, a renewed reason to toast.

References

1. M. Kaeberlein, M. McVey, L. Guarente, *Genes Dev.* **13**, 2570 (1999).
2. H. A. Tissenbaum, L. Guarente, *Nature* **410**, 227 (2001).
3. B. Rogina, S. L. Helfand, *Proc. Natl. Acad. Sci. U.S.A.* **101**, 15998 (2004).
4. B. P. Hubbard *et al*., *Science* **339**, 1216 (2013).
5. H. Yuan, R. Marmorstein, *J. Biol. Chem.* **287**, 42428 (2012).
6. K. T. Howitz *et al*., *Nature* **425**, 191 (2003).
7. J. C. Milne *et al*., *Nature* **450**, 712 (2007).
8. D. Beher *et al*., *Chem. Biol. Drug Des.* **74**, 619 (2009).
9. M. Pacholec *et al*., *J. Biol. Chem.* **285**, 8340 (2010).
10. M. Kaeberlein *et al*., *J. Biol. Chem.* **280**, 17038 (2005).
11. M. T. Borra, B. C. Smith, J. M. Denu, *J. Biol. Chem.* **280**, 17187 (2005).
12. J. A. Baur *et al*., *Nature* **444**, 337 (2006).
13. R. K. Minor *et al*., *Sci. Rep.* **1**, 70 (2011).
14. M. Pan, H. Yuan, M. Brent, E. C. Ding, R. Marmorstein, *J. Biol. Chem.* **287**, 2468 (2012).
15. S. J. Park *et al*., *Cell* **148**, 421 (2012).
16. C. X. Deng, *Int. J. Biol. Sci.* **5**, 147 (2009).
17. H. Kang *et al*., *Mol. Cell* **44**, 203 (2011).

10.1126/science.1236463

NEUROSCIENCE

Caffeine Boosts Bees' Memories

Lars Chittka and Fei Peng

Caffeine in floral nectar enhances the memory of bees for the flowers' scent by altering response properties of neurons in the bee brain.

Pollination systems are biological markets, where flower visitors choose between flower species on the basis of their quality, such as the sweetness and amount of nectar per flower. Plants in turn compete for pollinators and advertise their product through colorful visual displays and scents. A key challenge in floral advertising is that signals must be not only attractive but also memorable (*1*): The more distinct a flower signal, the more likely a pollinator is to remember it, increasing the probability that pollinators will visit more flowers of this species while ignoring competing flower species. On page 1202 of this issue, Wright *et al*. (*2*) report that

Psychology Division, School of Biological and Chemical Sciences, Queen Mary University of London, Mile End Road, London E1 4NS, UK. E-mail: l.chittka@qmul.ac.uk

CREDIT: Y. HAMMOND/SCIENCE

Downloaded from www.sciencemag.org on March 8, 2013

Published by AAAS

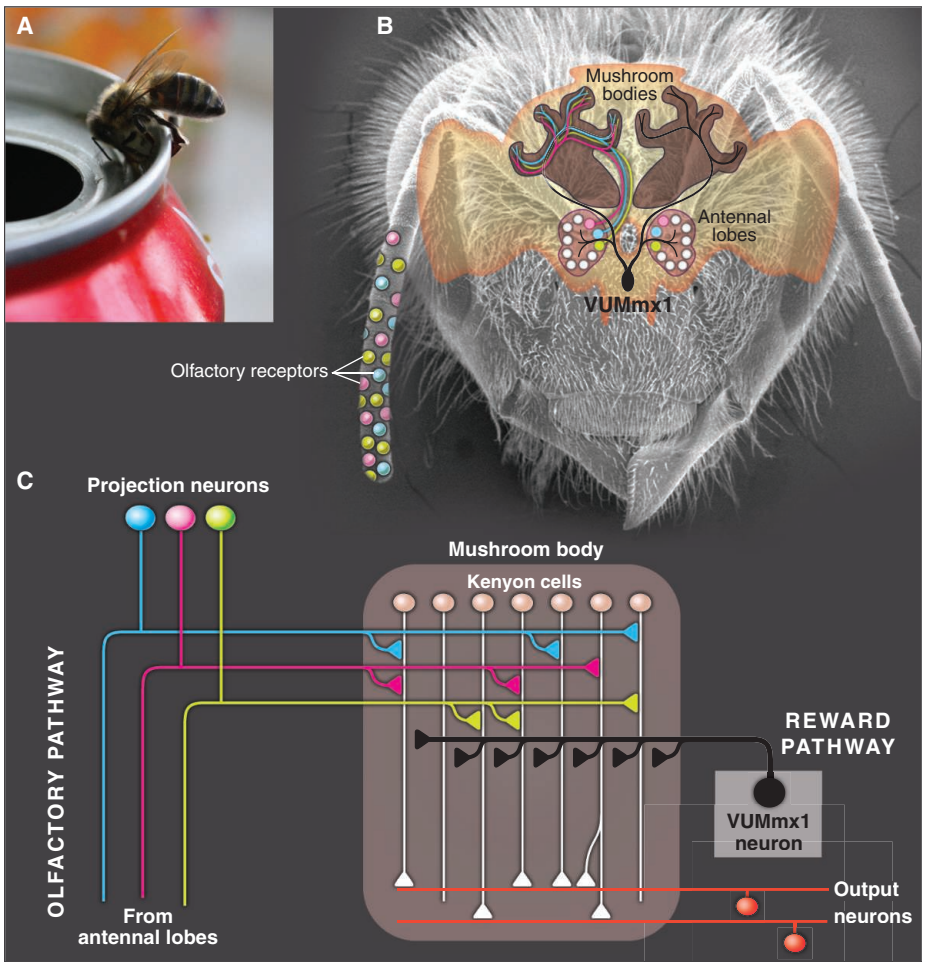

Caffeine junkies of the wild? (A) Honeybees often consume caffeinated drinks from discarded cans. Wright *et al*. show that some plants manipulate the memory of bees by adding caffeine to their nectar. **(B)** Various antennal odorant receptor types, each responsive to specific chemicals, send information to the mushroom bodies via the antennal lobes (*12*). A ventral unpaired neuron (VUMmx1) mediating the sucrose reward signal also connects to mushroom bodies (*9*). [Adapted from (*6*)] **(C)** In the odor-learning circuitry in the bee brain, projection neurons connect to Kenyon cells in the mushroom bodies (*12*). As Wright *et al*. show (*2*), simultaneous input to Kenyon cells from olfactory and reward pathways might strengthen synaptic connections between Kenyon cells and output neurons and between projection neurons and Kenyon cells. Caffeine increases transmission at the synapses between projection neurons and Kenyon cells and also enhances Kenyon cell excitability, facilitating the formation of long-term memories for floral scents (*2*).

some plant species appear to gain an unfair advantage in this competitive market by manipulating the memory of bees with psychoactive drugs.

Many plants contain alkaloids such as caffeine and nicotine. Their bitter taste deters herbivores; at high concentrations, they are toxic. The nectars of some flowers, in addition to various sugars, also contain such secondary compounds (*3*). This presents a puzzle, because pollinators typically reject bitter nectar (*4*). However, at low concentrations, bees appear to prefer caffeine-containing nectar (see the figure, panel A) (*3*). Wright *et al*. show that caffeine concentrations in the nectar of various *Coffea* and *Citrus* flower species never exceed levels at which they might deter bees. Hence, flowers are careful not to leak too much bitterness into the sweetness of their nectar. But why is there caffeine in nectar at all?

In mammals, caffeine is a cognitive enhancer (*5*). Wright *et al*. show that caffeine also has a dramatic effect on the long-term memory of bees. The authors trained bees to associate a floral scent with a sucrose reward. If, during training, the reward droplet contained caffeine, twice as many bees remembered the scent 3 days later.

The olfactory receptors of insects are distributed along their antennae (see the figure, panel B). Receptor cell axons extend to the primary olfactory centers, the antennal lobes (*6*). From the antennal lobes, projection neurons connect to the mushroom bodies, which mediate sensory integration and learning in insect brains (*7*). The mushroom bodies of honeybees contain about 370,000 so-called Kenyon cells. The projection neurons appear to release acetylcholine as the primary neurotransmitter, which binds to acetylcholine receptors in Kenyon cell dendrites (*8*). The mushroom bodies also receive information about sugary rewards from the bee's mouthparts by way of the VUMmx1 neuron, the single neuron that constitutes the reward pathway in bee olfactory learning (*9*).

Wright *et al*. found that caffeine increases the excitability of Kenyon cells. Blocking the acetylcholine receptors of Kenyon cells reverses the caffeine effect. This makes it likely that the effects of caffeine are due to increased activity of projection neurons from the antennal lobes.

The authors propose that the increased activation of Kenyon cells could be due to the interaction of caffeine and adenosine receptors in projection neurons. In mammals, adenosine acts as an inhibitory neuromodulator, and caffeine is a known antagonist of adenosine (*5*). The application of DPCPX (an antagonist of adenosine receptors) to bee brains produces a similar excitation of Kenyon cells as caffeine, indicating that the observed effects of caffeine on long-term memory could indeed be via blocking of adenosine receptors (*2*).

It is thus conceivable that caffeine facilitates strengthening of synaptic connections between Kenyon cells and olfactory projection neurons activated by a particular floral scent, especially under the modulatory influence of signals from the reward pathway (see the figure, panel C) (*7*). Connections between Kenyon cells and other neurons further downstream could also be affected (*2*).

The discovery of the cognitive effects of psychoactive drugs in floral nectar opens new perspectives in the competitive race between plant species to lure pollinators. Because these substances occur in many plant tissues (as deterrents to herbivores), they could be added to nectar at little extra cost to the plant, with profound effects on pollinator behavior. If as a result of caffeine ingestion, bees remember the traits of the flowers better, they might be more likely to stay faithful to these flowers and disregard others. Further research may show whether drugs in nectar not only influence pollinator preference via enhanced memory for floral traits but also might have addictive effects. These would be recognizable by drug seeking despite known adverse

PHOTO CREDITS: (PANEL A) AZIZ ALMUTAIRI/UNIVERSITY OF MASSACHUSETTS; MICROGRAPH (PANEL B), AXEL BROCKMANN/NCBS BANGALORE

Downloaded from www.sciencemag.org on March 8, 2013

Published by AAAS

effects [such as predation risk at flowers (*10*)], relapses after periods of abstinence, or withdrawal symptoms (*11*).

References

1. A. Gumbert, J. Kunze, L. Chittka, *Proc. Biol. Sci.* **266**, 1711 (1999).
2. G. A. Wright *et al.*, *Science* **339**, 1202 (2013).
3. N. Singaravelan, G. Nee'man, M. Inbar, I. Izhaki, *J. Chem. Ecol.* **31**, 2791 (2005).
4. L. Chittka, A. G. Dyer, F. Bock, A. Dornhaus, *Nature* **424**, 388 (2003).
5. S. Simons, D. Caruana, M. Zhao, S. Dudek, *Nat. Neurosci.* **15**, 23 (2012).
6. L. Chittka, A. Brockmann, *PLoS Biol.* **3**, e137 (2005).
7. B. Hourcade, T. S. Muenz, J. C. Sandoz, W. Rössler, J. M. Devaud, *J. Neurosci.* **30**, 6461 (2010).
8. S. Oleskevich, *J. Neurophysiol.* **82**, 1091 (1999).
9. M. Hammer, *Nature* **366**, 59 (1993).
10. T. C. Ings, L. Chittka, *Curr. Biol.* **18**, 1520 (2008).
11. M. O. Parker, C. H. Brennan, *Behaviour* **149**, 1037 (2012).
12. M. Giurfa, *Trends Neurosci.* **36**, (2013); 10.1016/j.tins.2012.12.011

10.1126/science.1234411

MATHEMATICS

Getting the Jump on Explosive Percolation

An analytical approach to explosive dynamical percolation yields general conditions for the transition to be a continuous or discontinuous process.

Robert M. Ziff

Percolation refers to the formation of long-range connectedness or conductivity in random systems. Simple models for percolation were independently devised in the areas of polymer science (*1*) and mathematics (*2*) in the 1940s and '50s, and have been both a persistent theoretical challenge and an enduring practical paradigm ever since. In the past decade, percolation has become a central problem in probability theory, and has figured in the work of two recent Fields medalists (*3*). A recent and somewhat controversial development concerns looking at the dynamics of percolation under various global bond selection rules and how percolating systems make the transition from being disconnected (or comprising a group of disconnected clusters) to being fully connected. It had been shown that the transition can proceed explosively, in which the transition is discontinuous (*4*), but that scenario was later challenged when it was shown that for some specific systems, such a transition is in fact continuous. On page 1185 of this issue, Cho *et al.* (*5*) show analytically and numerically that the explosive percolation transition can be either continuous or discontinuous, depending on the bias against certain "bridging" bonds and the dimensionality of the system.

In standard percolation, the probability P_∞ that a given point is part of a percolating cluster is a continuous function of the bond occupation probability p, the probability that a bond is conducting or open. P_∞ is zero for cases where $p < p_c$ but rapidly grows for $p > p_c$, where p_c is the percolation threshold that signals the onset of long-range connectivity. In an infinite system and for p slightly greater than p_c, P_∞ behaves as $P_\infty \approx (p - p_c)^\beta$, where β is a fractional power, such as $5/36 \approx 0.139$ in two dimensions (*6*), so the derivative dP_∞/dp is infinite at p_c. Being continuous, the percolation transition can be considered to be a kind of second-order phase transition.

Bonds can be added one at a time and clusters merged as they are added, leading to a dynamical percolation transition. Achlioptas *et al.* (*4*) introduced a new model of percolation in which two candidate unoccupied bonds are simultaneously considered, and only the one that joins the smaller cluster-size sum or product is added. Simulating this model, they found that the percolation transition is delayed to a higher value of p, but then occurs in an explosive and seemingly discontinuous manner, more akin to a first-order phase transition. Similar behavior is observed in many other systems, including regular lattices, when a variety of bond-addition rules are used (*7–10*).

Distinguishing a discontinuity from a sharp continuous transition in a finite system can be tricky, however. In 2010, da Costa *et al.* (*11*) showed theoretically that the random-graph model was in fact continuous under a modified product rule, but with a very small β (~0.056), which makes it nearly indistinguishable from a discontinuous transition. More investigation and proofs of the continuity followed for a variety of systems (*12*, *13*), and it is now generally accepted that the original two-choice product rule leads to a continuous transition, but it wasn't previously proven for a Euclidean lattice such as the simple square lattice.

Still, there remain some undoubtedly discontinuous explosive transitions out there. For example, a simple model of joining only the bond that gives the smallest product over all bonds in the system is discontinuous—the last bond joins two huge clusters together. A hierarchical long-range model also shows a discontinuity (*14*).

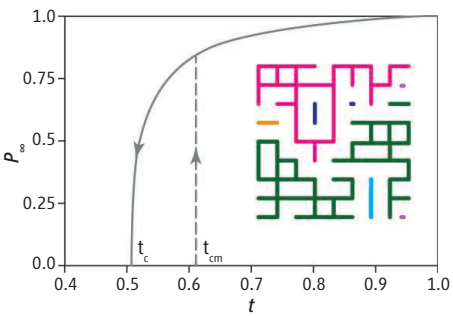

Joining the dots. Schematic of the probability P_∞ that a point belongs to the spanning cluster versus the occupation probability t, for regular percolation of $m = 1$ (solid line) and for a typical case with $m > 1$ (dashed line). A jump in P_∞ for $m > 1$ is evident. (**Inset**) A typical bond configuration showing a later stage where most of the sites belong to two distinct clusters. The algorithm preferentially puts new bonds along edges that do not connect the two clusters.

Cho *et al.* introduce a model of percolation with a new global constraint on a Euclidean lattice: If a candidate bond causes the system to percolate from one side to another, then the model biases against it. Specifically, m candidate bonds are chosen simultaneously, and if any are nonbridging, then one such bond is chosen randomly and occupied. If they are all bridge bonds, then one of those is chosen and occupied. Equivalently, just one unoccupied bond can be chosen and occupied (if it is a nonbridge bond) or occupied with an appropriate probability (if it is a bridge bond).

Now, $m = 1$ corresponds to standard percolation with critical bond occupancy t_c. For $m > 1$, Cho *et al.* observe that percolation is delayed until a later occupancy $t_m > t_c$, but

Department of Chemical Engineering, University of Michigan, Ann Arbor, MI 48109, USA. E-mail: rziff@umich.edu

Published by AAAS

then, once the boundary between the two large clusters has been breached, bridging bonds cease to exist, and the system follows essentially the behavior for $m = 1$. Thus, there is a jump in P_∞ and the system shows a discontinuity (see the figure).

However, when going to larger systems, some telling behavior is found. For m less than a critical value m_c, t_m decreases to the standard percolation value t_c and the discontinuity disappears. Likewise, when, for $m > m_c$, t_m increases to 1, the explosive percolation occurs but only at full occupancy. Cho *et al*. relate m_c theoretically to the backbone fractal dimension and predict $m_c \approx 2.55$, which is consistent with their extensive simulations.

The work of Cho *et al*. shows the importance of taking the infinite-size limit and explains some of the confusing and contradictory behavior seen in this field previously. Exactly at $m = m_c$, the discontinuity in the transition persists with a critical occupancy t_{cm} less than 1, so in this special case a nontrivial discontinuous transition on an infinite Euclidean lattice evidently exists. Investigating the nature of this transition and finding other models that can be tuned to a similar tricritical state is a rich area for future research.

References and Notes

1. P. J. Flory, *J. Am. Chem. Soc.* **63**, 3091 (1941).
2. S. Broadbent, J. Hammersley, *Proc. Camb. Philos. Soc.* **53**, 629 (1957).
3. Fields Medal winners S. Smirnov, 2010, and W. Werner, 2006.
4. D. Achlioptas, R. M. D'Souza, J. Spencer, *Science* **323**, 1453 (2009).
5. Y. S. Cho, S. Hwang, H. J. Herrmann, B. Kahng, *Science* **339**, 1185 (2013).
6. D. Stauffer, A. Aharony, *Introduction to Percolation Theory* (CRC Press, Boca Raton, FL, 1994).
7. R. M. Ziff, *Phys. Rev. Lett.* **103**, 045701 (2009).
8. Y. S. Cho, J. S. Kim, J. Park, B. Kahng, D. Kim, *Phys. Rev. Lett.* **103**, 135702 (2009).
9. F. Radicchi, S. Fortunato, *Phys. Rev. Lett.* **103**, 168701 (2009).
10. N. A. M. Araújo, J. S. Andrade Jr., R. M. Ziff, H. J. Herrmann, *Phys. Rev. Lett.* **106**, 095703 (2011).
11. R. A. da Costa, S. N. Dorogovtsev, A. V. Goltsev, J. F. F. Mendes, *Phys. Rev. Lett.* **105**, 255701 (2010).
12. O. Riordan, L. Warnke, *Science* **333**, 322 (2011).
13. P. Grassberger, C. Christensen, G. Bizhani, S.-W. Son, M. Paczuski, *Phys. Rev. Lett.* **106**, 225701 (2011).
14. S. Boettcher, V. Singh, R. M. Ziff, *Nat. Commun.* **3**, 787 (2012).

10.1126/science.1235032

IMMUNOLOGY

Guilty by Association

Fingerprinting regulatory T cells in tumors reveals that they are specific for organ-expressed antigens.

Nikhil S. Joshi and Tyler Jacks

Developing tumors face a multifaceted immune response that can ultimately "edit" the tumor by eliminating cells that cannot evade antitumor responses. Consequentially, tumors employ many mechanisms to evade immune responses, including expression of inhibitory chemokines or cytokines and recruitment of immunosuppressive cells such as regulatory T cells (T_{regs}) (*1*, *2*). T_{regs} are known for suppressing immune responses and maintaining immune homeostasis, but are also often found in the tumor microenvironment where their presence correlates with poorer patient outcomes. Moreover, acute T_{reg} depletion in transplant models of cancer results in more potent antitumor immune responses. Thus, T_{regs} are considered important players in tumor development. However, relatively little is known about why T_{regs} infiltrate tumors or how they are formed. On page 1219 of this issue, Malchow *et al.* (*3*) address these questions and discover that developing tumors do not elicit novel T_{reg} responses, but rather they recruit and/or expand T_{reg} populations naturally found within the tissue from which the tumor arises.

Tumors can elicit T cell responses because they have distinct protein expression relative to normal cells (*4*). T cells bearing antigen-specific surface T cell receptors (TCRs) recognize tumor antigens displayed on the cell surface, which results in T cell activation, proliferation, and destruction of target cells. Multiple layers of regulation exist to avoid T cells that recognize "self antigens" and target healthy cells. This regulation starts in the thymus, where developing T cells with TCRs that recognize self antigens are deleted or become immunosuppressive T_{regs} (*5*). Although the complete pathway for developing these "natural" T_{regs} (nT_{regs}) is unclear, it involves a molecule called autoimmune regulator (Aire), which is expressed by specialized thymic epithelial cells and helps them express a variety of tissue-restricted self antigens. In this way, developing T cells are first exposed to these antigens before leaving the thymus (*5*). Tissue-specific self antigens are thought to be critical for the function and localization of some nT_{regs}, but how they affect tumor-infiltrating T_{regs} is less well understood. Complicating matters, T_{regs} can also be generated post-thymically from conventional T cells, when they are exposed to antigen in the presence of immunosuppressive molecules such as transforming growth factor–β. Induced T_{regs} (iT_{regs}) are critical to maintaining immune tolerance to environmental antigens (e.g., commensal bacteria), and it has been suggested that immunosuppressive factors within the tumor microenvironment could convert tumor-specific T cells into iT_{regs}. Furthermore, because nT_{regs} and iT_{regs} can differ in plasticity (*6*), it is plausible that one population could be more amenable to therapeutic modulation. Thus, it is important to identify the antigens recognized by tumor-associated T_{regs} and to determine the role of antigen recognition in their development and function.

To address the role of antigen recognition, Malchow *et al.* used an elegant system for sequencing the TCRs expressed by tumor-infiltrating T_{regs} and conventional T cells. Like fingerprints, these TCR sequences distinguished different T cell clones present within the tumor microenvironment. Using a genetically engineered mouse model of prostate tumor development, they found that tumors were consistently infiltrated by T_{reg} populations bearing a single TCR (called MJ23), which differed from TCRs present on conventional tumor-infiltrating T cells. Furthermore, this TCR was specific for an antigen expressed in normal prostate tissue. Thus, this T_{reg} population was not selected for on the basis of expression of a novel antigen by a developing tumor, but was instead capable of recognizing an antigen expressed by the tissue from which the tumor arose.

The authors went on to show that the MJ23 TCR was sufficient to drive T_{reg} development within the thymus and that this process required the function of Aire. This led to the accumulation of T_{regs} within prostate-draining lymph nodes of male mice, regardless of whether they had a tumor. MJ23 TCR expression also caused nT_{reg} development in female mice, which lack prostate tissues but likely carry the gene that encodes the rel-

Koch Institute for Integrative Cancer Research, Department of Biology, and Howard Hughes Medical Institute, Massachusetts Institute of Technology, Cambridge, MA 02139, USA. E-mail: tjacks@mit.edu

Downloaded from www.sciencemag.org on March 8, 2013

Published by AAAS

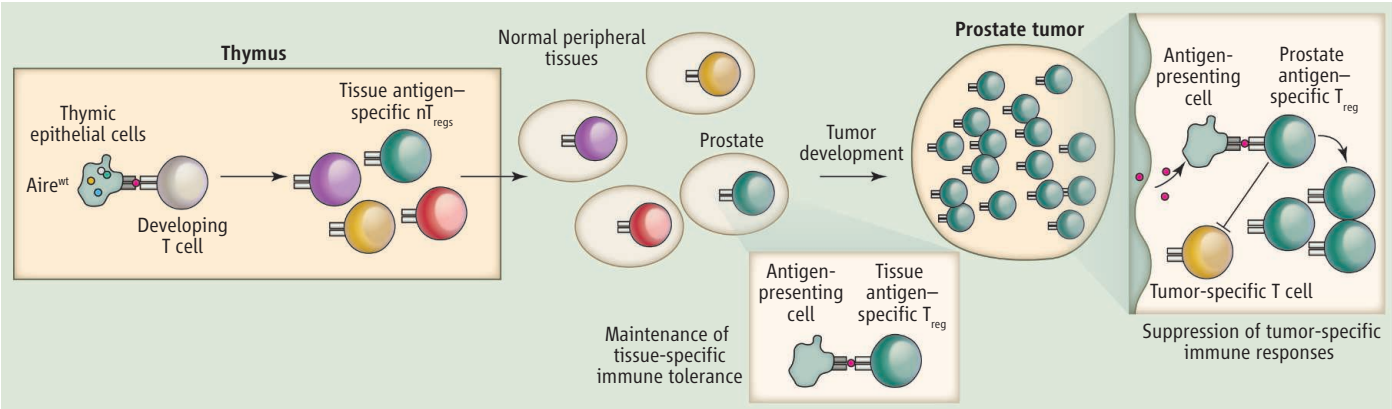

Tissue-specific T_{regs} suppress tumor-specific immune responses. In the thymus, specialized epithelial cells help generate "tissue-specific" T_{regs} with TCRs that recognize specific self antigens. After leaving the thymus, these T_{regs} preferentially accumulate in peripheral tissues according to tissue-restricted expression of self antigens. If a tumor develops, these T_{regs} infiltrate the developing tumor and inhibit tumor-specific immune responses.

evant antigen. These data suggest a model in which populations of tissue-specific T_{regs} arise during thymic development and then accumulate within those peripheral tissues on the basis of antigen recognition (see the figure). As tumors develop, these preexisting tissue-resident T_{regs} are recruited into and/or expanded within the tumor microenvironment, potentially allowing them to exert local immunosuppression. Thus, recognition of tissue-restricted antigens can play a central role in T_{reg} infiltration into tumors (and likely their function), even though the T_{regs} and antigens exist independent of tumor formation.

This study raises additional questions that bear on the role of T_{regs} and cancer development. For example, it would be interesting to know whether the tissue-specific T_{regs} found in the prostate tumor actively suppress antitumor immune responses. Likewise, what is their function in non–tumor-bearing animals? Given that this study makes a convincing case for tissue-resident T_{regs} in this genetically engineered mouse model of prostate cancer, are these findings generalizable to other tumor types and settings? In particular, it will be important to test whether natural, tissue-specific T_{regs} are the predominant population in tumors derived from other tissues and in tumors with higher mutation rates (i.e., carrying more tumor neoantigens) or increased expression of tumor-specific antigens. Indeed, previous work suggested that tumor-infiltrating T_{reg} populations would be a mixture of cells specific for tumor-specific neoantigens and tumor-associated antigens (*7*, *8*). It will also be interesting to determine whether T_{regs} that infiltrate distant metastases are specific for antigens expressed in the original tumor tissue or the tissue in which the metastasis seeded. Metastatic disease accounts for more than 80% of all cancer deaths, so therapies that target T_{regs} in both metastases and primary tumors will likely be more efficacious in treating disease. Understanding the broader set of mechanisms that govern the localization and function of T_{regs} in cancer will help guide the development of appropriate therapies that target this important class of cells in cancer patients.

References

1. D. M. Pardoll, *Nat. Rev. Cancer* **12**, 252 (2012).
2. S. P. Kerkar, N. P. Restifo, *Cancer Res.* **72**, 3125 (2012).
3. S. Malchow *et al.*, *Science* **339**, 1219 (2013).
4. O. J. Finn, *N. Engl. J. Med.* **358**, 2704 (2008).
5. C. S. Hsieh, H. M. Lee, C. W. Lio, *Nat. Rev. Immunol.* **12**, 157 (2012).
6. S. Z. Josefowicz, L. F. Lu, A. Y. Rudensky, *Annu. Rev. Immunol.* **30**, 531 (2012).
7. H. Y. Wang *et al.*, *Immunity* **20**, 107 (2004).
8. H. Y. Wang, G. Peng, Z. Guo, E. M. Shevach, R. F. Wang, *J. Immunol.* **174**, 2661 (2005).

10.1126/science.1235528

MATERIALS SCIENCE

Exceptional Properties by Design

A nanocomposite with a unique combination of attributes heralds an era of new possibilities in materials design.

Min Zhou

Materials, be they natural or human-made, come with characteristic combinations of mechanical properties. For example, ceramics have high stiffness but break easily, metals have high strength but limited ability to deform elastically, and polymers can recover from large deformations but carry relatively low stresses. Materials scientists have long tried to make materials that combine desirable properties in unusual ways. One such material is the nanocomposite reported by Hao *et al.* (*1*) on page 1191 of this issue. This material combines high strength, high recoverable strain, low stiffness, and biocompatibility. It may find application in dental braces, cardiac pacemakers, implantable devices, and flexible medical instruments.

Materials scientists and engineers use mechanical property maps (see the figure) to identify materials with particular combinations of attributes (*2*). These maps delineate ranges of accessible properties for bulk materials as well as low-dimensional materials (such as thin films and nanowires). Materials with previously unseen combinations of attributes can be designed by forming composites of different materials. The trick lies in making the constituents work together to yield a desired combination of behaviors. For example, nanowires are strong and have elastic strain limits on the order of 6 to 7%. Large elastic strains

School of Mechanical Engineering and School of Materials Science and Engineering, Georgia Institute of Technology, Atlanta, GA 30332, USA, and World Class University (WCU) Program on Multiscale Mechanical Design, School of Mechanical and Aerospace Engineering, Seoul National University, Seoul 151-744, Korea. E-mail: min.zhou@gatech.edu

Published by AAAS

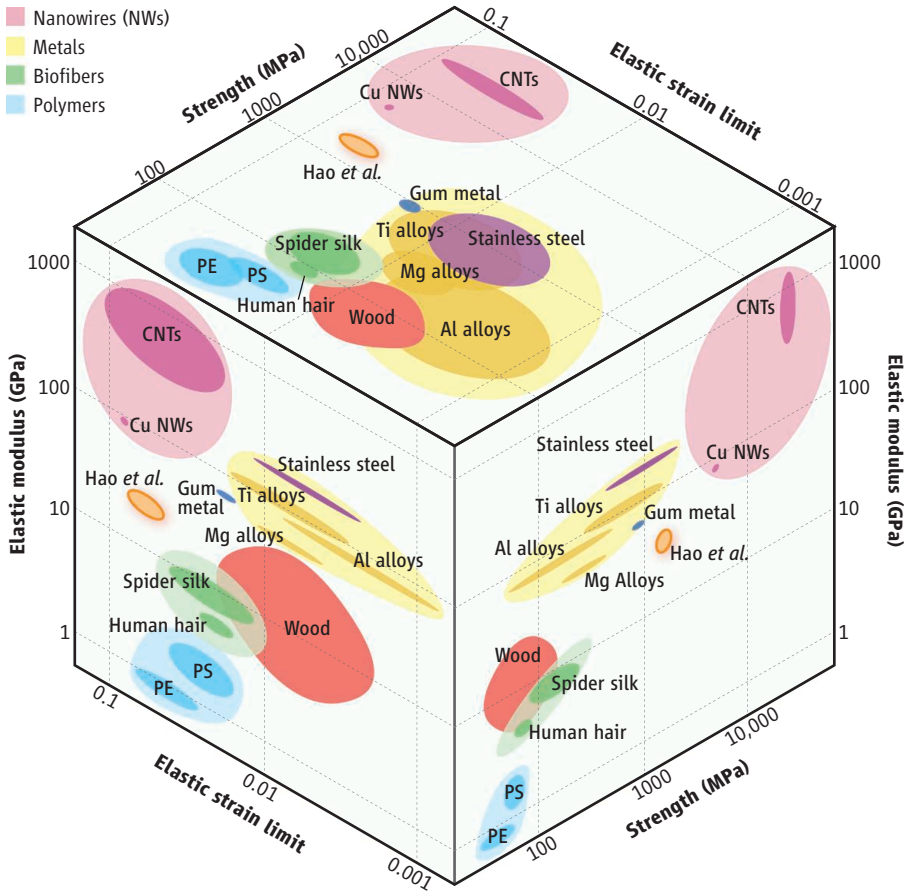

Find the spot. Mechanical property maps allow identification and selection of materials with desired combinations of attributes. The nanocomposite developed by Hao *et al.*, a bulk material consisting of niobium nanowires embedded in a nickel-titanium matrix, falls outside the domain of existing bulk materials and inside the domain of nanowires (see top and left faces of cube). This material is more flexible than other bulk materials with similar strength or stiffness. It may be useful for medical instruments and implantable devices. PE, polyethylene; PS, polystyrene; CNTs, carbon nanotubes.

allow a material to be flexible, adapt to and recover from different shapes, and store and release more energy. These are attractive attributes for sensors, actuators, and flexible devices. However, individual nanowires are too small to be used directly in applications that require bulk materials. How can their exceptional properties be translated into bulk form?

Hao *et al*. approached this challenge by creating a nanostructured composite consisting of niobium (Nb) nanowires embedded in a nickel-titanium (NiTi) matrix. The authors first performed careful calculations of how the nanowires and the matrix deformation can work together and how to condition the residual stresses in the material, and then subjected the material to cycles of stretch and release. This process leaves the Nb nanowires in tension and the NiTi matrix in compression even when the overall material is not under external forces. Thus, when the material is stretched, the matrix merely becomes less compressed or slightly stretched, allowing different parts of the material to deform and recover without the formation of defects (which marks the end of elasticity).

By engineering the structure of the interfaces between the fibers and the matrix at the atomistic level and controlling residual stresses, the authors can take advantage of the large elastic deformations of the nanowires in a bulk material setting, effectively coaxing the pseudoelastic deformation (each cycle of which involves the loss of some energy while the original size and shape of the material are recovered) of the NiTi matrix to go along with the elastic deformation (full recovery of mechanical work as well as size and shape) of the nanowires.

Previous attempts to do this were not successful (*3*). The key is to avoid lattice mismatch and defect generation by involving only coordinated shear deformation of lattices that does not change the relative positions of atoms. The resulting material occupies unique spots in the strength-stiffness, strength–elastic strain limit, and stiffness–elastic strain limit maps of all existing materials (see the figure).

As Hao *et al*.'s results show, design and engineering at the atomistic level can yield new materials with novel and desirable attributes. Can the envelope be pushed farther out to achieve, say, recoverable strains on the order of 15% or more in a bulk material? Such materials would be attractive as shock absorbers and energy storage devices.

Strains of ~6% approach the theoretical elastic limits of metal nanowires (*4*) and metallic glasses (*5*). However, nanowires of various other materials exhibit recoverable strains up to 15% through phase transformations (*6*, *7*) or even 50% through lattice reorientations (*8*, *9*). Taking advantage of these phenomena means that the resulting materials are likely to be pseudoelastic, as is the shape memory NiTi matrix in the Hao *et al*. nanocomposite. Pseudoelasticity would not be an issue for applications such as dental braces and medical implants. In fact, the ability to dissipate energy is required for many applications such as damping.

Materials development has historically been largely a trial-and-error empirical process that is expensive and time-consuming. Laboratory synthesis alone cannot explore material configurations not yet in existence. Computational design through modeling and simulation is making the concept of materials by design a reality (*10*, *11*); integrated computations, synthesis, and experiments are accelerating the development of new materials from the bottom up (*11*, *12*). In the future, we are likely to see more materials that, like the nanocomposite of Hao *et al*., push the boundaries of possibility.

References and Notes

1. S. Hao *et al*., *Science* **339**, 1191 (2013).
2. M. F. Ashby, *Materials Selection in Mechanical Design* (Butterworth Heinemann, Amsterdam, 2005).
3. Y. Dzenis, *Science* **319**, 419 (2008).
4. Y. Yue, P. Liu, Z. Zhang, X. Han, E. Ma, *Nano Lett.* **11**, 3151 (2011).
5. L. Tian *et al*., *Nature Commun.* **609**, 1 (2012).
6. A. J. Kulkarni, M. Zhou, K. Sarasamak, S. Limpijumnong, *Phys. Rev. Lett.* **97**, 105502 (2006).
7. J. Wang *et al*., *Phys. Rev. B* **76**, 172103 (2007).
8. W. Liang, M. Zhou, F. J. Ke, *Nano Lett.* **5**, 2039 (2005).
9. H. S. Park, K. Gall, J. A. Zimmerman, *Phys. Rev. Lett.* **95**, 255504 (2005).
10. G. B. Olson, *Science* **277**, 1237 (1997).
11. D. L. McDowell, G. B. Olson, *Sci. Modell. Simul.* **15**, 207 (2008).
12. T. E. Jones, M. E. Eberhart, S. Imlay, C. Mackey, G. B. Olson, *Phys. Rev. Lett.* **109**, 125506 (2012).

Acknowledgments: Supported by the NSF Center for Computational Materials Design and the WCU program of Korea. I thank Y. F. Gao, C. J. Lammi, A. Barua, S. Kim, and Y. Li for assistance.

10.1126/science.1236378

Published by AAAS

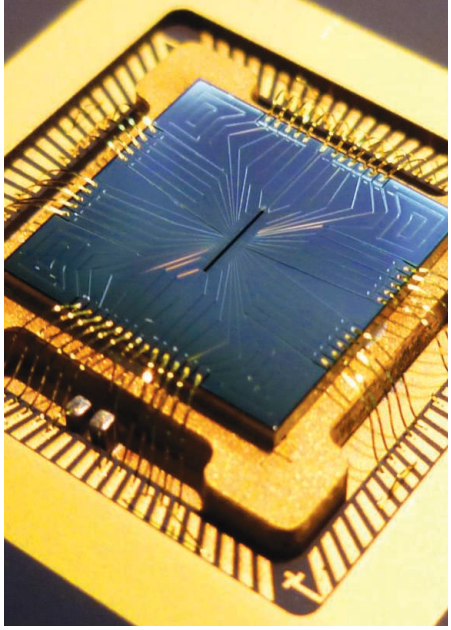

PHOTO: CURT SUPLEE AND EMILY EDWARDS, JOINT QUANTUM INSTITUTE AND UNIVERSITY OF MARYLAND; CHIP FABRICATION: SANDIA NATIONAL LABORATORIES WITH SUPPORT FROM THE INTELLIGENCE ADVANCED RESEARCH PROJECTS ACTIVITY

INTRODUCTION

The Future of Quantum Information Processing

IN A WORLD OVERWHELMED BY INCREASING AMOUNTS OF DATA, FINDING NEW WAYS to store and process information has become a necessity. Conventional silicon-based electronics has experienced rapid and steady growth, thanks to the progressive miniaturization of its basic component, the transistor, but that trend cannot continue indefinitely.

In conventional devices, information is stored and manipulated in binary form: The elementary components of these devices—the so-called bits—have two states, each of which encodes the binary 0 or 1. To move beyond the binary system, one can exploit the laws of quantum mechanics. A quantum-mechanical object with two energy levels at its disposal can occupy either of those two levels, but also an arbitrary combination ("superposition") of the two, much like an electron in a two-slit experiment can go through both slits at once. This results in infinitely many quantum states that a single quantum bit, or "qubit," can take; together with another strange property of quantum mechanics—entanglement—it allows for a much more powerful information platform than is possible with conventional components.

Quantum information processing (QIP) uses qubits as its basic information units. QIP has many facets, from quantum simulation, to cryptography, to quantum computation, which is expected to solve problems more complex than those within the capabilities of conventional computers. To be useful for QIP, a qubit needs to be both isolated from its environment and tightly controllable, which places stringent requirements on its physical realization. But this is only the first step; to build a quantum computer, for example, we must also have a scalable architecture and error correction that can be performed in parallel with computation; in addition, efficient quantum algorithms must exist for solving the problem at hand—a considerable theoretical challenge.

A number of qubit types have been proposed and experimentally realized that satisfy at least some of these criteria, and tremendous progress has been made over the past decade in improving the figures of merit, such as the coherence time. In this special section, four Reviews look into the future of QIP in some of its most promising physical realizations. On p. 1164, Monroe and Kim discuss the challenges of scaling trapped ion architectures to hundreds and thousands of qubits and beyond. Devoret and Schoelkopf (p. 1169) speculate on the future of superconducting circuits, whereas Awschalom *et al.* (p. 1174) focus on the many promising qubit flavors based on spins in semiconductors. Finally, Stern and Lindner (p. 1179) lay out the prospects for quantum computation using the entirely different approach of topologically protected states.

The future of QIP appears bright in spite of the many remaining challenges. As a bonus, overcoming these challenges will probably also advance basic research.

– JELENA STAJIC

Online

sciencemag.org

Podcast interview with author D. D. Awschalom (http://scim.ag/pod_6124a).

Quantum Information Processing

CONTENTS

Reviews

1164 Scaling the Ion Trap Quantum Processor
C. Monroe and J. Kim

1169 Superconducting Circuits for Quantum Information: An Outlook
M. H. Devoret and R. J. Schoelkopf

1174 Quantum Spintronics: Engineering and Manipulating Atom-Like Spins in Semiconductors
D. D. Awschalom et al.

1179 Topological Quantum Computation—From Basic Concepts to First Experiments
A. Stern and N. H. Lindner

See also Science *Podcast*

Science

Published by AAAS

REVIEW

Scaling the Ion Trap Quantum Processor

C. Monroe[1]* and J. Kim[2,3]

Trapped atomic ions are standards for quantum information processing, serving as quantum memories, hosts of quantum gates in quantum computers and simulators, and nodes of quantum communication networks. Quantum bits based on trapped ions enjoy a rare combination of attributes: They have exquisite coherence properties, they can be prepared and measured with nearly 100% efficiency, and they are readily entangled with each other through the Coulomb interaction or remote photonic interconnects. The outstanding challenge is the scaling of trapped ions to hundreds or thousands of qubits and beyond, at which scale quantum processors can outperform their classical counterparts in certain applications. We review the latest progress and prospects in that effort, with the promise of advanced architectures and new technologies, such as microfabricated ion traps and integrated photonics.

Quantum physics can be distilled to two disjointed and counterintuitive rules. First, an isolated quantum system is represented by a "wave function," or a mathematical entity that evolves according to a wave equation and is shaped with external controls. Second, when a quantum system interacts with a measurement apparatus or its surrounding environment, the wave function probabilistically and irreversibly "collapses" into a particular state. The incompatibility of these two quantum rules is seen most clearly in a quantum superposition state, in which, for instance, an isolated particle's wave function is delocalized between two or more positions. The second rule ensures that such states are never directly seen in the macroscopic world. However, when a system is left isolated without interacting with its environment, the (microscopic) superposition persists and can be exploited to store massive amounts of information in parallel.

A quantum information processor encodes information in an array of quantum bits or qubits, which can hold superpositions of classical bit values 0 and 1. When N qubits are prepared in their most general state, we have a quantum superposition of all 2^N N-bit binary numbers. Such a superposition is typically "entangled" in the sense that certain qubit values are correlated with others, even though they yield random outcomes when measured individually. A quantum computer manipulates this exponential amount of information by interfering pieces of this complex superposition through controlled interactions, or quantum logic gate operations. A final measurement of the system can then yield information pertaining to all 2^N states. For merely $N = 400$ qubits, we find that the encoded information of $2^{400} \sim 10^{120}$ values is more than the number of fundamental particles in the universe; such a computation could never be performed without the parallel processing enabled by quantum mechanics. In a sense, entanglement between qubits acts as an invisible wiring that can potentially be exploited to solve certain problems that are intractable otherwise (*1*).

The requirements for large-scale quantum computer hardware are daunting, given the exponential sensitivity of such large superpositions to errors and leaks to the environment. However, there exist error-correction codes that allow arbitrarily complex quantum superposition states to be generated and stabilized (*1*), giving us hope that useful fault-tolerant quantum computers will eventually be realized despite the steep technical requirements far beyond current experimental capability.

In the search for quantum information processing hardware, one needs qubits that are extremely well isolated from the environment yet can be precisely controlled with external fields to affect interferences through the operations of quantum logic gates. Moreover, we must ultimately couple the qubits to the outside world in the strongest possible sense by performing a measurement that collapses any superposition onto definite values. These conflicting stringent requirements restrict potential quantum hardware to exotic microscopic systems. In this Review, we consider the most fundamental of these platforms—electromagnetically trapped atoms (*2*)—and speculate how this system may be scaled to hundreds or thousands of interacting qubits in the coming years.

Entangling Trapped Atomic Ion Qubits

Individual atoms are natural carriers of quantum information because they are standards: An isolated atom of carbon, for example, is exactly the same in Washington as it is in London or anywhere else. Isolation can be provided by confining atoms in an evacuated environment with electromagnetic traps, suspending atoms in free space so that they do not uncontrollably interact with background atoms, molecules, or surfaces. There are several compelling proposals for quantum computer architectures based on trapped neutral atoms and optical lattices, although the weak interaction between neutral atoms leads to difficulties in controlling their entanglement, and research in this area is still exploratory (*3*). Here, we focus on the trapping of electrically charged atoms, or ions, for which high-fidelity quantum operations and measurements are now commonplace.

The typical ion trap geometry for quantum information purposes is the linear radio frequency (rf) Paul trap, in which nearby electrodes hold static and dynamic electrical potentials that lead to an effective harmonic confinement of the ions, like a bowl full of mutually repelling marbles (*2*). When ions are laser-cooled to very low temperatures in such a trap, the ions form a linear crystal of qubits, with the Coulomb repulsion balancing the external confinement force (Fig. 1A). Ions are typically loaded into traps by creating a neutral atomic flux of the desired particle and ionizing them once in the trapping volume. Ions can remain confined for months, with lifetimes often limited by the level of vacuum. Elastic collisions with residual background gas occur roughly once per hour per ion at typical ultrahigh-vacuum pressures ($\sim 10^{-11}$ torr) and do not necessarily eject the ion, although inelastic collisions can change the species of the trapped ion. Cryogenic chambers can virtually eliminate these collision events by further reducing the background pressure.

Appropriate atomic ion species should have a strong closed optical transition that allows for laser-cooling of the motion, qubit state initialization, and efficient qubit readout. This rules out almost anything other than simple atomic ions with a lone outer electron, such as the alkaline-earths (Be^+, Mg^+, Ca^+, Sr^+, and Ba^+) and particular transition metals (Zn^+, Hg^+, Cd^+, and Yb^+). Qubits are represented by two stable electronic levels within each ion, sometimes characterized by an effective spin with the two states $|\uparrow\rangle$ and $|\downarrow\rangle$ corresponding to bit values 0 and 1.

The reduced energy level diagram of $^{171}Yb^+$ is shown in Fig. 2, B and C, in which the qubit levels $|\uparrow\rangle$ and $|\downarrow\rangle$ are represented by the stable hyperfine levels in the ground electronic state, separated by frequency $\nu_{HF} = 12.642\ 812$ GHz. The excited electronic states $|e\rangle$ and $|e'\rangle$ are themselves split by a smaller hyperfine coupling and separated from the ground states by an optical interval. Laser radiation tuned just below resonance in these optical transitions allows Doppler laser cooling to confine ions near the bottom of the trap. Other more sophisticated forms of laser cooling can bring the ions to nearly at rest in the trap (*4*). When a bichromatic laser beam resonant with both $|\uparrow\rangle \leftrightarrow |e\rangle$ and $|\uparrow\rangle \leftrightarrow |e'\rangle$ transitions is applied to the atom, it rapidly falls into the state $|\downarrow\rangle$ and no longer interacts with the light

[1]Joint Quantum Institute (JQI), Department of Physics, University of Maryland, and National Institute of Standards and Technology, College Park, MD 20742, USA. [2]Department of Electrical and Computer Engineering, Duke University, Durham, NC 27708, USA. [3]Applied Quantum Technologies, Durham, NC 27707, USA.

*To whom correspondence should be addressed. E-mail: monroe@umd.edu

Downloaded from www.sciencemag.org on March 8, 2013

field (Fig. 1B), allowing the initialization of a qubit with essentially 100% fidelity. When a single laser resonant with the transition $|\uparrow\rangle \leftrightarrow |e\rangle$ is applied, the closed-cycling optical transition causes an ion in the $|\uparrow\rangle$ state to fluoresce strongly, whereas an ion in the $|\downarrow\rangle$ state stays dark because the laser is far from its resonance (Fig. 1C). The collection of even a small fraction of this fluoresence allows for the detection of the atomic qubit state with near-perfect efficiency. Other atomic species have similar initialization/detection schemes.

Coulomb-Based Gates and the Quantum CCD

The motion of many trapped ions is coupled through the Coulomb interaction, much like an array of pendulums connected by springs. A natural way to implement entangling quantum logic gates between ions in a crystal is thus to use the motion as an intermediary (Fig. 2A) by applying qubit state–dependent optical or microwave dipole forces to the ion (or ions) (*4*–*7*).

We assume that the qubit levels respond to an external field E by experiencing an equal and opposite energy shift $\pm\mu E$—for example, through the Stark effect for electric fields or the Zeeman effect for magnetic fields, in which case μ is an effective dipole moment of the qubit. When the field is inhomogeneous, this gives rise to a qubit state–dependent force along the x direction $F_x = \pm\mu E'(x)$, where the sign depends on the qubit state, and $E'(x)$ is the gradient of the applied field along x. For a plane wave radiation field with amplitude E_0 and wave vector k along x, $F_x = \pm hk\Omega$, where h is Planck's constant, and the Rabi frequency $\Omega = \mu E_0/h$ parametrizes the field-qubit coupling. Because this force acts differently on the two qubit states, it can coherently map the qubit state to the collective motion of N ions, with characteristic speed $R_{\text{gate}} = \Omega\sqrt{\nu_R/\nu}$ (*4*, *7*). In this expression, $\nu_R = hk^2/(8\pi^2 M)$ is the recoil frequency of the ion crystal associated with momentum transfer from the field, M is the total mass of the ions, and ν is the frequency of harmonic oscillation of the collective motional mode along the x direction. Thus, a qubit superposition within the ion is transformed to a superposition of the ion's position. When applied to multiple ions, this fundamental operation allows gates to be performed between separated ions, mediated through the motion (*5*, *6*). Current experiments with a few ions have realized entangled state fidelities of greater than 99% (*8*) and operate in the range $R_{\text{gate}} \sim 10$ to 100 kHz; with available ultrafast optical fields, it should be possible to operate gates in the gigahertz range (*9*).

As the number of ions N in the crystal grows, the gate speed slows down as $R_{\text{gate}} \sim 1/\sqrt{N}$ from the mass term. For large crystals, there will also be crosstalk between the many modes of collective motion. Background errors such as the decoherence (heating) of the motional modes (*10*) or fluctuating fields that add random phases to the qubits will become important at longer times; thus, there will be practical limits on the size of a single crystal for the performance of faithful quantum gates. Individual optical addressing of ions (*11*) and pulse-shaping techniques (*12*) can mitigate these errors to achieve the full control of single crystals ranging from $N = 10$ to 100 qubits. This should allow the implementation of quantum simulations (*13*) in a regime in which classical modeling of certain many-body systems, such as frustrated spin networks, becomes intractable. It would also enable the construction of error-correcting encoded qubits that might form block primitives of an eventual fault-tolerant quantum computer.

In order to scale beyond 10 to 100 trapped ion qubits, we turn to a multiplexed architecture called the quantum charge-coupled device (QCCD) (*14*). This involves the sequential entanglement of small numbers of ions through their collective motion in a single chain and the classical shuttling of individual ions between different trapping zones to propagate the entanglement, as depicted in Fig. 2B. The QCCD architecture requires exquisite control of the ion positions during shuttling and may require additional atomic ion species to act as "refrigerator" ions to quench the excess motion from shuttling operations (*15*). Rudimentary versions of the QCCD idea have been used in many quantum information applications, such as teleportation and small quantum algorithms (*7*), and recent experiments have shown the reliable, repeatable, and coherent shuttling of ion qubits over millimeter distances in microseconds (*16*, *17*) and through complex two-dimensional junctions (Fig. 2, C and D) (*18*, *19*). The QCCD approach will push current state-of-the-art quantum information processing experiments to territories where elementary quantum error correction and simple quantum algorithms can be implemented. However, scaling to thousands or more qubits in the QCCD may be challenging because of the complexity of interconnects, diffraction of optical beams, and the extensive hardware required for qubit control.

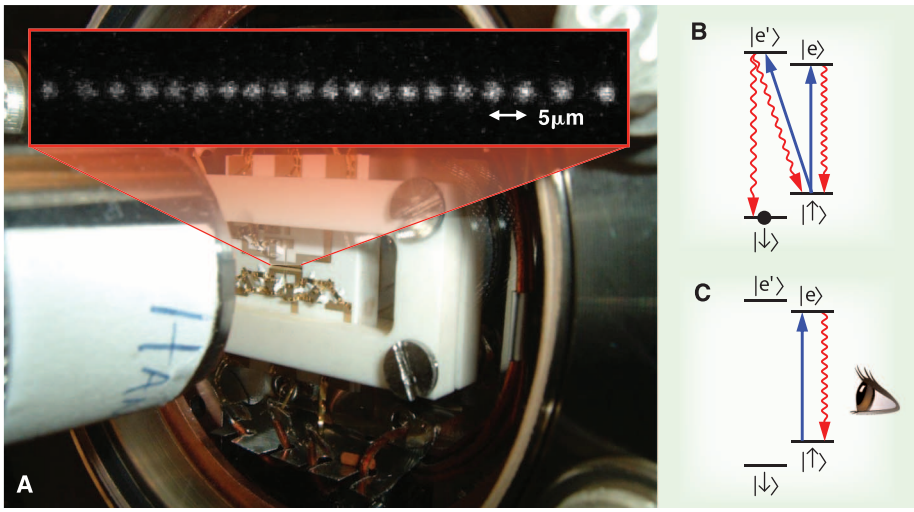

Fig. 1. (**A**) Vacuum chamber that houses electrodes for the trapping of atomic ions with a linear crystal of 20 confined atomic $^{171}Yb^+$ ions laser cooled to be nearly at rest. The atoms are illuminated with laser radiation tuned to a resonance in $^{171}Yb^+$, and the fluorescence is imaged onto a camera. The separation of the ions is determined by a balance between the external confinement force and Coulomb repulsion. (**B** and **C**) Reduced energy level diagram of each $^{171}Yb^+$ atomic ion, showing the atomic hyperfine levels $|\uparrow\rangle$ and $|\downarrow\rangle$ that represent a qubit. The electronic excited states $|e\rangle$ and $|e'\rangle$ are separated from the ground states by an energy corresponding to an optical wavelength of 369.53 nm, with all allowed transitions indicated by the downward red arrows. Applied laser radiation (upward blue arrows) drives these transitions for (B) initialization to state $|\downarrow\rangle$ and (C) fluorescence detection of the qubit state ($|\uparrow\rangle$, fluorescence, $|\downarrow\rangle$, no fluorescence).

Photonic Gates and Joining Remote Crystals

To scale beyond the QCCD in a modular architecture, one can link separate registers of trapped ion chains with photonic interfaces. In this scheme, an entangled qubit pair is first generated between the two registers, which is then used to implement a two-qubit gate between two ions that belong to each register (*20*). This approach is not limited to trapped ions and can be generalized to other physical systems with strong optical transitions (*3*).

A pair of trapped ion qubit registers [termed elementary logic units (ELUs)] can be entangled with each other by using propagating photons emitted by a subset of ions from each register, designated to be "communication qubits." Each communication qubit is driven to an excited state with near unit probability $p_e \sim 1$ by using a fast laser pulse, so that at most one photon emerges following appropriate radiative selection rules (Fig. 2E). The photon carries its qubit through two distinguishable internal photonic states (such as polarization or optical frequency) (*21*, *22*). For example, the joint state of a communication qubit and emitted photonic qubit can be written $|\downarrow\rangle_i|\nu_\downarrow\rangle_i + |\uparrow\rangle_i|\nu_\uparrow\rangle_i$, where $|\nu_\downarrow\rangle_i$ and $|\nu_\uparrow\rangle_i$ denote the frequency qubit states of a single photon

Downloaded from www.sciencemag.org on March 8, 2013

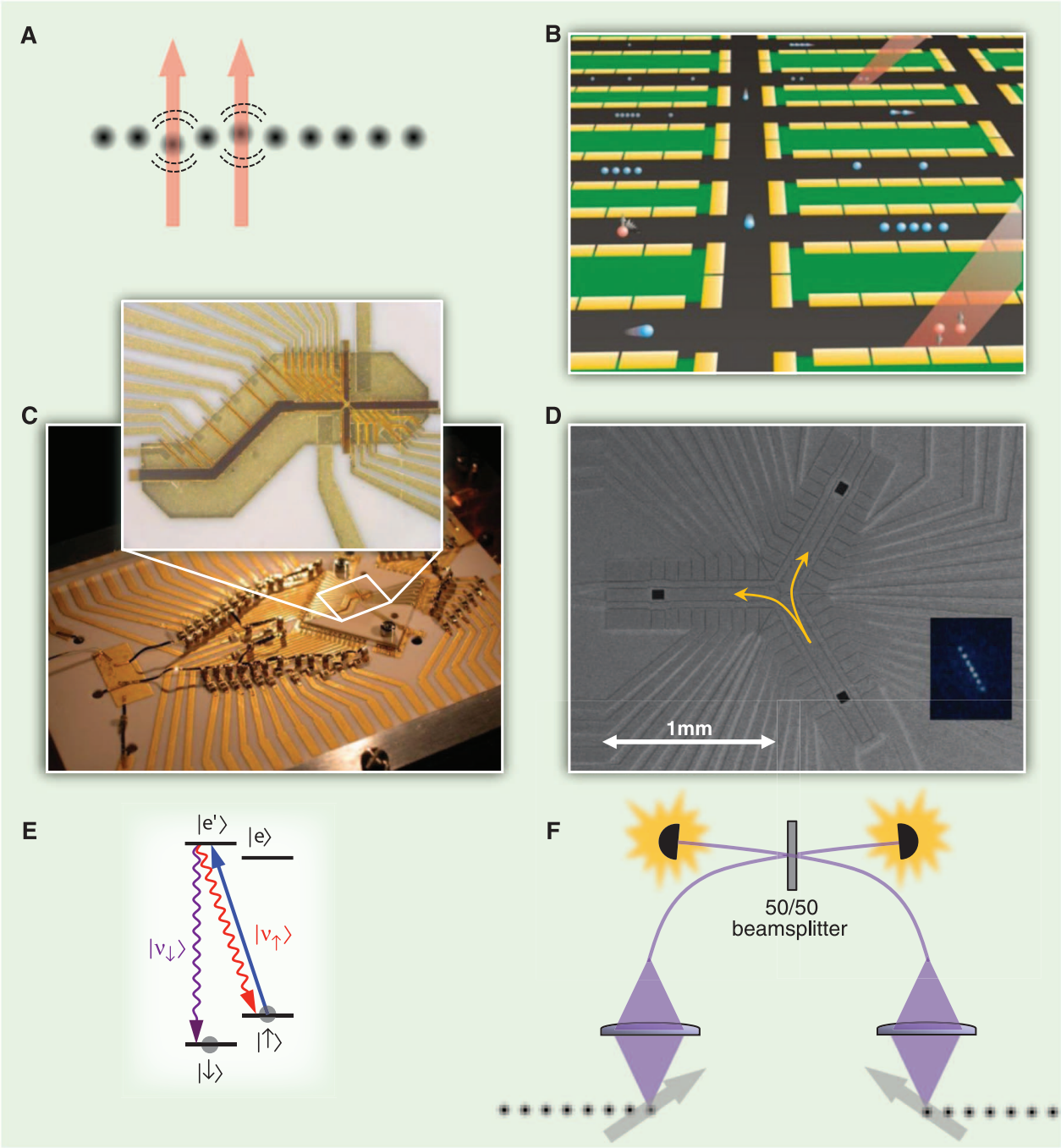

Fig. 2. (**A**) Optical dipole forces (red) displace two ions depending on their qubit states, and the resulting modulation of the Coulomb interaction allows the implementation of the controlled-NOT gate between these two ions. (**B**) Concept of a quantum CCD trap, in which ions can be shuttled between various zones. Ions can be entangled within a small crystal using laser forces as in (A) and then moved to different zones to propagate the entanglement to other ion crystals. Additional zones can be used for the loading of ions or qubit state detection. In principle, any pair of ions can be brought together through a web of ion trap channels, and a separate ion species can be used for sympathetic cooling to quench any residual motion from the shuttling procedure. [Image credit: National Institute of Standards and Technology] (**C**) Ion trap structure for the shuttling of ions through a junction. [Main image adapted with permission from (*18*); copyright 2011 by the American Physical Society] (**D**) Surface ion trap structure for shuttling ions through a three-channel junction. Inset shows an image of a trapped ion chain in lower right-hand sector. [Adapted with permission from (*19*); publisher: Institute of Physics] (**E**) Energy levels of trapped ion excited with a fast laser pulse (blue upward arrow) that produces single photon whose color, represented by the state $|\nu_\uparrow\rangle$ or $|\nu_\downarrow\rangle$, is entangled with the resultant qubit state $|\uparrow\rangle$ or $|\downarrow\rangle$, respectively. (**F**) Two "communication qubit" ions, immersed in separate crystals of other ions, each produce single photons when driven by laser pulses (blue). With some probability, the photons arrive at the 50/50 beamsplitter and then interfere. If the photons are indistinguishable (in polarization and color), then they always leave the beamsplitter along the same path. The simultaneous detection of photons at the two output detectors means that the photons were different colors, but because there is no knowledge of which color photon came from which ion emitter, this coincidence detection heralds the entanglement of the trapped ion qubits.

Downloaded from www.sciencemag.org on March 8, 2013

emitted by the i-th communication qubit. Here, we assume that the two photonic frequencies are distinguishable, or $|\nu_\uparrow - \nu_\downarrow| >> \gamma$, where γ is the radiative linewidth of the excited state. When two communication qubits i and j are excited in this way, and their photons are mode-matched on a 50/50 beamsplitter (Fig. 2F), the entanglement of the memories is heralded by the joint (coincidence) detection of photons at output detectors, creating the entangled state $|\downarrow\rangle_i|\uparrow\rangle_j - |\uparrow\rangle_j|\downarrow\rangle_i$ (*21–24*). This entanglement link succeeds with probability $p = (p_e F\eta_D)^2/2$, where F is the fraction of light collected from each emitter, and η_D is the single photon detector efficiency. Even though this is a probabilistic link, the detected photons indicate success, and the resulting entanglement between the ions can subsequently be used for deterministic quantum information processing. The mean connection rate is given by Rp, where R is the repetition rate of the initialization/excitation process, limited by the emission rate γ. For typical atomic transitions into free space with $\gamma \sim 10^8$/s, light collection fraction $F \sim 1$ to 10%, and detector efficiency $\eta_D \sim 20\%$, we find typical connection rates of 1 to 1000 Hz, with substantial gains possible with better photon collection strategies (*25*).

In practice, the communication qubit must be well isolated from the neighboring memory qubit ions so that scattered light from the excitation laser or the emitted photons themselves do not disturb the other memory qubits in each register. Although physical separation of the ions can provide the requisite isolation, a better solution is to use two different atomic species (*26*) to eliminate this crosstalk—for instance, $^{171}Yb^+$ for the memory qubit and $^{138}Ba^+$ for the communication qubit. Here, the communication qubits from separate registers become entangled via the photonic channel, and then the qubits within the communication ions are coherently mapped to neighboring memory qubits through Coulomb gates as described above.

New Technology for Scalability and Modularity

Scalable ion traps will require precision electrode structures, with as many discrete electrodes as trapped ion qubits, suggesting the use of micrometer-scale surface chip traps (*27*, *28*) that can be fabricated by using standard semiconductor processing techniques (*29*). Highly complex surface traps that can handle several tens of ions over tens of trapping zones have been fabricated and tested (Fig. 3, A and B) (*19*, *30*, *31*), with loading of up to ~10 ions with high-fidelity qubit preparation, detection, and single-qubit gate operations. Multi-qubit entangling operations in microscopic traps are more challenging because the ions experience higher levels of electric field noise from closer electrodes, causing motional decoherence during the gate operation. Although the source of this noise is still not well understood (*10*), it seems to scale roughly as $1/d^4$, where d is the characteristic distance from the ions to the nearest electrode (*32*). This motional heating can be quenched at cryogenic temperatures (*32*, *33*) or with adequate treatment of the trap surface (*34*), so this problem does not appear to be a fundamental limitation.

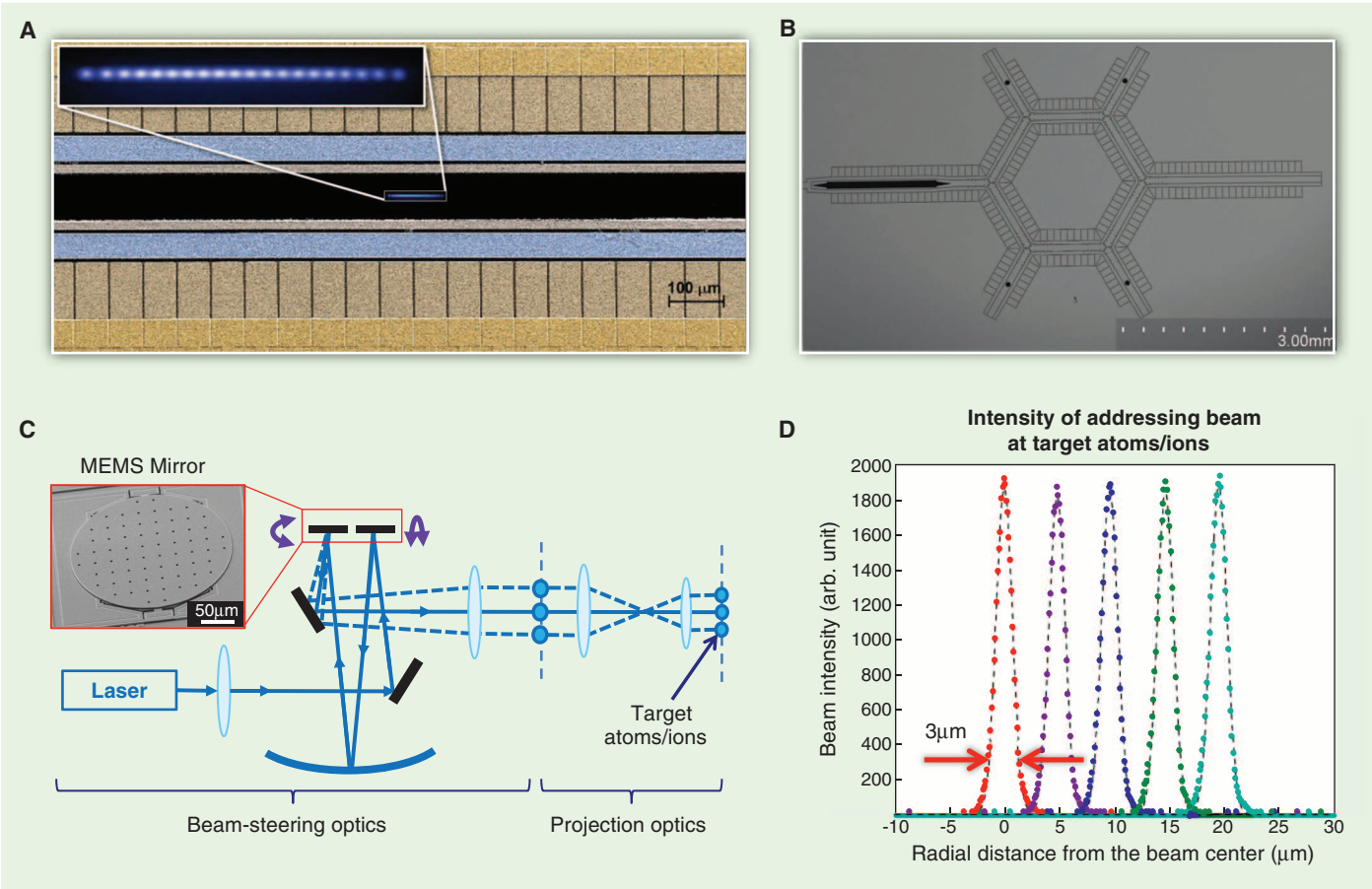

Fig. 3. (**A**) Scanning electron micrograph of a microfabricated linear trap with a long slot, with superimposed image of 20-ion chain in an anharmonic well (inset). The blue rails are RF electrodes and the rest are segments of static electrodes. [Courtesy GTRI] (**B**) Circulator trap with six junctions and two linear sections on either side for qubit manipulation. The other four short sections can be used as loading zones (of multiple ion species, if necessary), and the six junctions enable reordering of ions in the chain. [Courtesy Sandia National Laboratories] (**C**) Technology for individual optical addressing of ions in a linear chain. A control laser beam bounces off two MEMS mirrors tilting in orthogonal directions (inset) and can be steered over a two-dimensional space at the target atoms or ions. (**D**) The resulting profile of a ~3-µm diameter beam at 369.5 nm with a steering range of ~20 µm measured at the site of the ions.

Downloaded from www.sciencemag.org on March 8, 2013

Although the technology of trapping large numbers of ions has progressed, scaling the ability to individually address the qubits in the chain remains a challenge. Individual addressing of single atoms in an array via steering the control beam by using either electro-optic (EO) or acousto-optic deflectors has been demonstrated for small arrays (*35*, *36*). For larger atomic arrays, fast scanning mirrors provide an attractive solution (*37*, *38*). The advances in micro-electromechanical systems (MEMS) technology enable micromirror-based optical systems capable of independently steering multiple beams over the same atomic array (Fig. 3C).

A single ion chain (or several chains on a chip connected through the QCCD architecture) with an optical interface (Fig. 2F) can serve as a processor node (ELU) of a distributed quantum multicomputer, in which two-qubit gates between ions that belong to different ELUs are realized by using the photonic gate (*39*). When a large number ($\sim 10^3$) of such ELUs are connected through a reconfigurable photonic network supported by an optical crossconnect switch (*40*), a scalable quantum computer with up to $\sim 10^6$ qubits can be constructed (Fig. 4A). This architecture allows entanglement between any pair of ELUs in the processor with operations running in parallel, and distance-independent logic gate operations between any two qubits in the system. Such features are crucial for efficiently executing quantum algorithms that require nonlocal gates among the qubits and ensuring fault-tolerant quantum computation (*39*).

By conveying the photonic link over long distances, entanglement can be distributed between high-quality ion memory qubits separated by the distance traveled by the photons. Combined with the ability to perform local logic gates and high-fidelity measurements, each chip can thus serve as a quantum repeater node (Fig. 4B) that enables distribution of quantum entanglement over macroscopic distances by means of successive entanglement swapping (*41*). The photons adequate for carrying quantum information from ion qubits tend to have wavelengths in the ultraviolet or in the visible part of the spectrum, which is far from ideal for long-distance transmission. Quantum frequency converters can be used to translate the wavelength of the photon for better transmission (*42*). Shown in Fig. 4C is a schematic of a chain of quantum repeaters that enable entangled qubit pair distribution over macroscopic distances, which can be used for various quantum communication protocols, including quantum key distribution (QKD).

A major challenge in both modular quantum computer and quantum repeater applications is the slow rate of entanglement generation for the photonic gate, which is dominated by the low collection efficiency of the emitted photons. Continual efforts to improve collection of emitted photons into a single-mode fiber, involving the integration of ion traps with optical components such as mirrors (*43*), high numerical aperture lenses (*44*), and optical cavities (*45*), may boost the entanglement generation rate up by several orders of magnitude to above the decoherence rates of ion qubits.

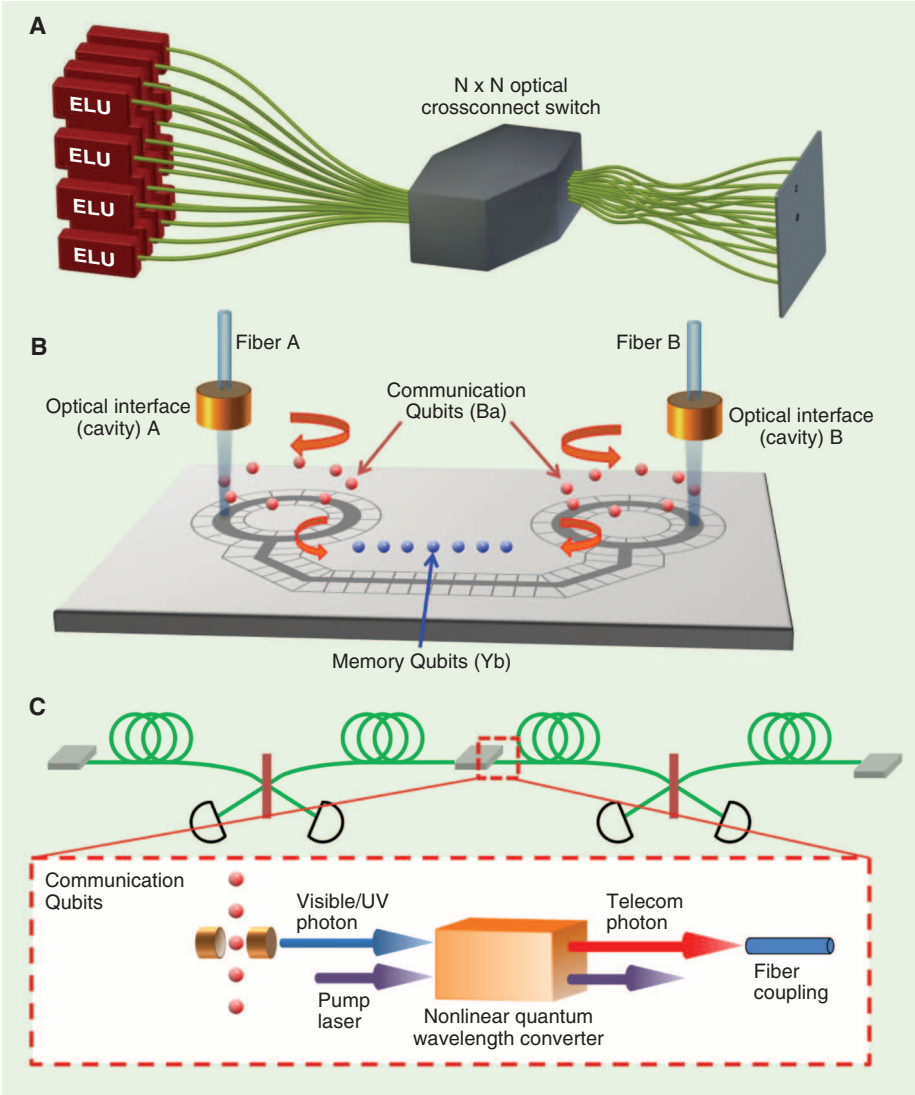

Fig. 4. Advanced quantum information systems with trapped ion technology. (**A**) Modular distributed quantum computer. Several ELUs are connected through a photonic network by using an optical crossconnect switch, inline fiber beamsplitters, and a photon-counting imager (*39*). [Adapted with permission from (*46*)] (**B**) Trapped ion quantum repeater node made up of communication qubit ions (such as Ba^+) and memory qubit ions (such as Yb^+), with two optical interfaces per node. Multiple communication qubits are used per optical interface to inject photons into the optical channel, while the results for successful entanglement generation at the detectors are reported back to this node. Only qubits corresponding to successful events will be transported to the memory qubit region for use in quantum repeater protocol. (**C**) A chain of quantum repeater nodes can distribute quantum entanglement over macroscopic distances. The photons generated by the ions must be converted to telecommunication wavelengths for long-distance transport, which can be achieved by nonlinear optical processes.

Outlook

The past decade has seen a number of small quantum information processors based on trapped ions, but in the coming years, we may see trapped ion devices used for applications that are difficult or impossible to perform using conventional technology. A quantum simulator that involves more than ~30 qubits may soon be able to predict behavior of interacting spin systems that is not tractable by a classical computer. Distribution of high-quality entangled qubit pairs over macroscopic distances by using trapped ion quantum repeaters may lead to new applications, such as long-distance QKD and multipartite entanglement distribution, as well as fundamental results, such as a loophole-free test of quantum nonlocality.

With the advent of microfabricated ion trap chips integrated with photonic components, modular ion trap quantum computer architectures

Downloaded from www.sciencemag.org on March 8, 2013

may lead to even larger quantum computers that can ultimately be put to use in materials design, communications, and high-performance computation. As quantum systems are made ever larger, they ultimately tend toward classical behavior because the quantum nature of the system quickly disappears even at the presence of tiny amounts of dissipation. Whether we find that the strange rules of quantum physics indeed persist to much larger systems, or perhaps a new order emerges, the trapped ion platform for quantum information processing is expected to provide the leading experimental playground in which to explore the evolution of complex quantum systems.

References and Notes

1. M. A. Nielsen, I. L. Chuang, *Quantum Computation and Quantum Information* (Cambridge Univ. Press, Cambridge, 2000).
2. C. R. Monroe, D. J. Wineland, *Sci. Am.* **299**, 64 (2008).
3. T. D. Ladd *et al.*, *Nature* **464**, 45 (2010).
4. D. Leibfried, R. Blatt, C. Monroe, D. Wineland, *Rev. Mod. Phys.* **75**, 281 (2003).
5. J. I. Cirac, P. Zoller, *Phys. Rev. Lett.* **74**, 4091 (1995).
6. A. Sørensen, K. Mølmer, *Phys. Rev. Lett.* **82**, 1971 (1999).
7. R. Blatt, D. Wineland, *Nature* **453**, 1008 (2008).
8. J. Benhelm, G. Kirchmair, C. F. Roos, R. Blatt, *Nat. Phys.* **4**, 463 (2008).
9. J. J. García-Ripoll, P. Zoller, J. I. Cirac, *Phys. Rev. Lett.* **91**, 157901 (2003).
10. Q. A. Turchette *et al.*, *Phys. Rev. A* **61**, 063418 (2000).
11. H. Häffner, C. Roos, R. Blatt, *Phys. Rep.* **469**, 155 (2008).
12. S.-L. Zhu, C. Monroe, L.-M. Duan, *Europhys. Lett.* **73**, 485 (2006).
13. J. Ignacio Cirac, P. Zoller, *Nat. Phys.* **8**, 264 (2012).
14. D. Kielpinski, C. Monroe, D. J. Wineland, *Nature* **417**, 709 (2002).
15. M. D. Barrett *et al.*, *Phys. Rev. A* **68**, 042302 (2003).
16. A. Walther *et al.*, *Phys. Rev. Lett.* **109**, 080501 (2012).
17. R. Bowler *et al.*, *Phys. Rev. Lett.* **109**, 080502 (2012).
18. R. B. Blakestad *et al.*, *Phys. Rev. A* **84**, 032314 (2011).
19. D. L. Moehring *et al.*, *New J. Phys.* **13**, 075018 (2011).
20. D. Gottesman, I. L. Chuang, *Nature* **402**, 390 (1999).
21. C. Simon, W. T. M. Irvine, *Phys. Rev. Lett.* **91**, 110405 (2003).
22. D. L. Moehring *et al.*, *Nature* **449**, 68 (2007).
23. C. Cabrillo, J. I. Cirac, P. Garcia-Fernandez, P. Zoller, *Phys. Rev. A* **59**, 1025 (1999).
24. L. Slodicka *et al.*, http://arxiv.org/abs/1207.5468 (2012).
25. T. Kim, P. Maunz, J. Kim, *Phys. Rev. A* **84**, 063423 (2011).
26. P. O. Schmidt *et al.*, *Science* **309**, 749 (2005).
27. J. Chiaverini *et al.*, *Quant. Inf. Comp.* **5**, 419 (2005).
28. S. Seidelin *et al.*, *Phys. Rev. Lett.* **96**, 253003 (2006).
29. J. Kim *et al.*, *Quant. Inf. Comput.* **5**, 515 (2005).
30. J. Amini *et al.*, *New J. Phys.* **12**, 033031 (2010).
31. J. T. Merrill *et al.*, *New J. Phys.* **13**, 103005 (2011).
32. L. Deslauriers *et al.*, *Phys. Rev. Lett.* **97**, 103007 (2006).
33. J. Labaziewicz *et al.*, *Phys. Rev. Lett.* **101**, 180602 (2008).
34. D. A. Hite *et al.*, *Phys. Rev. Lett.* **109**, 103001 (2012).
35. F. Schmidt-Kaler *et al.*, *Nature* **422**, 408 (2003).
36. D. D. Yavuz *et al.*, *Phys. Rev. Lett.* **96**, 063001 (2006).
37. C. Knoernschild *et al.*, *Appl. Phys. Lett.* **97**, 134101 (2010).
38. C. Weitenberg *et al.*, *Nature* **471**, 319 (2011).
39. C. Monroe *et al.*, http://arxiv.org/abs/1208.0391 (2012).
40. J. Kim *et al.*, *IEEE Photon. Technol. Lett.* **15**, 1537 (2003).
41. H.-J. Briegel, W.Dür, J. I. Cirac, P. Zoller, *Phys. Rev. Lett.* **81**, 5932 (1998).
42. K. De Greve *et al.*, *Nature* **491**, 421 (2012).
43. P. F. Herskind *et al.*, *Opt. Lett.* **36**, 3045 (2011).
44. A. Jechow, E. W. Streed, B. G. Norton, M. J. Petrasiunas, D. Kielpinski, *Opt. Lett.* **36**, 1371 (2011).
45. M. Steiner, H. M. Meyer, C. Deutsch, J. Reichel, M. Köhl, http://arxiv.org/abs/1211.0050 (2012).
46. L.-M. Duan, C. Monroe, *Rev. Mod. Phys.* **82**, 1209 (2010).

Acknowledgments: This work was supported by the U.S. Army Research Office (ARO) award W911NF0710576 with funds from the Defense Advanced Research Projects Agency (DARPA) Optical Lattice Emulator Program, ARO award W911NF0410234 with funds from the Intelligence Advanced Research Projects Activity Multi-Qubit Coherent Operations program, ARO Multidisciplinary University Initiative award W911NF0910406 on Hybrid Quantum Optical Circuits, Army Contracting Command award W31P4Q1210017 with funds from the DARPA Quiness Program, and the NSF Physics Frontier Center at JQI.

10.1126/science.1231298

Downloaded from www.sciencemag.org on March 8, 2013

REVIEW

Superconducting Circuits for Quantum Information: An Outlook

M. H. Devoret[1,2] and R. J. Schoelkopf[1]*

The performance of superconducting qubits has improved by several orders of magnitude in the past decade. These circuits benefit from the robustness of superconductivity and the Josephson effect, and at present they have not encountered any hard physical limits. However, building an error-corrected information processor with many such qubits will require solving specific architecture problems that constitute a new field of research. For the first time, physicists will have to master quantum error correction to design and operate complex active systems that are dissipative in nature, yet remain coherent indefinitely. We offer a view on some directions for the field and speculate on its future.

The concept of solving problems with the use of quantum algorithms, introduced in the early 1990s (*1*, *2*), was welcomed as a revolutionary change in the theory of computational complexity, but the feat of actually building a quantum computer was then thought to be impossible. The invention of quantum error correction (QEC) (*3*–*6*) introduced hope that a quantum computer might one day be built, most likely by future generations of physicists and engineers. However, less than 20 years later, we have witnessed so many advances that successful quantum computations, and other applications of quantum information processing (QIP) such as quantum simulation (*7*, *8*) and long-distance quantum communication (*9*), appear reachable within our lifetime, even if many discoveries and technological innovations are still to be made.

Below, we discuss the specific physical implementation of general-purpose QIP with superconducting qubits (*10*). A comprehensive review of the history and current status of the field is beyond the scope of this article. Several detailed reviews on the principles and operations of these circuits already exist (*11*–*14*). Here, we raise only a few important aspects needed for the discussion before proceeding to some speculations on future directions.

Toward a Quantum Computer

Developing a quantum computer involves several overlapping and interconnecting stages (Fig. 1). First, a quantum system has to be controlled sufficiently to hold one bit of quantum information long enough for it to be written, manipulated, and read. In the second stage, small quantum algorithms can be performed; these two stages require that the first five DiVincenzo criteria be satisfied (*15*). The following, more complex stages, however, introduce and require QEC (*3*–*6*). In the third stage, some errors can be corrected by quantum nondemolition readout of error syndromes such as parity. It also becomes possible to stabilize the qubit by feedback into any arbitrary state (*16*, *17*), including dynamical ones (*18*–*21*). This stage was reached first by trapped ions (*22*), by Rydberg atoms (*16*), and most recently by superconducting qubits (*23*–*25*). In the next (fourth) stage, the goal is to realize a quantum memory, where QEC realizes a coherence time that is longer than any of the individual components. This goal is as yet unfulfilled in any system. The final two stages in reaching the ultimate goal of fault-tolerant quantum information processing (*26*) require the ability to do all single-qubit operations on one logical qubit (which is an effective qubit protected by active error correction mechanisms), and the ability to perform gate operations between several logical qubits; in both stages the enhanced coherence lifetime of the qubits should be preserved.

Superconducting Circuits: Hamiltonians by Design

Unlike microscopic entities—electrons, atoms, ions, and photons—on which other qubits are based, superconducting quantum circuits are based on the electrical (LC) oscillator (Fig. 2A) and are macroscopic systems with a large number

[1]Departments of Applied Physics and Physics, Yale University, New Haven, CT 06520, USA. [2]College de France, Place Marcelin Berthelot, F-75005 Paris, France.

*To whom correspondence should be addressed. E-mail: robert.schoelkopf@yale.edu

of (usually aluminum) atoms assembled in the shape of metallic wires and plates. The operation of superconducting qubits is based on two robust phenomena: superconductivity, which is the frictionless flow of electrical fluid through the metal at low temperature (below the superconducting phase transition), and the Josephson effect, which endows the circuit with nonlinearity without introducing dissipation or dephasing.

The collective motion of the electron fluid around the circuit is described by the flux Φ threading the inductor, which plays the role of the center-of-mass position in a mass-spring mechanical oscillator (*27*). A Josephson tunnel junction transforms the circuit into a true artificial atom, for which the transition from the ground state to the excited state ($|g\rangle$-$|e\rangle$) can be selectively excited and used as a qubit, unlike in the pure LC harmonic oscillator (Fig. 2B). The Josephson junction can be placed in parallel with the inductor, or can even replace the inductor completely, as in the case of the so-called "charge" qubits. Potential energy functions of various shapes can be obtained by varying the relative strengths of three characteristic circuit energies associated with the inductance, capacitance, and tunnel element (Fig. 2, B and C). Originally, the three basic types were known as charge (*28*, *29*), flux (*30*–*33*), and phase (*34*, *35*). The performance of all types of qubits has markedly improved as the fabrication, measurement, and materials issues affecting coherence have been tested, understood, and improved. In addition, there has been a diversification of other design variations, such as the quantronium (*36*, *37*), transmon (*38*, *39*), fluxonium (*40*), and "hybrid" (*41*) qubits; all of these are constructed from the same elements but seek to improve performance by reducing their sensitivity to decoherence mechanisms encountered in earlier designs. The continuing evolution of designs is a sign of the robustness and future potential of the field.

When several of these qubits, which are nonlinear oscillators behaving as artificial atoms, are coupled to true oscillators (photons in a microwave cavity), one obtains, for low-lying excitations, an effective multiqubit, multicavity system Hamiltonian of the form

$$\frac{H_{\text{eff}}}{\hbar} = \sum_j \omega_j^q b_j^+ b_j + \frac{\alpha_j (b_j^+ b_j)^2}{2} + \sum_m \omega_m^r a_m^+ a_m + \sum_{j,m} \chi_{j,m} b_j^+ b_j a_m^+ a_m \quad (1)$$

describing anharmonic qubit mode amplitudes indexed by j coupled to harmonic cavity modes indexed by m (*42*). The symbols a, b, and ω refer to the mode amplitudes and frequency, respectively. When driven with appropriate microwave signals, this system can perform arbitrary quantum operations at speeds determined by the nonlinear interaction strengths α and χ, typically (*43*, *44*) resulting in single-qubit gate times within 5 to 50 ns ($\alpha/2\pi \approx 200$ MHz) and two-qubit entangling gate times within 50 to 500 ns ($\chi/2\pi \approx 20$ MHz). We have neglected here the weak induced anharmonicity of the cavity modes.

Proper design of the qubit circuit to minimize dissipation coming from the dielectrics surrounding the metal of the qubit, and to minimize radiation of energy into other electromagnetic modes or the circuit environment, led to qubit transition quality factors Q exceeding 1 million or coherence times on the order of 100 μs, which in turn make possible hundreds or even thousands of operations in one coherence lifetime (see Table 1). One example of this progression, for the case of the Cooper-pair box (*28*) and its descendants, is shown in Fig. 3A. Spectacular improvements have also been accomplished for transmission line resonators (*45*) and the other types of qubits, such the phase qubit (*35*) or the flux qubit (*46*). Rather stringent limits can now be placed on the intrinsic capacitive (*47*) or inductive (*43*) losses of the junction, and we construe this to mean that junction quality is not yet the limiting factor in the further development of superconducting qubits.

Nonetheless, it is not possible to reduce dissipation in a qubit independently of its readout and control systems (*39*). Here, we focus on the most useful and powerful type of readout, which is called a "quantum nondemolition" (QND) measurement. This type of measurement allows a continuous monitoring of the qubit state (*48*, *49*). After a strong QND measurement, the qubit is left in one of two computational states, $|g\rangle$ or $|e\rangle$, depending on the result of the measurement, which has a classical binary value indicating g or e. There are three figures of merit that characterize this type of readout. The first is QND-ness, the probability that the qubit remains in the same state after the measurement, given that the qubit is initially in a definite state $|g\rangle$ or $|e\rangle$. The second is the intrinsic fidelity, the difference between the probabilities—given that the qubit is initially in a definite state $|g\rangle$ or $|e\rangle$—that the readout gives the correct and wrong answers (with this definition, the fidelity is zero when the readout value is uncorrelated with the qubit state). The last and most subtle readout figure of merit is efficiency, which characterizes the ratio of the number of controlled and uncontrolled information channels in the readout. Maximizing this ratio is of utmost importance for performing remote entanglement by measurement (*50*).

Like qubit coherence, and benefiting from it, progress in QND performance has been spectacular (Fig. 3B). It is now possible to acquire more than $N = 2000$ bits of information from a qubit before it decays through dissipation (Fig. 3A), or, to phrase it more crudely, read a qubit once in a time that is a small fraction ($1/N$) of its lifetime. This is a crucial capability for undertaking QEC in the fourth stage of Fig. 1, because in order to fight errors, one has to monitor qubits at a pace faster than the rate at which they occur. Efficiencies in QND superconducting qubit readout are also progressing rapidly and will soon routinely exceed 0.5, as indicated by recent experiments (*25*, *51*).

Is It Just About Scaling Up?

Up to now, most of the experiments have been relatively small scale (only a handful of interacting qubits or degrees of freedom; see Table 1). Furthermore, almost all the experiments so far are

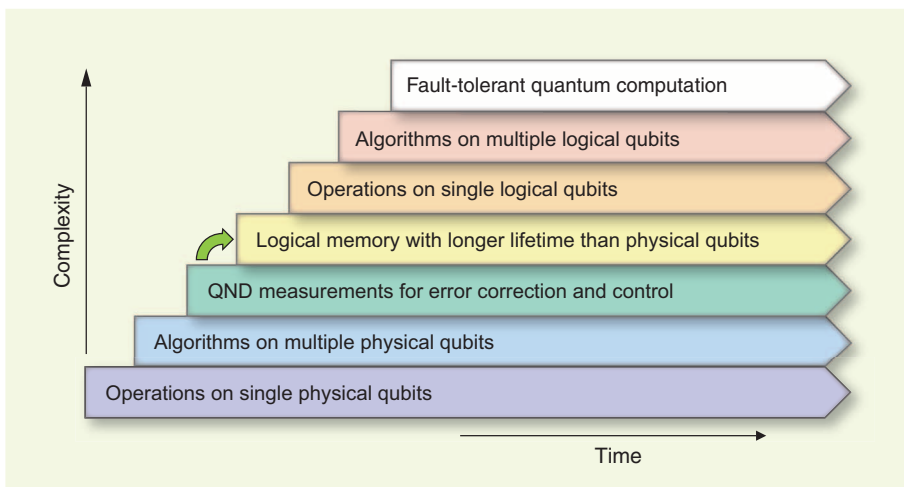

Fig. 1. Seven stages in the development of quantum information processing. Each advancement requires mastery of the preceding stages, but each also represents a continuing task that must be perfected in parallel with the others. Superconducting qubits are the only solid-state implementation at the third stage, and they now aim at reaching the fourth stage (green arrow). In the domain of atomic physics and quantum optics, the third stage had been previously attained by trapped ions and by Rydberg atoms. No implementation has yet reached the fourth stage, where a logical qubit can be stored, via error correction, for a time substantially longer than the decoherence time of its physical qubit components.

Downloaded from www.sciencemag.org on March 8, 2013

"passive"—they seek to maintain coherence only long enough to entangle quantum bits or demonstrate some rudimentary capability before, inevitably, decoherence sets in. The next stages of QIP require one to realize an actual increase in the coherence time via error correction, first only during an idle "memory" state, but later also in the midst of a functioning algorithm. This requires building new systems that are "active," using continuous measurements and real-time feedback to preserve the quantum information through the startling process of correcting qubit errors without actually learning what the computer is calculating. Given the fragility of quantum information, it is commonly believed that the continual task of error correction will occupy the vast majority of the effort and the resources in any large quantum computer.

Using the current approaches to error correction, the next stages of development unfortunately demand a substantial increase in complexity, requiring dozens or even thousands of physical qubits per bit of usable quantum information, and challenging our currently limited abilities to design, fabricate, and control a complex Hamiltonian (second part of Table 1). Furthermore, all of the DiVincenzo engineering margins on each piece of additional hardware still need to be maintained or improved while scaling up. So is advancing to the next stage just a straightforward engineering exercise of mass-producing large numbers of exactly the same kinds of circuits and qubits that have already been demonstrated? And will this mean the end of the scientific innovations that have so far driven progress forward?

We argue that the answers to both questions will probably be "No." The work by the community during the past decade and a half, leading up to the capabilities summarized in the first part of Table 1, may indeed constitute an existence proof that building a large-scale quantum computer is not physically impossible. However, identifying the best, most efficient, and most robust path forward in a technology's development is a task very different from merely satisfying oneself that it should be possible. So far, we have yet to see a dramatic "Moore's law" growth in the complexity of quantum hardware. What, then, are the main challenges to be overcome?

Simply fabricating a wafer with a large number of elements used today is probably not the hard part. After all, some of the biggest advantages of superconducting qubits are that they are merely circuit elements, which are fabricated in clean rooms, interact with each other via connections that are wired up by their designer, and are controlled and measured from the outside with electronic signals. The current fabrication requirements for superconducting qubits are not particularly daunting, especially in comparison to modern semiconductor integrated circuits (ICs). A typical qubit or resonant cavity is a few millimeters in overall size, with features that are mostly a few micrometers (even the smallest Josephson junction sizes are typically 0.2 μm on a side in a qubit). There is successful experience with fabricating and operating superconducting ICs with hundreds to thousands of elements on a chip, such as the transition-edge sensors with SQUID (superconducting quantum interference device) readout amplifiers, each containing several Josephson junctions (*52*), or microwave kinetic inductance detectors composed of arrays of high-Q ($>10^6$) linear resonators without Josephson junctions, which are being developed (*53*) and used to great benefit in the astrophysics community.

Nonetheless, designing, building, and operating a superconducting quantum computer presents substantial and distinct challenges relative to semiconductor ICs or the other existing versions of superconducting electronics. Conventional microprocessors use overdamped logic, which provides a sort of built-in error correction. They do not require high-Q resonances, and clocks or narrowband filters are in fact off-chip and provided by special elements such as quartz crystals. Therefore, small interactions between circuit elements may cause heating or offsets but do not lead to actual bit errors or circuit failures. In contrast, an integrated quantum computer will be essentially a very large collection of very high-Q, phase-stable oscillators, which need to interact only in the ways we program. It is no surprise that the leading quantum information technology has been and today remains the trapped ions, which are the best clocks ever built. In contrast with the ions, however, the artificially made qubits of a superconducting quantum computer will never be perfectly identical (see Table 1). Because operations on the qubits need to be controlled accurately to several significant digits, the properties of each part of the computer would first need to be characterized with some precision, have control signals tailored to match, and remain stable while the rest of the system is tuned up and then operated. The need for high absolute accuracy might therefore be circumvented if we can obtain a very high stability of qubit parameters (Table 1); recent results (*43*) are encouraging and exceed expectations, but more information is needed. The power of electronic control circuitry to tailor waveforms, such as composite pulse sequence techniques well known from nuclear magnetic resonance (*54*), can remove first-order sensitivity to variations in qubit parameters or in control signals, at the expense of some increase in gate time and a requirement for a concomitant increase in coherence time.

Even if the problem of stability is solved, unwanted interactions or cross-talk between the parts of these complex circuits will still cause problems. In the future, we must know and control the Hamiltonian to several digits, and for many qubits. This is beyond the current capability (~1 to 10%; see Table 1). Moreover, the number of measurements and the amount of data required

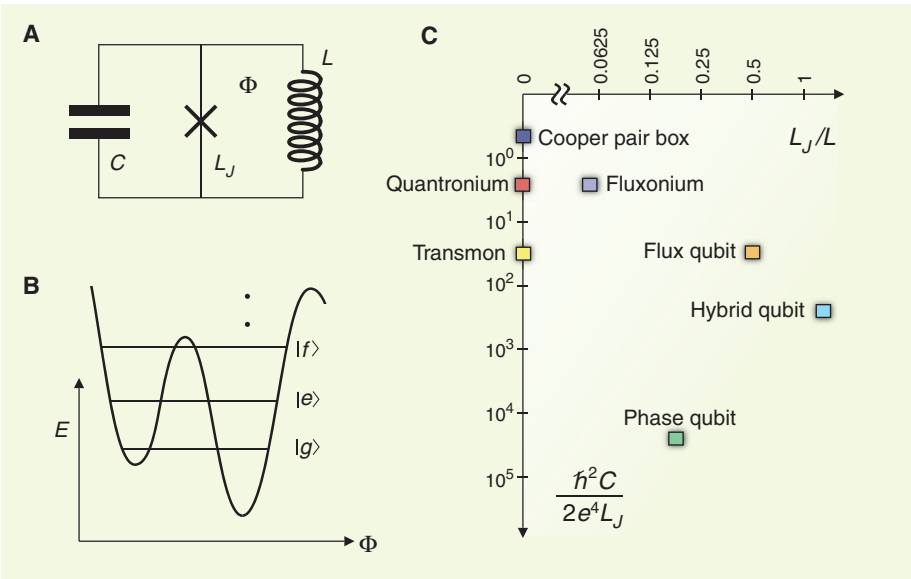

Fig. 2. (**A**) Superconducting qubits consist of simple circuits that can be described as the parallel combination of a Josephson tunnel element (cross) with inductance L_J, a capacitance C, and an inductance L. The flux Φ threads the loop formed by both inductances. (**B**) Their quantum energy levels can be sharp and long-lived if the circuit is sufficiently decoupled from its environment. The shape of the potential seen by the flux Φ and the resulting level structure can be varied by changing the values of the electrical elements. This example shows the fluxonium parameters, with an imposed external flux of ¼ flux quantum. Only two of three corrugations are shown fully. (**C**) A Mendeleev-like but continuous "table" of artificial atom types: Cooper pair box (*29*), flux qubit (*33*), phase qubit (*35*), quantronium (*37*), transmon (*39*), fluxonium (*40*), and hybrid qubit (*41*). The horizontal and vertical coordinates correspond to fabrication parameters that determine the inverse of the number of corrugations in the potential and the number of levels per well, respectively.

Downloaded from www.sciencemag.org on March 8, 2013

to characterize a system of entangled qubits appears to grow exponentially with their number, so the new techniques for "debugging" quantum circuits (*55*) will have to be further developed. In the stages ahead, one must design, build, and operate systems with more than a few dozen degrees of freedom, which, as a corollary to the power of quantum computation, are not even possible to simulate classically. This suggests that large quantum processors should perhaps consist of smaller modules whose operation and functionality can be separately tested and characterized.

A second challenge in Hamiltonian control (or circuit cross-talk) is posed by the need to combine long-lived qubits with the fast readout, qubit reset or state initialization, and high-speed controls necessary to perform error correction. This means that modes with much lower Q (~1000 for a 50-ns measurement channel) will need to be intimately mixed with the long-lived qubits with very high Q (~10^6 to 10^9), which requires exquisite isolation and shielding between the parts of our high-frequency integrated circuit. If interactions between a qubit and its surroundings cause even 0.1% of the energy of a qubit to leak into a low-Q mode, we completely spoil its lifetime. Although the required levels of isolation are probably feasible, these challenges have not yet been faced or solved by conventional superconducting or semiconducting circuit designers. In our view, the next stages of development will require appreciable advances, both practical and conceptual, in all aspects of Hamiltonian design and control.

What Will We Learn About Active Architectures During the Next Stage?

How long might it take to realize robust and practical error correction with superconducting circuits? This will depend on how rapidly the experimental techniques and capabilities (Fig. 3, A and B) continue to advance, but also on the architectural approach to QEC, which might considerably modify both the necessary circuit complexity and the performance limits (elements of Table 1) that are required. Several different approaches exist that are theoretically well developed (*1*, *2*) but remain relatively untested in the real world.

The canonical models for QEC are the stabilizer codes (*3*–*6*). Here, information is redundantly encoded in a register of entangled physical qubits (typically, at least seven) to create a single logical qubit. Assuming that errors occur singly, one detects them by measuring a set of certain collective properties (known as stabilizer operators) of the qubits, and then applies appropriate additional gates to undo the errors before the desired information is irreversibly corrupted. Thus, an experiment to perform gates between a pair of logically encoded qubits might take a few dozen qubits, with hundreds to thousands of individual operations. To reach a kind of "break-even" point and perform correctly, it is required that there should be less than one error on average during a single pass of the QEC. For a large calculation, the codes must then be concatenated, with each qubit again being replaced by a redundant register, in a treelike hierarchy. The so-called error-correction threshold, where the resources required for this process of expansion begin to converge, is usually estimated (*26*) to lie in the range of error rates of 10^{-3} to 10^{-4}, requiring values of 10^3 to 10^4 for the elements of Table 1. Although these performance levels and complexity requirements might no longer be inconceivable, they are nonetheless beyond the current state of the art, and rather daunting.

A newer approach (*56*–*58*) is the "surface code" model of quantum computing, where a large number of identical physical qubits are connected in a type of rectangular grid (or "fabric"). By having specific linkages between groups of four adjacent qubits, and fast QND measurements of their parity, the entire fabric is protected against errors. One appeal of this strategy is that it requires a minimum number of different types of elements, and once the development of the elementary cell is successful, the subsequent stages of development (the fourth, fifth, and sixth stages in Fig. 1) might simply be achieved by brute-force scaling. The second advantage is that the allowable error rates are appreciably higher, even on the order of current performance levels (a couple of percent). However, there are two drawbacks: (i) the resource requirements (between 100 and 10,000 physical qubits per logical qubit) are perhaps even higher than in the QEC codes (*58*), and (ii) the desired emergent properties of this fabric are obtained only after hundreds, if not thousands, of qubits have been assembled and tested.

A third strategy is based on modules of nested complexity. The basic element is a small register (*50*) consisting of a logical memory qubit, which stores quantum information while performing the usual kind of local error correction, and some additional communication qubits that can interact with the memory and with other modules. By entangling the communication qubits, one can distribute the entanglement and eventually perform a general computation between modules. Here, the operations between the communication bits can have relatively high error rates, or even be probabilistic and sometimes fail entirely, provided that the communication schemes have some modest redundancy and robustness. The adoption of techniques from cavity quantum electrodynamics (QED) (*59*) and the advantages for

Table 1. Superconducting qubits: Desired parameter margins for scalability and the corresponding demonstrated values. Desired capability margins are numbers of successful operations or realizations of a component before failure. For the stability of the Hamiltonian, capability is the number of Ramsey shots that meaningfully would provide one bit of information on a parameter (e.g., the qubit frequency) during the time when this parameter has not drifted. Estimated current capability is expressed as number of superconducting qubits, given best decoherence times and success probabilities. Demonstrated successful performance is given in terms of the main performance characteristic of successful operation or Hamiltonian control (various units). A reset qubit operation forces a qubit to take a particular state. A Rabi flop denotes a single-qubit π rotation. A swap to bus is an operation to make a two-qubit entanglement between distant qubits. In a readout qubit operation, the readout must be QND or must operate on an ancilla without demolishing any memory qubit of the computer. Stability refers to the time scale during which a Hamiltonian parameter drifts by an amount corresponding to one bit of information, or the time scale it would take to find all such parameters in a complex system to this precision. Accuracy can refer to the degree to which a certain Hamiltonian symmetry or property can be designed and known in advance, the ratio by which a certain coupling can be turned on and off during operation, or the ratio of desired to undesired couplings. Yield is the number of quantum objects with one degree of freedom that can be made without failing or being out of specification to the degree that the function of the whole is compromised. Complexity is the overall number of interacting, but separately controllable, entangled degrees of freedom in a device. Question marks indicate that more experiments are needed for a conclusive result. Values given in rightmost column are compiled from recently published data and improve on a yearly basis.

Requirement for scalability	Desired capability margins	Estimated current capability	Demonstrated successful performance
QI operation			
Reset qubit	10^2 to 10^4	50	Fidelity ≥ 0.995 (*17*)
Rabi flop	10^2 to 10^4	1000	Fidelity ≥ 0.99 (*69*, *70*)
Swap to bus	10^2 to 10^4	100	Fidelity ≥ 0.98 (*71*)
Readout qubit	10^2 to 10^4	1000	Fidelity ≥ 0.98 (*51*)
System Hamiltonian			
Stability	10^6 to 10^9	?	$\delta f/f$ in 1 day < 2×10^{-7} (*43*)
Accuracy	10^2 to 10^4	10 to 100	1 to 10% (*43*)
Yield	>10^4	?	?
Complexity	10^4 to 10^7	10?	1 to 10 qubits (*61*)

Downloaded from www.sciencemag.org on March 8, 2013

routing microwave photons with transmission lines [now known as circuit QED (*12*, *44*, *60*)] might make on-chip versions of these schemes with superconducting circuits an attractive alternative. Although this strategy can be viewed as less direct and requires a variety of differing parts, its advantage is that stringent quality tests are easier to perform at the level of each module, and hidden design flaws might be recognized at earlier stages. Finally, once modules with sufficient performance are in hand, they can then be programmed to realize any of the other schemes in an additional "software layer" of error correction.

Finally, the best strategy might include ideas that are radically different from those considered standard fare in quantum information science. Much may be gained by looking for shortcuts that are hardware-specific and optimized for the particular strengths and weaknesses of a particular technology. For instance, all of the schemes described above are based on a "qubit register model," where one builds the larger Hilbert space and the required redundancy from a collection of many individual two-level systems. But for superconducting circuits, the "natural units" are oscillators with varying degrees of nonlinearity, rather than true two-level systems. The use of noncomputational states beyond the first two levels is of course known in atomic physics, and has already been used as a shortcut to two- and three-qubit gates in superconducting circuits (*23*, *61*). Under the right conditions, the use of nonlinear oscillators with many accessible energy levels could replace the function of several qubits without introducing new error mechanisms. As a concrete example of the power of this approach, a recent proposal (*62*) for using a cavity as a protected memory requires only one ancilla and one readout channel—a real decrease in complexity.

How architectural choices like these affect our ability to perform error-corrected information processing will be a key scientific question occupying this field in the near future, and will probably take several years to resolve. The knowledge garnered in this process has the potential to substantially change the resources required for building quantum computers, quantum simulators, or quantum communication systems that are actually useful.

The Path Forward

The field of QIP with superconducting circuits has made dramatic progress, and has already demonstrated most of the basic functionality with reasonable (or even surprising) levels of performance. Remarkably, we have not yet encountered any fundamental physical principles that would prohibit the building of quite large quantum processors. The demonstrated capabilities of superconducting circuits, as in trapped ions and cold atoms, mean that QIP is beginning what may be one of its most interesting phases of development. Here, one enters a true terra incognita for complex quantum systems, as QEC becomes more than a theoretical discipline. As in the past, this era will include new scientific innovations and basic questions to be answered. Even if this stage is successful, there will remain many further stages of development and technical challenges to be mastered before useful quantum information processing could become a reality. However, we think it is unlikely to become a purely technological enterprise, like sending a man to the Moon, in the foreseeable future. After all, even the Moore's law progression of CMOS integrated circuits over the past four decades has not brought the end of such fields as semiconductor physics or nanoscience, but rather enabled, accelerated, and steered them in unanticipated directions. We feel that future progress in quantum computation will always

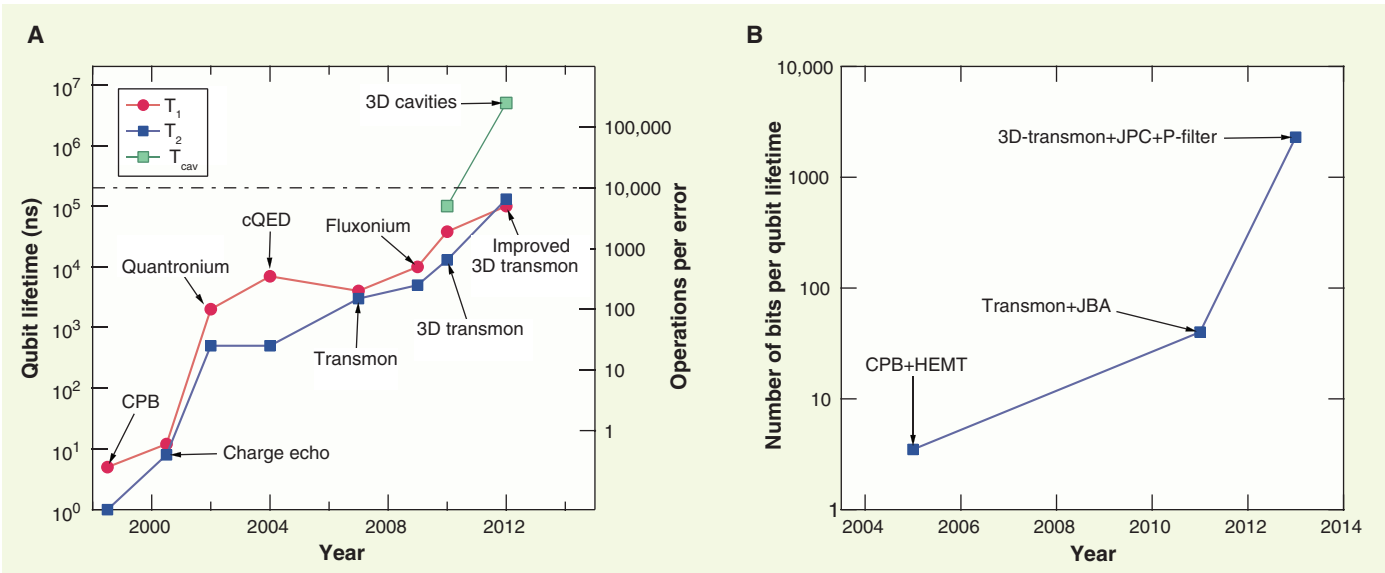

Fig. 3. Examples of the "Moore's law" type of exponential scaling in performance of superconducting qubits during recent years. All types have progressed, but we focus here only on those in the leftmost part of Fig. 2C. (**A**) Improvement of coherence times for the "typical best" results associated with the first versions of major design changes. The blue, red, and green symbols refer to qubit relaxation, qubit decoherence, and cavity lifetimes, respectively. Innovations were introduced to avoid the dominant decoherence channel found in earlier generations. So far an ultimate limit on coherence seems not to have been encountered. Devices other than those in Fig. 2C: charge echo (*63*), circuit QED (*44*), 3D transmon (*43*), and improved 3D transmon (*64*, *65*). For comparison, superconducting cavity lifetimes are given for a 3D transmon and separate 3D cavities (*66*). Even longer times in excess of 0.1 s have been achieved in similar 3D cavities for Rydberg atom experiments [e.g., (*67*)]. (**B**) Evolution of superconducting qubit QND readout. We plot versus time the main figure of merit, the number of bits that can be extracted from the qubit during its T1 lifetime (this number combines signal-to-noise ratio and speed). This quantity can also be understood as the number of measurements, each with one bit of precision, that would be possible before an error occurs. Data points correspond to the following innovations in design: a Cooper-pair box read by off-resonance coupling to a cavity whose frequency is monitored by a microwave pulse analyzed using a semiconductor high–electron mobility transistor amplifier (CPB+HEMT) [also called dispersive circuit QED (*68*)], an improved amplification chain reading a transmon using a superconductor preamplifier derived from the Josephson bifurcation amplifier (transmon+JBA) (*49*), and further improvement with another superconductor preamplifier derived from the Josephson parametric converter (*51*) combined with filter in 3D transmon cavity eliminating Purcell effect (3D-transmon+JPC+P-filter). Better amplifier efficiency, optimal signal processing, and longer qubit lifetimes are expected to maintain the rapid upward trend.

Downloaded from www.sciencemag.org on March 8, 2013

require the robust, continual development of both scientific understanding and engineering skill within this new and fascinating arena.

References and Notes

1. M. A. Nielsen, I. L. Chuang, *Quantum Computation and Quantum Information* (Cambridge Univ. Press, Cambridge, 2000).
2. N. D. Mermin, *Quantum Computer Science* (Cambridge Univ. Press, Cambridge, 2007).
3. P. W. Shor, *Phys. Rev. A* **52**, R2493 (1995).
4. A. Steane, *Proc. R. Soc. London Ser. A* **452**, 2551 (1996).
5. E. Knill, R. Laflamme, *Phys. Rev. A* **55**, 900 (1997).
6. D. Gottesman, thesis, California Institute of Technology (1997).
7. S. Lloyd, *Science* **273**, 1073 (1996).
8. See, for example, J. I. Cirac, P. Zoller, Goals and opportunities in quantum simulations. *Nat. Phys.* **8**, 264 (2012) and other articles in this special issue.
9. H. J. Kimble, *Nature* **453**, 1023 (2008).
10. Direct quantum spin simulations, such as aimed at by the machine constructed by D-Wave Systems Inc., are outside the scope of this article.
11. M. H. Devoret, J. M. Martinis, *Quant. Inf. Proc.* **3**, 381 (2004).
12. R. J. Schoelkopf, S. M. Girvin, *Nature* **451**, 664 (2008).
13. J. Clarke, F. K. Wilhelm, *Nature* **453**, 1031 (2008).
14. J. Q. You, F. Nori, *Phys. Today* **58**, 42 (2005).
15. D. P. DiVincenzo, *Fortschr. Phys.* **48**, 771 (2000).
16. C. Sayrin *et al.*, *Nature* **477**, 73 (2011).
17. K. Geerlings *et al.*, http://arxiv.org/abs/1211.0491 (2012).
18. R. Vijay *et al.*, *Nature* **490**, 77 (2012).
19. K. W. Murch *et al.*, *Phys. Rev. Lett.* **109**, 183602 (2012).
20. S. Diehl *et al.*, *Nat. Phys.* **4**, 878 (2008).
21. J. T. Barreiro *et al.*, *Nature* **470**, 486 (2011).
22. P. Schindler *et al.*, *Science* **332**, 1059 (2011).
23. M. D. Reed *et al.*, *Nature* **482**, 382 (2012).
24. D. Ristè, C. C. Bultink, K. W. Lehnert, L. DiCarlo, *Phys. Rev. Lett.* **109**, 240502 (2013).
25. P. Campagne-Ibarq *et al.*, http://arxiv.org/abs/1301.6095 (2013).
26. J. Preskill, http://arxiv.org/abs/quant-ph/9712048 (1997).
27. M. H. Devoret, in *Quantum Fluctuations*, S. Reynaud, E. Giacobino, J. Zinn-Justin, Eds. (Elsevier Science, Amsterdam, 1997).
28. V. Bouchiat, D. Vion, P. Joyez, D. Esteve, M. H. Devoret, *Phys. Scr.* **1998**, 165 (1998).
29. Y. Nakamura, Yu. A. Pashkin, J. S. Tsai, *Nature* **398**, 786 (1999).
30. J. E. Mooij *et al.*, *Science* **285**, 1036 (1999).
31. C. H. van der Wal *et al.*, *Science* **290**, 773 (2000).
32. J. R. Friedman, V. Patel, W. Chen, S. K. Tolpygo, J. E. Lukens, *Nature* **406**, 43 (2000).
33. I. Chiorescu, Y. Nakamura, C. J. Harmans, J. E. Mooij, *Science* **299**, 1869 (2003).
34. J. M. Martinis, S. Nam, J. Aumentado, C. Urbina, *Phys. Rev. Lett.* **89**, 117901 (2002).
35. J. Martinis, *Quant. Inf. Proc.* **8**, 81 (2009).
36. A. Cottet *et al.*, *Physica C* **367**, 197 (2002).
37. D. Vion *et al.*, *Science* **296**, 886 (2002).
38. J. Koch *et al.*, *Phys. Rev. A* **76**, 042319 (2007).
39. A. A. Houck *et al.*, *Phys. Rev. Lett.* **101**, 080502 (2008).
40. V. E. Manucharyan, J. Koch, L. I. Glazman, M. H. Devoret, *Science* **326**, 113 (2009).
41. M. Steffen *et al.*, *Phys. Rev. Lett.* **105**, 100502 (2010).
42. S. E. Nigg *et al.*, *Phys. Rev. Lett.* **108**, 240502 (2012).
43. H. Paik *et al.*, *Phys. Rev. Lett.* **107**, 240501 (2011).
44. A. Wallraff *et al.*, *Nature* **431**, 162 (2004).
45. A. Megrant *et al.*, *Appl. Phys. Lett.* **100**, 113510 (2012).
46. J. Bylander *et al.*, *Nat. Phys.* **7**, 565 (2011).
47. Z. Kim *et al.*, *Phys. Rev. Lett.* **106**, 120501 (2011).
48. A. Palacios-Laloy *et al.*, *Nat. Phys.* **6**, 442 (2010).
49. R. Vijay, D. H. Slichter, I. Siddiqi, *Phys. Rev. Lett.* **106**, 110502 (2011).
50. L. M. Duan, B. B. Blinov, D. L. Moehring, C. Monroe, *Quantum Inf. Comput.* **4**, 165 (2004).
51. M. Hatridge *et al.*, *Science* **339**, 178 (2013).
52. D. Bintley *et al.*, *Proc. SPIE* **8452**, 845208 (2012).
53. J. Zmuidzinas, *Annu. Rev. Condens. Matter Phys.* **3**, 169 (2012).
54. J. Jones, NMR Quantum Computation (nmr.physics.ox.ac.uk/pdfs/lhnmrqc.pdf).
55. M. P. da Silva, O. Landon-Cardinal, D. Poulin, *Phys. Rev. Lett.* **107**, 210404 (2011).
56. S. Bravyi, A. Yu. Kitaev, *Quantum Computers Comput.* **2**, 43 (2001).
57. M. H. Freedman, D. A. Meyer, *Found. Comput. Math.* **1**, 325 (2001).
58. A. G. Fowler, M. Mariantoni, J. M. Martinis, A. N. Cleland, *Phys. Rev. A* **86**, 032324 (2012).
59. S. Haroche, J. M. Raimond, *Exploring the Quantum: Atoms, Cavities, and Photons* (Oxford Univ. Press, Oxford, 2006).
60. C. Eichler *et al.*, *Phys. Rev. Lett.* **106**, 220503 (2011).
61. M. Mariantoni *et al.*, *Nat. Phys.* **7**, 287 (2011).
62. Z. Leghtas *et al.*, http://arxiv.org/abs/1207.0679.
63. Y. Nakamura, Y. A. Pashkin, T. Yamamoto, J. S. Tsai, *Phys. Rev. Lett.* **88**, 047901 (2002).
64. A. Sears *et al.*, *Phys. Rev. B* **86**, 180504 (2012).
65. C. Rigetti *et al.*, *Phys. Rev. B* **86**, 100506 (2012).
66. M. Reagor *et al.*, http://arxiv.org/abs/1302.4408 (2013).
67. S. Kuhr *et al.*, *Appl. Phys. Lett.* **90**, 164101 (2007).
68. A. Wallraff *et al.*, *Phys. Rev. Lett.* **95**, 060501 (2005).
69. E. Magesan *et al.*, *Phys. Rev. Lett.* **109**, 080505 (2012).
70. E. Lucero *et al.*, *Phys. Rev. Lett.* **100**, 247001 (2008).
71. J. M. Chow *et al.*, *Phys. Rev. Lett.* **109**, 060501 (2012).

Acknowledgments: We thank L. Frunzio, S. Girvin, L. Glazman, and L. Jiang for their contributions. Supported by the U.S. Army Research Office, U.S. National Security Agency Laboratory for Physical Science, U.S. Intelligence Advanced Research Projects Activity, NSF, and Yale University.

10.1126/science.1231930

Downloaded from www.sciencemag.org on March 8, 2013

REVIEW

Quantum Spintronics: Engineering and Manipulating Atom-Like Spins in Semiconductors

David D. Awschalom,[1]* Lee C. Bassett,[1] Andrew S. Dzurak,[2] Evelyn L. Hu,[3] Jason R. Petta[4]

The past decade has seen remarkable progress in isolating and controlling quantum coherence using charges and spins in semiconductors. Quantum control has been established at room temperature, and electron spin coherence times now exceed several seconds, a nine–order-of-magnitude increase in coherence compared with the first semiconductor qubits. These coherence times rival those traditionally found only in atomic systems, ushering in a new era of ultracoherent spintronics. We review recent advances in quantum measurements, coherent control, and the generation of entangled states and describe some of the challenges that remain for processing quantum information with spins in semiconductors.

In a marriage of quantum physics, information theory, and nanoscale engineering, quantum information science endeavors to build machines that can use the power of quantum mechanics for practical purposes. Such machines have great potential, including cryptography guaranteed by the laws of physics, quantum-enhanced sensing and imaging technology, and quantum computers able to crack problems inaccessible to even the most powerful classical computers of the foreseeable future.

The complexity of building quantum machines is a fantastic challenge, and recent years have seen a vast array of proposals for quantum information processing in diverse systems. Although specific requirements vary considerably, there are a few generalized prerequisites for quantum computers (*1*). The target quantum system must be controllable, in the sense that it can be initialized, manipulated, and read out to achieve a computation; it must be correctable, such that unavoidable errors can be detected and compensated; and it must be scalable, such that a linear increase in the effective size of the system—corresponding to an exponential increase in computing power—does not require an exponential increase of resources. The first two requirements require some degree of isolation of the quantum system from its environment, to keep quantum information from "leaking away" (decohering) at a rate faster than the computation is achieved. Because no system is entirely free of decoherence, the goal of most approaches is to balance the need for isolation with the ability to accurately and quickly control the system, ideally in architectures with potential for scaling to larger systems once the fundamentals are established.

[1]Center for Spintronics and Quantum Computation, University of California, Santa Barbara, Santa Barbara, CA 93106, USA. [2]Centre for Quantum Computation and Communication Technology, School of Electrical Engineering and Telecommunications, The University of New South Wales, Sydney 2052, Australia. [3]School of Engineering and Applied Sciences, Harvard University, Cambridge, MA 02138, USA. [4]Department of Physics, Princeton University, Princeton, NJ 08544, USA.

*To whom correspondence should be addressed. E-mail: awsch@physics.ucsb.edu

Nature's own atoms and ions, isolated in vacuum, served as the first quantum information test beds, with many groundbreaking experiments in atomic and optical physics demonstrating exquisite control of individual quantum systems. Inspired by this success, solid-state physicists have recently developed a wide array of "designer atoms" based on semiconductor nanostructures whose quantum states can also be coherently controlled (*2*). The spins of individual electrons and nuclei, in particular, offer a promising combination of environmental isolation and controllability, with wide flexibility in terms of materials and design. Furthermore, solid-state technologies offer the promise of large-scale integration using fabrication processes developed by the semiconductor industry (*3*). Approaches are markedly varied, employing different materials, temperatures, device structures, and both electrical and optical measurements. We focus on several key advances of the past few years in controlling quantum coherence and entanglement in several semiconductor architectures, and outline the major challenges and goals ahead.

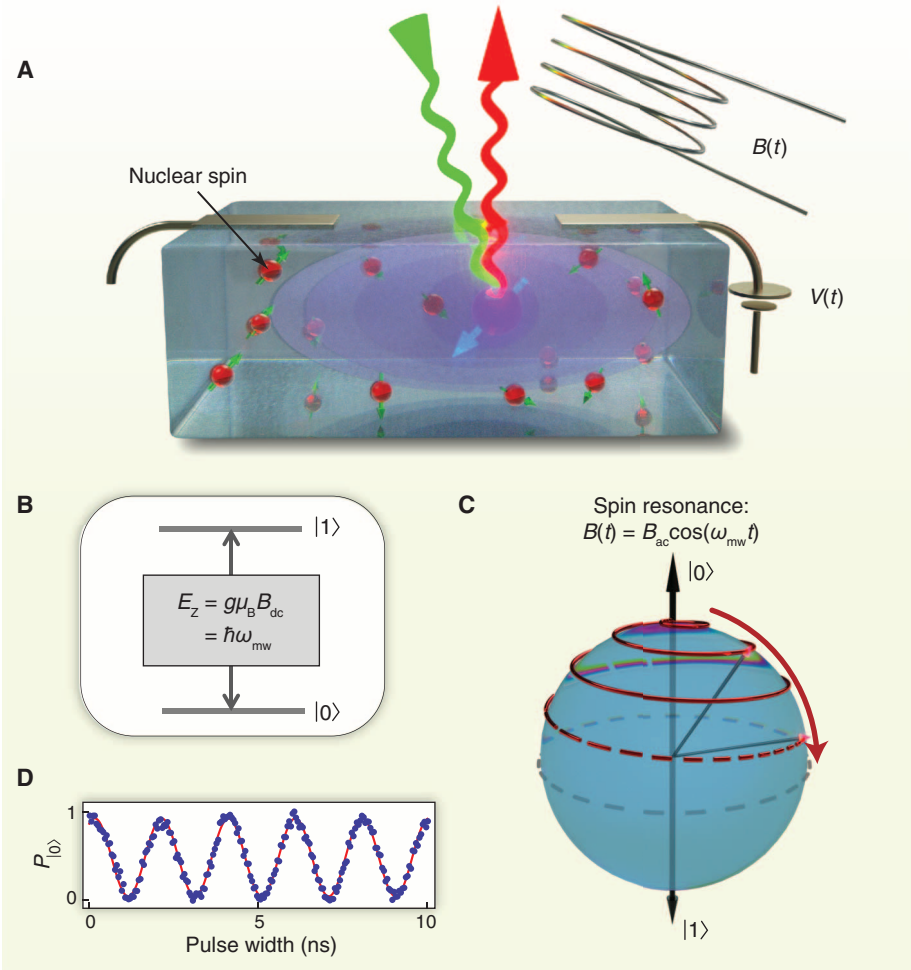

Fig. 1. (**A**) Single electron spins (blue arrow) can be confined in solid-state systems and manipulated with various "control knobs," including gate voltages [$V(t)$], microwave magnetic fields [$B(t)$], and light (green and red wiggly arrows). Quantum coherence is lost (fading purple cloud) through interactions with the local environment of, for example, nuclear spins (green arrows), phonons, or leaky mirrors in a cavity. Recent advances in materials science have made it possible to achieve electron spin coherence times up to several seconds (*15*), rivaling those traditionally found only in atomic systems. (**B**) A single electron spin placed in a dc magnetic field, B_{dc}, forms a quantum bit with states $|0\rangle$ and $|1\rangle$ corresponding to parallel and antiparallel spin alignment to the field, split by the Zeeman energy E_Z. (**C**) The application of an oscillating magnetic field $B(t)$ perpendicular to B_{dc} and resonant with the Zeeman energy causes the qubit to oscillate between states $|0\rangle$ and $|1\rangle$ at the Rabi frequency (changing the qubit amplitude, θ), while the phase ϕ accumulates due to precession in B_{dc}. (**D**) Rabi nutations of a single electronic spin in diamond, measured optically, showing the probability to measure the state $|0\rangle$ as a function of the width of an ac magnetic field pulse. Conventional electron spin resonance has focused on the dynamics of large ensembles of $\gtrsim 10^{15}$ spins; it has recently become possible to coherently control single-spin dynamics. [Originally published in (*60*) and adapted with permission]

Spin Qubits for Computation

The spin carried by a single electron is a prototypical quantum bit, or qubit (Fig. 1A). In an external magnetic field, B_{dc}, the spin's energy levels are quantized into states where the magnetic moment points either parallel or antiparallel to the magnetic field. These two states are separated by the Zeeman energy, $E_Z = g\mu_B B_{dc}$, where g is the Landé g factor and μ_B is the Bohr magneton (Fig. 1B). By identifying one spin orientation as "0" and the other as "1," spins can serve as the logical elements for Boolean computation. Even as classical bits, spins offer advantages over today's charge-based microprocessors and form the basis for emerging technologies termed spintronics. The more ambitious goal of building a spin-based quantum computer requires not only manipulation of the spin eigenstates $|0\rangle$ and $|1\rangle$ but also coherent superpositions of the form $|\psi\rangle = \cos(\theta/2)|0\rangle + e^{i\phi}\sin(\theta/2)|1\rangle$, where both the amplitude, θ, and the phase, ϕ, must be controlled with high precision. Most challengingly, quantum computing requires the creation and coherent control of nonclassical correlations—i.e., entanglement—between distinct qubits in the device and preservation of these fragile many-body states on time scales long enough to perform calculations. At the few-qubit level, both of these goals have been met in recent years.

As qubits, spins in semiconductors have distinct technical advantages. Host-dependent band structure and spin-orbit interactions imprint critical characteristics on spins in different materials, providing widely tunable qubit properties. Particularly in materials where spin-orbit coupling is weak, spins are relatively insensitive to many sources of decoherence in solid-state systems, including electrical noise and thermal vibrations of the semiconductor lattice. Furthermore, experimental methods for coherent control of single-spin qubit states are now established (Fig. 1C), building on decades of research in magnetic resonance. Figure 2 shows examples of four types of spin qubits featured in current research. Despite vastly different methods for production and individual advantages and challenges of the different systems, coherent quantum control of individual qubits has been demonstrated in all cases, and in several systems entangled multiqubit devices have been realized in recent years.

Following a proposal based on spins in quantum dots (*4*), the first semiconductor qubits were based on group III/V materials (*5*), taking advantage of the well-developed growth of ultrapure GaAs/AlGaAs heterostructures. Heterostructures provide the means to confine electrons and/or holes into reduced dimensions, to the ultimate limit of a zero-dimensional "box"—a quantum dot (QD)—containing a single spin. QDs can be formed either through top-down approaches

Downloaded from www.sciencemag.org on March 8, 2013

in which nanofabricated surface electrodes deplete charges from a buried two-dimensional electron gas (Fig. 2A) or through bottom-up growth techniques in which small islands of a III/V alloy, typically InAs, self-assemble on a GaAs surface (Fig. 2B).

The small magnetic moment of the electron renders it highly insensitive to the local environment, leading to long spin coherence times. At the same time, however, rapid spin control using conventional electron spin resonance requires large ac magnetic field amplitudes that are difficult to produce in cryogenic environments. Qubit selectivity is also exacerbated in nanoscale devices (Fig. 2A), where each spin needs to be individually controlled without disturbing its nearest neighbors only ≈50 nm away. Two approaches have been developed to circumvent these challenges. The first is to use quantum interference of two-electron spin states for rapid quantum control. By rapidly tuning through an avoided crossing in the energy-level diagram, two electrons in a correlated (e.g., singlet) state can be "split" and then recombined after a free evolution time, enabling nanosecond spin rotations without the application of an electron spin resonance field (*6*). Another approach to single-spin control harnesses the strong spin-orbit interactions intrinsic to materials such as InAs and InSb. With such "spin-orbit qubits," it is possible to perform spin rotations using electric rather than magnetic fields, which are easier to generate and localize in a device (*7*).

Self-assembled QDs in III/V materials confine both electrons and holes and can therefore support optical transitions between a ground-state spin qubit configuration (e.g., a single electron or hole) and optically excited "excitons" with additional bound electron-hole pairs. Strong spin-orbit interactions give rise to optical transitions with strict spin- and polarization-dependent selection rules, and relatively large optical dipole moments (compared with atoms) make these transitions highly efficient. These key features enable coherent optical control of the QD spin state using ultrafast (picosecond-scale) pulses of light (*8*, *9*) and the generation of entanglement between the qubit spin state and a single photon emitted by the QD (*10*, *11*). Such light-matter coupling is the key to building distributed networks of qubit nodes with coherent information transfer mediated by photons.

Only a few years ago, the intrinsic "spin bath" of host nuclear spins in III/V materials was the primary impediment to achieving long spin coherence times in these systems. This problem has been practically solved through the use of dynamical decoupling protocols that can extend the useful coherence time by orders of magnitude (*12*–*14*). Still, it helps to remove as many potential noise sources as possible. Group IV semiconductors can be isotopically purified to provide a nearly spin-free environment consisting only of spin-zero nuclei such as ^{12}C and ^{28}Si, and weaker spin-orbit coupling than in III/V materials reduce susceptibility to electrical and thermal noise. With recent reports of electron-spin coherence times measured in seconds (*15*) and nuclear spin coherence times of minutes (*16*) for neutral donor atoms in ^{28}Si, for example, these materials are poised to have a major role in coming years.

Silicon, the dominant material used for conventional microprocessor chips, was identified early on as a prime candidate for quantum information processing through several proposals to use the electron and/or nuclear spins of individual donor atoms, particularly phosphorus, as spin qubits (*17*, *18*). The first such single-atom qubit in silicon (Fig. 2C) used the spin of a phosphorus donor electron implanted into a silicon chip as the qubit (*19*). An adjacent metal-oxide-semiconductor–based single-electron transistor implements a spin-to-charge conversion protocol for initialization and readout (*20*) similar to that developed for III/V quantum dots (*21*), and coherent control is achieved through electron spin resonance using an integrated microwave transmission line. Fabricated using a silicon substrate with the natural 4.7% isotopic fraction of ^{29}Si, the spin coherence time of the device in (*19*) was limited by the nuclear spin bath to $T_2 \approx 200$ μs, but it is anticipated that similar devices constructed from isotopically enriched ^{28}Si substrates will open a path to the exceptional coherence times (≈1 s) that have been measured for bulk ^{28}Si:P ensembles (*15*). The device depicted in Fig. 2C has also been used to demonstrate a nuclear spin qubit (*22*) based on the ^{31}P dopant nucleus. These nuclear spins could serve as long-lived quantum memories (*18*) in future quantum processors.

In some ways, dopant-based qubits in silicon represent a powerful combination of both top-down and bottom-up fabrication approaches, because a natural and highly reproducible qubit (a single atom) is controllably placed within a nanofabricated electronic device. At the same

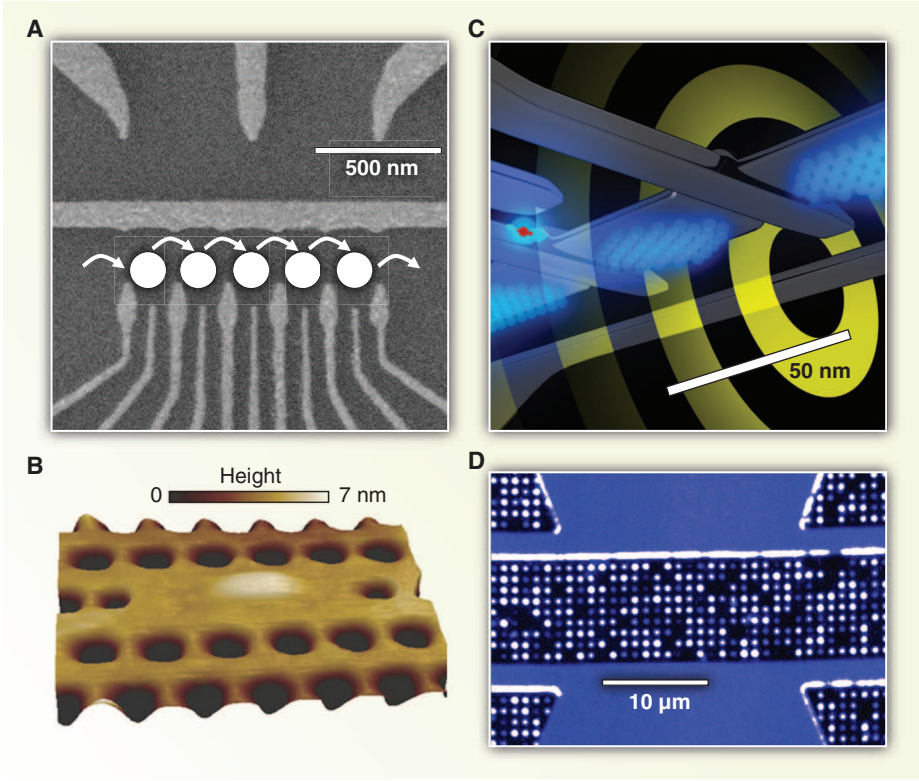

Fig. 2. Semiconductor qubit architectures. (**A**) Scanning electron microscope image of a gate-defined quintuple QD in a GaAs/AlGaAs heterostructure. Each QD is designed to contain one or two electron spins. (**B**) Atomic force microscope image of a single self-assembled InAs QD strongly coupled to a GaAs photonic crystal cavity, which is used to confine photons to small regions of space. Originally published in (*46*) and adapted with permission. (**C**) Schematic of a spin qubit device based on a single phosphorus dopant atom (red) implanted in silicon (*19*). The qubit electron spin is initialized and measured electronically through spin-dependent tunnel coupling to a nanofabricated single-electron transistor (gray) and manipulated using pulsed ac magnetic fields (yellow concentric circles) delivered by an integrated microwave transmission line. Image credit: W. Algar-Chuklin. (**D**) Confocal microscope image showing an array of implanted nitrogen vacancy centers in diamond aligned to a microwave transmission line. [Adapted with permission from (*61*); copyright (2010) American Chemical Society]

Downloaded from www.sciencemag.org on March 8, 2013

time, artificial atoms formed using gate electrodes in analogy with QDs in III/V heterostructures have also met with success (*18*). Coherent oscillations between two-electron singlet and triplet states of a double QD defined in a Si/SiGe heterostructure were demonstrated in 2012 (*23*), in direct analogy with experiments in III/V QDs (*21*). The measured dephasing time $T_2^* \approx 360$ ns was more than an order of magnitude longer than in GaAs thanks to the much weaker hyperfine coupling in natural silicon, and further improvements are expected for devices using isotopically enriched ^{28}Si.

Another group IV material with great promise for quantum information technology is diamond. With its large 5.5 eV band gap, diamond supports a plethora of optically active point defects, many of which are paramagnetic and could therefore serve as spin qubits. The most intensely studied of these is the nitrogen-vacancy (NV) center, consisting of a substitutional nitrogen atom adjacent to a vacancy in the diamond crystal. In its negatively charged ground state, the NV center is an electron spin triplet, and a special set of optical transitions facilitate the initialization and measurement of its spin state simply through optical excitation and fluorescence detection, respectively (*24*). Diamond's unique properties, particularly weak spin-orbit interactions, an extremely high Debye temperature (limiting spin-lattice relaxation), and the large band gap that energetically isolates interband electronic states, endow NV center spins with remarkable coherence properties that persist up to room temperature. Furthermore, isotopic purification of spin-free ^{12}C diamond leads to ultralong coherence times, up to several milliseconds at room temperature (*25*). With on-chip microwave-frequency waveguides enabling quantum control operations on subnanosecond time scales (*26*), more than one million coherent operations can be performed within the NV center's spin coherence time.

A key feature of NV center spin qubits is access not only to the electronic spin state but also to the individual nuclear spins of the intrinsic nitrogen atom and proximal ^{13}C nuclei (*27*). This makes each NV center a small "quantum register" consisting of several individually addressable nuclear spin qubits with exceptional coherence properties that can be initialized (*28*), measured nondestructively in a single shot (*29*), and even entangled (*30*) through their interactions with the electron spin. These nuclear spins could act as operational qubits in their own right, with the electron spins serving as ancillary qubits for initialization and readout, or as integrated quantum memory nodes associated with each electronic spin qubit. A room-temperature quantum memory consisting of a single ^{13}C nucleus weakly coupled to an NV center has been demonstrated with coherence exceeding 1 s (*31*). At temperatures $\lesssim$10 K, coherent optical transitions enable nondestructive single-shot spin measurements (*32*), coherent control (*33*), and spin-photon entanglement (*34*), with promise for integrating distributed NV center nodes within a large-scale optical network.

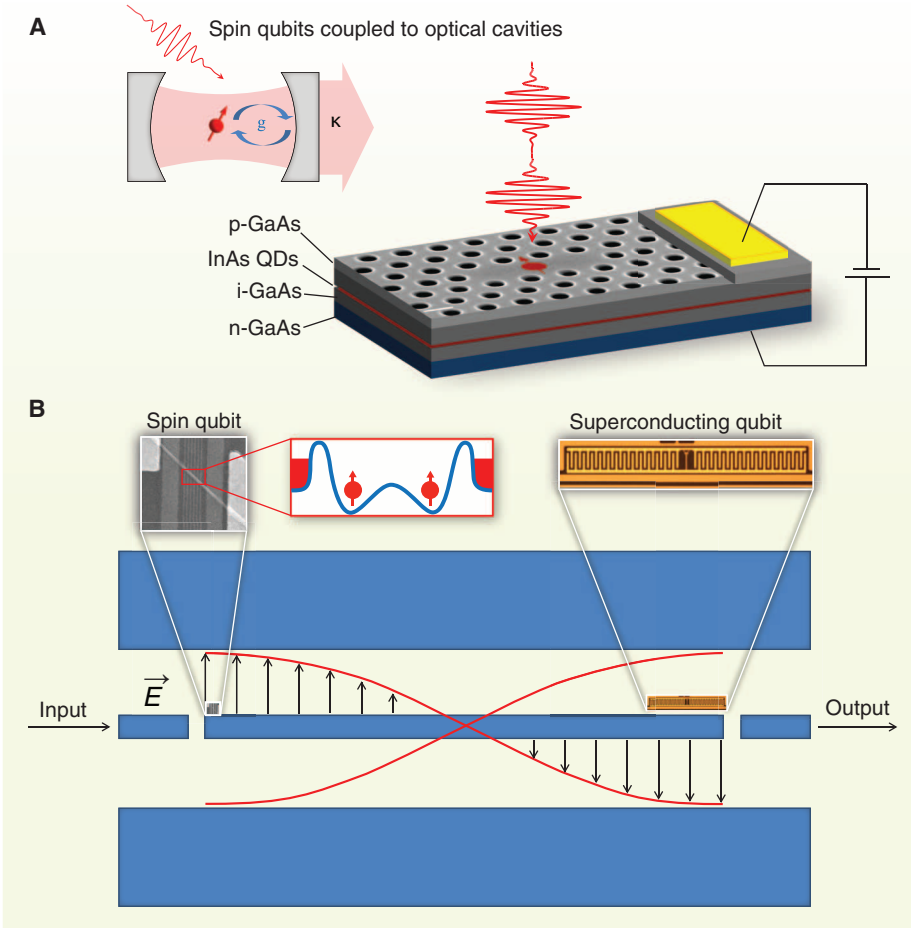

Fig. 3. (**A**) Cavity quantum electrodynamics with optical photons. (Upper left) Schematic of a single spin embedded within an optical cavity. If the qubit-cavity coupling strength, *g*, dominates over both qubit decoherence and the loss rate of photons from the cavity, κ, the system is in the strong coupling regime. (Lower right) Schematic of a photonic crystal cavity integrated with a diode structure used to realize coherent optical control of a cavity-coupled QD spin (*48*). [Image courtesy of D. Gammon, U.S. Naval Research Laboratory] (**B**) Superconducting qubits and spin qubits have quantum transitions in the microelectron volt range, closely matching the energy of microwave photons. This cartoon depicts a circuit quantum electrodynamics architecture that is used to couple a spin qubit to a superconducting qubit via a microwave cavity.

Scalable Architectures

With high-fidelity control of individual spin qubits now routine in many semiconductor systems, solid-state devices are poised to reach their full potential for integration and scalability. Nevertheless, a pressing challenge is the development of a robust two-qubit gate that can be scaled up to link many computational nodes into a larger network. One approach is to fabricate multiple qubits close enough together to use "direct" interactions such as magnetic dipole-dipole or electrostatic coupling to generate an entangling gate—for example, to implement a "surface code" computation using nearest-neighbor interactions only (*35*, *36*). This has been achieved both for pairs of lithographic quantum dot qubits in GaAs (*37*) and for NV center spins (*38*), although in both cases the gate time is rather long, limiting the entanglement fidelity. Furthermore, for applications in quantum communication and distributed quantum computing, it is desirable to be able to implement two-qubit gates between spins that are spatially separated beyond the reach of nearest-neighbor interactions. Such long-range coupling requires a "quantum bus" to transmit quantum information between local nodes. Although ideas exist for using nanomechanical resonators (*39*), "chains" of fixed spins (*40*), or electrons themselves carried by travelling QDs (*41*, *42*) as such a bus, an obvious choice of "flying qubit" to transmit information is the photon.

Photons are an excellent means of linking physical nodes within a network (*43*). They are capable of rapid propagation, low dissipation,

Downloaded from www.sciencemag.org on March 8, 2013

and low signal loss via integrated waveguides or fibers leading to or from the outside world. Furthermore, high-quality solid-state optical cavities mediate the coupling strength between spin qubits and photons (*44*), providing tools for photon-based selective readout and state preparation. When a qubit is optimally matched to an optical cavity—in the "strong coupling" regime (Fig. 3A)—the coherent interaction between the qubit and the cavity modes dominates over other, dissipative processes, such as the loss of photons from the cavity or the emission of qubit excitations to competing states. Notably, progress in the design and fabrication of dielectric optical cavities over the past decade has allowed the achievement of strong coupling between microcavities and semiconductor QDs (*45*, *46*). Strongly coupled systems produce entangled qubit-cavity states, such that the resulting photons carry the signature of the quantum state of the qubit, allowing long-distance propagation of that physical state information throughout the network. Although tremendous progress has been made in controlling purely photonic behavior with high-Q cavities and optically active QDs (*47*), it has remained a challenge to study cavity-coupled spin qubits. Promisingly, a photonic crystal cavity device integrated with a diode structure (Fig. 3A), necessary to tune the charge state of embedded QDs, has enabled coherent optical control of cavity-coupled spin qubits (*48*).

For "emerging" materials like diamond, where new fabrication techniques are required, cavity coupling to NV centers and other optical qubits still has much room for progress (*49*). Even without well-developed optical cavities, however, photons can still mediate coherent information transfer between distant qubits. A protocol has recently been developed to generate heralded entanglement between two NV center electron spins in separate cryostats 3 m apart (*50*). Using the dc Stark effect to tune the NV center optical transitions (*51*), a pair of indistinguishable photons is prepared, each entangled with their source NV center spins. By performing joint quantum measurements on the photons, the spin-photon entanglement is "swapped" to generate an entangled state of the two spins. Given the ability to initialize, measure, and entangle nuclear spin quantum registers local to each NV center (*28*–*30*), this protocol could enable long-distance quantum teleportation of spin states, quantum repeaters, and extended quantum networks.

Although optically active qubits such as self-assembled QDs and NV centers lend themselves naturally to photonic coupling, electronic qubits can also couple to photons, particularly those in the microwave regime. In fact, typical spin resonance frequencies of electronic spins in moderate magnetic fields are in the gigahertz range, closely matched to existing microwave resonator designs and even superconducting qubit architectures (*52*). A first step toward implementing "circuit quantum electrodynamics" with spin qubits was the recent demonstration of coupling between an InAs spin-orbit qubit and a superconducting resonator (*53*). Superconducting resonators have been effectively used to couple superconducting qubits that are separated by nearly a centimeter (*54*) and could similarly link semiconductor spins either to each other or to superconducting qubits (Fig. 3B).

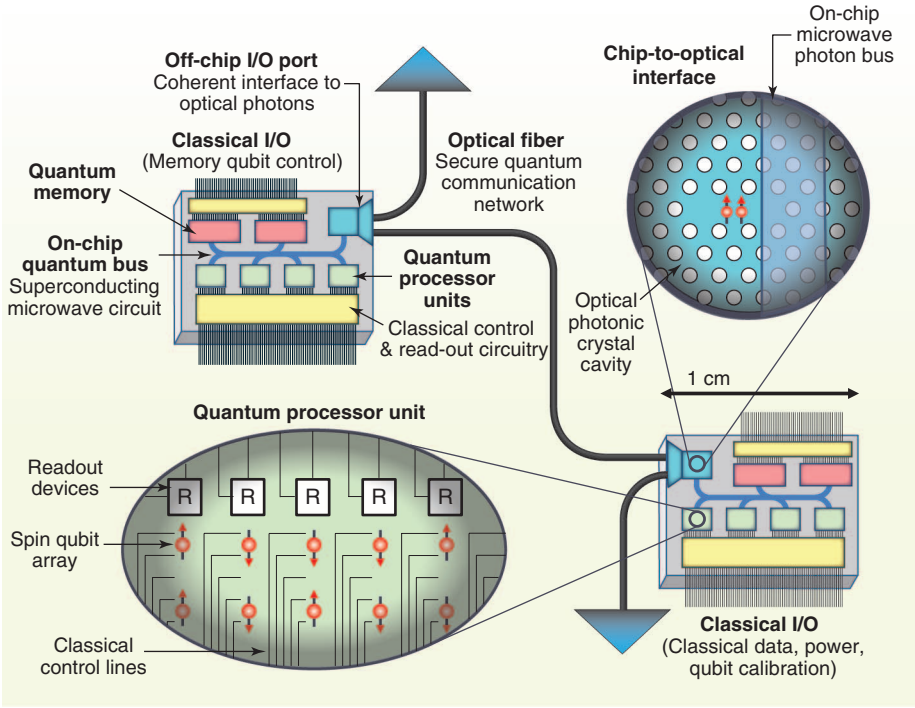

Fig. 4. A future integrated quantum device architecture might consist of quantum processor units comprising arrays of single-spin qubits, locally coupled on-chip using either photonic or microwave cavities. Photonic crystal cavities could be used to interface electron spins with optical photons, allowing long-distance transfer of quantum information via an optical fiber. Quantum memory might be located remotely from the processor units as depicted here or integrated with the processor qubits by using the nuclear spins of individual atoms. Classical circuitry provides qubit readout and calibration.

Outlook

It is tempting to view the wide array of systems under development as a race to find the "optimal" qubit, but this is likely to be the wrong perspective. Each implementation has relative strengths and weaknesses for different applications, and it could well serve to use each to its advantage. Modern computers comprise many types of logical implementations, including transistor logic, data transfer busses, and a large variety of memory nodes optimized either for fast access or long-term storage. A similar hybrid future could be in store for quantum computers, as envisaged in Fig. 4. Computational qubits will be chosen that are fast and easily coupled together, whereas memory nodes should be long lived but each need to be coupled to only one computational node. This might mean that the memory is not physically separated but is instead intrinsic to each computational node, being, for example, the nuclear spin of an NV center in diamond (*55*) or a phosphorus donor in silicon (*22*). Although optical interconnects are likely to serve as ports to transfer quantum information to and from the outside world, on-chip communication could be accomplished through either optical waveguides or superconducting microwave circuitry.

Although many challenges remain on the road to constructing a "useful" quantum computer, the pace of discovery seems to be accelerating, and spins in semiconductors are poised to play a major role. Several materials systems and architectures have already come to fruition, but others waiting in the wings might prove to be even better for some applications. For example, the remarkable properties of the diamond NV center motivates the search for other impurity-based spin systems with similar properties, possibly in more versatile host materials (*56*). Indeed, optically addressable defect spins with room-temperature coherence have recently been discovered in silicon carbide (*57*), which boasts well-developed techniques for heteroepitaxy and fabrication of complex structures. These and other material systems, such as rare-earth ions in crystals (*58*) and II/VI semiconductors (*59*), are likely to be a major focus in coming years.

Downloaded from www.sciencemag.org on March 8, 2013

The breadth of research in solid-state quantum information science is largely what makes the field so exciting. Advances achieved in one system are often directly applicable to many others, and solving the challenges that arise leads to breakthroughs that carry over to other fields of science and engineering. Clearly, the synergies between solid state and atomic physics are accelerating discoveries and demonstrations in both fields. Besides the potential we already recognize for quantum machines, our quest for greater control over quantum systems will surely lead to new materials and applications we have yet to imagine, just as the pioneers of classical computing could not have predicted exactly how the digital revolution has shaped our information age.

References and Notes

1. T. D. Ladd *et al.*, *Nature* **464**, 45 (2010).
2. R. Hanson, D. D. Awschalom, *Nature* **453**, 1043 (2008).
3. G. E. Moore, *Electronics* **38**, 114 (1965).
4. D. Loss, D. P. DiVincenzo, *Phys. Rev. A* **57**, 120 (1998).
5. R. Hanson, L. P. Kouwenhoven, J. R. Petta, S. Tarucha, L. M. K. Vandersypen, *Rev. Mod. Phys.* **79**, 1217 (2007).
6. J. R. Petta, H. Lu, A. C. Gossard, *Science* **327**, 669 (2010).
7. S. Nadj-Perge, S. M. Frolov, E. P. A. M. Bakkers, L. P. Kouwenhoven, *Nature* **468**, 1084 (2010).
8. J. Berezovsky, M. H. Mikkelsen, N. G. Stoltz, L. A. Coldren, D. D. Awschalom, *Science* **320**, 349 (2008).
9. D. Press, T. D. Ladd, B. Zhang, Y. Yamamoto, *Nature* **456**, 218 (2008).
10. W. B. Gao, P. Fallahi, E. Togan, J. Miguel-Sanchez, A. Imamoglu, *Nature* **491**, 426 (2012).
11. K. De Greve *et al.*, *Nature* **491**, 421 (2012).
12. G. de Lange, Z. H. Wang, D. Ristè, V. V. Dobrovitski, R. Hanson, *Science* **330**, 60 (2010).
13. C. A. Ryan, J. S. Hodges, D. G. Cory, *Phys. Rev. Lett.* **105**, 200402 (2010).
14. H. Bluhm *et al.*, *Nat. Phys.* **7**, 109 (2011).
15. A. M. Tyryshkin *et al.*, *Nat. Mater.* **11**, 143 (2011).
16. M. Steger *et al.*, *Science* **336**, 1280 (2012).
17. B. E. Kane, *Nature* **393**, 133 (1998).
18. J. J. L. Morton, D. R. McCamey, M. A. Eriksson, S. A. Lyon, *Nature* **479**, 345 (2011).
19. J. J. Pla *et al.*, *Nature* **489**, 541 (2012).
20. A. Morello *et al.*, *Nature* **467**, 687 (2010).
21. J. R. Petta *et al.*, *Science* **309**, 2180 (2005).
22. J. J. Pla *et al.*, http://arxiv.org/abs/1302.0047.
23. B. M. Maune *et al.*, *Nature* **481**, 344 (2012).
24. F. Jelezko, T. Gaebel, I. Popa, A. Gruber, J. Wrachtrup, *Phys. Rev. Lett.* **92**, 076401 (2004).
25. G. Balasubramanian *et al.*, *Nat. Mater.* **8**, 383 (2009).
26. G. D. Fuchs, V. V. Dobrovitski, D. M. Toyli, F. J. Heremans, D. D. Awschalom, *Science* **326**, 1520 (2009).
27. L. Childress *et al.*, *Science* **314**, 281 (2006).
28. M. V. G. Dutt *et al.*, *Science* **316**, 1312 (2007).
29. P. Neumann *et al.*, *Science* **329**, 542 (2010).
30. W. Pfaff *et al.*, *Nat. Phys.* **9**, 29 (2013).
31. P. C. Maurer *et al.*, *Science* **336**, 1283 (2012).
32. L. Robledo *et al.*, *Nature* **477**, 574 (2011).
33. B. B. Buckley, G. D. Fuchs, L. C. Bassett, D. D. Awschalom, *Science* **330**, 1212 (2010).
34. E. Togan *et al.*, *Nature* **466**, 730 (2010).
35. L. Trifunovic *et al.*, *Phys. Rev. X* **2**, 011006 (2012).
36. R. Raussendorf, J. Harrington, *Phys. Rev. Lett.* **98**, 190504 (2007).
37. M. D. Shulman *et al.*, *Science* **336**, 202 (2012).
38. F. Dolde *et al.*, http://arxiv.org/abs/1212.2804 (2012).
39. P. Rabl *et al.*, *Nat. Phys.* **6**, 602 (2010).
40. S. Bose, *Contemp. Phys.* **48**, 13 (2007).
41. R. P. G. McNeil *et al.*, *Nature* **477**, 439 (2011).
42. S. Hermelin *et al.*, *Nature* **477**, 435 (2011).
43. H. J. Kimble, *Nature* **453**, 1023 (2008).
44. K. J. Vahala, *Nature* **424**, 839 (2003).
45. J. P. Reithmaier *et al.*, *Nature* **432**, 197 (2004).
46. K. Hennessy *et al.*, *Nature* **445**, 896 (2007).
47. I. Fushman *et al.*, *Science* **320**, 769 (2008).
48. S. G. Carter *et al.*, http://arxiv.org/abs/1211.4540 (2012).
49. I. Aharonovich, A. D. Greentree, S. Prawer, *Nat. Photonics* **5**, 397 (2011).
50. H. Bernien *et al.*, http://arxiv.org/abs/1212.6136 (2012).
51. L. C. Bassett, F. J. Heremans, C. G. Yale, B. B. Buckley, D. D. Awschalom, *Phys. Rev. Lett.* **107**, 266403 (2011).
52. A. Wallraff *et al.*, *Nature* **431**, 162 (2004).
53. K. D. Petersson *et al.*, *Nature* **490**, 380 (2012).
54. L. DiCarlo *et al.*, *Nature* **467**, 574 (2010).
55. G. D. Fuchs, G. Burkard, P. V. Klimov, D. D. Awschalom, *Nat. Phys.* **7**, 789 (2011).
56. J. R. Weber *et al.*, *Proc. Natl. Acad. Sci. U.S.A.* **107**, 8513 (2010).
57. W. F. Koehl, B. B. Buckley, F. J. Heremans, G. Calusine, D. D. Awschalom, *Nature* **479**, 84 (2011).
58. R. Kolesov *et al.*, http://arxiv.org/abs/1301.5215 (2013).
59. T. D. Ladd, K. Sanaka, Y. Yamamoto, A. Pawlis, K. Lischka, *Phys. Status Solidi B* **247**, 1543 (2010).
60. G. D. Fuchs *et al.*, *Nat. Phys.* **6**, 668 (2010).
61. D. M. Toyli, C. D. Weis, G. D. Fuchs, T. Schenkel, D. D. Awschalom, *Nano Lett.* **10**, 3168 (2010).

Acknowledgments: D.D.A., L.C.B., and E.L.H. acknowledge support from the Air Force Office of Scientific Research and the Defense Advanced Research Projects Agency (DARPA); A.S.D. from the Australian Research Council (project CE11E0096) and the U.S. Army Research Office (contract W911NF-08-1-0527); and J.R.P. from the Sloan and Packard Foundations, Army Research Office grant W911NF-08-1-0189, NSF grants DMR-0819860 and DMR-0846341, and DARPA QuEST grant HR0011-09-1-0007.

10.1126/science.1231364

Downloaded from www.sciencemag.org on March 8, 2013

REVIEW

Topological Quantum Computation—From Basic Concepts to First Experiments

Ady Stern[1]* and Netanel H. Lindner[2,3]

Quantum computation requires controlled engineering of quantum states to perform tasks that go beyond those possible with classical computers. Topological quantum computation aims to achieve this goal by using non-Abelian quantum phases of matter. Such phases allow for quantum information to be stored and manipulated in a nonlocal manner, which protects it from imperfections in the implemented protocols and from interactions with the environment. Recently, substantial progress in this field has been made on both theoretical and experimental fronts. We review the basic concepts of non-Abelian phases and their topologically protected use in quantum information processing tasks. We discuss different possible realizations of these concepts in experimentally available solid-state systems, including systems hosting Majorana fermions, their recently proposed fractional counterparts, and non-Abelian quantum Hall states.

The principal obstacles on the road to quantum computing are noise and decoherence. By noise, we mean imperfections in the execution of the operations on the qubits (quantum bits). Decoherence arises when the quantum system that encodes the qubits becomes entangled with its environment, which is a bigger, uncontrolled system. There are two approaches to tackling these barriers. One is based on complete isolation of the computer from its environment, careful elimination of noise, and protocols for quantum correction of unavoidable errors. Enormous progress has been achieved in this direction in the past few years. The other approach, which is at the root of topological quantum computation, is very different. It uses a non-Abelian state of matter (*1*–*10*) to encode and manipulate quantum information in a nonlocal manner. This nonlocality endows the information with immunity to the effects of noise and decoherence (*2*–*6*).

Non-Abelian States of Matter

Several properties define a non-Abelian state of matter (*1*, *2*, *6*–*10*). It is a quantum system whose

[1]Department of Condensed Matter Physics, Weizmann Institute of Science, Rehovot 76100, Israel. [2]Institute of Quantum Information and Matter, California Institute of Technology, Pasadena, CA 91125, USA. [3]Department of Physics, California Institute of Technology, Pasadena, CA 91125, USA.

*To whom correspondence should be addressed. E-mail: adiel.stern@weizmann.ac.il

ground state is separated from the excited part of the spectrum by an energy gap. The elementary particles of the system may form collective composite particles, known as "non-Abelian anyons." When that occurs, the ground state becomes degenerate. In the limit of a large number of anyons, N, the ground-state degeneracy is λ^N, and the anyon is said to have a "quantum dimension" of λ. This degeneracy is not a result of any obvious symmetry of the system. As such, it is robust and cannot be lifted with the application of any local perturbation (*11*).

Transformations between the degenerate ground states may be induced by exchanging the anyons' positions. The canonical example is that of a two-dimensional (2D) system, where anyons may be regarded as point particles. Imagine a set of anyons that are initially positioned on a plane at $(R_1 \ldots R_N)$. They are made to move along a set of trajectories $[R_1(t) \ldots R_N(t)]$ that ends with their positions permuted. The motion is slow enough not to excite the system out of the subspace of ground states. When viewed in a 3D plot, the set of trajectories, known also as world lines, $R_i(t)$ look like entangled strands of spaghetti. A "braid" is defined as a set of spaghetti configurations that can be deformed to one another without spaghetti strands being cut. Remarkably, the unitary transformation implemented by the motion of the anyons depends only on the braid and is independent of the details of the trajectories. These unitary transformations must satisfy a set of conditions that result from their topological nature, such as the Yang-Baxter equation (Fig. 1A).

Notably, for the braid in which two anyons of types a and b are encircled by a third that is far away (Fig. 1B), the corresponding transformation will not be able to resolve the two anyons' types; from a distance they would look as if they "fused" to one anyon, of type c. The fusion of a pair of non-Abelian anyons may result in several different outcomes that are degenerate in energy when the anyons are far away from one another (leading to the ground-state degeneracy). The degeneracy is split when the fused anyons get close. The list of cs to which any a-b pair may fuse constitutes the "fusion rules." For each anyon of type a, there is an "anti-anyon" $\bar{a}$ such that the two may annihilate one another, or be created as a pair.

Topological Quantum Computation

The properties of non-Abelian states that are important for our discussion are the quantum dimensions of the anyons, the unitary transformations that they generate by braiding, and their fusion rules. Different non-Abelian systems differ in these properties. To turn a non-Abelian system into a quantum computer, we first create pairs of anyons and anti-anyons from the "vacuum," the state of zero anyons. In the simplest computational model, a qubit is composed of a group of several anyons, and its two states, $|0\rangle$ and $|1\rangle$, are two possible fusion outcomes of these anyons. (A qudit is formed if there are more than two possible fusion outcomes.) The creation from the vacuum initializes qubits in a well-defined state. The unitary gates are implemented by the braid transformations (Fig. 1C). At the end of the computation, the state is read off by measuring the fusion outcome of the anyons (*2*–*6*).

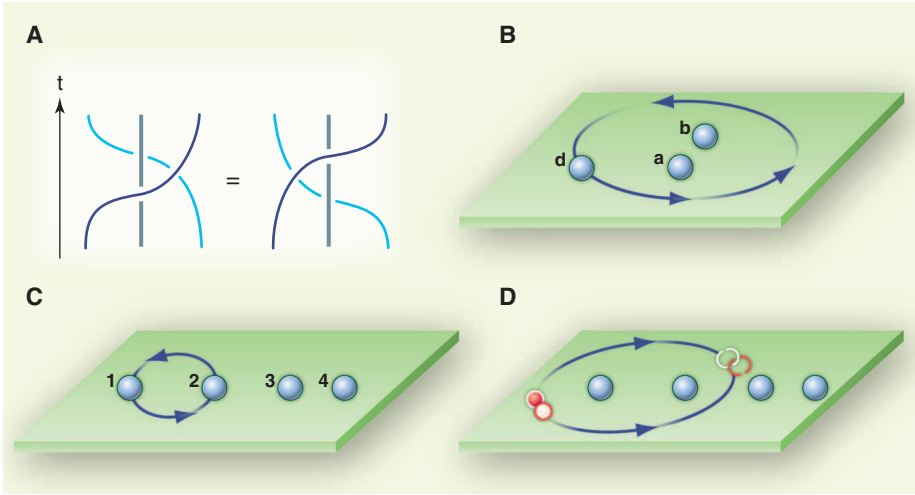

Fig. 1. (**A**) The Yang-Baxter equation states that two exchange paths that can be deformed into each other without cutting the world lines of the particles (blue curves) define the same braid. (**B**) Two anyons labeled a and b are encircled by a third anyon d. The resulting transformation depends only on the fusion outcome of a and b. (**C**) A canonical construction for a qubit, in a system of Ising anyons, consists of four anyons that together fuse to the vacuum. The two possible states can then be labeled by the fusion charge, say, of the left pair. A single qubit $\pi/4$ gate can be used by exchanging anyons 1 and 2 (depicted), whereas a Hadamard gate can be used by exchanging anyons 2 and 3. Such a construction can be realized using Majorana fermions. (**D**) Decoherence of information encoded in the ground-state space. Thermal and quantum fluctuations nucleate a quasiparticle-antiquasiparticle pair (red, white). The pair encircles two anyons encoding quantum information, and annihilates. The result of the process depends on the fusion charge of the two anyons, leading to decoherence of the encoded quantum information.

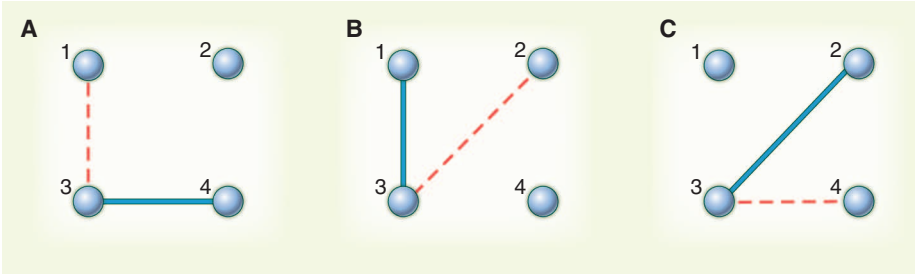

Fig. 2. Braiding in a system hosting Majorana fermions (zero modes or their fractionalized counterparts). For a manipulation of the subspace of ground states to lead to a topological result, the number of ground states should remain fixed. (**A**) Two zero modes initially at locations 1 and 2 are to be interchanged. A pair of coupled zero modes, 3 and 4, is created from the vacuum and may reside, for example, at the two ends of a short wire. As long as 3 and 4 are coupled (blue line), they are not zero modes and do not change the degeneracy of the ground state. Next, location 1 is coupled to 3 and 4 (red dashed line). The coupled system of 1, 3, and 4 must still harbor a zero mode. Thus, this step does not vary the degeneracy of the ground state, but it does redistribute the wave function of that zero mode among the three coupled sites. Location 4 is then decoupled from 1 and 3, and the localized zero mode is now at location 4. The outcome is then that 1 was copied to location 4. (**B**) In a similar fashion, 2 is copied to location 1. (**C**) Finally, 1 is copied from location 4 to location 2. At the end of this series, 3 and 4 are again coupled to one another, but 1 and 2 have been interchanged.

Downloaded from www.sciencemag.org on March 8, 2013

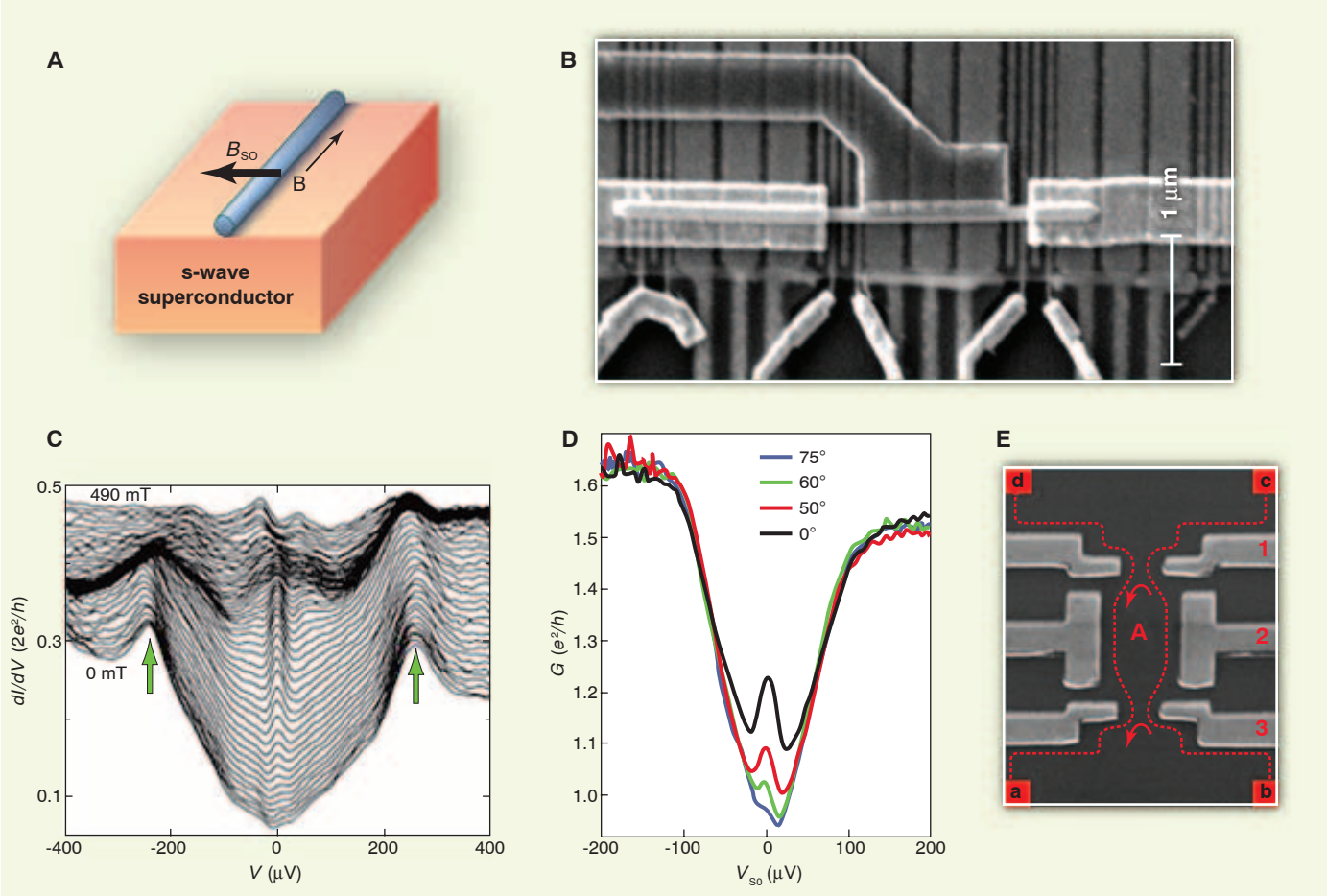

Fig. 3. Majorana end modes in a quantum wire. (**A**) A schematic plot of the sample: a quantum wire lying on a superconductor. B is the magnetic field that couples to the electron's spin, and B_{so} is the effective magnetic field induced by spin-orbit scattering. (**B**) A picture of the sample. Scale bar, 1 μm. (**C** and **D**) The measured differential conductance as a function of voltage at a range of magnetic fields (C) and magnetic field orientation (D) in the experiments reported in (*28*) and (*29*), respectively. The peak at zero voltage may be a sign of a Majorana fermion zero mode. (**E**) The experimental device of the type used in (*50*, *58*) to measure interference of quasiparticles in the ν = 5/2 state. The periodicity of the interference pattern as a function of magnetic field and gate voltage reflects the non-Abelian nature of the quasiparticles (*54*–*56*). Indicated are the interference loop (A), the interfering trajectories (dashed lines), ohmic contacts (a to d), and gates (numbered). [(A), (B), and (C) reprinted from (*28*); (D) reprinted from (*29*) by permission of Macmillan Publishers Ltd., copyright 2012; (E) reprinted from (*58*)]

The process outlined above is immune to noise and decoherence. The only mechanism that may alter the quantum state of the qubit in an uncontrolled fashion is a quantum or thermal fluctuation that creates an anyon–anti-anyon pair from the vacuum; the pair braids around two of the qubit's anyons, and finally annihilates (Fig. 1D). The probability for such a process decreases exponentially with decreasing temperature and with increasing distance between the anyons.

A quantum computer needs to have a minimal set of gates that allow it to efficiently approximate any unitary transformation in its space of logical states. Such a set is commonly called universal (*12*, *13*). For example, a universal set may be composed of two single-qubit gates and a two-qubit controlled-not gate (CNOT). For some non-Abelian states, all of these gates may be carried out in a topologically protected way (*2*, *4*–*6*). Fortunately, even when that is not the case, universality may still be obtained by combining topological and nontopological operations, as shown below (*14*, *15*).

Zero Modes and Majorana Fermions

A useful concept for understanding the stability of the degeneracy of the ground state in non-Abelian systems is that of localized "zero modes" (*16*, *17*). These are operators that act only within the subspace of ground states, and whose operation is confined to a localized spatial region. Generally, the number of independent operators that transfer the system between orthogonal ground states must be even. Thus, when there is only one such operator acting within a given spatial region, it must be Hermitian (note that Hermitian conjugation does not change the location of the operator). Consequently, it must have a partner in a different spatial region. If the system is subjected to a perturbation that acts locally within one of the regions, the local zero mode cannot be eliminated, because its partner is not subjected to that perturbation.

The position and wave function of the zero modes depend on the parameters of the system. Braiding operations are carried out by a cyclic trajectory in this parameter space. The braiding of world lines in two dimensions (*18*, *19*) is a particular example of topologically distinct classes of cyclic trajectories in the parameter space. More generally, the unitary transformation applied by a cycle is determined by the topological class to which the cycle belongs. This allows for braiding operations in systems that are not 2D, such as networks of 1D wires (*20*–*22*) (Fig. 2).

The simplest non-Abelian states of matter, those that carry Majorana fermions (*16*, *17*), can

Downloaded from www.sciencemag.org on March 8, 2013

be explained using the concept of zero modes. Such systems usually combine spin-orbit coupling, superconductivity, and Zeeman coupling to the electron spin (*23*–*27*). In superconductors, operators that take the system from one energy state to another are superpositions of electron creation and annihilation operators. In certain conditions, localized zero modes occur, in which the amplitude for the creation and annihilation operators is equal in magnitude, and the resulting operator is Hermitian. These operators are commonly referred to as Majorana fermions. The non-Abelian state of matter occurs when the zero modes are spatially separated from one another. Like all zero modes, Majorana fermions occur in pairs. A pair of Majorana fermions form a complex conventional fermion that spans a Hilbert space of two dimensions. The quantum dimension of a single Majorana fermion is therefore $\sqrt{2}$.

Because a superconductor is gapped, Majorana fermions in a superconducting system can only occur where the superconducting gap closes locally. In 2D systems, Majorana fermions are to be found in vortex cores (*16*, *18*), whereas in 1D systems they are to be found at the interfaces between different types of superconductivity, or at the system's ends (*17*). In vortex cores of s-wave superconductors, the presence of two spin directions per each electronic state does not allow for an isolated Majorana fermion zero mode. The places to look for isolated Majorana fermions are superconductors with only one spin direction per each electronic state. Examples are superconductors with spin-polarized p-wave pairing (*16*, *17*), surfaces of 3D and edges of 2D topological insulators (*23*, *24*), and 2D/1D systems featuring both spin-orbit and Zeeman couplings (*25*–*27*) in proximity to superconductors.

Recent experiments (*28*–*32*) support the existence of Majorana fermions at the ends of semiconducting wires in which strong spin-orbit coupling, together with Zeeman coupling of the spin to a magnetic field, creates a range of densities at which spin degeneracy is removed. The wires are made superconducting through their proximity to a superconductor, and zero modes are expected to form at their ends, which are separated from metallic contacts by potential barriers. When a current is driven through the wires in the absence of the end modes, the combination of the barriers and the superconducting gap suppresses the current at low voltages. The Majorana end modes allow current to flow, resulting in a sharp peak in the wires' differential conductance at zero voltage. This peak was observed in several experiments (Fig. 3) and its characteristics are consistent with Majorana end modes in quantum wires.

Although these are encouraging observations, it is still too early to identify them unambiguously as originating from Majorana fermions. The wires used in the experiments were short enough that coupling between the two ends may be expected to split the degeneracy between the end modes. Future experiments may observe the decay of this splitting with increasing wire length. Different measurements using the Josephson effect, Coulomb blockade, and scanning tunneling microscopes may provide additional information.

The Majorana fermions on the ends of quantum wires offer useful insights into the physics of non-Abelian systems. In the absence of the Majorana fermions, the ground state of a clean superconducting wire has an even number of electrons paired to Cooper pairs. Adding another electron is costly in energy, because this electron has no pairing partner. When the two Majorana fermions are localized at the ends of the wire, the odd electron can join at no cost of energy. The two degenerate ground states are then of different electron parities. When there are N wires, there are $2N$ zero modes and 2^N states, with each wire having either an even or odd number of electrons. This manner of counting explains the quantum dimension of $\sqrt{2}$.

Magic State Distillation and Surface Codes

Majorana fermions realize fusion and braiding rules analogous to those of "Ising anyons." Interchanging Majorana fermions at the ends of the same wire is equivalent to rotating the wire; this preserves the parity of the electron number while implementing a relative phase shift of $\pi/2$ between states of different parities. The braiding of two Majorana fermions of two different wires (Fig. 2) leads to a unitary transformation that takes the two wires from a state of well-defined parities to a state that is a superposition of even and odd parities, with equal probabilities. For example, the state $|\text{even1},\text{even2}\rangle$ is transformed to the state $1/\sqrt{2}\ [|\text{even1},\text{even2}\rangle \pm i|\text{odd1},\text{odd2}\rangle]$, where the sign of the second term depends on the details of the interchange. Because only two types of interchanges are possible—intrawire and interwire—there is no topologically protected way to turn two wires that start, say, at even parities $|\text{even1},\text{even2}\rangle$ into an arbitrary superposition of the

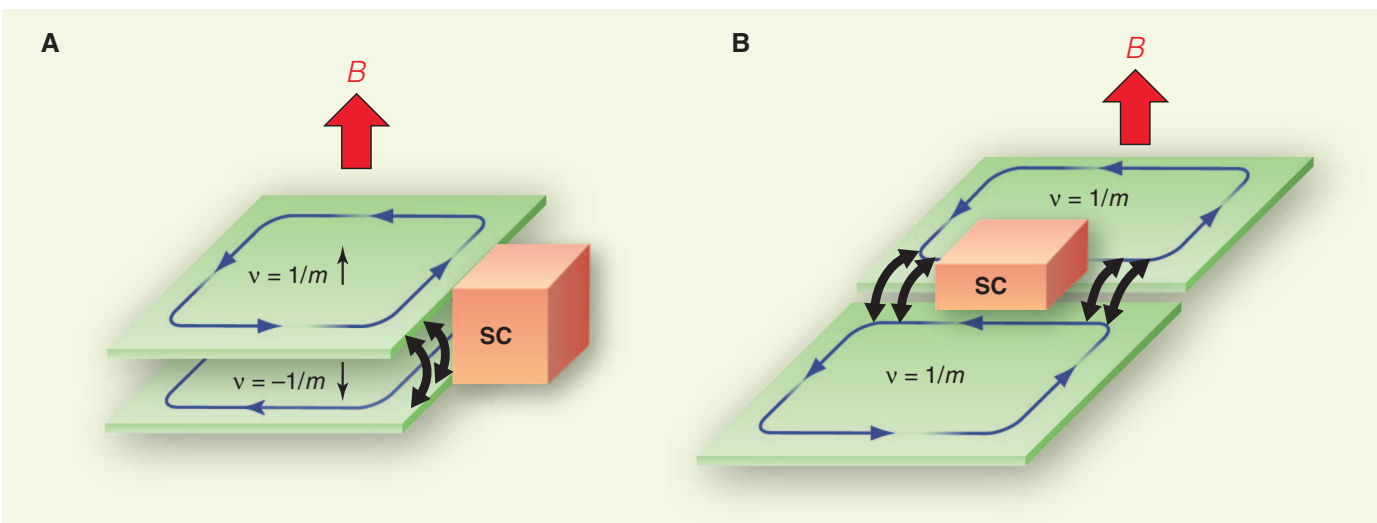

Fig. 4. Fractionalized Majorana zero modes at the interface between the superconductor and tunneling regions. (**A**) An electron-hole bilayer where the two layers are in a FQHE where the Hall conductivities are quantized at $\nu = \pm 1/m$ (in units of e^2/h), where m is an odd integer. The direction of the edge modes is indicated by the blue arrows. An s-wave superconductor (SC; orange) coupled to the edge of the two-layer system can gap the edge modes. In nonsuperconducting regions, spin-flipping electron tunneling between the top and bottom layer (black arrows) opens a gap on the edge. These can be enhanced by coupling the edge to a ferromagnet. Two layers of graphene may be a possible realization for such a system. (**B**) Single-layer realization, with a trench cut in a FQHE state with $\nu = 1/m$ exposing counterpropagating edge states. In spin-polarized quantum Hall states, spin-orbit interaction would couple these modes to a superconductor.

Downloaded from www.sciencemag.org on March 8, 2013

type $a|\text{even1,even2}\rangle \pm b|\text{odd1,odd2}\rangle$, with $|a| \neq |b|$. Topological quantum computation with Majorana fermions is therefore not universal (*4–6*). Using topologically protected braiding and measurement operations, Majorana fermions may carry out a set of gates known as the "Clifford gates." This set is generated by the single-qubit Hadamard gate, the single-qubit Pauli matrices, and the two-qubit CNOT gate (the latter requires a parity measurement of two qubits) (*13*). The gap to universal quantum computation may be bridged by adding a single-qubit gate that rotates the qubit by an angle $\pi/8$ (values other than $\pi/8$ are also possible).

Although topologically protected operations cannot implement the missing gate, they are able to approximate this gate with an arbitrarily small error, using a protocol called "magic state distillation" (*14*, *15*). The protocol consists of three key steps. First, nontopological operations create a large number of resource qubits in a "noisy" version of the state $|\psi_M\rangle = 1/\sqrt{2}\,[|0\rangle + \exp(i\pi/4)|1\rangle]$. [Note that there is no known way to accurately create the state $|\psi_M\rangle$ by using Clifford gates (i.e., topologically protected operations) alone.]

In the second step, one almost accurate qubit in the state $|\psi_M\rangle$ is distilled, using only topologically protected operations, from a large number of the noisy resource states. The possibility to do this endows $|\psi_M\rangle$ with the affectionate name "magic state." The distillation protocol is based on the concept of a "stabilizer" quantum error-correcting code (*33*). A quantum error-correcting code uses n physical qubits that span a space of 2^n states to represent one logical qubit. A unitary transformation takes a state of a single "logical" qubit and encodes it in this 2^n-dimensional space. As long as only a limited number of errors occur in the encoded state, they may be detected and corrected by measurements carried out on the n-qubit system, without disturbing the encoded quantum information.

In a stabilizer code, Pauli measurements and Clifford operations are sufficient for information encoding, decoding, and error correction. In the particular stabilizer code used for magic state distillation, Clifford operations can transform n qubits in the state $|\psi_M\rangle$ to an encoded logical state. Therefore, this code can be used to take n of the qubits that are noisy yet close enough to the state $|\psi_M\rangle$, encode them, detect the errors in their combined n-qubit state, keep only the error-free instances, and decode back to a single-qubit state. This entire step may be done in a topologically protected manner. Because the number of detectable errors is limited, this procedure cannot yield perfect magic states. However, the output is closer to the desired $|\psi_M\rangle$ than are the input resource states. This step can be applied repeatedly until the required level of accuracy is reached.

In the third and final step, the distilled magic states are used as ancillary qubits in order to apply the single-qubit rotation that is missing in the Clifford gates set. This is accomplished by measuring the joint parity of the logical qubit and the ancilla in the state $|\psi_M\rangle$. If the initial state of the logical qubit is $\alpha\,|0\rangle + \beta|1\rangle$, the measurement entangles the qubit and the ancilla either to the state $1/\sqrt{2}\,[\alpha|00\rangle + \beta\,\exp(i\pi/4)|11\rangle]$ or to $1/\sqrt{2}\,[\exp(i\pi/4)\alpha\,|01\rangle + \beta|10\rangle]$, depending on its outcome. A CNOT operation then disentangles the qubit from the ancilla, resulting in the required operation on the logical qubit. Magic state distillation complements the set of Clifford gates and opens the way to universal quantum computation based on Majorana fermions. The optimization of distillation protocols is currently under study (*34*).

In any physical realization of topological quantum computing, we must still expect an inevitable amount of errors. A promising approach for dealing with these errors is to incorporate topological qubits into a particularly fault-tolerant class of stabilizer codes, known as "surface codes." These codes consist of a 2D or 3D array of qubits (*3*, *35*). In surface codes, the states used to encode the logical qubit are the ground states of a Hamiltonian that describes couplings between different physical qubits in the array. This Hamiltonian gives rise to Abelian anyons. Two Abelian anyons have only one fusion outcome and therefore do not have the full advantages of their non-Abelian counterparts. Nonetheless, the surface codes do offer an enhanced robustness to decoherence and noise. The logical quantum information is encoded by the presence or absence of Abelian anyons on holes cut out in the array. An error occurring in a surface code amounts to creating an excited anyon–anti-anyon pair, which can be located and corrected by performing Pauli measurements and Clifford operations on the code's qubits. The error tolerance of surface codes can be several orders of magnitude better than most other known types of quantum error-correcting codes, but it comes at the price of the large number of physical qubits needed to encode a single logical qubit.

The ideas outlined above have inspired several proposals for hybrid structures of topological and nontopological components. These structures either combine nonprotected superconducting qubits or charge qubits with protected Majorana qubits, or combine protected quantum Hall interferometric gates with nonprotected parts (*36–41*). The role of the nontopological parts is limited to the operations that cannot be carried out in a protected manner, requiring effective and fast control of the coupling of the nontopological and topological parts.

Non-Abelian Anyons in Quantum Hall Systems

Non-Abelian anyons with properties richer than those of Majorana fermions are known in several systems. Below, we survey non-Abelian anyons on the edges of Abelian quantum Hall systems (*42–47*) and non-Abelian quantum Hall states (*1*, *2*, *10*, *16*, *48*).

The 2D gapped bulk of the quantum Hall effect is accompanied by 1D gapless edge modes. These modes occur at the interface of a quantum Hall state with the vacuum, between quantum Hall states of different filling factors, or even between quantum Hall states of the same filling factor and different spin polarization. We focus here on cases where gapless modes flow in both directions; these modes may be gapped by a perturbation that induces backscattering between them. One such case (Fig. 4A) is bilayer electron-hole system, in which the electrons and the holes are subjected to the same magnetic field and have the same densities. Because of their opposite charges, the two layers carry counterpropagating edge modes in physical proximity. When the values of the quantized Hall conductivities at the two layers (in units of e^2/h) are $\nu = \pm 1/m$, there is one mode flowing in each of the layers; in more complicated cases, there may be several such modes. Counterpropagating edge modes can also be realized in single-layer systems (Fig. 4B).

For $\nu = \pm 1/m$, the two counterpropagating edge modes may be gapped when they are both coupled either to a superconductor or to a ferromagnet (Fig. 4). In the two-layer case, the superconductor exchanges pairs of electrons with the two layers, one electron with each layer, whereas the ferromagnet scatters an electron from one layer to the other. In more complicated cases, there may be other ways to gap the edges, even with no superconductivity present. If different regions of the edge are gapped by different mechanisms, zero modes may appear at the interfaces between these regions. For $m = 1$, these are Majorana fermion zero modes, with quantum dimension $\sqrt{2}$. For the fractional case $m > 1$, the emerging anyons have a larger quantum dimension of $\sqrt{2m}$. In these cases, the regions on the edge that are coupled to superconductors form "superconducting quantum wires" and are otherwise surrounded by an insulating bulk. Their charge is then quantized modulo the charge of a Cooper pair. The quantization unit is the elementary charge of the surrounding medium, which is $1/m$ of the electron charge, resulting in $2m$ possible charge values.

The non-Abelian anyons that are realized on the gapped edges of Abelian quantum Hall systems may be braided using operations of the form outlined in Fig. 2. The unitary transformations that are realized by such braiding are richer than those realized by Majorana fermions. Unfortunately, these systems do not allow for universal quantum computation; however, they are robust to electronic noise and allow all Clifford operations to be performed using braiding. The precise computational potential of the non-Abelian anyons on edges of Abelian quantum Hall states has not yet been fully explored (*47*).

With respect to universal quantum computation, the most powerful anyons may be realized in the fractional quantum Hall effect (FQHE), in particular for states in the Landau level range of $2 < \nu < 4$. The non-Abelian anyons

Downloaded from www.sciencemag.org on March 8, 2013

in this system are fractionally charged quasiparticles. Despite the differences between these and the systems described above in the context of Majorana fermions, there are similarities in the path that may lead to the formation of non-Abelian anyons. In both systems, the interaction between electrons leads to states that may be viewed as a Bose-Einstein condensate. For superconductors, the condensed particles are Cooper pairs composed of two electrons each. For non-Abelian FQHE states, the condensed bosons are clusters of k electrons, with $k + 2$ magnetic flux quanta attached. The attached flux transmutes the electrons into Abelian anyons, and k of these anyons form the boson that condenses. The resulting state is a candidate state for Landau level fillings of $\nu = L + [2/(k + 2)]$ and $\nu = L + [k/(k + 2)]$, where L is the number of filled inert Landau levels. On the basis of numerical analysis, the most likely range of fillings where these states may be energetically favorable to other states has $L = 2$. These states are usually referred to as the Moore-Read state (for $k = 2$) (*1*) and the Read-Rezayi states (for $k \geq 3$) (*48*).

Similar to Majorana fermions, Moore-Read non-Abelian quasiparticles (*1*) have the quantum dimension of $\sqrt{2}$. For the Read-Rezayi states, the fractional statistics of the k anyons makes the counting of the ground states quite complicated. Briefly, the quantum dimension of the resulting non-Abelian anyons is $2 \cos[\pi/(k + 2)]$, which is not a square root of an integer. The transformations implemented when the non-Abelian anyons of $k \neq 2$ or 4 are braided are rich enough to enable a universal set of quantum gates.

Numerical and experimental evidence (Fig. 3E) supports the identification of the $\nu = 5/2$ state as a Moore-Read state (*49–52*). Experimental investigation of states with $k \geq 3$ has so far been hindered by their fragility, reflected in a small energy gap and strong sensitivity to disorder.

The non-Abelian anyons realized by fractionally charged quasiparticles in FQHE states are full-fledged quantum dynamical degrees of freedom, in contrast to those realized by zero modes confined to vortices or interfaces between phases. This difference is reflected in the way of measuring the fusion outcome of two anyons. For a pair of zero modes at two ends of a superconducting wire, the outcome can be measured by interfering a vortex around the superconductor and then measuring the phase shift induced by the Aharonov-Casher effect (*53*). In contrast, for the FQHE anyons, qubit measurements can be carried out by interfering the anyons themselves (*54–56*). We note that the unitary transformations required for topological quantum computing can be simulated using only measurements of fusion outcomes (instead of performing braiding operations) (*57*).

Outlook

The field of topological quantum computation is in its infancy. On the experimental side, there has been substantial recent progress in the study of systems that host Majorana fermions. So far, this study has mostly attempted to demonstrate the existence of these Majorana fermions. In the near future, one may expect further experiments aimed at nailing down the identification of these systems as non-Abelian, together with the development of methods to control, manipulate, and braid the anyons. Concurrently, one may expect experimental attempts to form hybrids of topological and nontopological qubits. These experiments will surely benefit from detailed theoretical modeling of the experimental systems. Future theoretical studies will hopefully propose novel non-Abelian systems that could be realized experimentally. These studies will benefit from an ongoing effort to classify non-Abelian states and explore the underlying mathematical structures. On the quantum computer science front, much remains to be understood regarding the computational power of various types of non-Abelian systems. Future studies may refine the distinction between universal and nonuniversal quantum computation, and distinguish between more and less powerful schemes for nonuniversal quantum computation.

References and Notes

1. G. Moore, N. Read, *Nucl. Phys. B* **360**, 362 (1991).
2. C. Nayak, S. H. Simon, A. Stern, M. Freedman, S. Das Sarma, *Rev. Mod. Phys.* **80**, 1083 (2008), and references therein.
3. A. Yu. Kitaev, *Ann. Phys.* **303**, 2 (2003).
4. M. H. Freedman, M. Larsen, Z. Wang, *Comm. Math. Phys.* **227**, 605 (2002).
5. M. Freedman, C. Nayak, K. Walker, *Phys. Rev. B* **73**, 245307 (2006).
6. J. Preskill, Lecture Notes on Quantum Computation (www.theory.caltech.edu/~preskill/ph219/topological.pdf).
7. A. Stern, *Nature* **464**, 187 (2010).
8. J. Alicea, *Rep. Prog. Phys.* **75**, 076501 (2012).
9. A. Kitaev, *Ann. Phys.* **321**, 2 (2006).
10. C. Nayak, F. Wilczek, *Nucl. Phys. B* **479**, 529 (1996).
11. The degeneracy of the ground state is never perfect. The energy splitting between the different ground states is exponentially small in the ratio of the anyons' separation and a (system-dependent) microscopic length scale. It can thus be made arbitrarily small by increasing this separation.
12. A. Yu. Kitaev, *Russ. Math. Surv.* **52**, 1191 (1997).
13. M. A. Nielsen, I. L. Chuang, *Quantum Computation and Quantum Information* (Cambridge Univ. Press, Cambridge, 2000).
14. S. Bravyi, A. Yu. Kitaev, *Phys. Rev. A* **71**, 022316 (2005).
15. S. Bravyi, *Phys. Rev. A* **73**, 042313 (2006).
16. N. Read, D. Green, *Phys. Rev. B* **61**, 10267 (2000).
17. A. Yu. Kitaev, *Phys. Uspekhi* **44** (suppl. 10), 131 (2001).
18. D. A. Ivanov, *Phys. Rev. Lett.* **86**, 268 (2001).
19. A. Stern, F. von Oppen, E. Mariani, *Phys. Rev. B* **70**, 205338 (2004).
20. J. Alicea, Y. Oreg, G. Refael, F. von Oppen, M. P. A. Fisher, *Nat. Phys.* **7**, 412 (2011).
21. B. I. Halperin *et al.*, *Phys. Rev. B* **85**, 144501 (2012).
22. J. D. Sau, D. J. Clarke, S. Tewari, *Phys. Rev. B* **84**, 094505 (2011).
23. L. Fu, C. L. Kane, *Phys. Rev. Lett.* **100**, 096407 (2008).
24. L. Fu, C. L. Kane, *Phys. Rev. B* **79**, 161408 (2009).
25. J. D. Sau, R. M. Lutchyn, S. Tewari, S. Das Sarma, *Phys. Rev. Lett.* **104**, 040502 (2010).
26. R. M. Lutchyn, J. D. Sau, S. Das Sarma, *Phys. Rev. Lett.* **105**, 077001 (2010).
27. Y. Oreg, G. Refael, F. von Oppen, *Phys. Rev. Lett.* **105**, 177002 (2010).
28. V. Mourik *et al.*, *Science* **336**, 1003 (2012).
29. A. Das *et al.*, *Nat. Phys.* **8**, 887 (2012).
30. A. D. K. Finck, D. J. Van Harlingen, P. K. Mohseni, X. Li, K. Jung, http://arXiv.org/abs/1212.1101 (2012).
31. L. P. Rokhinson, X. Liu, J. K. Furdyna, *Nat. Phys.* **8**, 795 (2012).
32. M. T. Deng *et al.*, *Nano Lett.* **12**, 6414 (2012).
33. D. Gottesman, http://arxiv.org/abs/quant-ph/9705052 (1997).
34. G. Duclos-Cianci, K. M. Svore, http://arXiv.org/abs/1210.1980 (2012).
35. E. Dennis, A. Yu. Kitaev, A. Landahl, J. Preskill, *J. Math. Phys.* **43**, 4452 (2002).
36. F. Hassler, A. R. Akhmerov, C.-Y. Hou, C. W. J. Beenakker, *N. J. Phys.* **12**, 125002 (2010).
37. P. Bonderson, D. J. Clarke, C. Nayak, K. Shtengel, *Phys. Rev. Lett.* **104**, 180505 (2010).
38. E. Grosfeld, A. Stern, *Proc. Natl. Acad. Sci. U.S.A.* **108**, 11810 (2011).
39. L. Jiang, C. L. Kane, J. Preskill, *Phys. Rev. Lett.* **106**, 130504 (2011).
40. P. Bonderson, R. M. Lutchyn, *Phys. Rev. Lett.* **106**, 130505 (2011).
41. F. Hassler, A. R. Akhmerov, C. W. J. Beenakker, *N. J. Phys.* **13**, 095004 (2011).
42. N. H. Lindner, E. Berg, G. Refael, A. Stern, *Phys. Rev. X* **2**, 041002 (2012).
43. D. J. Clarke, J. Alicea, K. Shtengel, *Nat. Commun.* **4**, 1348 (2013).
44. M. Cheng, *Phys. Rev. B* **86**, 195126 (2012).
45. A. Vaezi, *Phys. Rev. B* **87**, 035132 (2013).
46. M. Barkeshli, C.-M. Jian, X.-L. Qi, *Phys. Rev. B* **87**, 045130 (2013).
47. M. B. Hastings, C. Nayak, Z. Wang, http://arXiv.org/abs/1210.5477 (2012).
48. N. Read, E. Rezayi, *Phys. Rev. B* **54**, 16864 (1996).
49. M. Storni, R. H. Morf, S. Das Sarma, *Phys. Rev. Lett.* **104**, 076803 (2010).
50. R. L. Willett, L. N. Pfeiffer, K. W. West, *Phys. Rev. B* **82**, 205301 (2010).
51. A. Bid *et al.*, *Nature* **466**, 585 (2010).
52. S. An *et al.*, http://arXiv.org/abs/1112.3400 (2011).
53. Y. Aharonov, A. Casher, *Phys. Rev. Lett.* **53**, 319 (1984).
54. S. Das Sarma, M. Freedman, C. Nayak, *Phys. Rev. Lett.* **94**, 166802 (2005).
55. A. Stern, B. I. Halperin, *Phys. Rev. Lett.* **96**, 016802 (2006).
56. P. Bonderson, A. Kitaev, K. Shtengel, *Phys. Rev. Lett.* **96**, 016803 (2006).
57. P. Bonderson, M. Freedman, C. Nayak, *Ann. Phys.* **324**, 787 (2009).
58. R. L. Willett, C. Nayak, K. Shtengel, L. N. Pfeiffer, K. W. West, http://arXiv.org/abs/1301.2639 (2013).

Acknowledgments: We thank C. Nayak and J. Preskill for helpful discussions, and the Kavli Institute for Theoretical Physics for their hospitality. Supported by the U.S.-Israel Binational Science Foundation, the Minerva foundation, and Microsoft Station Q (A.S.); Defense Advanced Research Projects Agency award N66001-12-1-4034 and the Institute for Quantum Information and Matter, an NSF Physics Frontiers Center, with support of the Gordon and Betty Moore Foundation (N.H.L.); and NSF grant PHY11-25915.

10.1126/science.1231473

Downloaded from www.sciencemag.org on March 8, 2013

Avoiding a Spanning Cluster in Percolation Models

Y. S. Cho,[1] S. Hwang,[1] H. J. Herrmann,[2] B. Kahng[1]*

When dynamics in a system proceeds under suppressive external bias, the system can undergo an abrupt phase transition, as can happen when an epidemic spreads. Recently, an explosive percolation (EP) model was introduced to understand such phenomena. The order of the EP transition has not been clarified in a unified framework covering low-dimensional systems and the mean-field limit. We introduce a stochastic model in which a rule for dynamics is designed to avoid the formation of a spanning cluster through competitive selection in Euclidean space. We use heuristic arguments to show that in the thermodynamic limit and depending on a control parameter, the EP transition can be either continuous or discontinuous if $d < d_c$ and is always continuous if $d \geq d_c$, where d is the spatial dimension and d_c is the upper critical dimension.

The notion of percolation transition (PT) (*1*) is widely applied in a variety of disciplines; it explains the formation of a spanning cluster connecting two opposite sides of a system in Euclidean space, such as occurs in metal-insulator or sol-gel transitions. Alternatively, percolation can also be interpreted as the formation of a macroscopic cluster in the system, and this concept has been used to model the spread of epidemics (*2*) and the formation of opinions within social networks (*3*). These two pictures may be regarded as the same, but they can lead to different evolution processes in Euclidean space. Here, we study an abrupt PT (*4*) from these two perspectives.

One of the models in the more general second category is the classic Erdős and Rényi (ER) (*5*) model, in which the evolution proceeds as follows: Starting with N isolated nodes, an edge is connected between a randomly selected unconnected pair of nodes at each time step. Then, as the number of connected edges is increased, a macroscopic cluster is generated at the percolation threshold, and its size is increased continuously. Recently, the ER model was modified by imposing additionally a so-called product rule or sum rule, which suppresses the formation of a large cluster (*4*). Because of this suppressive bias, the percolation threshold is delayed; thus, when the giant cluster eventually emerges, it does so explosively. Hence, this model has been called the explosive percolation (EP) model. This result has attracted much interest (*6*–*23*), including openings toward other subjects such as synchronization phenomena (*23*), jamming in the Internet (*24*), and analysis of real-world networks (*25*). Initially, this explosive PT was regarded as a discontinuous transition; however, it was recently found that the transition is continuous in the thermodynamic limit (*9*), followed by a mathematical proof (*10*) and extensive supporting simulations (*11*–*13*). The random graph in fact represents the mean-field description of the model on a Euclidean lattice. EP problems in Euclidean space have also been considered, and the numerical results suggest discontinuous percolations (*14*). Because of the absence of analytic results, the order of explosive PT in Euclidean space has not yet been determined. Under this circumstance, it is of interest to clarify the order of the explosive PT in Euclidean space and on random graphs in a unified manner.

The product rule or sum rule was inspired by an idea first mathematically developed in (*26*, *27*) to investigate the power of multiple choices in random processes. These ideas were refined to what is called an Achlioptas process, in which one chooses the best among randomly given multiple options to avoid the formation of a certain target pattern (*28*). Here, we choose the spanning cluster rather than the giant cluster as the target pattern of the PT in Euclidean space. Surprisingly, this choice, while keeping the strategy of choosing the best among several options, enables us to determine analytically the order of the explosive PT for the spanning cluster in the thermodynamic limit. In this spanning cluster–avoiding (SCA) model, the transition can be either discontinuous or continuous below the upper critical dimension, depending on the number of potential bonds m introduced in the dynamic rule, and it is continuous above the upper critical dimension (i.e., in the mean-field limit). Thus, the appearance of an abrupt PT can be clarified within a unified scheme. Moreover, the analytic results and the methodology used in the SCA model can serve as a platform for understanding the PTs for other models showing abrupt transitions, such as the product rule (*4*) and the Gaussian model (*18*). In fact, the general mechanism underneath the abrupt PT is that by throttling spanning, the finite clusters can become very dense, so that when they finally merge to a percolating configuration, a substantial fraction of sites is immediately involved in the largest cluster.

We begin by introducing an adequate suppressing rule in Euclidean space. Starting with a d-dimensional regular square lattice of linear size L having $N = L^d$ nodes and $N_b = zN$ unoccupied bonds, where z is the coordination number divided by 2, we randomly choose at each time step m unoccupied bonds. They are classified into two types: bridge and nonbridge bonds. Bridge bonds are those that would form a spanning cluster if occupied. We want to avoid bridge bonds being occupied, and thus one of the nonbridge bonds is randomly selected and occupied (Fig. 1A). If the m potential bonds are all bridge bonds, then one of them is selected randomly and occupied (Fig. 1B). Once a spanning cluster is created, no more restrictions are imposed on the occupation of bonds. This procedure continues until all bonds are occupied. The selection rule among multiple options is inspired by the best-of-m model (*19*). We denote the number and the fraction of occupied bonds as ℓ and $t = \ell/zN$, respectively. By analogy to ordinary percolation, t can be interpreted as an occupation probability, and also as

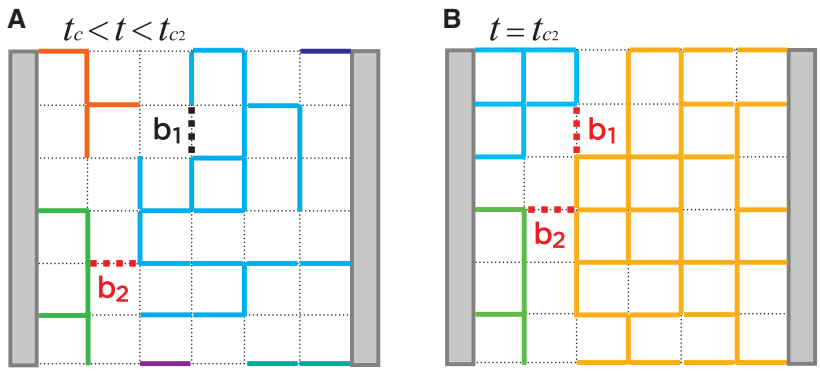

Fig. 1. (**A**) Dynamics of the SCA model on a square lattice. For the case $m = 2$, two empty bonds, b_1 and b_2 (shown as dashed lines), are randomly selected. If one of them is a bridge bond (b_2), by which a spanning cluster would be formed, then the nonbridge bond (b_1) is chosen. (**B**) At $t = t_{c2}$, two bridge bonds can be selected for the first time. Then, one of them is taken randomly and a spanning cluster is formed.

[1]Department of Physics and Astronomy, Seoul National University, Seoul 151-747, Korea. [2]Computational Physics for Engineering Materials, Institute for Building Materials, ETH Zürich, 8093 Zürich, Switzerland.

*To whom correspondence should be addressed. E-mail: bkahng@snu.ac.kr

Downloaded from www.sciencemag.org on March 8, 2013

the time of our dynamic system. We define ℓ_{cm} as the number of occupied bonds when a bridge bond is occupied for the first time. The percolation threshold is $t_{cm} \equiv \ell_{cm}/N_b$, which for $m > 1$ is larger than the percolation threshold t_c of ordinary percolation.

We performed extensive numerical simulations for various system sizes L and parameter values m to see (i) how the order parameter $G_m(t)$—the fraction of sites (nodes) belonging to the spanning cluster—behaves as a function of t and m, and (ii) how the percolation threshold t_{cm} averaged over configurations depends on m, L, and dimension d. Then, extrapolating these results, we determined the order of the PT under the suppressing rule in the thermodynamic limit.

We now briefly show numerical results and then theoretical results, of which derivations are presented in (*29*). First, for a given m, $G_m(t) = 0$ for $t < t_{cm}$. For $t_c < t < t_{cm}$, a spanning cluster is not created because of the suppressing rule, whereas it is formed in ordinary percolation. However, for $m > 1$ and $t > t_{cm}$, once one bridge bond is occupied, no further bonds are suppressed and thus the spanning cluster is not modified. Thus, $G_m(t)$ follows the curve of $G_1(t)$ for $t > t_{cm}$ (Fig. 2A). Therefore, there exists a finite discontinuity $G_1(t_{cm})$ at t_{cm}. In the reverse evolution, dynamics proceeds under the bias of sustaining the spanning cluster. For this case, evolution can be understood as the opposite procedure—that is, from occupation to deletion of bonds. Then, the spanning cluster can sustain up to $1 - t_{cm}$, but its size reduces to N_{BB}/N_b, where N_{BB} is the number of bridge bonds. In the thermodynamic limit, the fraction N_{BB}/N_b is zero in the interval $[1 - t_{cm}, 1 - t_c]$ for $d < 6$ (*20*). Thus, the order parameter behaves as shown in Fig. 2B.

Next, we plot the percolation threshold for systems with linear size L, $t_{cm}(L)$, versus L for several values of m. We find that $t_{cm}(L)$ decreases and converges to t_c as L increases for $m = 2$, and that $t_{cm}(L)$ increases and converges to 1 as L increases for $m \geq 3$ in two dimensions. More generally, we find that there exists a critical value $m_c(d) = d/(d - d_{BB})$ for $d > d_{BB}$, where d_{BB} is the fractal dimension of the set of bridge bonds (*20*), such that if $m < m_c$, $t_{cm}(L)$ decreases and converges to t_c as L increases, and if $m > m_c$, $t_{cm}(L)$ increases and converges to 1 as L increases. This is shown in Fig. 2C for two dimensions, and in fig. S2, A and C, for three and four dimensions, respectively. The analytic solution for $m_c(d)$ is presented in (*29*). It is estimated that $m_c(d) \approx 2.55 \pm 0.01$ ($d = 2$), 5.98 ± 0.07 ($d = 3$), 16.99 ± 5.23 ($d = 4$), 50 ($d = 5$), and ∞ ($d = 6$). For $d = 5$, the standard deviation is larger than the mean value. d_{BB} is equal to d in $d = 6$, which is thus the upper critical dimension, and the formula for m_c is valid for $d < d_c = 6$. To simulate for noninteger m cases, once we select an unoccupied bond randomly, and if that bond is a bridge bond, then it is occupied with the probability $q(t)^{1-(1/m)}$, where $q(t)$ is the probability that m potential bonds are all bridge bonds. Otherwise, it is always occupied. This dynamic process can be implemented without choosing m different unoccupied bonds, but by choosing just one bond.

Subsequently, we check the convergence rates for $t_{cm}(L) - t_c$ and $1 - t_{cm}(L)$ as a function of L. We obtain power-law behaviors, $t_{cm}(N) - t_c \sim N^{-1/\bar{\nu}_<}$ and $1 - t_{cm}(N) \sim N^{-1/\bar{\nu}_>}$, where the exponents $\bar{\nu}_<$ and $\bar{\nu}_>$ are derived analytically (*29*) as $1/\bar{\nu}_< = [1 - (m/m_c)]/(m\zeta + 1)$ and $1/\bar{\nu}_> = [(m/m_c) - 1]/(m - 1)$. The exponent $\bar{\nu}$ is rewritten as $d\nu$, where d is the spatial dimension and ν is the exponent characterizing the scaling relation between length scale L and the occupation probability t. These results are shown in Fig. 2, D and E, for two dimensions, and in fig. S2, B and D, for three and four dimensions, respectively. We show in (*29*) that the standard deviation for the statistical fluctuations of the critical point $t_{cm}(N)$ behaves in the same manner as $\sigma_< \sim N^{-1/\bar{\nu}_<}$ for $m < m_c$ and $\sigma_> \sim N^{-1/\bar{\nu}_>}$ for $m > m_c$, and this is confirmed

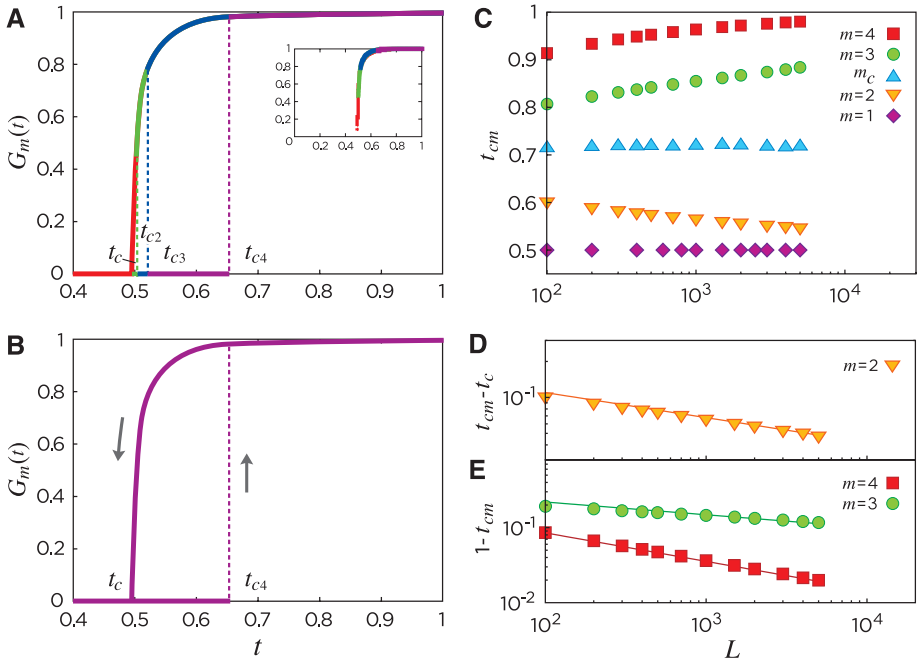

Fig. 2. (**A**) Schematic plot of the spanning cluster size $G_m(t)$ versus t, the number of attached bonds per N_b for the SCA model, with $m = 1$ (red), 2 (green), 3 (blue), and 4 (purple). Inset: Same plot with real data, which are obtained after averaging over the samples containing nonzero $G_m(t)$ at each time t. Data are obtained for a system size of $N = 10^6$ in two dimensions. (**B**) Hysteresis curve of the order parameter in forward and backward evolution. (**C**) Plot of $t_{cm}(L)$ versus L for various values of m. (**D**) Plot of $t_{cm}(L) - t_c$ for $m = 2$ versus L, which is the case $m < m_c$. (**E**) Plot of $1 - t_{cm}(L)$ for $m = 3$ and 4 versus L, which is the case $m > m_c$. Solid lines are guidelines with the slopes theoretically predicted. All data are averaged over 10^4 configurations.

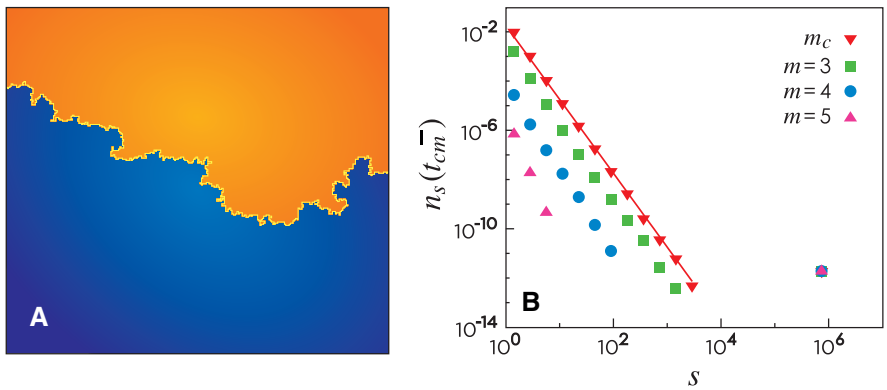

Fig. 3. (**A**) Plot of the giant and second largest clusters just before the percolation threshold t_{c4}^- for $m = 4$. Clusters are compact and the boundary is self-affine, with fractal dimension $d_{BB} \approx 1.22$. In general, for sufficiently large m, only very few clusters remain at $t_{cm}^-(N)$. (**B**) Plot of n_s versus s at t_{cm}^- for $m = 3$, 4, 5, and $m_c \approx 2.55$ in two dimensions. Simulations are performed for $N = 10^6$, and the data are averaged over 10^3 configurations. The solid line is a guideline with slope −3.

Downloaded from www.sciencemag.org on March 8, 2013

numerically in fig. S1B. Note that at a tricritical point m_c, $t_{cm_c}(L \to \infty)$ is finite; for example, $t_{cm_c}(\infty) \approx 0.72$ in two dimensions, which is neither t_c nor unity, and the fluctuation is large and independent of N.

On the basis of the above results, we come to the conclusion that for $d < d_c = 6$, the percolation threshold in the limit $N \to \infty$ is t_c for $m < m_c$, finite t_{cm} at $m = m_c$, and 1 for $m > m_c$ [(*29*), equations 8 to 10]. For $d \geq d_c$, $m_c \to \infty$, and for finite m, $t_{cm} \to t_c$ (*29*). We conclude that when m is finite, the PT is continuous in the limit $N \to \infty$. In statistical physics, it is known that mean-field results above the upper critical dimension are equivalent to the solution on sparse random graphs. From this perspective, our result for $d > d_c$ is comparable to previous results for the EP model (*10*) on random graphs.

For the SCA model in the regime $m > m_c$ at $t^-_{cm}(L)$, we find that there are only a few clusters and that they are compact (Fig. 3A). Thus, the cluster size distribution at $t^-_{cm}(L)$ decays rapidly in the region of small cluster size and exhibits a peak in the region of large cluster size (Fig. 3B). The interface between clusters forms naturally along the bridge bonds and is self-affine. Because of the presence of already macroscopically grown but not yet spanning clusters, the order parameter is increased drastically when occupying a bridge bond. Finally, we note that for $d \geq d_c$, a discontinuous PT can take place if m varies with the system size N. We obtain a characteristic value $m_c \sim \ln N$ such that when m increases with N slower than m_c, the PT is continuous, and when m increases with N faster than m_c, the PT is discontinuous. They occur at t_c and 1, respectively [see (*29*)].

For the product rule (*4*), the nature of the PT is similar to the mean-field behavior of the SCA model in low dimensions such as $d = 2$. Under the best-of-m strategy, when m varies with the system size as $m > m_c \sim \ln N$, clusters are also compact and the number of clusters is limited to a finite value, and thus a discontinuous PT can take place. However, for a fixed m and in the thermodynamic limit, the PT is continuous [see (*29*)].

References and Notes

1. D. Stauffer, A. Aharony, *Introduction to Percolation Theory* (Taylor & Francis, London, ed. 2, 1994).
2. R. Pastor-Satorras, A. Vespignani, *Phys. Rev. Lett.* **86**, 3200 (2001).
3. M. Girvan, M. E. J. Newman, *Proc. Natl. Acad. Sci. U.S.A.* **99**, 7821 (2002).
4. D. Achlioptas, R. M. D'Souza, J. Spencer, *Science* **323**, 1453 (2009).
5. P. Erdös, A. Rényi, *Publ. Math. Inst. Hungar. Acad. Sci* **5**, 17 (1960).
6. R. M. Ziff, *Phys. Rev. Lett.* **103**, 045701 (2009).
7. Y. S. Cho, J. S. Kim, J. Park, B. Kahng, D. Kim, *Phys. Rev. Lett.* **103**, 135702 (2009).
8. F. Radicchi, S. Fortunato, *Phys. Rev. Lett.* **103**, 168701 (2009).
9. R. A. da Costa, S. N. Dorogovtsev, A. V. Goltsev, J. F. F. Mendes, *Phys. Rev. Lett.* **105**, 255701 (2010).
10. O. Riordan, L. Warnke, *Science* **333**, 322 (2011).
11. P. Grassberger, C. Christensen, G. Bizhani, S.-W. Son, M. Paczuski, *Phys. Rev. Lett.* **106**, 225701 (2011).
12. H. K. Lee, B. J. Kim, H. Park, *Phys. Rev. E* **84**, 020101(R) (2011).
13. N. Bastas, K. Kosmidis, P. Argyrakis, *Phys. Rev. E* **84**, 066112 (2011).
14. W. Choi, S.-H. Yook, Y. Kim, *Phys. Rev. E* **84**, 020102 (2011).
15. K. Panagiotou, R. Spöhel, A. Steger, H. Thomas, *Electron. Notes Discrete Math.* **38**, 699 (2011).
16. Y. S. Cho, B. Kahng, *Phys. Rev. Lett.* **107**, 275703 (2011).
17. W. Chen, R. M. D'Souza, *Phys. Rev. Lett.* **106**, 115701 (2011).
18. N. A. M. Araújo, H. J. Herrmann, *Phys. Rev. Lett.* **105**, 035701 (2010).
19. N. A. M. Araújo, J. S. Andrade Jr., R. M. Ziff, H. J. Herrmann, *Phys. Rev. Lett.* **106**, 095703 (2011).
20. K. J. Schrenk, N. A. M. Araújo, J. S. Andrade Jr., H. J. Herrmann, *Sci. Rep.* **2**, 348 (2012).
21. J. Nagler, A. Levina, M. Timme, *Nat. Phys.* **7**, 265 (2011).
22. H. D. Rozenfeld, L. K. Gallos, H. A. Makse, *Eur. Phys. J. B* **75**, 305 (2010).
23. J. Gómez-Gardeñes, S. Gómez, A. Arenas, Y. Moreno, *Phys. Rev. Lett.* **106**, 128701 (2011).
24. D. D. Martino, L. Dall'Asta, G. Bianconi, M. Marsili, *Phys. Rev. E* **79**, 015101(R) (2009).
25. R. K. Pan, M. Kivelä, J. Saramäki, K. Kaski, J. Kertész, *Phys. Rev. E* **83**, 046112 (2011).
26. Y. Azar, A. Z. Broder, A. R. Karlin, E. Upfal, *SIAM J. Comput.* **29**, 180 (1999).
27. M. Mitzenmacher, *IEEE Trans. Parallel Distrib. Syst.* **12**, 1094 (2001).
28. O. Riordan, L. Warnke, *Ann. Appl. Probab.* **22**, 1450 (2012).
29. See supplementary materials on *Science* Online.

Acknowledgments: We thank the referees for useful comments. Supported by National Research Foundation grant 2010-0015066 awarded through the Acceleration Research Program, the Seoul Science Foundation, and the Global Frontier Program (Y.S.C.).

Supplementary Materials

www.sciencemag.org/cgi/content/full/339/6124/1185/DC1
Supplementary Text
Figs. S1 to S11
Table S1

27 September 2012; accepted 28 January 2013
10.1126/science.1230813

Emergence of a Measurement Basis in Atom-Photon Scattering

Yinnon Glickman, Shlomi Kotler, Nitzan Akerman, Roee Ozeri*

After measurement, a wave-function is postulated to collapse on a predetermined set of states—the measurement basis. Using quantum process tomography, we show how a measurement basis emerges in the evolution of the electronic spin of a single trapped atomic ion after spontaneous photon scattering and detection. This basis is determined by the excitation laser polarization and the direction along which the photon was detected. Quantum tomography of the combined spin-photon state reveals that although photon scattering entangles all superpositions of the measurement-basis states with the scattered photon polarization, the measurement-basis states themselves remain classically correlated with it. Our findings shed light on the process of quantum measurement in atom-photon interactions.

The interaction between quantum systems and their environment results in decoherence and reduction of quantum superpositions to classical statistical ensembles. On the other hand, probing a fraction of the environment (environments by nature are too large to be monitored as a whole) yields information about the system state. The back-action on the system can then result in the emergence of a measurement basis. The measurement basis states will be those that are classically correlated with the detected environment modes, whereas their superpositions will be entangled with the environment (*1*, *2*). Thus, decoherence, measurement, and entanglement all partake in the quantum measurement process.

Because atomic systems can be well isolated from their environment and coherently controlled with good fidelity, they are a good experimental platform for the study of such fundamental quantum phenomena. In a typical experiment, a bipartite atomic superposition is controllably coupled to its environment and monitored in order to investigate different facets of decoherence and measurement. Examples include the study of decoherence due to coupling to engineered reservoirs by using trapped atomic ions (*3*) or the observation of the progressive decoherence of the measurement apparatus by using the interaction between atoms and a microwave cavity (*4*).

A natural environment for atomic systems is the electromagnetic vacuum to which they couple via spontaneous photon scattering. The effect of light scattering on the coherence of atomic interferometers showed that scattered photons expose the path an atom has taken (*5*–*7*). Photon scattering by trapped atomic ions, in which the direction and magnitude of the internal angular momentum of an atom become correlated with a scattered photon, results in spin decoherence (*8*–*10*). State-selective florescence by use of resonant laser light was used to measure the internal electronic state of atoms with a very small error probability (*11*–*13*). Last, the entanglement between a single atom and a spontaneously scattered photon was recently observed (*10*, *14*, *15*). In all of these experiments, decoherence, measurement, and entanglement

Department of Physics of Complex Systems, Weizmann Institute of Science, Rehovot 76100, Israel.

*To whom correspondence should be addressed. E-mail: roee.ozeri@weizmann.ac.il

Downloaded from www.sciencemag.org on March 8, 2013

were separately explored. However, the full dynamics of measurement of the atomic state by the electromagnetic vacuum environment was not observed. We show that a measurement basis emerges in the spin-state space of a single trapped atomic ion when photons are scattered and detected, in a process in which decoherence, measurement, and entanglement are intertwined.

We used the electronic spin, in the $5s^2S_{1/2}$ ground level, of a single trapped $^{88}Sr^+$ ion (Fig. 1). The ion was trapped and laser-cooled in a linear Paul trap. A weak magnetic field, applied in the $\hat{z}$ direction, removed the degeneracy between the two spin states by $\hbar\omega_0$, where $\omega_0/2\pi$ = 3.5 MHz, and $\hbar$ is Planck's constant h divided by 2π. Spin initialization, readout, and rotations were carried out by a combination of optical and radio frequency (rf) pulses (*13*, *16*, *17*). To ensure that the spin direction was well defined in the lab frame of reference, we reset the phase of our rf oscillator at the beginning of each repetition of the experiment. Subsequent to this initialization procedure, the spin performed Larmor precession around the $\hat{z}$ direction at ω_0.

Spin-photon interactions were induced by a 422-nm laser beam resonant with the $5s^2S_{1/2} \rightarrow 5s^2P_{1/2}$ transition (21 MHz spectral width) and polarized in the $\hat{z}$ direction (Fig. 1, inset). The ion scattered a photon from this beam with a probability between 0.05 and 0.1. Outgoing photons were detected from a direction perpendicular to the excitation laser direction ($\hat{x}$ direction). The outgoing photon polarization was fully characterized by a polarization analysis unit. The overall detection efficiency of scattered photons was measured to be roughly 1/400. We post-selected only those repetitions of the experiment in which a single photon was recorded. To investigate spin dynamics due to photon scattering, it is important to know the spin direction within the Larmor precession cycle at the moment the photon was scattered. To this end, we recorded the phase of our local oscillator—tuned to the Larmor precession frequency ω_0—at the time the scattered photon was recorded (*10*).

Photon scattering transfers the electron between two spin 1/2 manifolds ($5s^2S_{1/2} \rightarrow 5p^2P_{1/2}$). It is therefore convenient to think of the coupling between these manifolds in terms of spin 1/2 (Pauli) operators. In events in which a single photon was emitted into a direction $\hat{k}$, the spin degrees of freedom in the ground and excited states are coupled via a single application of the spin operator $i(\vec{\sigma} \cdot \vec{E})$ (*2*). Here, $\vec{\sigma}$ is a vector of the Pauli spin 1/2 operators, and $\vec{E}$ is the polarization vector of the emitted photon. In the case of absorption, the coupling operator is $-i\vec{\sigma} \cdot \vec{E}$ (*17*). It is instructive to study the reduced spin evolution, after photon emission, by using a circular photon polarization basis. In this case, the two spin operators that correspond to the emitted photon polarization components are $\vec{\sigma} \cdot \vec{E}_{\pm}{}^* = \sigma_{\pm}$, the spin ladder operators in the $\vec{k}$ direction. This means that spin states that initially point along the emitted photon propagation direction can emit circularly polarized photons but only with the helicity parallel to their spin. After emission of a circularly polarized photon, the spin direction reverses but remains aligned with the photon $\vec{k}$ vector. This is a simple manifestation of angular momentum conservation in the photon emission process. To evaluate spin evolution in the full scattering process, one has to account for photon absorption as well. Here, spin evolution depends on the polarization of the excitation laser and its

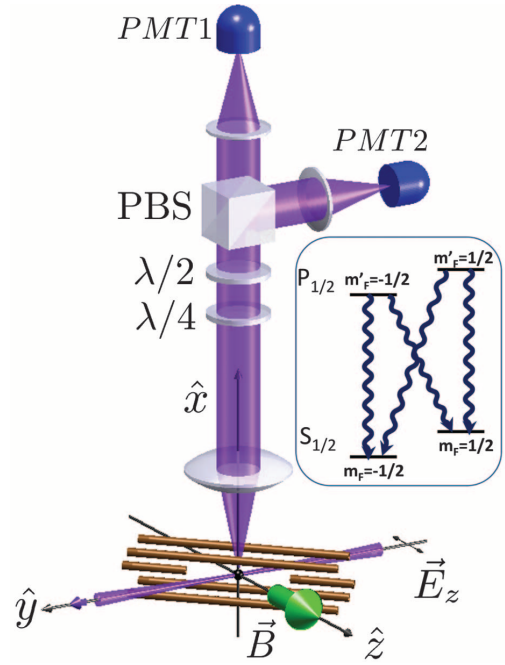

Fig. 1. Schematic of the experimental setup. A single $^{88}Sr^+$ ion is trapped in a linear Paul trap (*15*). The magnetic field is aligned along $\hat{z}$. (Inset) A schematic level structure of the $5s^2S_{1/2}$ and the $5p^2P_{1/2}$ electronic levels. The transition between these two levels is excited by a weak resonant beam, propagating along $\hat{y}$ and linearly polarized along $\hat{z}$. Scattered photons are collected along the $\hat{x}$ direction, and their polarization is analyzed by using half- and quarter-wave retardation plates and a PBS. The two ports of the PBS are directed toward two photo multiplier tube (PMT) detectors.

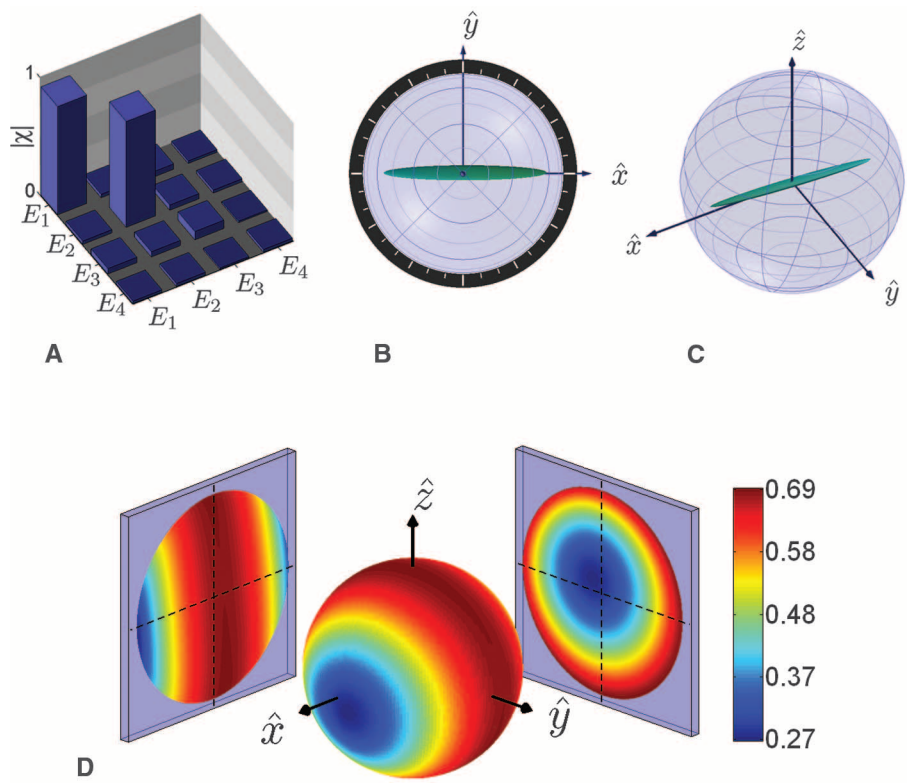

Fig. 2. Collapse of spin states. (**A**) The absolute value of the elements of the reconstructed process matrix, in the basis $E_1 = |\hat{x}\rangle\langle\hat{x}| = (I + \sigma_x)/2$, $E_2 = |-\hat{x}\rangle\langle-\hat{x}| = (I-\sigma_x)/2$ (projections on the $|\pm\hat{x}\rangle$ states), $E_3 = -i\sigma_y$, and $E_4 = \sigma_z$. (**B** and **C**) Two view points on the surface on which the Bloch sphere of initial spin states is mapped after photon detection. (**D**) The von Neumann entropy of post-scattering spin states plotted on the Bloch sphere of initial spin states.

Downloaded from www.sciencemag.org on March 8, 2013

direction relative to that of the scattered photon. In our experiment, the ion is excited with a laser beam that is linearly polarized in the $\vec{z}$ direction and photons are detected in the $\vec{x}$ direction (Fig. 1). The effect of a sequence of absorption and emission on the combined state of spin and emitted photons can then be expressed by an application of $\vec{\sigma}\cdot\vec{E} = \sigma_z$ followed by $S_{\text{emit}} = \vec{\sigma}_{(+,x)}\otimes a^{\dagger}_{\vec{x},\vec{E}_+} + \vec{\sigma}_{(-,x)}\otimes a^{\dagger}_{\vec{x},\vec{E}_-}$, where $\vec{\sigma}_{(\pm,x)} = \sigma_y \mp i\sigma_z$ are the spin raising and lowering operators in the $\hat{x}$ direction. The spin-photon combined state after absorption and subsequent photon emission in the $\vec{x}$ direction hence evolves under

$$S_{\text{scatt}} = \vec{\sigma}_{(+,x)}\vec{\sigma}_z\otimes a^{\dagger}_{\vec{x},\vec{E}_+} + \vec{\sigma}_{(-,x)}\vec{\sigma}_z\otimes a^{\dagger}_{\vec{x},\vec{E}_-} = |-\hat{x}\rangle\langle-\hat{x}|\otimes a^{\dagger}_{\vec{x},\vec{E}_+} + |\hat{x}\rangle\langle\hat{x}|\otimes a^{\dagger}_{\vec{x},\vec{E}_-} \quad (1)$$

The spin of the ion is therefore projected along the emitted photon direction every time a photon with a circular polarization is detected. The pair of states $|\pm\hat{x}\rangle$ constitutes a measurement basis. These states are invariant under photon scattering (in the $\vec{x}$ direction), and therefore their entropy does not increase in the process. States that are initialized along this direction do not—whereas their superpositions do—entangle with the scattered photon polarization.

The correlation between the scattered photon and the basis along which spin states collapse can be well understood by angular momentum conservation arguments. Absorption of a $\hat{z}$-polarized photon flips $\hat{x}$-polarized spins (*18*). Circularly polarized emitted photons require full $\hbar$ angular momentum transfer along $\hat{x}$. The detection of circularly polarized photons therefore both measures and flips the spin in this direction. Spin states that are initially pointing in the $\hat{x}$ direction remain invariant under absorption followed by emission while the photon polarization measures the atomic spin along this direction. By post-selecting events in which the photon was scattered in a different direction, the basis along which the atomic spin is measured will change accordingly. Therefore, under continuous photon scattering from a linearly polarized beam, and without post-selection of a well-defined photon scattering direction, all resulting measurement directions will average to result in complete spin depolarization. An unpolarized excitation laser would have a similar effect.

We performed spin quantum process tomography (QPT) of post-selected events in which a single photon was detected. Typically, QPT is performed in a frame of reference that is rotating together with the spin. In this work, however, spin evolution due to photon scattering is determined by directions in the lab frame of reference. To faithfully perform QPT in the lab frame, we perform it stroboscopically with the spin Larmor precession. To this end, rather than analyzing all recorded events we limited our analysis to events that occurred within a $2\pi/32$-radian phase interval of our local oscillator. The direction of the spin at the moment of scattering, in these events, was spread over an angular span that equals this phase interval. Choosing other phase intervals of similar width yield identical results (*17*). We found that the process matrix is mostly composed of nearly equal contributions of projections on the $|+\hat{x}\rangle$ and $|-\hat{x}\rangle$ states, which is in agreement with Eq. 1. This is seen in Fig. 2A, in which the absolute value of the entries of the reconstructed process matrix is displayed. It is written by using the basis elements $|\hat{x}\rangle\langle\hat{x}| = (I+\sigma_x)/2$, $|-\hat{x}\rangle\langle-\hat{x}| = (I-\sigma_x)/2$ (projections on the $|\pm\hat{x}\rangle$ states), $-i\sigma_y$, and σ_z. The collapse of the spin wave function is best depicted in the Bloch sphere geometric representation. Each point on the surface of the Bloch sphere represents a pure state, whereas mixed states are represented as points within the sphere volume (*19*). After photon scattering, all prescattering pure states, represented by the Bloch sphere surface, are mapped onto a different surface, which is contained within the sphere. The reconstructed process matrix can be used to calculate the surface onto all pure spin state are mapped (Fig. 2, B and C). An elongated ellipsoid clearly marks the emergence of a spin measurement basis. We chose the direction along which the pointer basis emerges to be the $\hat{x}$ axis, thus coinciding this coordinate system with the lab coordinate system (Fig. 1). The 1:11 aspect ratio between the spheroid length along the emergent basis and its radial size is dictated by the finite local oscillator phase interval in our data, the finite numerical aperture of our photon collection lens, and quantum projection noise (*17*). The von Neumann entropy $S(\rho) = -\text{Tr}[\rho\ln(\rho)]$ of all post-scattering states is shown in the color map in Fig. 2D. This is also the increase in entropy due to photon scattering. Spin states along the $\hat{x}$ direction indeed experience the minimal increase in entropy, which is in accordance with the predictability sieve criteria in decoherence theory (*1*). Other states, on the other hand, acquire entropy, demonstrating that without any knowledge of the scattered photon, the process of photon scattering is in general irreversible.

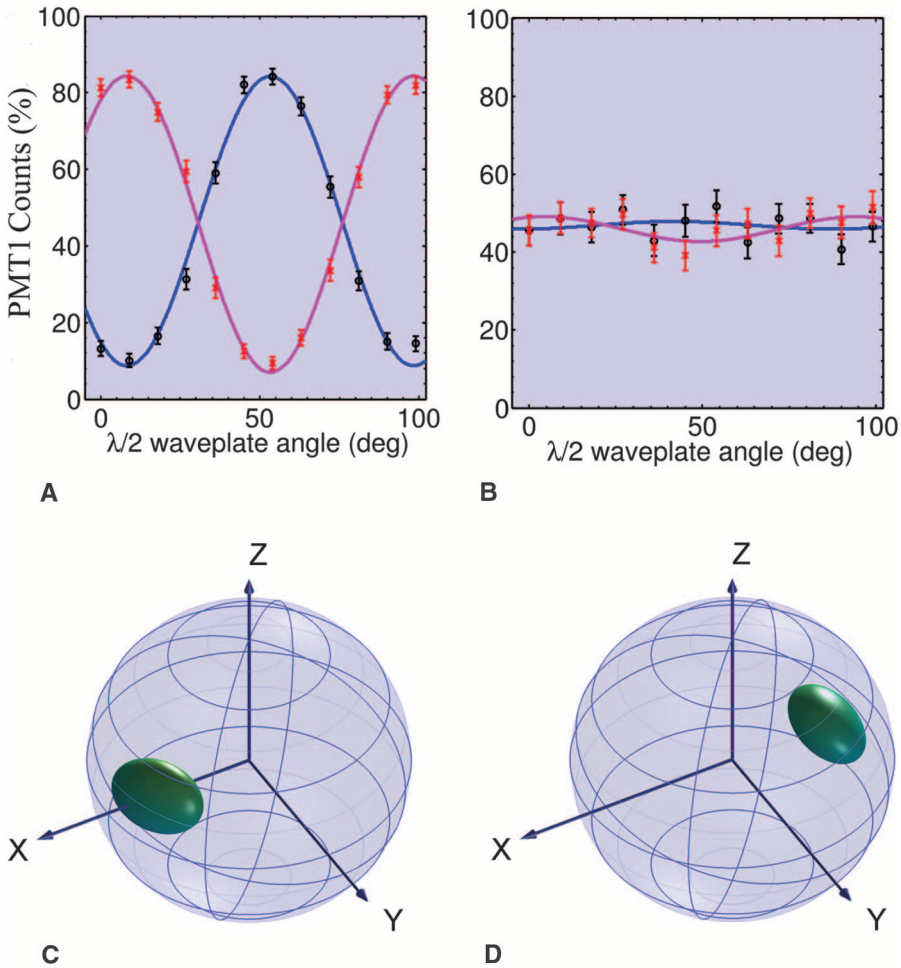

Fig. 3. Spin measurement via photon polarization detection. A quarter-wave retardation plate transformed the circular polarization of scattered photons into linear. The abscissa is the angle of the half-wave retardation plate, which is subsequently rotating the photon polarization direction with respect to that of the PBS. The ordinate is the probability of detecting photons on one port of the PBS when the spin is initialized to (**A**) the $|\hat{x}\rangle$ (solid red circles) or $|-\hat{x}\rangle$ (solid black circles) states or (**B**) the $|\pm Y\rangle$ states. (**C** and **D**) The surfaces representing all post-scattering states in which right or left circularly polarized photons were detected, respectively.

Downloaded from www.sciencemag.org on March 8, 2013

In order to prove that the $|\pm\hat{x}\rangle$ states on the poles of the emerging ellipsoid are a measurement basis, we analyzed the polarization of photons that were scattered by different initial spin states. According to Eq. 1, the $|\pm\hat{x}\rangle$ states scatter photons with a pure circular polarization, whereas other initial spin states become entangled with the photon polarization. The latter case leads to a statistical mixture of photon polarization measurement outcomes. The results of our photon polarization measurements are shown in Fig. 3. Here, we aligned a quarter-wave retardation plate so that it transformed the $|E_{\pm}\rangle$ states to an orthogonal linear basis. A proceeding half-wave plate rotated this linear polarization with respect to the basis of a polarization beam splitter (PBS). The probability of photon detection on a given port of the PBS versus the half-wave plate rotation angle is shown in Fig. 3A. Here, the spin is initialized to the $|\hat{x}\rangle$ (solid red circles) or $|-\hat{x}\rangle$ (solid black circles) states. As expected from a pure polarization state, this probability sinusoidally oscillates as the polarization is rotated. The blue and magenta solid lines are a sinusoidal fit to our data. Furthermore, whenever the two wave plates transform the emitted circular polarization to match the PBS basis, a clear correlation between the measured polarization and the initial spin state is observed. Similar data with the spin initialized to the $|\pm\hat{y}\rangle$ states is shown in Fig. 3B. As expected from a fully mixed polarization state, the photon detection probability on a given PBS port is independent of polarization rotation indicating a lack of classical correlation between the photon polarization state and the initial spin state. Alternatively, we performed spin QPT conditioned on the detection of right or left circularly polarized photons. The surfaces onto which all pure states are mapped are shown in Fig. 3, C (right-circular) and D (left-circular). Indeed, conditioned on the detection of a right circularly polarized photon, all initial states collapsed to the $|\hat{x}\rangle$ state, and conditioned on the detection of a left circularly polarized photon, all initial states collapsed to the $|-\hat{x}\rangle$ state.

Starting with an initial spin state other than $|\pm\hat{x}\rangle$, we have seen that both the spin state and the photon polarization state decohere into statistical mixtures. This decoherence is the result of spin-photon entanglement. To observe this entanglement, we preformed quantum state tomography of the combined spin-photon state. The reconstructed spin-photon density matrices for six different initial spin states are presented in Fig. 4, A to F: $|\pm\hat{z}\rangle$, $|\pm\hat{x}\rangle$, and $|\pm\hat{y}\rangle$. We plotted the density matrices using the $|\pm\hat{x}\rangle$ and $|E_{\pm}\rangle$ states as a basis. As seen, whenever the spin was initialized along $\pm\hat{x}$ the resulting spin-photon density matrices represent approximately separable states. Alternatively, spin states that were initially oriented along the $\pm\hat{y}$ or $\pm\hat{z}$ directions resulted in highly entangled states. We quantified the amount of atom-photon entanglement using the concurrence entanglement monotone, $C(\rho)$ (*20*). All atom-photon final density matrices were evaluated by means of linear combinations of the six reconstructed density matrices. A color map of the calculated concurrence values plotted on the Bloch sphere of initial spin states is presented in Fig. 4G. The minimum entanglement ($C < 0.03$) is along the $\hat{x}$ direction, whereas the maximally entangled states ($C \cong 0.7$) are along the sphere circumference in the $\hat{y}\hat{z}$ plane, which is consistent with the observed entropy increase shown in Fig. 2D.

We have shown that the back action of the observation of the atomic spin with light aligned it with our observation direction. States that were

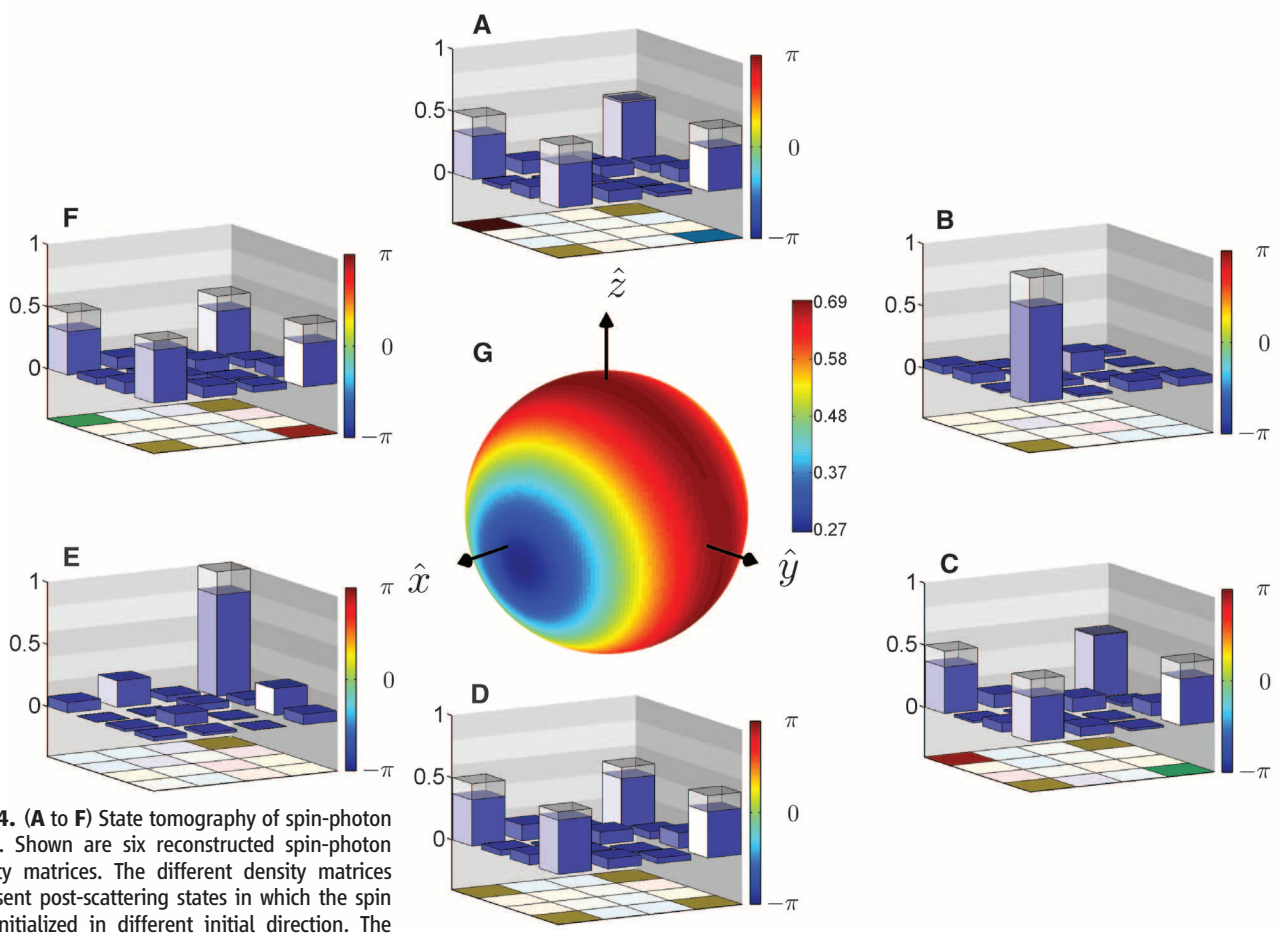

Fig. 4. (**A** to **F**) State tomography of spin-photon states. Shown are six reconstructed spin-photon density matrices. The different density matrices represent post-scattering states in which the spin was initialized in different initial direction. The different spin initial states are (A) $|\hat{z}\rangle$, (B) $|-\hat{x}\rangle$, (C) $|\hat{y}\rangle$, (D) $|-\hat{z}\rangle$, (E) $|\hat{x}\rangle$, and (F) $|-\hat{y}\rangle$. The density matrices are written in the basis of the product states $|\pm\hat{x}\rangle\otimes|E_{\pm}\rangle$. The solid bars are absolute values of entries of the reconstructed density matrices, whereas the transparent bars correspond to the values predicted with Eq. 1. The phases of the different entries are represented by different colors below the bars and according to the color map on the right. (**G**) A color map of the measured concurrence of every post-scattering spin-photon state. The map is plotted on the Bloch sphere of all initial pure spin directions.

Downloaded from www.sciencemag.org on March 8, 2013

initially aligned with this direction emitted pure circularly polarized photons and remained invariant under scattering. Their superpositions, on the other hand, became entangled with the scattered photon polarization. States that are invariant under coupling to the environment are of interest, not only because of their importance in the quantum measurement process but also because of their potential use for quantum control purposes. Invariant states can span decoherence-free subspaces in which quantum information can be protected (*21*). It would be therefore interesting to search for multi-spin states that are invariant under photon scattering, and detection, by using larger arrays of trapped ions.

References and Notes

1. W. H. Zurek, *Rev. Mod. Phys.* **75**, 715 (2003).
2. This mechanism is different than the process of ein-selection in decoherence theory, in which the mutual interaction between a quantum system, a measurement apparatus, and their environment results in the emergence of a preferred basis (*1*).
3. C. J. Myatt *et al.*, *Nature* **403**, 269 (2000).
4. M. Brune *et al.*, *Phys. Rev. Lett.* **77**, 4887 (1996).
5. M. S. Chapman *et al.*, *Phys. Rev. Lett.* **75**, 3783 (1995).
6. M. Mei, M. Weitz, *Phys. Rev. Lett.* **86**, 559 (2001).
7. D. A. Kokorowski, A. D. Cronin, T. D. Roberts, D. E. Pritchard, *Phys. Rev. Lett.* **86**, 2191 (2001).
8. R. Ozeri *et al.*, *Phys. Rev. Lett.* **95**, 030403 (2005).
9. H. Uys *et al.*, *Phys. Rev. Lett.* **105**, 200401 (2010).
10. N. Akerman, S. Kotler, Y. Glickman, R. Ozeri, *Phys. Rev. Lett.* **109**, 103601 (2012).
11. D. B. Hume, T. Rosenband, D. J. Wineland, *Phys. Rev. Lett.* **99**, 120502 (2007).
12. A. H. Myerson *et al.*, *Phys. Rev. Lett.* **100**, 200502 (2008).
13. A. Keselman, Y. Glickman, N. Akerman, S. Kotler, R. Ozeri, *New J. Phys.* **13**, 073027 (2011).
14. B. B. Blinov, D. L. Moehring, L. M. Duan, C. Monroe, *Nature* **428**, 153 (2004).
15. J. Volz *et al.*, *Phys. Rev. Lett.* **96**, 030404 (2006).
16. N. Akerman, S. Kotler, Y. Glickman, A. Keselman, R. Ozeri, *App. Phys. B*, 10.1007/s00340-011-4807-6 (2011).
17. Materials and methods are available as supplementary materials on *Science* Online.
18. Cohen-Tannoudji, Claude and Diu, Bernard and Laloe, Frank, *Quantum Mechanics* (Wiley-Interscience 2006), Vol. 2, p. 1048.
19. M. A. Nielsen, I. L. Chuang, *Quantum Computation and Quantum Information* (Cambridge Univ. Press, Cambridge, 2000).
20. M. B. Plenio, S. Virmani, *Quant. Inf. Comput.* **7**, 1 (2007).
21. D. A. Lidar, I. L. Chuang, K. B. Whaly, *Phys. Rev. Lett.* **81**, 2594 (1998).

Acknowledgments: Y.G. and S.K. have equally contributed to this work. We thank N. Davidsson and D. Stamper-Kurn for useful comments on the manuscript. We gratefully acknowledge the support by the Israeli Science Foundation, the Minerva Foundation, the German-Israeli Foundation for scientific research, the Crown Photonics Center, and M. Kushner Schnur, Mexico.

Supplementary Materials
www.sciencemag.org/cgi/content/full/339/6124/1187/DC1
Materials and Methods
Figs. S1 to S4

3 September 2012; accepted 2 January 2013
10.1126/science.1229650

A Transforming Metal Nanocomposite with Large Elastic Strain, Low Modulus, and High Strength

Shijie Hao,[1] Lishan Cui,[1]* Daqiang Jiang,[1] Xiaodong Han,[2]* Yang Ren,[3]* Jiang Jiang,[1] Yinong Liu,[4] Zhenyang Liu,[1] Shengcheng Mao,[2] Yandong Wang,[5] Yan Li,[6] Xiaobing Ren,[7,8] Xiangdong Ding,[7] Shan Wang,[1] Cun Yu,[1] Xiaobin Shi,[1] Minshu Du,[1] Feng Yang,[1] Yanjun Zheng,[1] Ze Zhang,[2,9] Xiaodong Li,[10] Dennis E. Brown,[11] Ju Li[7,12]*

Freestanding nanowires have ultrahigh elastic strain limits (4 to 7%) and yield strengths, but exploiting their intrinsic mechanical properties in bulk composites has proven to be difficult. We exploited the intrinsic mechanical properties of nanowires in a phase-transforming matrix based on the concept of elastic and transformation strain matching. By engineering the microstructure and residual stress to couple the true elasticity of Nb nanowires with the pseudoelasticity of a NiTi shape-memory alloy, we developed an in situ composite that possesses a large quasi-linear elastic strain of over 6%, a low Young's modulus of ~28 gigapascals, and a high yield strength of ~1.65 gigapascals. Our elastic strain-matching approach allows the exceptional mechanical properties of nanowires to be exploited in bulk materials.

It is challenging to develop bulk materials that exhibit a large elastic strain, a low Young's modulus, and a high strength because of the intrinsic trade-off relationships among these properties (*1*, *2*). A low Young's modulus in a single-phase material usually means weak interatomic bonding and thus low strength. Because of the initiation of dislocation activity and/or early failure caused by structural flaws, the elastic strain of bulk metals is usually limited to less than 1%. Because freestanding nanowires have ultrahigh elastic strain limits (4 to 7%) and yield strengths (*3*–*9*), it is expected that composites made with nanowires will have exceptional mechanical properties. However, the results obtained so far have been disappointing (*10*), primarily because the intrinsic mechanical properties of nanowires have not been successfully exploited in bulk composites (*10*–*12*). A typical example is the Nb nanowire–Cu matrix composite, in which the nanowires are well dispersed and well aligned, with strong interfacial bonding. The elastic strain limit achieved in the Nb nanowires in this type of composite is only ~1.5% (*13*, *14*), far below what may be expected of freestanding nanowires (*3*–*9*).

To optimize the retention of nanowire properties in a composite, we hypothesize that the matrix should not deform via sharp microscopic defects such as cracks or dislocations but rather should be rubbery or gluelike, which suggests the use of a shape-memory alloy (SMA) as the matrix. There are two main differences between an SMA matrix and a conventional, plastically deforming metal matrix. First, macroscopically, SMA supports a large pseudoelastic strain of ~7% by stress-induced martensitic transformation (SIMT) (*15*, *16*), which is a strain magnitude comparable to nanowire elasticity (*3*–*9*). Use of an SMA as the matrix allows one to match the high pseudoelasticity of the SMA with the high elasticity of nanowires, as illustrated in Fig. 1A. Second, SIMT and dislocation slip are fundamentally different processes at the atomic scale. Whereas the inelastic shear strain between two adjacent atomic planes approaches 100% after dislocation slip (*17*), the atomic-level inelastic or transformation strain is ~10% after SIMT in typical SMAs such as NiTi (*16*). Therefore, inelastic strain incompatibilities (which must be compensated for by the elastic strain field to maintain cohesion) are much milder at the SMA-nanowire interface than at typical dislocation–piled-up interfaces.

To verify this hypothesis, we selected Nb nanowires to be combined with a NiTi SMA. The NiTi-Nb system with ~20 atomic % Nb undergoes eutectic solidification into a microstructure consisting of fine Nb lamellae (*18*), which can be converted into Nb nanowires through severe plastic deformation. In this study, an ingot with a composition of $Ni_{41}Ti_{39}Nb_{20}$ (atomic %) was prepared by means of vacuum induction

[1]State Key Laboratory of Heavy Oil Processing, China University of Petroleum, Beijing 102249, China. [2]Institute of Microstructure and Properties of Advanced Materials, Beijing University of Technology, Beijing 100124, China. [3]X-ray Science Division, Argonne National Laboratory, Argonne, IL 60439, USA. [4]School of Mechanical and Chemical Engineering, The University of Western Australia, Crawley, WA 6009, Australia. [5]State Key Laboratory for Advanced Metals and Materials, University of Science and Technology Beijing, Beijing 100083, China. [6]School of Materials Science and Engineering, Beihang University, Beijing 100191, China. [7]State Key Laboratory for Mechanical Behavior of Materials and Frontier Institute of Science and Technology, Xi'an Jiaotong University, Xi'an 710049, China. [8]Ferroic Physics Group, National Institute for Materials Science, Tsukuba, 305-0047 Ibaraki, Japan. [9]State Key Laboratory of Silicon Materials, Zhejiang University, Hangzhou 310058, China. [10]Department of Mechanical Engineering, University of South Carolina, Columbia, SC 29208, USA. [11]Department of Physics, Northern Illinois University, De Kalb, IL 60115, USA. [12]Department of Nuclear Science and Engineering and Department of Materials Science and Engineering, Massachusetts Institute of Technology, Cambridge, MA 02139, USA.

*To whom correspondence should be addressed. E-mail: lishancui63@126.com (L.C.); xdhan@bjut.edu.cn (X.H.); ren@aps.anl.gov (Y.R.); liju@mit.edu (J.L.)

Downloaded from www.sciencemag.org on March 8, 2013

melting (fig. S1). Macroscopic wires of the in situ composite (nanowire in situ composite with SMA, hereinafter referred to as NICSMA) with diameters of 0.3 to 1.0 mm were subsequently fabricated by forging, wire-drawing, and annealing (Fig. 1B) (*19*). The typical microstructure of NICSMA (Fig. 1, C to E) consists of Nb nanowires formed in situ with a mean diameter of 60 nm, well dispersed and well aligned in the NiTi matrix along the wire axial direction, with well-bonded interfaces. The selected-area electron diffraction (SAED) pattern (Fig. 1F) is indexed to body-centered cubic Nb and B2-NiTi phases. The phase components of the composite were further characterized by high-energy x-ray diffraction (HE-XRD) (fig. S2) and energy-dispersive x-ray spectroscopic analysis (fig. S3). Both SAED and HE-XRD demonstrate that the Nb nanowires are well oriented with its [110] direction parallel to the wire axial direction. Figure 1, G and H, shows the morphologies of freestanding Nb nanowires obtained by removing the NiTi matrix via electrolytic etching (fig. S4), revealing that the Nb nanowires have lengths ranging from 1 to 100 μm and a mean aspect ratio exceeding 100.

In situ synchrotron HE-XRD (fig. S5) was carried out on NICSMA at room temperature. The evolution of the diffraction peaks for B2-NiTi (211) and B19′-NiTi (001) (fig. S6) indicates that the NiTi matrix underwent an elastic deformation followed by SIMT during tensile loading. Figure 2A shows the evolution of *d*-spacing strain with respect to the applied macroscopic strain for the Nb (220) plane perpendicular to the loading direction, illustrating that the Nb nanowires exhibited a tensile elastic strain of 4.2% when embedded in the SIMT matrix. This elastic strain limit of the Nb nanowires is comparable to that of freestanding nanowires (*3*–*9*). Furthermore, the elastic strain limits of the nanowires embedded in the SIMT matrix increase gradually with decreasing nanowire diameter. The maximum elastic strain limit of the Nb nanowires observed (fig. S7) was 6.5% (the red curve in Fig. 2A). In contrast, we found that, whenever the NiTi matrix deformed by dislocation slip instead of by SIMT after the initial elastic deformation (fig. S8), the elastic strain limits of the Nb nanowires are greatly reduced to ~1.3% (the black curve in Fig. 2A). Figure 2B shows a comparison of the elastic strain limits of (a) Nb nanowires in the matrix deforming by dislocation slip (*13*, *14*, *20*–*22*), (b) Nb nanowires in the matrix deforming by SIMT, and (c) some freestanding nanowires (*3*–*9*).

After pretreatment with a tensile strain cycle of 9.5%, the bulk NICSMA exhibited a large quasi-linear elastic strain of over 6%, a low Young's modulus of ~28 GPa, and a high yield strength of minimum 1.65 GPa within the temperature range of 15° to 50°C (Fig. 3, A and B). In comparison with other known bulk metals with low Young's moduli—for example, Mg, Al, and Ti alloys and gum metals (*1*, *2*, *23*, *24*)—the yield strength of NICSMA is superior. Figure 3, C and D, shows general comparisons of the elastic strain limit, Young's modulus, and yield strength of NICSMA and other metals (*1*, *2*, *23*–*25*) and human bones (*23*). NICSMA occupies a unique spot on a chart of the mechanical properties of various bulk materials (fig. S9) and possesses good cytocompatibility (figs. S10 and S11) and corrosion resistance in a physiological environment (fig. S12).

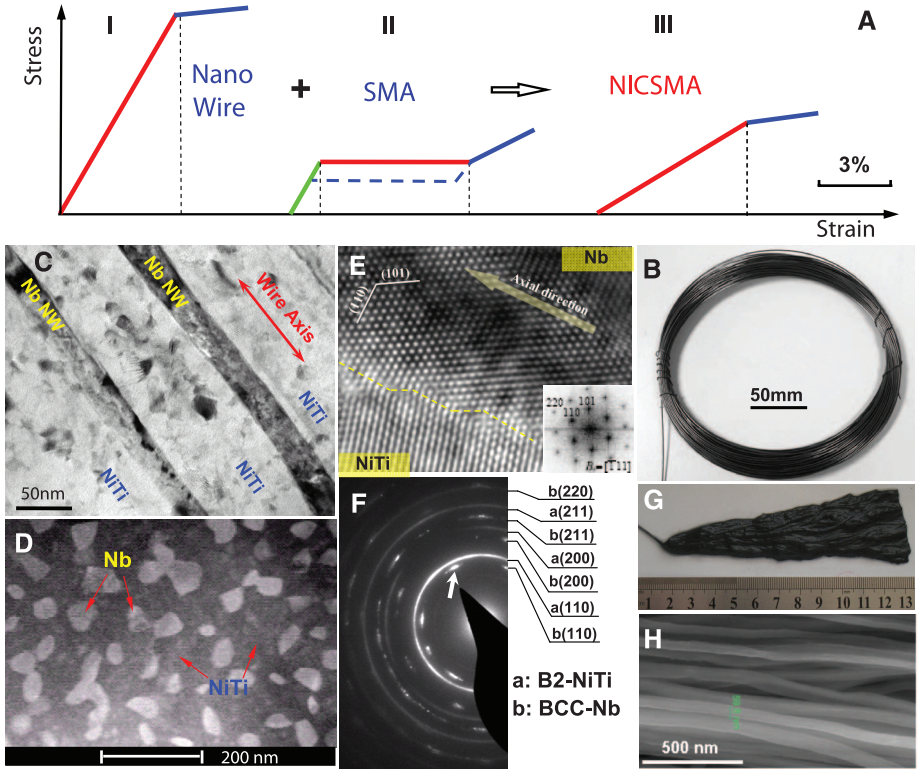

Fig. 1. (**A**) Schematic of the design concept of NICSMA. Schematic tensile stress-strain curves of a high-strength metallic nanowire (I), an SMA (II), and a NICSMA (III). (**B**) A coil of NICSMA wire with a diameter of 0.5 mm. (**C**) Transmission electron microscopy (TEM) image of a longitudinal section of NICSMA wire. NW indicates nanowire. (**D**) Scanning TEM image of the cross section of NICSMA wire (bright regions, cross sections of Nb nanowires; dark regions, NiTi matrix). (**E**) High-resolution TEM image of the interface between the Nb nanowire and the NiTi matrix. (**F**) SAED pattern from a longitudinal section of NICSMA wire. (**G**) Macroscopic appearance of a bundle of freestanding Nb nanowires. (**H**) Scanning electron microscopy image of the freestanding Nb nanowires.

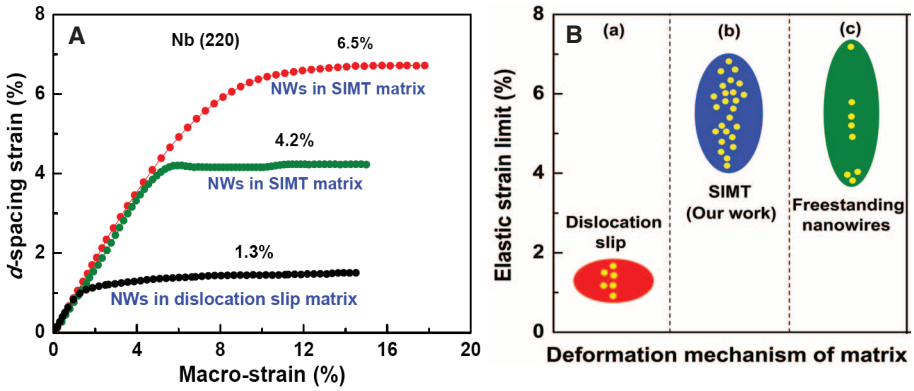

Fig. 2. Elastic strain limits of nanowires. (**A**) Evolution of the *d*-spacing strain with respect to the applied macroscopic strain for the Nb (220) plane perpendicular to the loading direction in the NICSMA wires in which the NiTi matrix deformed by SIMT and dislocation slip. The green curve (with a maximum strain of 4.2%) corresponds to the sample shown in Fig. 1 with 60-nm-diameter Nb nanowires. The red curve (with a maximum strain of 6.5%) corresponds to a different sample (fig. S7), with even narrower Nb nanowires. (**B**) Comparison of the elastic strain limits of (a) Nb nanowires embedded in the matrix deforming by dislocation slip (*13*, *14*, *20*–*22*), (b) Nb nanowires embedded in the matrix deforming by SIMT, and (c) some freestanding nanowires (*3*–*9*).

Downloaded from www.sciencemag.org on March 8, 2013

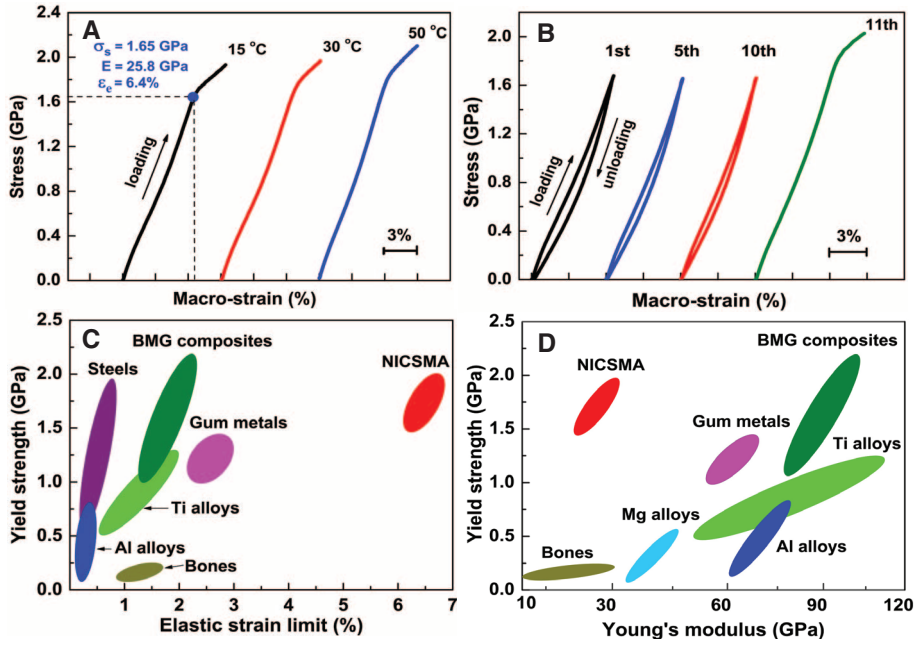

Fig. 3. Typical macroscopic mechanical properties of NICSMA. (**A**) Tensile stress-strain curves of a pretreated NICSMA at 15°, 30°, and 50°C. σ_S, yield strength; E, Young's modulus; ε_e, elastic strain limit. (**B**) Cyclic tensile stress-strain curves of a pretreated NICSMA at room temperature. (**C**) Comparison of the yield strengths and elastic strain limits of different materials. (**D**) Comparison of the yield strengths and Young's moduli of different materials.

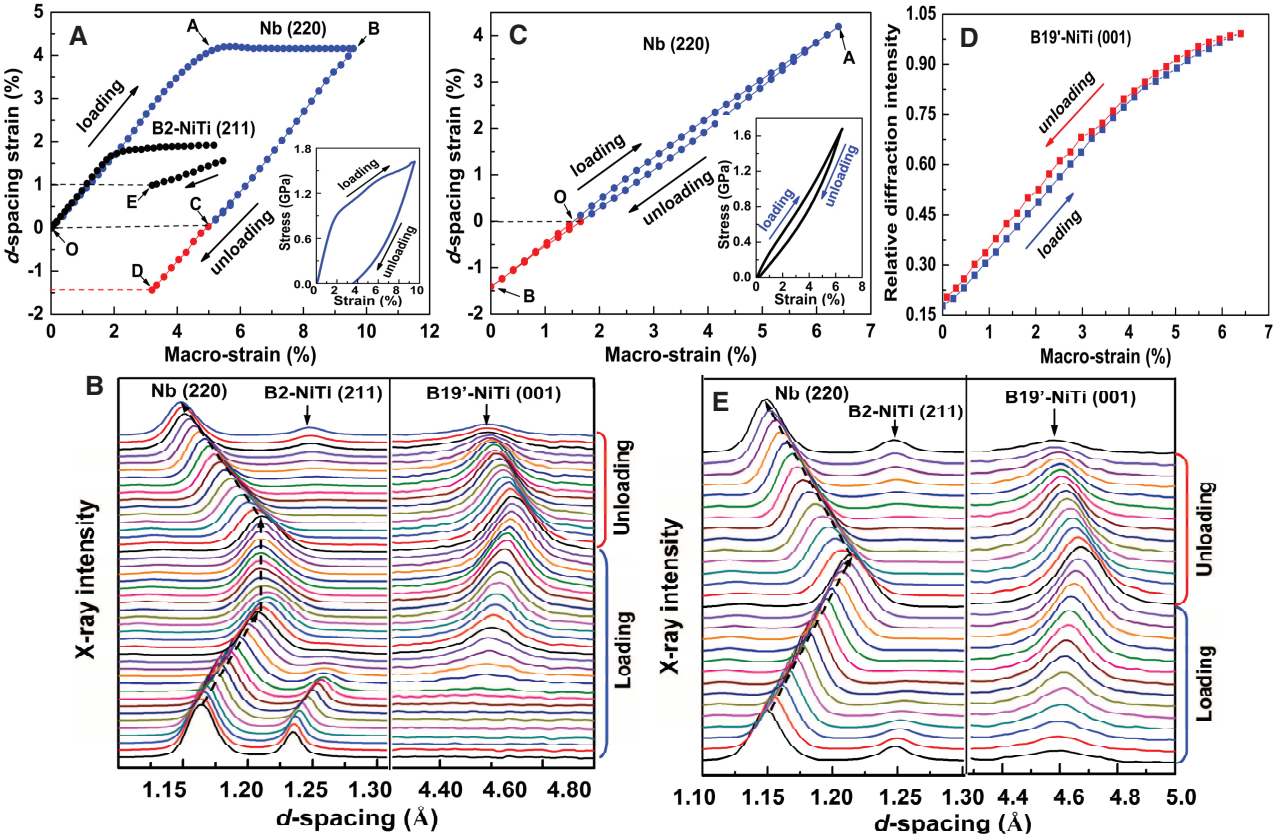

Fig. 4. Microscopic responses of NICSMA revealed by in situ synchrotron HE-XRD. (**A**) Evolution of the *d*-spacing strain for Nb (220) and B2-NiTi (211) planes perpendicular to the loading direction during the pretreatment. (Inset) The macroscopic stress-strain curve of the pretreatment. (**B**) Evolution of the diffraction peaks of Nb (220), B2-NiTi (211), and B19′-NiTi (001) during the pretreatment. (**C**) Evolution of the *d*-spacing strain for Nb (220) plane perpendicular to the loading direction during the subsequent tensile cycle. (Inset) The cyclic stress-strain curve. (**D**) Evolution of the relative intensity of the B19′-NiTi (001) diffraction peak during the subsequent tensile cycle. The relative intensity is defined as the ratio of the integrated area of the B19′-NiTi (001) diffraction peak at a given applied strain to that of the B19′-NiTi (001) diffraction peak at the maximum applied strain. (**E**) Evolution of the diffraction peaks of Nb (220), B2-NiTi (211), and B19′-NiTi (001) during the subsequent tensile cycle. The B2-versus-B19′ peak intensity changes continuously, indicating continuous SIMT throughout the tensile loading.

Downloaded from www.sciencemag.org on March 8, 2013

In situ synchrotron HE-XRD was used to characterize the deformation and phase transformation evolutions of the Nb nanowires and the NiTi matrix, during the pretreatment (Fig. 4A, inset) and the subsequent tensile cycle (Fig. 4C, inset). After the pretreatment, the Nb nanowires sustained an elastic compressive strain of –1.4% (point D), whereas the NiTi matrix sustained an elastic tensile strain of 1% (point E) (Fig. 4A). There is also some retained B19′ phase in the matrix (Fig. 4B). These results can be understood as follows. Upon removal of the pretreatment load, the plastically deformed Nb nanowires (A to B in Fig. 4A) hindered the recovery of the NiTi matrix because of the B19′→B2 transformation (*15*, *16*), which caused large residual strains in the nanowires and the SMA with some retained B19′ phase. This demonstrates that strong coupling between the nanowires and the matrix took place during the pretreatment. In the subsequent tensile cycle (Fig. 4C), the elastic strain achieved in the Nb nanowires was up to 5.6% (A to B), consisting of the preexisting elastic compressive strain of –1.4% (O to B) and an elastic tensile strain of 4.2% (O to A). The NiTi matrix went through continuous SIMT throughout the tensile loading and exhibited an ultralow tangential effective modulus (Fig. 4, D and E) rather than undergoing an initial elastic deformation followed by an abrupt SIMT transition, as would occur in a monolithic SMA (*16*). The continuous SIMT can be ascribed to the contribution of the preexisting internal tensile stress and the retained B19′ phase in the matrix. Upon unloading, the NiTi matrix underwent a reverse transformation from the stress-induced martensite to the parent phase (Fig. 4, D and E), introducing a small hysteresis in the stress-strain curve resulting from energy dissipation during the process. The experimental evidence presented above demonstrates that the Nb nanowires experienced an ultrawide elastic strain of 4.2% – (–1.4%) = 5.6%, which closely matches the phase transformation strain of ~7% of NiTi. This matching of elastic and transformation strains results in the extraordinary properties of NICSMA.

References and Notes

1. M. F. Ashby, *Materials Selection in Mechanical Design* (Butterworth-Heinemann, Burlington, VT, 2005).
2. T. Saito *et al.*, *Science* **300**, 464 (2003).
3. E. W. Wong, P. E. Sheehan, C. M. Lieber, *Science* **277**, 1971 (1997).
4. T. Zhu, J. Li, *Prog. Mater. Sci.* **55**, 710 (2010).
5. Y. Yue, P. Liu, Z. Zhang, X. Han, E. Ma, *Nano Lett.* **11**, 3151 (2011).
6. G. Richter *et al.*, *Nano Lett.* **9**, 3048 (2009).
7. L. Tian *et al.*, *Nat Commun.* **3**, 609 (2012).
8. K. Koziol *et al.*, *Science* **318**, 1892 (2007).
9. D. A. Walters *et al.*, *Appl. Phys. Lett.* **74**, 3803 (1999).
10. Y. Dzenis, *Science* **319**, 419 (2008).
11. P. Podsiadlo *et al.*, *Science* **318**, 80 (2007).
12. J. N. Coleman, U. Khan, Y. K. Gun'ko, *Adv. Mater.* **18**, 689 (2006).
13. L. Thilly *et al.*, *Acta Mater.* **57**, 3157 (2009).
14. V. Vidal *et al.*, *Scr. Mater.* **60**, 171 (2009).
15. K. Otsuka, C. M. Wayman, Eds., *Shape Memory Materials* (Cambridge Univ. Press, Cambridge, 1998).
16. K. Otsuka, X. Ren, *Prog. Mater. Sci.* **50**, 511 (2005).
17. S. Ogata, J. Li, S. Yip, *Science* **298**, 807 (2002).
18. M. Piao, S. Miyazaki, K. Otsuka, *Mater. Trans. Jpn. Inst. Met.* **33**, 337 (1992).
19. See supplementary materials on *Science* Online.
20. C. C. Aydıner, D. W. Brown, N. A. Mara, J. Almer, A. Misra, *Appl. Phys. Lett.* **94**, 031906 (2009).
21. L. Thilly *et al.*, *Appl. Phys. Lett.* **88**, 191906 (2006).
22. C. Scheuerlein, U. Stuhr, L. Thilly, *Appl. Phys. Lett.* **91**, 042503 (2007).
23. M. Niinomi, M. Nakai, *Int. J. Biomater.* **2011**, 1 (2011).
24. M. Niinomi, *Metall. Mater. Trans. A Phys. Metall. Mater. Sci.* **33**, 477 (2002).
25. D. C. Hofmann *et al.*, *Nature* **451**, 1085 (2008).

Acknowledgments: We thank G. H. Wu, H. B. Xu, and Y. F. Zheng for valuable discussions on the deformation mechanism of NICSMA. This work is supported by the key program project of National Natural Science Foundation of China (NSFC) (51231008), the National 973 programs of China (2012CB619400 and 2009CB623700), and the NSFC (51071175, 51001119, 50831001, and 10825419). J.L. also acknowledges support by NSF DMR-1008104 and DMR-1120901. X.D.H. acknowledges support by the Beijing High-level Talents (PHR20100503), the Beijing PXM201101420409000053, and Beijing 211 project. D.E.B. acknowledges support by the Institute for NanoScience, Engineering, and Technology (INSET) of Northern Illinois University. Use of the Advanced Photon Source was supported by the U.S. Department of Energy, Office of Science, under contract no. DE-AC02-06CH11357.

Supplementary Materials

www.sciencemag.org/cgi/content/full/339/6124/1191/DC1
Materials and Methods
Figs. S1 to S12
References (*26*–*30*)

9 August 2012; accepted 10 January 2013
10.1126/science.1228602

Terrestrial Accretion Under Oxidizing Conditions

Julien Siebert,[1]* James Badro,[2] Daniele Antonangeli,[1] Frederick J. Ryerson[2,3]

The abundance of siderophile elements in the mantle preserves the signature of core formation. On the basis of partitioning experiments at high pressure (35 to 74 gigapascals) and high temperature (3100 to 4400 kelvin), we demonstrate that depletions of slightly siderophile elements (vanadium and chromium), as well as moderately siderophile elements (nickel and cobalt), can be produced by core formation under more oxidizing conditions than previously proposed. Enhanced solubility of oxygen in the metal perturbs the metal-silicate partitioning of vanadium and chromium, precluding extrapolation of previous results. We propose that Earth accreted from materials as oxidized as ordinary or carbonaceous chondrites. Transfer of oxygen from the mantle to the core provides a mechanism to reduce the initial magma ocean redox state to that of the present-day mantle, reconciling the observed mantle vanadium and chromium concentrations with geophysical constraints on light elements in the core.

The depletion of siderophile (i.e., "iron-loving") elements in Earth's mantle relative to chondrites can constrain the redox state of accreting materials during terrestrial accretion and core differentiation (*1*–*4*). For example, metal-silicate partitioning experiments at atmospheric pressure indicate that the observed depletion of slightly siderophile elements (SSEs) such as V and Cr can only be produced at conditions more reducing than those required to account for the abundance of moderately siderophile elements (such as Ni, Co, and W) or highly siderophile elements (*5*). Using metal-silicate partition coefficients obtained at pressures up to 25 GPa, homogeneous accretion models posit that metal-silicate equilibrium took place at the base of a deep terrestrial magma ocean at a single oxygen fugacity (fO_2) (*6*–*8*). However, the pressure-temperature (*P*-*T*) conditions required to produce the observed depletions for V and Cr (at the present-day fO_2) require temperatures that greatly exceed that of the mantle liquidus (*2*, *4*, *9*, *10*). Such conditions are physically inconsistent with the magma ocean hypothesis, where the *P*-*T* conditions at the base of a magma ocean necessarily lie between the mantle solidus and liquidus, thereby creating a rheological boundary that enables the metal to pond and equilibrate with the silicate melt.

To satisfy this rheological constraint and SSE abundance patterns, recent models of core formation constrain metal-silicate equilibration to the *P*-*T* conditions of the peridotite liquidus and invoke early accretion of highly reduced materials with a FeO-poor silicate component (*2*, *4*, *10*, *11*). These initially low fO_2 conditions (~IW-4, corresponding to 4 log fO_2 units below the iron-wüstite buffer) enhance the siderophile character of the SSEs at the relevant *P*-*T* conditions. Subsequent, gradual oxidation of the mantle to ~IW-2 over the course of core formation is required to account for moderately siderophile element abundances and, most important, to reach the current mantle FeO content [8 weight percent (wt %) FeO in silicate]. Under reducing conditions, silicon is likely to be the only light element entering the core in large amounts (*10*–*12*). This scenario relies on extensive pressure and temperature extrapolation of SSE partitioning data, as existing results are restricted to rela-

[1]Institut de Minéralogie et de Physique des Milieux Condensés, Université Pierre et Marie Curie, UMR CNRS 7590, Institut de Physique du Globe de Paris, 75005 Paris, France. [2]Institut de Physique du Globe de Paris, Université Paris Diderot, 75005 Paris, France. [3]Lawrence Livermore National Laboratory, Livermore, CA 94551, USA.

*To whom correspondence should be addressed. E-mail: julien.siebert@impmc.upmc.fr

tively low-*P*, low-*T* conditions (up to 25 GPa and 3000 K) and do not cover a large fraction of the *P-T* conditions relevant to core-mantle equilibrium in a deep magma ocean (up to 60 GPa and 4000 K) (*13*, *14*). Should the solubility of additional components, such as oxygen, be enhanced in this *P-T* range, their influence on the thermodynamics of the metallic phase would not be captured by extrapolation.

Here, we present partitioning data for V and Cr at the conditions directly equivalent to the full range of *P-T* conditions relevant to core formation and metal-silicate equilibration at the base of a deep magma ocean (Fig. 1). The experiments were performed in a laser-heated diamond anvil cell (LHDAC) (*15*) between 35 and 74 GPa and between 3100 and 4400 K. We found that the mantle concentration of Cr and V can be satisfied in a single high-*P*, high-*T* equilibrium (Fig. 1) in relatively oxidizing conditions. In fact, core formation is a continuous process taking place over the course of accretion, with the core and mantle continuously growing and segregating from one another (*2*, *4*). Metal-silicate partition coefficients for SSEs along any possible thermodynamic path (*P*, *T*, composition) hypothesized during core formation are required to accurately calculate mantle siderophile trace element concentrations. The *P-T* conditions of core formation necessarily increase as Earth grows, but there is no robust constraint on the evolution and composition of accretionary material. The composition of these materials does, however, establish the initial oxidation state of Earth's interior—an important variable controlling metal-silicate equilibrium. Hence, siderophile element partitioning provides a diagnostic by which the composition of accretionary materials may be inferred.

Plausible accretionary composition models coupled with core formation scenarios can be tested against observables to constrain better the nature of the building blocks of Earth. For any core formation model, the primary metrics are (i) that final silicate mantle composition coincides with present-day mantle compositions, and (ii) that the composition of the core is consistent with geophysical observations. In terms of composition, the most important influence on partitioning is fO_2, which describes the redox state of the accretionary environment and controls the FeO content of the silicate magma ocean. The effect of core formation on the siderophile trace element concentration in the mantle cannot be determined unless the partition coefficient is known as a function of *P*, *T*, and fO_2. The Fe-normalized partition coefficient (K_D) of an element M can be parameterized as

$$\log \frac{D_M}{D_{Fe^{\frac{n}{2}}}} = \log K_D = a + \frac{b}{T} + \frac{c \cdot P}{T} - \log \frac{\gamma_M}{\gamma_{Fe^{\frac{n}{2}}}} \quad (1)$$

where *n* is the valence of element M, γ_{Fe} and γ_M are the activity coefficients of iron and cation M

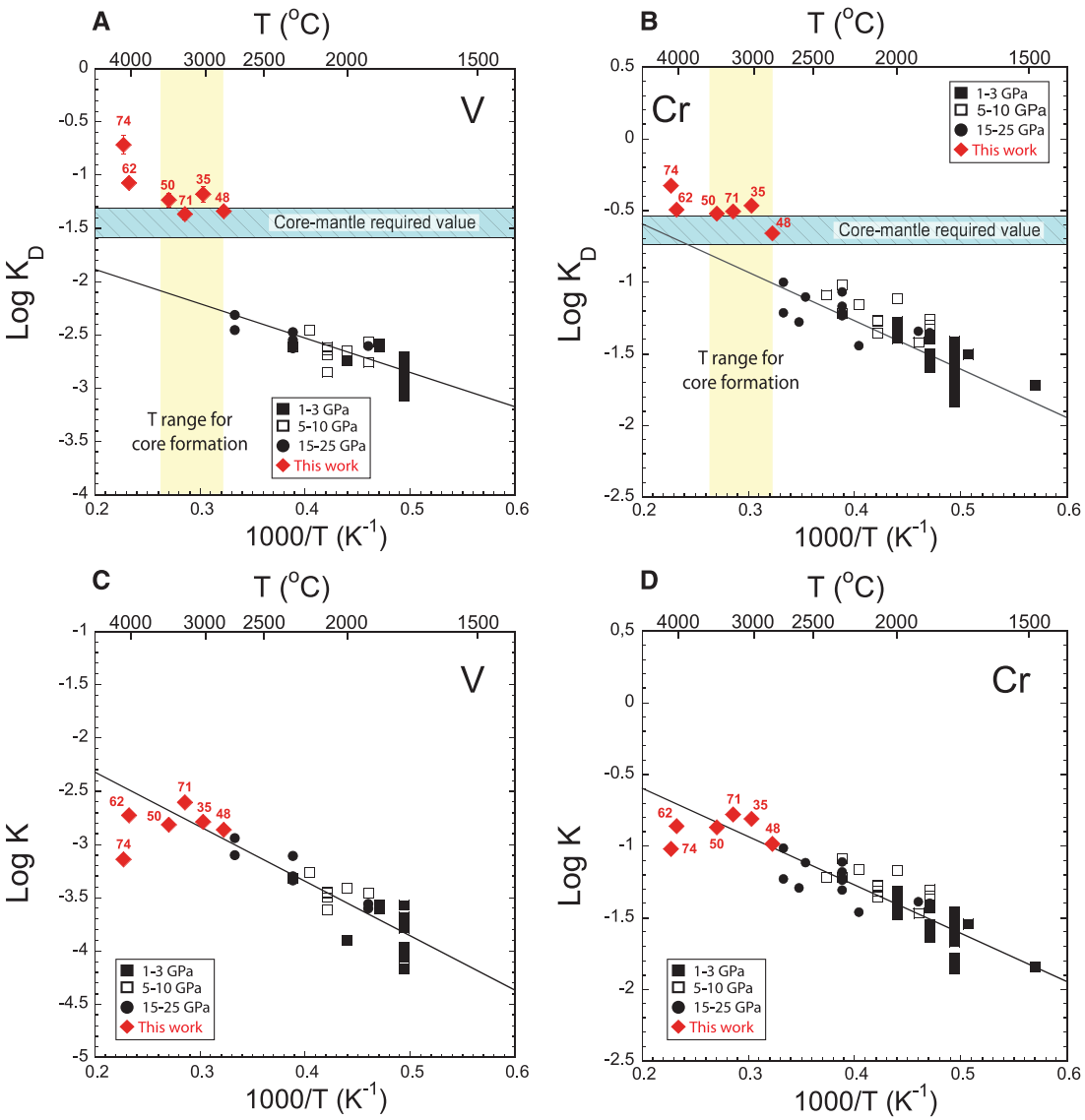

Fig. 1. (**A** and **B**) Exchange coefficients (K_D) for V (A) and Cr (B) plotted as a function of reciprocal temperature: this work (red diamonds with labeled pressure conditions in GPa) and other studies (*2*, *9*, *10*, *16*–*19*) at different pressure conditions. Where no error bars are shown, the uncertainties do not exceed the symbol size. The solid lines are the result of least-squares regressions of previous lower-pressure partitioning data (*2*, *9*, *10*, *16*–*19*). The partitioning data from our DAC experiments, well above the low-pressure regression, are attributed to the influence of oxygen solubility in the metal on the activity coefficients of Cr and V in the metal. (**C** and **D**) Equilibrium constant *K* [i.e., K_D corrected for activity coefficients (*15*), $K = K_D \cdot (\gamma_M/\gamma_{Fe}^{n/2})$] for V (C) and Cr (D) as a function of reciprocal temperature. This is the same data set as in (A) and (B), except that the exchange coefficient has been corrected for the activity coefficients of Fe, Cr, and V. These values depend strongly on oxygen content in the metallic phase. All data (O-bearing and O-depleted) fall on a single linear trend, showing the consistency of our activity model. Note that it is difficult to correct the activity in metals that are too O-rich, like our point at 74 GPa that has the highest O content in the metal (17 wt %), which falls systematically below the trend; however, high oxygen concentration increases the siderophile behavior of V and Cr.

in the metal phase, respectively, and a, b, and c are regression constants.

In accord with results from large-volume press (LVP) experiments at lower pressure (*2*, *9*, *10*, *16*–*19*), we see that the K_D values for Cr and V obtained in the LHDAC both increase with temperature between 35 and 74 GPa and are relatively insensitive to pressure (Fig. 1, A and B). However, the results of our experiments show that Cr and V are more siderophile (higher K_D) than would be expected from the extrapolation of lower-P, lower-T data and directly match the terrestrial target values (Fig. 1, A and B). Indeed, all of our data lie above the trend extrapolated from lower-P, lower-T LVP experiments. This is due to another important parameter that influences metal-silicate partitioning: the presence of minor constituents in the metallic phase, which in turn affects the activity coefficients of the siderophile elements (the last term in Eq. 1). In the high-P, high-T, high-fO_2 (~IW-1) conditions of our experiments (*15*), large amounts of oxygen (between 3.7 and 17 wt %) are present in the metallic phase (tables S2 and S3). This alters the activities of Cr and V in iron (*20*, *21*) and explains the disparity between our results and those extrapolated from lower-P experiments in which the metallic phases contain negligible oxygen. We used the epsilon formalism (*22*) to calculate the activity coefficients

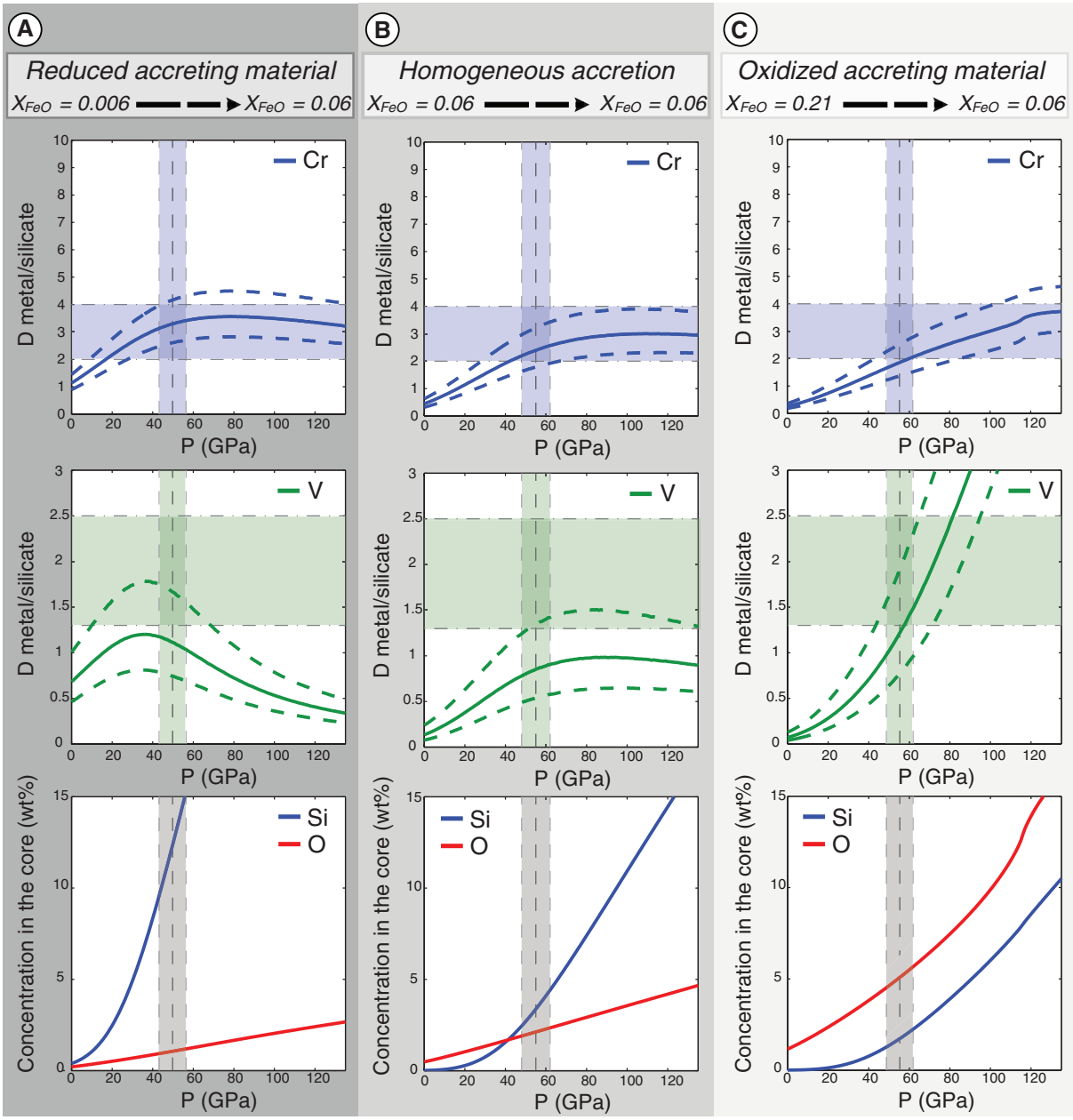

Fig. 2. Final core-mantle partition coefficients of Cr and V (D_{Cr} and D_V, top and middle rows) resulting from continuous core formation, as a function of final magma ocean pressure (i.e., depth). Solid lines show the evolution of the average partition coefficients; dashed lines define the uncertainty envelope calculated by Monte Carlo propagation of all uncertainties listed in table S4. The horizontal shaded bars represent the observed terrestrial target values for Cr and V (*9*). The bottom row shows the concentrations of O and Si in the core. The calculations are performed along three different oxygen fugacity paths: (**A**) the highly reduced model, (**B**) the homogeneous accretion model, and (**C**) the oxidized model. The relative size of the magma ocean with respect to that of the whole mantle was varied from a shallow magma ocean (final pressure of 0 GPa) to a global magma ocean (final pressure of 135 GPa). The gray vertical shaded bars show the pressure range where Cr and V abundances match the target values, along with additional constraints from Ni and Co partitioning (*15*). They show that the core must have formed at a final pressure between 40 and 60 GPa.

for Cr and V due to the incorporation of oxygen, correcting both the LHDAC and lower-P data (*2*, *9*, *10*, *16–19*) to obtain an equilibrium constant $K = K_D \cdot (\gamma_M/\gamma_{Fe}^{n/2})$, where γ_M is the activity coefficient for element M at the relevant oxygen concentration. The low-P and high-P data follow a linear trend (Fig. 1, C and D), supporting our contention that the apparent discrepancy between the low-P and high-P values of K_D (Fig. 1, A and B) is entirely due to the change in activity coefficient resulting from enhanced oxygen solubility in our experiments. The regression constants a, b, and c and activity models using LVP data [for experiments with metal phases containing no additional light elements such as C and S (*2*, *9*, *10*, *16–19*)] combined with our data are reported in table S4 (*15*).

We used the results of our regression in a continuous core formation model (*2*, *4*) to evaluate the influence of oxidation state on the core-mantle evolution of SSEs (*15*). We explored all possible magma ocean depths (from 0 to 100% of the mantle) and all possible geotherms relevant to the base of that magma ocean (temperatures between the mantle solidus and liquidus) (*23*, *24*). Three accretionary models distinguished by the compositions of accretionary components and oxidation/reduction paths during planetary growth were considered: (i) a reduced model (*4*, *10*), in which the initial 28% of accretion is characterized by the addition of highly reduced material (0.6 wt % FeO in the mantle) followed by continuous oxidation to yield a mantle with the current FeO content of 8 wt %; (ii) a homogeneous accretion model, in which the FeO content of the mantle is constant and equal to its present value over the entire course of accretion; and (iii) an oxidized model, in which Earth accretes from oxidized material, such as carbonaceous chondrites or a mixture (21% FeO in the mantle) of chondrites (*25*), and is then gradually reduced (through O solubility in the core) until the FeO content of the mantle reaches the present-day value.

The partition coefficients D_V and D_{Cr} evolve as a function of magma ocean depth (Fig. 2) for the three accretionary scenarios (fig. S2 reports results for D_{Ni} and D_{Co}). We find that the redox state of the accreting material only slightly influences the acceptable range of magma ocean depths, 50 to 56 (±7) GPa. In contrast to previous investigations (*2*, *4*, *9–11*, *26*), we show that the terrestrial SSE partition coefficients (V and Cr) can be satisfied with any of our three accretion models. On the basis of our data, there is no requirement that accretion must have occurred under highly reducing conditions in order to explain present-day mantle siderophile trace element concentrations. This contradicts previous claims (*2*, *4*, *10*, *11*) that V and Cr constrain the redox conditions of core formation and terrestrial accretion to allow only the highly reduced model.

The fO_2 path during terrestrial accretion also strongly affects the concentration of light elements in the core. On the basis of our LHDAC partitioning experiments, we calculate the O and Si concentrations in the core (table S5) and find that the highly reduced model leads to excessively high concentrations of silicon in the core, above 10 wt %, along with less than 1 wt % oxygen (Fig. 2, bottom row). The constant FeO–homogeneous accretion model leads to a core containing 2.5 to 5.5 wt % Si and 2 to 2.5 wt % O, whereas the oxidized path yields an oxygen-rich core with 4.5 to 5.5 wt % O and 1.5 to 2.2 wt % Si. The Si content of the core in the highly reduced model (>10 wt %) is incompatible with cosmochemical and geophysical constraints. Indeed, cosmochemical models (*27–29*) suggest that the upper limit for Si content in the core is 8 wt %. High-pressure measurements of sound velocities in iron and iron alloys indicate that the core must contain between 1 and 4 wt % Si for it to be compatible with seismic radially averaged wave speeds and densities (*30*, *31*).

Terrestrial accretion under relatively oxidizing conditions requires a mechanism for reducing the mantle to yield an oxidation state and FeO concentration compatible with present-day conditions. Because our model requires large concentrations of oxygen in the core, transferring FeO from the silicate mantle to the core solves both problems: reducing FeO in the mantle and increasing O in the core, while at the same time rendering the SSEs more siderophile because of the thermodynamic influence of enhanced oxygen solubility on their activities. This mechanism of FeO solubility in the core has been proposed to explain the difference in mantle redox between Earth and Mars (*32*).

A mutually compatible solution to the problems of light elements in the core and trace siderophile element concentrations in the mantle is a major discriminant in validating various models of accretion and core formation. On this basis, we show that it is unlikely that Earth formed under highly reduced conditions, such as those found in enstatite chondrites. Conversely, accretion under oxidized conditions similar to those of the most common meteorites (e.g., ordinary and/or carbonaceous chondrites) is consistent with the siderophile trace element concentrations in the mantle and with the geophysical constraints on the composition of the core. Finally, accretion of large objects (planetesimals and planetary embryos) that had redox conditions similar (~IW-2.3) to those of Earth also satisfies the geochemical and geophysical constraints, while at the same time proving the most realistic in terms of dynamical planetary formation models (*33*).

References and Notes

1. H. S. C. O'Neill, *Geochim. Cosmochim. Acta* **55**, 1159 (1991).
2. J. Wade, B. J. Wood, *Earth Planet. Sci. Lett.* **236**, 78 (2005).
3. H. Wänke, T. Gold, *Philos. Trans. R. Soc. London Ser. A* **303**, 287 (1981).
4. B. J. Wood, M. J. Walter, J. Wade, *Nature* **441**, 825 (2006).
5. A. E. Ringwood, *Geochim. Cosmochim. Acta* **30**, 41 (1966).
6. C. K. Gessmann, D. C. Rubie, *Earth Planet. Sci. Lett.* **184**, 95 (2000).
7. J. Li, C. B. Agee, *Nature* **381**, 686 (1996).
8. K. Righter, M. J. Drake, G. Yaxley, *Phys. Earth Planet. Inter.* **100**, 115 (1997).
9. J. Siebert, A. Corgne, F. J. Ryerson, *Geochim. Cosmochim. Acta* **75**, 1451 (2011).
10. B. J. Wood, J. Wade, M. R. Kilburn, *Geochim. Cosmochim. Acta* **72**, 1415 (2008).
11. D. C. Rubie *et al.*, *Earth Planet. Sci. Lett.* **301**, 31 (2011).
12. A. Ricolleau, Y. Fei, A. Corgne, J. Siebert, J. Badro, *Earth Planet. Sci. Lett.* **310**, 409 (2011).
13. J. Siebert, J. Badro, D. Antonangeli, F. J. Ryerson, *Earth Planet. Sci. Lett.* **321–322**, 189 (2012).
14. M. A. Bouhifd, A. P. Jephcoat, *Earth Planet. Sci. Lett.* **307**, 341 (2011).
15. See supplementary materials on *Science* Online.
16. N. L. Chabot, C. B. Agee, *Geochim. Cosmochim. Acta* **67**, 2077 (2003).
17. C. K. Geßmann, D. C. Rubie, *Geochim. Cosmochim. Acta* **62**, 867 (1998).
18. U. Mann, D. J. Frost, D. C. Rubie, *Geochim. Cosmochim. Acta* **73**, 7360 (2009).
19. J. Wade, B. J. Wood, *Nature* **409**, 75 (2001).
20. A. Corgne, J. Siebert, J. Badro, *Earth Planet. Sci. Lett.* **288**, 108 (2009).
21. A. E. Ringwood, T. Kato, W. Hibberson, N. Ware, *Nature* **347**, 174 (1990).
22. Z. Ma, *Metall. Mater. Trans. B* **32**, 87 (2001).
23. D. Andrault *et al.*, *Earth Planet. Sci. Lett.* **304**, 251 (2011).
24. G. Fiquet *et al.*, *Science* **329**, 1516 (2010).
25. C. Fitoussi, B. Bourdon, *Science* **335**, 1477 (2012).
26. A. Corgne, S. Keshav, B. J. Wood, W. F. McDonough, Y. Fei, *Geochim. Cosmochim. Acta* **72**, 574 (2008).
27. C. J. Allègre, J. P. Poirier, E. Humler, A. W. Hofmann, *Earth Planet. Sci. Lett.* **134**, 515 (1995).
28. M. Javoy *et al.*, *Earth Planet. Sci. Lett.* **293**, 259 (2010).
29. W. F. McDonough, in *The Mantle and Core*, R. W. Carlson, Ed., vol. 2 of *Treatise on Geochemistry*, H. Holland, K. K. Turekian, Eds. (Elsevier-Pergamon, Oxford, 2003), pp. 547–568.
30. D. Antonangeli *et al.*, *Earth Planet. Sci. Lett.* **295**, 292 (2010).
31. J. Badro *et al.*, *Earth Planet. Sci. Lett.* **254**, 233 (2007).
32. D. C. Rubie, C. K. Gessmann, D. J. Frost, *Nature* **429**, 58 (2004).
33. K. J. Walsh, A. Morbidelli, S. N. Raymond, D. P. O'Brien, A. M. Mandell, *Nature* **475**, 206 (2011).

Acknowledgments: The research leading to these results has received funding from the European Research Council (ERC) under the European Community's Seventh Framework Programme (FP7/2007-2013)/ERC grant agreement 207467. This work was performed under the auspices of the Lawrence Livermore National Laboratory, U.S. Department of Energy, under contract DE-AC52 07NA27344 and was supported by the Office of Basic Energy Sciences, Geosciences Research Program (F.J.R.). The Focused Ion Beam (FIB) facility of the IMPMC is supported by Région Ile de France grant SESAME 2006 N°I-07-593/R, INSU-CNRS, Institut de Physique (INP) CNRS, University Pierre et Marie Curie–Paris 6, and French National Research Agency (ANR) grant ANR-07-BLAN-0124-01 (J.B.). We thank I. Esteve for assistance during sample preparation with the FIB, and G. Garbarino for assistance on the high-pressure beamline (ID27) of the European Synchrotron Radiation Facility.

Supplementary Materials

www.sciencemag.org/cgi/content/full/science.1227923/DC1
Materials and Methods
Supplementary Text
Figs. S1 and S2
Tables S1 to S5
References (*34–50*)

25 July 2012; accepted 20 December 2012
Published online 10 January 2013;
10.1126/science.1227923

A Reconstruction of Regional and Global Temperature for the Past 11,300 Years

Shaun A. Marcott,[1] Jeremy D. Shakun,[2] Peter U. Clark,[1] Alan C. Mix[1]

Surface temperature reconstructions of the past 1500 years suggest that recent warming is unprecedented in that time. Here we provide a broader perspective by reconstructing regional and global temperature anomalies for the past 11,300 years from 73 globally distributed records. Early Holocene (10,000 to 5000 years ago) warmth is followed by ~0.7°C cooling through the middle to late Holocene (<5000 years ago), culminating in the coolest temperatures of the Holocene during the Little Ice Age, about 200 years ago. This cooling is largely associated with ~2°C change in the North Atlantic. Current global temperatures of the past decade have not yet exceeded peak interglacial values but are warmer than during ~75% of the Holocene temperature history. Intergovernmental Panel on Climate Change model projections for 2100 exceed the full distribution of Holocene temperature under all plausible greenhouse gas emission scenarios.

Placing present climate into a historical perspective beyond the instrumental record is important for distinguishing anthropogenic influences on climate from natural variability (*1*). Proxy-based temperature reconstructions of the past 1500 years suggest that the warming of the past few decades is unusual relative to preanthropogenic variations (*2*, *3*), but whether recent warming is anomalous relative to variability over the entirety of the Holocene interglaciation (the past 11,500 years) (*4*) has yet to be established.

The 73 globally distributed temperature records used in our analysis are based on a variety of paleotemperature proxies and have sampling resolutions ranging from 20 to 500 years, with a median resolution of 120 years (*5*). We account for chronologic and proxy calibration uncertainties with a Monte Carlo–based randomization scheme (*6*). Our data set exhibits several important strengths, as well as limitations, as compared to global and hemispheric reconstructions of the past 1500 years (*2*, *3*, *7*, *8*). For example, whereas reconstructions of the past millennium rapidly lose data coverage with age, our coverage increases with age (Fig. 1, G and H). Published reconstructions of the past millennium are largely based on tree rings and may underestimate low-frequency (multicentury-to-millennial) variability because of uncertainty in detrending (*9*) [although progress is being made on this front (*10*)], whereas our lower-resolution records are well suited for reconstructing longer-term changes. Terrestrial records dominate reconstructions of the past millennium, whereas our stack is largely derived from marine archives (~80%). Unlike the reconstructions of the past millennium, our proxy data are converted quantitatively to temperature before stacking, using independent core-top or laboratory-culture calibrations with no post-hoc adjustments in variability.

We took the 5° × 5° area-weighted mean of the 73 records to develop a global temperature stack for the Holocene (referred to as the $\text{Standard}_{5\times5}$ reconstruction) (Fig. 1, A and B). To compare our $\text{Standard}_{5\times5}$ reconstruction with modern climatology, we aligned the stack's mean for the interval 510 to 1450 yr B.P. (where yr B.P. is years before 1950 CE) with the same interval's mean of the global Climate Research Unit error-in-variables (CRU-EIV) composite temperature record (*2*), which is, in turn, referenced to the 1961–1990 CE instrumental mean (Fig. 1A). We then assessed the sensitivity of the temperature reconstruction to several averaging schemes, including an arithmetic mean of the data sets, a 30° × 30° area-weighted mean, a 10° latitudinal weighted mean, and a calculation of 1000 jackknifed stacks that randomly exclude 50% of the records in each realization (Fig. 1, C and D, and fig. S4). Although some differences exist at the centennial scale among the various methods (Fig. 1, C and D), they are small (<0.2°C) for most of the reconstructions, well within the uncertainties of our $\text{Standard}_{5\text{x}5}$ reconstruction, and do not affect the long-term trend in the reconstruction.

In addition to the previously mentioned averaging schemes, we also implemented the RegEM algorithm (*11*) to statistically infill data gaps in records not spanning the entire Holocene, which is particularly important over the past several centuries (Fig. 1G). Without filling data gaps, our $\text{Standard}_{5\times5}$ reconstruction (Fig. 1A) exhibits 0.6°C greater warming over the past ~60 yr B.P. (1890 to 1950 CE) than our equivalent infilled 5° × 5° area-weighted mean stack (Fig. 1, C and D). However, considering the temporal resolution of our data set and the small number of records that cover this interval (Fig. 1G), this difference is probably not robust. Before this interval, the gap-filled and unfilled methods of calculating the stacks are nearly identical (Fig. 1D).

Because the relatively low resolution and time-uncertainty of our data sets should generally suppress higher-frequency temperature variability, an important question is whether the Holocene stack adequately represents centennial- or millennial-scale variability. We evaluated this question in two ways. First, we generated a single mean zero, unit variance white-noise time series and used it in place of our 73 records. The white-noise records were then perturbed through Monte Carlo simulations using the resolution and chronological uncertainty specific to each proxy record as well as a common 1°C proxy uncertainty. We composited a $\text{Standard}_{5\text{x}5}$ global stack from these synthetic records and calculated the ratio between the variances of the stack and the input white noise as a function of frequency to derive a gain function. The results suggest that at longer periods, more variability is preserved, with essentially no variability preserved at periods shorter than 300 years, ~50% preserved at 1000-year periods, and nearly all of the variability preserved for periods longer than 2000 years (figs. S17 and S18). Second, spectral analysis indicates that the variance of the Holocene proxy stack approaches that of the global CRU-EIV reconstruction of the past 1500 years (*2*) at millennial time scales and longer (figs. S20 and S23).

Our global temperature reconstruction for the past 1500 years is indistinguishable within uncertainty from the Mann *et al*. (*2*) reconstruction; both reconstructions document a cooling trend from a warm interval (~1500 to 1000 yr B.P.) to a cold interval (~500 to 100 yr B.P.), which is approximately equivalent to the Little Ice Age (Fig. 1A). This similarity confirms that published temperature reconstructions of the past two millennia capture long-term variability, despite their short time span (*3*, *12*, *13*). Our median estimate of this long-term cooling trend is somewhat smaller than in Mann *et al*. (*2*) though, which may reflect our bias toward marine and lower-latitude records.

The $\text{Standard}_{5\text{x}5}$ reconstruction exhibits ~0.6°C of warming from the early Holocene (11,300 yr B.P.) to a temperature plateau extending from 9500 to 5500 yr B.P.. This warm interval is followed by a long-term 0.7°C cooling from 5500 to ~100 yr B.P. (Fig. 1B). Extratropical Northern Hemisphere sites (30° to 90°N), in particular from the North Atlantic sector, contribute most of the variance to the global signal; temperatures in this region decrease by ~2°C from 7000 yr B.P. to ~100 yr B.P. (Fig. 2H). By comparison, the low latitudes (30°N to 30°S) exhibit a slight warming of ~0.4°C from 11,000 to 5000 yr B.P., with temperature leveling off thereafter (Fig. 2I), whereas the extratropical Southern Hemisphere (30°S to 90°S) cooled ~0.4°C from about 11,000 to 7000 yr B.P., followed by relatively constant temperatures except for some possible strong multicentennial variability in the past 2500 years (Fig. 2J). The Southern Hemisphere is represented by fewer data sets (n = 11) than the equatorial (n = 33)

[1]College of Earth, Ocean, and Atmospheric Sciences, Oregon State University, Corvallis, OR 97331, USA. [2]Department of Earth and Planetary Sciences, Harvard University, Cambridge, MA 02138, USA.

*To whom correspondence should be addressed. E-mail: marcotts@science.oregonstate.edu

Downloaded from www.sciencemag.org on March 8, 2013

and Northern Hemisphere (n = 29) regions, providing fewer constraints on characterizing the variability in our reconstruction for this region.

Trends in regional temperature reconstructions show strong similarities with high-resolution precipitation records, consistently associating greater warmth with greater wetness (Fig. 2, H to J). For example, extratropical Northern Hemisphere mid-to-high–latitude temperature correlates well with records of Asian monsoon intensity (*14*, *15*) and the position of the Atlantic intertropical convergence zone (*16*) (Fig. 2H), tropical temperatures track precipitation proxies from speleothems in Borneo (*17*) and Indonesia (*18*) (Fig. 2I), and extratropical Southern Hemisphere temperatures parallel

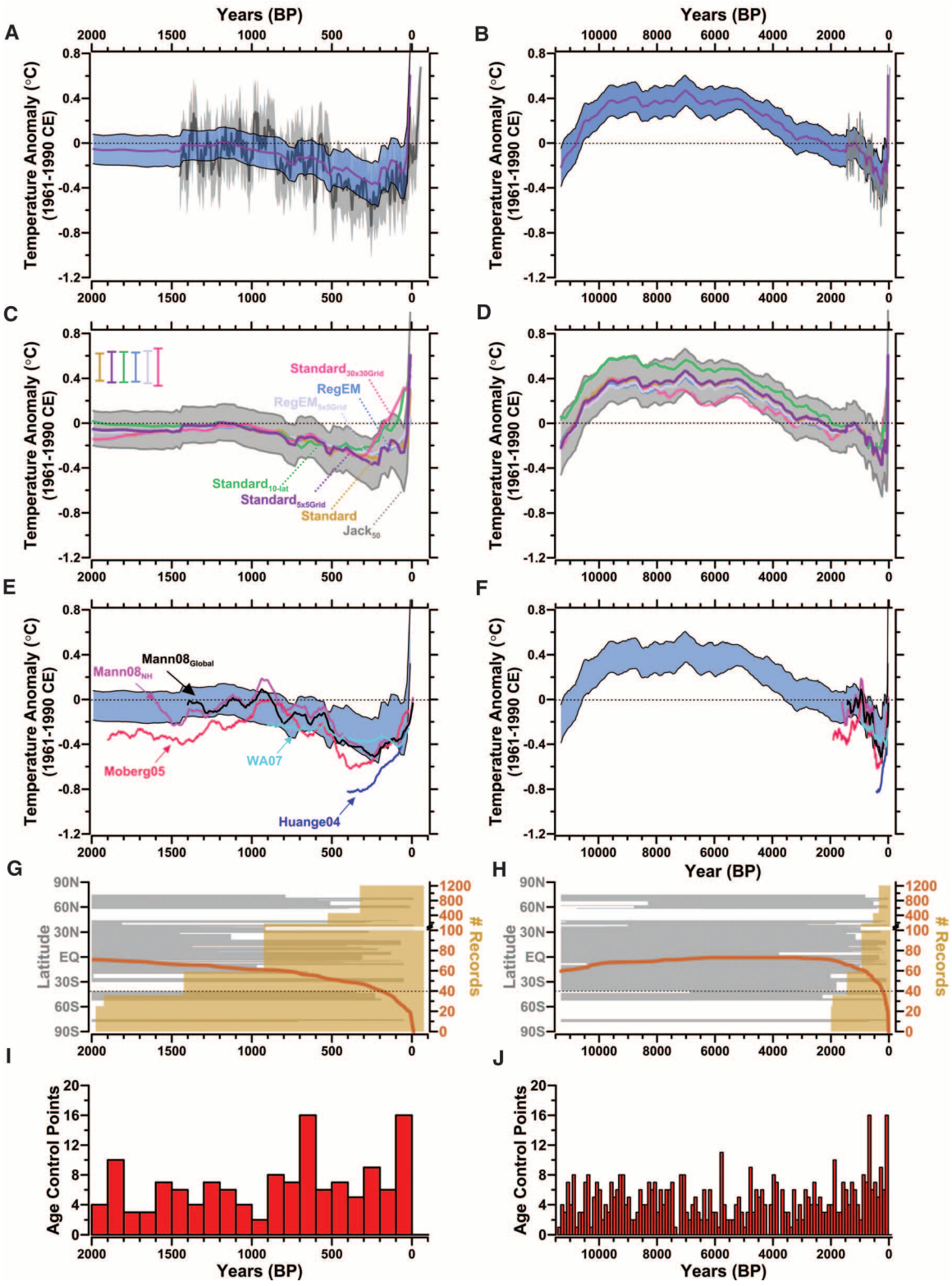

Fig. 1. Comparison of different methods and reconstructions of global and hemispheric temperature anomalies. (**A** and **B**) Globally stacked temperature anomalies for the 5° × 5° area-weighted mean calculation (purple line) with its 1σ uncertainty (blue band) and Mann *et al.*'s global CRU-EIV composite mean temperature (dark gray line) with their uncertainty (light gray band). (**C** and **D**) Global temperature anomalies stacked using several methods (Standard and Standard$_{5x5Grid;\ 30x30Grid;\ 10\text{-}lat}$: Arithmetic mean calculation, area-weighted with a 5° × 5° grid, area-weighted with a 30° × 30° grid, and area-weighted using 10° latitude bins, respectively; RegEM and RegEM$_{5x5Grid}$: Regularized expectation maximization algorithm-infilled arithmetic mean and 5° × 5° area-weighted). The gray shading [50% Jackknife (Jack$_{50}$)] represents the 1σ envelope when randomly leaving 50% of the records out during each Monte Carlo mean calculation. Uncertainties shown are 1σ for each of the methods. (**E** and **F**) Published temperature anomaly reconstructions that have been smoothed with a 100-year centered running mean, Mann08$_{Global}$ (*2*), Mann08$_{NH}$ (*2*), Moberg05 (*3*), WA07 (*8*), Huange04 (*36*), and plotted with our global temperature stacks [blue band as in (A)]. The temperature anomalies for all the records are referenced to the 1961–1990 instrumental mean. (**G** and **H**) Number of records used to construct the Holocene global temperature stack through time (orange line) and Mann *et al.*'s (*2*) reconstruction (gold vertical bars). Note the *y* axis break at 100. The latitudinal distribution of Holocene records (gray horizontal bars) through time is shown. (**I** and **J**) Number of age control points (e.g., ^{14}C dates) that constrain the time series through time.

Downloaded from www.sciencemag.org on March 8, 2013

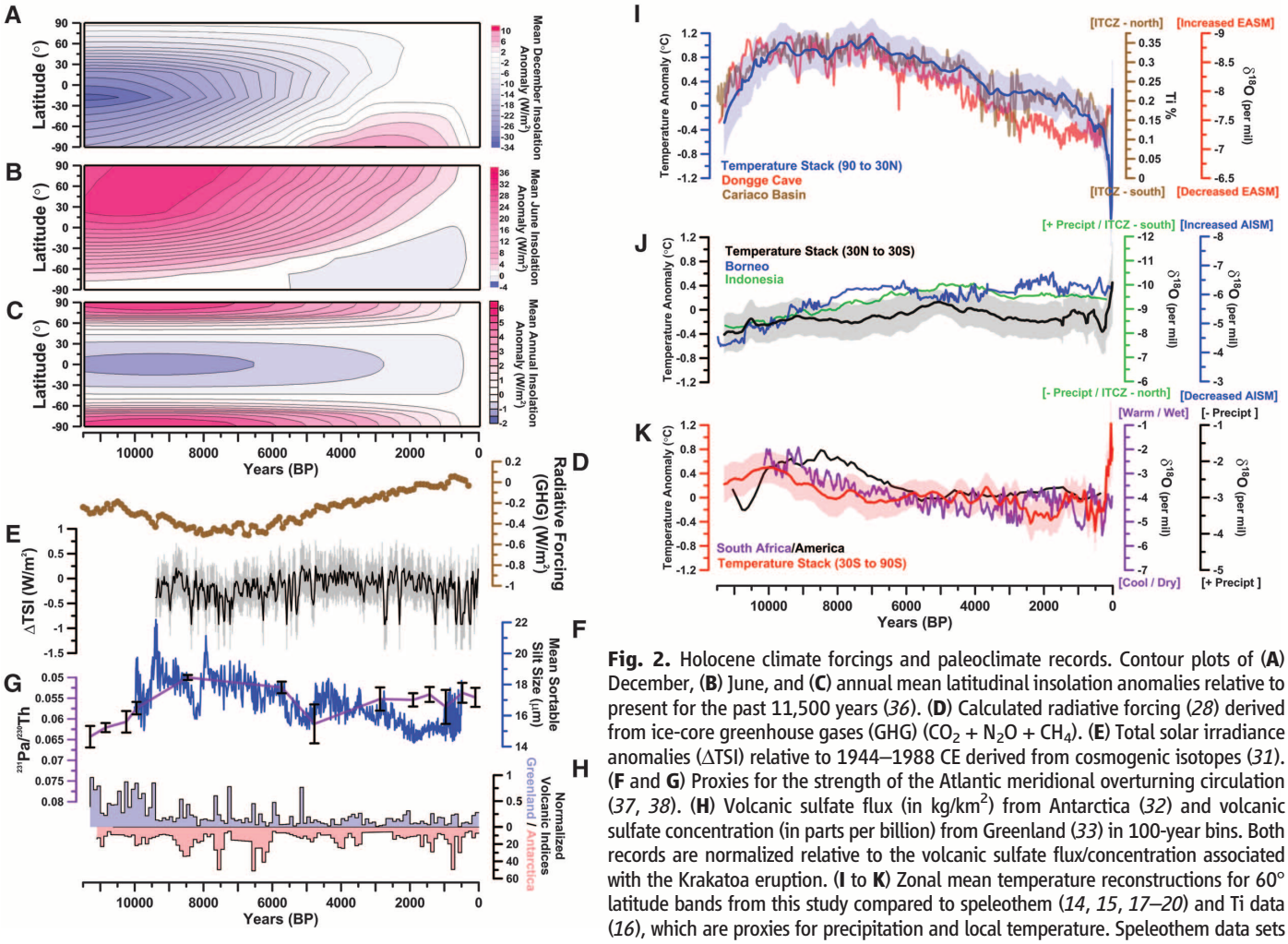

Fig. 2. Holocene climate forcings and paleoclimate records. Contour plots of (**A**) December, (**B**) June, and (**C**) annual mean latitudinal insolation anomalies relative to present for the past 11,500 years (*36*). (**D**) Calculated radiative forcing (*28*) derived from ice-core greenhouse gases (GHG) ($CO_2 + N_2O + CH_4$). (**E**) Total solar irradiance anomalies (ΔTSI) relative to 1944–1988 CE derived from cosmogenic isotopes (*31*). (**F** and **G**) Proxies for the strength of the Atlantic meridional overturning circulation (*37*, *38*). (**H**) Volcanic sulfate flux (in kg/km^2) from Antarctica (*32*) and volcanic sulfate concentration (in parts per billion) from Greenland (*33*) in 100-year bins. Both records are normalized relative to the volcanic sulfate flux/concentration associated with the Krakatoa eruption. (**I** to **K**) Zonal mean temperature reconstructions for 60° latitude bands from this study compared to speleothem (*14*, *15*, *17*–*20*) and Ti data (*16*), which are proxies for precipitation and local temperature. Speleothem data sets were smoothed with a seven-point running mean for clarity. ITCZ, Intertropical Convergence Zone; EASM, East Asian Summer Monsoon; AISM, Australian-Indonesian Summer Monsoon.

speleothem proxies of precipitation and temperature from South Africa (*19*) and South America (*20*) that are independent of our reconstruction.

The general pattern of high-latitude cooling in both hemispheres opposed by warming at low latitudes is consistent with local mean annual insolation forcing associated with decreasing orbital obliquity since 9000 years ago (Fig. 2C). The especially pronounced cooling of the Northern Hemisphere extratropics, however, suggests an important role for summer insolation in this region, perhaps through snow-ice albedo and vegetation feedbacks (*21*, *22*). Such a mechanism that mediates seasonal insolation is plausible at these latitudes, where the fraction of continental landmasses relative to the ocean is high (~50% land from 30° to 90°N; 25% land from 30°N to 30°S; 15% land from 30° to 90°S).

We cannot fully exclude the possibility of a seasonal proxy bias in our temperature reconstructions (*23*), but a sensitivity experiment with an intermediate-complexity model (fig. S8) suggests that the effects of such a bias would probably be modest in the global reconstruction. The dominance of the northern signal in our global stack is consistent with Milankovitch theory, in which summer insolation would drive the planet toward eventual future glacial inception in the Northern Hemisphere (*24*), excluding any anthropogenic influence. Models support our finding of a global mean cooling in response to an obliquity decrease, though of lesser magnitude (*25*), and also support the idea about the sensitivity of the northern high latitudes to summer insolation (*21*).

Additional effects probably further influenced the evolution of climate through the Holocene. In the early-to-middle Holocene, the deglaciating Northern Hemisphere ice sheets would have modulated warming of the northern high latitudes relative to peak seasonal insolation (*26*, *27*). Radiative forcing by greenhouse gases (primarily CO_2) rose 0.5 W/m^2 during the mid-to-late Holocene (Fig. 2D), which would be expected to yield ~0.4°C warming for a mid-range climate sensitivity (*28*). Response to such forcing may have been offset by opposing orbital insolation forcing that was greater than greenhouse gas forcing by up to one (annual) to two (seasonal) orders of magnitude over the course of the Holocene (Fig. 2, A to C). Northward heat transport in the Atlantic basin by the meridional overturning circulation (MOC) may have weakened since the middle Holocene (*29*), contributing to the strong cooling in the North Atlantic while dampening cooling in the mid-to-high latitude Southern Hemisphere due to the bipolar seesaw (*30*). Insofar as winter conditions influence the sources and strength of deepwater formation, a weakening MOC may partly reflect the increase in high northern-latitude winter insolation over the Holocene (Fig. 2A). Total solar irradiance reconstructed from cosmogenic isotopes (*31*) also varied by 0.5 to 1 W/m^2, and volcanic eruptions occurred throughout the duration of the Holocene (*32*, *33*), although most of this variance is at higher frequencies than those resolved by our stacked temperature records, and the scaling of both is poorly constrained.

Although our temperature stack does not fully resolve variability at periods shorter than 2000 years, such high-frequency changes would only modestly broaden the statistical distribution of Holocene temperatures (Fig. 3 and fig. S22). Moreover, we suggest that accounting for any spatial or seasonal biases in the stack would tend to reduce its

Downloaded from www.sciencemag.org on March 8, 2013

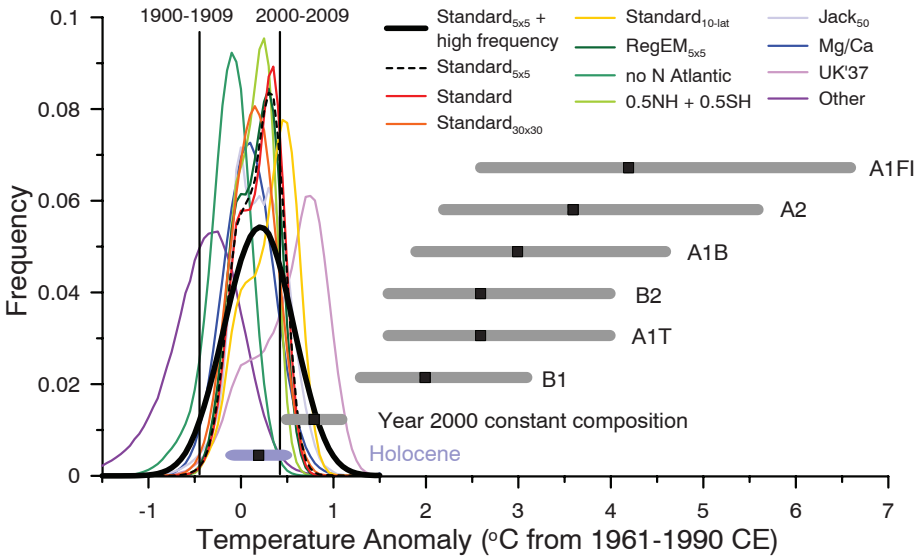

Fig. 3. Holocene temperature distribution compared to modern temperature and future projections. Shown are relative frequency plots of Holocene temperature anomalies in 0.05°C bins using multiple data subsets and reconstructions (colored lines), instrumental means for 1900–1909 and 2000–2009 CE (vertical black lines), 2100 CE projections based on various emissions scenarios (*35*) (black squares and gray bars give the best estimate and 66% confidence interval), and the Holocene median and 66% range from $Standard_{5\times5}$ + high-frequency stack (black square and blue bar). Projections in (*35*) were referenced to 1980–1999 CE, whereas we reference them to 1961–1990 CE here. Data sets are divided by proxy type: UK'37, Mg/Ca, and the remainder (Other); method: arithmetic mean (Standard) and RegEM; weighting: equal Northern and Southern Hemisphere weighting (0.5NH + 0.5SH), 5° × 5°grid, and 30° × 30°grid; exclusion of data sets: no North Atlantic and $Jack_{50}$; and high-frequency addition: red noise with the same power spectrum as Mann *et al.* (*2*) added to the global stack (supplementary materials).

variability because of the cancellation of noise in a large-scale mean and the opposing nature of seasonal insolation forcing over the Holocene, causing the Holocene temperature distribution to contract.

Our results indicate that global mean temperature for the decade 2000–2009 (*34*) has not yet exceeded the warmest temperatures of the early Holocene (5000 to 10,000 yr B.P.). These temperatures are, however, warmer than 82% of the Holocene distribution as represented by the $Standard_{5\times5}$ stack, or 72% after making plausible corrections for inherent smoothing of the high frequencies in the stack (*6*) (Fig. 3). In contrast, the decadal mean global temperature of the early 20th century (1900–1909) was cooler than >95% of the Holocene distribution under both the $Standard_{5\times5}$ and high-frequency corrected scenarios. Global temperature, therefore, has risen from near the coldest to the warmest levels of the Holocene within the past century, reversing the long-term cooling trend that began ~5000 yr B.P. Climate models project that temperatures are likely to exceed the full distribution of Holocene warmth by 2100 for all versions of the temperature stack (*35*) (Fig. 3), regardless of the greenhouse gas emission scenario considered (excluding the year 2000 constant composition scenario, which has already been exceeded). By 2100, global average temperatures will probably be 5 to 12 standard deviations above the Holocene temperature mean for the A1B scenario (*35*) based on our $Standard_{5\times5}$ plus high-frequency addition stack (Fig. 3).

Strategies to better resolve the full range of global temperature variability during the Holocene, particularly with regard to decadal to centennial time scales, will require better chronologic constraints through increased dating control. Higher-resolution sampling and improvements in proxy calibration also play an important role, but our analysis (fig. S18) suggests that improvements in chronology are most important. Better constraints on regional patterns will require more data sets from terrestrial archives and both marine and terrestrial records representing the mid-latitudes of the Southern Hemisphere and central Pacific.

References and Notes

1. E. Jansen *et al.*, in *Climate Change 2007: The Physical Science Basis. Contribution of Working Group I to the Fourth Assessment Report of the Intergovernmental Panel on Climate Change,* S. Solomon *et al.*, Eds. (Cambridge Univ. Press, Cambridge, 2007), pp. 433–497.
2. M. E. Mann *et al.*, *Proc. Natl. Acad. Sci. U.S.A.* **105**, 13252 (2008).
3. A. Moberg, D. M. Sonechkin, K. Holmgren, N. M. Datsenko, W. Karlén, *Nature* **433**, 613 (2005).
4. H. Wanner *et al.*, *Quat. Sci. Rev.* **27**, 1791 (2008).
5. The majority of the data sets can be found at NOAA National Climate Data Center (www.ncdc.noaa.gov/paleo/paleo.html) and the PANGAEA data repository (www.pangaea.de/). Sources for all data sets are available online (*6*).
6. Materials, methods, and supporting data are available as supplementary materials on *Science* Online.
7. J. Esper, E. R. Cook, F. H. Schweingruber, *Science* **295**, 2250 (2002).
8. C. M. Ammann, E. R. Wahl, *Clim. Change* **85**, 71 (2007).
9. J. Esper, D. C. Frank, R. J. S. Wilson, *EOS* **85**, 113, 120 (2004).
10. J. Esper *et al.*, *Nat. Clim. Change* 10.1038/nclimate1589 (2012).
11. T. Schneider, *J. Clim.* **14**, 853 (2001).
12. E. R. Wahl, C. M. Ammann, *Clim. Change* **85**, 33 (2007).
13. E. R. Wahl, D. M. Ritson, C. M. Ammann, *Science* **312**, 529, author reply 529 (2006).
14. C. A. Dykoski *et al.*, *Earth Planet. Sci. Lett.* **233**, 71 (2005).
15. Y. Wang *et al.*, *Science* **308**, 854 (2005).
16. G. H. Haug, K. A. Hughen, D. M. Sigman, L. C. Peterson, U. Röhl, *Science* **293**, 1304 (2001).
17. J. W. Partin, K. M. Cobb, J. F. Adkins, B. Clark, D. P. Fernandez, *Nature* **449**, 452 (2007).
18. M. L. Griffiths *et al.*, *Nat. Geosci.* **2**, 636 (2009).
19. K. Holmgren *et al.*, *Quat. Sci. Rev.* **22**, 2311 (2003).
20. F. W. Cruz Jr. *et al.*, *Nature* **434**, 63 (2005).
21. H. Renssen *et al.*, *Clim. Dyn.* **24**, 23 (2005).
22. A. Ganopolski, C. Kubatzki, M. Claussen, V. Brovkin, V. Petoukhov, *Science* **280**, 1916 (1998).
23. G. Leduc, R. Schneider, J.-H. Kim, G. Lohmann, *Quat. Sci. Rev.* **29**, 989 (2010).
24. P. C. Tzedakis, J. E. T. Channell, D. A. Hodell, H. F. Kleiven, L. C. Skinner, *Nat. Geosci.* 10.1038/ngeo1358 (2012).
25. D. F. Mantsis, A. C. Clement, A. J. Broccoli, M. P. Erb, *J. Clim.* **24**, 2830 (2011).
26. D. S. Kaufman *et al.*, *Quat. Sci. Rev.* **23**, 529 (2004).
27. F. C. Ljungqvist, *Geografia* **116**, 91 (2011).
28. V. Ramaswamy *et al.*, Eds., *Radiative Forcing Of Climate Change. Climate Change 2001: The Scientific Basis. Contribution of Working Group I to the Third Assessment Report of the Intergovernmental Panel on Climate Change* (Cambridge Univ. Press, New York, 2001).
29. B. A. A. Hoogakker *et al.*, *Paleoceanography* **26**, PA4214 (2011).
30. W. S. Broecker, *Paleoceanography* **13**, 119 (1998).
31. F. Steinhilber *et al.*, *Proc. Natl. Acad. Sci. U.S.A.* **109**, 5967 (2012).
32. E. Castellano *et al.*, *J. Geophys. Res.* **110**, D06114 (2005).
33. G. A. Zielinski, P. A. Mayewski, L. D. Meeker, S. Whitlow, M. S. Twickler, *Quat. Res.* **45**, 109 (1996).
34. P. Brohan, J. J. Kennedy, I. Harris, S. F. B. Tett, P. D. Jones, *J. Geophys. Res.* **111**, D12106 (2006).
35. G. A. Meehl *et al.*, in *Climate Change 2007: The Physical Science Basis. Contribution of Working Group I to the Fourth Assessment Report of the Intergovernmental Panel on Climate Change,* S. Solomon *et al.*, Eds. (Cambridge Univ. Press, Cambridge, 2007), pp. 747–845.
36. S. Huang, *Geophys. Res. Lett.* **31**, L13205 (2004).
37. A. Berger, M.-F. Loutre, *Quat. Sci. Rev.* **10**, 297 (1991).
38. J. F. McManus, R. Francois, J.-M. Gherardi, L. D. Keigwin, S. Brown-Leger, *Nature* **428**, 834 (2004).

Acknowledgments: We thank J. Alder, T. Bauska, E. Brook, C. Buizert, V. Ersek, S. Hostetler, P. Huybers, N. Pisias, J. Rosen, G. Schmidt, A. Schmittner, M. Tingley, and our reviewers for invaluable insight and helpful discussion. The data sets provided by T. Barrows, J.-H. Kim, Y. Kubota, I. Larocque, G. Leduc, M. McGlone, T. Rodrigues, C. Rühlemann, J. Sachs, R. Schneider, H. Seppä, J. Tierney, M. Yamamoto, B. Vinther, and C. Waelbrock, as well as the data sets compiled from the National Oceanic and Atmospheric Administration Climate Data Center and PANGAEA databases, made this research possible. Funding for this work was provided by the NSF Paleoclimate Program for the Paleovar Project.

Supplementary Materials

www.sciencemag.org/cgi/content/full/339/6124/1198/DC1
Supplementary Text
Figs. S1 to S26
References

27 July 2012; accepted 4 January 2013
10.1126/science.1228026

Downloaded from www.sciencemag.org on March 8, 2013

Caffeine in Floral Nectar Enhances a Pollinator's Memory of Reward

G. A. Wright,[1*] D. D. Baker,[2] M. J. Palmer,[3] D. Stabler,[1,2] J. A. Mustard,[4] E. F. Power,[1,2] A. M. Borland,[2] P. C. Stevenson[5,6]

Plant defense compounds occur in floral nectar, but their ecological role is not well understood. We provide evidence that plant compounds pharmacologically alter pollinator behavior by enhancing their memory of reward. Honeybees rewarded with caffeine, which occurs naturally in nectar of *Coffea* and *Citrus* species, were three times as likely to remember a learned floral scent as were honeybees rewarded with sucrose alone. Caffeine potentiated responses of mushroom body neurons involved in olfactory learning and memory by acting as an adenosine receptor antagonist. Caffeine concentrations in nectar did not exceed the bees' bitter taste threshold, implying that pollinators impose selection for nectar that is pharmacologically active but not repellent. By using a drug to enhance memories of reward, plants secure pollinator fidelity and improve reproductive success.

Many drugs commonly consumed by humans are produced by plants as a form of toxic defense against herbivores (*1*, *2*). Although plant-derived drugs like caffeine or nicotine are lethal in high doses (*3*–*5*), at low doses they have pharmacological effects on mammalian behavior. For example, low doses of caffeine are mildly rewarding and enhance cognitive performance and memory retention (*6*). Caffeine has been detected in low doses in the floral nectar and pollen of *Citrus* (*7*), but whether it has an ecological function is unknown.

Two caffeine-producing plant genera, *Citrus* and *Coffea*, have large floral displays with strong scents and produce more fruits and seeds when pollinated by bees (*8*, *9*). If caffeine confers a selective advantage when these plants interact with pollinators, we might expect it to be commonly encountered in nectar. We measured caffeine in the nectar of three species of *Coffea* (*C. canephora*, *C. arabica*, and *C. liberica*) and four species of *Citrus* (*C. paradisi*, *C. maxima*, *C. sinensis*, and *C. reticulata*) using liquid chromatography–mass spectrometry (*10*) (fig. S1A). When caffeine was present, its concentration ranged from 0.003 to 0.253 mM. The median caffeine concentration in both genera was not significantly different (Fig. 1A, Mann-Whitney, $Z = -1.09$, $P = 0.272$). Caffeine was more common in the nectar of *C. canephora* than in that of *C. arabica* or *C. liberica* (*Coffea*: logistic regression $\chi_2^2 = 11.1$, $P = 0.004$); it was always present in *Citrus* nectar. The mean total nectar sugar concentration ranged from 0.338 to 0.843 M (Fig. 1B; see fig S1B for individual sugars). Caffeine concentration in nectar did not correlate with total sugar concentration (Pearson's $r = 0.063$, $P = 0.596$).

We hypothesized that caffeine could affect the learning and memory of foraging pollinators. To test this, we trained individual honeybees to associate floral scent with 0.7 M sucrose and seven different concentrations of caffeine and tested their olfactory memory. Using a method for classical conditioning of feeding responses (proboscis extension reflex) (*11*), we trained bees for six trials with 30 s between each pairing of odor with reward. This intertrial interval approximated the rate of floral visitation exhibited by honeybees foraging from multiple flowers on a single *Citrus* tree (see methods). The presence of low doses of caffeine in reward had a weak effect on the rate of learning (Fig. 2A), but it had a profound effect on long-term memory. When rewarded with solutions containing nectar levels of caffeine, three times as many bees remembered the conditioned scent 24 hours later and responded as if it predicted reward (Fig. 2B, logistic regression, $\chi_7^2 = 41.9$, $P < 0.001$). Twice as many bees remembered it 72 hours later (Fig. 2C). This improvement in memory performance was not due to a general increase in olfactory sensitivity resulting from caffeine consumption (fig. S2A). Indeed, the effect of caffeine on long-term

[1]Centre for Behaviour and Evolution, Institute of Neuroscience, Newcastle University, Newcastle upon Tyne NE1 7RU, UK. [2]School of Biology, Newcastle University, Newcastle upon Tyne NE1 7RU, UK. [3]Division of Neuroscience, Medical Research Institute, Ninewells Medical School, University of Dundee, Dundee DD1 9SY, UK. [4]School of Life Sciences, Arizona State University, Tempe, AZ 85287, USA. [5]Jodrell Laboratory, Royal Botanic Gardens, Kew, Surrey TW9 3AB, UK. [6]Natural Resources Institute, University of Greenwich, Chatham, Kent ME4 4TB, UK.

*To whom correspondence should be addressed. E-mail: jeri.wright@ncl.ac.uk

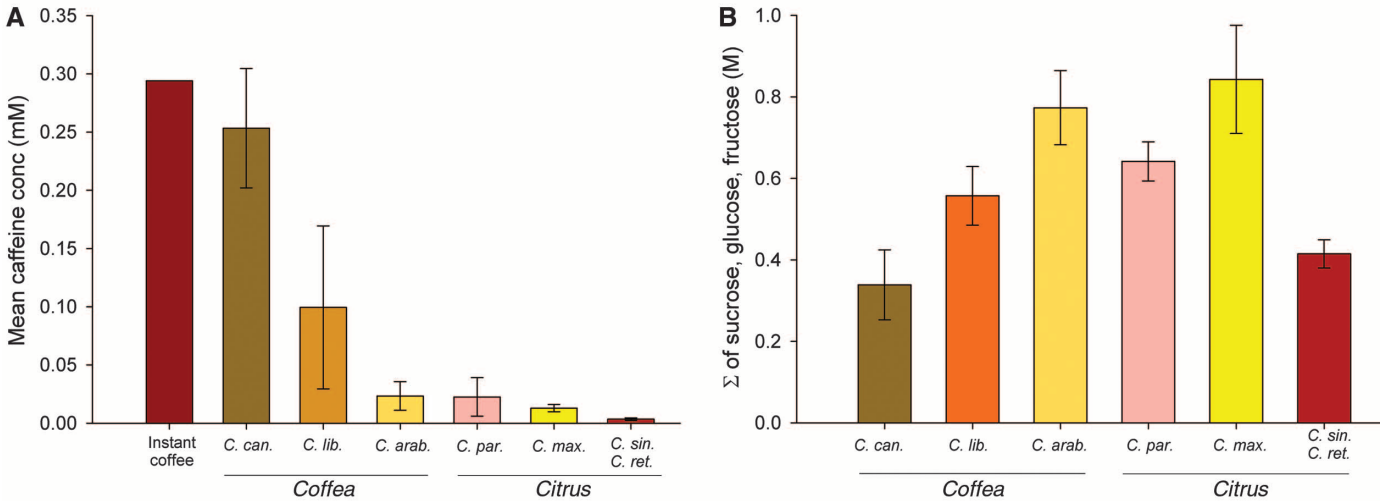

Fig. 1. (**A**) Caffeine concentration in *Coffea* and *Citrus* spp. and a cup of instant coffee. Caffeine concentration depended on species within each genus (*Coffea*: Kruskal-Wallis, $\chi_2^2 = 28.1$, $P < 0.001$; *Citrus*: Kruskal-Wallis, $\chi_2^2 = 6.98$, $P = 0.030$); *C. canephora* had the highest mean concentration of all species sampled. (**B**) The sum of the concentration of sucrose, glucose, and fructose (total nectar sugars) depended on species (one-way analysis of variance: $F_{5,\ 161} = 4.64$, $P < 0.001$) and was greatest in *Citrus maxima* and hybrids (citron, lemons, clementines). [*C. can.*, *Coffea canephora*, $N = 34$; *C. lib.*, *Coffea liberica*, $N = 31$; *C. arab.*, *Coffea arabica*, $N = 27$; *C. par.*, *Citrus paradisi* and hybrids, $N_{cp} = 17$; *C. max.*, *Citrus maxima* and hybrids, $N = 5$; *C. sin.* and *C. ret.*, *Citrus sinensis* and *Citrus reticulata*, $N_{CS} = 7$, $N_{CR} = 5$ (data for these two species were pooled).] Mean responses ± SE.

Downloaded from www.sciencemag.org on March 8, 2013

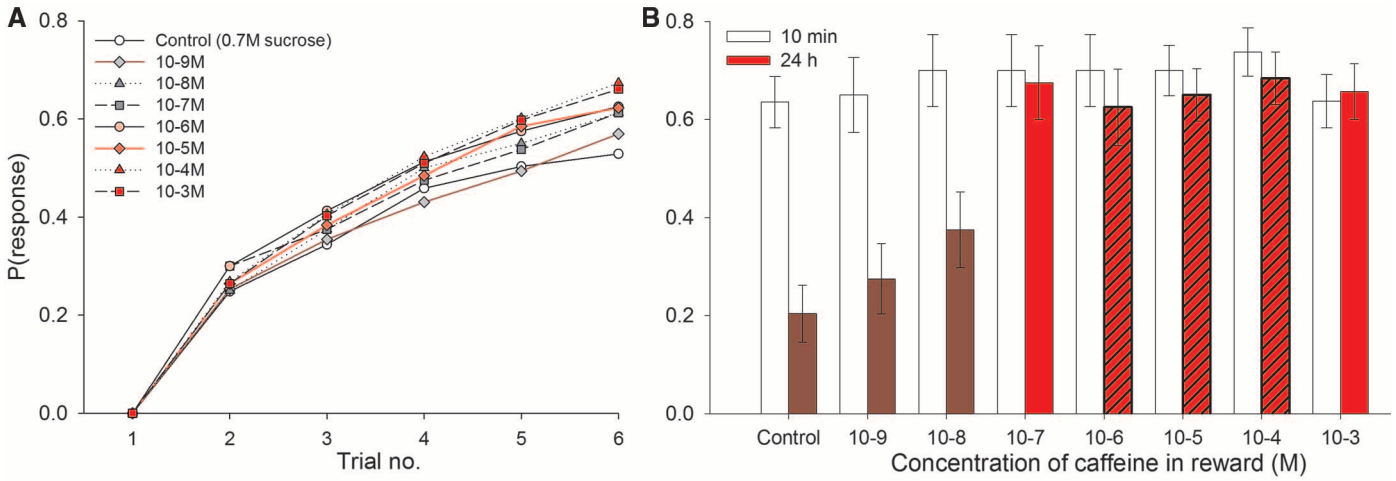

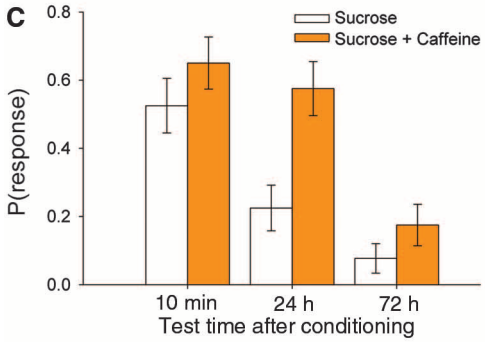

Fig. 2. (**A**) The rate of learning of bees conditioned with an odor stimulus paired with a 0.7 M sucrose reward containing caffeine. The rate of learning was slightly greater for the bees fed caffeine in reward during conditioning (logistic regression, $\chi_1^2 = 4.85$, $P = 0.028$). $N \geq 79$ for all groups. (**B**) Memory recall test for odors at 10 min (white bars) or 24 hours (red bars) after bees had been trained as in (A). Bright red bars indicate that the response at 24 hours was significantly different from the control (0.7 M sucrose) (least-squares contrasts: $P < 0.05$); dark red bars were not significantly different. Nectar levels of caffeine are indicated by hatching. $N > 79$ for each group. (**C**) Bees fed 0.1 mM caffeine in sucrose (orange bars) were more likely to remember the conditioned odor than sucrose alone (white bars) (logistic regression, $\chi_1^2 = 9.04$, $P < 0.003$) at 24 hours and 72 hours after conditioning. $N = 40$ per group.

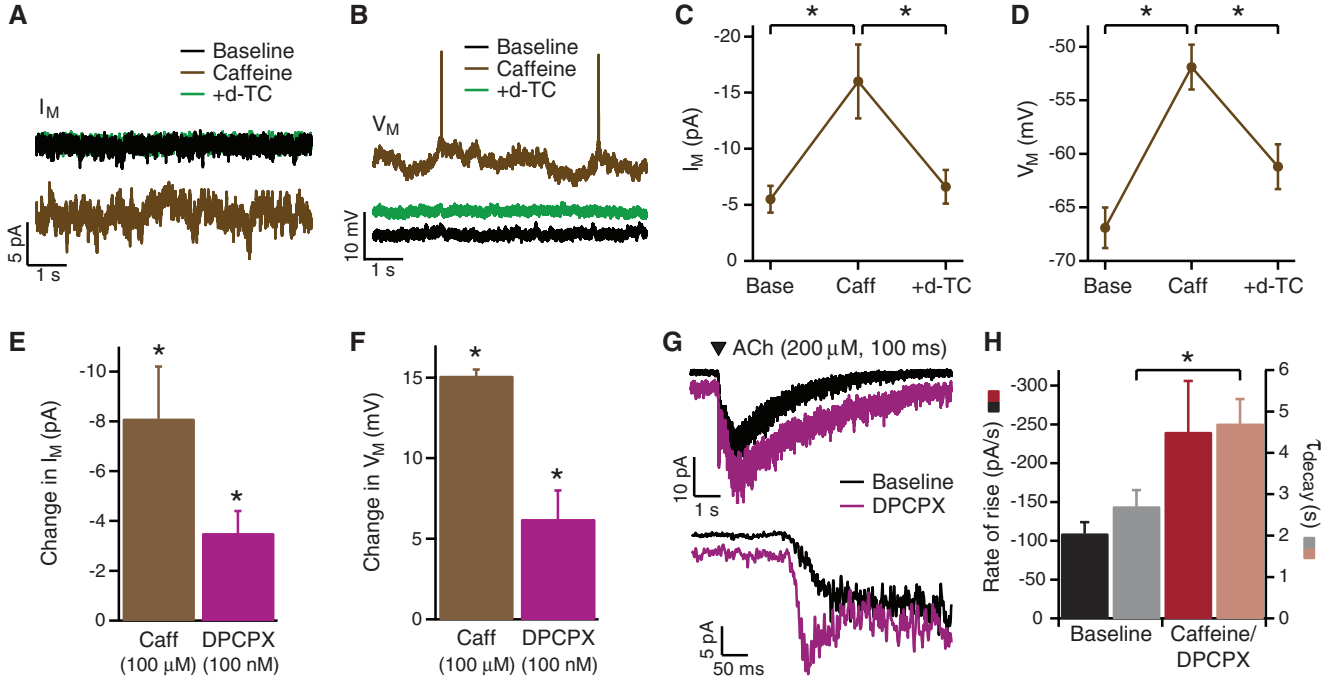

Fig. 3. The effect of caffeine on Kenyon cells. (**A** and **B**) Example traces from a KC in intact honeybee brain recorded under voltage-clamp [(A), $V_H = -73$ mV) and current-clamp [(B), at resting V_M), showing the increase in I_M and depolarization evoked by bath application of caffeine (100 μM) and subsequent reversal by the nAChR antagonist d-TC (500 μM). (**C** and **D**) Mean data showing the reversal by d-TC (500 μM) of the effect of caffeine (Caff; 100 μM) on I_M [(C); $N = 6$, $t_5 = 4.03$, $P = 0.010$; $t_5 = 4.07$, $P = 0.010$] and V_M [(D); $N = 6$, $t_5 = 34.1$, $P < 0.001$; $t_5 = 12.0$, $P < 0.001$]. (**E** and **F**) Comparison of the mean effects of caffeine and DPCPX on I_M [(E); Caff: $N = 10$, $t_9 = 3.84$, $P = 0.004$; DPCPX: $N = 6$, $t_5 = 4.04$, $P = 0.010$] and V_M [(F) Caff: $N = 6$, $t_5 = 34.1$, $P < 0.001$; DPCPX: $N = 6$, $t_5 = 3.39$, $P = 0.019$]. (**G** and **H**) Example traces [(G); rising phase shown on an expanded time scale below] and mean data [(H); rate of rise: $N = 6$, $t_5 = 2.20$, $P = 0.079$; τ_{decay}: $N = 9$, $t_8 = 3.54$, $P = 0.008$] showing that DPCPX (100 nM) and caffeine (100 μM) slowed the decay and, in six of nine KCs, potentiated the fast component of the response evoked by exogenous ACh. (Student's paired t test used in all comparisons.) Mean responses ± SE.

Downloaded from www.sciencemag.org on March 8, 2013

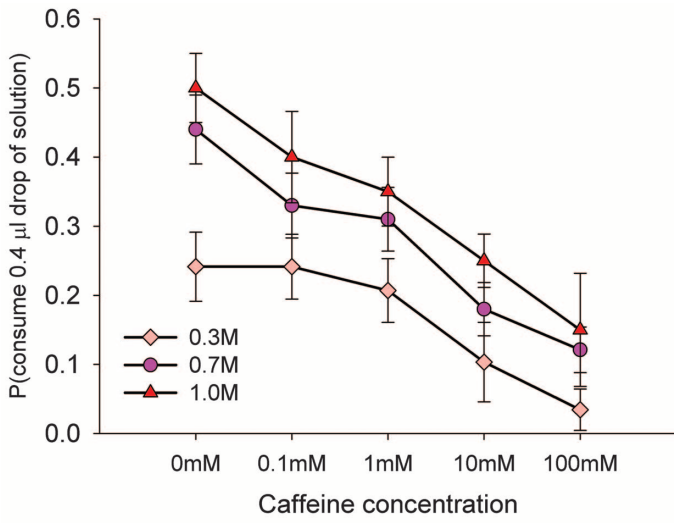

Fig. 4. Bees are more likely to reject sucrose solutions containing caffeine at concentrations greater than 1 mM (logistic regression, χ_4^2 = 23.4, $P < 0.001$; for 0.7 and 1.0 M, 1 mM caffeine versus sucrose post hoc, $P < 0.05$; for 0.3 M, 100 mM caffeine versus sucrose post hoc, $P < 0.05$). Bees were less likely to drink 0.3 M sucrose (pale pink diamonds) than 0.7 M (pink circles) or 1.0 M solutions (red triangles) (logistic regression, $\chi_2^2 = 8.69$, $P = 0.013$). Mean responses ± SE. $N_{0.3M} = 29$, $N_{0.7M} = 100$, $N_{1.0M} = 20$.

olfactory memory in bees was greater than that produced by high concentrations of sucrose when the same experimental methods were used (e.g., 2.0 M, fig. S2B).

Caffeine's influence on cognition in mammals is in part mediated by its action as an adenosine receptor antagonist (*6*). In the hippocampal CA2 region, inhibition of adenosine receptors by caffeine induces long-term potentiation (*12*), a key mechanism of memory formation (*13*). The Kenyon cells (KCs) in mushroom bodies of the insect brain are similar in function to hippocampal neurons: They integrate sensory input during associative learning, exhibit long-term potentiation, and are involved in memory formation (*14*–*16*). To determine whether nectar-caffeine doses affect mushroom body function, we made whole-KC recordings in the intact honeybee brain. Caffeine (100 μM) evoked a small increase in the holding current (I_M) and depolarized KC membrane potential (V_M) toward the action potential firing threshold, by increasing nicotinic acetylcholine receptor (nAChR) activation (Fig. 3, A to D). To determine whether the observed effects of caffeine were due to interactions with adenosine receptors, we applied the adenosine receptor antagonist DPCPX and observed that it similarly increased I_M and depolarized V_M, but to a lesser extent (Fig. 3, E and F). Both caffeine and DPCPX affected KC response kinetics evoked by brief, local application of ACh, increasing the activation rate and slowing the decay (Fig. 3, G and H). Our data show that caffeine modulates cholinergic input via a postsynaptic action, but could act via presynaptic adenosine receptors to potentiate ACh release (*17*). The resulting increase in KC excitability should lead to an increased probability of action potential firing in response to sensory stimulation (*18*), thereby facilitating the induction of associative synaptic plasticity in KCs (*19*). The enhanced activation of KCs may also facilitate plasticity at synapses with mushroom body extrinsic neurons (*20*), which exhibit spike-timing–dependent plasticity (*21*). In this way, a "memory trace" could be formed for the odor associated with reward during and after conditioning (*22*, *23*).

Caffeine is bitter tasting to mammals and is both toxic (*24*) and repellent to honeybees at high concentrations (*25*, *26*). If bees can detect caffeine, they might learn to avoid flowers offering nectar containing it (*27*). We found that honeybees were deterred from drinking sucrose solutions containing caffeine at concentrations greater than 1 mM (Fig. 4); they also have neurons that detect caffeine in sensilla on their mouthparts (fig. S3). However, nectar concentrations did not exceed 0.3 mM (0.058 mg/ml), even though levels of caffeine in vegetative and seed tissues of *Coffea* have been reported to be as great as 24 mg/ml (*28*). This implies that pollinators drive selection toward concentrations of caffeine that are not repellent but still pharmacologically active.

Our data show that plant-produced alkaloids like caffeine have a role in addition to defense: They can pharmacologically manipulate a pollinator's behavior. When bees and other pollinators learn to associate floral scent with food while foraging (*29*), they are more likely to visit flowers bearing the same scent signals. Such behavior increases their foraging efficiency (*30*) while concomitantly leading to more effective pollination (*31*, *32*). Our experiments suggest that by affecting a pollinator's memory, plants reap the reproductive benefits arising from enhanced pollinator fidelity.

References and Notes

1. R. J. Sullivan, E. H. Hagen, P. Hammerstein, *Proc. Biol. Sci.* **275**, 1231 (2008).
2. J. B. Harborne, *Introduction to Ecological Biochemistry* (Academic Press, London, ed. 4, 1993).
3. R. G. Hollingsworth, J. W. Armstrong, E. Campbell, *Nature* **417**, 915 (2002).
4. M. Okamoto, T. Kita, H. Okuda, T. Tanaka, T. Nakashima, *Pharmacol. Toxicol.* **75**, 1 (1994).
5. T. Rudolph, K. Knudsen, *Acta Anaesthesiol. Scand.* **54**, 521 (2010).
6. A. Nehlig, *Neurosci. Biobehav. Rev.* **23**, 563 (1999).
7. J. A. Kretschmar, T. W. Baumann, *Phytochemistry* **52**, 19 (1999).
8. T. H. Ricketts, G. C. Daily, P. R. Ehrlich, C. D. Michener, *Proc. Natl. Acad. Sci. U.S.A.* **101**, 12579 (2004).
9. D. W. Roubik, *Nature* **417**, 708 (2002).
10. Materials and methods are available in the supplementary materials in *Science* Online.
11. M. E. Bitterman, R. Menzel, A. Fietz, S. Schafer, *J. Comp. Psychol.* **97** 107–119 (1983).
12. S. B. Simons, D. A. Caruana, M. L. Zhao, S. M. Dudek, *Nat. Neurosci.* **15**, 23 (2012).
13. R. G. M. Morris, E. Anderson, G. S. Lynch, M. Baudry, *Nature* **319**, 774 (1986).
14. M. Heisenberg, *Nat. Rev. Neurosci.* **4**, 266 (2003).
15. S. Oleskevich, J. D. Clements, M. V. Srinivasan, *J. Neurophysiol.* **78**, 528 (1997).
16. N. J. Strausfeld, L. Hansen, Y. S. Li, R. S. Gomez, K. Ito, *Learn. Mem.* **5**, 11 (1998).
17. B. Sperlágh, E. S. Vizi, *Curr. Top. Med. Chem.* **11**, 1034 (2011).
18. J. Perez-Orive *et al.*, *Science* **297**, 359 (2002).
19. P. Szyszka, A. Galkin, R. Menzel, *Front. Syst. Neurosci.* **2**, 3 (2008).
20. R. Menzel, G. Manz, *J. Exp. Biol.* **208**, 4317 (2005).
21. S. Cassenaer, G. Laurent, *Nature* **482**, 47 (2012).
22. D. S. Galili, A. Lüdke, C. G. Galizia, P. Szyszka, H. Tanimoto, *J. Neurosci.* **31**, 7240 (2011).
23. P. Szyszka *et al.*, *J. Neurosci.* **31**, 7229 (2011).
24. A. Detzel, M. Wink, *Chemoecology* **4**, 8 (1993).
25. J. A. Mustard, L. Dews, A. Brugato, K. Dey, G. A. Wright, *Behav. Brain Res.* **232**, 217 (2012).
26. N. Singaravelan, G. Nee'man, M. Inbar, I. Izhaki, *J. Chem. Ecol.* **31**, 2791 (2005).
27. G. A. Wright *et al.*, *Curr. Biol.* **20**, 2234 (2010).
28. H. Ashihara, A. Crozier, *Trends Plant Sci.* **6**, 407 (2001).
29. G. A. Wright, F. P. Schiestl, *Funct. Ecol.* **23**, 841 (2009).
30. L. Chittka, A. Gumbert, J. Kunze, *Behav. Ecol.* **8**, 239 (1997).
31. R. Hopkins, M. D. Rausher, *Science* **335**, 1090 (2012).
32. W. E. Kunin, *Ecology* **74**, 2145 (1993).

Acknowledgments: We thank staff at Centro Agronomico Tropicale de Investigacion et Ensenanza in Costa Rica for access to the *Coffea* collections and at Technological Education Institute of Crete for access to *Citrus* orchards; M. Thomson, K. Smith, F. Marion-Poll, and A. Popescu for help with the data collection; M. Thompson for beekeeping; and J. Harvey and C. Connolly for project support. This work was funded in part by the Linnean Society of London and by a UK government Insect Pollinators Initiative grant BB/I000968/1 to G.A.W. and a separate grant to C. Connolly (BB/1000313/1). Methods and additional data are available in the online supplementary materials. All data are archived on the Natural Environment Research Council Environmental Information Data Centre.

Supplementary Materials

www.sciencemag.org/cgi/content/full/339/6124/1202/DC1
Materials and Methods
Supplementary Text
Figs. S1 to S3
References (*33*–*36*)

14 August 2012; accepted 21 December 2012
10.1126/science.1228806

Downloaded from www.sciencemag.org on March 8, 2013

Prairie Dogs Disperse When All Close Kin Have Disappeared

John L. Hoogland

Because competition decreases inclusive fitness among kin, Hamilton and May predicted that the presence of nearby kin should induce the dispersal of individuals from the natal territory, independent of pressures to avoid inbreeding. Many studies support this landmark prediction, but research over 31 years with prairie dogs reveals the opposite pattern: Young females are 12.5 times more likely to disperse in the absence of mother and siblings for one species, and 5.5 times more likely for another species. Such striking patterns probably occur because cooperation among kin is more important than competition among kin for young prairie dogs. The inability to cooperate with close kin, due to their absence, prompts a search for a new territory where cooperation might be less crucial for survival and reproduction.

Natal dispersal, the emigration from an individual's territory of birth, has important consequences for demography, gene flow, range expansion, conservation, and population dynamics (*1*–*8*). Natal dispersal occurs in plants and animals across all taxa, but the identification of factors that drive dispersal has nonetheless been difficult (*1*, *2*, *5*). Because kin within the natal territory compete for resources, Hamilton and May (*9*) predicted that the presence of nearby kin should induce natal dispersal, irrespective of attempts to avoid inbreeding. When kin of the natal territory engage in cooperative behaviors (*10*–*12*), however, the benefits of cooperation might outweigh the costs of competition; if so, then the absence of kin might induce natal dispersal (*3*–*8*, *10*–*13*). Studies of several diverse species support Hamilton and May's (*9*) seminal prediction that the presence of nearby kin induces natal dispersal (*14*–*16*), but data for the shaping of natal dispersal by cooperation among kin are scarce. In field research spanning 31 years, I investigated the effect of nearby kin on natal philopatry (i.e., remaining in the natal territory) and natal dispersal of prairie dogs of three species that inhabit grassland ecosystems of the western United States: black-tailed (*Cynomys ludovicianus*, from 1975 to 1988), Gunnison's (*C. gunnisoni*, from 1989 to 1995), and Utah (*C. parvidens*, from 1996 to 2005) (*17*–*20*).

Prairie dogs are large (300 to 900 g for adults, which are ≥1 year old), colonial, diurnal, burrowing, herbivorous rodents of the squirrel family (Sciuridae) (*17*–*20*). Colonies of all three species contain territorial, contiguous family groups called clans, which typically contain one sexually mature male, two to five sexually mature females, and one or two sexually immature yearling males (*17*–*20*). Prairie dogs are excellent models for a study of natal dispersal because they are easy to live-trap, mark, and observe, and because dispersers usually move only short distances to nearby territories (*17*–*21*). My results come from the tracking of wild prairie dogs living under natural conditions, including all 2036 female offspring and all 2102 male offspring from 1093 litters. Of these, 907 females and 744 males survived for ≥12 months, enabling me to score them for dispersal or nondispersal (table S1). Of these 1651 survivors, 1315 (79.6%) showed natal philopatry and 336 (20.4%) showed natal dispersal (table S1). When dispersal occurred during the period when research assistants and I were at the study colony from March through June of every year, young prairie dogs always moved alone [$N > 100$ dispersers; see also (*17*–*21*)].

For females of all three species, the probability of natal dispersal varied inversely and strongly with the number of close kin (mother, littermate sisters, and littermate brothers) within the natal territory (Fig. 1A). These striking inverse relationships resulted directly from the number of nearby close kin per se rather than from the number of nearby conspecifics, because a multiple logistic regression showed that the probability of natal dispersal did not vary significantly with clan size (the number of adults within the same territory, including not only close kin but also more distant kin and immigrants) for any species (for each species, $t \leq 0.839$, $P \geq 0.297$, $N \geq 228$ dispersers and nondispersers). When compared to

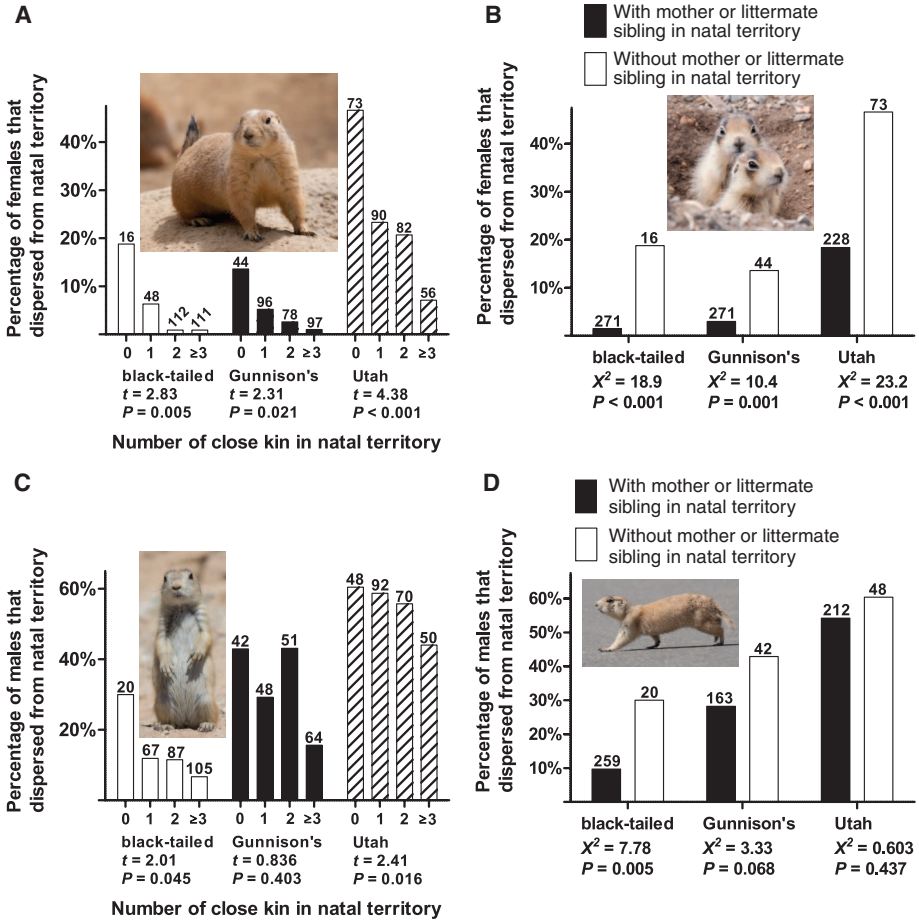

Fig. 1. (**A**) Percentage of females that dispersed versus the number of close kin (mother, littermate sister, or littermate brother) in the natal territory. (**B**) Percentage of females that dispersed from the natal territory versus the presence or absence of close kin in that territory. (**C**) Percentage of males that dispersed versus the number of close kin in the natal territory. (**D**) Percentage of males that dispersed from the natal territory versus the presence or absence of close kin in that territory. For (A) and (C), values for t and P are from a multiple logistic regression that also considered the effect of clan size. For (B) and (D), values for X^2 and P are from a 2 × 2 chi-square test (df = 1). All P values in the text and for Figs. 1 and 2 and fig. S1 are from two-tailed statistical tests. [Photos by Elaine Miller Bond]

University of Maryland Center for Environmental Science, Appalachian Laboratory, Frostburg, MD 21532, USA. E-mail: hoogland@al.umces.edu

Downloaded from www.sciencemag.org on March 8, 2013

females with ≥1 close kin within the natal territory, females with 0 nearby close kin were 12.5 times more likely to disperse for black-tailed prairie dogs, 5.5 times more likely for Gunnison's prairie dogs, and 2.5 times more likely for Utah prairie dogs (Fig. 1B).

Like young female prairie dogs, young males also were more likely to disperse when few or no close kin were present within the natal territory (Fig. 1, C and D). The effect of nearby close kin was weaker for males, however, and natal dispersal was significantly more common for males than for females for all three species (Fig. 2). Because of this sexual asymmetry in the frequency of dispersal and because both males and females were reluctant to copulate with close kin of the opposite sex living in the same territory (*17–20*), the frequency of incest with parents, offspring, or littermate siblings was <5% for black-tailed and Gunnison's prairie dogs and <10% for Utah prairie dogs (*17–20*). Figures 1 and 2 indicate that the reduced opportunity to cooperate with close kin and the importance of avoiding incest have both been important in the evolution of dispersal patterns of prairie dogs.

Determination of father-offspring kinships was more difficult than determination of mother-offspring and sibling-sibling kinships, because a female frequently copulated with more than one male during the period of 5 to 6 hours on the single day each year when she was sexually receptive (*18*, *20*, *21*). For the black-tailed prairie dog, the only species for which I had good behavioral and genetic information on paternity (*18*), natal dispersal by females was not significantly affected by the presence of the biological father in the natal territory ($X^2 = 1.26$, $P = 0.261$, $N = 278$ dispersers and nondispersers).

The absence of close kin within the natal territory almost always encouraged dispersal by females, but the magnitude of the effect of each type of close kin varied (fig. S1). For example, female dispersal was significantly more likely in the absence of ≥1 littermate sister for all three species, and the disappearance of the mother significantly increased female dispersal for two of the three species. The absence of ≥1 littermate brother tended to induce female dispersal for two species, but the effect was not significant for any species.

Clan territories were usually contiguous, and most prairie dogs (>50% for both sexes for all three species) dispersed into an adjacent territory (*17–21*). Consequently, the typical costs of dispersal such as increased vulnerability to predation (*2*, *5*, *9*, *18*) were probably lower for prairie dogs than for most other animals that usually disperse into more distant territories. This factor helps to explain why local dispersal in the absence of close kin within the natal territory was common and easy to document for the three species of prairie dogs (Figs. 1 and 2).

Some interactions among kin are competitive and costly, whereas others are cooperative and enhance survivorship and reproductive success (*4*, *8–13*, *22*, *23*). For prairie dogs of all three species, competitive interactions with close kin of the same clan are frequent, and include fighting and chasing, ritualized disputes at territorial boundaries, and aggressive behaviors to commit or defend against infanticide (*17–20*, *24*). Counteracting these competitive interactions are frequent cooperative behaviors among close kin, including the excavation and maintenance of elaborate burrow systems for rearing offspring and protection from predators and inclement weather; alarm calling when a large predator such as a coyote (*Canis latrans*) attacks; working together to chase a small predator such as a long-tailed weasel (*Mustela frenata*); and shared defense of the home territory against trespassing prairie dogs from adjacent territories (*17–20*). Another important cooperative behavior is communal nursing (the suckling of non-offspring), which can be life-saving for the unweaned offspring of close kin when the mother of those offspring dies from predation or some other cause (*18*, *25*).

When the benefits of cooperation with kin within the natal territory exceed the costs of competition with those kin, the presence of close kin should promote natal philopatry, and the absence of close kin should promote natal dispersal. Natal philopatry of one or both sexes is common across many taxa (*1–8*, *22*, *23*, *26–29*), but only one other study under natural conditions has shown that natal dispersal is significantly more common when cooperating close kin are absent from the natal territory. Female yellow-bellied marmots (*Marmota flaviventris*, $N = 231$ dispersers and nondispersers) were about 1.5 times more likely to disperse from the natal territory when the mother had disappeared [(*30*); see also (*7*) for supporting results from 23 laboratory-born desert night lizards, *Xantusia vigilis*, released into the wild].

When a young prairie dog's mother and littermate siblings all disappear because of death or dispersal, then the opportunity to benefit from cooperation with close kin within the natal territory also disappears; perhaps the absence of nearby close kin indicates that the natal territory is seriously inferior for some reason (such as recurring predation). In response to the absence of close kin within the natal territory, the results from this study show that young prairie dogs of three species are more likely to disperse in search of a new territory. When available, the best choice for a new territory might be one with the mother or a littermate sibling that has dispersed there previously, so that cooperation with close kin is again possible; 1 female black-tailed prairie dog, 3 female Gunnison's prairie dogs, and 10 female Utah prairie dogs made this choice. This option usually is not available, however, so the best alternative for most dispersers is probably a territory with more resources per individual, a lower probability of predation, or fewer intrusions by prairie dogs from adjacent territories. The absence of close kin in the natal territory is thus a proximate cause of natal dispersal by prairie dogs, but the ultimate cause is presumably the opportunity to find either a new territory that offers the benefits of cooperation with close kin that dispersed there previously (rare), or a new territory in which survivorship and reproductive success might be less dependent on cooperation with close kin (common).

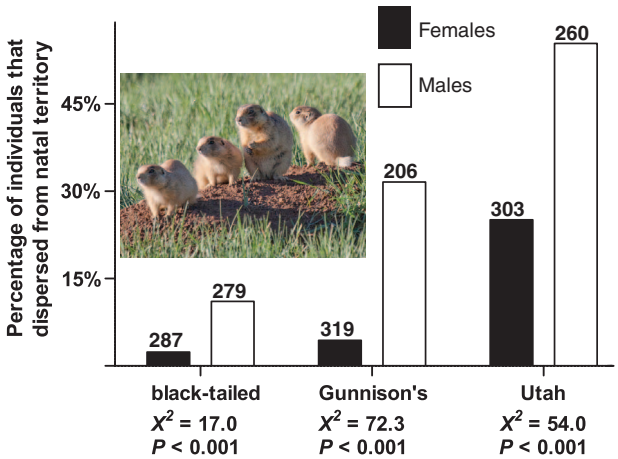

Fig. 2. Sexual asymmetry in natal dispersal for three species of prairie dogs. Values for X^2 and P are from a 2 × 2 chi-square test (df = 1). [Photo by Elaine Miller Bond]

References and Notes

1. K. E. Holekamp, *Ecology* **56**, 365 (1986).
2. N. C. Stenseth, W. Z. Lidicker, Eds., *Animal Dispersal: Small Mammals as a Model* (Springer, New York, 2012).
3. F. S. Dobson, A. T. Smith, W. X. Gao, *Behav. Ecol.* **9**, 622 (1998).
4. X. Lambin, J. Aars, S. B. Piertney, in *Dispersal*, J. Clobert, E. Danchin, A. A. Shondt, J. D. Nichols, Eds. (Oxford Univ. Press, New York, 2001), pp. 110–122.
5. D. E. Bowler, T. G. Benton, *Biol. Rev. Camb. Philos. Soc.* **80**, 205 (2005).
6. L. J. Lawson Handley, N. Perrin, *Mol. Ecol.* **16**, 1559 (2007).
7. A. R. Davis, *Behav. Ecol.* **23**, 18 (2012).
8. T. H. Clutton-Brock, D. Lukas, *Mol. Ecol.* **21**, 472 (2012).
9. W. D. Hamilton, R. M. May, *Nature* **269**, 578 (1977).
10. W. D. Hamilton, *J. Theor. Biol.* **7**, 1 (1964).
11. R. Axelrod, W. D. Hamilton, *Science* **211**, 1390 (1981).
12. S. A. West, I. Pen, A. S. Griffin, *Science* **296**, 72 (2002).
13. T. G. Platt, J. D. Bever, *Trends Ecol. Evol.* **24**, 370 (2009).
14. J. J. Jacquot, S. H. Vessey, *Behav. Ecol. Sociobiol.* **37**, 407 (1995).
15. J. C. Moore, A. Loggenberg, J. M. Greeff, *Biol. Lett.* **2**, 17 (2006).
16. J. Cote, J. Clobert, P. S. Fitze, *Proc. Natl. Acad. Sci. U.S.A.* **104**, 9703 (2007).

Downloaded from www.sciencemag.org on March 8, 2013

17. J. L. Hoogland, *Science* **215**, 1639 (1982).
18. J. L. Hoogland, *The Black-tailed Prairie Dog: Social Life of a Burrowing Mammal* (Univ. of Chicago Press, Chicago, 1995).
19. J. L. Hoogland, *J. Mammal.* **80**, 243 (1999).
20. J. L. Hoogland, in *Rodent Societies*, J. O. Wolff, P. W. Sherman, Eds. (Univ. of Chicago Press, Chicago, 2007), pp. 438–450.
21. Details about my materials and methods are available as supplementary materials on *Science* Online.
22. J. B. Silk, *Philos. Trans. R. Soc. London Ser. B* **362**, 539 (2007).
23. J. C. Mitani, J. Call, P. M. Kappeler, R. Palombit, J. B. Silk, *The Evolution of Primate Societies* (Univ. of Chicago Press, Chicago, 2012).
24. J. L. Hoogland, *Behaviour* **69**, 1 (1979).
25. J. L. Hoogland, *Behav. Ecol. Sociobiol.* **63**, 1621 (2009).
26. P. J. Greenwood, *Anim. Behav.* **28**, 1140 (1980).
27. P. M. Waser, W. T. Jones, *Q. Rev. Biol.* **58**, 355 (1983).
28. W. D. Koenig, D. Van Vuren, P. N. Hooge, *Trends Ecol. Evol.* **11**, 514 (1996).
29. C. M. Arnaud, F. S. Dobson, J. O. Murie, *Mol. Ecol.* **21**, 493 (2012).
30. K. B. Armitage, D. H. Van Vuren, A. Ozgul, M. K. Oli, *Ecology* **92**, 218 (2011).

Acknowledgments: I thank J. Hoogland for encouraging me to reexamine my information on dispersal; my 150+ research assistants over the 31 years of research (especially my four offspring); and D. Boesch, K. Fuller, R. Gardner, R. Morgan, and L. Pitelka of the University of the Maryland Center for Environmental Science (UMCES) for the opportunity for long-term comparative research. Financial support was provided by Colorado Parks and Wildlife, the Denver Zoological Foundation, Environmental Defense, the Eppley Foundation, the Harry Frank Guggenheim Foundation, the National Fish and Wildlife Foundation, the National Geographic Society, NSF, Princeton University, the Ted Turner Foundation, UMCES, and the Universities of Michigan and Minnesota. For help with the manuscript, I thank R. Alexander, D. Blumstein, D. Bowler, C. Brown, J. Clobert, T. H. Clutton-Brock, A. Davis-Robosky, F. S. Dobson, L. Handley, K. Holekamp, A. Hoogland, S. Keller, X. Lambin, M. Oli, P. Sherman, N. Solomon, and D. Van Vuren. Data for this report are archived as supplementary materials on *Science* Online.

Supplementary Materials
www.sciencemag.org/cgi/content/full/339/6124/1205/DC1
Materials and Methods
Fig. S1
Tables S1 and S2
References (*31–38*)

18 October 2012; accepted 23 January 2013
10.1126/science.1231689

Gene Transfer from Bacteria and Archaea Facilitated Evolution of an Extremophilic Eukaryote

Gerald Schönknecht,[1,2]*† Wei-Hua Chen,[3,4]† Chad M. Ternes,[1]† Guillaume G. Barbier,[5]†‡ Roshan P. Shrestha,[5]†§ Mario Stanke,[6] Andrea Bräutigam,[2] Brett J. Baker,[7] Jillian F. Banfield,[8] R. Michael Garavito,[9] Kevin Carr,[10] Curtis Wilkerson,[5,10] Stefan A. Rensing,[11]|| David Gagneul,[12] Nicholas E. Dickenson,[13] Christine Oesterhelt,[14] Martin J. Lercher,[3,15] Andreas P. M. Weber[2,5,15]*

Some microbial eukaryotes, such as the extremophilic red alga *Galdieria sulphuraria*, live in hot, toxic metal-rich, acidic environments. To elucidate the underlying molecular mechanisms of adaptation, we sequenced the 13.7-megabase genome of *G. sulphuraria*. This alga shows an enormous metabolic flexibility, growing either photoautotrophically or heterotrophically on more than 50 carbon sources. Environmental adaptation seems to have been facilitated by horizontal gene transfer from various bacteria and archaea, often followed by gene family expansion. At least 5% of protein-coding genes of *G. sulphuraria* were probably acquired horizontally. These proteins are involved in ecologically important processes ranging from heavy-metal detoxification to glycerol uptake and metabolism. Thus, our findings show that a pan-domain gene pool has facilitated environmental adaptation in this unicellular eukaryote.

Although bacteria and archaea usually dominate extreme environments, hot and extremely acidic habitats are typically devoid of photosynthetic bacteria. Instead, eukaryotic unicellular red algae of the Cyanidiophyceae are the principal photosynthetic organisms in these ecological niches (*1*). Cyanidiophyceae can grow at pH 0 to 4 and temperatures up to 56°C, close to the upper temperature limit for eukaryotic life (*2*). *Galdieria sulphuraria* is a unique member of the Cyanidiophyceae, displaying high salt and metal tolerance and exhibiting extensive metabolic versatility (*3*, *4*). *G. sulphuraria* naturally inhabits volcanic hot sulfur springs, solfatara soils, and anthropogenic hostile environments. In habitats with high concentrations of arsenic, aluminum, cadmium, mercury, and other toxic metals, *G. sulphuraria* frequently represents up to 90% of total biomass and almost all the eukaryotic biomass (*1*, *5*).

To understand the molecular mechanisms underlying *G. sulphuraria*'s extremophilic and metabolically flexible lifestyle (Fig. 1), we determined its genome sequence (13.7 Mb; table S1) (*6*). The only member of the Cyanidiophyceae for which a genome sequence was previously available, *Cyanidioschyzon merolae* (*7*), diverged from *G. sulphuraria* about 1 billion years ago, which approximates the evolutionary distance between fruit flies and humans (see fig. S1 and supplementary materials). *C. merolae* maintains a strictly photoautotrophic lifestyle and does not tolerate high salt or metal concentrations; it differs markedly from *G. sulphuraria* in ecology, cell biology, and physiology. Accordingly, we find orthologs for only 42% of the 6623 *G. sulphuraria* proteins in *C. merolae*, and only 25% of both genomes constitute syntenic blocks (fig. S2). Coding sequences make up 77.5% of the *G. sulphuraria* genome, resulting in a median intergenic distance of 20 base pairs (bp) (fig. S3). Protein-coding genes contain on average two introns (fig. S4), with median lengths of 55 bp (fig. S5). Thus, the *G. sulphuraria* genome is highly condensed by comparison with that of *C. merolae* and most other eukaryotes.

Eukaryotic innovations usually arise through gene duplications and neofunctionalizations, which lead to expansion of existing gene families (*8*). In contrast, archaea and bacteria commonly adapt through horizontal gene transfer (HGT) from other lineages (*9*). HGT has also been observed in some unicellular eukaryotes (*10*); however, to our knowledge, horizontally acquired genes have not been linked to fitness-relevant traits in free-living eukaryotes (*11*). Phylogenetic analyses of *G. sulphuraria* genes using highly stringent criteria indicate at least 75 separate gene acquisitions from archaea and bacteria (supplementary materials). The origin of these *G. sulphuraria* genes from HGT is supported by the finding that compared to the genomic average, they have

[1]Department of Botany, Oklahoma State University, Stillwater, OK 74078, USA. [2]Institute of Plant Biochemistry, Heinrich-Heine-Universität Düsseldorf, 40225 Düsseldorf, Germany. [3]Institute for Computer Science, Heinrich-Heine-Universität Düsseldorf, 40225 Düsseldorf, Germany. [4]European Molecular Biology Laboratory (EMBL) Heidelberg, EMBL, Meyerhofstrasse 1, 69117 Heidelberg, Germany. [5]Department of Plant Biology, 612 Wilson Road, Michigan State University, East Lansing, MI 48824, USA. [6]Institut für Mathematik und Informatik, Ernst Moritz Arndt Universität Greifswald, Walther-Rathenau-Straße 47, 17487 Greifswald, Germany. [7]Department of Earth and Environmental Sciences, 4011 CC Little Building, 1100 North University Avenue, University of Michigan, Ann Arbor, MI 48109, USA. [8]Department of Earth and Planetary Science, Department of Environmental Science, Policy, and Management, University of California, Berkeley CA 94720–4767, USA. [9]Department of Biochemistry and Molecular Biology, 603 Wilson Road, Michigan State University, East Lansing, MI 48824, USA. [10]Research Technology Support Facility, Plant Biology Laboratories, 612 Wilson Road, Michigan State University, East Lansing, MI 48824, USA. [11]Faculty of Biology and BIOSS Centre for Biological Signalling Studies, University of Freiburg, Schänzlestrasse 1, 79104 Freiburg, Germany. [12]UMR USTL-INRA 1281 "Stress Abiotiques et Différenciation des Végétaux cultivés," Université de Lille 1, 59650 Villeneuve d'Ascq Cédex, France. [13]Department of Microbiology and Molecular Genetics, Oklahoma State University, Stillwater, OK 74078, USA. [14]CyanoBiofuels GmbH, Magnusstrasse 11, 12489 Berlin, Germany. [15]Cluster of Excellence on Plant Sciences (CEPLAS), Heinrich-Heine-Universität Düsseldorf, 40225 Düsseldorf, Germany.

*To whom correspondence should be addressed. E-mail: gerald.schoenknecht@okstate.edu (G.S.); andreas.weber@uni-duesseldorf.de (A.P.M.W.)
†These authors contributed equally to this work.
‡Permanent address: Novozymes, Inc, 1445 Drew Avenue, Davis, CA 95618, USA.
§Permanent address: Scripps Institution of Oceanography, University of California, San Diego, CA 92037, USA.
||Permanent address: Faculty of Biology, Philipps-University Marburg, 35032 Marburg, Germany.

Downloaded from www.sciencemag.org on March 8, 2013

significantly fewer introns (mean 0.8 versus 2.06, $P = 0.0012$, Mann-Whitney test; fig. S6), slightly higher GC content (40.6% versus 39.9%, $P = 0.0030$, Student's t test; fig. S7), and deviating oligonucleotide usage ($P = 0.00034$, Mann-Whitney test; fig. S7). Gene transfers can be traced to a broad range of donor taxa (fig. S8 and table S4), with a significant enrichment from extremophile bacteria ($P = 7.8 \times 10^{-9}$, Fisher's exact test). The genome of *G. sulphuraria* thus shows notable contributions from a pan-domain gene pool.

The two largest *G. sulphuraria* protein families form a monophyletic branch within the so-called archaeal ATPases (adenosine triphosphatases) (Fig. 2A). These soluble ATPases have not been observed in other eukaryotes. Phylogenetic analyses indicate that *G. sulphuraria* acquired an ancestral ATPase gene from archaea, followed by duplications and diversification into separate families (fig. S11). Genes encoding the different families cluster in pairs on the *G. sulphuraria* genome (Fig. 2B). Pairs of homologous ATPase genes that are transcribed together are observed in archaeal genomes (*12*). Although their physiological function is unknown (*13*), archaeal ATPases may contribute to heat tolerance. We found a correlation between ATPase gene copy number and optimal growth temperature across thermophilic and hyperthermophilic archaea (Fig. 2C). These findings suggest that *G. sulphuraria*'s adaptation to heat may have been facilitated by the acquisition and subsequent expansion of an archaeal ATPase gene family.

G. sulphuraria's tolerance to high salinity is also likely to have been facilitated by HGT. Resistance to salt stress requires the removal of Na^+ from the cytosol and an increase of osmolarity using compatible solutes in the cytosol. In addition to several Na^+:H^+ antiporters of eukaryotic origin, *G. sulphuraria* encodes two monovalent cation:proton antiporters that appear to have been acquired from bacteria (fig. S13). Furthermore, genes encoding sarcosine dimethylglycine methyltransferase (SDMT) appear to originate from halophilic cyanobacteria (fig. S14). These enzymes allow the production of the compatible solute betaine from glycine (*14*), which indeed accumulates in *G. sulphuraria* under salt stress (fig. S15).

How does *G. sulphuraria* maintain near-neutral cytosolic pH against a 10^6-fold H^+ gradient across its plasma membrane (*15*, *16*)? There is no evidence for an enhanced capacity to pump H^+ out of the cytosol (which would be an energetically intense strategy). Yet, there are indications of a reduced H^+ permeability of the plasma membrane. For *G. sulphuraria*, one voltage-gated ion channel gene was identified in the genome, compared to three in *C. merolae* (table S3) and 16 or more in other unicellular algae. Voltage-gated ion channels allow single-file diffusion of water, and therefore have a very high conductance for protons. A plasma membrane devoid of proton-conducting voltage-gated ion channels probably

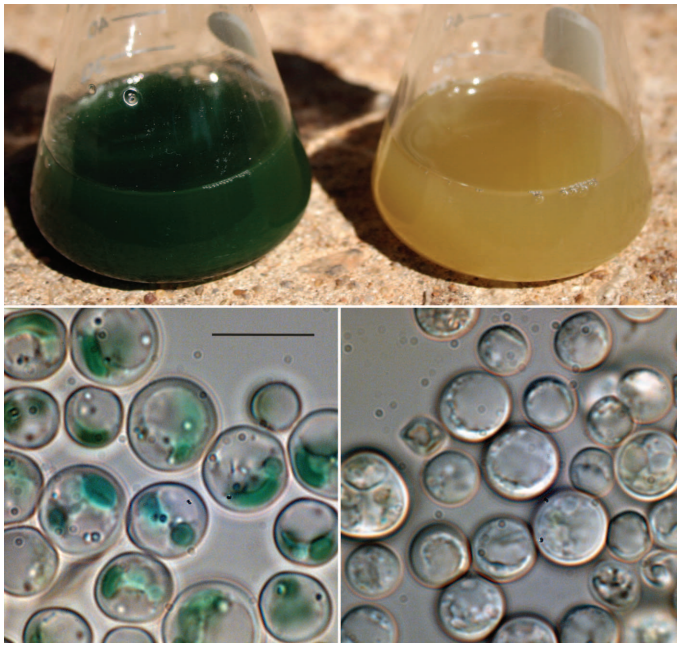

Fig. 1. Photoautotrophic (left) and heterotrophic (right) *G. sulphuraria* cells. Cell cultures (top) and light microscopic images (bottom; bar represents 10 μm) of *G. sulphuraria* cells grown under continuous illumination in the absence of glucose (left) or in darkness in the presence of 200 mM glucose (right).

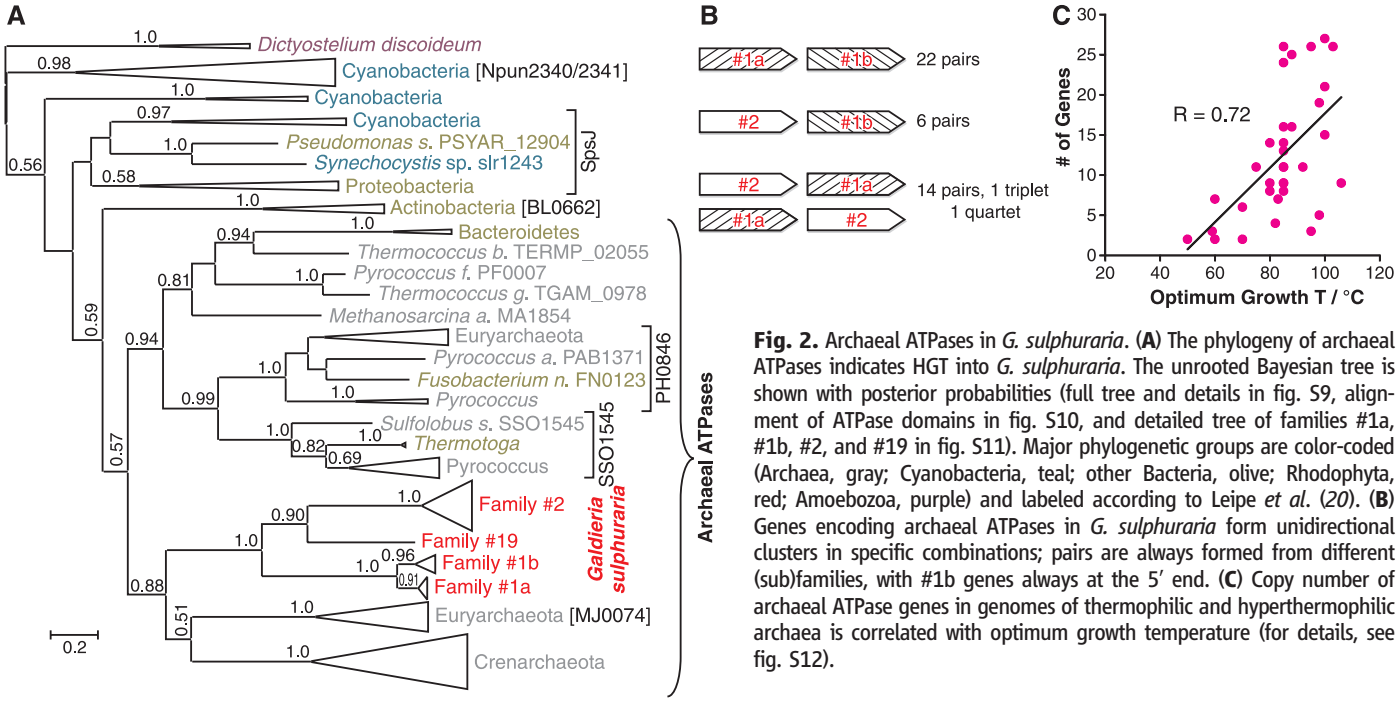

Fig. 2. Archaeal ATPases in *G. sulphuraria*. (**A**) The phylogeny of archaeal ATPases indicates HGT into *G. sulphuraria*. The unrooted Bayesian tree is shown with posterior probabilities (full tree and details in fig. S9, alignment of ATPase domains in fig. S10, and detailed tree of families #1a, #1b, #2, and #19 in fig. S11). Major phylogenetic groups are color-coded (Archaea, gray; Cyanobacteria, teal; other Bacteria, olive; Rhodophyta, red; Amoebozoa, purple) and labeled according to Leipe *et al.* (*20*). (**B**) Genes encoding archaeal ATPases in *G. sulphuraria* form unidirectional clusters in specific combinations; pairs are always formed from different (sub)families, with #1b genes always at the 5′ end. (**C**) Copy number of archaeal ATPase genes in genomes of thermophilic and hyperthermophilic archaea is correlated with optimum growth temperature (for details, see fig. S12).

Downloaded from www.sciencemag.org on March 8, 2013

has a low H^+ permeability, preventing the acidification of the cell interior even at very high external H^+ concentrations. *G. sulphuraria* shows an expansion of both, the intracellular chloride channel (CLIC) family and the chloride carrier/channel (ClC) family (table S3), which do not conduct protons.

G. sulphuraria copes with toxic metals typically found in volcanic areas and acid mine drainage by a variety of metal transporters (table S3). Different plasma membrane uptake systems for divalent metal cations permit the selective uptake of essential metals (such as iron or copper) at high concentrations of toxic metals (such as aluminum or cadmium). *G. sulphuraria* can also neutralize biohazardous metals, making it potentially useful in biotechnological applications. For example, *G. sulphuraria* arsenite methyltransferases can biotransform arsenic, which is often found at very high concentrations in geothermal environments, into less toxic and possibly gaseous methyl derivatives (*17*). In addition, two intronless *G. sulphuraria* genes encode the bacterial arsenical membrane protein pump, ArsB. The sequences most similar to *G. sulphuraria* ArsB are from thermoacidophilic bacteria (Fig. 3), again indicating a central role for HGT in extremophilic adaptation. Mercury is found at concentrations up to 200 μg/g in soils from which *G. sulphuraria* has been isolated. *G. sulphuraria* can reduce cytotoxic Hg^{2+} into less toxic metallic mercury. The enzyme responsible, mercuric reductase, was also most likely acquired horizontally from Proteobacteria (fig. S17).

In total, 5.2% of *G. sulphuraria* genes encode membrane transport proteins (mostly metabolite transporters), which is more than has been discovered in most other eukaryotes (fig. S18). Gene family expansions (table S3) are found, for example, in sugar porters (fig. S19), amino acid/auxin permeases (fig. S20), and putative acetate transporters (fig. S21); these three protein families are among the 20 largest in *G. sulphuraria* (table S2). Further major expansions were found in amino acid–polyamine–organocation transporters (fig. S22), glycoside-pentoside-hexuronide:cation symporters, and glycerol uptake facilitators (fig. S23). Together, these metabolite transporters are likely to be essential for the exceptional ability of *G. sulphuraria* to grow heterotrophically on many different metabolites. In contrast, most other unicellular algae, including *C. merolae*, are strictly (or almost strictly) photoautotrophic.

Again, phylogenetic analyses indicate that HGT contributed to *G. sulphuraria*'s enormous metabolic flexibility. All acetate permeases (fig. S21) appear to originate from bacteria, whereas some of the amino acid–polyamine–organocation transporters (fig. S22) seem to stem from thermoacidophilic archaea. *G. sulphuraria* can grow heterotrophically on glycerol as sole carbon source (*3*) using a family of five glycerol uptake facilitators and a family of three glycerol dehydrogenases; both families apparently originate from HGT (figs. S23 and S24).

Some of *G. sulphuraria*'s metabolic pathways appear to be conserved from a heterotrophic last common eukaryotic ancestor, but subsequently were lost from other photosynthetic eukaryotes. For example, animals (metazoa) use the methylmalonyl–coenzyme A pathway for the degradation of odd-numbered chain fatty acids and leucine. Whereas green plants and *C. merolae* lack this pathway, it is present in *G. sulphuraria*, as well as in diatoms and brown algae. Furthermore, green plants, diatoms, and brown algae synthesize the essential nicotinamide adenine dinucleotide precursor quinolinate from aspartate. In contrast, *G. sulphuraria* and *C. merolae* produce quinolinate from tryptophan by way of kynurenine, a pathway common to animals and fungi.

G. sulphuraria contains a number of metabolite transporter families that group with fungi and show less similarity to metabolite transporter families from more closely related organisms (figs. S19, S20, and S25). This unexpected phylogenetic trace could be explained by the loss of genes present in the common eukaryotic ancestor from other clades, by HGT from unsequenced bacteria or archaea into both eukaryotic lineages, or by HGT between fungi and *G. sulphuraria*. We currently cannot distinguish between these alternative hypotheses owing to limited taxon representation in sequence databases.

G. sulphuraria can also survive saprophytically by excreting catabolic enzymes that decompose extracellular organic polymers into small metabolites for uptake by plasma membrane transporters. Proteomics (*18*) and/or bioinformatics analyses (supplementary materials) indicate excretion of aspartyl proteases, which cleave peptide bonds at acidic pH; β-galactosidases (fig. S26) and glucoamylases, which degrade polysaccharides; and acid phosphatases (fig. S27), which remove phosphate groups from organic molecules. These excreted enzymes lack orthologs in other photosynthetic eukaryotes, but show homology to excreted enzymes encoded by fungi or bacteria. In particular, *G. sulphuraria* may have acquired acid phosphatases (fig. S27) and some β-galactosidases (fig. S26) from bacteria.

Extensive gene transfer appears to have been key to the genomic evolution of a metabolically versatile, extremophilic, red alga. Numerous proteins acquired through HGT interact with *G. sulphuraria*'s physico-chemical and metabolic environment. Protein families acquired horizontally by *G. sulphuraria* are 3-fold enriched in membrane transporters (10.5% for HGT families, $P = 0.010$, Fisher's exact test) and 14-fold enriched in protein families also found in extremophilic bacteria or archaea (86.8% for HGT families, $P = 1.5 \times 10^{-22}$). These findings for *G. sulphuraria* mirror the results of a previous systematic study, which showed that proteobacterial adaptation relies on the horizontal acquisition of genes that function at the bacteria's interface to the environment (*19*). Whereas the importance of HGT for evolution of Bacteria and Archaea is well established, adaptation of a eukaryotic extremophile by gene transfer from Bacteria and Archaea is unexpected and shines a new light on the evolution of unicellular eukaryotes.

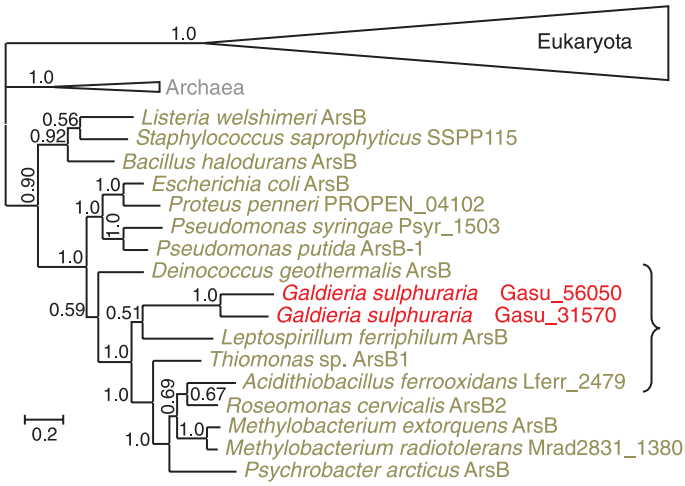

Fig. 3. The phylogeny (Bayesian tree) of bacterial arsenical resistance efflux pumps (ArsB) indicates HGT into *G. sulphuraria* (full tree and details in fig. S16). The curly bracket marks *G. sulphuraria* and four thermophilic and/or acidophilic bacteria (in olive), which live in the same environment as *G. sulphuraria* and from which taxa the algal ArsB may have derived.

References and Notes

1. W. N. Doemel, T. D. Brock, *J. Gen. Microbiol.* **67**, 17 (1971).
2. L. J. Rothschild, R. L. Mancinelli, *Nature* **409**, 1092 (2001).
3. W. Gross, C. Schnarrenberger, *Plant Cell Physiol.* **36**, 633 (1995).
4. V. Reeb, D. Bhattacharya, in *Red Algae in the Genomic Age,* J. Seckbach, D. J. Chapman, Eds. (Springer, Netherlands, 2010), pp. 409–426.
5. G. Pinto, C. Ciniglia, C. Cascone, A. Pollio, in *Algae and Cyanobacteria in Extreme Environments,* J. Seckbach, Ed. (Springer, Dordrecht, Netherlands, 2007), vol. 11, pp. 487–502.
6. Materials and methods are available as supplementary materials on *Science* Online.
7. M. Matsuzaki *et al.*, *Nature* **428**, 653 (2004).
8. H. Innan, F. Kondrashov, *Nat. Rev. Genet.* **11**, 97 (2010).
9. T. J. Treangen, E. P. C. Rocha, *PLoS Genet.* **7**, e1001284 (2011).
10. C. Bowler *et al.*, *Nature* **456**, 239 (2008).
11. P. J. Keeling, *Curr. Opin. Genet. Dev.* **19**, 613 (2009).

Downloaded from www.sciencemag.org on March 8, 2013

12. R. Overbeek *et al.*, *Nucleic Acids Res.* **33**, 5691 (2005).
13. E. V. Koonin, *Science* **275**, 1489 (1997).
14. J. G. McCoy *et al.*, *Proteins Struct. Funct. Bioinformatics* **74**, 368 (2009).
15. I. Enami, H. Akutsu, Y. Kyogoku, *Plant Cell Physiol.* **27**, 1351 (1986).
16. W. Gross, *Hydrobiologia* **433**, 31 (2000).
17. J. Ye, C. Rensing, B. P. Rosen, Y.-G. Zhu, *Trends Plant Sci.* **17**, 155 (2012).
18. C. Oesterhelt, S. Vogelbein, R. P. Shrestha, M. Stanke, A. P. M. Weber, *Planta* **227**, 353 (2008).
19. C. Pál, B. Papp, M. J. Lercher, *Nat. Genet.* **37**, 1372 (2005).
20. D. D. Leipe, E. V. Koonin, L. Aravind, *J. Mol. Biol.* **343**, 1 (2004).

Acknowledgments: This work was made possible by NSF grant EF 0332882 (to A.P.M.W.). Partial support came from the Deutsche Forschungsgemeinschaft (DFG) (CRC TR1, IRTG 1525/1 and WE2231/7-1 to A.P.M.W., EXC 1028 to M.J.L. and A.P.M.W., CRC 680 to M.J.L., and a DFG Mercator Fellowship to G.S.). G.S. appreciates support from NSF (MCB 0925298) and the College of Arts and Sciences, Oklahoma State University (OSU). We thank M. Hanikenne and E. Koonin for helpful discussion, and A. Doust and P. Pelser for advice on phylogenetic analyses. We are grateful to B. Sears for introduction to and assistance with CsCl purification of bisbenzamide-treated nuclear DNA. Some of the computing for this project was performed at the OSU High Performance Computing Center. Sequence data have been deposited at DNA Data Bank of Japan, EMBL, and GenBank under accession ADNM00000000 (SRA012465). The version described in this paper is the first version, ADNM01000000.

Supplementary Materials
www.sciencemag.org/cgi/content/full/339/6124/1207/DC1
Materials and Methods
Supplementary Text
Figs. S1 to S27
Tables S1 to S3
Additional Data Table S4
References (*21–79*)

18 October 2012; accepted 8 January 2013
10.1126/science.1231707

Cell Death from Antibiotics Without the Involvement of Reactive Oxygen Species

Yuanyuan Liu and James A. Imlay*

Recent observations have suggested that classic antibiotics kill bacteria by stimulating the formation of reactive oxygen species (ROS). If true, this notion might guide new strategies to improve antibiotic efficacy. In this study, the model was directly tested. Contrary to the hypothesis, antibiotic treatment did not accelerate the formation of hydrogen peroxide in *Escherichia coli* and did not elevate intracellular free iron, an essential reactant for the production of lethal damage. Lethality persisted in the absence of oxygen, and DNA repair mutants were not hypersensitive, undermining the idea that toxicity arose from oxidative DNA lesions. We conclude that these antibiotic exposures did not produce ROS and that lethality more likely resulted from the direct inhibition of cell-wall assembly, protein synthesis, and DNA replication.

In recent decades, the growing number of antibiotic-resistant pathogens has spurred efforts to further understand and improve the efficacy of the basic antibiotic classes. Most clinically used antibiotics target cell-wall assembly, protein synthesis, or DNA replication. However, recent reports have raised the possibility that although these antibiotics block growth by directly inhibiting the targets mentioned above, they may owe their lethal effects to the indirect creation of reactive oxygen species (ROS) that then damage bacterial DNA (*1–10*).

The evidence supporting this proposal included the observation that cell-penetrating dyes were oxidized more quickly inside antibiotic-treated bacteria (*3–8*). Furthermore, iron chelators (*3*, *4*, *7–9*), which suppress hydroxyl-radical–generating Fenton chemistry, and thiourea (*4*, *6*, *8–10*), a potential scavenger of hydroxyl radicals, lessened toxicity. Mutations that diminish fluxes through the tricarboxylic acid cycle were protective (*3–5*), suggesting a key role for respiration, and DNA-repair mutants were somewhat sensitive (*4*, *8*). Systems analysis of aminoglycoside-treated *Escherichia coli* suggested a model that fits these data (*5*). It was postulated that interference with ribosome progression would release incomplete polypeptides, some of which are translocated to the cell membranes where they might trigger envelope stress. The Arc regulatory system is perturbed, potentially accelerating respiration and thereby increasing the flux of superoxide and hydrogen peroxide into the cell interior. These two oxidants have known sequelae that ultimately lead to DNA damage. Specifically, superoxide and hydrogen peroxide damage the iron-sulfur clusters of dehydratases (*11*, *12*), releasing iron atoms and elevating the pool of intracellular unincorporated iron (*13*, *14*). This iron can then react with hydrogen peroxide in the Fenton reaction, generating hydroxyl radicals that either directly damage DNA (*15*) or indirectly oxidize the deoxynucleotide pool, which is subsequently incorporated into DNA (*16*). This scenario could explain the observed oxidation of intracellular dyes, protection by scavengers and chelators, a requirement for respiration, and the sensitivity of DNA-repair mutants.

This model is plausible, so we devised experiments to directly test the molecular events that underpin it. The bacterial strain (*E. coli* MG1655), growth medium (LB), and antibiotic doses were chosen to match those of previous studies (*4*). Kanamycin was used to target translation, ampicillin to block cell-wall synthesis, and norfloxacin to disrupt DNA replication.

Superoxide and hydrogen peroxide are generated inside cells when flavoenzymes inadvertently transfer a fraction of their electron flux directly to molecular oxygen (*15*, *17*). Thus, neither of these ROS can be formed under anoxic

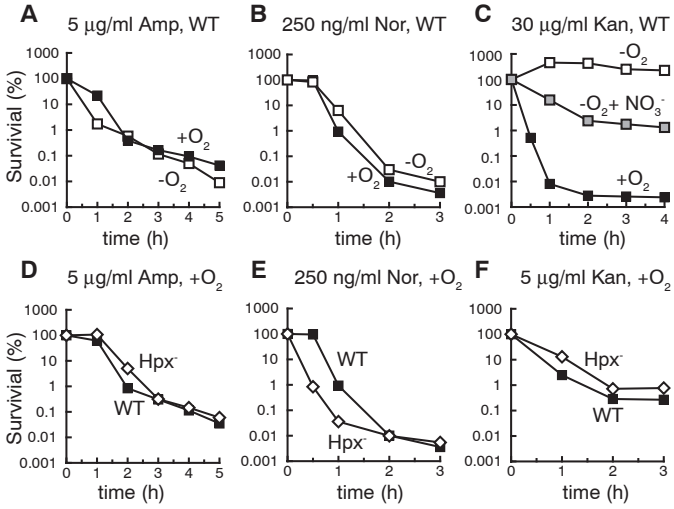

Fig. 1. Antibiotic efficacy does not require oxygen or H_2O_2. (**A** to **C**) Wild-type cells were treated with ampicillin (A), norfloxacin (B), or kanamycin (C) in the presence (solid squares) or absence (open squares) of oxygen. In (C), anoxic killing was also tested in the presence of 40 mM KNO_3 (gray squares). (**D** to **F**) Wild-type cells (solid squares, MG1655) and congenic Hpx^- cells (open diamonds, AL427) were treated with antibiotics ampicillin (D), norfloxacin (E), or kanamycin (F). Results are representative of at least three biological replicates.

Department of Microbiology, University of Illinois, Urbana, IL 61801, USA.

*To whom correspondence should be addressed. E-mail: jimlay@illinois.edu

Downloaded from www.sciencemag.org on March 8, 2013

conditions. We found, however, that ampicillin and norfloxacin were as lethal to cells in an anaerobic chamber as to cells in air-saturated medium (Fig. 1, A to C). Anoxia sharply diminished the toxicity of kanamycin, but lethal activity was partially restored at high kanamycin doses when nitrate was provided as an alternative respiratory substrate. This pattern mirrors the effects of oxygen and nitrate upon kanamycin import, which is governed by the magnitude of the proton motive force (*18*, *19*). Thus, ROS were not required for the lethal actions of kanamycin, and they made no apparent contribution at all to the toxicity of ampicillin and norfloxacin.

Hydroxyl radicals are formed inside cells when ferrous iron transfers electrons to H_2O_2, so hydroxyl-radical stress is greatest when either H_2O_2 or ferrous concentrations are high. An *E. coli* mutant that lacks catalase and peroxidase activities (denoted Hpx^-) cannot scavenge H_2O_2 and more easily accumulates it to toxic levels; substantial damage to proteins and to DNA ensues (*12*, *20*, *21*). However, this mutant was not more sensitive to ampicillin or kanamycin than were wild-type cells (Fig. 1, D and F). It was more sensitive to norfloxacin, an effect that might result from the preexisting DNA damage in the scavenger mutant, coupled with the inhibitory effect of norfloxacin on DNA metabolism (*22*) (Fig. 1E).

We directly tested the prediction that antibiotic treatment would augment respiration and thereby increase superoxide and H_2O_2 formation. The respiratory chain is normally a minor source (<20%) of these oxidants (*17*), so a very large flux increase would be needed to substantially amplify total intracellular oxidant production. However, measurements of oxygen consumption with a Clark-type electrode showed that respiration slowly declined, rather than increased, when cells were treated with kanamycin (Fig. 2A). This trend persisted throughout the period during which the number of viable cells declined by >99%. Norfloxacin had little effect on respiration. Ampicillin transiently increased respiration, perhaps by causing envelope damage that dissipated the back-pressure of the proton motive force, before cell lysis ended metabolism. In no case did respiration accelerate enough to be a sufficient explanation for toxicity.

E. coli features a transcription factor, OxyR, that is activated by H_2O_2 whenever its levels approach the concentrations (0.5 to 1 μM) sufficient to damage enzymes or DNA (*23*). The OxyR regulon includes genes whose products assist in H_2O_2 scavenging (*katG* and *ahpCF*), free-iron control (*dps*, *fur*, and *yaaA*), and enzyme protection (*mntH* and *sufABCDE*) (*15*, *24*). When cells were treated with ampicillin and norfloxacin, they accumulated lethal damage within 1 hour; however, real-time quantitative reverse transcription polymerase chain reaction (qRT-PCR) analysis indicated that OxyR-controlled genes were not induced (Fig. 2B). These antibiotic-treated cells robustly activated *katG*, *ahpC*, and *yaaA* when exogenous H_2O_2 was added as a control. (After 1 hour, kanamycin-treated cells failed to respond even to authentic H_2O_2, perhaps because OxyR protein was depleted in these translationally blocked cells.) This result was confirmed by measurements of *katG::lacZ* expression (Fig. 2, C and D). Thus, neither ampicillin nor norfloxacin create enough H_2O_2 stress to trigger the natural H_2O_2 sensor within the cell.

The rate of intracellular H_2O_2 formation can be directly measured using catalase/peroxidase mutants. Endogenous H_2O_2 rapidly diffuses from these cells out into the growth medium, and the rate of its accumulation can be quantified by direct assay (fig. S1) (*17*). When cells were treated with lethal concentrations of kanamycin and ampicillin, H_2O_2 production did not increase (Fig. 2, E to H). In norfloxacin-treated cells H_2O_2 formation increased slightly (<2-fold) after 1 hour but not at all within the first 30 min when >99% of cells accumulated lethal damage. In contrast, when cells were treated with a nonlethal dose of the redox-cycling drug paraquat, H_2O_2 production was stimulated ~7-fold. We conclude that these classic bactericidal antibiotics did not promote H_2O_2 formation.

There is one other way that hydroxyl-radical formation might be accelerated: by increases in the amount of unincorporated iron. Iron can accumulate inside cells under conditions of superoxide stress, due to the destruction of labile enzymic iron-sulfur clusters (*13*, *14*), and this mechanism was postulated to occur during antibiotic exposure (*4*). We monitored the status of 6-phosphogluconate dehydratase, an iron-sulfur

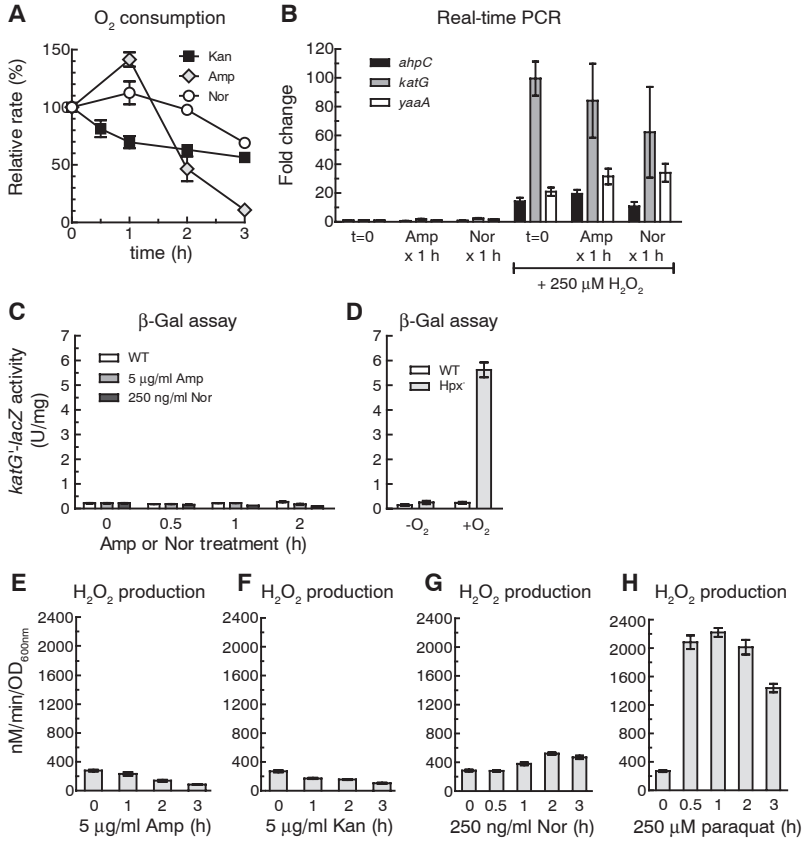

Fig. 2. Antibiotics do not create H_2O_2 stress. (**A**) O_2 consumption rates were not substantially elevated by antibiotic treatment. Oxygen consumption by wild-type cells was measured with a Clark-type electrode before and during exposure to 5 μg/ml kanamycin, 5 μg/ml ampicillin, or 250 ng/ml norfloxacin. Respiration rates were normalized to optical density. (**B**) The OxyR regulon was not induced by ampicillin (5 μg/ml) or norfloxacin (250 ng/ml). mRNA was collected from naïve and antibiotic-exposed wild-type cells, and the expression of OxyR-responsive genes was quantified by qRT-PCR. Signals were normalized to that of the housekeeping gene *gapA*, and fold inductions were calculated. Where indicated, cultures were additionally treated with exogenous H_2O_2 at room temperature for 10 min before mRNA collection. (**C** and **D**) Expression of a *katG'::lacZ* fusion was measured in exponential-phase wild-type cells (AL441) before and after antibiotic incubations (C). As a positive control, expression was measured in wild-type and Hpx^- cells (AL494) before ($-O_2$) and after ($+O_2$) 1-hour aeration (D). (**E** to **H**) Classic antibiotics—ampicillin (E), kanamycin (F), and norfloxacin (G)—did not promote H_2O_2 formation. Aerobic Hpx^- cells (AL427) were treated with antibiotic, and at designated time points samples were collected and the ongoing rate of H_2O_2 production was measured. The redox-cycling compound paraquat (H) was included as a positive control; this dose was insufficient to cause cell death (viable counts increased for >3 hours). Data in this figure are reported as the means and SEM from at least three independent experiments.

Downloaded from www.sciencemag.org on March 8, 2013

enzyme that quickly loses activity in superoxide-stressed cells. We observed that the overall enzyme activity diminished during hours of antibiotic treatment, but the fraction of enzymes with incomplete clusters did not significantly rise (Fig. 3, A to C). In contrast, in control mutants that lack superoxide dismutase, the entire enzyme population was inactive due to cluster damage.

Levels of intracellular unincorporated iron were directly imaged by whole-cell electron paramagnetic resonance (EPR) spectroscopy (*14*). These levels did not rise in kanamycin- or norfloxacin-treated cells (Fig. 3, D and E). (Levels could not be measured after ampicillin treatment, as lysing cells could not be concentrated for the measurement.) In contrast, free-iron levels were increased 4-fold in *fur* regulatory mutants that oversynthesize iron import systems (Fig. 3F). Notably, although these *fur* mutants were slightly more sensitive to ampicillin, they were actually more resistant to kanamycin and norfloxacin (fig. S2). This result, also observed by others (*3*), indicates that intracellular free-iron levels do not correlate with antibiotic sensitivity.

DNA is substantially damaged when hydroxyl radicals are rapidly formed inside cells, and mutants that are deficient in the excision or recombinational repair of oxidative DNA lesions are particularly vulnerable (*15*). The extreme sensitivity of *recA* and *polA* mutants to exogenous H_2O_2 is illustrated in fig. S3A. However, *recA* strains exhibited little or no hypersensitivity to killing doses of kanamycin or ampicillin, suggesting that these antibiotics have little effect upon the rate of DNA damage (Fig. 3, G and H). The *recA* mutants were hypersensitive to norfloxacin (Fig. 3I), as expected, because this antibiotic directly introduces DNA strand breaks by interrupting the catalytic cycle of topoisomerases. The *polA* mutants were actually more resistant to kanamycin and ampicillin than were wild-type strains (fig. S3B), a phenomenon that likely reflects the slower growth rate of this mutant. In sum, these data indicate that, unlike H_2O_2 stress, these antibiotics do not introduce lethal damage into the DNA of cells.

Other workers noted that lower doses (1 to 2 μg/ml) of ampicillin slowly kill *recA* mutants while being merely bacteriostatic to wild-type strains (*4*, *8*). We reproduced that result (fig. S4A). However, this behavior also occurred under anoxic conditions, when ROS are nonexistent (fig. S4B). The slight sensitivity of *recA* mutants may reflect defects in septation from their innate replication problems. At higher doses of ampicillin, i.e., at doses sufficient to kill wild-type bacteria, recombination proficiency had little or no impact on death rate.

Collectively, these data indicate that the known mechanisms of oxidative stress by ROS were not involved in causing the death of antibiotic-treated cells. Oxygen was dispensable for toxicity, and neither OxyR activity nor direct measurements of H_2O_2 formation indicated that ROS were formed at accelerated rates. Further, no customary markers of oxidative damage—enzyme damage, increases in free-iron levels, or hypersensitivity of DNA-repair mutants—were detected.

Fluorescein-based dyes such as hydroxyphenyl fluorescein are more quickly oxidized within antibiotic-treated cells than in control cells, and this fact has been regarded as evidence that hydroxyl radicals are present (*25*). Indeed, thiourea, a presumptive scavenger of hydroxyl radicals, diminished the antibiotic-augmented fluorescence. However, we observed that although thiourea efficiently blocked dye oxidation in a simple in vitro Fenton system, ethanol—another hydroxyl-radical scavenger of similar efficiency (*26*)—failed to do so, even at far higher doses (fig. S5, A and B). This result implies that the dye was actually oxidized by the high-valence iron (FeO^{2+}) initially formed by the Fenton reaction, rather than by the hydroxyl radical to which it decomposes; thiourea, a sulfur compound, may have re-reduced the metal before it oxidized the dye. Indeed, the dye was very rapidly oxidized by horseradish peroxidase (fig. S5C), which has an analogous high-valence metal intermediate but does not release hydroxyl radicals (*27*). The dye was even oxidized by ferricyanide, a ferric-iron chelate of moderate oxidizing potential (+0.44 V) (fig. S5E). Finally, the fluorescence of the oxidized dye

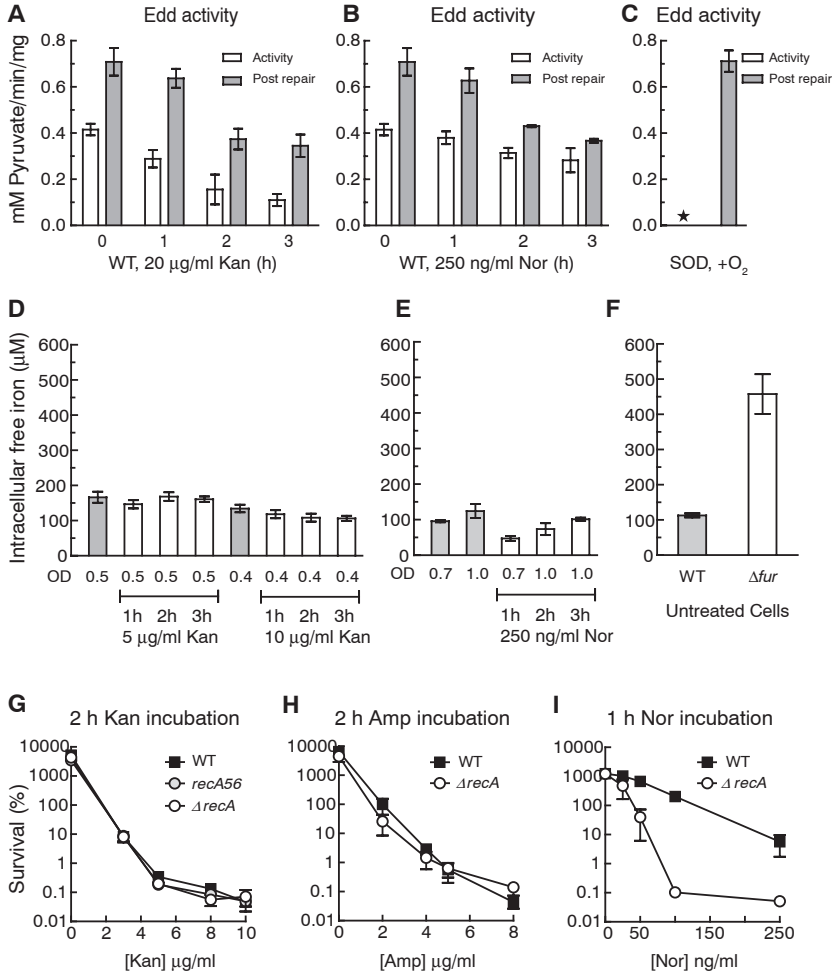

Fig. 3. Antibiotic lethality does not correlate with levels of unincorporated iron. (**A** to **C**) The superoxide-sensitive enzyme Edd was not damaged by cell exposure to kanamycin or norfloxacin. Wild-type cells growing in aerobic LB with 0.2% gluconate were incubated with lethal doses of kanamycin (A) (20 μg/ml) or norfloxacin (B) (250 ng/ml), and Edd activity was measured before (open bar) and after (closed bar) in vitro cluster repair with ferrous iron/dithiothreitol. (C) represents control data from a superoxide dismutase (SOD)–deficient strain (KI232). The star denotes <4% normal activity. (**D** to **F**) Kanamycin (D) and norfloxacin (E) did not increase intracellular iron levels. The levels of intracellular unincorporated iron in wild-type cells were determined by whole-cell EPR analysis before and during antibiotic exposure. Gray bars represent iron levels in untreated cells at similar optical densities. (F) Levels of unincorporated iron were measured in untreated congenic wild-type cells (MG1655) and Δ*fur* mutants (Jem913). (**G** to **I**) DNA-repair mutants are not hypersensitive to antibiotic doses that kill wild-type cells. Wild-type cells (solid squares) and *recA* mutants (open circles) were treated with the indicated doses of kanamycin (G) or ampicillin (H) for 2 hours, or norfloxacin (I) for 1 hour. Fig. S3A demonstrates the hypersensitivity of *recA* mutants to authentic H_2O_2. Data in this figure are reported as the means and SEM from at least three independent experiments.

Downloaded from www.sciencemag.org on March 8, 2013

product was itself quenched after the fact by addition of the same doses of thiourea that were used in antibiotic studies (fig. S5D); this effect cannot be due to hydroxyl-radical scavenging activity. Thus, it is plausible that fluorescein-based dyes are predominantly oxidized in vivo by oxidized enzymic metal centers, which may be more prominent in antibiotic-treated cells as metabolism fails. In any case, one must be cautious in interpreting the oxidation of these dyes inside cells.

Finally, cell protection by either thiourea or iron chelators cannot be regarded as diagnostic of lethal Fenton chemistry. Both agents suppressed antibiotic sensitivity even under anaerobic conditions (fig. S6), when death occurs through pathways that do not involve ROS. We conjecture that they did so by reducing growth and/or metabolic rates. In general, it is unlikely that exogenous agents like thiourea could substantially diminish the lifetimes of hydroxyl radicals in vivo, because these radicals already react at nearly diffusion-limited rates with intracellular biomolecules that are collectively at molar concentrations (*28*). Iron chelators have pleiotropic effects, including the repression of tricarboxylic acid–cycle and respiratory enzymes (*29*), and may thereby diminish the membrane potential that drives aminoglycoside uptake. Synthesis of these enzymes is also repressed when cells are fed glucose, and this treatment analogously diminished kanamycin sensitivity (fig. S7). Thus, it is advisable to follow up experiments that rely upon these agents with ones that employ more direct markers of oxidative stress.

We conclude that under our experimental conditions, these major classes of antibiotics did not exert their lethal actions through the known mechanisms of oxidative stress. Of course, this does not preclude the possibility that antibiotics trigger mechanisms of stress that do not involve the ROS that were tested here.

References and Notes

1. I. Albesa, M. C. Becerra, P. C. Battán, P. L. Páez, *Biochem. Biophys. Res. Commun.* **317**, 605 (2004).
2. M. Goswami, S. H. Mangoli, N. Jawali, *Antimicrob. Agents Chemother.* **50**, 949 (2006).
3. D. J. Dwyer, M. A. Kohanski, B. Hayete, J. J. Collins, *Mol. Syst. Biol.* **3**, 91 (2007).
4. M. A. Kohanski, D. J. Dwyer, B. Hayete, C. A. Lawrence, J. J. Collins, *Cell* **130**, 797 (2007).
5. M. A. Kohanski, D. J. Dwyer, J. Wierzbowski, G. Cottarel, J. J. Collins, *Cell* **135**, 679 (2008).
6. B. W. Davies *et al.*, *Mol. Cell* **36**, 845 (2009).
7. J. Yeom, J. A. Imlay, W. Park, *J. Biol. Chem.* **285**, 22689 (2010).
8. J. J. Foti, B. Devadoss, J. A. Winkler, J. J. Collins, G. C. Walker, *Science* **336**, 315 (2012).
9. X. Wang, X. Zhao, M. Malik, K. Drlica, *J. Antimicrob. Chemother.* **65**, 520 (2010).
10. S. S. Grant, B. B. Kaufmann, N. S. Chand, N. Haseley, D. T. Hung, *Proc. Natl. Acad. Sci. U.S.A.* **109**, 12147 (2012).
11. C. F. Kuo, T. Mashino, I. Fridovich, *J. Biol. Chem.* **262**, 4724 (1987).
12. S. Jang, J. A. Imlay, *J. Biol. Chem.* **282**, 929 (2007).
13. S. I. Liochev, I. Fridovich, *Free Radic. Biol. Med.* **16**, 29 (1994).
14. K. Keyer, J. A. Imlay, *Proc. Natl. Acad. Sci. U.S.A.* **93**, 13635 (1996).
15. J. A. Imlay, *Annu. Rev. Biochem.* **77**, 755 (2008).
16. M. Yamada *et al.*, *Mol. Microbiol.* **86**, 1364 (2012).
17. L. C. Seaver, J. A. Imlay, *J. Biol. Chem.* **279**, 48742 (2004).
18. S. B. Vakulenko, S. Mobashery, *Clin. Microbiol. Rev.* **16**, 430 (2003).
19. H. W. Taber, J. P. Mueller, P. F. Miller, A. S. Arrow, *Microbiol. Rev.* **51**, 439 (1987).
20. J. M. Sobota, J. A. Imlay, *Proc. Natl. Acad. Sci. U.S.A.* **108**, 5402 (2011).
21. S. Park, X. You, J. A. Imlay, *Proc. Natl. Acad. Sci. U.S.A.* **102**, 9317 (2005).
22. K. Drlica, *Curr. Opin. Microbiol.* **2**, 504 (1999).
23. F. Aslund, M. Zheng, J. Beckwith, G. Storz, *Proc. Natl. Acad. Sci. U.S.A.* **96**, 6161 (1999).
24. M. Zheng *et al.*, *J. Bacteriol.* **183**, 4562 (2001).
25. K. Setsukinai, Y. Urano, K. Kakinuma, H. J. Majima, T. Nagano, *J. Biol. Chem.* **278**, 3170 (2003).
26. M. Anbar, P. Neta, *Int. J. Appl. Radiat. Isot.* **18**, 493 (1967).
27. K. Ikemura *et al.*, *J. Am. Chem. Soc.* **130**, 14384 (2008).
28. M. J. Davies, *Biochim. Biophys. Acta* **1703**, 93 (2005).
29. E. Massé, C. K. Vanderpool, S. Gottesman, *J. Bacteriol.* **187**, 6962 (2005).

Acknowledgments: We thank D. Hassett (University of Cincinnati) for helpful conversations about this topic, and J. Collins, G. Walker, and members of their laboratories for generously sharing ideas, unpublished data, and strains. We also thank M. Nilges of the Illinois EPR Research Center for assistance. This work was supported by GM49060 from the National Institutes of Health. The authors declare no conflict of interest.

Supplementary Materials

www.sciencemag.org/cgi/content/full/339/6124/1210/DC1
Materials and Methods
Figs. S1 to S7
Table S1
References (*30*–*36*)

14 November 2012; accepted 24 January 2013
10.1126/science.1232751

Killing by Bactericidal Antibiotics Does Not Depend on Reactive Oxygen Species

Iris Keren, Yanxia Wu, Julio Inocencio, Lawrence R. Mulcahy, Kim Lewis*

Bactericidal antibiotics kill by modulating their respective targets. This traditional view has been challenged by studies that propose an alternative, unified mechanism of killing, whereby toxic reactive oxygen species (ROS) are produced in the presence of antibiotics. We found no correlation between an individual cell's probability of survival in the presence of antibiotic and its level of ROS. An ROS quencher, thiourea, protected cells from antibiotics present at low concentrations, but the effect was observed under anaerobic conditions as well. There was essentially no difference in survival of bacteria treated with various antibiotics under aerobic or anaerobic conditions. This suggests that ROS do not play a role in killing of bacterial pathogens by antibiotics.

Bactericidal antibiotics are an essential component of our antimicrobial arsenal. However, even the best bactericidal antibiotics have limited efficacy against dormant persister cells, specialized survivors that are phenotypic variants of the wild type (*1*, *2*). Bactericidal antibiotics from each of the three main classes have unique mechanisms of killing. Fluoroquinolones convert DNA gyrase/topoisomerase into an endonuclease (*3*); aminoglycosides cause mistranslation, leading to production of toxic peptides (*4*, *5*); and β-lactams lead to autolysis (*6*, *7*). In dormant persisters, targets of these antibiotics have limited activity, resulting in tolerance (*2*). Understanding the detailed mechanism of killing is essential for developing better therapeutics. Recently, an alternative unified mechanism of antibiotic killing was proposed (*8*, *9*), according to which bactericidal compounds, irrespective of their mode of action, induce formation of reactive oxygen species (ROS) by activating the electron transport chain, which kills bacterial cells. The initial study reported that antibiotics induce ROS production and that their quenching by thiourea protects *Escherichia coli* cells from killing (*8*). Subsequent studies report ROS-dependent killing in different bacterial species and detail the mechanism leading to cell death (*10*–*15*). The ROS hypothesis of antibiotic killing became widely accepted but does not account for many observations. For example, mutants lacking ROS production have not been reported among drug resistant clinical isolates, and *Streptococcus pneumoniae*, which is highly susceptible to killing by bactericidal antibiotics, lacks an electron transport chain (*16*, *17*), the proposed source of ROS. Thus, we decided to reexamine the role of ROS in cell death and consequently found that killing by antibiotics is unrelated to ROS production.

Thiourea was reported to protect *E. coli* from killing by norfloxacin, a fluoroquinolone antibiotic (*8*). Norfloxacin was used at a fairly low concentration (0.25 μg/ml), only two to four times as high as the minimal inhibitory concentration (MIC). The peak plasma concentration of norfloxacin has been reported to range from 1.3 to 1.6 μg/ml, with a half-life of 3 to 7 hours (*18*). We therefore examined the effect of thiourea on killing at a range of antibiotic concentrations that included clinically achievable levels.

Antimicrobial Discovery Center, Department of Biology, Northeastern University, Boston, MA 021156, USA.

*To whom correspondence should be addressed. E-mail: k.lewis@neu.edu

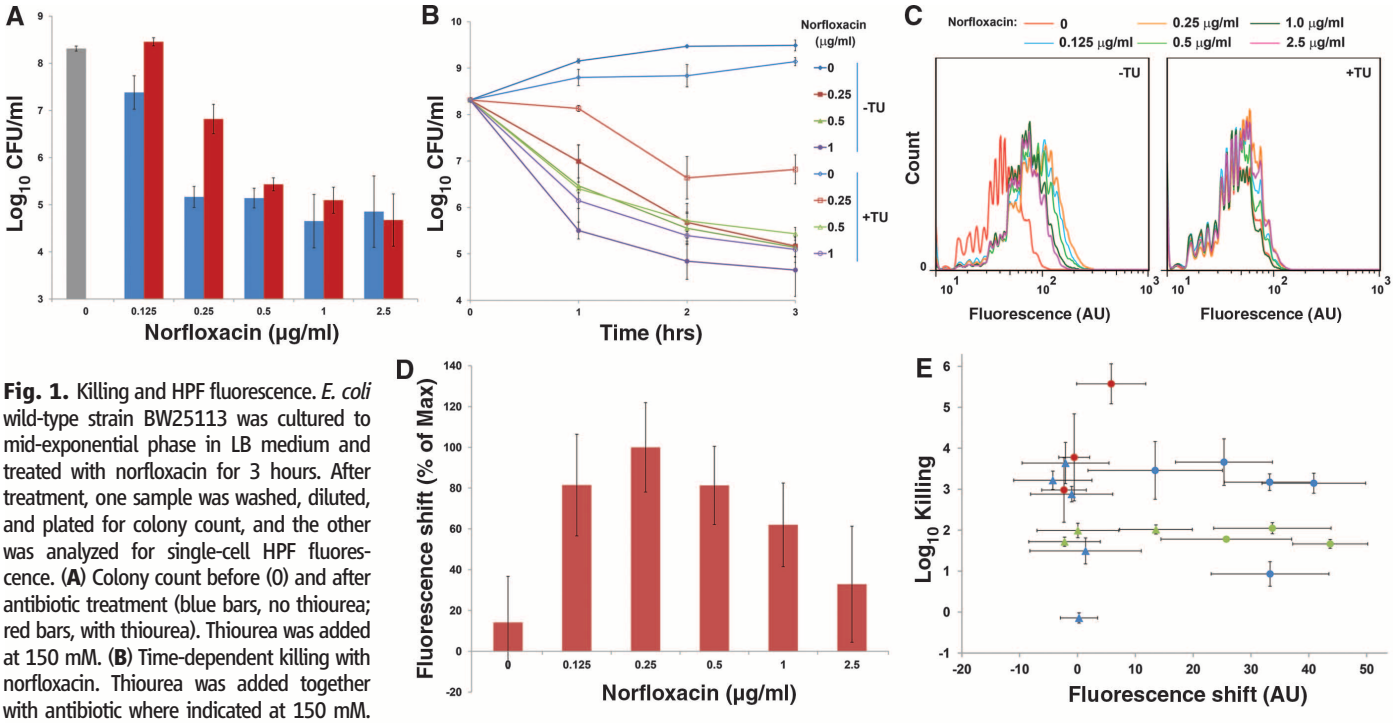

Fig. 1. Killing and HPF fluorescence. *E. coli* wild-type strain BW25113 was cultured to mid-exponential phase in LB medium and treated with norfloxacin for 3 hours. After treatment, one sample was washed, diluted, and plated for colony count, and the other was analyzed for single-cell HPF fluorescence. (**A**) Colony count before (0) and after antibiotic treatment (blue bars, no thiourea; red bars, with thiourea). Thiourea was added at 150 mM. (**B**) Time-dependent killing with norfloxacin. Thiourea was added together with antibiotic where indicated at 150 mM. (**C**) HPF fluorescence after treatment with norfloxacin. HPF was present at 5 μM, and thiourea was added at 150 mM together with antibiotic (right panel). (**D**) Relationship between HPF fluorescence and the concentration of norfloxacin. The graph is based on data from (C). (**E**) Lack of a relationship between HPF fluorescence and killing (blue circles, norfloxacin; blue triangles, norfloxacin with thiourea; green circles, ampicillin; green triangles, ampicillin with thiourea, red circles, kanamycin). The graph is based on data from (A) to (C).

Thiourea was added to an exponentially growing culture of *E. coli* together with antibiotic, and a sample was taken for a colony count 3 hours later, as described in (*8*). In the control without thiourea, the number of live cells decreased sharply with increasing concentrations of antibiotic, reaching a characteristic plateau of surviving persisters at 0.25 μg/ml of norfloxacin (Fig. 1A). Addition of thiourea increased the norfloxacin MIC twofold, from 0.06 μg/ml to 0.125 μg/ml. At low concentrations of norfloxacin, thiourea protected cells from killing, which was probably due to its effect on the MIC. This protective effect disappeared at higher concentrations, starting with 0.5 μg/ml. Protection by thiourea was only observed at 0.25 μg/ml but not at higher concentrations of norfloxacin in a time-dependent killing experiment (Fig. 1B). Thiourea was also reported to protect cells from killing by β-lactams and aminoglycosides administered at low levels (*8*). Similar to experiments with norfloxacin, we did observe a protection by thiourea at low concentrations of ampicillin or the fluoroquinolone ofloxacin, but this effect disappeared at higher, clinically relevant levels, and there was no protection against kanamycin (fig. S1).

Antibiotics have been reported to increase production of ROS, as measured by increased fluorescence of a hydroxyphenyl fluorescein (HPF) dye (*8*). We similarly examined samples from cultures treated with norfloxacin for ROS production using HPF as a detector. Single-cell analysis by a flow cytometer showed a shift in HPF fluorescence in response to antibiotic treatment (Fig. 1C and fig. S2). The greatest shift was observed at 0.25 μg/ml of norfloxacin, the level at which it was used in the previous studies (*8*, *10*). As the concentration of norfloxacin was increased above 0.25 μg/ml the shift in fluorescence decreased. At the highest concentration of antibiotic tested, 2.5 μg/ml, there was no difference in HPF

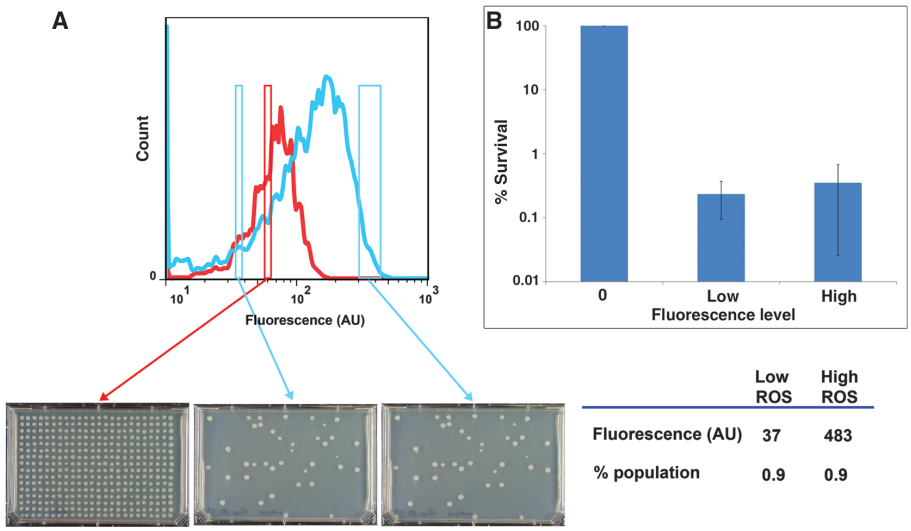

Fig. 2. HPF fluorescence is not an indicator of cell death. Mid-exponential phase cultures were treated with 0.25 μg/ml norfloxacin for 3 hours. (**A**) Single cells were sorted with a fluorescence-activated cell sorter based on fluorescence. The HPF fluorescence histogram before addition of antibiotic is shown in red, and the one after treatment with norfloxacin is in blue. The red rectangle indicates the gate corresponding to the part of the population from which single cells were spotted on an agar plate. The blue rectangles indicate the two gates corresponding to the part of the population from which cells were spotted on an agar plate. Each gate corresponds to 0.9% of the population. Fifty cells per spot were sorted from each gate onto a 384-point grid of an LB agar plate. (**B**) The average level of survival of each population (n = 3 ± SD), calculated based on data from Fig. 3A.

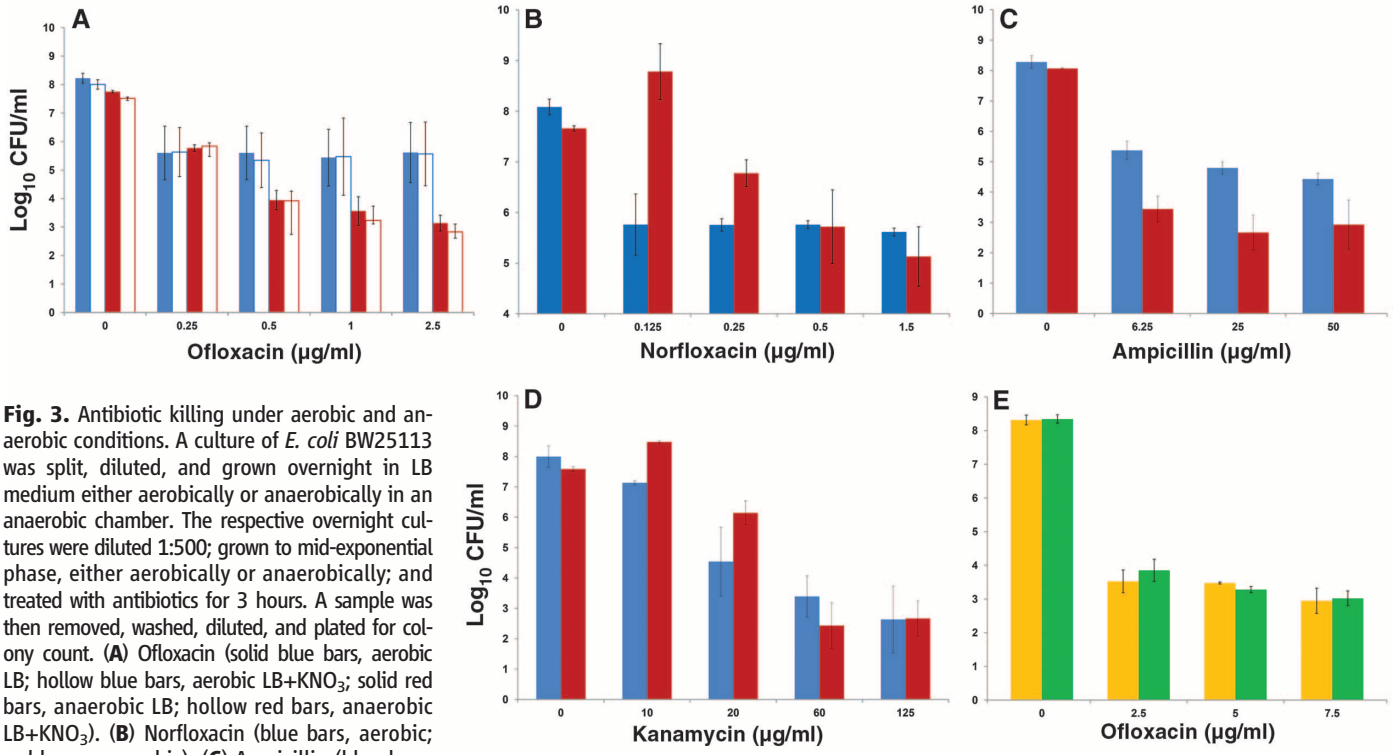

Fig. 3. Antibiotic killing under aerobic and anaerobic conditions. A culture of *E. coli* BW25113 was split, diluted, and grown overnight in LB medium either aerobically or anaerobically in an anaerobic chamber. The respective overnight cultures were diluted 1:500; grown to mid-exponential phase, either aerobically or anaerobically; and treated with antibiotics for 3 hours. A sample was then removed, washed, diluted, and plated for colony count. (**A**) Ofloxacin (solid blue bars, aerobic LB; hollow blue bars, aerobic LB+KNO_3; solid red bars, anaerobic LB; hollow red bars, anaerobic LB+KNO_3). (**B**) Norfloxacin (blue bars, aerobic; red bars, anaerobic). (**C**) Ampicillin (blue bars, aerobic; red bars, anaerobic). (**D**) Kanamycin (blue bars, aerobic; red bars, anaerobic). (**E**) *P. aeruginosa* PAO1 was cultured similarly to *E. coli* in LB medium, aerobically or anaerobically (in the presence of KNO_3), and treated with ofloxacin (yellow bars, aerobic; green bars, anaerobic).

fluorescence between treated and untreated cells (Fig. 1D). Addition of thiourea quenched the HPF signal (Fig. 1C). However, there was no correlation between the level of HPF fluorescence and the extent of killing by norfloxacin (Fig. 1, D and E) or ampicillin (Fig. 1E); HPF fluorescence did not change in cells treated with kanamycin (Fig. 1E). Similar results were observed with a different strain of *E. coli* (fig. S3).

To examine the relationship between ROS and killing more directly, cells from a population treated with norfloxacin were sorted onto nutrient medium to determine the level of survival in relation to HPF fluorescence. In a control, 384 cells from a culture containing HPF but no antibiotic were sorted onto a rectangular LB agar plate and produced 384 colonies (red arrow, Fig. 2, A and B), showing the high fidelity of the process. After treatment with norfloxacin at 0.25 μg/ml, 0.9% of the population representing highly fluorescent cells, and 0.9% of low-fluorescent cells, were sorted. At this concentration, norfloxacin killed 99.9% of the population, which required us to sort 50 cells per spot (19,200 total cells per plate) to observe survivors with a reasonable probability. The plates were incubated overnight, and the surviving cells formed colonies (Fig. 2A). There was no difference in recovery; 34 spots (out of 384 seeded) yielded colonies from the low-fluorescence fraction (0.18% survival), and 37 spots from the high-fluorescence fraction produced growth (0.19% survival). The 10-fold difference in HPF fluorescence among these groups of cells, however, was substantial, showing no relationship between survival and ROS. Similar results were obtained with ampicillin (fig. S4).

Apart from reports of a correlation between HPF measurements and killing and protective effects of thiourea, several observations have linked ROS production more directly with the action of bactericidal antibiotics. It has been proposed that antibiotics induce the tricarboxylic acid (TCA) cycle and respiratory chain–dependent ROS production, and TCA mutants show improved survival (*8*). Antibiotic-dependent ROS production has been reported to oxidize the guanine pool, leading to double-strand DNA breaks and death (*10*). It was also claimed that antibiotic tolerance in *Pseudomonas aeruginosa* biofilms was due to increased oxidative stress tolerance (*12*) and that killing of *E. coli*, *Mycobacterium tuberculosis*, and *P. aeruginosa* is potentiated in the presence of oxygen and reduced in an oxygen-limited environment (*11*). We reasoned that examining the effectiveness of antibiotics under aerobic compared to anaerobic conditions would be the most direct way to test these claims.

E. coli grows well under anaerobic conditions using fermentation to produce adenosine triphosphate and can also use alternative electron acceptors such as nitrate for anaerobic respiration (*19*). To investigate the action of antibiotics under anaerobic conditions, we used ofloxacin, which is employed in treating both aerobic and anaerobic pathogens. Killing by ofloxacin was more effective under anaerobic conditions, in contradiction to the ROS hypothesis (Fig. 3A). Inclusion of nitrate had no effect; why ofloxacin killed better under anaerobic conditions is unclear. Norfloxacin MIC was 0.125 μg/ml under aerobic conditions and 0.25 μg/ml under anaerobic conditions. As expected, there was no killing by norfloxacin below MIC at anaerobic conditions, but killing was comparable at aerobic or anaerobic conditions at ≥0.5 μg/ml (Fig. 3B). There was more killing by ampicillin under anaerobic as compared to aerobic conditions (Fig. 3C). Killing by kanamycin was slightly higher under aerobic conditions at a low concentration of antibiotic (Fig. 3D). This is expected because aminoglycosides require proton motive force for transport into the cell (*20*). At higher levels of kanamycin, there was no difference in killing between aerobic and anaerobic conditions. We also tested killing of *P. aeruginosa* under anaerobic conditions. Killing by ofloxacin was the same under aerobic versus anaerobic conditions (Fig. 3E).

Our findings raise the question, what is the source of discrepancy between this study and the reports linking cell death to ROS production by antibiotics? There seem to be several factors responsible for this disagreement. The use of very low concentrations of antibiotics, at or slightly above the MIC, is prone to producing errors, because the accepted error in determining the MIC is 100% (*21*). In some experiments performed with the same concentration of antibiotic, no killing would result because of variation in the MIC. The variation in the level of surviving persisters can be high among biological replicates (*22*). The use of thiourea to quench

ROS is also problematic. According to our data, thiourea mildly inhibits cell growth (Fig. 1B), indicating that this compound may have nonspecific effects, such as slowing down cell metabolism, which would lead to increased tolerance to killing. Indeed, we observed protective effect of thiourea from antibiotic killing even under anaerobic conditions (fig. S5). Reports of mutants in the TCA cycle being more resistant to killing could similarly result from these cells having a slower metabolism. Finally, the use of HPF as a detector of ROS is only valid if this dye is a specific detector. However, we find that antibiotics cause a shift in HPF fluorescence under anaerobic conditions (fig. S6). Dying cells apparently produce some products to which HPF responds.

Taken together, our results show that killing by antibiotics is unrelated to ROS production. This finding will refocus efforts on unanswered questions on the mechanism of killing by antibiotics. For example, we do not know how β-lactams induce autolysis, nor how exactly mistranslation caused by aminoglycosides leads to cell death. Better understanding of cell death will guide the development of advanced cures to treat recalcitrant infectious diseases (*23*).

References and Notes

1. I. Keren, D. Shah, A. Spoering, N. Kaldalu, K. Lewis, *J. Bacteriol.* **186**, 8172 (2004).
2. K. Lewis, *Annu. Rev. Microbiol.* **64**, 357 (2010).
3. D. C. Hooper, *Clin. Infect. Dis.* **32** (suppl. 1), S9 (2001).
4. B. D. Davis, L. L. Chen, P. C. Tai, *Proc. Natl. Acad. Sci. U.S.A.* **83**, 6164 (1986).
5. M. A. Kohanski, D. J. Dwyer, J. Wierzbowski, G. Cottarel, J. J. Collins, *Cell* **135**, 679 (2008).
6. K. W. Bayles, *Nat. Rev. Microbiol.* **5**, 721 (2007).
7. T. Uehara, T. Dinh, T. G. Bernhardt, *J. Bacteriol.* **191**, 5094 (2009).
8. M. A. Kohanski, D. J. Dwyer, B. Hayete, C. A. Lawrence, J. J. Collins, *Cell* **130**, 797 (2007).
9. D. J. Dwyer, M. A. Kohanski, J. J. Collins, *Curr. Opin. Microbiol.* **12**, 482 (2009).
10. J. J. Foti, B. Devadoss, J. A. Winkler, J. J. Collins, G. C. Walker, *Science* **336**, 315 (2012).
11. S. S. Grant, B. B. Kaufmann, N. S. Chand, N. Haseley, D. T. Hung, *Proc. Natl. Acad. Sci. U.S.A.* **109**, 12147 (2012).
12. D. Nguyen *et al.*, *Science* **334**, 982 (2011).
13. T. R. Sampson *et al.*, *Antimicrob. Agents Chemother.* **56**, 5642 (2012).
14. Y. Liu *et al.*, *Antimicrob. Agents Chemother.* **56**, 6048 (2012).
15. X. Wang, X. Zhao, *Antimicrob. Agents Chemother.* **53**, 1395 (2009).
16. B. Poolman, *FEMS Microbiol. Rev.* **12**, 125 (1993).
17. J. Hoskins *et al.*, *J. Bacteriol.* **183**, 5709 (2001).
18. R. C. Rowen, D. J. Michel, J. C. Thompson, *Pharmacotherapy* **7**, 92 (1987).
19. G. Unden, J. Bongaerts, *Biochim. Biophys. Acta* **1320**, 217 (1997).
20. P. D. Damper, W. Epstein, *Antimicrob. Agents Chemother.* **20**, 803 (1981).
21. J. M. Andrews, *J. Antimicrob. Chemother.* **48** (suppl. 1), 5 (2001).
22. C. Wiuff *et al.*, *Antimicrob. Agents Chemother.* **49**, 1483 (2005).
23. K. Lewis, *Nature* **485**, 439 (2012).

Acknowledgments: The authors thank V. Isabella for helpful discussion of the manuscript. This work was supported by NIH grant T-R01AI085585-01 and by Army Research Office grants W9911NF-09-1-0265 and 55631-LS-RIP.

Supplementary Materials
www.sciencemag.org/cgi/content/full/339/6124/1213/DC1
Materials and Methods
Figs. S1 to S6
Reference (*24*)

13 November 2012; accepted 24 January 2013
10.1126/science.1232688

Evidence for a Common Mechanism of SIRT1 Regulation by Allosteric Activators

Basil P. Hubbard,[1] Ana P. Gomes,[1,2] Han Dai,[3] Jun Li,[1] April W. Case,[3] Thomas Considine,[3] Thomas V. Riera,[3] Jessica E. Lee,[4] Sook Yen E,[4] Dudley W. Lamming,[1]* Bradley L. Pentelute,[5] Eli R. Schuman,[3] Linda A. Stevens,[6] Alvin J. Y. Ling,[1] Sean M. Armour,[1] Shaday Michan,[1]† Huizhen Zhao,[7] Yong Jiang,[7] Sharon M. Sweitzer,[7] Charles A. Blum,[3] Jeremy S. Disch,[3] Pui Yee Ng,[3] Konrad T. Howitz,[8]‡ Anabela P. Rolo,[2,9] Yoshitomo Hamuro,[4] Joel Moss,[6] Robert B. Perni,[3] James L. Ellis,[3] George P. Vlasuk,[3] David A. Sinclair[1,10]§

A molecule that treats multiple age-related diseases would have a major impact on global health and economics. The SIRT1 deacetylase has drawn attention in this regard as a target for drug design. Yet controversy exists around the mechanism of sirtuin-activating compounds (STACs). We found that specific hydrophobic motifs found in SIRT1 substrates such as PGC-1α and FOXO3a facilitate SIRT1 activation by STACs. A single amino acid in SIRT1, Glu[230], located in a structured N-terminal domain, was critical for activation by all previously reported STAC scaffolds and a new class of chemically distinct activators. In primary cells reconstituted with activation-defective SIRT1, the metabolic effects of STACs were blocked. Thus, SIRT1 can be directly activated through an allosteric mechanism common to chemically diverse STACs.

The nicotinamide adenine dinucleotide (NAD^+)–dependent deacetylase SIRT1 is implicated in the prevention of many age-related diseases such as cancer, Alzheimer's disease, and type 2 diabetes (*1*). At the cellular level, SIRT1 controls DNA repair and apoptosis, circadian clocks, inflammatory pathways, insulin secretion, and mitochondrial biogenesis (*2*, *3*).

Naturally occurring STACs such as resveratrol (*4*) and chemically unrelated synthetic STACs activate SIRT1 in vitro by lowering its peptide Michaelis constant (K_M) and produce pharmacological changes consistent with SIRT1 activation (*4*–*7*). However, the legitimacy of STACs as direct SIRT1 activators has been widely debated. In previous studies, STACs increased SIRT1 activity toward fluorophore-tagged substrates but not toward corresponding nontagged peptides (*8*–*11*). One explanation was that STACs were binding to the fluorophore-linked substrate, which would not occur in vivo (*10*). Alternatively, the fluorescent groups might mimic a property of natural substrates. Given that the fluorophores used in previous studies are bulky and hydrophobic (*4*, *5*), we tested whether these moieties might substitute for hydrophobic amino acids in endogenous substrates.

We used a SIRT1 activity assay whereby the reaction product nicotinamide was converted to 1-alkylthio–substituted isoindoles via the nicotinamidase PNC1 (*12*) and ortho-phthalaldehyde (OPT) (*13*) (fig. S1, A to E). A second assay measured the SIRT1 product *O*-acetyl adenosine diphosphate ribose (OAcADPR) by mass spectrometry (*14*) (fig. S2, A to E).

A series of STACs, including STAC-1 (SRT1460) (*5*) and STAC-2 [compound 22 in (*15*)] (fig. S3), activated SIRT1 with an aminomethylcoumarin (AMC)–tagged peptide serving as a substrate via a peptide K_M-lowering mechanism, similar to the action of resveratrol (fig. S4, A to C, and tables S1 and S2) (*4*). The AMC moiety mediated activation only when it was directly adjacent to the acetylated Lys^9 of histone 3 (H3K9) at the +1 position (*16*); this finding demonstrates that the fluorophore has a positional requirement (Fig. 1A and fig. S5A). The fluorophore moieties at

[1]Department of Genetics, Harvard Medical School, Boston, MA 02115, USA. [2]Center for Neurosciences and Cell Biology, Department of Life Sciences, University of Coimbra, Coimbra 3004-517, Portugal. [3]Sirtris, a GSK Company, Cambridge, MA 02139, USA. [4]ExSAR Corporation, Monmouth Junction, NJ 08852, USA. [5]Department of Chemistry, Massachusetts Institute of Technology, Cambridge, MA 02139, USA. [6]NIH Cardiovascular and Pulmonary Branch/National Heart, Lung and Blood Institute, Bethesda, MD 20892, USA. [7]GlaxoSmithKline, Collegeville, PA 19426, USA. [8]BIOMOL Research Laboratories Inc., Plymouth Meeting, PA 19462, USA. [9]Department of Biology, University of Aveiro, Aveiro 3810-193, Portugal. [10]Department of Pharmacology, University of New South Wales, Sydney, NSW 2052, Australia.

*Present address: Whitehead Institute for Biomedical Research, Cambridge, MA 02142, USA.
†Present address: Instituto Nacional de Geriatría, Institutos Nacionales de Salud, México D.F. 04510, México.
‡Present address: Reaction Biology Corporation, Malvern, PA 19355, USA.
§To whom correspondence should be addressed. E-mail: david_sinclair@hms.harvard.edu

Downloaded from www.sciencemag.org on March 8, 2013

positions +1 (*4*) or +6 (*5*) were dispensable if replaced with naturally occurring hydrophobic amino acids (*15*) (Fig. 1B and fig. S5B).

We then tested whether native peptide sequences might also support activation (*17*–*24*). Sequences from two SIRT1 substrates supported STAC-mediated activation: mouse peroxisome proliferator–activated receptor γ coactivator 1α Lys^{778} (PGC-1α–K778) (*22*) and human forkhead box O3a protein Lys^{290} (FOXO3a-K290) (*19*) (Fig. 1C). STAC-mediated activation was dose-dependent (Fig. 1D), and relative activation was similar between the SIRT1 assays (fig. S5C).

Isothermal titration calorimetry (ITC) did not detect binding between saturating amounts of PGC-1α peptide (2 mM) and STAC-1 (100 μM) or STAC-2 (50 μM), arguing against activation driven solely by substrate enhancement (fig. S6, A and B) (*15*). Kinetic analysis of SIRT1 activation by STAC-2 with the FOXO3a-K290 substrate revealed that rate enhancement was mediated primarily through a lowering of peptide K_M (fig. S6C). Thus, the mechanism of activation appeared to be independent of the substrate used.

The PGC-1α–K778 peptide contains aromatic, hydrophobic amino acids at the +1 and +6 positions (relative to the acetylated lysine), as does the FOXO3a-K290 peptide at position +1. Alanine substitution of either the Tyr at the +1 position or the Phe at the +6 position of the PGC-1α peptide reduced activation, and substitution of both abolished activation completely (Fig. 2A). Similarly, for FOXO3a, substitution of the Trp at the +1 position blocked activation (Fig. 2B), but substitution of several N-terminal residues did not (Fig. 2, A and B). A global search of nuclear acetylated proteins, conforming to the sequences X_6-K(Ac)-{Y,W,F}-X_5, X_6-K(Ac)-X_5-{Y,W,F} (*16*), and the union of the two sets, identified more than 400 sequences (fig. S7A). We tested five of these native sequences and found that three of them supported activation: metallothionein-like 5 (MTL5), peptidylprolyl isomerase A (PPIA), and eukaryotic translation initiation factor 2α (eIF2α) (*25*) (fig. S7B).

An alternative peptide sequence from FOXO3a (encompassing Lys^{242}) was sequentially altered to resemble the FOXO3a-K290 sequence. Substitution of the Ser at +1 with Trp did not impart the ability to activate (fig. S7C) unless in combination with a Pro substitution at the +2 position (fig. S7C). Thus, a hydrophobic residue at the +1 position is necessary but not sufficient for activation.

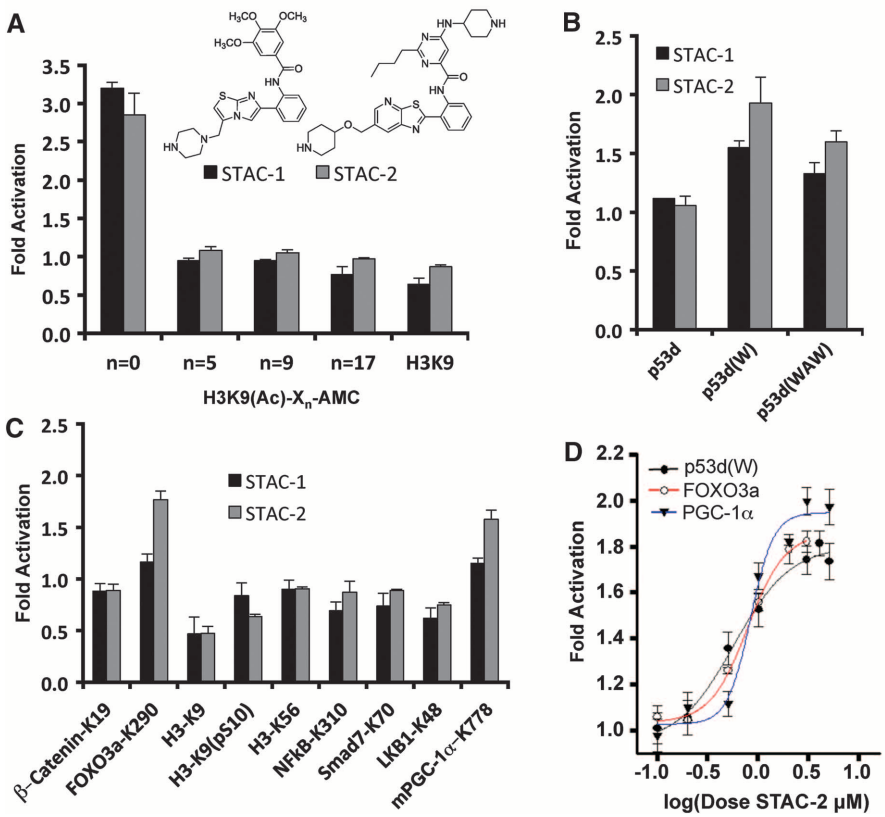

Fig. 1. SIRT1 activation by STACs on native peptide sequences. (**A**) SIRT1 activation by 50 μM STAC-1 or 5 μM STAC-2 with peptides bearing an AMC moiety at the indicated positions, where X_n represents the number of amino acids between the acetylated lysine and the AMC. (**B**) SIRT1 activation by STACs on hydrophobic patch peptides. Complete amino acid sequences of peptides bearing tryptophan (W) or tryptophan and alanine substitutions (WAW) are provided in the supplementary materials. (**C**) SIRT1 activation on native peptide sequences of known targets (detailed in the supplementary materials). (**D**) Dose-response curves for STAC-2 as measured by PNC1-OPT assay; data are means ± SEM (n = 3).

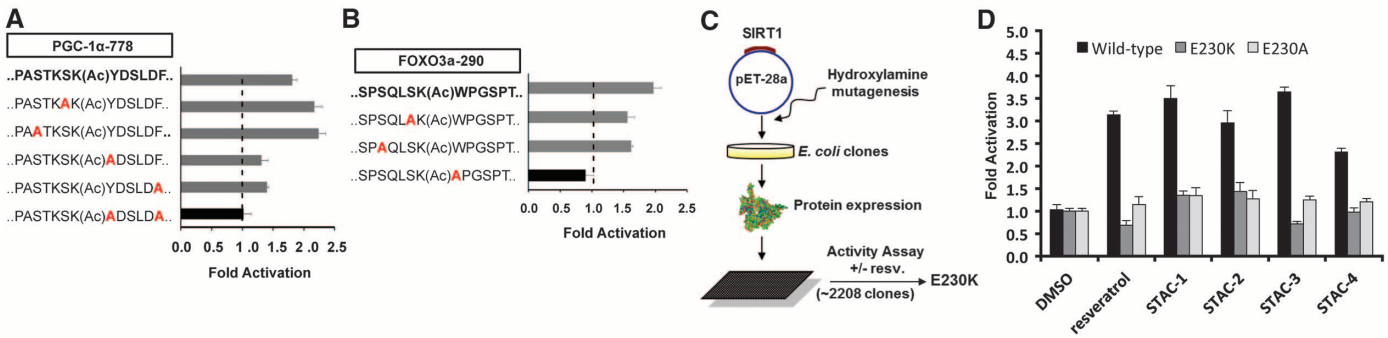

Fig. 2. Substrate sequence requirements and regions on SIRT1 necessary for activation. (**A** and **B**) SIRT1 activation by STAC-2 on peptides derived from PGC-1α–K778 (A) and FOXO3a-K290 (B) as measured by PNC1-OPT assay; data are means ± SEM (n = 3). (**C**) Biochemical screen for activation-compromised mutants. A bacterial expression plasmid (pET28a) carrying the SIRT1 gene was mutagenized and used to generate recombinant SIRT1 proteins that were screened for activity in the presence or absence of resveratrol using an AMC-based assay. (**D**) Activation of wild-type SIRT1, E230K, and E230A mutants by 40 μM resveratrol, 50 μM STAC-1, 5 μM STAC-2, 5 μM STAC-3, and 10 μM STAC-4 as measured by an AMC assay; data are means ± SD (n = 3). Dimethyl sulfoxide (DMSO) was used as a control.

Downloaded from www.sciencemag.org on March 8, 2013

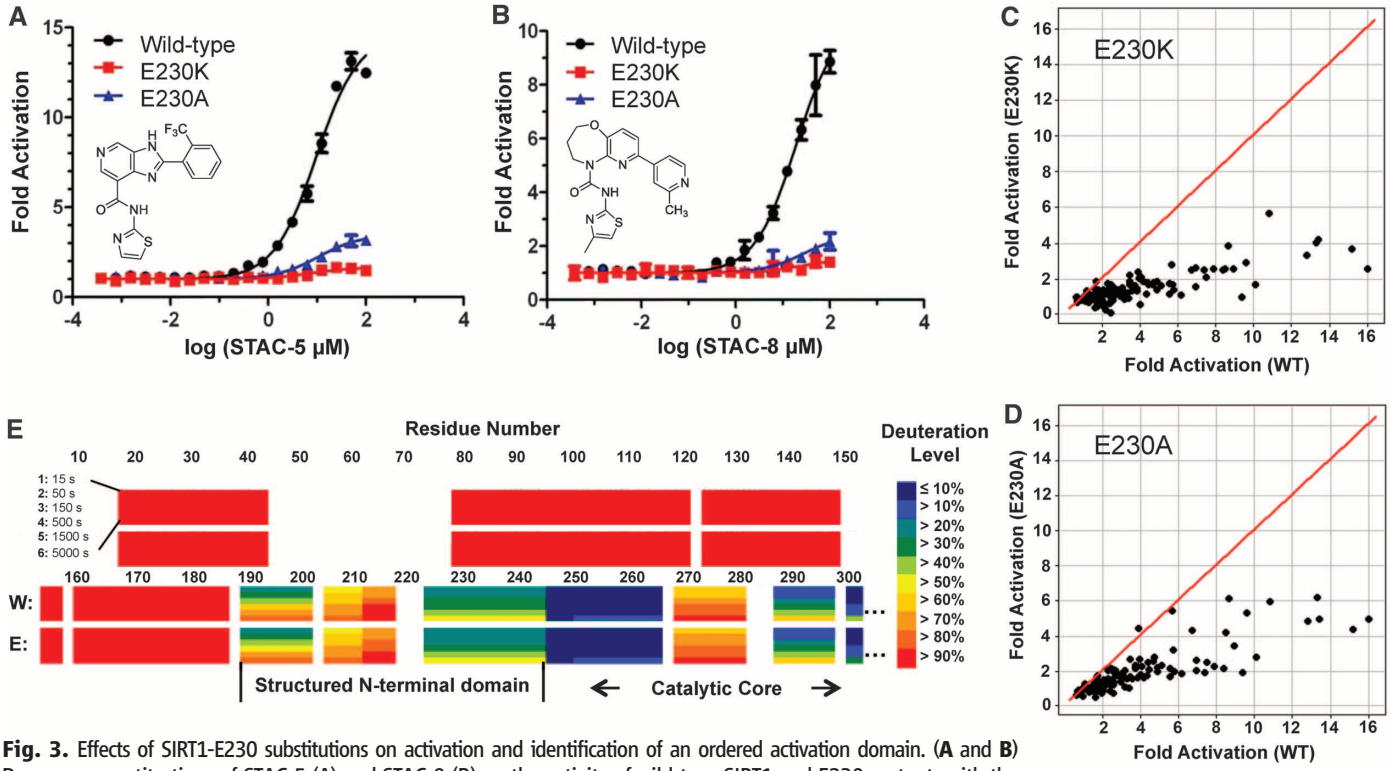

Fig. 3. Effects of SIRT1-E230 substitutions on activation and identification of an ordered activation domain. (**A** and **B**) Dose-response titrations of STAC-5 (A) and STAC-8 (B) on the activity of wild-type SIRT1 and E230 mutants with the Trp 5-mer peptide serving as the substrate, as measured by mass spectrometry–based OAcADPR assay. The sequence of the Trp 5-mer peptide is included in the supplementary materials. data are means ± SD (n = 3). (**C** and **D**) Relative activation by a chemically diverse, 117-compound set (25 μM) using the Trp 5-mer substrate for wild-type versus E230K (C) or wild-type versus E230A (D), as measured by OAcADPR assay (n = 2). The red line represents $y = x$ correlation. (**E**) HDXMS heat map of deuteration levels of wild-type (W) and SIRT1-E230K (E) N termini at six different time points (15 to 5000 s).

These data were consistent with an allosteric mechanism of SIRT1 activation (*4*, *15*). To elucidate the determinants of activation in SIRT1, we screened for SIRT1 mutant proteins lacking activation (Fig. 2C). The ability of SIRT1 to be activated by resveratrol was attenuated in one mutant that substituted a lysine for a glutamate at position 230 (E230K), whether an AMC-tagged substrate (Fig. 2D) or a natural amino acid substrate was used (fig. S8A). Substitution of Glu^{230} with Lys or Ala attenuated SIRT1 activation by 117 chemically diverse STACs, independent of the substrate used (Fig. 2D, Fig. 3, A to D, fig. S8, B and C, and tables S3 and S4).

Glu^{230} is immediately N-terminal to the catalytic core of SIRT1 and is conserved from flies to humans (fig. S8D). The E230K substitution did not impair the basal catalytic activity of SIRT1, nor did it significantly alter the maximum velocity of reaction (V_{max}), the Michaelis constant for NAD^+ ($K_{M\ NAD^+}$), or the K_M for several peptides (fig. S9, A to E) or the median inhibitory concentration (IC_{50}) values for several SIRT1 inhibitors (fig. S10, A to E and table S5). Secondary structural elements, thermal denaturation profiles (fig. S11, A to C and table S6), melting temperatures (fig. S12, A and B), and intracellular localization patterns (fig. S13A) of wild-type and SIRT1-E230K were also similar.

To examine the entire structure of SIRT1, we used hydrogen-deuterium exchange mass spectrometry (HDXMS). No changes in protein dynamics were detected between wild-type and SIRT1-E230K. The catalytic core domain showed slow exchange, consistent with a well-defined structure (fig. S14, A and B). The N and C termini showed fast exchange (fig. S14A), except for a small C-terminal region around residue 650 recently implicated in the regulation of SIRT1 activity (*26*, *27*) and a small rigid N-terminal region, residues 190 to 244, encompassing Glu^{230} (Fig. 3E and fig. S14A).

The variable median effective concentration (EC_{50})/dissociation constant (K_d) ratios indicate that the majority of synthetic STACs do not interact strongly with SIRT1 and likely bind to a steady-state form such as the enzyme-substrate complex (*15*). SIRT1 truncations of the first 183 residues did not disrupt STAC binding, but truncations to residues 195 and 225 did, coincident with a loss of activation (table S7), whereas the E230K substitution had variable effects on STAC binding (fig. S15). Together, these data indicate that SIRT1 has a structured N-terminal domain that is required for STAC binding that encompasses Glu^{230}, an amino acid critical for activation across a broad class of STACs.

Resveratrol and synthetic STACs increase mitochondrial function in a SIRT1-dependent manner (*28*–*30*). However, it is unclear whether this is a direct or indirect effect of STACs on SIRT1. We therefore reconstituted primary SIRT1 knockout (KO) myoblasts (*30*) with wild-type mouse SIRT1 or mouse SIRT1-E222K (the murine equivalent of human SIRT1-E230K) (Fig. 4A and fig. S16A). STACs increased mitochondrial mass and adenosine triphosphate (ATP) content in wild-type but not SIRT1 KO myoblasts (Fig. 4, B and C, and fig. S16B). In myoblasts carrying SIRT1-E222K, the effects of STACs on mitochondrial mass and ATP levels were also blocked (Fig. 4, B and C, and fig. S16B). In SIRT1 KO mouse embryonic fibroblasts (MEFs) reconstituted with SIRT1-E222K (fig. S17A), the ability of STACs to increase mitochondrial mass, ATP, and mitochondrial DNA copy number was also blocked (fig. S17, B to D, and fig. S18A). At these concentrations, there was no evidence for SIRT1-independent adenosine monophosphate (AMP)–activated protein kinase phosphorylation (fig. S19A) (*30*) or inhibition of phosphodiesterase isoforms (table S8). These findings argue against these pathways directly mediating the effects of STACs.

The data presented here favor a mechanism of direct "assisted allosteric activation" mediated by an N-terminal activation domain in SIRT1 (fig. S20, A and B) that is responsible for at least some of the physiological effects of STACs. Thus, allosteric activation of SIRT1 by STACs remains a viable therapeutic intervention strategy for many diseases associated with aging.

Downloaded from www.sciencemag.org on March 8, 2013

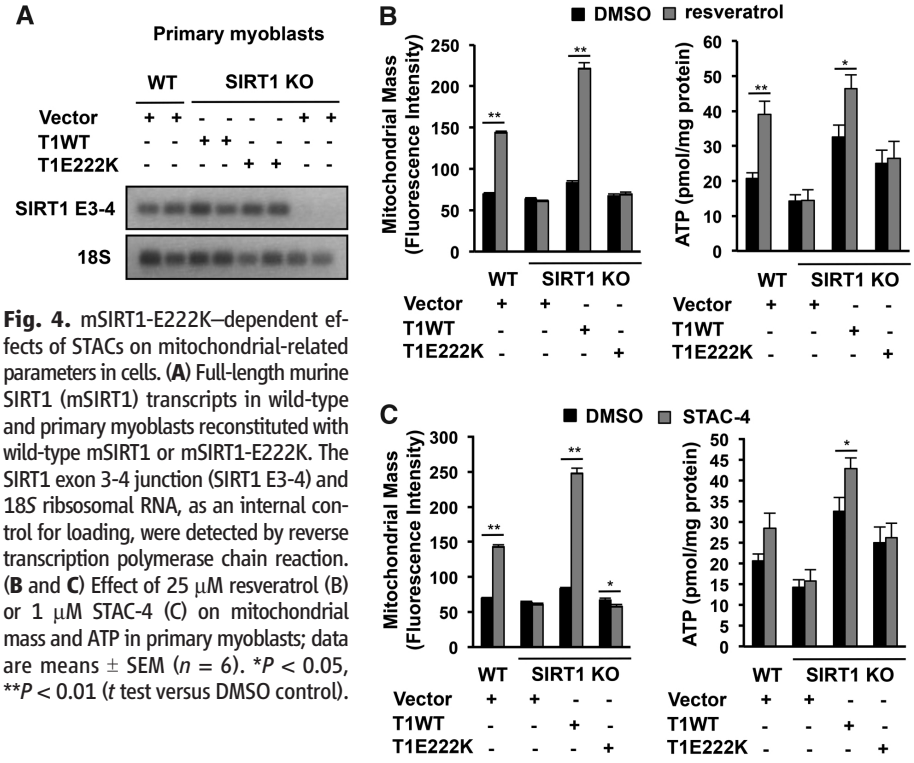

Fig. 4. mSIRT1-E222K–dependent effects of STACs on mitochondrial-related parameters in cells. (**A**) Full-length murine SIRT1 (mSIRT1) transcripts in wild-type and primary myoblasts reconstituted with wild-type mSIRT1 or mSIRT1-E222K. The SIRT1 exon 3-4 junction (SIRT1 E3-4) and 18*S* ribsosomal RNA, as an internal control for loading, were detected by reverse transcription polymerase chain reaction. (**B** and **C**) Effect of 25 μM resveratrol (B) or 1 μM STAC-4 (C) on mitochondrial mass and ATP in primary myoblasts; data are means ± SEM (n = 6). *P < 0.05, **P < 0.01 (t test versus DMSO control).

References and Notes

1. C. Sebastian, K. F. Satterstrom, M. C. Haigis, R. Mostoslavsky, *J. Biol. Chem.* **287**, 42444 (2012).
2. M. C. Haigis, D. A. Sinclair, *Annu. Rev. Pathol.* **5**, 253 (2010).
3. A. Chalkiadaki, L. Guarente, *Nat. Rev. Endocrinol.* **8**, 287 (2012).
4. K. T. Howitz *et al.*, *Nature* **425**, 191 (2003).
5. J. C. Milne *et al.*, *Nature* **450**, 712 (2007).
6. J. A. Baur *et al.*, *Nature* **444**, 337 (2006).
7. R. K. Minor *et al.*, *Sci. Rep.* **1**, 70 (2011).
8. M. Kaeberlein *et al.*, *J. Biol. Chem.* **280**, 17038 (2005).
9. M. T. Borra, B. C. Smith, J. M. Denu, *J. Biol. Chem.* **280**, 17187 (2005).
10. M. Pacholec *et al.*, *J. Biol. Chem.* **285**, 8340 (2010).
11. D. Beher *et al.*, *Chem. Biol. Drug Des.* **74**, 619 (2009).
12. M. Ghislain, E. Talla, J. M. François, *Yeast* **19**, 215 (2002).
13. K. Sugawara, F. Oyama, *J. Biochem.* **89**, 771 (1981).
14. A. A. Sauve, C. Wolberger, V. L. Schramm, J. D. Boeke, *Annu. Rev. Biochem.* **75**, 435 (2006).
15. H. Dai *et al.*, *J. Biol. Chem.* **285**, 32695 (2010).
16. Single-letter abbreviations for amino acid residues: A, Ala; C, Cys; D, Asp; E, Glu; F, Phe; G, Gly; H, His; I, Ile; K, Lys; L, Leu; M, Met; N, Asn; P, Pro; Q, Gln; R, Arg; S, Ser; T, Thr; V, Val; W, Trp; Y, Tyr; X, any amino acid.
17. A. Vaquero *et al.*, *Mol. Cell* **16**, 93 (2004).
18. R. Firestein *et al.*, *PLoS ONE* **3**, e2020 (2008).
19. A. Brunet *et al.*, *Science* **303**, 2011 (2004).
20. S. Kume *et al.*, *J. Biol. Chem.* **282**, 151 (2007).
21. F. Lan, J. M. Cacicedo, N. Ruderman, Y. Ido, *J. Biol. Chem.* **283**, 27628 (2008).
22. J. T. Rodgers *et al.*, *Nature* **434**, 113 (2005).
23. F. Yeung *et al.*, *EMBO J.* **23**, 2369 (2004).
24. C. Das, M. S. Lucia, K. C. Hansen, J. K. Tyler, *Nature* **459**, 113 (2009).
25. H. S. Ghosh, B. Reizis, P. D. Robbins, *Sci. Rep.* **1**, 150 (2011).
26. H. Kang *et al.*, *Mol. Cell* **44**, 203 (2011).
27. M. Pan, H. Yuan, M. Brent, E. C. Ding, R. Marmorstein, *J. Biol. Chem.* **287**, 2468 (2012).
28. Z. Gerhart-Hines *et al.*, *EMBO J.* **26**, 1913 (2007).
29. M. Bernier *et al.*, *J. Biol. Chem.* **286**, 19270 (2011).
30. N. L. Price *et al.*, *Cell Metab.* **15**, 675 (2012).

Acknowledgments: Supported by the Glenn Foundation for Medical Research, the Ellison Medical Foundation, the Juvenile Diabetes Research Foundation, the United Mitochondrial Disease Foundation, NIH and NIAID grants, an NSERC fellowship (B.P.H.), the Portuguese Science and Technology Foundation (A.P.G.), the Intramural Research Program, and NIH/NHLBI (L.A.S. and J.M.). D.A.S. is a consultant and inventor on patents licensed to Sirtris, a GSK company. H.D., A.W.C., T.C., T.V.R., E.R.S., H.Z., Y.J., S.M.S., C.A.B., J.S.D., P.Y.N., R.B.P., J.L.E., and G.P.V. are employees of Sirtris, a GSK company. Dedicated to the memories of Jana Perni and Harmon Rasnow. A patent application on the PNC1-OPT sirtuin assay has been filed by Harvard Medical School with D.A.S. and B.P.H. as inventors. Patent applications related to sirtuin activators have been filed by Sirtris and Biomol. Natural Sirt1 activators will be provided upon request. Synthetic STACs are provided under a material transfer agreement from Sirtris.

Supplementary Materials

www.sciencemag.org/cgi/content/full/339/6124/1216/DC1
Materials and Methods
Figs. S1 to S20
Tables S1 to S8
Reference (*31*)

4 October 2012; accepted 18 January 2013
10.1126/science.1231097

Downloaded from www.sciencemag.org on March 8, 2013

Aire-Dependent Thymic Development of Tumor-Associated Regulatory T Cells

Sven Malchow,[1] Daniel S. Leventhal,[1] Saki Nishi,[1] Benjamin I. Fischer,[1] Lynn Shen,[1] Gladell P. Paner,[1] Ayelet S. Amit,[1] Chulho Kang,[2] Jenna E. Geddes,[3]* James P. Allison,[3]† Nicholas D. Socci,[4] Peter A. Savage[1]‡

Despite considerable interest in the modulation of tumor-associated Foxp3$^+$ regulatory T cells (T_{regs}) for therapeutic benefit, little is known about the developmental origins of these cells and the nature of the antigens that they recognize. We identified an endogenous population of antigen-specific T_{regs} (termed MJ23 T_{regs}) found recurrently enriched in the tumors of mice with oncogene-driven prostate cancer. MJ23 T_{regs} were not reactive to a tumor-specific antigen but instead recognized a prostate-associated antigen that was present in tumor-free mice. MJ23 T_{regs} underwent autoimmune regulator (Aire)–dependent thymic development in both male and female mice. Thus, Aire-mediated expression of peripheral tissue antigens drives the thymic development of a subset of organ-specific T_{regs}, which are likely coopted by tumors developing within the associated organ.

Regulatory T (T_{reg}) cells are critical for the prevention of autoimmunity, the maintenance of immune homeostasis, and the suppression of antitumor immune responses (*1*, *2*). For many human cancers, the density of T_{regs} within tumor lesions is predictive of poor clinical outcome (*3*), suggesting that T_{regs} play a functional role in cancer progression. In this study, we set out to establish a tractable animal model in which a single specificity of naturally occurring tumor-associated T_{regs} could be studied in the context of a genetically driven mouse model of autochthonous cancer. In order to identify an endogenous tumor-associated T_{reg} response, we analyzed the immune response in TRAMP mice, which develop prostatic adenocarcinoma because of the transgenic expression of the model oncogene SV40 T antigen in the prostate (*4*, *5*). Unlike the prostates of tumor-free mice, which contain very few

[1]Department of Pathology, University of Chicago, Chicago, IL 60637, USA. [2]Cancer Research Laboratory, University of California, Berkeley, CA 94720, USA. [3]Department of Immunology, Howard Hughes Medical Institute, Memorial Sloan-Kettering Cancer Center, New York, NY 10021, USA. [4]Bioinformatics Core, Memorial Sloan-Kettering Cancer Center, New York, NY 10021, USA.

*Present address: Department of Immunology, Harvard Medical School, Boston, MA 02115, USA.
†Present address: Department of Immunology, The University of Texas MD Anderson Cancer Center, Houston, TX 77030, USA.
‡To whom correspondence should be addressed. E-mail: psavage@bsd.uchicago.edu

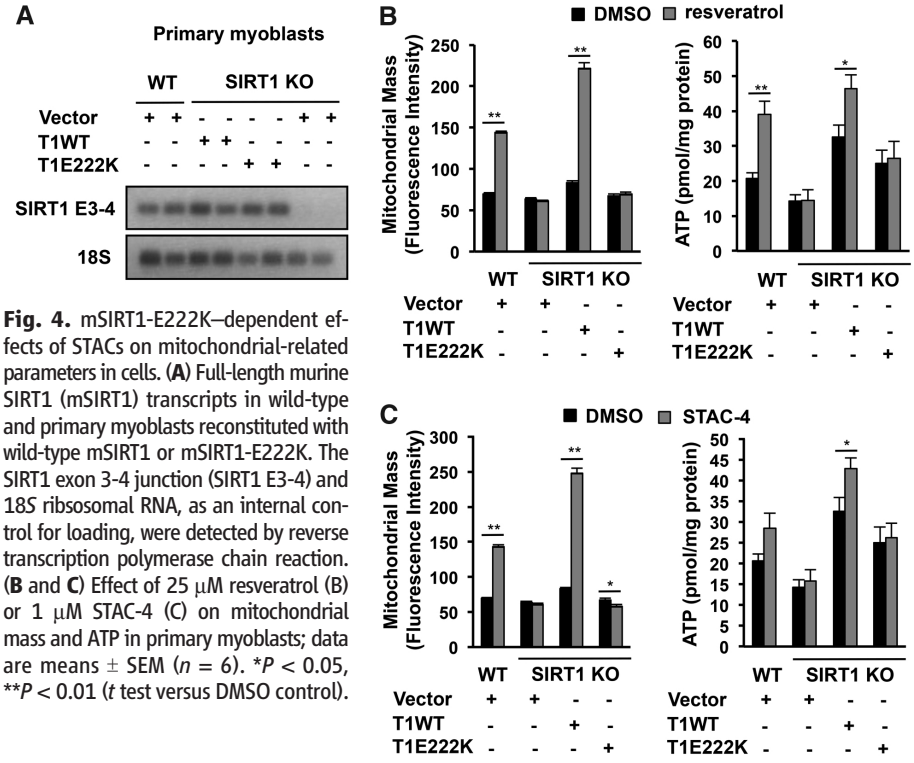

Fig. 4. mSIRT1-E222K–dependent effects of STACs on mitochondrial-related parameters in cells. (**A**) Full-length murine SIRT1 (mSIRT1) transcripts in wild-type and primary myoblasts reconstituted with wild-type mSIRT1 or mSIRT1-E222K. The SIRT1 exon 3-4 junction (SIRT1 E3-4) and 18*S* ribsosomal RNA, as an internal control for loading, were detected by reverse transcription polymerase chain reaction. (**B** and **C**) Effect of 25 μM resveratrol (B) or 1 μM STAC-4 (C) on mitochondrial mass and ATP in primary myoblasts; data are means ± SEM (n = 6). *P < 0.05, **P < 0.01 (t test versus DMSO control).

References and Notes

1. C. Sebastian, K. F. Satterstrom, M. C. Haigis, R. Mostoslavsky, *J. Biol. Chem.* **287**, 42444 (2012).
2. M. C. Haigis, D. A. Sinclair, *Annu. Rev. Pathol.* **5**, 253 (2010).
3. A. Chalkiadaki, L. Guarente, *Nat. Rev. Endocrinol.* **8**, 287 (2012).
4. K. T. Howitz *et al.*, *Nature* **425**, 191 (2003).
5. J. C. Milne *et al.*, *Nature* **450**, 712 (2007).
6. J. A. Baur *et al.*, *Nature* **444**, 337 (2006).
7. R. K. Minor *et al.*, *Sci. Rep.* **1**, 70 (2011).
8. M. Kaeberlein *et al.*, *J. Biol. Chem.* **280**, 17038 (2005).
9. M. T. Borra, B. C. Smith, J. M. Denu, *J. Biol. Chem.* **280**, 17187 (2005).
10. M. Pacholec *et al.*, *J. Biol. Chem.* **285**, 8340 (2010).
11. D. Beher *et al.*, *Chem. Biol. Drug Des.* **74**, 619 (2009).
12. M. Ghislain, E. Talla, J. M. François, *Yeast* **19**, 215 (2002).
13. K. Sugawara, F. Oyama, *J. Biochem.* **89**, 771 (1981).
14. A. A. Sauve, C. Wolberger, V. L. Schramm, J. D. Boeke, *Annu. Rev. Biochem.* **75**, 435 (2006).
15. H. Dai *et al.*, *J. Biol. Chem.* **285**, 32695 (2010).
16. Single-letter abbreviations for amino acid residues: A, Ala; C, Cys; D, Asp; E, Glu; F, Phe; G, Gly; H, His; I, Ile; K, Lys; L, Leu; M, Met; N, Asn; P, Pro; Q, Gln; R, Arg; S, Ser; T, Thr; V, Val; W, Trp; Y, Tyr; X, any amino acid.
17. A. Vaquero *et al.*, *Mol. Cell* **16**, 93 (2004).
18. R. Firestein *et al.*, *PLoS ONE* **3**, e2020 (2008).
19. A. Brunet *et al.*, *Science* **303**, 2011 (2004).
20. S. Kume *et al.*, *J. Biol. Chem.* **282**, 151 (2007).
21. F. Lan, J. M. Cacicedo, N. Ruderman, Y. Ido, *J. Biol. Chem.* **283**, 27628 (2008).
22. J. T. Rodgers *et al.*, *Nature* **434**, 113 (2005).
23. F. Yeung *et al.*, *EMBO J.* **23**, 2369 (2004).
24. C. Das, M. S. Lucia, K. C. Hansen, J. K. Tyler, *Nature* **459**, 113 (2009).
25. H. S. Ghosh, B. Reizis, P. D. Robbins, *Sci. Rep.* **1**, 150 (2011).
26. H. Kang *et al.*, *Mol. Cell* **44**, 203 (2011).
27. M. Pan, H. Yuan, M. Brent, E. C. Ding, R. Marmorstein, *J. Biol. Chem.* **287**, 2468 (2012).
28. Z. Gerhart-Hines *et al.*, *EMBO J.* **26**, 1913 (2007).
29. M. Bernier *et al.*, *J. Biol. Chem.* **286**, 19270 (2011).
30. N. L. Price *et al.*, *Cell Metab.* **15**, 675 (2012).

Acknowledgments: Supported by the Glenn Foundation for Medical Research, the Ellison Medical Foundation, the Juvenile Diabetes Research Foundation, the United Mitochondrial Disease Foundation, NIH and NIAID grants, an NSERC fellowship (B.P.H.), the Portuguese Science and Technology Foundation (A.P.G.), the Intramural Research Program, and NIH/NHLBI (L.A.S. and J.M.). D.A.S. is a consultant and inventor on patents licensed to Sirtris, a GSK company. H.D., A.W.C., T.C., T.V.R., E.R.S., H.Z., Y.J., S.M.S., C.A.B., J.S.D., P.Y.N., R.B.P., J.L.E., and G.P.V. are employees of Sirtris, a GSK company. Dedicated to the memories of Jana Perni and Harmon Rasnow. A patent application on the PNC1-OPT sirtuin assay has been filed by Harvard Medical School with D.A.S. and B.P.H. as inventors. Patent applications related to sirtuin activators have been filed by Sirtris and Biomol. Natural Sirt1 activators will be provided upon request. Synthetic STACs are provided under a material transfer agreement from Sirtris.

Supplementary Materials

www.sciencemag.org/cgi/content/full/339/6124/1216/DC1
Materials and Methods
Figs. S1 to S20
Tables S1 to S8
Reference (*31*)

4 October 2012; accepted 18 January 2013
10.1126/science.1231097

Aire-Dependent Thymic Development of Tumor-Associated Regulatory T Cells

Sven Malchow,[1] Daniel S. Leventhal,[1] Saki Nishi,[1] Benjamin I. Fischer,[1] Lynn Shen,[1] Gladell P. Paner,[1] Ayelet S. Amit,[1] Chulho Kang,[2] Jenna E. Geddes,[3]* James P. Allison,[3]† Nicholas D. Socci,[4] Peter A. Savage[1]‡

Despite considerable interest in the modulation of tumor-associated Foxp3$^+$ regulatory T cells (T_{regs}) for therapeutic benefit, little is known about the developmental origins of these cells and the nature of the antigens that they recognize. We identified an endogenous population of antigen-specific T_{regs} (termed MJ23 T_{regs}) found recurrently enriched in the tumors of mice with oncogene-driven prostate cancer. MJ23 T_{regs} were not reactive to a tumor-specific antigen but instead recognized a prostate-associated antigen that was present in tumor-free mice. MJ23 T_{regs} underwent autoimmune regulator (Aire)–dependent thymic development in both male and female mice. Thus, Aire-mediated expression of peripheral tissue antigens drives the thymic development of a subset of organ-specific T_{regs}, which are likely coopted by tumors developing within the associated organ.

Regulatory T (T_{reg}) cells are critical for the prevention of autoimmunity, the maintenance of immune homeostasis, and the suppression of antitumor immune responses (*1*, *2*). For many human cancers, the density of T_{regs} within tumor lesions is predictive of poor clinical outcome (*3*), suggesting that T_{regs} play a functional role in cancer progression. In this study, we set out to establish a tractable animal model in which a single specificity of naturally occurring tumor-associated T_{regs} could be studied in the context of a genetically driven mouse model of autochthonous cancer. In order to identify an endogenous tumor-associated T_{reg} response, we analyzed the immune response in TRAMP mice, which develop prostatic adenocarcinoma because of the transgenic expression of the model oncogene SV40 T antigen in the prostate (*4*, *5*). Unlike the prostates of tumor-free mice, which contain very few

[1]Department of Pathology, University of Chicago, Chicago, IL 60637, USA. [2]Cancer Research Laboratory, University of California, Berkeley, CA 94720, USA. [3]Department of Immunology, Howard Hughes Medical Institute, Memorial Sloan-Kettering Cancer Center, New York, NY 10021, USA. [4]Bioinformatics Core, Memorial Sloan-Kettering Cancer Center, New York, NY 10021, USA.

*Present address: Department of Immunology, Harvard Medical School, Boston, MA 02115, USA.
†Present address: Department of Immunology, The University of Texas MD Anderson Cancer Center, Houston, TX 77030, USA.
‡To whom correspondence should be addressed. E-mail: psavage@bsd.uchicago.edu

T_{reg} cells (which are identified as $CD4^+Foxp3^+$), a substantial population of T_{regs} can be detected in the prostate tumors of TRAMP mice (fig. S1). We used an experimental system involving T cell antigen receptor alpha chain (TCRα) repertoire analysis of T cell populations from TRAMP mice expressing the $Foxp3^{gfp}$ (where gfp indicates green fluorescent protein) reporter (*6*) and a fixed, transgenic (tg) TCRβ chain. The fixed TCRβ used in this study was a TCRβ chain that was found to be recurrently expressed by $CD4^+Foxp3^+$ T_{regs} isolated from the prostates of TRAMP mice (fig. S2) and will be referred to hereafter as TCRβtg. TCR complementarity-determining region 3 (CDR3) length-distribution analysis of cDNA from purified $CD4^+Foxp3^+$ and $CD4^+Foxp3^{neg}$ T cells from the prostate tumors of $TRAMP^{+/-}$ $Foxp3^{gfp}$ TCRβtg males revealed a substantial overrepresentation of $CD4^+Foxp3^+$ T cells expressing a Vα2 (TRAV14) TCRα chain with a CDR3 of nine amino acids in length (as defined by International Immunogenetics Information System, www.imgt.org) (Fig. 1A, denoted in red). Deep sequencing of these samples revealed that the identical TCRα chain, of CDR3 sequence LYYNQGKLI (where G indicates Gly; I, Ile; K, Lys; L, Leu; N, Asn; Q, Gln; and Y, Tyr), was recurrently expressed by $Foxp3^+$ T_{regs} (Fig. 1B), indicating that T_{regs} of a single specificity are recurrently enriched within TRAMP prostate tumors. In many prostate samples, the Vα2-LYYNQGKLI TCR chain was encoded by a single nucleotide sequence (fig. S3), suggesting that, in many cases, tumor-infiltrating T_{regs} of this specificity may originate from a single clone.

A survey of different anatomical sites of $TRAMP^{+/-}$ $Foxp3^{gfp}$ TCRβtg mice using CDR3 length-distribution analysis revealed that the overrepresentation of T_{regs} expressing a $V\alpha2^+$ TCRα chain of nine amino acids in length was observed in the prostate tumor and prostate-draining periaortic lymph nodes but was not detected over background in nondraining brachial lymph nodes (Fig. 1C). Thus, T_{regs} of this specificity are not expanded systemically in tumor-bearing mice but are instead selectively enriched in the prostate tumor environment.

In order to gain insight into the antigen specificities of polyclonal tumor-infiltrating $CD4^+$ T cells, we determined the extent of overlap of the $V\alpha2^+$ TCR repertoire for T cell subsets isolated from the prostate tumors of $TRAMP^{+/-}$ $Foxp3^{gfp}$ TCRβtg mice. Repertoire overlap was assessed by using the Morisita-Horn (MH) similarity index (*7–11*), for which a value of 1 indicates identity and a value of 0 denotes complete dissimilarity (Fig. 1D). The analysis revealed that the TCR repertoire of $CD4^+Foxp3^+$ and $CD4^+Foxp3^{neg}$ populations isolated from a particular prostate tumor were largely distinct and nonoverlapping (MH = 0.07 ± 0.10 SD; Fig. 1D, samples intersecting at red lines), implying that the antigens recognized by tumor-infiltrating T_{regs} are different from those recognized by conventional $CD4^+$ T cells. Second, the TCR repertoire of $CD4^+Foxp3^+$ cells isolated from the prostates of different mice exhibited a high degree of similarity from mouse

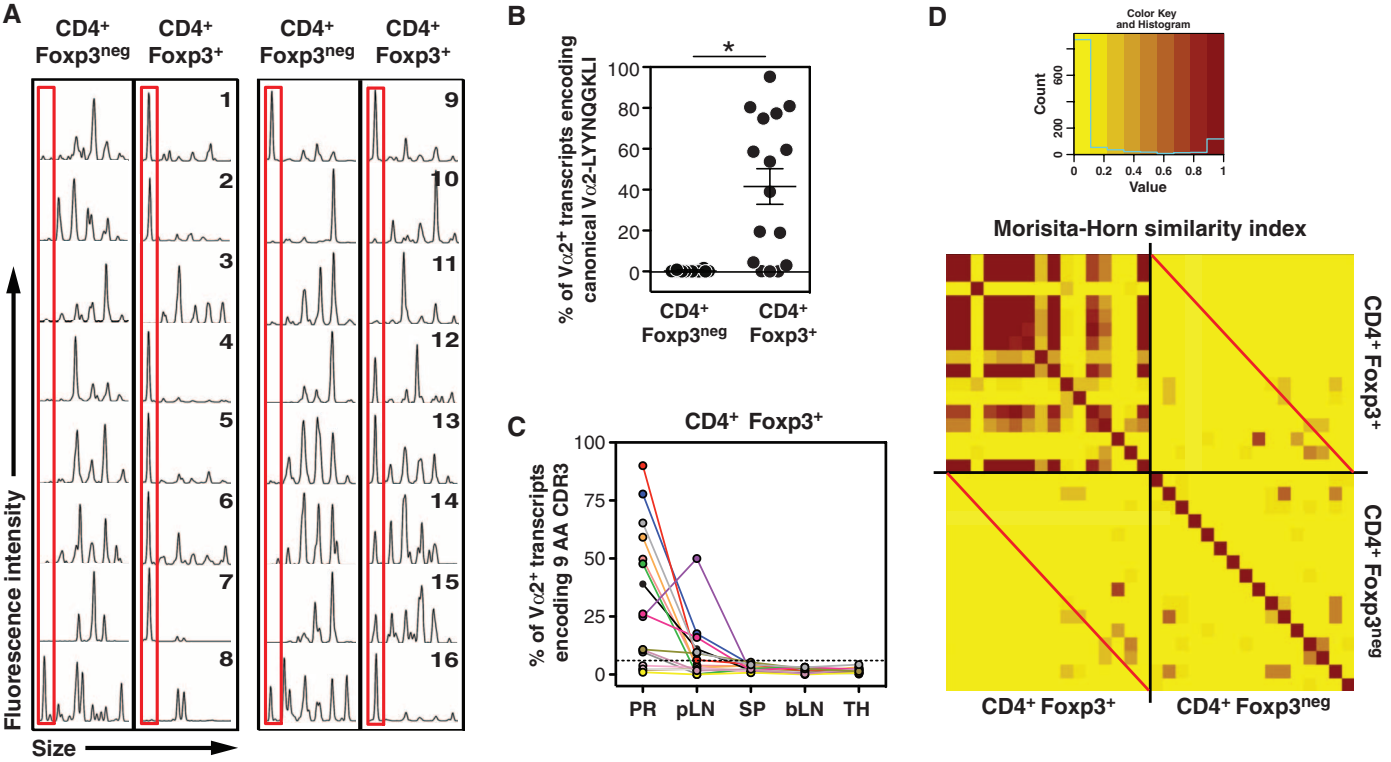

Fig. 1. $CD4^+Foxp3^+$ T_{regs} expressing a canonical TCR are recurrently enriched in TRAMP prostate tumors. Analysis of Vα2 (TRAV14)$^+$ TCRα chains in tumor-bearing $TRAMP^{+/-}$ $Foxp3^{gfp}$ TCRβtg mice. $CD4^+Foxp3^{neg}$ and $CD4^+Foxp3^+$ T cells were purified by fluorescence-activated cell sorting (FACS) from different anatomical sites of ~27-week-old male mice, and cDNA was subjected to molecular analysis. (**A**) CDR3 length-distribution analysis of $V\alpha2^+$ TCRα chains of T cell subsets isolated from prostate tumors. The mouse number is indicated. The red boxes denote TCRα transcripts encoding a CDR3 of nine amino acids (AA) in length. (**B**) $V\alpha2^+$ TCRα transcripts from the indicated populations were polymerase chain reaction (PCR)–amplified and subjected to deep sequencing (*24*). The percentage of all $V\alpha2^+$ TCRα transcripts encoding the canonical Vα2-LYYNQGKLI chain is plotted for each sample. The mean ± SEM is indicated. The asterisk indicates $P < 0.05$ (*t* test). (**C**) Plots of the percentage of $V\alpha2^+$ transcripts encoding a CDR3 of nine AAs (based on peak area) for $CD4^+Foxp3^+$ T cells isolated from different anatomical sites of the mice depicted in (A). PR, prostate; pLN, periaortic lymph nodes; SP, spleen; bLN, brachial lymph nodes; TH, thymus. Samples from each mouse are color-coded. The plot does not depict data from mice 1 and 2 and includes data from two additional mice (numbers 17 and 18). Samples with values above the indicated threshold (dashed line) are considered overrepresented. This threshold is defined as the mean percent peak area plus three standard deviations for $V\alpha2^+$ TCRα transcripts encoding a nine-AA CDR3 from the spleen of female TCRβtg mice. (**D**) Heat map of the MH similarity index for prostatic T cell subsets from mice 1 to 16. Samples are oriented in ascending numerical order, from top to bottom and left to right (not shown). A motif table of predicted amino acid sequences is presented in table S1. $CD4^+Foxp3^{neg}$ and $CD4^+Foxp3^+$ subsets from the same prostate tumor intersect at the red diagonal lines. Data are pooled from $N = 3$ independent FACS experiments.

to mouse (MH = 0.38 ± 0.39 SD; Fig. 1D, upper left quadrant). Although a substantial proportion of this similarity was due to the recurrent enrichment of the Vα2-LYYNQGKLI TCR, additional TCRα chains were identified that were recurrently expressed by prostatic Foxp3$^+$ T_{regs} (fig. S4). This finding suggests that TRAMP prostate tumors do not recruit polyclonal T_{regs} of arbitrary specificity but instead are associated with the reproducible enrichment of T_{regs} of distinct specificities.

To facilitate the study of T cells expressing the canonical Vα2-LYYNQGKLI TCRα chain paired with the fixed TCRβ chain (hereafter referred to as MJ23 T cells), we generated transgenic mice expressing the MJ23 TCRαβ heterodimer. In female MJ23tg *Rag1*$^{-/-}$ mice, CD4$^+$ T cells in the periphery were phenotypically naïve (Fig. 2A and fig. S5). Moreover, Foxp3$^+$ MJ23tg cells were not detected above background in the thymus and periphery of these mice (Fig. 2, A and B, and fig. S5). In contrast, analysis of tumor-free male MJ23tg *Rag1*$^{-/-}$ mice revealed spontaneous accumulation of activated CD44^{hi} CD4$^+$ MJ23tg T cells in the prostate and prostate-draining periaortic lymph nodes (Fig. 2, A and B, and fig. S5), indicative of MJ23 reactivity to an autoantigen at these sites. In the prostate, T cell accumulation was observed in both the stroma and the epithelium and was associated with disruption of the basement membrane of prostatic glands (Fig. 2C). The presence of activated CD4$^+$ T cells was accompanied by the concomitant appearance of a percentage of CD4$^+$Foxp3$^+$ T cells (Fig. 2, A and B, and fig. S5). Foxp3$^+$ cells exhibited in vitro suppressive activity (fig. S6) and phenotypic characteristics of T_{regs} (fig. S7), including expression of neuropilin-1 (supplementary text and figs. S7 and S8). Taken together, our data demonstrate that MJ23 T_{regs}, identified on the basis of their enrichment in mouse prostate tumors, are not reactive to a unique tumor-specific antigen but instead recognize a self antigen associated with the organ of cancer origin.

In other experiments, CD11c$^+$ dendritic cells isolated from TRAMP prostate tumors induced robust proliferation of MJ23tg T cells ex vivo (Fig. 2D) but did not stimulate OT-II transgenic T cells expressing an irrelevant class II–restricted TCR (*12*). These data provide direct evidence that prostate tumors contain the antigen recognized by MJ23 T cells.

In order to study the development of MJ23tg T cells at physiological clonal frequencies, we generated chimeric animals in which bone marrow cells from MJ23tg *Rag1*$^{-/-}$ donors were engrafted into host mice at low frequencies (<1%), and the development and distribution of MJ23tg T cells was assessed (Fig. 3 and fig. S9). Analysis of B6 male and tumor-bearing TRAMP male hosts revealed that Foxp3$^+$ MJ23tg T_{regs} developed in the thymus (Fig. 3, A and B). The efficiency of development varied from mouse to mouse and was inversely correlated with the frequency of MJ23tg precursors (Fig. 3B), a finding that is consistent with previously published studies (*13*, *14*). In other experiments, OT-II *Rag1*$^{-/-}$ precursors did not develop efficiently into Foxp3$^+$ cells in the thymus, demonstrating the specificity of MJ23tg T_{reg} development (fig. S10). In the periphery of male chimeras, Foxp3$^+$ MJ23tg cells were distributed

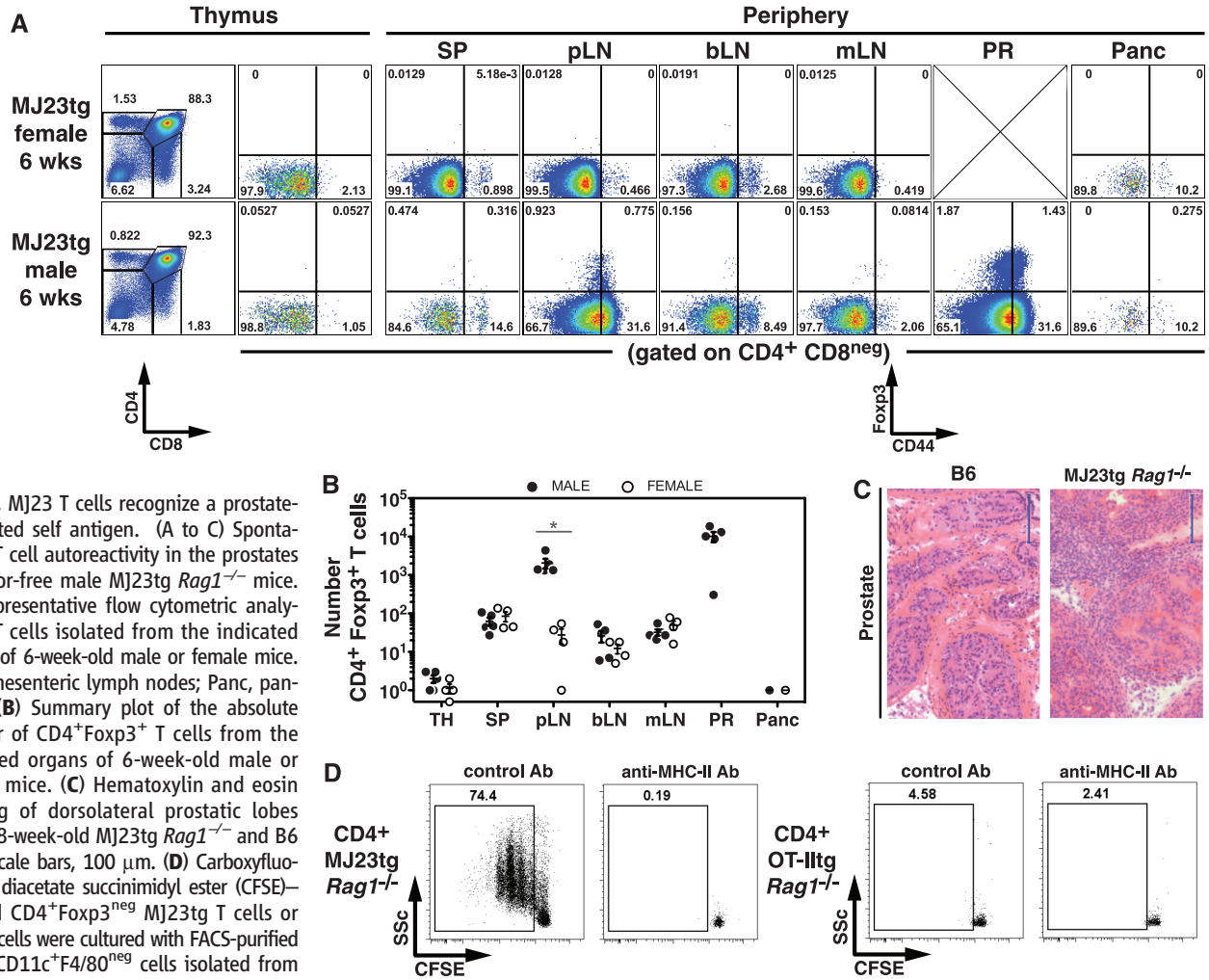

Fig. 2. MJ23 T cells recognize a prostate-associated self antigen. (A to C) Spontaneous T cell autoreactivity in the prostates of tumor-free male MJ23tg *Rag1*$^{-/-}$ mice. (**A**) Representative flow cytometric analyses of T cells isolated from the indicated organs of 6-week-old male or female mice. mLN, mesenteric lymph nodes; Panc, pancreas. (**B**) Summary plot of the absolute number of CD4$^+$Foxp3$^+$ T cells from the indicated organs of 6-week-old male or female mice. (**C**) Hematoxylin and eosin staining of dorsolateral prostatic lobes from 18-week-old MJ23tg *Rag1*$^{-/-}$ and B6 mice. Scale bars, 100 μm. (**D**) Carboxyfluorescein diacetate succinimidyl ester (CFSE)–labeled CD4$^+$Foxp3^{neg} MJ23tg T cells or OT-IItg cells were cultured with FACS-purified CD45$^+$CD11c$^+$F4/80^{neg} cells isolated from TRAMP prostate tumors in the presence of recombinant mouse interleukin-2 (IL-2). In addition, MHC-II antibody (Ab) or isotype control antibody was added to the culture. Dilution of CFSE was assessed by flow cytometry on day 4. The mean ± SEM is indicated. Asterisks indicate $P <$ 0.05. For (A) and (B), data are pooled from $N = 2$ independent experiments. For (B), *t* tests were used to compare data from male and female mice at each site. Data in (D) are representative of $N = 7$ independent experiments.

throughout the secondary lymphoid organs but were preferentially enriched in the prostate-draining periaortic lymph nodes (Fig. 3C), a finding consistent with evidence of reactivity to a prostate-associated antigen (Fig. 2). Very few donor-derived MJ23tg T_{regs} were observed in the prostate (Fig. 3, A and C), likely reflecting competition with endogenous MJ23 T_{regs} (supplementary text and fig. S11). Upon intravenous transfer of naïve $CD4^+Foxp3^{neg}$ MJ23tg T cells into TRAMP males, the induction of Foxp3 expression by MJ23tg cells was negligible (fig. S12), suggesting that antigen exposure in the periphery does not favor the development of induced T_{regs}. Taken together, our results demonstrate that expression of the MJ23 TCR facilitates T_{reg} development in the thymus of male hosts. Thus, T cells of this specificity encounter the antigen(s) driving T_{reg} development during maturation in the thymus, before their exposure to the prostate or tumor environment.

On the basis of our data indicating that MJ23 T cells are reactive to a prostate-associated antigen, we anticipated that $Foxp3^+$ MJ23tg T_{regs} would not develop in B6 female hosts. Unexpectedly, $Foxp3^+$ MJ23tg T_{regs} developed in the thymus of chimeric B6 females (Fig. 3, A and B, and fig. S9). In the periphery of female mice, $Foxp3^+$ MJ23tg T cells were broadly distributed in the spleen and all lymph nodes examined, but selective enrichment in the periaortic lymph nodes was not observed in female hosts (Fig. 3C). In order to elucidate the mechanisms underlying MJ23tg T_{reg} development in both male and female mice, we examined the role of autoimmune regulator (Aire) in development. *Aire* encodes a transcriptional regulator that drives the ectopic expression of peripheral tissue-specific antigens by medullary thymic epithelial cells and is critical for the maintenance of immune tolerance (*15–17*). Analysis of MJ23tg development in chimeric mice in which MJ23tg precursors were engrafted into $Aire^{+/+}$ or $Aire^{-/-}$ hosts revealed that

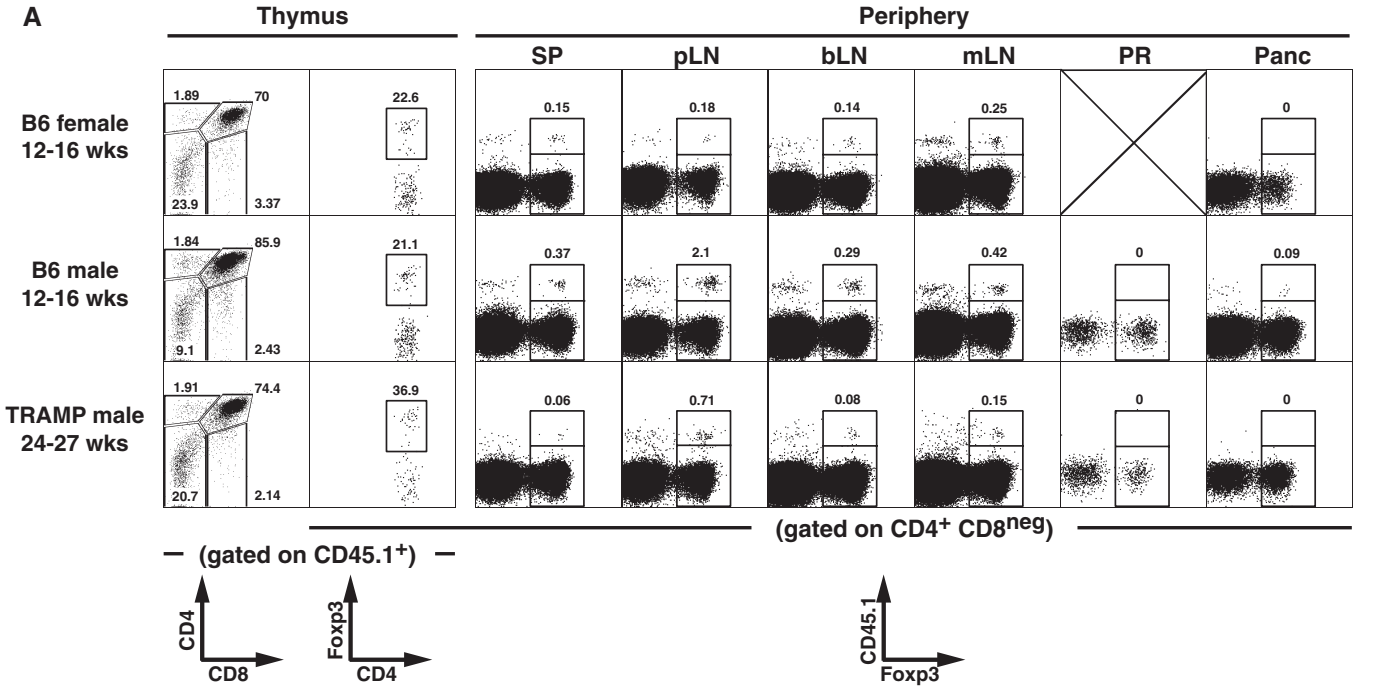

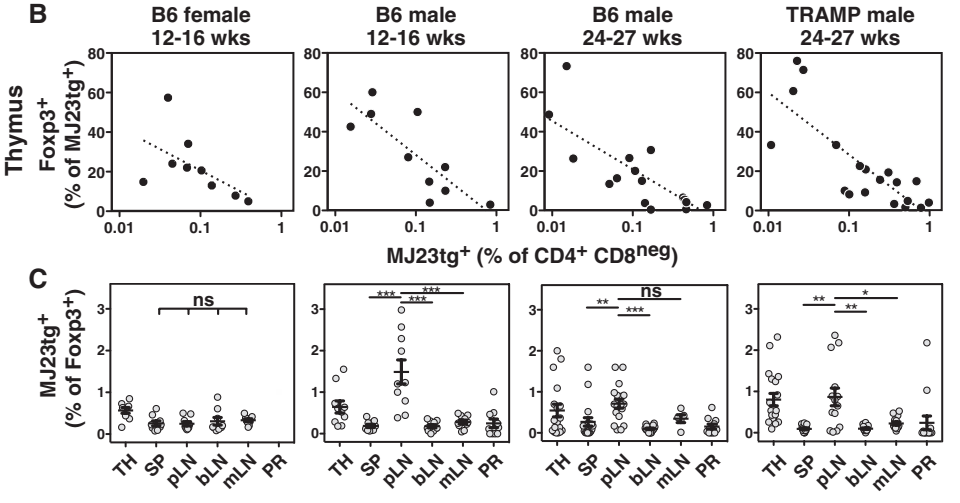

Fig. 3. Thymic development of MJ23 T_{regs}. The MJ23 TCR facilitates thymic T_{reg} development at low clonal frequencies. T cell–depleted bone marrow cells from MJ23tg *Rag1*$^{-/-}$ $CD45.1^+$ female donor mice were engrafted, along with polyclonal "filler" cells from B6 females ($CD45^{.2/.2}$), into sublethally irradiated $CD45^{.2/.2}$ recipient mice. This approach resulted in seeding of MJ23tg precursors at a low frequency (<1%). Six weeks post-engraftment, the fate of MJ23tg cells was analyzed. (**A**) Representative flow cytometric analyses of $CD45.1^+$ MJ23tg T cells from different anatomical sites of male or female mice of the indicated ages and strain. Abbreviations are the same as in Fig. 2. For the thymus, the left column (CD4 versus CD8) depicts undepleted samples; the right column (Foxp3 versus CD4) depicts CD8-depleted samples. For the periphery, the percentage of all $CD4^+Foxp3^+$ T cells that are $CD45.1^+$ ($MJ23tg^+$) is indicated. (**B**) Summary plots of the "efficiency" of MJ23tg T_{reg} development in the thymus, in which the percentage of $CD4^+CD8^{neg}$ $CD45.1^+$ MJ23tg cells that express Foxp3 is plotted versus the frequency of $CD45.1^+$ MJ23tg thymocytes (as a percentage of all $CD4^+CD8^{neg}$ cells) for cells isolated from host mice of the indicated strain, gender, and age. Dashed lines indicate best-fit semi-log curves. (**C**) Summary plots of the percentage of $CD45.1^+$ MJ23tg T cells among all $CD4^+Foxp3^+$ cells isolated from various organs of the indicated hosts. The mean ± SEM is shown. Asterisks indicate $P < 0.05$; ns, not significant. Analysis of variance was used to compare the secondary lymphoid sites (spleen and lymph nodes) within chimeric hosts of a given type. Data are pooled from at least $N = 3$ independent experiments.

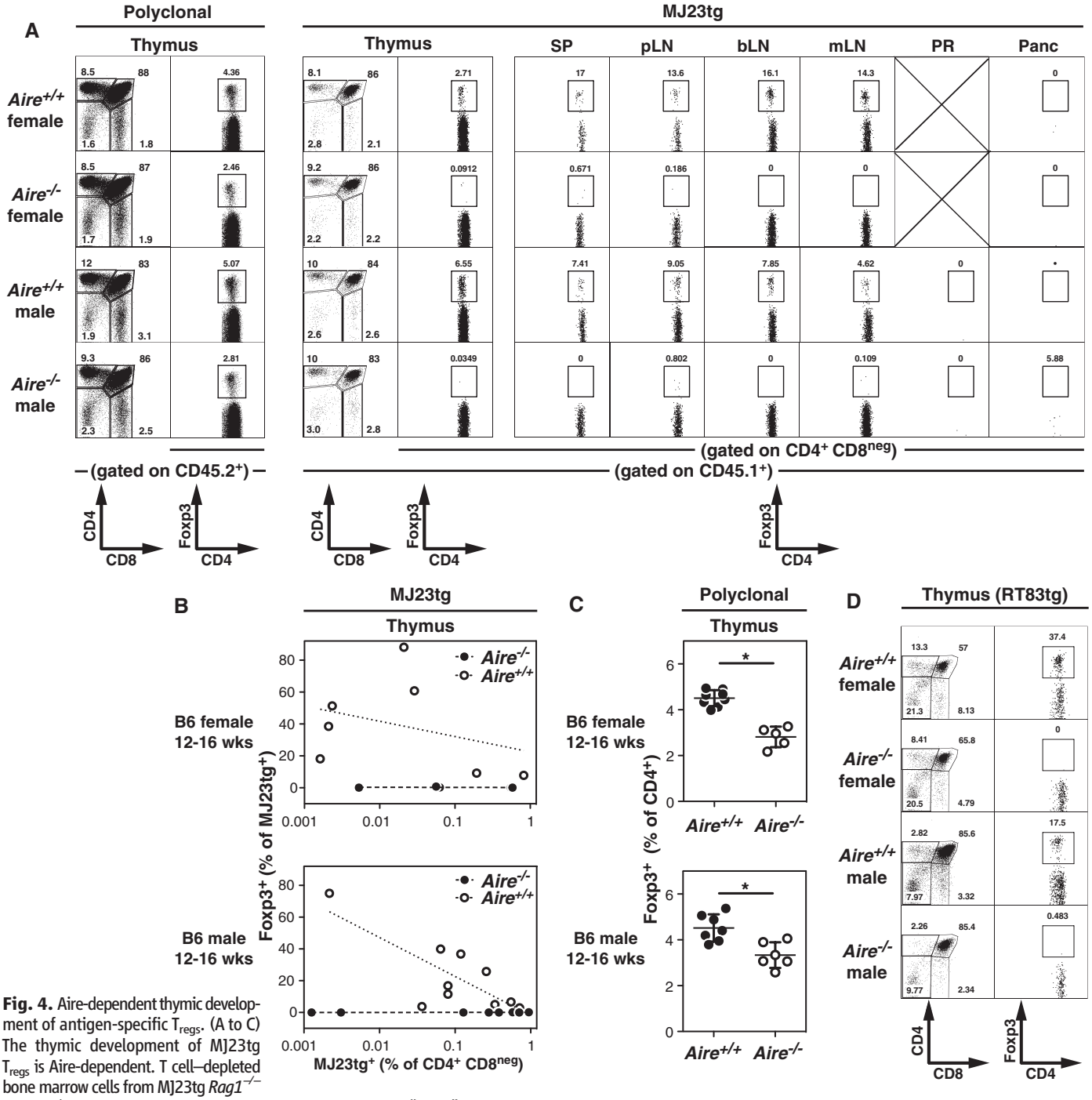

Fig. 4. Aire-dependent thymic development of antigen-specific T_{regs}. (A to C) The thymic development of MJ23tg T_{regs} is Aire-dependent. T cell–depleted bone marrow cells from MJ23tg *Rag1*$^{-/-}$ CD45.1^{+} female donor mice were engrafted, along with "filler" cells from *Aire*$^{-/-}$ females (CD45$^{.2/.2}$), into sublethally irradiated *Aire*$^{-/-}$ or *Aire*$^{+/+}$ recipient mice (CD45$^{.2/.2}$), both male and female. Six weeks post-engraftment, the fate of MJ23tg cells was analyzed. (**A**) Representative flow cytometric analyses of CD45.2^{+} polyclonal T cells (left) and CD45.1^{+} MJ23tg T cells from different anatomical sites of 12- to 16-week-old male or female mice of the indicated *Aire* genotype. Abbreviations are the same as in Figs. 1 and 2. The percentages of CD4^{+} cells that are Foxp3^{+} are shown. For the thymus, the left column (CD4 versus CD8) depicts undepleted samples; the right column (Foxp3 versus CD4) depicts CD8-depleted samples. (**B**) Summary plots of the "efficiency" of MJ23tg T_{reg} development, in which the percentage of CD45.1^{+} MJ23tg cells that express Foxp3 is plotted versus the frequency of CD45.1^{+} MJ23tg thymocytes (as a percentage of all CD4^{+}CD8^{neg} cells) for cells isolated from host mice of the indicated sex and genotype. Dashed lines indicate best-fit semilog curves. (**C**) Summary plots of the percentage of CD45.2^{+} polyclonal CD4^{+}CD8^{neg} thymocytes that express Foxp3 in chimeric mice of the indicated sex and genotype. The mean ± SEM is shown. Asterisks indicate $P < 0.05$ for the comparison of *Aire*$^{-/-}$ versus *Aire*$^{+/+}$ mice (*t* test). Data in (A) to (C) are pooled from $N = 3$ independent experiments. (**D**) Aire-dependent thymic development of RT83tg T_{regs}. RT83tg bone marrow chimeras were generated in *Aire*$^{-/-}$ or *Aire*$^{+/+}$ hosts, as described above for MJ23tg T cells. Representative flow cytometric analyses of CD45.1^{+} RT83tg T cells from the thymus of 12- to 16-week-old male or female mice of the indicated *Aire* genotype. The percentage of CD4^{+} cells that are Foxp3^{+} is shown. For the thymus, the left column (CD4 versus CD8) depicts undepleted samples; the right column (Foxp3 versus CD4) depicts CD8-depleted samples. Data in (D) are pooled from $N = 2$ independent experiments.

Foxp3$^+$ MJ23tg T_{regs} failed to develop in the thymus and periphery of *Aire*$^{-/-}$ hosts, both male and female (Fig. 4, A and B). In addition, *Aire*$^{-/-}$ hosts exhibited a reduction in the percentage of thymic T_{regs} relative to *Aire*$^{+/+}$ hosts, consistent with previous reports (*15*, *18*), but were not characterized by a complete deficiency of polyclonal T_{regs} (Fig. 4, A and C). Despite the lack of MJ23tg T_{reg} development, mature CD4$^+$Foxp3^{neg} MJ23tg T cells developed in *Aire*$^{-/-}$ hosts (Fig. 4A and fig. S13), indicating that T cells of this specificity are not dependent on Aire for their positive selection into the CD4$^+$ lineage. This result also suggests that the thymic development of T_{regs} reactive to an Aire-dependent antigen may require both the recognition of self peptide/major histocompatibility complex (MHC) ligands for positive selection and the recognition of an additional Aire-dependent antigen for commitment to the T_{reg} lineage. Similar experiments using a second naturally occurring tumor-infiltrating T_{reg} TCR, termed RT83, demonstrated that Aire is required for the thymic development of RT83tg T_{regs} (Fig. 4D and fig. S14). Thus, our data demonstrate that Aire is critical for the thymic development of multiple naturally occurring T_{reg} specificities. These findings are consistent with a model in which the Aire-mediated expression of peripheral tissue-restricted antigens by thymic epithelial cells drives the development of a subset of tissue-specific or organ-specific T_{regs} (*19*).

Although there is substantial evidence demonstrating that Aire plays a critical role in the deletion of autoreactive thymocytes reactive to peripheral tissue antigens (*15*, *20*–*22*), a definitive role for Aire in the thymic selection of naturally occurring T_{regs} has not been previously established. Here, we provide direct evidence that Aire is critical for the thymic development of T_{regs} of naturally arising specificities. Thus, the integration of available evidence suggests a dual role for Aire in the maintenance of immune tolerance, in which Aire drives both the deletion of autoreactive T cells and the development of a subset of Foxp3$^+$ T_{regs}.

Our data support a model in which a tumor does not drive the de novo conversion of tumor-specific CD4$^+$ effector T cells into induced Foxp3$^+$ T_{regs} but instead recruits preexisting thymic-derived T_{regs} reactive to Aire-dependent self antigens associated with the organ of cancer origin. Thus, a developing neoplasm coopts endogenous mechanisms that have evolved to preserve the integrity of the host by maintaining organ-specific immune tolerance.

References and Notes

1. S. Z. Josefowicz, L. F. Lu, A. Y. Rudensky, *Annu. Rev. Immunol.* **30**, 531 (2012).
2. M. D. Vesely, M. H. Kershaw, R. D. Schreiber, M. J. Smyth, *Annu. Rev. Immunol.* **29**, 235 (2011).
3. R. J. deLeeuw, S. E. Kost, J. A. Kakal, B. H. Nelson, *Clin. Cancer Res.* **18**, 3022 (2012).
4. N. M. Greenberg *et al.*, *Proc. Natl. Acad. Sci. U.S.A.* **92**, 3439 (1995).
5. J. R. Gingrich, R. J. Barrios, B. A. Foster, N. M. Greenberg, *Prostate Cancer Prostatic Dis.* **2**, 70 (1999).
6. J. D. Fontenot *et al.*, *Immunity* **22**, 329 (2005).
7. J. Wong, D. Mathis, C. Benoist, *J. Exp. Med.* **204**, 2039 (2007).
8. J. Wong *et al.*, *J. Immunol.* **178**, 7032 (2007).
9. C. S. Hsieh, Y. Zheng, Y. Liang, J. D. Fontenot, A. Y. Rudensky, *Nat. Immunol.* **7**, 401 (2006).
10. S. K. Lathrop, N. A. Santacruz, D. Pham, J. Luo, C. S. Hsieh, *J. Exp. Med.* **205**, 3105 (2008).
11. A. E. Magurran, *Ecological Diversity and Its Measurement* (Princeton Univ. Press, Princeton, NJ, 1988).
12. M. J. Barnden, J. Allison, W. R. Heath, F. R. Carbone, *Immunol. Cell Biol.* **76**, 34 (1998).
13. J. L. Bautista *et al.*, *Nat. Immunol.* **10**, 610 (2009).
14. M. W. Leung, S. Shen, J. J. Lafaille, *J. Exp. Med.* **206**, 2121 (2009).
15. M. S. Anderson *et al.*, *Immunity* **23**, 227 (2005).
16. M. S. Anderson *et al.*, *Science* **298**, 1395 (2002).
17. D. Mathis, C. Benoist, *Annu. Rev. Immunol.* **27**, 287 (2009).
18. Y. Lei *et al.*, *J. Exp. Med.* **208**, 383 (2011).
19. K. Aschenbrenner *et al.*, *Nat. Immunol.* **8**, 351 (2007).
20. A. Liston, S. Lesage, J. Wilson, L. Peltonen, C. C. Goodnow, *Nat. Immunol.* **4**, 350 (2003).
21. R. T. Taniguchi *et al.*, *Proc. Natl. Acad. Sci. U.S.A.* **109**, 7847 (2012).
22. J. DeVoss *et al.*, *J. Exp. Med.* **203**, 2727 (2006).
23. V. Kouskoff, K. Signorelli, C. Benoist, D. Mathis, *J. Immunol. Methods* **180**, 273 (1995).
24. Materials and methods are available as supplementary materials on *Science* Online.

Acknowledgments: We thank A. Bendelac, T. Gajewski, R. Gottschalk, and S. Quezada for critical reading of the manuscript; A. Rudensky for Foxp3^{gfp} reporter mice (*6*); C. Benoist for cassette vectors for TCRα and TCRβ transgenic mice (*23*); L. Degenstein for transgenic mouse production; and A. Thomas and N.-L. Yin for deep TCR sequence analysis. The data presented in this manuscript are tabulated in the main paper and in the supplementary materials. This work was partially funded by the following sources (to P.A.S.): R01 (1R01CA160371-01), a Cancer Research Institute Investigator Award, a Cancer Research Foundation Young Investigator Award, an American Cancer Society Institutional Research Grant (IRG-58-004), and the University of Chicago Comprehensive Cancer Center (including Support Grant P30 CA14599). N.D.S. was supported by MSKCC Comprehensive Cancer Center (Support Grant P30 CA008748). J.P.A. was supported by funding from the Howard Hughes Medical Institute.

Supplementary Materials

www.sciencemag.org/cgi/content/full/339/6124/1219/DC1
Materials and Methods
Supplementary Text
Figs. S1 to S14
Table S1
References (*25*–*28*)

11 December 2012; accepted 16 January 2013
10.1126/science.1233913

BENCHTOP CENTRIFUGES

The new range of compact, benchtop centrifuges is ideally suited to most essential applications in life-science laboratories. The models available are designed to suit all applications and budgets and include the important features and benefits of a robust sealed housing, fully programmable microprocessor control, smooth, brushless motors, and near silent running. They are also fitted with a lid lock to prevent accidental opening during operation, while the inner bowl is a self-contained unit designed for easy wipe-down and disinfection should a breakage or spillage occur. The entry level MC-5000 model is a low-speed (max 5,000 rpm) option, which is available with or without a 'load auto-balance' function. At the other end of the scale is the more sophisticated MC16000R model which is ideal for most molecular biological laboratories for use in cell separation and DNA applications.

Medline Scientific

For info: +44-(0)-1865-400321 | www.medlinescientific.com

BOTTLETOP DISPENSERS

The new 0.2–2 mL size of Brand Seripettor and Seripettor Pro bottle-top dispensers join the previously available 1–10 mL and 2.5–25 mL sizes. These durable, yet economical dispensers are a great choice for laboratories that do not need all of the convenience features of a Dispensette. An inexpensive replaceable wiping seal dispensing cartridge renews the wearing parts for long life. One extra cartridge is included with the dispenser.

BrandTech Scientific

For info: 888-522-2726 | www.brandtech.com

LIGHT-SENSITIVE SAMPLE STORAGE

A new range of black screw-top centrifuge tubes provides secure storage of light sensitive materials. Manufactured from black, RNAse/DNase-free polypropylene, the tubes are fully resistant to most organic solvents, can be autoclaved, and enable high integrity storage of samples and reagents down to -80°C. Available initially in 15 mL and 50 mL sizes, the black centrifuge tubes are supplied sterile and include a recessed HDPE lid that prevents leakage. Each tube includes a frosted area to enable marking for easy identification.

Asynt

For info: +44-(0)-1638-781709 | www.asynt.com

MICROPLATE DATA ACQUISITION AND ANALYSIS SOFTWARE

SoftMax Pro 6 GxP Software is designed for data acquisition and analysis from microplate readers in regulated environments. The software supports the SpectraMax Paradigm Multi-Mode Detection Platform and FilterMax F3/F5 Microplate Readers. SoftMax Pro 6 GxP Software facilitates easy upgrades for existing users from previous software versions with its unique "plug-in" feature that allows existing databases to be integrated without the need to reestablish and revalidate the whole system. A custom-designed validation package supports the software such as printable IQ-OQ worksheets, extensive tests for data analysis features, easy-to-follow instructions, and ready-to-use sample data to streamline the software validation process making it easy and fast to validate this powerful data analysis tool. The new software package also incorporates editors to enable easy creation of intricate protocols, such as the Syntax Helper formula writing tool, and a robust data analysis package with over 15 curve fits, effectively eliminating the need for additional software purchase and validation.

Molecular Devices

For info: 800-635-5577 | www.moleculardevices.com

HIGH-INTENSITY UV VIEWING CABINETS

Spectroline CX-20 and CX-21 high-intensity ultraviolet (UV) viewing cabinets guarantee maximum UV irradiance and fluorescent contrast because they are designed for peak efficiency. The CX-20 and CX-21 cabinets combine separate long-wave and short-wave 8-watt UV light sources with uniquely designed specular aluminum reflectors to assure maximum intensity and exceptional fluorescent contrast. Both units have removable bottom panels so they can be easily placed over large objects or, to provide greater illumination, over a Spectroline UV transilluminator. The cabinets' housings are made of vinyl-clad aluminum for maximum durability. The flexible, contoured viewing eyepiece has a UV-absorbing window for comfort and safety. The window also eliminates "blue haze" interference and increases contrast between the fluorescent area and the background. Loading and unloading plates and gels is simple. Soft rubber curtains on both sides of the CX-20 allow easy entrance to its interior.

Spectroline

For info: 800-274-8888 | www.spectroline.com

CLONING KIT

The Gibson Assembly Cloning Kit and online primer design tool, NEBuilder, is designed for the cloning of DNA fragments using the Gibson Assembly approach. This kit includes NEB's robust Gibson Assembly Master Mix and NEB 5-alpha competent *E. coli* for fragment assembly and transformation in less than two hours. Gibson Assembly enables the rapid assembly of multiple DNA fragments using a one-step, isothermal reaction. The Gibson Assembly Cloning Kit includes protocols for primer design, and has been optimized for the assembly of one or more DNA fragments into a linearized vector. Alongside this new kit, NEB has also developed NEBuilder, an online primer design tool, specifically for use in Gibson Assembly.

New England Biolabs

For info: 800-632-5227 | www.nebgibson.com

Electronically submit your new product description or product literature information! Go to **www.sciencemag.org/products/newproducts.dtl** for more information.

Newly offered instrumentation, apparatus, and laboratory materials of interest to researchers in all disciplines in academic, industrial, and governmental organizations are featured in this space. Emphasis is given to purpose, chief characteristics, and availability of products and materials. Endorsement by *Science* or AAAS of any products or materials mentioned is not implied. Additional information may be obtained from the manufacturer or supplier.

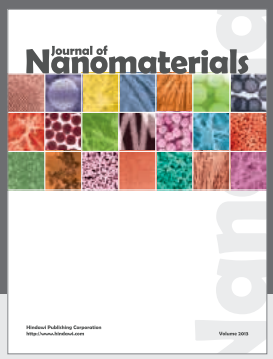

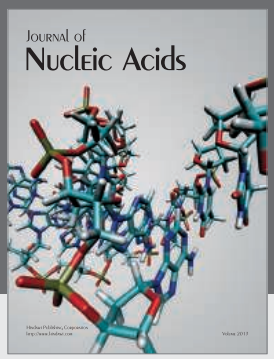

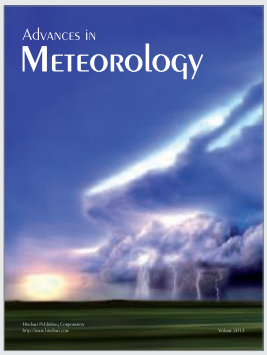

Hindawi

Submit your manuscripts at
http://www.hindawi.com

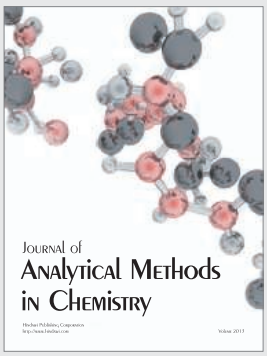

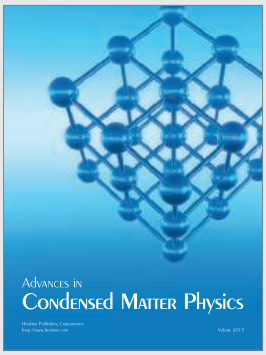

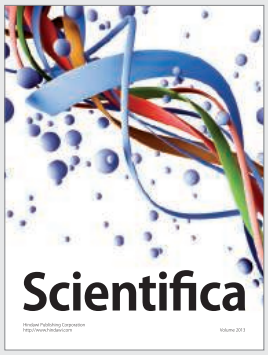

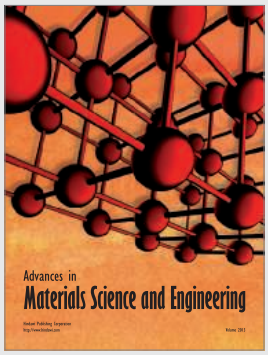

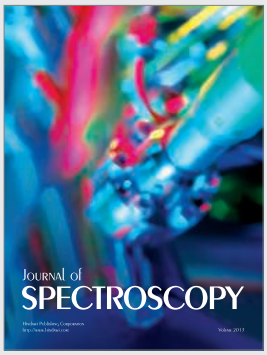

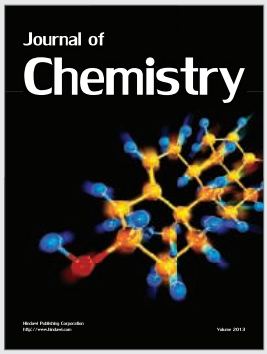

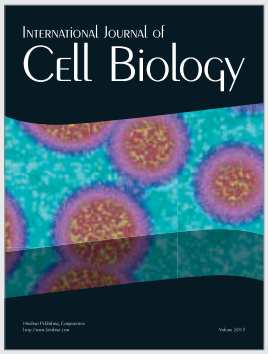

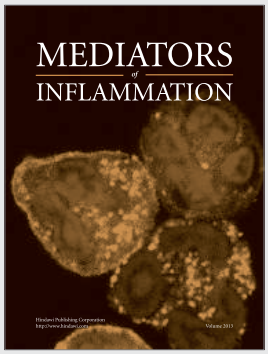

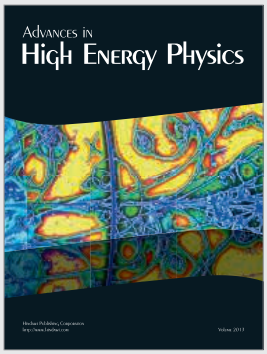

cell sciences®

cytokine center

Browse our web site of recombinant proteins, including cytokines, growth factors, chemokines and neurotrophins. Daily shipping and competitive pricing are offered. Bulk quantities of many proteins available. Cell Sciences also carries corresponding antibodies and ELISA kits.

www.cellsciences.com

LIST OF PROTEINS

4-1BBL
4-1BB Receptor
6 Ckine
ACAD8
ACAT2
gAcrp30/Adipolean
Activin A
ACY1
ADAT1
Adiponectin
ADRP
AITRL
Akt1
Alpha-Feto Protein (AFP)
Alpha-Galactosidase A
Angiopoietin-1 (Ang-1)
Angiopoietin-2 (Ang-2)
Angiostatin K1-3
Annexin-V
apo-SAA
Apoliprotein A-1
Apoliprotein E2
Apoliprotein E3
Apoliprotein E4
APRIL
Artemin
ATF2
Aurora A
Aurora B
BAFF
BAFF Receptor
BCA-1 / BLC / CXCL13
BCMA
BD-1
BD-2
BD-3
BDNF
Bivalirudin
BMP-2
BMP-4
BMP-7
BMP-13
sBMPR-1A
Brain Natriuretic Protein
BRAK
Breast Tumor Antigen
C5a
C5L2 Peptide
C-10
C-Reactive Protein
C-Src
Calbindin D-9K
Calbindin D-28K
Calbindin D-29K
Calmodulin
Calcitonin Acetate
Carbonic Anhydrase III
Carcino-embryonic Antigen
Cardiotrophin-1
Caspase-3
Caspase-6
CD4
CD14
CD22
CD40 Ligand / TRAP
CD95 / sFas Ligand
CD105 / Endoglin
CHIPS
CNTF
Collagen
CREB
CTACK/CCL27
CTGF
CTGFL/WISP-2
CTLA-4/Fc
CXCL16
Cytokeratin 8
DEP-1
Desmopressin
Disulfide Oxidoreductase
E-selectin
ECGF
EGF
Elafin/SKALP
EMAP-II
ENA-78
Endostatin
Enteropeptidase
Eotaxin
Eotaxin-2
Eotaxin-3 (TSC)
EPHB2
EPHB4
Eptifbatide
Erk-2
Erythropoietin (EPO)
Exodus-2
Fas Ligand
Fas Receptor
FGF-1 (acidic)
FGF-2 (basic)
FGF-4
FGF-5
FGF-6
FGF-7/ KGF
FGF-8
FGF-9
FGF-10
FGF-16
FGF-17
FGF-18
FGF-19
FGF-20
sFGFR-1 (IIIc) / Fc Chimera
sFGFR-2 (IIIc) / Fc Chimera
sFGFR-3 / Fc Chimera
sFGFR-4 / Fc Chimera
sFlt-1 (native)
sFlt-1 (D3)
sFlt-1 (D4)
sFlt-1 (D5)
sFlt-1 (D7)
Flt3-Ligand
sFlt-4
sFlt-4/ Fc Chimera
Follistatin
FSH
Fractalkine/ CX3C
G-CSF
α-Galactosidase A
Galectin-1
Galectin-3
Gastrointestinal CA
GCP-2
GDF-3
GDF-9
GDF-11
GDNF
GLP-1
Glucagon
Goserelin
GM-CSF
GPBB
GROα
GROβ
GROγ
GRO/MGSA
Growth Hormone
Growth Hormone BP
GST-p21/WAF-1
HB-EGF
HCC-1
HGF
Histdyl-tRNA synthetase
Histrelin
HRG1-β1
I-309
I-TAC
IFN-α
IFN-α A
IFN-α 2a
IFN-α 2b
IFN-β
IFN-γ
IFN-Omega
IGF-I
IGF-II
proIGF-II
IGFBP-1
IGFBP-2
IGFBP-3
IGFBP-4
IGFBP-4
IGFBP-5
IGFBP-6
IGFBP-7
IL-1α
IL-1β
IL-2
IL-3
IL-4
sIL-4 Receptor
IL-5
IL-6
sIL-6 Receptor
IL-7
IL-8 (72 a.a.)
IL-8 (77 a.a.)
IL-9
IL-10
IL-11
IL-12
IL-13
IL-13 analog
IL-15
IL-16 (121 a.a.)
IL-16 (130 a.a.)
IL-17
IL-17B
IL-17D
IL-17E
IL-17F
IL-19
IL-20
IL-22
IL-31
Insulin
IP-10
JE
JNK2a1
JNK2a2
KC / CXCL1
KGF
L-asparaginase
LAG-1
LALF Peptide
LAR-PTP
LC-1
LBP
LD-78β
LDH
LEC/NCC-4
Leptin
LIGHT
LIX
LKM
LL-37
Lymphotactin
sLYVE-1
M-CSF
MCP-1 (MCAF)
MCP-2
MCP-3
MCP-4
MCP-5
MDC (67 a.a.)
MDC (69 a.a.)
MDH
MEC
Mek-1
MIA
Midkine
MIG / CXCL9
MIP-1α / CCL3
MIP-1β / CCL4
MIP-3 / CCL23
MIP-3α / CCL20
MIP-3β / CCL19
MIP-4 (PARC) / CCL18
MIP-5 / CCL15
MMP-3
MMP-7
MMP-13
Myostatin
Nanog
NAP-2
Neurturin
NFAT-1
beta-NGF
NOGGIN
NOV
NP-1
NT-1/BCSF-3
NT-3
NT-4
Ocreotide
Oncostatin M
Osteoprotegerin (OPG)
OTOR
Oxytocin
p38-α
Parathyroid Hormone
PDGF-AA
PDGF-AB
PDGF-BB
Persephin
PF-4
PIGF-1
PIGF-2
PKA α-subunit
PKC-α
PKC-γ
Pleiotrophin
PLGF-1
Polymyxin B (PMB)
PRAS40
PRL-1
PRL-2
PRL-3
Prokineticin-2
Prolactin
Protirelin
PTHrP
PTP1B
PTP-IA2
PTP-MEG2
PTP-PEST
sRANK
sRANKL
RANTES
RELM-α
RELM-β
Resistin
RPTPβ
RPTPγ
RPTPμ
SCF
SCGF-α
SCGF-β
SDF-1α
SDF-1β
Secretin
SF20
SHP-2
STAT1
c-Src
TACI
TARC
TC-PTP
TECK
TFF2
TGF-α
TGF-β1
TGF-β2
TGF-β3
Thymosin α1
sTIE-1/Fc Chimera
sTIE-2/Fc Chimera
TL-1A
TNF-α
TNF-β
sTNFR1
sTNFR2
TPO
TRAIL/Apo2L
sTRAIL R-1 (DR4)
sTRAIL R-2 (DR5)
TSH
TSLP
TWEAK
TWEAK Receptor
Urokinase
VEGF121
VEGF145
VEGF165
VEGF-C
VEGF-C I525
EG-VEGF
VEGF-E
HB-VEGF-E
sVEGFR-1
sVEGFR-2
sVEGFR-3
WISP-1
WISP-2
WISP-3
WNT-1

CELL SCIENCES INC • 480 NEPONSET STREET, BUILDING 12A, CANTON, MA 02021 • INFO@CELLSCIENCES.COM

TOLL FREE: (888) 769-1246 • TEL: (781) 828-0610 • FAX: (781) 828-0542 • WEB: WWW.CELLSCIENCES.COM

NEW ENGLAND BioLabs® Inc.
enabling technologies in the life sciences

Make ends meet.

Gibson Assembly™ Cloning Kit

New England Biolabs has revolutionized your laboratory's standard cloning methodology. The Gibson Assembly Cloning Kit combines the power of the Gibson Assembly Master Mix with NEB 5-alpha Competent *E. coli*, enabling fragment assembly and transformation in just under two hours. Save time, without sacrificing efficiency.

Making ends meet is now quicker and easier than ever before, with the Gibson Assembly Cloning Kit from NEB.

Gibson Assembly Cloning Kit provides robust transformation efficiencies

Assembly reactions containing 25 ng of linear pUC19 vector and 0.04 pmol of each fragment were performed following individual suppliers' recommended protocols and using the competent cells provided with the kit. The total number of recombinant colonies was calculated per 25 ng of linear pUC19 vector added to the assembly reaction.

NEBuilder™ for Gibson Assembly

Visit **NEBGibson.com** to view the latest tutorials and to try our primer design tool.

IN-FUSION® is a registered trademark of Clontech Laboratories, Inc.
GENEART® is a registered trademark of Life Technologies, Inc.
GIBSON ASSEMBLY™ is a trademark of Synthetic Genomics, Inc.

SYNTHETIC GENOMICS®

Some components of this product are manufactured by New England Biolabs, Inc. under license from Synthetic Genomics, Inc.

sysmex

Accelerate drug discovery

Prospective Protein Provider

ProCube

A new solution offering the speed, quality, and flexibility to transform protein production.

If you need to produce a variety of proteins efficiently in a short period of time, ProCube offers a total solution.
Designed to meet the rigorous demands of laboratory testing,
from gene construction to protein expression, refining and immobilization,
ProCube brings speed, quality, and flexibility to your drug discovery and development project.

http://procube.sysmex.co.jp

Sysmex Corporation

LightCycler®

Reveal Your qPCR Super Powers!

Introducing the LightCycler® 96 Real-Time PCR System

Price: $28,900 US

- **Innovative optics for accurate results**
  Simultaneously capture 96 wells of data for maximum well-to-well consistency.
- **Intuitive touchscreen interface and powerful data analysis software**
  Speed time to results with an advanced yet easy-to-use system designed for both novices and experienced users.
- **Built on 14 years of real-time PCR excellence**
  Rely on Roche's expertise in providing fast, flexible, and accurate real-time PCR systems that enable research breakthroughs.

Become a qPCR Superhero with the NEW LightCycler® 96 Real-Time PCR System from Roche! See the video at *www.lightcycler96.com*

Contact your Roche representative or call **800 262 1640** for more information.

For life science research only.
Not for use in diagnostic procedures.

LIGHTCYCLER is a trademark of Roche.

Roche Diagnostics Corporation
Roche Applied Science
Indianapolis, Indiana

Roche

© 2013 Roche Diagnostics.
All rights reserved.

What — You *Don't* Dip and Read™?!

Do less and get more from your ELISAs

- Quantitate 96 protein samples in 15 minutes, not hours
- Take advantage of a 4-log dynamic range and dilute less
- Run automated assays without wash steps or overnight incubations
- Analyze crude samples with less prep
- Get information-rich direct binding data, not end-point results
- Develop new assays in a few hours, not weeks

The Octet® Platform

Octet Systems with Dip and Read assays.
No hassle, label-free ELISAs.

fortéBIO®
A Division of **Pall Life Sciences**

PALL® Life Sciences

www.fortebio.com • 1.888.OCTET-75

Fast. Accurate. EASY.

if you are looking for research funding, apply today.

If your work is in need of funding, today - maybe the two of us should meet. **Please go to www.lls.org to find out more.**

someday is today

LEUKEMIA & LYMPHOMA SOCIETY®
fighting blood cancers

When it comes to scan rates, the faster the better.

Think again!

Thermo Scientific Q Exactive identified more low abundance proteins than QTOF.

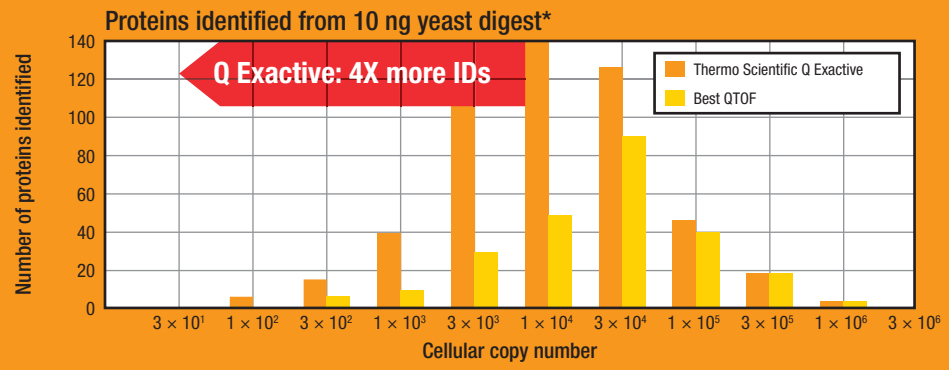

Exactive Plus LC-MS

Q Exactive LC-MS/MS

LTQ Orbitrap XL Hybrid FTMS

Orbitrap Velos Pro Hybrid MS

Orbitrap Elite Hybrid MS

Some manufacturers will try to convince you that you need to scan as fast as possible to obtain the most data from complex mixtures. The reality? Very fast scanning often leads to poor data quality. **Thermo Scientific™ Orbitrap™ mass spectrometers** deliver the highest effective scan rate for consistent, high quality spectra to access low-abundance proteins, making them the most desirable choice for complex samples. Learn about Orbitrap productivity and see how much more you can discover.

• visit haste makes waste at thermoscientific.com/scanspeed

* Hao Z, Zhang Y, Eliuk S, Blethrow J, Horn D, Zabrouskov V, Kellmann M, and Huhmer A. A Quadrupole-Orbitrap Hybrid Mass Spectrometer Offers Highest Benchtop Performance for In-Depth Analysis of Complex Proteomes; Thermo Scientific Application Note 552; April 2012.

Thermo SCIENTIFIC

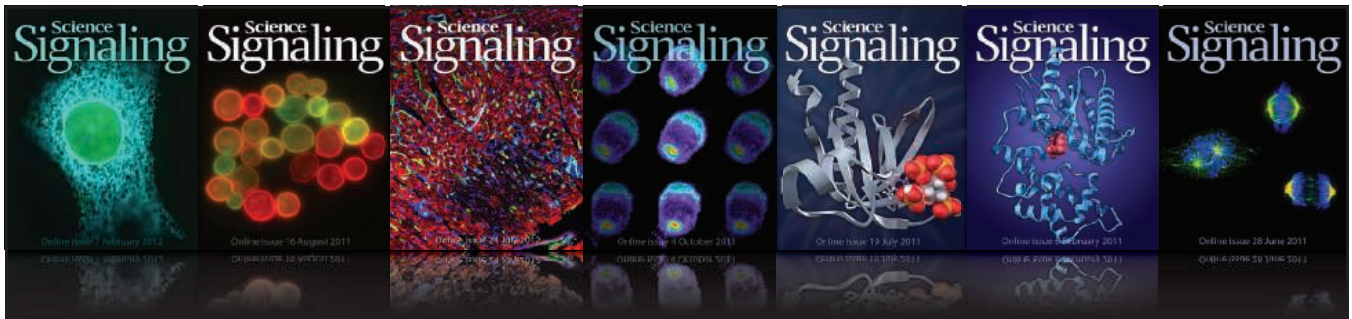

Science Signaling

The Leading Journal of Cell Signaling

- Peer-reviewed Research Articles and Resources
- Perspectives, Reviews, Protocols, and an interactive Database of Cell Signaling
- Recommend *Science Signaling* to your institution's library
  ScienceSignaling.org/recommend

ScienceSignaling.org

Focus on Careers
Postdocs

Produced by the *Science*/AAAS Custom Publishing Office

Opportunity Knocks:
But Which Door Should You Open?

In This Issue

Game-changing career opportunities for postdocs are everywhere. Whether it is a paper to write, a fellowship to chase, or an informal conversation to have, any opportunity could be "the one"—the one that grants you access to a satisfying job, a prolific alliance, or a novel research insight. After you network, go to the right conferences, have coffee with the right people, and apply for several appointments, how do you pick which avenues to pursue?

See the full story on page 1228.

Upcoming Features

Regional Focus: Germany—March 22

Cancer Research Careers:
Academia vs. Industry—March 29

Biotech and Pharma: Forging
Academic Collaborations—April 12

AAAS *Travels*

MONGOLIA
July 5-19, 2013
Genghis Khan to the Gobi Desert

Discover the expansive landscapes and the proud heritage of Mongolia. Explore the Orkhon Valley Cultural Landscape, the Gun-Galuut Nature Reserve, and Gobi Desert, site of the Flaming Cliffs dinosaur site. Horse racing, archery, and other activities of the Naadam Festival will be a treat! $3,995 + air.

For a detailed brochure, please call (800) 252-4910
All prices are per person twin share + air

BETCHART EXPEDITIONS Inc.
17050 Montebello Rd, Cupertino, CA 95014
Email: AAASInfo@betchartexpeditions.com
www.betchartexpeditions.com

eppendorf & Science

PRIZE FOR NEURO BIOLOGY

2012 Winner
Dr. Marlene R. Cohen
Assistant Professor
University of Pittsburgh

Application Deadline
June 15, 2013

Call for Entries

Eppendorf & Science Prize for Neurobiology
The annual Eppendorf & Science Prize for Neurobiology, an international award, honors young scientists for their outstanding contributions to neurobiological research. The winner and finalists are selected by a committee of independent scientists, chaired by Science's Senior Editor, Dr. Peter Stern. To be eligible, you must be 35 years of age or younger.

You could be next to win this prize and to receive
> Prize money of US$25,000
> Publication of your work in Science
> Full support to attend the Prize Ceremony held in conjunction with the Annual Meeting of the Society for Neuroscience in the USA
> An invitation to visit Eppendorf in Hamburg, Germany

It's easy to apply!

Learn more at: www.eppendorf.com/prize

eppendorf Science AAAS

eppendorf® and the eppendorf Logo are registered trademarks of Eppendorf AG, Hamburg, Germany. All rights reserved, including graphics and images. Copyright © 2013 by Eppendorf AG.
AAAS® and Science® are registered trademarks of the American Society for the Advancement of Science, USA. Kurstin Roe Photography.

BENCHTOP CENTRIFUGES

The new range of compact, benchtop centrifuges is ideally suited to most essential applications in life-science laboratories. The models available are designed to suit all applications and budgets and include the important features and benefits of a robust sealed housing, fully programmable microprocessor control, smooth, brushless motors, and near silent running. They are also fitted with a lid lock to prevent accidental opening during operation, while the inner bowl is a self-contained unit designed for easy wipe-down and disinfection should a breakage or spillage occur. The entry level MC-5000 model is a low-speed (max 5,000 rpm) option, which is available with or without a 'load auto-balance' function. At the other end of the scale is the more sophisticated MC16000R model which is ideal for most molecular biological laboratories for use in cell separation and DNA applications.

Medline Scientific

For info: +44-(0)-1865-400321 | www.medlinescientific.com

BOTTLETOP DISPENSERS

The new 0.2–2 mL size of Brand Seripettor and Seripettor Pro bottle-top dispensers join the previously available 1–10 mL and 2.5–25 mL sizes. These durable, yet economical dispensers are a great choice for laboratories that do not need all of the convenience features of a Dispensette. An inexpensive replaceable wiping seal dispensing cartridge renews the wearing parts for long life. One extra cartridge is included with the dispenser.

BrandTech Scientific

For info: 888-522-2726 | www.brandtech.com

LIGHT-SENSITIVE SAMPLE STORAGE

A new range of black screw-top centrifuge tubes provides secure storage of light sensitive materials. Manufactured from black, RNAse/DNase-free polypropylene, the tubes are fully resistant to most organic solvents, can be autoclaved, and enable high integrity storage of samples and reagents down to -80°C. Available initially in 15 mL and 50 mL sizes, the black centrifuge tubes are supplied sterile and include a recessed HDPE lid that prevents leakage. Each tube includes a frosted area to enable marking for easy identification.

Asynt

For info: +44-(0)-1638-781709 | www.asynt.com

MICROPLATE DATA ACQUISITION AND ANALYSIS SOFTWARE

SoftMax Pro 6 GxP Software is designed for data acquisition and analysis from microplate readers in regulated environments. The software supports the SpectraMax Paradigm Multi-Mode Detection Platform and FilterMax F3/F5 Microplate Readers. SoftMax Pro 6 GxP Software facilitates easy upgrades for existing users from previous software versions with its unique "plug-in" feature that allows existing databases to be integrated without the need to reestablish and revalidate the whole system. A custom-designed validation package supports the software such as printable IQ-OQ worksheets, extensive tests for data analysis features, easy-to-follow instructions, and ready-to-use sample data to streamline the software validation process making it easy and fast to validate this powerful data analysis tool. The new software package also incorporates editors to enable easy creation of intricate protocols, such as the Syntax Helper formula writing tool, and a robust data analysis package with over 15 curve fits, effectively eliminating the need for additional software purchase and validation.

Molecular Devices

For info: 800-635-5577 | www.moleculardevices.com

HIGH-INTENSITY UV VIEWING CABINETS

Spectroline CX-20 and CX-21 high-intensity ultraviolet (UV) viewing cabinets guarantee maximum UV irradiance and fluorescent contrast because they are designed for peak efficiency. The CX-20 and CX-21 cabinets combine separate long-wave and short-wave 8-watt UV light sources with uniquely designed specular aluminum reflectors to assure maximum intensity and exceptional fluorescent contrast. Both units have removable bottom panels so they can be easily placed over large objects or, to provide greater illumination, over a Spectroline UV transilluminator. The cabinets' housings are made of vinyl-clad aluminum for maximum durability. The flexible, contoured viewing eyepiece has a UV-absorbing window for comfort and safety. The window also eliminates "blue haze" interference and increases contrast between the fluorescent area and the background. Loading and unloading plates and gels is simple. Soft rubber curtains on both sides of the CX-20 allow easy entrance to its interior.

Spectroline

For info: 800-274-8888 | www.spectroline.com

CLONING KIT

The Gibson Assembly Cloning Kit and online primer design tool, NEBuilder, is designed for the cloning of DNA fragments using the Gibson Assembly approach. This kit includes NEB's robust Gibson Assembly Master Mix and NEB 5-alpha competent *E. coli* for fragment assembly and transformation in less than two hours. Gibson Assembly enables the rapid assembly of multiple DNA fragments using a one-step, isothermal reaction. The Gibson Assembly Cloning Kit includes protocols for primer design, and has been optimized for the assembly of one or more DNA fragments into a linearized vector. Alongside this new kit, NEB has also developed NEBuilder, an online primer design tool, specifically for use in Gibson Assembly.

New England Biolabs

For info: 800-632-5227 | www.nebgibson.com

Electronically submit your new product description or product literature information! Go to **www.sciencemag.org/products/newproducts.dtl** for more information.

Newly offered instrumentation, apparatus, and laboratory materials of interest to researchers in all disciplines in academic, industrial, and governmental organizations are featured in this space. Emphasis is given to purpose, chief characteristics, and availability of products and materials. Endorsement by *Science* or AAAS of any products or materials mentioned is not implied. Additional information may be obtained from the manufacturer or supplier.

STAY INFORMED! STAY CONNECTED!

Get more from your AAAS membership

Are you currently registered to receive e-mails from AAAS and *Science*?

E-mail is the primary way that AAAS communicates with our members about AAAS programs, new member benefits, invitations to special events, and, of course, the latest news and research being published in *Science*.

Sign up today to receive e-mails from AAAS and ensure that you are getting the most out of your membership and *Science* subscription.*

To get started visit: **promo.aaas.org/stayconnected**
You'll need your AAAS Member number. Find it above your name on your *Science* mailing label.

Don't miss a thing. Sign up for e-mail communications from AAAS today!

Science AAAS

*AAAS follows CAN-SPAM and European Safe Harbor guidelines for protecting your privacy. We will never sell your e-mail address and you can opt-out of receiving e-mails at any time.

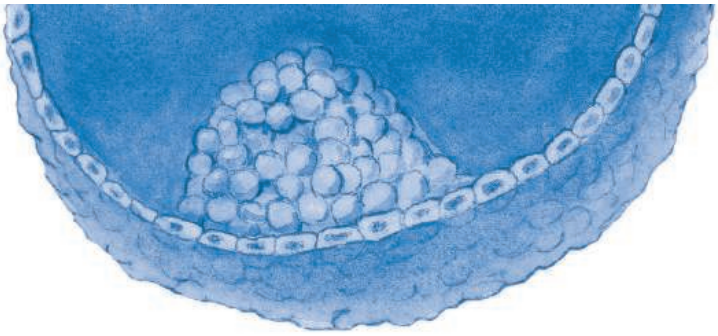

More differentiation
With less variation

- ✓ **Defined Culture Matrix & Specialized Media**
  to reduce cell culture variability
- ✓ **Premium Quality Cytokines & Growth Factors**
  to obtain consistent expansion & differentiation results
- ✓ **High Performance Antibodies**
  to assess differentiation mechanisms & markers

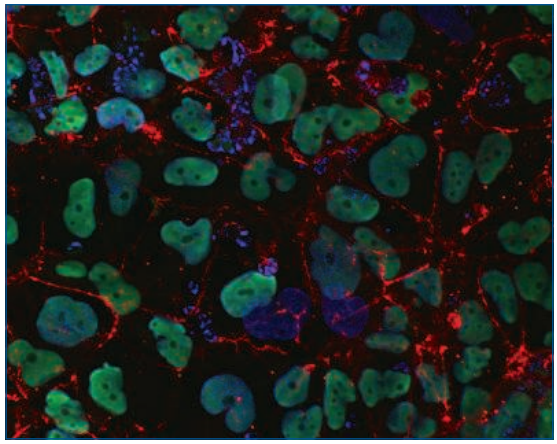

SOX17 (green) & Claudin-6 (red) in iPS2 human induced pluripotent stem cells differentiated to definitive endoderm using R&D Systems Recombinant Human Activin A & Wnt-3a.

Increase the Probability of Experimental Consistency & Success

www.RnDSystems.com/StemCells

Stem cell experiments require significant time, effort, and funding. The use of low quality or undefined reagents can introduce unwanted experimental variability that can compromise the validity of new data and question previous conclusions. To increase the probability of experimental consistency and success, R&D Systems manufactures premium quality reagents for stem cell culture, expansion, and differentiation.

R&D SYSTEMS®

For research use only. Not for use in diagnostic procedures.

There's only one

Science Careers Advertising

For full advertising details, go to ScienceCareers.org and click For Employers, or call one of our representatives.

Tracy Holmes
Worldwide Associate Director
Science Careers
Phone: +44 (0) 1223 326525

THE AMERICAS

E-mail: advertise@sciencecareers.org
Fax: 202-289-6742

Tina Burks
United States/Canada/South America
Phone: 202-326-6577

Marci Gallun
Sales Administrator
Phone: 202-326-6582

Online Job Posting Questions
Phone: 202-312-6375

EUROPE / INDIA / AUSTRALIA / NEW ZEALAND / REST OF WORLD

E-mail: ads@science-int.co.uk
Fax: +44 (0) 1223 326532

Lucy Nelson
Phone: +44 (0)1223 326527

Kelly Grace
Phone: +44 (0) 1223 326528

JAPAN

Yuri Kobayashi
Phone: +81-(0)90-9110-1719
E-mail: ykobayas@aaas.org

CHINA / KOREA / SINGAPORE / TAIWAN / THAILAND

Ruolei Wu
Phone: +86-1367-1015-294
E-mail: rwu@aaas.org

All ads submitted for publication must comply with applicable U.S. and non-U.S. laws. *Science* reserves the right to refuse any advertisement at its sole discretion for any reason, including without limitation for offensive language or inappropriate content, and all advertising is subject to publisher approval. *Science* encourages our readers to alert us to any ads that they feel may be discriminatory or offensive.

Science Careers
From the journal *Science* AAAS

ScienceCareers.org

Stony Brook University

POSTDOCTORAL POSITIONS

Stony Brook anticipates the following postdoctoral positions being available

• BIOCHEMISTRY AND CELL BIOLOGY

Structural biology of macromolecular complexes by crio-EM and X-ray crystallography
Dr. Huilin Li, WC-R-7758-13-02-S

• GEOSCIENCE

Theoretical and computational crystallography, mineral physics and materials design
Dr. Artem Oganov, WC-S-7763-13-02-S

• MOLECULAR GENETICS

The role of lipids in infectious disease
Dr. Maurizio Del Poeta, HS-R-7757-13-02-S

• NEUROBIOLOGY AND BEHAVIOR

Motoneuron Physiology and Plasticity
Dr. William Collins, WC-R-7723-13-02-S

Cortical processing of chemosensory information and reward
Dr. Alfredo Fontanini, WC-R-7729-13-02-S

Molecular Mechanisms of Neuronal Phenotype control
Dr. Simon Halegoua, WC-R-7731-13-02-S

Glial function in Health and Disease
Dr. Joel Levine, WC-R-7722-13-02-S

Experience-dependent plasticity in cortical circuits
Dr. Arianna Maffei, WC-R-7730-13-02-S

Synaptic Mechanisms in the Retina
Dr. Gary Mathews, WC-R-7726-13-02-S

Functional Capacity of the Damaged Spinal Cord
Dr. Lorne Mendell, WC-R-7727-13-02-S

Electrophysiological and Optogenetic Studies of Central Cholinergic Circuits
Dr. Lorna Role, WC-R-7724-13-02-S

Developmental molecular cellular Neurobiology
Dr. Maya Shelly, WC-R-7765-13-02-S

Regulation of Neural Gene Expression
Dr. Howard Sirotkin, WC-R-7728-13-02-S

Molecular Structure of Glutamate Signaling
Dr. Lonnie Wollmuth, WC-R-7725-13-02-S

• PATHOLOGY

Stem cell development; generate/differentiate umbilical cord mesenchymal stem cell
Dr. Yupo Ma, WC-R-7767-13-02-S

• PHARMACOLOGICAL SCIENCES

Cancer, Lipid biology, diabetes, mitochondria, and neuropharmacology
Dr. Michael Frohman, HS-R-7766-13-02-S

Molecular toxicology, cancer, genomics
Dr. Arthur Grollman, HS-R-7760-13-02-S

Toxicology, Cancer, Genetic Association Testing, Mouse Models
Dr. Thomas Rosenquist, HS-R-7759-13-02-S

• PSYCHOLOGY

Postdoctoral fellow in developmental clinical cognitive neuroscience (ERP/fMRI) of depression
Dr. Greg Hajcak, WC-R-7783-13-02-S

To apply online and for information, visit *www.stonybrook.edu/jobs* under category "K" or mail résumés to:
Human Resource Services, 390 Administration Building
Stony Brook University, Stony Brook, NY 11794-0751

Stony Brook University/SUNY is an affirmative action, equal opportunity educator and employer.

Postdoc and research **opportunities** in Brazil

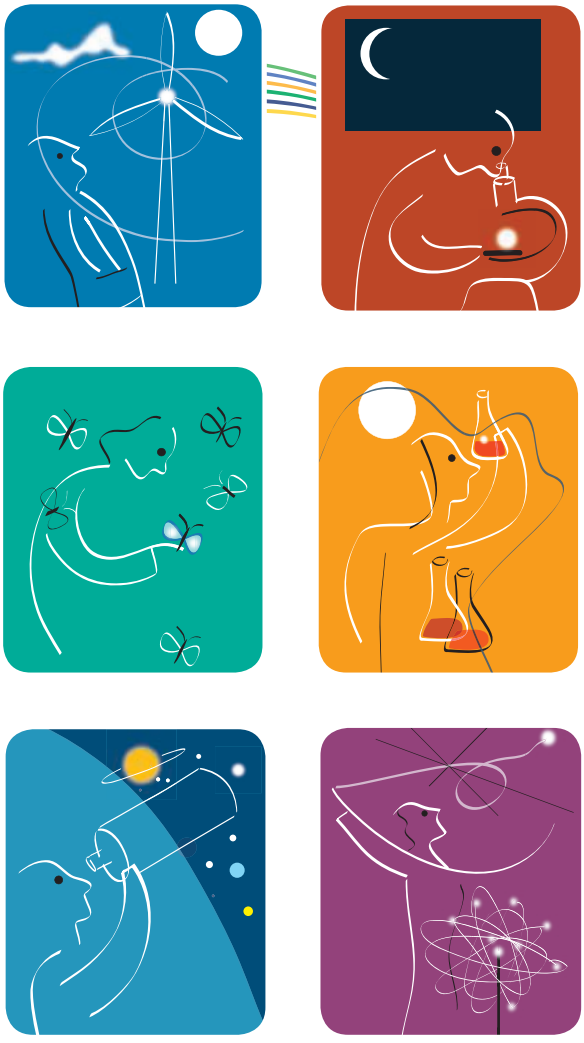

About us

Fifty percent of all science created in Brazil is produced in the State of São Paulo. The state hosts three of the most important Latin American universities: USP, UNICAMP and UNESP. Other universities and 19 research institutes are also located in São Paulo, among them the renowned Instituto Tecnológico de Aeronáutica (ITA), Instituto Nacional de Pesquisas Espaciais (INPE) and Laboratório Nacional de Luz Síncrotron, besides most of Brazilian Industrial P&D.

The São Paulo Research Foundation (FAPESP), one of the leading Brazilian agencies dedicated to the support of research, has ongoing programs and support mechanisms to bring researchers from abroad to excellence centers in São Paulo.

The **Young Investigators Awards** is part of FAPESP's strategy to strengthen the State research institutions, favoring the creation of new research groups. See more about it at www.fapesp.br/yia.

FAPESP **Post-Doctoral Fellowship** is aimed at distinguished researchers with a recent doctorate degree and a successful research track record. The fellowship enables the development of research within higher education and research institutions in São Paulo. Postdoc fellowships are available when calls for applications are issued internationally, or as individual fellowships requested on demand.

In the first case, positions are advertised at www.fapesp.br/oportunidades/ and candidates are selected through international competition. In the second, the proposal must represent an addition to a pre-existent research group and should be developed in association with faculty in higher education and research institutions in São Paulo. More information at www.fapesp.br/en/5427.

Location: São Paulo, SP, Brazil

Primary Contact Details:
Rua Pio XI, 1500 Alto da Lapa 05468-901
São Paulo, SP – Brazil
Phone: +55-11-3838-4000
URL: www.fapesp.br

Key Research Areas
Earth Sciences
Engineerings
Exact Sciences
Life Sciences
Physical Sciences
Social Sciences

FAPESP 50 YEARS

FAPESP
SÃO PAULO RESEARCH FOUNDATION

Opportunity Knocks: But Which Door Should You Open?

Game-changing career opportunities for postdocs are everywhere. Whether it is a paper to write, a fellowship to chase, or an informal conversation to have, any opportunity could be "the one"—the one that grants you access to a satisfying job, a prolific alliance, or a novel research insight. After you network, go to the right conferences, have coffee with the right people, and apply for several appointments, how do you pick which avenues to pursue?

By Alaina G. Levine

Matthew Wund

"It's never too late to think about and explore options that may make you really happy and excited to come into work every day."

Melanie Sinche

Shortly after receiving his Ph.D., **Lakshmi Reddi** ran into a researcher from South Korea while he was on route to the restroom. The scholar was visiting his department to give a talk in an area with seemingly very little connection to Reddi's expertise, but he cornered him nonetheless, because "as a doctoral student I had made it an issue to attend talks in areas other than mine and to cultivate learning from people who didn't speak the same language as I do," he recalls. That ad hoc assembly in the antechamber led to a discussion about innovative avenues to solving the engineering problems perplexing Reddi at the time. And later, it paved the way for a series of rich collaborations between Reddi and the visiting Korean engineer, resulting in multiple co-authored grants.

Reddi, now the dean of the graduate school at Florida International University, realized early on that "hundreds of opportunities that could connect my research to other areas" would have been lost if he had been only focused on his own day-to-day activities as a researcher and not on also keeping his eyes open to new opportunities. "It takes a new paradigm to cultivate this type of thinking," he admits. "Now I tell my students: don't think it's a time-intensive process—change your thinking about where the research opportunities are."

Keeping your options open to game-changers, whether they are opportunities to apply for fellowships, serve on committees, referee a journal paper, or just talk to someone in or out of your area of expertise, is a necessity if you want to advance in science. "The number one job of a postdoc is not to be a postdoc anymore," says **Matthew Wund,** assistant professor of biology at the College of New Jersey. And the output one generates from all the tasks required of a postdoc—research, publishing, and presenting at conferences—is only part of the equation that gets one ahead. It is "really stressful" to say no to any opportunity, whether it is as overtly concrete as a job offer to something more amorphous like engaging a visiting scholar, he concedes. "Who knows whether that conversation in a hallway could lead to a job?"

But how do you find balance? "The scariest thing about the postdoc is that you have to do all the work *and* get a job," concedes **Prosanta Chakrabarty,** assistant professor of biology and curator of ichthyology at Louisiana State University (LSU). And how do you know which opportunities to pursue and which to let go? At Argonne National Laboratory, which hosts 320 postdocs, "we try to emphasize that part of their job here is to get a job," says continued>

Upcoming Features

Regional Focus: Germany—March 22

Cancer Research Careers: Academia vs. Industry—March 29

Biotech and Pharma: Forging Academic Collaborations—April 12

CREDITS: (FROM TOP) © ISTOCKPHOTO.COM/ ; PHOTO: ANNA MAZZARELLA; PHOTO BY STEPHAN LIESKE

Accelerate your impact

Keep your world moving forward

EMERGING LEADERS IN SCIENCE

In the Emerging Leaders in Science (ELS) rotational program, you'll be immersed in a comprehensive, cross-functional experience with a world leader in agricultural biotechnology. You'll work with and be mentored by some of Monsanto's most talented scientific leaders – and emerge prepared to lead the way to agricultural innovation.

Monsanto's Emerging Leaders in Science (ELS) rotational program allows you to apply your research and leadership experience across our Global Technology (R&D) organization. The program consists of three, one-year rotational assignments within your selected strategic scientific focus area. Following successful completion of the three-year program, you'll be placed in a key role within Monsanto's Technology Organization.

For more details on the program and to apply visit:
monsanto.com/emergingleadersinscience

MONSANTO

Monsanto is an equal opportunity employer; we value a diverse combination of ideas, perspectives and cultures.
EEO/AA EMPLOYER M/F/D/V © 2013 Monsanto Company

Career Feature: March 29

Ads accepted until March 25 if space is still available.

This special feature looks at how academia and industry are more closely coordinating their research in the fight against cancer.

- Reach 700,000 readers worldwide
- Bonus distributions to the AACR Meeting and Career Fair, the ACS Meeting and the NSTA Meeting

To book your ad:
E-mail: advertise@sciencecareers.org
Or telephone us:
US: 202-326-6582
Europe/RoW: +44 (0) 1223 326500
Japan: +81-(0)-90-9110-1719
China/Korea/Singapore/Taiwan/Thailand: +86-1367-1015-294

Department of Health and Human Services
National Institutes of Health
National Institute on Aging

The National Institute on Aging (NIA), a major research component of the National Institutes of Health (NIH) and the Department of Health and Human Services (HHS), is recruiting postdoctoral fellows with interests in Alzheimer's disease (AD) and/or age-associated memory impairment (AAMI) in the Unit of Clinical and Translational Neuroscience, within the Laboratory of Behavioral Neuroscience.

This research represents an exciting new initiative within the NIA intramural research program (IRP) to enhance our understanding of disease mechanisms underlying risk factors for AD/AAMI, discover biologically relevant biomarkers that accurately reflect neuropathology and identify potential targets for effective disease modification/intervention. These studies combine multimodal neuroimaging methods to delineate changes in brain structure/function associated with risk factors for AD/AAMI (***for eg: Effect of complement CR1 on brain amyloid burden during aging and its modification by APOE genotype. Biol Psych. 2013, 73(5):422-428; Alzheimer risk variant CLU and brain function during aging. Biol Psych. 2013, 73(5):399-405***) and employ mass spectrometry-based proteomic/metabolomic techniques for the identification of biomarkers related to pathological endophenotypes associated with neurodegeneration (***for eg: Association of plasma clusterin concentration with severity, pathology, and progression in Alzheimer disease. Arch Gen Psychiatry. 2010, 67(7):739-48***). The research benefits from the unique and rich longitudinal dataset available in the Baltimore Longitudinal Study of Aging (BLSA) as well as complementary patient cohorts such as AddNeuroMed that are available as part of ongoing international collaborations (***for eg: Plasma biomarkers of brain atrophy in Alzheimer's disease. PLoS One. 2011;6(12):e28527***).

The successful candidate will have research interests in the related fields of neuroscience, human biology or cognition. Experience with analysis of neuropsychological or neuroimaging data, and/or biomarker identification with strong writing skills are desirable. Preference will be given to individuals who are able to work independently and within a team. Those with experience in structural MRI and/or PET imaging in humans will be preferred. Fellowship duration is typically 3-4 years. Candidates must have a Ph.D. in neuroscience/neuroimaging or M.D., with less than five years of postdoctoral research experience. The position is located in Baltimore, MD, a city with a stimulating scientific and cultural environment, with proximity to the Johns Hopkins medical campus. Salary is commensurate with experience and accomplishments.

To apply, please send curriculum vitae, a brief description of research interests, and three letters of reference to: **Madhav Thambisetty, MD, Ph.D., Unit of Clinical and Translational Neuroscience, Laboratory of Behavioral Neuroscience**, at **thambisettym@mail.nih.gov** or at **Biomedical Research Center, 251 Bayview Blvd, Suite 100, Room 4B317, Baltimore, MD 21224-6825**.

HHS and NIH are Equal Opportunity Employers.
The NIH is dedicated to building a diverse community in its training and employment programs.

Kristene Henne, postdoctoral programs coordinator. So pursuing other opportunities to progress is something that is promoted and encouraged. "Certain collaborative opportunities, even in the next lab, people might not be aware of without having conversations," she stresses.

But whether you consider opportunities before, during, or even after the postdoc, a strategic approach to selecting opportunities still needs to be part of your career planning process. "It's never too late to think about and explore options that may make you really happy and excited to come into work every day," says **Melanie Sinche,** director of the Faculty of Arts and Sciences Office of Postdoctoral Affairs at Harvard University.

"Know the skills that help you answer the interesting research questions. Have your top priorities in mind and seek to maximize learning opportunities. Everything else is details."

— Nadia Stegeman

Metrics for Opportunity Selection

Selecting opportunities doesn't have to be as rigorous a process as science itself, but it should involve proper planning, self-assessment, and awareness of available and needed resources, like money or time. **Christina Ragan,** a postdoc at Michigan State University, bases some of her strategy for choosing opportunities on how time-intensive they are. When she first began her appointment, she erroneously believed that she had lots of extra time because she wasn't taking any classes or teaching, so she sought out myriad outside opportunities to volunteer and network. "But that time gets sucked up so quickly," she says with a laugh. She realized that she needed to adjust her schedule considerably based on her immediate needs and responsibilities to conduct research and publish. As a result, Ragan now commits herself to only one outreach activity a semester, and has cut back on active networking for now as well. "As my career progresses, a different amount of time will be spent on different priorities," she says.

For any opportunity, **Eric Brown,** deputy group leader in the Physics Division of Los Alamos National Laboratory, advises weighing "the potential return on investment (ROI) versus the time you would put in and whether you've done something that can achieve this goal in a different way." An example of a respectable investment of time would be while you are at a conference, attend meet-and-greets with senior members of the professional society. "You're already there, so it's good ROI," he concludes.

Opportunities on your own campus can also deliver great ROI. "Often people don't take advantage of or understand that there's a wealth of information at your university, and people really do want to see you succeed," says **Cheryl B. Schrader,** chancellor of Missouri University of Science and Technology. For example, there are numerous professional development training resources for tenure-track faculty at universities that can often be shared by postdocs. **Lorraine Tracey** realized the potential goldmine of internal advancement resources while a postdoc at St. Jude Children's Research Hospital. In pursuit of a career as a medical science liaison for a pharmaceutical company, she sought out the chance to participate in clinical shadowing and conduct lab tours to learn and practice coveted skills like communication, time management, and relationship building, and to gain a better understanding of clinical practice. To optimize her time, Tracey stayed within the borders of the institution.

But "thinking local" should be only one metric for choosing opportunities. Doing a thorough self-assessment and understanding your career aspirations and the steps to achieving these objectives is also a key component to prioritizing, says **Nadia Stegeman,** an NIH-funded postdoc at Oregon State University. "Know the skills that help you answer the interesting research questions," she says. "Have your top priorities in mind and seek to maximize learning opportunities. Everything else is details." In her case, she aspires to a career as a conservation medicine/field forensics veterinary consultant who assesses the health of a population or ecosystem, so she narrowed down her opportunities to those that allowed her to sharpen her clinical skills in evaluations of population health and toxicology. "Don't let school get in the way of your education," Stegeman cautions. "You are responsible for gaining those skills. Be bold. If you want something, say it and go after it."

Keep Up Your Output

Of course as you hunt opportunities, you have to make certain you are still doing what is anticipated of you by your boss. "It's so easy to get bogged down in opportunities and think you have to respond to everything," notes Brown. "Nothing can derail a postdoc faster than if they follow every opportunity out there at the expense of what they need to do in their research."

"Be upfront with your advisor about what they expect and the mechanisms you should use to meet those expectations," says Stegeman. By clarifying your promises, you also reduce restrictions on tracking other opportunities, she continues. A carefully worded discussion with your PI can articulate the message/request that if you meet certain expectations, then the rest of your time can be spent on other activities to move your career forward. "If you don't communicate your goals and your desired skill set, your advisor will never know and you both will suffer from this lack of communication," she warns.

Having a tool handy, like "My Individual Development Plan" (MyIDP.sciencecareers.org), through which you have solidified and organized your goals and needs, can be especially helpful when having that conversation with your advisor, notes Tracey, chair of the board of the National Postdoctoral Association. For example, if you desire the chance to chat with other scientists who are not in your immediate discipline, if it is on your plan, "it could be eye-opening to your PI," she says. The ability for your manager to see essentially in black and white how these discussions will serve you (and perhaps even them as well), "can make your time in the lab more flexible to pursue these other opportunities."

In fact, the more you can illuminate how your investment in pursuing a particular opportunity can provide hard benefits to your advisor, the more you may end up with time and other resources to explore them. This can even be a metric for determining whether you should investigate an opportunity in the first place. "Demonstrate that it's a win-win," encourages Schrader. continued>

CREDIT: PHOTO BY PATRICK INACIO PINA

National Socio-Environmental Synthesis Center

SESYNC (să-sink) is dedicated to fostering synthesis that brings together diverse forms of knowledge from the natural and social sciences to generate insights into the behavior and management of interlinked systems of people and nature

Postdoctoral Fellowship Program
Applications due May 1, 2013
Please visit:
http://www.sesync.org/postdoctoral-fellows-program
for further details

The National Socio-Environmental Synthesis Center (SESYNC), located in Annapolis, Maryland, invites applications for 2 year postdoctoral fellowships that begin September 2013. Fellows will undertake independent social, environmental, or cyber-infrastructure synthesis projects that are consistent with the mission of SESYNC. In addition to leading independent synthesis research, SESYNC fellows spend part of their time (~30%) on collaborative center activities. We seek a diverse group of postdoctoral fellows with PhDs in social, natural, and computational sciences.

The University of Maryland is an Equal Opportunity Employer. Minorities and Women Are Encouraged to Apply.

NREL
NATIONAL RENEWABLE ENERGY LABORATORY

POSTDOCTORAL CANDIDATES

The National Renewable Energy Laboratory (NREL) Chemical and Materials Science Center (5900) seeks highly qualified postdoctoral candidates in the areas of chemical and nanoscale sciences, experimental materials science, and theoretical materials science.

Through fundamental and applied research, the Center provides scientific understanding, discovery, and innovative solutions for energy conversion, storage, and utilization including solar electricity and fuels, advanced batteries, fuel cells, solid-state lighting, smart windows, and energy efficiency.

Interested applicants can find additional information and apply for Requisition #2978 or search other openings at www.nrel.gov/employment.

NREL is an equal employment opportunity employer.

NREL is a national laboratory of the U.S. Department of Energy, Office of Energy Efficiency and Renewable Energy, operated by the Alliance for Sustainable Energy, LLC.

University of Michigan
Medical School

POSTDOCTORAL
TRAINING OPPORTUNITIES
www.med.umich.edu/postdoc

The University of Michigan Medical School is an outstanding training environment that combines world-class faculty and innovative programs of research with a rich academic tradition. For two decades Michigan has ranked among the top 10 medical schools in NIH research funding. This research effort is enhanced by 27 NIH-sponsored training programs that support Postdoctoral Scholars.

The University of Michigan recognizes the essential contributions Postdoctoral Scholars make to the University's research mission. We offer a comprehensive career development program for our Postdoctoral Scholars to help guide their choices as they prepare themselves for independent careers. We welcome inquiries from graduate students nearing completion of the Ph.D. degree regarding opportunities for postdoctoral training in the following areas:

- Alcoholism Research
- Biology of Aging
- Biology of Drug Abuse
- Cancer Biology
- Cardiovascular Research
- Cell and Molecular Dermatology
- Clinical and Basic Neuroscience
- Endocrine Dysfunction
- Endocrinology and Metabolism
- Environmental Toxicology
- Experimental Immunology
- Genome Sciences
- Hearing, Balance and Chemical Senses
- Imaging Science in Biomedicine
- Lung Disease
- Lung Immunopathology
- Medical Rehabilitation Research
- Microbial Pathogenesis
- Molecular Hematology
- Nephrology Research
- Organogenesis
- Reproductive Sciences
- Research in Gastroenterology
- Substance Abuse
- Tissue Engineering and Regeneration
- Urology Research
- Vision Research

One way to explore these programs is to attend the *Postdoc Preview* on U-M's campus on June 27-27, 2013. The *Preview* weekend will introduce outstanding upper-level graduate students in the biomedical sciences to the breadth and excitement of postdoctoral research and training at Michigan.

Apply online by April 15, 2013 at
www.med.umich.edu/postdoc/preview

The University of Michigan is an equal opportunity, affirmative action employer.

Featured Participants

Argonne National Laboratory
www.anl.gov

Florida International University
www.fiu.edu

Harvard University
www.harvard.edu

Los Alamos National Laboratory
www.lanl.gov

Louisiana State University
www.lsu.edu

Michigan State University
www.msu.edu

Missouri University of Science and Technology
www.mst.edu

National Postdoctoral Association
www.nationalpostdoc.org

Oregon State University
www.oregonstate.edu

St. Jude Children's Research Hospital
www.stjude.org

The College of New Jersey
tcnj.pages.tcnj.edu

University of Cologne
www.uni-koeln.de

Cheryl Schrader

Prosanta Chakrabarty

Are You Moving Forward?

It is critical to know that for every opportunity you explore, you are moving one step closer to your goal. But how do you quantify this? Reddi suggests that one litmus test is whether or not you are getting feedback from your activities. For example if you publish a paper, "are you getting reprint requests? Are you getting requests to share your research?" he asks. "If it is always one-way traffic, that's assuredly not going to get you anywhere. The single most important factor is how well others are respecting your work, how well you are needed in the field, and how well you are known."

"Every step of the way to becoming a star you have to have those publications," confirms Chakrabarty. And yet, as you begin to have significant output, you also have to ensure that others know about it. "In grad school, I didn't think strategically," admits Wund. "I thought that if my research is cool, everybody else will think that too. I soon realized I had to develop soft skills."

Networking and self-promotion are two of those essential skills that not only must be learned, but also must be pursued as opportunities of their own. Schrader argues that "raising the visibility of you and your group's accomplishments" is paramount. "Establishing your uniqueness will move the whole group (and field) forward," she says. One opportunity that affords you the chance to build your "brand," or promise of value, in this regard is to volunteer to be a technical reviewer for conference papers or a journal. "If you do this type of professional activity, you can very quickly become recognized as an expert. Establishing your technical expertise in a particular niche is very important early on."

But be strategic about your networking endeavors in particular, cautions both Schrader and Chakrabarty. "The postdoc is a short time frame," says Schrader. Prioritize your networking actions by looking for (1) leaders who are most directly related to your area of expertise, (2) institutions that have the best fit for the careers you want to pursue, or (3) support groups that will give you the help you need to succeed, she advises. Mentors also play a key role in helping postdocs assess the value of certain opportunities.

If You Think They are Slipping Away…

The postdoc experience is a roller coaster. "You're going to be down at some point and you're going to be ecstatic at some point, and that's the nature of science," says Chakrabarty. "No one's going to pat you on the back. No one's going to tell you you're doing a good job. You have to figure it out yourself. The mistake people make is thinking that these opportunities happen on their own."

But don't think that just because you decline something now, that the chance is necessarily gone for good. "Some opportunities I have said no to, and they have come back and I was able to add more value the second time around," says Brown.

Tracey acknowledges that the fear of opportunities slipping away can consume postdocs, and she always seeks to bring her own career development decisions back to her plan. It's a way to parse opportunities, she suggests. "Try to understand what you want out of your career and where you want to be in 10–20 years."

On the other hand, not all undertakings will bring you directly to your career goal, and that's OK. "Many activities may lead to new options that will open up and more collaborative opportunities," says **Martin Prechtl,** a chemist with the University of Cologne, in Cologne, Germany. Although he jokingly admits, "Sometimes it's like a miracle to find the right job in academia because often it is difficult to predict where new positions will open in the next few years."

Indeed, Reddi emphasizes that you must incorporate a mindset of making connections and looking for opportunities, even if they don't seem to be leading to something very specific. The mere act of attending a talk "outside of your comfort zone," he says, helps to "cultivate this type of thinking, an attitude of connecting" with others which will bring its own rewards. And to those who express concern about not having enough time, the engineer offers this wisdom: "It doesn't take much time to light a candle. But after you light a candle, you can see everything in the room and how everything has its place among others."

Alaina G. Levine is a science writer and science careers consultant/speaker in Tucson, AZ.

DOI: 10.1126/science.opms.r1300129

CREDITS: (FROM LEFT) B.A. RUPERT/MISSOURI S&T; COURTESY OF PROSANTA CHAKRABARTY

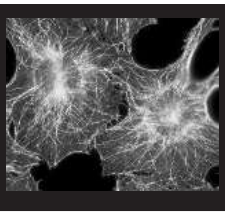

The NIH is the center of medical and behavioral research for the Nation ---making essential medical discoveries that improve health and save lives.

Chief Officer for Scientific Workforce Diversity
Office of the Director, National Institutes of Health
Department of Health and Human Services

Are you a top-level Scientific Researcher or Scientific Administrator seeking a career at one of the preeminent biomedical research institutes in the nation and the world? This position offers a unique and exciting opportunity for a leader to develop and implement initiatives enhancing diversity and promoting equity in the biomedical research enterprise, including NIH and other health and medical research entities. This position is expected, through the development of new programs, policies and practices and through cultural change, and shared responsibilities, to positively impact both the government and nongovernment workforces. The Chief Officer for Scientific Workforce Diversity serves as a member of the NIH Director's senior leadership team and will also serve as the co-chair to two newly formed Committees.

We are looking for applicants with a commitment to scientific excellence and the energy, enthusiasm, and innovative thinking necessary to lead within a dynamic and diverse organization. Applicants must possess an M.D., Ph.D., or equivalent doctoral degree in a scientific field related to biomedical research, plus expert stature in their discipline as demonstrated through their publication history and other contributions to their field. The strong candidate will have evidence of managerial, administrative, and mentoring ability. The full list of qualifications required can be found on the vacancy announcement located at **http://www.jobs.nih.gov/vacancies/executive.htm**.

The successful candidate for this position will be appointed at a salary commensurate with experience and accomplishments, and full Federal benefits, including leave, health and life insurance, retirement and savings plan (401K equivalent) will be provided.

If you are ready for an exciting leadership opportunity, please see the detailed vacancy announcement at http://www.jobs.nih.gov/vacancies/executive.htm
Applications are due by 11:59 p.m. on Tuesday, April 30, 2013.
Please contact Lynnita Jacobs at 301-402-4077 for questions and/or additional information.
DHHS AND NIH ARE EQUAL OPPORTUNITY EMPLOYERS

POSTDOCTORAL OPPORTUNITIES

Postdoctoral Fellow Opportunities

Geisinger Health System (GHS) is seeking Postdoctoral Fellows for multiple research areas.

- Postdoctoral Fellow for the laboratory of Anne Moon, MD, PhD to focus on the functions of Fgf and T-box transcription factors in vivo during mouse embryonic development
- Postdoctoral Fellow for the laboratory of Nikolaos Tapinos, MD, PhD with an interest in the fields of Molecular and Cellular Neuroscience
- Postdoctoral Fellow for the laboratory of Gerda E. Breitwieser, PhD to contribute to dissection of the novel mechanism(s) linking Calcium Sensing Receptor signaling and trafficking
- Postdoctoral Fellow to join a team focused on autism, neurodevelopmental disorders and genomics

Discover for yourself why Geisinger has been nationally recognized as a visionary model of integrated healthcare. For more information, please visit Join-Geisinger.org or contact: Jocelyn Heid, Department of Professional Staffing, at 1-800-845-7112 or jheid1@geisinger.edu.

GEISINGER
HEALTH SYSTEM

Follow us: f | LinkedIn

The Institute of Agriculture and Natural Resources at the University of Nebraska, is accepting applications for a Dryland Cropping Systems Specialist, a 50% research, 50% extension, 12-month, tenure-leading or tenured appointment at the Assistant, Associate, or Full Professor rank, located at the Panhandle Research and Extension Center (PHREC), Scottsbluff, Nebraska. Tenure home for this position is the Department of Agronomy and Horticulture, with administrative assignment to the PHREC. Rank and tenure will be based on experience and credentials of the successful applicant. If filled at the rank of Professor, the position is eligible for the endowed Fenster Professorship of Dryland Agriculture. Focus of this position will be developing and conducting relevant and responsive research and extension programs for the unique crops and cropping systems of the Central High Plains region and, in particular, the Nebraska Panhandle.

The successful candidate will be expected to develop a nationally and internationally recognized program in dryland cropping systems in a semi-arid, High Plains region, with a focus on efficiency, profitability and environmental management of dryland cropping systems with emphasis on appropriate cropping rotations, water management, weed control and soil conservation. The incumbent will participate in multi-disciplinary teams in alternative crops, pest and soil management, and livestock grazing programs; maintain a vigorous program supported through external grants and contracts, publish research results in peer-reviewed journals; and conduct relevant research and extension programs to convey research findings to clientele.

Requires Ph.D. degree or Ph.D. in place by date of hire, in Agronomy or closely related field.

To review the complete position details and apply for this position, go to: **http://employment.unl.edu**, search for requisition number **F_130078**. Click on "**Apply to this Job.**" Attach a letter of application, an overview of research and extension experience and interests, and a curriculum vitae. Arrange for 3 letters of reference to be sent via e-mail to: **sholman1@unl.edu**. Review of applications will begin on **April 22, 2013** and continue until the position is filled or the search is closed.

The University of Nebraska has an active National Science Foundation ADVANCE gender equity program, and is committed to a pluralistic campus community through Affirmative Action, Equal Opportunity, work-life balance, and dual careers.

POSITIONS OPEN

SCHOOL OF MEDICINE
UNIVERSITY of CALIFORNIA • IRVINE
Discover • Teach • Heal

POSTDOCTORAL SCHOLAR POSITION OPEN
School of Medicine
Department of Anatomy and Neurobiology
The University of California, Irvine

The laboratory of **Dr. Xiangmin Xu** at the University of California, Irvine (**website: http://xulab.anat.uci.edu/**) is funded by NIH and private foundation grants. One or two postdoctoral positions are available for young scientists with experimental training in systems or cellular neuroscience. Projects are to investigate cortical circuit organization and function using combined approaches such as electrophysiology, laser scanning photostimulation, optical imaging, and genetically modified rabies tracing. Applicants should be motivated for academic excellence, and will pursue projects in a relatively independent manner. A Ph.D. is required. Salaries and compensations will be competitive and commensurate with experience and accomplishments.

To apply, please contact:

Xiangmin Xu, Ph.D.
Assistant Professor
Department of Anatomy & Neurobiology
School of Medicine
University of California, Irvine
Irvine CA 92697-1275
Telephone: 949-824-0040 (office)
E-mail: xiangmin.xu@uci.edu

The University of California, Irvine is an Equal Opportunity Employer committed to excellence through diversity.

POSTDOCTORAL/RESEARCH ASSOCIATE POSITIONS in
Human and/or Mouse Immunology

Two postdoctoral positions are available to qualified applicants in the laboratory of **Dr. Janko Nikolich-Zugich** in the Department of Immunobiology, College of Medicine, University of Arizona. For description of laboratory interests and publications, see **website: http://immunobiology.arizona.edu/faculty/janko-nikolich-zugich-md-Ph.D**.

Qualified applicants will investigate T cell function and homeostasis in health, viral diseases, vaccination, and aging in a human and/or mouse model. Positions are also available to candidates interested in the broader role of inflammation and immunity in aging. Cellular immunology training is essential for this position.

Research in the Department and the University is supported by state-of-the-art core facilities including animal housing, FACS, DNA, Microarrays, Proteomics, and Imaging. University of Arizona is amongst the top 20 public research and education universities, boasting excellent departments and Centers, lively campus culture and life, and a blossoming recreation center. It is located in sunny Tucson, a city with a vibrant multicultural population of approximately 900,000, a strong economy, and business opportunities. Tucson is surrounded by a majestic desert and mountains rising to more than 9,000 feet.

Interested individuals should send inquiries/curriculum vitae and arrange for three letters of reference to be sent to:

Janko Nikolich-Zugich, M.D.-Ph.D.
Head, Department of Immunobiology
E-mail: nikolich@e-mail.arizona.edu

We deliver
customized job alerts.
www.ScienceCareers.org

POSITIONS OPEN

DREXEL UNIVERSITY
College of
Medicine
Biochemistry and Molecular Biology

POSTDOCTORAL FELLOW to
Investigate Synthetic Design of HIV-1 Env Peptidomimetic Antagonists

A postdoctoral position is available, contingent on grant funding, for recent Ph.D. recipient with demonstrated experience in peptidomimetic synthesis and the interest both to synthesize next generation nanomolar inhibitors targeting Env gp120 and to collaborate within a multidisciplinary research group to elucidate mechanisms of antagonist action. Interested candidates should send (1) a cover letter describing relationship of their experience and career goals to the available position and to the group research program, (2) resume, and (3) three support letters to: **Dr. Irwin Chaiken, Department of Biochemistry and Molecular Biology, Drexel University College of Medicine, 245 North 15th Street, M.S. 497, Philadelphia, PA 19102**.

E-mail: ichaiken@drexelmed.edu; website: http://www.drexelmed.edu/chaikengroup.

POSTDOCTORAL ASSOCIATE in
Maize Epigenomics
The Ohio State University

A position is available for understanding the molecular mechanisms governing heritable epigenomic variation. The research involves transcriptional and epigenomic profiling of maize as well as mutant characterization and molecular cloning. A Ph.D. in molecular-oriented biology, genetics, or biochemistry is required. Experience with plants, molecular genetics and computational biology is desired.

Applicants should electronically send their curriculum vitae and statement of research interest to **e-mail: hollick.3@osu.edu.**

Contact: **Dr. Jay Hollick, Department of Molecular Genetics, The Ohio State Univereisty, 500 Aronoff Laboratory, 318 W. 12th, Columbus, OH 43210**.

An NIH-funded **POSTDOCTORAL ASSOCIATE/RESEARCH ASSOCIATE POSITION** is available in the Department of Pediatrics at Baylor College of Medicine to study the molecular mechanisms of lung injury and abnormal lung development and angiogenesis by oxygen in newborn rodent models and cell lines. The successful candidate will use transgenic and knockout mice, cell lines, and apply state of the art molecular and cell biology techniques such as cloning, electrophorectic mobility shift assays, plasmid isolation, real time RT-PCR, chromatin immunoprecipitation, transfections, Western blotting, microarrays, RNA-seq, etc. Knowledge and skills in molecular biology research and angiogenesis would be highly desirable. Please send curriculum vitae to **Emily Pedraza** via **e-mail: emilyp@bcm.edu**.

Help employers find
you. Post your
resume/cv.
Science Careers
From the journal *Science* AAAS
www.ScienceCareers.org

Nontraditional Careers:
Opportunities Away From the Bench
Webinar

Want to learn more about exciting and rewarding careers outside of academic/industrial research? View a roundtable discussion that looks at the various career options open to scientists and strategies you can use to pursue a nonresearch career.

Now Available On Demand
www.sciencecareers.org/webinar

Produced by the *Science*/AAAS Business Office.
Science Careers
From the journal *Science* AAAS

UHN Princess Margaret Cancer Centre

Regenerative Medicine Scientist

The Ontario Cancer Institute (OCI) at the Princess Margaret Cancer Center is seeking an outstanding stem cell scientist, whose research program will be focused on developing a regenerative strategy to repair normal tissue injury, secondary to therapeutic ionizing radiation. The OCI is the largest cancer research center in Canada, and amongst one of the largest in North America. The OCI is part of the Princess Margaret Cancer Center, which houses the largest single institution Radiation Medicine Program, consulting on >8000 new cancer patients, and delivering >10,000 courses of radiation treatments each year.

We are seeking candidates who have an outstanding research track record in stem cell biology, in areas of neural, lung, intestinal or salivary gland regeneration, along with an understanding of the effects of ionizing radiation on normal tissues. The successful applicant will be expected to lead a world-class research program focused on this specific topic, with an emphasis on potential applications into the clinic. The OCI encompasses a broad spectrum of fundamental to translational cancer research programs, with significant strengths in stem cell biology, signal transduction, immunology, proteomics, structural biology, nanotechnology, radiation biology, hypoxia, and medical imaging.

The successful candidate will be eligible for appointment at the appropriate level in the Department of Radiation Oncology, Medical Biophysics, or related departments at the University. The position is available immediately, but the search will remain open until the position is filled.

Interested candidates should send their CV, as well as a description of their research interests and program, highlighting leadership experience or potential to:

Dr. Benjamin G. Neel
Director, Ontario Cancer Institute
oci @uhnresearch.ca
Please use the subject line: Regenerative Medicine Scientist

UHN Princess Margaret Cancer Centre

Chair in Inflammation

The **Ontario Cancer Institute** (OCI) at **Princess Margaret Cancer Centre and the Arthritis and Autoimmunity Research Centre (AARC) at the University Health Network** in Toronto, invite highly productive individuals to apply for the position of Scotiabank Chair in Inflammation Research at either the Scientist or Senior Scientist level. Research interests focused on inflammation pertaining to tumor biology and/or autoimmunity are encouraged. Applicants must have an M.D. and/or Ph.D. degree(s) and a proven track record, as evidenced by a number of high impact publications. The successful candidate will be expected to establish an original, competitive and independently funded research program, and to have a commitment to education in immunology.

OCI is the largest centre for cancer research in Canada covering the full spectrum of applied and fundamental research. The AARC is the most comprehensive research centre for autoimmune diseases in Canada, combining clinical and applied studies with basic science research. The downtown location provides an extraordinarily rich scientific environment, adjacent to other major academic institutions including the University of Toronto St. George campus, the Toronto General Research Institute, the Hospital for Sick Children, the Samuel Lunenfeld Research Institute, the Toronto Western Research Institute, and the Ontario Institute for Cancer Research,

The successful applicant will receive full salary commensurate with the position and a generous start up package. Applicants will also be eligible for appointment at the Associate or Full Professor level in the Department of Immunology at the University of Toronto.

Interested candidates should send their CV and a 2 page description of research interests to:

Inflammation Chair Search Committee,
Ontario Cancer Institute
620 University Ave
Toronto ON M5G 2M9
cwells@uhnresearch.ca

The Ontario Cancer Institute is the Research Institute of Princess Margaret Hospital, which, along with the AARC, Toronto General Hospital, Toronto Western Hospital and Toronto Rehabilitation Institute are members of the University Health Network, an Equal Opportunity Employer.

Idaho State UNIVERSITY

Dean, College of Science and Engineering

Pocatello, Idaho

Idaho State University seeks candidates for the position of Dean of the College of Science and Engineering. Idaho State University is a Carnegie-classified doctoral research high institution and attracts students from around the world to its Idaho campuses. The Dean is responsible for planning, budgeting, implementing, and evaluating its integrated programs of resident instruction, research, service and online educational programs. The College is comprised of the following departments; Biological Sciences, Chemistry, Computer Science, Geosciences, Mathematics, Physics, and a School of Engineering, which includes programs in Civil and Environmental Engineering, Electrical Engineering, Mechanical Engineering, Nuclear Engineering and Health Physics. The College of Science and Engineering is proud of its research that continues to expand through strong associations with research partners, both government and private sectors, and facilities that support multidisciplinary research. The College exemplifies the synergy that exists for collaboration between science and engineering.

Candidates should have a demonstrated competence in a field of study commonly included in a college of science and engineering with credentials and/or experience appropriate for a tenured appointment at the rank of professor in his or her discipline. Visionary leadership, creative response to opportunities, an understanding of the multiple missions and constituencies of the College, a commitment to diversity, and strong communication skills are selection criteria of great importance to the University. In addition, the successful candidate should have a demonstrated record of accomplishment in fundraising. The candidate should have substantial familiarity with the philosophy and responsibilities of a research-oriented institution with current or recent academic leadership experience at a Carnegie research high or very high university. Prior experience in managing a complex organization with responsibility for personnel, planning, program development, and resource allocation is desired.

At the main campus in Pocatello, and at locations in Meridian, Idaho Falls and Twin Falls, ISU offers access to high-quality education in more than 280 programs. Almost 14,500 students attend ISU, receiving education and training in those programs. Idaho State University faculty and students are leading the way in cutting-edge research and innovative solutions in the areas of energy, health sciences, nuclear research, engineering, technology, and biological sciences. Idaho State University combines exceptional academics amidst the grand natural beauty of the West.

For a complete job description and application instructions, visit us at https://isujobs.net/.

IDAHO STATE UNIVERSITY

ISU is an equal opportunity/affirmative action employer. We have an institution-wide commitment to inclusion and diversity and encourage all qualified individuals to apply. Veterans' preference.
Upon request, reasonable accommodations in the application process will be provided to individuals with disabilities.

AAAS is here –

bringing educational infrastructure to the developing world.

AAAS is helping the Rwandan government rebuild its educational infrastructure. By providing materials such as the Project 2061 *Atlas of Science Literacy*, lesson plans from Science NetLinks, and access to *Science* digital libraries, AAAS is helping the people of Rwanda work toward a future built around science and technology. If you're not yet a AAAS member, join us. Together we can make a difference.

To learn more, visit
aaas.org/plusyou/rwanda

AAAS + U = Δ

TEXAS BIOMEDICAL RESEARCH INSTITUTE | SNPRC Southwest National Primate Research Center

STEM CELL REGENERATIVE MEDICINE FACULTY POSITIONS

Southwest National Primate Research Center (SNPRC)

The SNPRC at the Texas Biomedical Research Institute invites applications and nominations for two faculty positions in stem cell regenerative medicine. Applicants and nominees are expected to have an interest in, and preferably experience with, nonhuman primate models. Major strengths of the SNPRC are in genetics and genomics, metabolic disorders, and infectious diseases. Several primate models of human diseases developed at SNPRC are ideally suited for translational research on stem cell regenerative medicine. The SNPRC has an outstanding diversity of primate resources, including large colonies of baboons, rhesus monkeys, common marmosets, and chimpanzees.

The SNPRC has close associations with the University of Texas Health Science Center at San Antonio and the University of Texas at San Antonio, including opportunities for roles in graduate education. A critical mass of stem cell regenerative medicine researchers exists at those institutions, together with the developing stem cell regenerative medicine program at the SNPRC. The SNPRC has a strong tradition in postdoctoral training.

Rank and salary will be nationally competitive and commensurate with experience. The laboratories and offices of the successful candidates will be located in the new SNPRC laboratory and administration facility, which is now under construction and expected to be ready for occupancy in March, 2014. The positions, as well as temporary laboratory and office space, are available immediately.

Applications and nominations should be sent to the **Chair, SNPRC Regenerative Medicine Search Committee, c/o Human Resources Office, P.O. Box 760549, San Antonio, TX 78245-0549**, and should include a letter outlining qualifications and research interests. Applications, but not nominations, must also include a CV, and the names and contact information for at least three references. Additional information about the SNPRC can be found at **www.snprc.org**. Additional information about Texas Biomed can be found at **www.txbiomed.org**.

EOE

Université Joseph Fourier GRENOBLE

Chair of Excellence in Cancer Translational Research

The Institute Albert Bonniot (IAB) (**http://iab.ujf-grenoble.fr/fr/**) seeks highly qualified applicants in the field of Cancer Translational Research for a three-year professor position, extendable to a permanent professor position at the University Joseph Fourier and the University Hospital of Grenoble.

The ideal candidate will be a senior scientist, oncologist or biologist (MD and or PhD) with highly recognized expertise in molecular biology applied to cancer. He/She will have an outstanding track record of publication in top-ranked journals. The conducted research should lead to innovative applied results by developing the synergy between the IAB and Grenoble Institute of Cancer Research (**http://girc.ujf-grenoble.fr/fr/**)teams to exploit the full potential of the Grenoble site in clinical aspects, biology, chemistry, physic and numeric science under the frame of a cancer theragnosis project.

This Chair of Excellence financed by University Joseph Fourier, the University Hospital of Grenoble, the Cancéropôle Lyon Auvergne Rhône-Alpes (CLARA) and the « Collectivités Locales » offers an attractive salary, leading to a permanent position in the University and the Hospital, with associated human (PhD students, post doc positions) and technical resources allowing a high level cancer translational project to be set up rapidly. A proficient level in French language is required given the translational projects to be led.

Potential candidates should send a CV and a project proposal before **March 29th 2013** (please download application: **http://iab.ujf-grenoble.fr/fr/**). Selected candidates will be interviewed by an international committee in May 2013.

For further information please contact: **Christian Brambilla**, Head of IAB: **christian.brambilla@ujf-grenoble.fr**

北京航空航天大學
BEIHANG UNIVERSITY

Faculty Positions Available in Beihang University, China

Established in 1952, Beihang University is one of top research-oriented universities in China, focusing on fundamental cutting edge research and high-level education. One of the first universities funded by China's "211" and "985" programs, it has seven national key laboratories and twenty-five provincial and ministerial key laboratories. Today, Beihang University is known for outstanding research and education in aviation and aerospace sciences, power and energy engineering, materials science, mechanics, information science, transportation science, instrumentation science, management science and law.

Beihang University is on a clear path to become a world-class university in many engineering and science disciplines. As part of Beihang's further pursuit for excellence in research and education, we have expanded our global search for the best research talent to join our International Research Institute for Multidisciplinary Science (IRIMS). Five independent international research centers (IRC) were established recently under the name of IRIMS. As the core part of IRIMS, IRCs are devoted to establish a world-class, advanced and multidisciplinary research platform.

Beihang University invites applications for full-time Professors, Associate Professors and excellent scientists. Preference will be given to candidates whose research emphasis demonstrates the potential to complement and advance the IRIMS existing research strengths. Successful candidates will be provided competitive salaries and start-up funds.

Positions Available

- Position offered by the Recruitment Program of Global Experts (1000 Plan Professorship)
- Position offered by the Chang Jiang Scholars Program
- Position offered by the Recruitment Program of Global Young Experts (1000 Plan Professorship for Young Talents)
- Position offered by Beihang University's Zhuoyue Program of Professors
- Position offered by Beihang University's Zhuoyue Program of Associate Professors.

Interested individuals should send curriculum vitae by email to **rscrcb@buaa.edu.cn**, with "Faculty Application" in the title. For more information, please visit the university's Human Resource Department website **http://rsc.buaa.edu.cn/**, or contact us by email **rscrcb@buaa.edu.cn** or by telephone **86-010-82317779**.

NYU NEUROSCIENCE

Valentino D.B. Mazzia MD, JD Professorship in Anesthesiology

The Department of Anesthesiology and the Neuroscience Institute of NYU Langone Medical Center are recruiting an outstanding MD/PhD or MD neuroscientist to become tenured Professor and Vice Chair of Research for the Department of Anesthesiology and a member of the Neuroscience Institute at NYU. Applicants should have an ongoing extramurally supported research program in any area of neuroscience related to anesthesiology, such as ion channel physiology, neuronal plasticity, mechanisms of pain, consciousness and higher cognitive function, etc. The candidate will be responsible for their own research program and expected to grow basic and clinical neuroscience research in the Department of Anesthesiology and to mentor junior faculty, residents, and students.

Please submit your CV with a statement describing your scientific and mentoring interests by email to:

Thomas.Blanck@nyumc.org
or to
Richard.Tsien@nyumc.org

Submission deadline: **May 30, 2013**

深圳大學
Shenzhen University

Institute of Molecular Medicine (IMM)

Distinguished Professor/full professor/Associate Professor/ Lecturer Positions

Institute of Molecular Medicine (IMM) of Shenzhen University is seeking applicants for ten or more positions of distinguished/full professors, associate professors and lecturers with outstanding scholarly achievements and with research expertise in the areas of molecular biology, cell biology, cancer biology, medicinal chemistry and/or other related disciplines. Researchers with experience in cancer stem cell, second-generation sequencing, NK cells, epigenetics, high-throughput screening and/or other cutting edge technologies are welcome to apply. Salary and benefits are highly competitive and commensurate with accomplishments and experience.

IMM is a brand new, modern, research-oriented and well-equipped medical research institute resided in Shenzhen which is right next to Hong Kong and is one of the top cities of China. The mission of IMM is to identify drug targets and to develop cures for diseases. The director of IMM is a 2012 recipient of the national 1000-talents Program. For publications of the IMM director, please see [**Cancer Cell** 2010, 18(3):258-67; **Nature Medicine** 2006,12(1):128-32 and **Nature** 1998, 395(6703):713-6].

The applicants will be expected to maintain a vigorous research program and participate in teaching and service for IMM. The successful candidate will possess a PhD and/or MD degree and also is fluent in both English and Chinese. Applicants should submit (1) curriculum vitae, (2) a description of research accomplishments and (3) an email title with the position intended to apply electronically to **jdlee@scripps.edu**, **jdleeszu@gmail.com** and **jdlee@szu.edu.cn**. Review of applications will begin immediately, and continue until the positions are filled. Details please see Job Ad in Shenzhen University Website (**http://szuhr.szu.edu.cn/**).

WEBINAR

The Future of High Throughput Assays

From Reporter Genes to qPCR

WEDNESDAY, MARCH 20, 2013

12 noon ET, 9 a.m. PT, 4 p.m. UK, 5 p.m. CET

In vitro high throughput screening in drug discovery has typically been accomplished using reporter gene assays, which offer a versatile, cost-effective, and technically simple way to screen in high throughput, and are amenable to miniaturization. However, these assays are unsuitable for screening primary cells and cannot assess impact on endogenous gene expression. Real-time (quantitative) PCR (qPCR) can overcome these drawbacks and has widespread and proven use in gene expression analysis at both low and medium throughput. Until now, the application of qPCR in high throughput screening (HTS) has been limited by an often laborious multistep process to generate suitable template, and high reagent cost due to large reaction volumes. Recent advances in streamlining the qPCR workflow, liquid handling, and instrumentation have enabled scientists to generate sensitive and cost-effective high throughput qPCR data in drug discovery processes.

During the webinar the expert panel will:

- Discuss the pros and cons of qPCR vs. traditional reporter gene assays in HTS
- Describe the advances in technology that have enabled the application of qPCR in HTS
- Outline the necessary steps required for fully automated implementation of qPCR technology in HTS
- Answer your questions live during the broadcast.

SPEAKERS

Andrea Weston, Ph.D.
Bristol-Myers Squibb
Wallingford, CT

Patrick Faloon, Ph.D.
Broad Institute of MIT and Harvard
Cambridge, MA

Daniel G. Sipes
Genomics Institute of the Novartis Research Foundation
San Diego, CA

REGISTER NOW!
webinar.sciencemag.org

Webinar sponsored by

Roche

Brought to you by the *Science*/AAAS Custom Publishing Office

Science AAAS

UNIQUE SETTING. UNPARALLELED LEARNING.

JANELIA FARM RESEARCH CAMPUS | CONFERENCES

SEP 22–25
MAMMALIAN CIRCUITS UNDERLYING TOUCH SENSATION
David Ginty, Steve Hsiao, Ellen Lumpkin, Karel Svoboda

SEP 29–OCT 2
METHODS IN CRYO-EM TO DEAL WITH DIFFICULT SAMPLES
Tamir Gonen, Niko Grigorieff

OCT 13–16
SYNAPTIC VESICLE BIOGENESIS
Pietro de Camilli, Volker Hauke, Tim Ryan

OCT 27–30
HORMONAL CONTROL OF CIRCUITS FOR COMPLEX BEHAVIORS
Lynn Riddiford, Scott Sternson, Jim Truman

NOV 17–20
SHAPING THE WAVES: ENGINEERING OPTICAL WAVEFRONT FOR BIOMEDICAL IMAGING
Meng Cui, Na Ji

Janelia conferences are small and specialized events intended to encourage rapid scientific advances and foster collaborative interactions. If you are interested in joining a robust dialogue among leading scientists, submit a research abstract today.

APPLICATION DEADLINE: 2 P.M. ET, MAY 15, 2013
www.janelia.org/conferences/sci

HHMI janelia farm research campus

PRIZES

The 2013 Martha T. Muse Prize for Science and Policy in Antarctica

The "Martha T. Muse Prize for Science and Policy in Antarctica" is a US$ 100,000 unrestricted award presented to an individual in the fields of Antarctic science or policy who has demonstrated potential for sustained and significant contributions that will enhance the understanding and/or preservation of Antarctica. The Prize is inspired by Martha T. Muse's passion for Antarctica and is intended to be a legacy of the International Polar Year 2007-2008.

The prize-winner can be from any country and work in any field of Antarctic science or policy. The goal is to provide recognition of the important work being done by the individual and to call attention to the significance of understanding Antarctica in a time of change. A website with further details, including the process of nomination, closing date and selection of the Prize recipients is available at **www.museprize.org**.

The Prize is awarded by the Tinker Foundation and administered by the Scientific Committee on Antarctic Research (SCAR).

TFI TINKER FOUNDATION INCORPORATED

Nominations open until 23 May 2013

SCAR

POSITIONS OPEN

The Norwegian University of Science and Technology (NTNU) in Trondheim represents academic eminence in technology and the natural sciences as well as in other academic disciplines ranging from the social sciences, the arts, medicine, architecture to fine art. Cross-disciplinary cooperation results in innovative breakthroughs and creative solutions with far-reaching social and economic impact.

Faculty of Medicine

Two Positions as Professor in Medicine

- **One 100 % permanent position as Professor in Medicine (Biochemistry/Molecular Biology).**
- **One 100 % temporary position as Professor in Medicine (Cell Biology) for five years with a possible extension.**

Both positions are administratively attached to the Department of Cancer Research and Molecular Medicine (IKM), with the Laboratory Centre as the place of work. For further information about the Department, see www.ntnu.edu/dmf/ikm

For further information about the position, please see the full announcement at www.jobbnorge.no or please contact: Professor Magne Børset, head of Department of Cancer Research and Molecular Medicine: Telephone +47 725 73 038, e-mail: magne.borset@ntnu.no

Applications are to be submitted electronically via www.jobbnorge.no (ID.No. DMF 108-12 or DMF 17-13) within the deadline of 2013-04-30.

Jobbnorge.no

NTNU Norwegian University of Science and Technology

Science Careers online @sciencecareers.org

AAAS is here – Science Funding, Climate Regulation, Human Rights.

Around the world, governments turn to AAAS as an objective, multidisciplinary scientific authority to educate public officials and judicial figures on today's most pressing issues. And this is just one of the ways that AAAS is committed to advancing science to support a healthy and prosperous world. Join us. Together we can make a difference.

To learn more, visit aaas.org/plusyou/policy

AAAS + U = Δ

AAAS is here – helping scientists achieve career success.

Every month, over 400,000 students and scientists visit ScienceCareers.org in search of the information, advice, and opportunities they need to take the next step in their careers.

A complete career resource, free to the public, *Science* Careers offers a suite of tools and services developed specifically for scientists. With hundreds of career development articles, webinars and downloadable booklets filled with practical advice, a community forum providing answers to career questions, and thousands of job listings in academia, government, and industry, *Science* Careers has helped countless individuals prepare themselves for successful careers.

As a AAAS member, your dues help AAAS make this service freely available to the scientific community. If you're not a member, join us. Together we can make a difference.

To learn more, visit **aaas.org/plusyou/sciencecareers**

AAAS + U = Δ

AAAS is here – promoting universal science literacy.

In 1985, AAAS founded Project 2061 with the goal of helping all Americans become literate in science, mathematics, and technology. With its landmark publications *Science for All Americans* and *Benchmarks for Science Literacy*, Project 2061 set out recommendations for what all students should know and be able to do in science, mathematics, and technology by the time they graduate from high school. Today, many of the state standards in the United States have drawn their content from Project 2061.

Every day Project 2061 staff use their expertise as teachers, researchers, and scientists to evaluate textbooks and assessments, create conceptual strand maps for educators, produce groundbreaking research and innovative books, CD-ROMs, and professional development workshops for educators, all in the service of achieving our goal of universal science literacy.

As a AAAS member, your dues help support Project 2061 as it works to improve science education. If you are not yet a AAAS member, join us. Together we can make a difference.

To learn more, visit **aaas.org/plusyou/project2061**

AAAS + U = Δ